# Olefin Metathesis Catalysts: From Decomposition to Redesign

Daniel Luis do Nascimento

Thesis submitted to the University of Ottawa
in partial fulfillment of the requirements for the degree of

Doctor of Philosophy

Ottawa-Carleton Chemistry Institute
Faculty of Science
University of Ottawa

## Table of Contents

## Table of Figures

## Table of Schemes

## Table of Charts



## Table of Tables

# Abstract

Olefin metathesis is arguably the most versatile catalytic route yet developed for the assembly of carbon-carbon bonds. Metathesis methodologies are attractive from both synthetic and ecological standpoints, because they employ unactivated double bonds. This reduces the total number of synthetic steps, and the associated generation of chemical wastes. The drive to deploy olefin metathesis in highly demanding contexts, including pharmaceutical manufacturing and chemical biology, puts severe pressure on catalyst lifetime and productivity. Understanding the relevant decomposition pathways is critical to achieve essential performance goals, and to enable informed catalyst redesign. This thesis work expands on significant prior advances that identified and quantified critical decomposition pathways for ruthenium catalysts stabilized by N-heterocyclic carbene (NHC) ligands. Because pristine catalyst materials are essential for mechanistic study, it focuses first on methods aimed at improving efficiency and purity in catalyst synthesis. Merrifield iodide resins were shown to function as efficient, selective phosphine scavengers in the production of clean second-generation catalysts from $PCy_3$-stabilized precursors.

The thesis then turns to mechanistic examination of decomposition pathways that underlie success and failure for leading NHC catalysts, for comparison with a new family of catalysts stabilized by cyclic (alkyl)(amino) carbene (CAAC) ligands. These represent the first in-depth mechanistic studies of the CAAC catalysts, which have attracted much attention for their breakthrough productivities in challenging metathesis reactions. The remarkable productivity of the CAAC catalysts is shown to originate in their resistance to decomposition of the key metallacyclobutane intermediate via β-elimination, and (to a lesser extent) in their resistance to attack by nucleophiles and Bronsted bases. Importantly, however, they are *more* susceptible to bimolecular decomposition. The latter behaviour, as well as their resistance to β-elimination, is traced to the strong trans influence of the CAACs relative to NHC ligands. This insight significantly advances our understanding of the fundamental properties governing both productivity and decomposition.

Finally, two new catalysts are developed, building on the principle that nucleophilic stabilizing ligands should be avoided in the precatalysts. In the first of these complexes, an *o*-dianiline ligand is employed to stabilize the precatalyst. This flexible, H-bonding chelate serves the further purpose of accelerating macrocyclization of flexible dienes that bear polar functionalities. As its H-bonding capacity also increases its sensitivity to trace water, however, an alternative catalyst architecture was pursued. The latter consists of a dimer bearing bulky Ru-indenylidene centers, in which a dative bond from a bridging chloride affords the fifth ligand essential to stabilize the precatalyst.

# Acknowledgements

First and foremost, I wish to thank Prof. Deryn Fogg for everything she has done to make this thesis possible. I am tremendously grateful for the comprehensive and rigorous training you provided. You taught me how to think critically and communicate my ideas effectively, two fundamental skills in science that I will carry for the rest of my life. I hope in my future group I can teach my students with the same level of rigour, passion and dedication you display every day. Before I came to Canada, I remember telling you I would do everything in my power to make the most of the opportunity you were giving me. I hope the work in this thesis reflects that promised dedication, and that you agree you made me more "hard-ass" than I was on arrival.

Secondly, I need to thank all past and present members of the Fogg lab. Each and every one of you enriched my graduate experience. Thank you for the daily discussions, constructive feedback on manuscripts and presentations, and willingness to lend a hand, especially when I was not in peak physical condition. A special thank you to Steph Ton, Alex Goudreault, Mason Guy, Danny Sheldon and Craig Day for the times we played soccer. As a Brazilian, you have no idea how those moments made me happy. I would like to thank all the members of the "breaky squad" for the relaxing breakfasts on Fridays. My body will miss the extravagantly high fat content of the "breakfast special" we always ordered (and regretted the next hour). Thank you Steph Rufh for coming up with this idea and I hope this tradition will be kept alive after my graduation. I would like to thank the senior members of the Fogg lab when I started (Carolyn Higman and Stephan Audoersch) for mentoring me when I joined the group. A special thank you to the amazing scientist Gwen Bailey for being so kind, so clever and so inspirational. For the present members Christian, Eliza, Nathan, Harrison and Pedro, I hope I have taught you well and I am sure you will do some really cool science in the coming years.

I also wish to recognize the hard work of the technical experts I have had the pleasure of working with: Drs. Glenn Facey and Peter Pallister (uOttawa NMR Facility Managers past and present) and Roxanne Clement (uOttawa High Throughput Facility Manager). I also thank the Government of Ontario and the University of Ottawa for the scholarship support they provided over the course of my graduate studies.

To my beloved friends from Brazil, whom I miss every day, you have a special place in my heart. I will always be by your side, even if I am in a different country.

To my family, I thank you for your unconditional love, support, encouragement, and understanding. I cannot wait to hug you all. Lastly, to my best friend Jihane, thank you for being by my side every step of the way, and for always believing in me - I truly could not have done it without you.

# *Dedication*

"Therefore, as God's chosen people, holy and dearly loved, clothe yourselves with compassion, kindness, humility, gentleness and patience. Bear with each other and forgive one another if any of you has a grievance against someone. Forgive as the Lord forgave you. And over all these virtues put on love, which binds them all together in perfect unity. Let the peace of Christ rule in your hearts, since as members of one body you were called to peace. And be thankful." — Colossians 3:12-15

"Revesti-vos, pois, como eleitos de Deus santos e amados de entranhas de misericórdia, de benignidade, humildade, mansidão, longanimidade. Suportando-vos uns aos outros e perdoando-vos uns aos outros, se alguém tiver queixa contra outro; assim como Cristo vos perdoou, assim fazei vós também. E sobre tudo isso revesti-vos de amor, que é o vínculo da perfeição. E a paz de Deus, para qual também fostes chamados em um corpo, domine em vossos corações; e sede agradecidos." — Colossenses 3:12-15

*In memory of Luiz Recchia and Gabriel Arab*

# List of Contributions

**Publications** (C = communication; F = full paper). Co-author names appear in order of contribution; the principal investigator (PI) is named last.

**10C.** G. Occhipinti, M. Foscato, **D. L. Nascimento**, V. R. Jensen, D. E. Fogg, Exploring the Metathesis Productivity of Olefin Metathesis Catalysts: A High Trans-Influence Carbene Prevents Decomposition via β-Hydride Elimination. **2021**, Manuscript in preparation.

**9C. D. L. Nascimento**, M. Foscato, G. Occhipinti, V. R. Jensen, D. E. Fogg, Bimolecular Coupling in Olefin Metathesis: Correlating Structure and Decomposition for Leading and Emerging Ruthenium-Carbene Catalysts. *J. Am. Chem. Soc*., **2021**, *143*, 11072–11079.

**8C.** C.O. Blanco, **D.L. Nascimento**, D.E. Fogg, Routes to High-Performing Ru-Iodide Catalysts for Olefin Metathesis: Phosphine Lability Is Key to Efficient Halide Exchange. *Organometallics.*, **2021**, *40*, 1811–1816.

**7C.** C.O. Blanco, J. Sims, **D.L. Nascimento**, A.Y. Goudreault, S. Steinmann, C. Michel, D.E. Fogg, The Impact of Water on Ru-Catalyzed Olefin Metathesis: Potent Deactivating Effects Even at Low Water Concentrations. *ACS Catal.*, **2021**, *11*, 893-899.

**6F. D.L. Nascimento**, I. Reim, M. Foscato, V.R. Jensen, D.E. Fogg, Challenging Metathesis Catalysts with Nucleophiles and Brønsted Base: Examining the Stability of State-of-the-Art Ruthenium Carbene Catalysts to Attack by Amines. *ACS Catal.*, **2020**, *10*, 11623-11633.

**5C.** A.Y. Goudreault, D. Walden, **D.L. Nascimento**, A.G. Botti, S. Steinmann, C. Michel, D.E. Fogg, Hydroxide-Induced Degradation of Olefin Metathesis Catalysts: A Challenge for Metathesis in Alkaline Media. *ACS Catal.*, **2020**, 10, 3838-3843.

**4C. D.L. Nascimento**, D.E. Fogg, Origin of the Breakthrough Productivity of Ruthenium-CAAC Catalysts in Olefin Metathesis *J. Am. Chem. Soc*., **2019**, *141*, 19236-19240.

**3C. D.L. Nascimento**, A. Gawin, R. Gawin, P.A. Gunka, J. Zachara, K. Skowerski, D.E. Fogg, Integrating Activity with Accessibility in Olefin Metathesis: An Unprecedentedly Reactive Ruthenium-Indenylidene Catalyst. *J. Am. Chem. Soc*., **2019**, *141*, 10626-10631.

**2C.** C.S. Higman,[†] **D.L. Nascimento**,[†] B.J. Ireland, G.A Bailey, , S.A. Audorsch, D.E. Fogg, Chelate-Assisted Ring-Closing Metathesis: A General Strategy for Macrocyclization at Ambient Temperature. *J. Am. Chem. Soc.*, **2018**, *140*, 1604−1607. ([†]Equal contributions).

**1F. D.L. Nascimento**, E.C Davy, D.E. Fogg, Merrifield Resin-Assisted Routes to Second-Generation Catalysts for Olefin Metathesis. *Catal. Sci. Technol.,* **2018**, *8*, 1535-1544.

**Selected Presentations** (O = oral, P = poster)

**8O. D.L. Nascimento**, D.E. Fogg (2020) Integrating Robustness and Productivity in Olefin Metathesis. Virtual Conference; *Ottawa-Carleton Chemistry Institute Day,* Ottawa, June 4.

**7O. D.L. Nascimento**, D.E. Fogg (2019) Integrating Catalyst Performance and Accessibility in Olefin Metathesis. *CCRI Technical Seminar,* Ottawa, Dec. 12.

**6O. D.L. Nascimento**, D.E. Fogg (2019) Integrating Catalyst Performance and Accessibility in Olefin Metathesis. *102nd Canadian Chemistry Conference*, Quebec City, June 3–7.

**5O. D.L. Nascimento**, D.E. Fogg (2018) H-Bonding-Assisted Metathesis Macrocyclization (H-BAMM): Cyclizing Large Rings Bearing Polar Functionalities. *Ottawa-Carleton Chemistry Institute Day,* Ottawa, May 22.

**4O. D.L. Nascimento**, D.E. Fogg (2017) Chelate-Assisted Ring-Closing Metathesis: A Strategy For Accelerated Macrocyclization At Ambient Temperatures. *50th Inorganic Discussion Weekend,* Toronto, Nov. 3-5.

**3P. D.L. Nascimento**, D.E. Fogg (2017) Merrifield Resins As Phosphine Scavengers In Olefin Metathesis. *Ottawa-Carleton Chemistry Institute Meeting*, Ottawa, May 25.

**2P. D.L. Nascimento**, D.E. Fogg (2017) Merrifield Resins as Synthetic Aids in The Production of Metathesis Catalysts. *100th Canadian Society for Chemistry Conference*, Toronto, May 28-June 1.

**1P. D.L. Nascimento**, D.E. Fogg (2016) Exploring "Phosphine Sponges" as Aids in Synthesis of Ru Metathesis Catalysts. 49th Inorganic Discussion Weekend, Hamilton, Nov. 4.

# List of Abbreviations

| | |
|---|---|
| CAAC | cyclic alkyl amino carbene |
| NHC | N-heterocyclic carbene |
| CM | cross-metathesis |
| COSY | correlation spectroscopy |
| Cy | cyclohexyl |
| DBU | 1,8-diazabicyclo[5.4.0]undec-7-ene |
| DFT | density functional theory |
| DMT | dimethyl terephthalate |
| ESI | electrospray ionization |
| Et | ethyl |
| equiv | equivalents |
| FID | flame-ionization detector |
| GC | gas chromatography |
| GC/MS | gas chromatography/mass spectrometry |
| $H_2$IMes | 1,3-bis-(2,4,6-trimethylphenyl)imidazolin-2-ylidene |
| HMBC | heteronuclear multiple bond coherence |
| HMQC | heteronuclear multiple quantum coherence |
| HPLC | high-performance liquid chromatography |
| KTp | potassium tris(1-pyrazolyl)borate |
| MALDI | matrix-assisted laser desorption/ionization |
| MCB | metallacyclobutane |
| Me | methyl |
| Mes | mesityl (i.e., 1,3,5-trimethylphenyl) |
| MS | mass spectrometry |
| N.D. | not determined |
| NHC | *N*-heterocyclic carbene |
| NMR | nuclear magnetic resonance |
| NOESY | nuclear Overhauser effect spectroscopy |
| N.R. | not reported |
| ORTEP | Oak Ridge thermal ellipsoid plot |
| Ph | phenyl |
| py | pyridine |
| RCM | ring-closing metathesis |
| mRCM | macrocyclization |
| THF | tetrahydrofuran |
| TMB | trimethoxybenzene |
| TOF | time-of-flight |
| UHP | ultra-high purity |
| XRD | X-ray diffraction |
| $^{i}$Pr | isopropyl |
| BMC | bimolecular coupling |
| SE | styrenyl ether |
| NSE | nitro styrenyl ether |
| pTSA | *p*-toluene sulfonic acid |

| | |
|---|---|
| MF-I | Merrifield iodide resin |
| MF-Cl | Merrifield chloride resin |
| NNDD | *N,N'*-dimesitylethane-1,2-diamine |
| NBS | *N*-bromosuccinimide |
| DME | dimethoxyethane |
| RT | room temperature |
| ROMP | ring opening metathesis polymerization |
| SHOP | shell higher olefin process |
| TLC | thin layer chromatography |
| TON | turnover number |
| HCV | hepatitis C virus |
| DBU | 1,8-Diazabicyclo[5.4.0]undec-7-ene |
| $NEt_3$ | triethylamine |
| ADMET | acyclic diene metathesis |
| GMP | Good Manufacturing Practices |
| tBVE | tert-butylvinylether |
| HOTf | triflic acid |
| ODA | ortho-dianiline |
| MO | methyl oleate |

# List of Compounds

## Ruthenium Complexes

| # | Structure | # | Structure |
|---|---|---|---|
| **GI** | 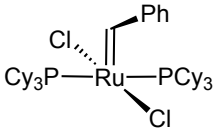 | **GII** | 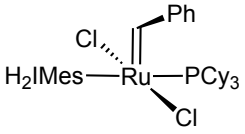 |
| **GII(I)** | 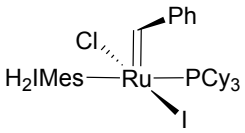 | **GII($I_2$)** | 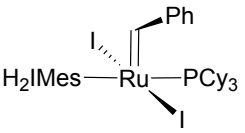 |
| **$d_{22}$-GII** | 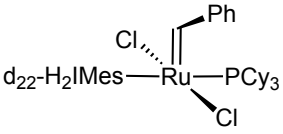 | **GIII** | 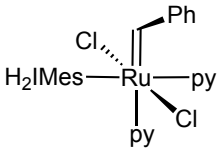 |
| **GIII'** | 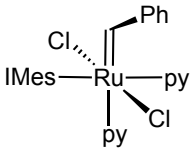 | **HI** | 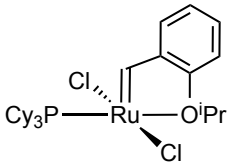 |
| **HI($I_2$)** | 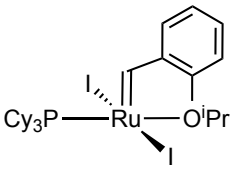 | **HII** | 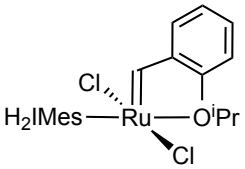 |
| **HII(I)** | 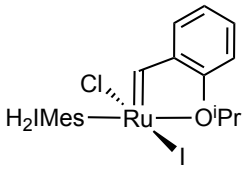 | **HII($I_2$)** | 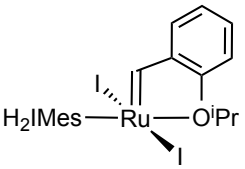 |
| **$d_{22}$-HII** | 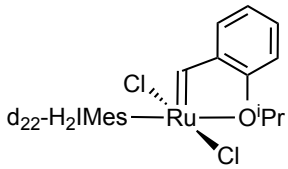 | **$^{13}$C-HII** | 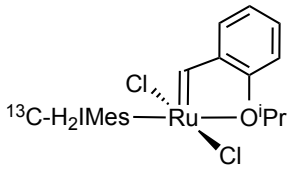 |

| | | | |
|---|---|---|---|
| **HII$^{P}$** | 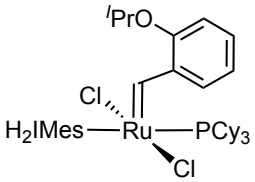 | **InC1$^{Ph}$** | 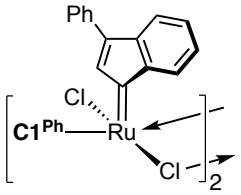 |
| **InI** | 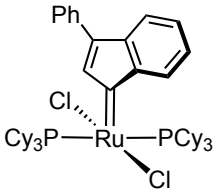 | **InII** | 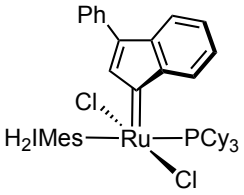 |
| **InII-I** | 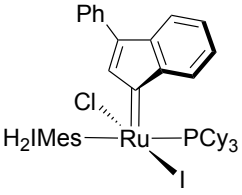 | **UC** | 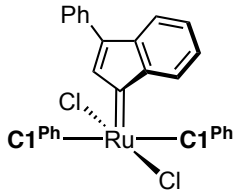 |
| **DAC1$^{Ph}$** | 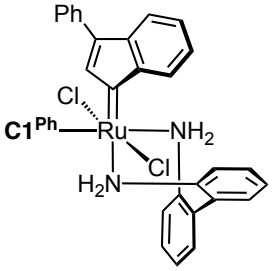 | **nG** | 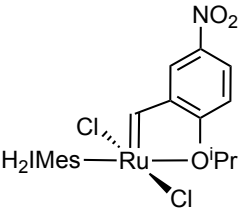 |
| **nG(I$_2$)** | 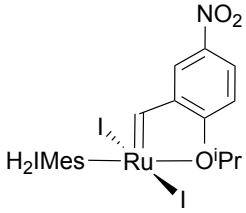 | **nGC1$^{Ph}$** | 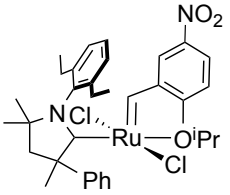 |
| **nGC2$^{Me}$** | 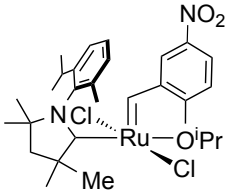 | **HC1$^{Me}$** | 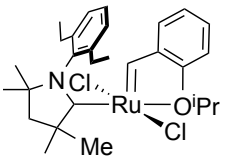 |
| **HC1$^{Ph}$** | 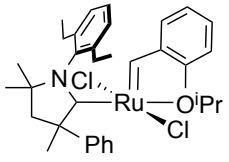 | **HC2$^{Me}$** | 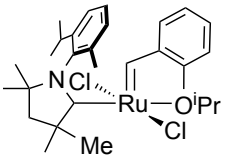 |

| | | | |
|---|---|---|---|
| **HC3$^{Ph}$** | 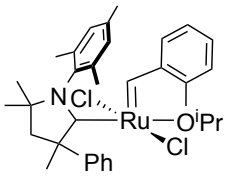 | **HC1$^{Ph}$($I_2$)** | 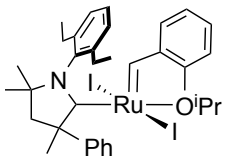 |
| **Cb$^{X}$** | 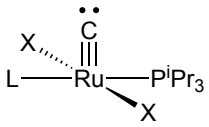 | **CbII** | 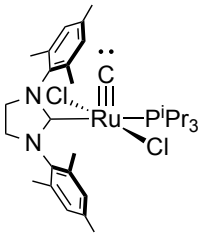 |
| **CbC1$^{Ph}$** | 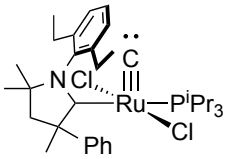 | **CbC1$^{Me}$** | 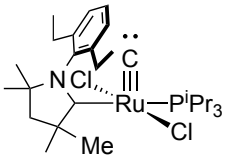 |
| **CbC2$^{Me}$** | 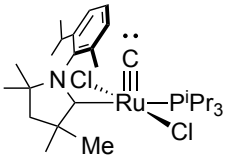 | **CbC3$^{Ph}$** | 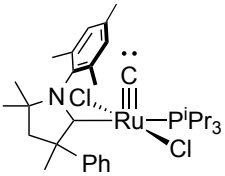 |
| **CbC1$^{Ph}$($I_2$)** | 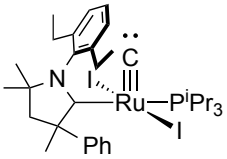 | **P$^{X}$** | 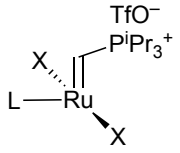 |
| **PII** | 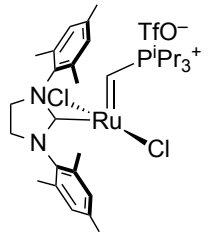 | **PII'** | 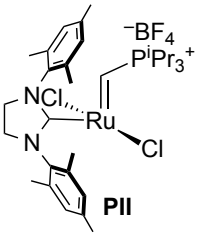 |
| **PC1$^{Ph}$** | 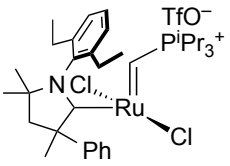 | **PC1$^{Me}$** | 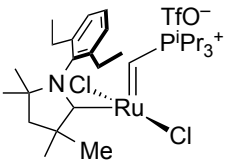 |

| | | | |
|---|---|---|---|
| **PC2$^{Me}$** | 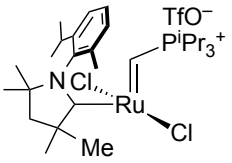 | **PC3$^{Ph}$** | 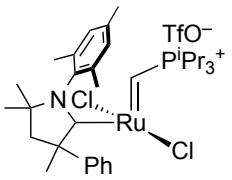 |
| **PC1$^{Ph}$($I_2$)** | 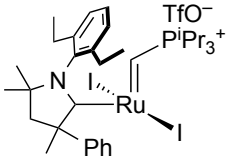 | **mC1$^{Ph}$** | 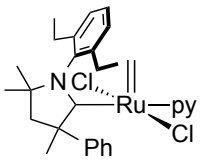 |
| **mGI*** | 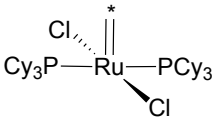 | **mGII** | 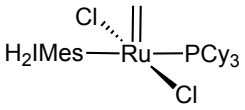 |
| **mGIII** | 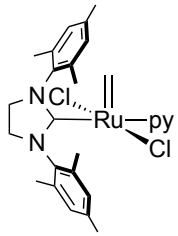 | **mC1$^{Me}$** | 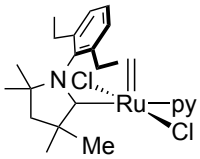 |
| **mC2$^{Me}$** | 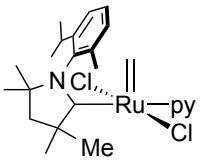 | **mC3$^{Ph}$** | 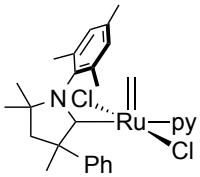 |
| **mC1$^{Ph}$** | 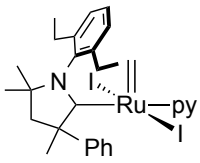 | **Ru-1** | 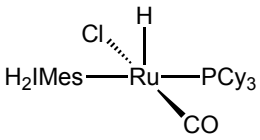 |
| **DA** | 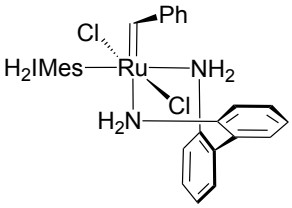 | **DA'** | 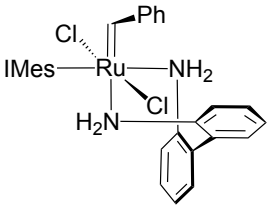 |

| | | | |
|---|---|---|---|
| **HODA** | 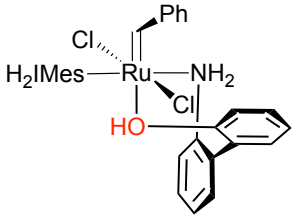 | **MeODA** | 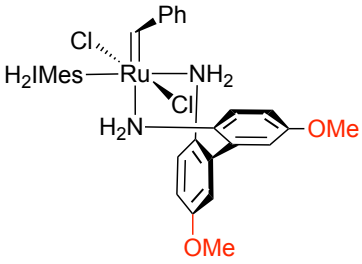 |
| **mDA** | 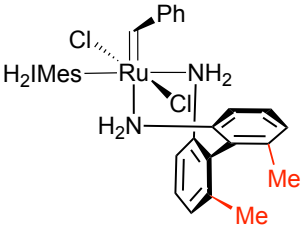 | **BrDA** | 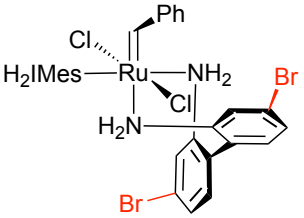 |
| **HC3$^{Me}$** | 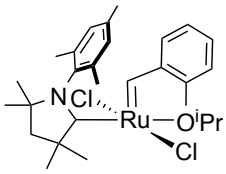 | **nGC3$^{Me}$** | 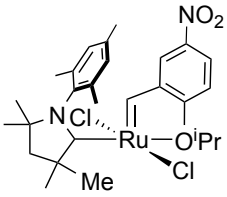 |
| **nGC3$^{Ph}$** | 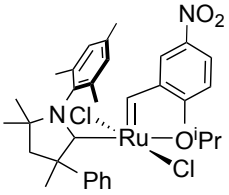 | | |

**Ruthenium Intermediates and Transition States**

| # | Structure | # | Structure |
|---|---|---|---|
| **A** | 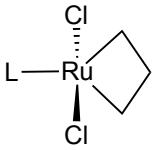 | **$A^R$** | 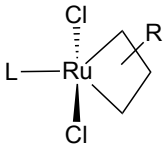 |
| **$A^X$** | 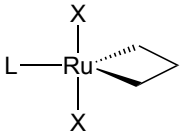 | **A'** | 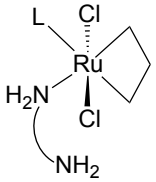 |
| **A-$H_2$IMes** | 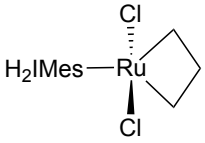 | **A*-$H_2$IMes** | 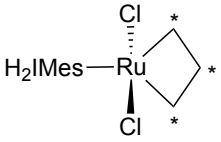 |
| **A–$C1^{Ph}$** | 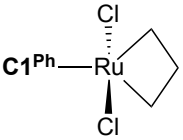 | **mBpy** | 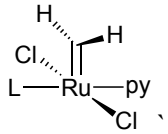 |
| **$mBpy^X$** | 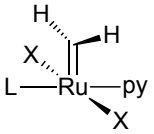 | **B** | 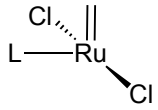 |
| **B'** | 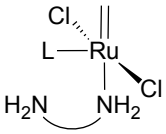 | **$\kappa^2$-B'** | 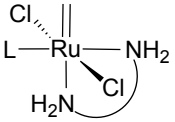 |
| **$B^X$** | 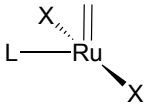 | **B–$H_2$IMes** | 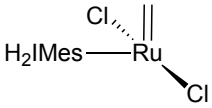 |
| **B–$C1^{Ph}$** | 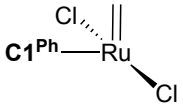 | **B-$C2^{Me}$** | 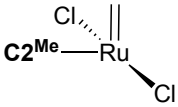 |
| **dimer1** | 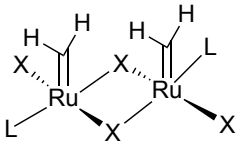 | **dimer2** | 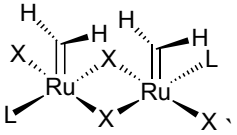 |

| | | | |
|---|---|---|---|
| **Ru-2** | 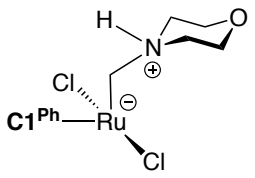 | **Ru-3-C1$^{Ph}$** | 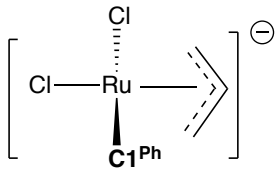 |
| **Ru-3-$H_2$IMes** | 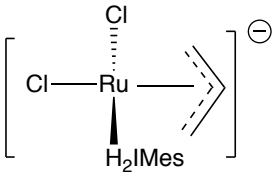 | **TS-1** | 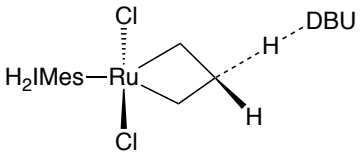 |
| **TS-2** | 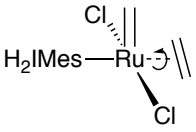 | **TS-3** | 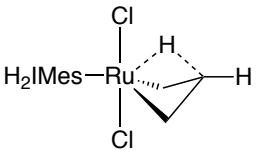 |

**Other Transition Metal Complexes**

| # | Structure | # | Structure |
|---|---|---|---|
| **Re-1** | 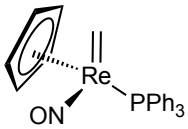 | **Re-2** | 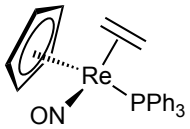 |
| **Re-3** | 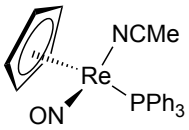 | **Mo-1** | 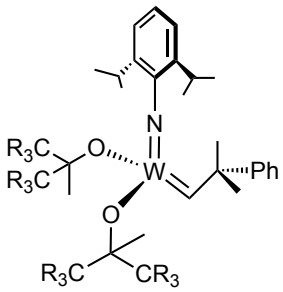 |

## Ligands

| # | Structure | # | Structure |
|---|---|---|---|
| **$H_2$IMes** | 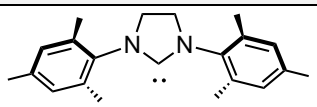 | **$d_{22}$-$H_2$IMes** | 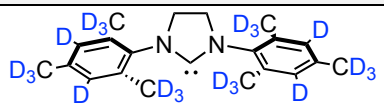 |
| **$^{13}$C-$H_2$IMes•HBr** | 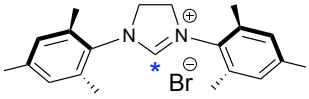 | **$^{13}$C-$H_2$IMes•$HBF_4$** | 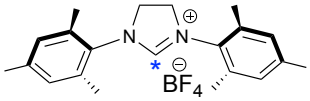 |
| **$^{13}$C-$H_2$IMes** | 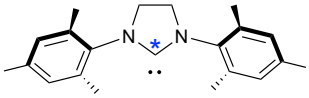 | **IMes** | 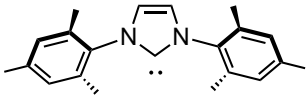 |
| **C2$^{Me}$•$BF_4$** | 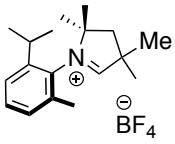 | **C2$^{Me}$** | 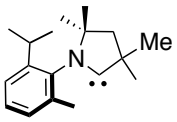 |
| **C1$^{Ph}$** | 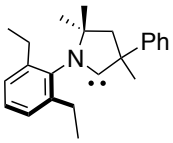 | **C1$^{Me}$** | 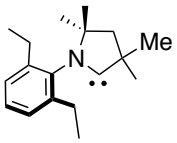 |
| **C3$^{Ph}$** | 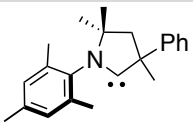 | **C3$^{Me}$** | 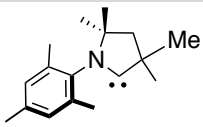 |
| ***o*-Dianiline (ODA)** | 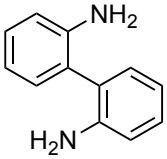 | | |

## Organic Compounds and Polymers

| # | Structure | # | Structure |
|---|---|---|---|
| **1** | 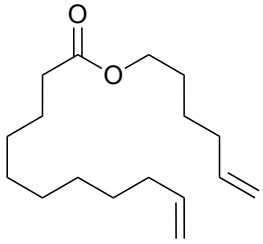 | **1'** | 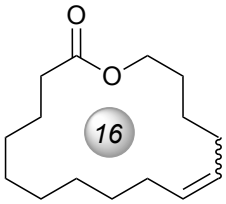 |
| **2** | 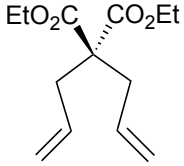 | **2'** | 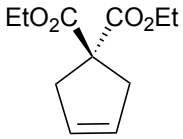 |
| **3** | 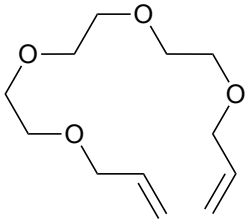 | **3'** | 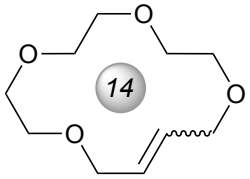 |
| **4** | 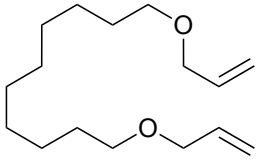 | **4'** | 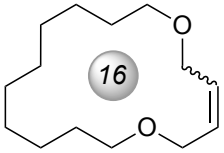 |
| **5** | 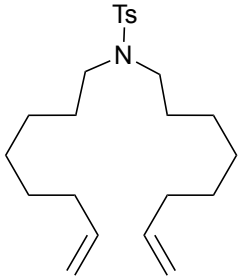 | **5'** | 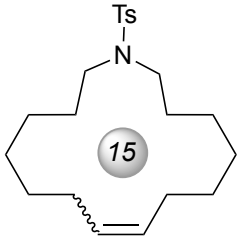 |
| **6** | 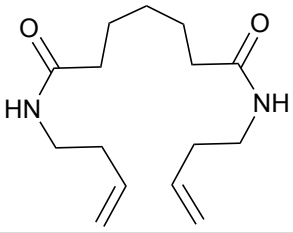 | **6'** | 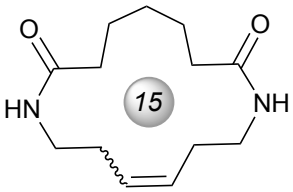 |
| **7** | 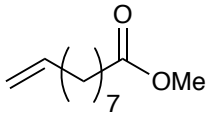 | **8** | 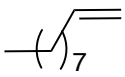 |

| | | | |
|---|---|---|---|
| **9** | 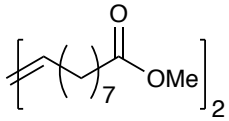 | **10** |  |
| **11** | 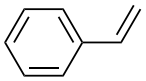 | **12** |  |
| **MO** | 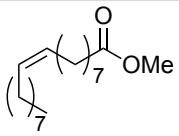 | **13** | 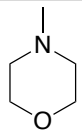 |
| **SE** | 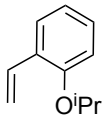 | **NSE** | 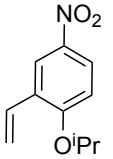 |
| **NSE'** | 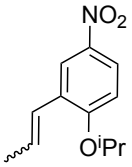 | **Feist's ester** | 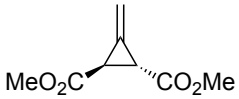 |
| **DMT** | 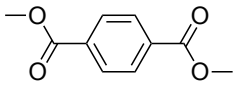 | **TMB** | 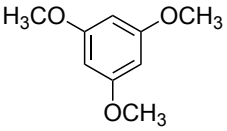 |
| **MF-Cl** | 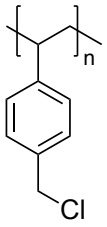 | **Amberlyst-15** | 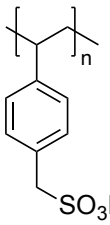 |
| **MF-I** | 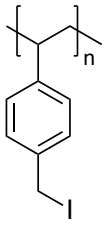 | **MF-I'** | 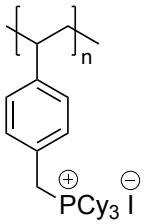 |

# Chapter 1. Introduction

## 1.1. Catalysis

The urgent need for a more sustainable society underscores the critical importance of catalytic technologies. A simple, widely-used description defines a catalyst as a species that lowers the activation energy of a chemical reaction without being consumed in the process. Commonly, equilibrium binding of substrate to catalyst is followed by further reaction steps involving a series of lower activation barriers, and finally the product dissociates, again via an equilibrium process (Scheme 1.1). The role of the catalyst is not merely lowering the energy barrier, but affording access to entirely new transition states and intermediates. Catalytic reactions can hence enable access to products that would otherwise be inaccessible, or energetically exorbitant. They thus play a key role in reducing the environmental footprint of chemical transformations.

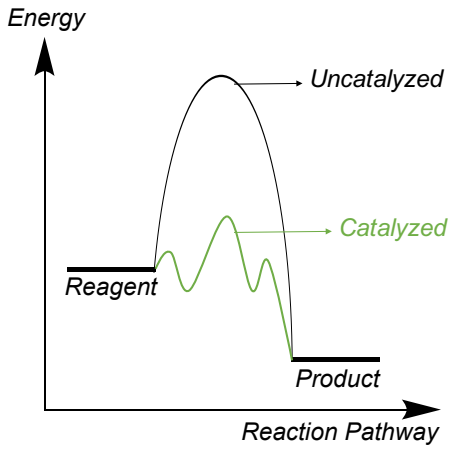


**Scheme 1.1. Positive impact of catalysis on energy demands for chemical transformations.**

Molecular catalysts now enable the production of commodity chemicals and polymers, specialty-grade molecules (e.g., perfumes and personal care products, and dyes), and pharmaceuticals.[1-3] They also play an increasingly important role in the capture and transformation of hazardous environmental contaminants,[4,5] and for energy storage.[6,7] The societal impact of catalysis is highlighted by the multiple Nobel Prizes in this area of science. Relevant to this thesis is that awarded to Yves Chauvin, Robert Grubbs, and Richard Schrock, "for development of the metathesis method in organic synthesis".

## 1.2. Olefin Metathesis

Olefin metathesis is an exceptionally versatile tool for the catalytic formation of $sp^2$-$sp^2$ C=C bonds.[8] In this reaction, a metal complex catalyzes the skeletal reorganization of alkenes to form

*References for Chapter 1 begin on p. 16*

new products (Scheme 1.2). In the absence of a catalyst, the [2+2] cycloaddition of two alkenes is symmetry-forbidden.

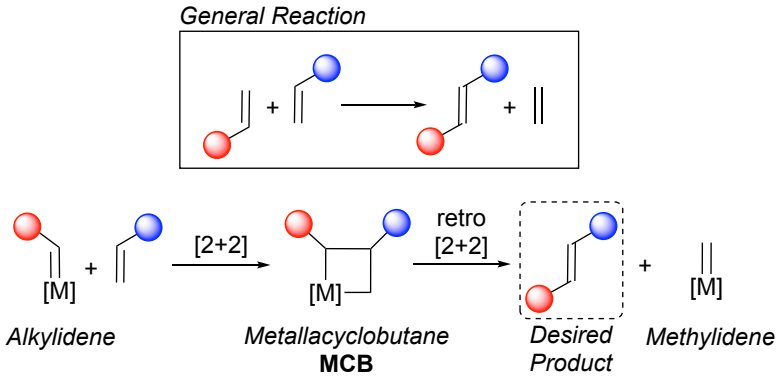


**Scheme 1.2. General scheme for olefin metathesis, following the Chauvin mechanism.**

The history of olefin metathesis dates back to 1956, when researchers at DuPont noticed formation of 1-butene and ethylene on passing propylene over Mo on alumina.[9] In 1960, Standard Oil filed a patent for the synthesis of ethylene and butenes from propylene, using a similar catalyst with an $Al^{i}Bu_3$ additive. In 1963, linear elastomeric polymers were observed on treating cyclopentene with $WCl_6$ and $AlEt_3$ (Scheme 1.3). The following year, Banks and Bailey at Phillips Petroleum reported the disproportionation of propylene to ethylene and butenes on heating with $Mo(CO)_6$ on alumina.[10] The term "olefin metathesis" was coined by Nissim Calderon of Goodyear Tire & Rubber in 1967, to describe the cleavage and reformation of alkene double bonds.[11]

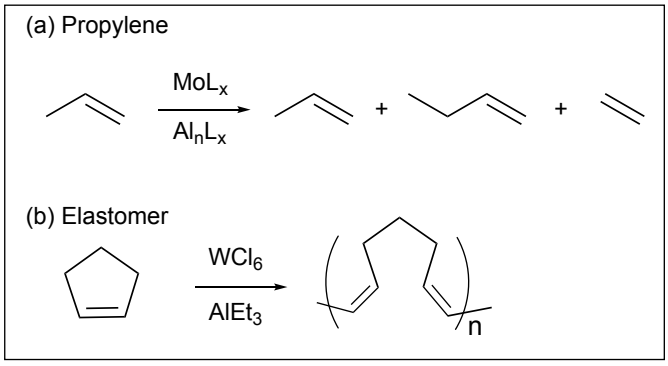


**Scheme 1.3. Exemplary olefin metathesis reactions in early discoveries.**

Calderon's proposal of a metal-bound cyclobutane as the key intermediate set off a boom in study of the reaction mechanism. In 1968, following work with propylene and $^{14}C$-tagged ethylene, Mol reported that "The ethene formed showed no radioactivity at all, in contrast with

*References for Chapter 1 begin on p. 16*

the butenes, which showed a specific radioactivity twice as much as that of the starting material". He suggested that a four-membered ring intermediate must be involved. In 1971, Pettit proposed that this could be a tetramethylene complex, with 4 methylene units on the central metal.[12] The issue with this idea was the required oxidation state of the metal. A year later,[13] Grubbs proposed a metallacyclopentane intermediate, based on evidence from Katz and Eaton that a species with a M–C σ-bond was involved.[14] The riddle was solved by Yves Chauvin, who observed that cross-metathesis of cyclopentene and 2-pentene gave chiefly C9, C10 and C11 products, in 1:2:1 ratio.[15] As the conventional mechanism predicted only C10, this was strong evidence for a *metallacyclobutane* intermediate. Importantly, his mechanism postulated exchange between the starting cyclic and acyclic olefins via a metal carbene, rather than a metal-bound cyclobutane intermediate, as proposed by Calderon.[11]

Less widely recognized is another critical Chauvin proposal: that metal carbenes* could be formed via α-hydride abstraction from a M–$CH_2R$ bond. This seminal work paved the way for Schrock's synthesis of the first well-defined metathesis-active metal complexes.

### 1.3. Catalyst Synthesis and Modification

Inspired by the work of his DuPont colleague Tebbe on titanium chemistry (specifically, development of the iconic "Tebbe dimer", $[Cp_2Ti–CH_2]_2$),[16,17] Schrock synthesized the first well-defined tantalum catalyst via α-hydride abstraction of a neopentyl ligand.[18] Over the next four decades, following a move to MIT, he developed a series of tungsten and molybdenum catalysts, culminating in remarkably tunable structures.[19,20] These complexes are now collectively known as the Schrock catalysts. Catalysts based on late transition metal salts also saw development. In 1974, Porri reported slow ROMP of norbornene with ruthenium and iridium salts in protic media; cyclopentene could also be polymerized, but required addition of $H_2$.[21,22] These discoveries led to implementation of the Norsorex Process for ROMP of norbornene, affording a very high molecular weight polymer still of interest for (e.g.) environmental remediation. Polymerization is promoted by $RuCl_3$/HCl in *t*-butanol: the combination of $RuCl_3$ and alcohol solvent was presumed to enable in situ formation of a ruthenium alkylidene species.[23] These discoveries are notable given that prior metathesis catalysts, including the important Schrock catalysts, are rapidly decomposed by protic contaminants.

In 1992, two advances by Grubbs revolutionized the field, opening the door to broad uptake of olefin metathesis via molecular catalysts. First, Nguyen and Grubbs described the first well-defined Ru alkylidene complex.[24] Secondly, Fu and Grubbs rediscovered ring-closing metathesis (RCM).[25] The latter, a key synthetic pathway to cyclic alkenes, had gone overlooked despite a

* The term "alkylidene" for the [M]=CRR' functionality was later coined by Schrock. It will be used henceforth in this thesis, to preclude the ambituities associated with Fischer carbenes, including N-heterocyclic carbenes that represent a critical ligand family. See next Section.

handful of reports from the 1970s and 1980s by Boelhouwer,[26,27] Villemin[28] Tsuji, and their co-workers.[29,30] A flurry of work on catalyst development followed, notably replacement of the arylphosphine ligands by the more electron-rich ligand $PCy_3$, and introduction of a benzylidene ligand. These advances gave the more active first-generation Grubbs catalyst (**GI**).[31] The enabling advantage of **GI** over catalysts based on the early and mid-transition metals was its ease of handling,[32] which enabled use of olefin metathesis by the practicing organic chemist. An important drawback, however, was the reduced activity of **GI** compared to Schrock catalysts (for specific structures, see Scheme 1.8, Section 1.6.2.1).[33] This early context leaves its mark on the area of Ru-catalyzed olefin metathesis to this day, in the form of a widespread preoccupation (at least among catalyst developers) with initiation rates. The limitations of this approach, alluded to in the first paragraph of this introduction, form a central part of this thesis.

While the first-generation Grubbs catalyst **GI** first made olefin metathesis practicable for organic chemists, a major boost occurred on replacing one $PCy_3$ ligand by a strongly donating N-heterocyclic carbene (NHC). The second-generation Grubbs catalysts (e.g., **GII**, Chart 1.1)[34] were followed by the indenylidene and Hoveyda derivatives **IndII** and **HII**, varying (respectively) in the alkylidene and stabilizing ancillary donor.[35,36] In 2004, Grela reported a faster-initiating version of **HII**.[37] Incorporation of a nitro group *para* to the ether site gave the catalyst **nG**, in which the electron-withdrawing nitro group weakens σ-donation from the ether ligand, enabling four-fold faster initiation.[38] Very recently, the introduction of cyclic (alkyl) (amino) carbenes (CAAC) has led to remarkable advances. These ligands enable breakthrough productivity for topical reactions discussed in Section 1.5.

**Chart 1.1. Leading ruthenium catalysts for olefin metathesis, current to 2015.**

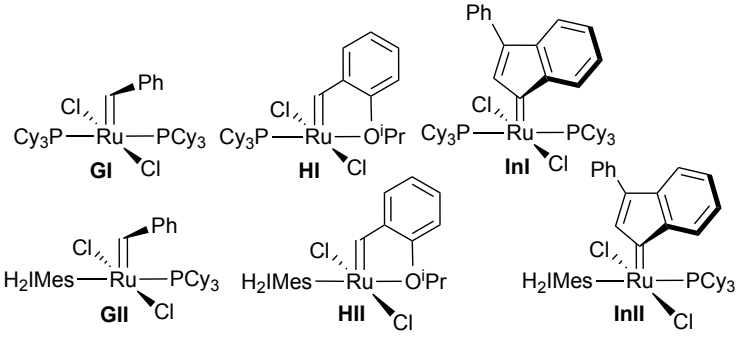


## 1.4. Carbene Ligands

Carbenes are neutral compounds containing a divalent carbon atom with a six-electron valence shell. This incomplete octet, combined with coordinative unsaturation, makes them Lewis acidic as well as Lewis basic. Efforts to isolate such entities date back to 1835,[39] but it was only in 1988 that Bertrand and co-workers synthesized a carbene that was sufficiently stable to isolate and characterize (Chart 1.2a).[40] Three years later, Arduengo synthesized a remarkably stable N-heterocyclic carbene in which two adamantyl substituents flank the carbene carbon (Chart

1.2b).[41] Due to its relative simplicity, Arduengo's methodology was readily adopted by other researchers, and a plethora of NHC ligands has appeared over the ensuing two decades.[39]

In general, these ligands have bulky N-aryl substituents adjacent to the carbene carbon, thus inhibiting dimerization (the Wanzlick equilibrium). The adjacent nitrogen atom provides further stabilization to the carbene. Its σ-electron withdrawing ability lowers the energy of the HOMO σ-orbital (best described as a $sp^2$-hybridized lone pair), while mesomerically donating electron density to the unoccupied LUMO p-orbital (Chart 1.3c). In the CAACs, one nitrogen atom is replaced by a σ-donating alkyl. This lowers the energy of the HOMO and raises that of the LUMO. The CAAC ligands are hence both more nucleophilic (σ-donating) and more electrophilic (π-accepting) than the NHCs (Chart 1.3d).[40,42] These changes dramatically increase metathesis activity. They also, however, increase challenges in handling. Both points are explored in this thesis work.

**Chart 1.2. Carbenes and their properties. (a) First isolated free carbene. (b) First "bottleable" carbene. (c) Stabilization of carbene carbon by adjacent nitrogens. (d) HOMO–LUMO orbitals energy for C2$^{Me}$, C1$^{Ph}$ and $H_2$IMes ligands.**

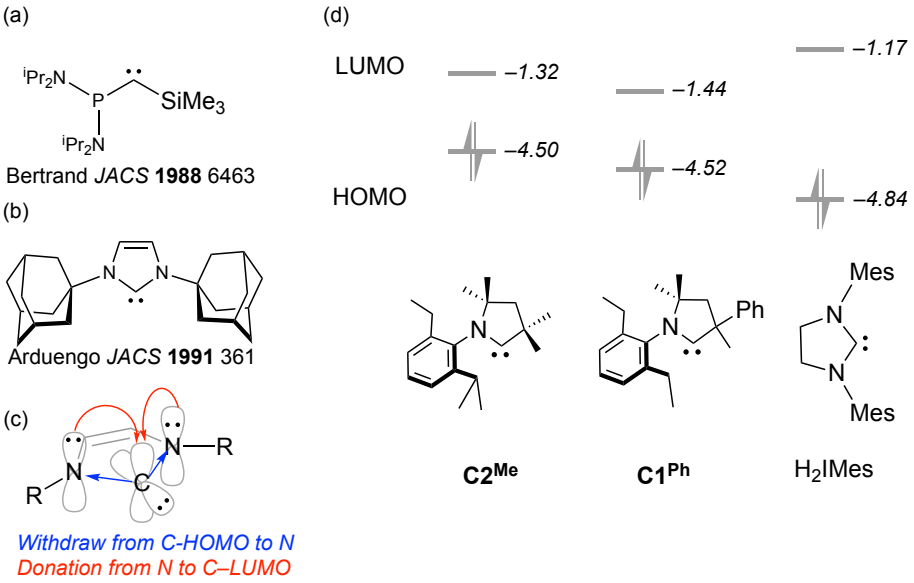


NHCs have found widespread applications in catalytic,[43] materials[44] and organocatalytic applications.[39] In the latter context, their ability to interact with aldehydes and induce an umpolung in the carbonyl group affords access to products otherwise difficult to obtain. NHC derivatives have also been studied in biomedical applications.[45]

In contrast, exploration of the CAAC ligands is still in development. Catalytic applications beyond metathesis include Au-catalyzed hydroamination of unactivated alkynes and allenes.[46] Their use in organocatalysis is limited by their higher basicity, which makes them poor leaving

groups.[45] However, their increased electrophilicity and smaller singlet−triplet gap enable stoichiometric activation of small molecules (CO, $H_2$, and $P_4$), including strong bonds (B−H, Si−H, N−H, and P−H). That is, CAAC ligands can behave like transition metals by undergoing oxidative addition. Owing to the need for re-reduction, however, no catalytic method has yet been developed.[40] More broadly, CAACs have been used to stabilize unusual diamagnetic and paramagnetic main group elements and transition-metal complexes. Also of interest is their use in functionalization of nanoscale, and bulk surfaces and preparation of organic light-emitting diodes (OLEDs).[40]

## 1.5. Types of Olefin Metathesis Reactions and Applications

### 1.5.1. Ring-Closing Metathesis

The broad term "olefin metathesis" covers multiple reaction categories. By far most important is ring-closing metathesis (RCM). First reported in 1980,[28,30] this methodology was brought to the attention of the broad synthetic community in 1992, in a seminal report by Fu and Grubbs.[25,47] The attraction of RCM lies in its astonishing simplicity: it obviates the need to install activating or leaving groups, and the associated waste in time and materials. While RCM is very broadly used, the synthesis of macrocycles via RCM (mRCM) is a particularly important sub-category, with applications in sectors ranging from fragrance and flavours[48] to pharmaceutical manufacturing[49,50] and chemical biology.[51]

RCM proceeds via a two-step pathway, involving installation of a diene on the metal center, followed by intramolecular coupling of two olefinic sites. Studies of mRCM by Jay Conrad of this group, however, demonstrated that oligomerization is kinetically preferred for the second-generation Ru catalysts, even at the high dilutions designed to favour intramolecular reaction (Scheme 1.4). The selectivity for macrocycles over oligomers is ultimately controlled by a concentration-dependent ring-chain equilibrium.[52,53] High dilutions come at a considerable price from an economic and sustainability perspective: moreover, by decreasing the rate of metathesis reaction, they promote competing catalyst decomposition.[54]

*References for Chapter 1 begin on p. 16*

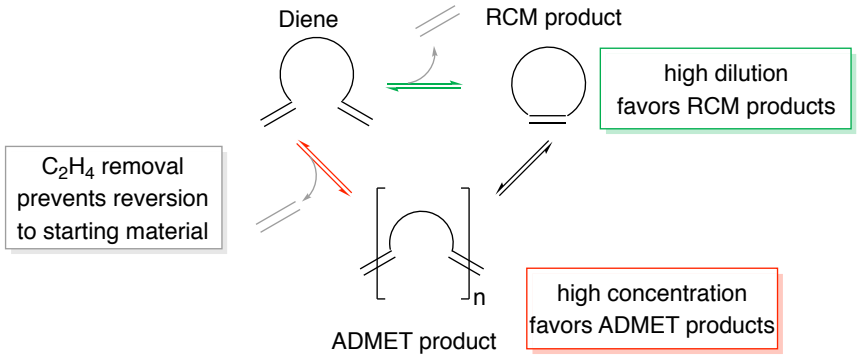


**Scheme 1.4. mRCM pathways. Direct cyclization (rare), equilibria in the presence of ethylene, and the concentration-dependent ring-equilibrium critical for the dominant catalysts in current use.**

Catalyst choice is reported to offer some success in improving selectivity at higher substrate concentrations,[55] but highly active catalystst that exhibit kinetic selectivity for macrocyclization remain to be developed. In an alternative approach, Grela reported mRCM at up to 400x higher concentrations using an unsymmetrical NHC catalyst, and removing macrocyclic product by vacuum distillation. To prevent loss of solvent, involatile paraffin oil was used as the reaction medium.[56] This is clearly operationally simpler than classic "infinite dilution" (Ziegler) strategies, in which the substrate is infused at the same rate it cyclizes. Catalyst decomposition, rather surprisingly, apparently did not degrade product selectivity. It is unclear whether this is due to the resistance of the catalysts to decomposition, or to the isomerization-inactivity of the ruthenium decomposition products.

Major advances toward the deployment of molecular metathesis catalysts in process chemistry were reported by Boehringer-Ingelheim Montreal.[57-61] Boehringer-Ingelheim was the first industrial concern to employ mRCM on large scale, in a campaign directed at synthesis of the drug candidate Ciluprevir. Substrate concentrations of 200 mM[62] were achieved after extensive reaction optimization, and protection of an amide group close to the olefinic site. While Ciluprevir ultimately failed in clinical trials, this work laid the foundation for much related chemistry aimed at production of macrocyclic APIs via mRCM. Many of these compounds are HCV inhibitor candidates, but other antiviral therapeutics include inhibitors for the human immunodeficiency virus (HIV) and the COVID virus.[62-65] A subsequent HCV drug, Simeprevir (Chart 1.3), was developed by Janssen Pharma using mRCM. Clinical trials were complete in 2013, and a manufacturing process was in place by 2014.[60] Simeprevir has been distributed globally, with sales amounting to $234 million USD in the first quarter of 2015 alone.[66] Janssen Pharma announced discontinuation of the drug in 2019, due to limited sales. Simeprevir was recently reinvestigated for its capacity to interact with SARS–CoV-2 proteins, in an effort aimed at rapidly redeploying existing antiviral agents as therapeutics for the treatment of COVID-19.

*References for Chapter 1 begin on p. 16*

**Chart 1.3. First example of an active pharmaceutical ingredient (API) accessed via mRCM.**

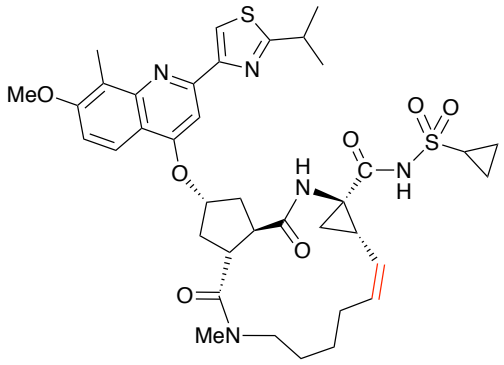


Simeprevir
Janssen

### 1.5.2. Cross-Metathesis

As shown by the Chauvin experiment described in Section 1.2, the intermolecular cross-metathesis (CM) reaction generates a mixture of olefins. Chatterjee and Grubbs proposed rules for predicting the selectivity of CM reactions.[67] Enhanced selectivity can be achieved by (1) mismatching the reactivity between the reacting olefins, and (2) using a catalyst with suitable reactivity. However, the selectivity issues are an inherent challenge for target-oriented synthesis. An exception is "ethenolysis", or the CM of internal olefins with ethylene to obtain α-olefin products.

CM using supported rhenium and tungsten catalysts has long been a critical technology in petroleum processing, which benefits from the absence of functional groups on the substrates, and highly sophisticated gas-separation technology. One of its highest-profile historical applications is the Shell Higher Olefin Process (SHOP, Scheme 1.5a). Developed by Keim at Royal Dutch Shell, the SHOP process makes use of the "olefin-shuffling" capacity of CM to upgrade the olefin stream produced via ethylene oligomerization to favour detergent-range olefins.[23] In this process, the desired chain lengths are removed, and undesired fractions are re-subjected to metathesis. Further petrochemical applications include the Phillips Process originated by Banks and Bailey, for production of butene from propene, and its reverse, the Olefin Conversion Technology process.[23]

Widely used to manipulate chain lengths for the petroleum refinery, CM has long drawn attention for its potential in what are now termed "biorefinery" applications. While applications of metathesis in oleochemistry date back to the 1970s,[26,27] and a further report by Mol appeared in 1981,[68] industrial interest took off with the development of more robust Ru catalysts. In 2013, Elevance (a joint venture between the agrochemical giant Cargill and the metathesis catalyst company Materia) reported the first shipments of oleochemicals from a purpose-built facility in Gresik, Indonesia. This pre-shale oil venture was aimed at transforming palm-oil lipids into

relatively high-value, detergent-range olefins, and specialty difunctional olefins with applications as (e.g.) lubricants, synthetic oils, and surfactants.[69]

The central idea, production of α-olefins from triglycerides via ethenolysis, was complicated by the extreme sensitivity of the first- and second-generation Ru catalysts to decomposition under ethylene (see Section 1.6).* To limit the proportion of the highly sensitive methylidene and unsubstituted metallacyclobutane, metathesis was carried out with 1-butene, rather than ethylene. Scheme 1.5b illustrates the process with oleic acid. The decene and dodecene co-products can be separated for use as lubricants or synthetic oils, or hydrogenated for use as fuels. The glyceride subunits are then separated by transesterification to obtain C13 and C11 products.[69] Little has been heard of Elevance since the advent of cheap shale oil and gas devastated the renewables industry. However, these technologies hold long-term potential, particularly if more sustainable lipid sources can be successfully harnessed.

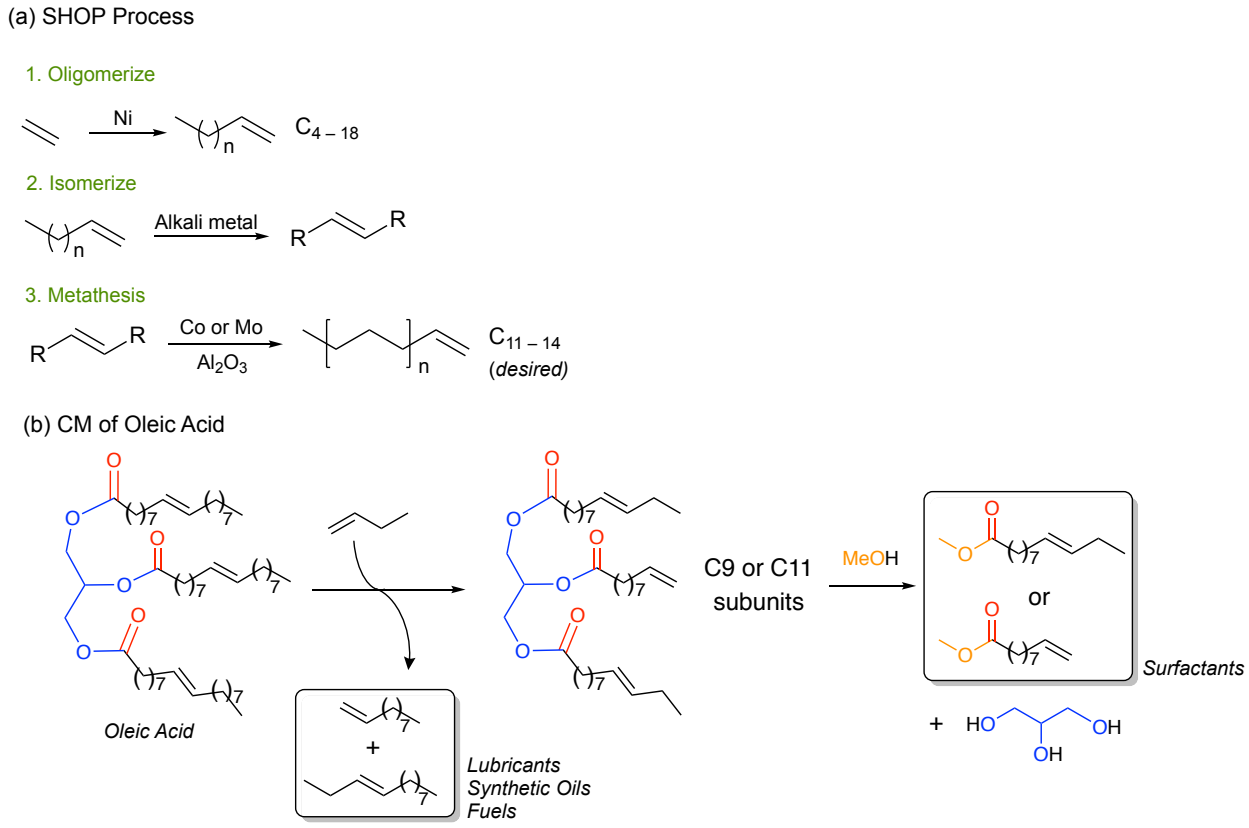


**Scheme 1.5. CM in industry. (a) The SHOP process. (b) Biorefinery applications.**

* Highly important in this context is the recent development of ethylene-tolerant CAAC catalysts: see later.

*References for Chapter 1 begin on p. 16*

### 1.5.3. ADMET and Ring-Opening Metathesis

As noted above, ADMET generates long-chain products, albeit with limited control over the distribution of chain lengths. A more powerful strategy for material synthesis is ring-opening polymerization (ROMP, Scheme 1.6) of strained cyclic monomers, in which reaction is driven by the relief of ring strain. Initiators that enable faster rates of initiation than propagation enable precise control over polymer molecular weights and microstructure. The propagating species in ROMP are alkylidenes, which are sterically protected against the decomposition pathways that plague the methylidene species critical to CM and RCM (see next section). ROMP applications are of tremendous interest given the ease with which polymers can be "decorated" with pendant functionalities. Early applications ranged from drug delivery[70] to tissue engineering,[71] ROMP-gel reagents,[72] tumor imaging[73] and cell signaling.[74] Although overshadowed for a period by the advent of RCM, ROMP has seen a remarkable resurgence in materials science in the past few years.[75] Of note, reports of catalyst instability are increasing as the sophistication of these applications increases (notwithstanding the greater steric protection of the propagating alkylidene). The source of the problems has seen limited study to date.

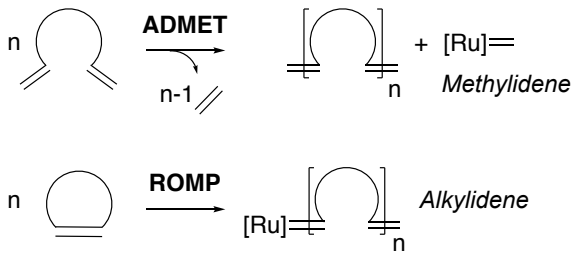


**Scheme 1.6. Comparison of ADMET and ring-opening metathesis polymerization (ROMP).**

Other metathesis reactions that go beyond the scope of this thesis involve enyne metathesis (i.e., alkene-alkyne coupling) and cyclopolymerization (alkyne-alkyne coupling). In these processes molecular or polymeric 1,3-conjugated dienes are formed, and the propagating species is a conjugated alkylidene.[76,77] These species may be susceptible to unique decomposition pathways.[78]

## 1.6. Catalyst Decomposition in Olefin Metathesis

### 1.6.1. Induced Decomposition

Despite the power and versatility of olefin metathesis, realization of its full potential is hampered by catalyst decomposition. Loss of the alkylidene or metallacyclobutane functionalities from the active species results in complete loss of metathesis activity. While a number of researchers have sought to tackle the problem of "reactivating" decomposed catalyst, success to date has been limited.[79a,80,81] Understanding catalyst decomposition pathways is hence critical.[79] Beyond

opportunities to improve productivity by controlling process chemistry – particularly for the readily-handled ruthenium catalysts – this approach is fundamental to informed catalyst redesign.

Prominent in reviews that describe decomposition of metathesis catalysts are studies in which decomposition pathways are inferred from the crystal structures of serendipitously-isolated ruthenium products.[79] While such structures can offer valuable clues, in the absence of mechanistic study they can also be deeply misleading. For example, an early clue that the chloride ligands enabled bimolecular decomposition emerged from work by Dino Amoroso from this group.[82,83] On the other hand, the plethora of cyclometallated products involving activation of the *o*-Me site of an $H_2$IMes ligand led to the widespread inference that NHC protection should be a core design goal.[84] In fact, cyclometallation is now known to occur *subsequent* to the key deactivating event.[85-87] Of greater value from a diagnostic perspective are the organic products of decomposition, which can report on the initial decomposition event.

Within the ruthenium catalysts, the first systematic studies of decomposition focused on the resting-state species formed by the Grubbs catalysts, $RuCl_2(L)(PCy_3)(=CH_2)$ (L = $PCy_3$, NHC). The key advance was the development by Justin Lummiss of this research group[88] of a clean, high-yield route to **mGII** (previously available in low yields; reportedly 36%[89,90] but in our hands, <20% in situ). The availability of this rare stable methylidene species,[88] and its $^{13}C$-labelled isotopologue,[91] offered the first opportunity for detailed examination of its decomposition chemistry. In a series of studies, Lummiss and colleagues documented that abstraction of the methylidene ligand by liberated $PCy_3$ is the dominant decomposition pathway, the marker for which is the phosphonium salt $[MePCy_3]Cl$.[85,86,91,92] The initial decomposition event involves nucleophilic attack of free $PCy_3$ on the methylidene ligand, forming a σ-alkyl species that could be isolated in near-quantitative yields for a first-generation complex,[85] and which was observed for the $H_2$IMes and IMes derivatives.[86] The methylphosphonium salt is then liberated by deprotonation of a mesityl *o*-methyl group: this accounts for the formation of a cyclometallated Ru product. Importantly, this pathway is greatly accelerated by adventitious donors (e.g., sterically accessible amines, as well as smaller oxygen donors such as water or ethers).[91,92] These promote $PCy_3$ dissociation from **mGII** via an associative pathway, overcoming the normally low lability of this ligand. This "donor-accelerated decomposition" accounts for many of the problems with productivity and reliability of Grubbs-class, $PCy_3$-stabilized catalysts.

Bulky bases such as DBU (1,8-diazabicyclo[5.4.0]undec-7-ene), in contrast, cause catalyst decomposition without liberation of $[MePCy_3]Cl$.[92] Deprotonation of the metallacyclobutane was postulated, and supported by subsequent studies of the phosphine-free catalyst **HII** by Benjamin Ireland, in which propenes were identified as the key organic marker for decomposition (Scheme 1.7).[93] Studies by Gwendolyn Bailey demonstrated similar behaviour for the $PCy_3$-stabilized catalysts in acrylate metathesis.[87] Here nucleophilic attack of free $PCy_3$ on the electron-deficient olefin forms a strongly basic enolate anion, which deprotonates the metallacyclobutane.

*References for Chapter 1 begin on p. 16*

Diagnostic for this pathway was the observation and quantitation of organic co-products evidencing attack of $PCy_3$ on the acrylate, including labelled isotopologues confirming deprotonation of the MCB.

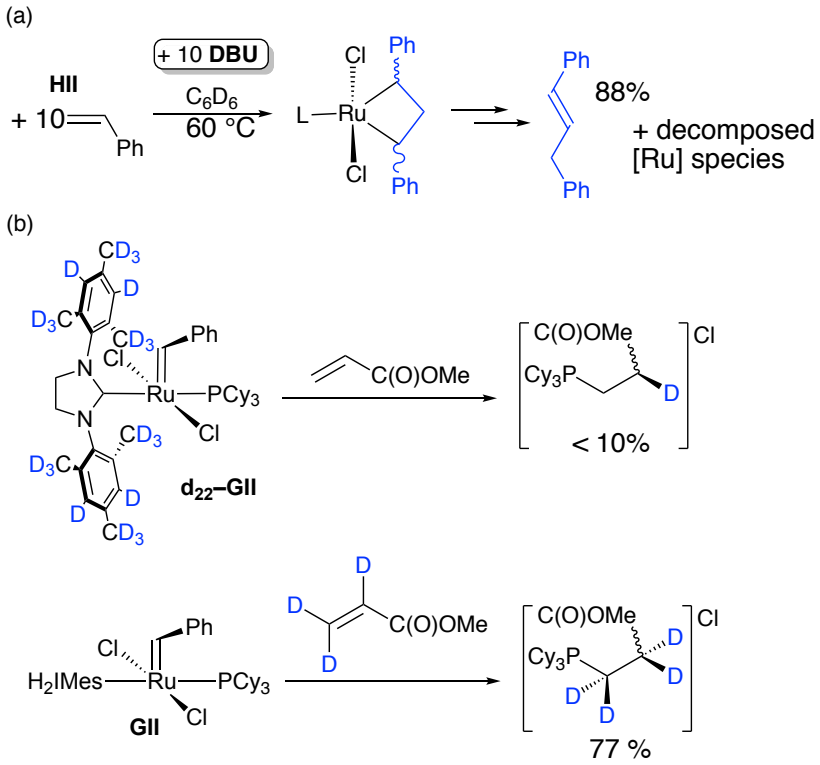


**Scheme 1.7. Decomposition of ruthenium metathesis catalysts by: (a) Brønsted base. (b) Nucleophiles. Labelling studies confirmed initial attack on the metallacyclobutane.**

The decomposition pathways above give insight into challenges that must be overcome for metathesis to be used reliably in synthetic contexts, in which contaminants are routinely present. While important in discovery operations, they become critical in manufacturing contexts. In pharmaceutical process chemistry, for example, amines and related nucleophiles or Brønsted bases represent key, performance-limiting contaminants. Such entities may be present in the reaction medium: for example, ppm levels of morpholine present in technical-grade toluene were identified as a key factor limiting metathesis productivity in Boehringer-Ingelheim's early production route to Ciluprevir.[60] More commonly, they are present as a consequence of upstream chemistry. *N*-methyl morpholine and $PPh_3$, for example, were found to impede synthesis of the hepatitis C virus (HCV) inhibitor Simeprevir,[49] while DBU and secondary amines had a similar effect in production of a cathepsin K inhibitor.[94] More broadly, contaminants are ubiquitous in chemical biology. In all of these contexts, understanding the nature of the decomposition pathways the induce is essential to the informed design of solutions or work-arounds.

*References for Chapter 1 begin on p. 16*

### 1.6.2. Intrinsic Decomposition

A second, major class of decomposition pathways, however, is intrinsic to the active species. Indeed, these are better known, having been a part of the landscape in olefin metathesis since its origin in early transition metal chemistry. In the group 4-7 systems, catalyst decomposition occurs via two main pathways: 1) bimolecular coupling of [M]=CHR intermediates, with elimination of the alkylidene as an olefin of the form RHC=CHR; and 2) β-H elimination of metallacyclobutane to yield propenes.[19,95]

While the four-coordinate methylidene is spectroscopically unobservable, Ti, Ta, W and Nb metallacyclobutane complexes have been isolated.[96] In the Ru systems, this species is observable at low temperatures, above which it is either fluxional or unstable to decomposition. The organic products of decomposition offer key markers that distinguish between the decomposition pathways operative: their identification and quantitation enables a major step toward understanding the relevant decomposition behaviour.

#### 1.6.2.1. Bimolecular Coupling (BMC)

Within the early and mid-transition metals, BMC was first studied for Re and Ta methylidenes,[97,98] followed by Mo and W catalysts (Scheme 1.8).[99-103] Ethylene quantitation was greatly facilitated by adduct formation.[97,98,101-103] Kinetic studies confirmed second-order behaviour over a wide range of concentrations and temperatures,[97,98] although the intimate mechanism remained unclear. In the Ru systems, studies of BMC are complicated by instability of the olefin adducts, which results in loss of the ethylene product to the headspace. An elegant strategy was developed by Gwendolyn Bailey, in which the four-coordinate methylidene **B** was trapped as a transiently-stabilized adduct.[104] In the Bailey protocol, the metallacyclobutane is generated from the Piers catalyst at low temperature,[105] following which a stabilizing ligand (initially *o*-dianiline, later pyridine) is added to collapse the MCB and form the adduct. The latter is precipitated at low temperature (– 110 °C) and filtered off under vacuum, thus also removing the ethylene required for initial synthesis of **A**. This is essential for quantitation of ethylene, and hence bimolecular coupling of **B**.

*References for Chapter 1 begin on p. 16*

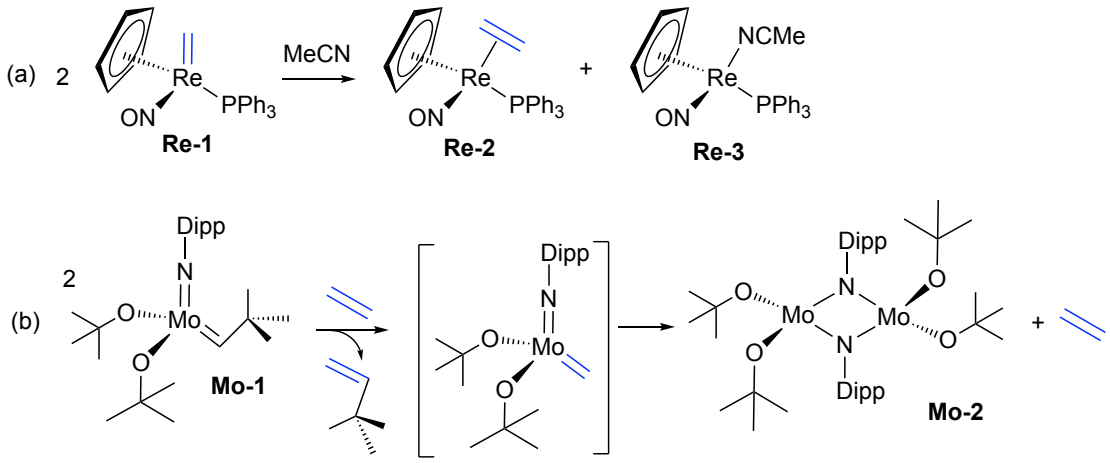


**Scheme 1.8. Leading studies of bimolecular decomposition in group 6-7 olefin metathesis.**

### 1.6.2.2. β-Hydride Elimination

Reports of decomposition of the metallacyclobutane via **β**-H elimination are rife in the earlier transition-metal catalysts, particularly once bulky ligands were introduced, limiting bimolecular decomposition.[101,103,106,107] A study by Janse van Rensburg from Sasol reported the first evidence for β-H elimination from **mGI**[*], while the Bespalova group likewise noted that propene forms in ethenolysis of **HII**.[108,109] DFT calculations by the Sasol group indicated that β-H elimination was energetically accessible, with an energy barrier (vs **A–$H_2$IMes**) of 24.3 kcal/mol.[109] Clear-cut labelling evidence for this pathway was reported in a groundbreaking study by the Piers group,[105] in which the ruthenacyclobutane intermediate was observed for the first time. Warming solutions of $^{13}$C-labelled **A*-$H_2$IMes** above –50 °C yielded $^{13}$C-propene, confirming its origin in the MCB ring carbons (Scheme 1.9). Gwendolyn Bailey of this research group expanded on this approach, as described in the previous section, to quantify β-elimination for the first time, and to assess its contribution relative to bimolecular coupling.

[*] This is surprising, given the dominance of methylidene abstraction by $PCy_3$ described in Section 1.6.1. It presumably reflects the presence of adventitious $O_2$, and sequestration of free $PCy_3$ as the oxide. Consistent with this inference is the prominent $O{=}PCy_3$ signal in $^{31}$P NMR spectra provided in the supporting information.

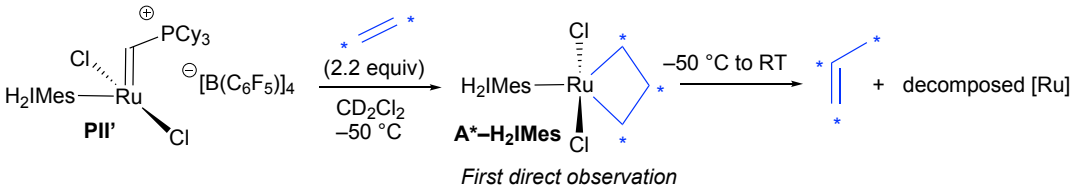


**Scheme 1.9. First observation of the metallacyclobutane intermediate in Ru-catalyzed olefin metathesis, and unambiguous labelling evidence for β-H elimination.**

## 1.6. Scope of Thesis

The drive to deploy olefin metathesis in highly demanding contexts, including pharmaceutical manufacturing and chemical biology, puts severe pressure on the lifetime and productivity of the purportedly robust ruthenium catalysts. Understanding the relevant decomposition pathways is critical to address such problems and, in the longer term, to enable informed catalyst redesign. At the outset of this thesis work, significant advances had been made in identifying and quantifying the critical decomposition pathways for the Ru-$H_2$IMes catalysts. The underlying factors, however – particularly those governing β-H elimination and bimolecular decomposition – remained obscure. Also new at that time was the discovery of the breakthrough metathesis productivities of the CAAC catalysts. These complementary perspectives set the context for the present thesis. This work sought to extend our understanding of decomposition pathways to the CAAC catalysts, and to uncover their origin.

Essential for mechanistic study are pristine materials. Described in Chapter 2 are synthetic methods aimed at improving clean, high-yield catalyst production. Chapter 3 turns to mechanistic examination of decomposition pathways that underlie success and failure for the $H_2$IMes and (in the first such studies) for the CAAC catalysts. In particular, the origin of the remarkable productivity of the CAAC catalysts is examined: first, with a focus on intrinsic decomposition, and secondly, assessing their robustness to nucleophiles and Brønsted bases. Some critical, very recent lessons arising from these findings will open up new directions. Chapter 4 builds on key lessons from the work of Lummiss and Bailey, to explore new paradigms for the design of metathesis catalysts. Finally, Chapter 5 highlights key advances and contributions of this thesis, and proposes avenues for future work. We are now entering a new stage in olefin metathesis, which will enable contexts and opportunities previously out of reach.

*References for Chapter 1 begin on p. 16*

## 1.7. References


(1) de Vries, J. G., Palladium-Catalysed Coupling Reactions. In *Top. Organomet. Chem.* (Organometallics as Catalysts in the Fine Chemical Industry), Beller, M.; Blaser, H.-U., Eds. Springer-Verlag Berlin, 2012; Vol. 42, pp 1–34.

(2) Busacca, C. A.; Fandrick, D. R.; Song, J. J.; Senanayake, C. H., The Growing Impact of Catalysis in the Pharmaceutical Industry. *Adv. Synth. Catal.* **2011**, *353*, 1825–1864.

(3) Hoff, R.; Mathers, R. T., *Handbook of Transition Metal Polymerization Catalysts*. Wiley: Hoboken, NJ, 2010.

(4) Wang, C.-C.; Li, J.-R.; Lv, X.-L.; Zhang, Y.-Q.; Guo, G., Photocatalytic Organic Pollutants Degradation in Metal–Organic Frameworks. *Energy Environ. Sci.* **2014**, *7*, 2831–2867.

(5) Lai Lyu, C. H., Heterogeneous Fenton Catalytic Water Treatment Technology and Mechanism. *Prog. Chem.* **2017**, *29*, 981–999.

(6) Crabtree, R. H., *Energy Production and Storage: Inorganic Chemical Strategies for a Warming World*. Wiley: Hoboken, NJ, 2010.

(7) Olah, G. A.; Goeppert, A.; Prakash, G. K. S., Chemical Recycling of Carbon Dioxide to Methanol and Dimethyl Ether: From Greenhouse Gas to Renewable, Environmentally Carbon Neutral Fuels and Synthetic Hydrocarbons. *J. Org. Chem.* **2009**, *74*, 487–498.

(8) (a) Grela, K., *Olefin Metathesis-Theory and Practice*. Wiley: Hoboken, NJ, 2014. (b) Grubbs, R. H.; Wenzel, A. G., *Handbook of Metathesis*. 2nd ed.; Wiley-VCH: Weinheim, 2015.

(9) Eleuterio, H. S., Olefin Metathesis: Chance Favors Those Minds That Are Best Prepared. *J. Mol. Catal.* **1991**, *65*, 55-61.

(10) Banks, R. L.; Bailey, G. C., Olefin Disproportionation. A New Catalytic Process. *Ind. Eng. Chem. Prod. Res. Dev.* **1964**, *3*, 170–173.

(11) Calderon, N.; Chen, H. Y.; Scott, K. W., Olefin Metathesis, A Novel Reaction for Skeletal Transformations of Unsaturated Hydrocarbons. *Tetrahedron Lett.* **1967**, 3327–3329.

(12) Lewandos, G. S.; Pettit, R., Mechanism of the Metal-Catalyzed Disproportionation of Olefins. *J. Am. Chem. Soc.* **1971**, *93*, 7087-7088.

(13) Grubbs, R. H.; Brunck, T. K., Possible Intermediate in the Tungsten-Catalyzed Olefin Metathesis Reaction. *J. Am. Chem. Soc.* **1972**, *94*, 2538-2540.

(14) Katz, T. J.; McGinnis, J., Mechanism of the Olefin Metathesis Reaction. *J. Am. Chem. Soc.* **1975**, *97*, 1592–1594.

(15) Hérisson, J. L.; Chauvin, Y., Catalysis of Olefin Transformations by Tungsten Complexes. II. Telomerization of Cyclic Olefins in the Presence of Acyclic Olefins. *Makromol. Chem.* **1971**, *141*, 161–176.

(16) Tebbe, F. N.; Parshall, G. W.; Reddy, G. S., Olefin Homologation with Titanium Methylene Compounds. *J. Am. Chem. Soc.* **1978**, *100*, 3611–3613.

(17) Thompson, R.; Nakamaru-Ogiso, E.; Chen, C.-H.; Pink, M.; Mindiola, D. J., Structural Elucidation of the Illustrious Tebbe Reagent. *Organometallics* **2014**, *33*, 429–432.

(18) Schrock, R. R., Alkylcarbene Complex of Tantalum by Intramolecular alpha-Hydrogen Abstraction. *J. Am. Chem. Soc.* **1974**, *96*, 6796–6797.

(19) Schrock, R. R.; Copéret, C., Formation of High-Oxidation-State Metal–Carbon Double Bonds. *Organometallics* **2017**, *36*, 1884–1892.

(20) Schrock, R. R., Recent Advances in High Oxidation State Mo and W Imido Alkylidene Chemistry. *Chem. Rev.* **2009**, *109*, 3211–3226.

(21) Rossi, R.; Diversi, P.; Lucherini, A.; Porri, L., Metathesis Reactions by Iridium Catalysts: Synthesis of cis-1,3-Dialkenylcyclopentanes. *Tetrahedron Lett.* **1974**, *15*, 879–882.

(22) Porri, L.; Rossi, R.; Diversi, P.; Lucherini, A., Ring-Opening Polymerization of Cycloolefins with Catalysts Derived from Ruthenium and Iridium. *Makromolekul. Chem.* **1974**, *175*, 3097–3115.

(23) Mol, J. C., Industrial Applications of Olefin Metathesis. *J. Mol. Catal. A* **2004**, *213*, 39–45.

(24) Nguyen, S. T.; Johnson, L. K.; Grubbs, R. H.; Ziller, J. W., Ring-Opening Metathesis Polymerization (ROMP) of Norbornene by a Group VIII Carbene Complex in Protic Media. *J. Am. Chem. Soc.* **1992**, *114*, 3974–3975.

(25) Fu, G. C.; Grubbs, R. H., The Synthesis of Nitrogen Heterocycles via Catalytic Ring-Closing Metathesis of Dienes. *J. Am. Chem. Soc.* **1992**, *114*, 7324–7325.

(26) van Dam, P. B.; Mittelmeijer, M. C.; Boelhouwer, C. J., Metathesis of Unsaturated Fatty Acid Esters by a Homogeneous Tungsten Hexachloride-Tetramethyltin Catalyst. *J. Chem. Soc., Chem. Commun.* **1972**, *22*, 1221–1222.

(27) Verkuijlen, E.; Boelhouwer, C., Metathesis of Unsaturated Fatty Esters. *Fett. Wiss. Technol.* **1977**, *79*, 444–447.

(28) Villemin, D., Synthesis of Macrolides via Metathesis. *Tetrahedron Lett.* **1980**, *21*, 1715–1718.

(29) Tsuji, J.; Hashiguchi, S., Metathesis Reactions of Unsaturated Esters Catalyzed by Homogeneous Tungsten Complexes. Syntheses of Civetone and Macrolides. *J. Organomet. Chem.* **1981**, *218*, 69–80.

(30) Tsuji, J.; Hashiguchi, S., Application of Olefin Metathesis to Organic Synthesis. Syntheses of Civetone and Macrolides. *Tetrahedron Lett.* **1980**, *21*, 2955–2958.

(31) Schwab, P.; Grubbs, R. H.; Ziller, J. W., Synthesis and Applications of $RuCl_2(=CHR')(PR_3)_2$: The Influence of the Alkylidene Moiety on Metathesis Activity. *J. Am. Chem. Soc.* **1996**, *118*, 100–110.

(32) Wolf, J.; Stuer, W.; Grunwald, C.; Werner, H.; Schwab, P.; Schulz, M., Ruthenium Trichloride, Tricyclohexylphosphine, 1-Alkynes, Magnesium, Hydrogen, and Water - Ingredients of an Efficient One-Pot Synthesis of Ruthenium Catalysts for Olefin Metathesis. *Angew. Chem., Int. Ed.* **1998**, *37*, 1124–1126.

(33) Schrock, R. R., High-Oxidation-State Molybdenum and Tungsten Alkylidyne Complexes. *Acc. Chem. Res.* **1986**, *19*, 342–348.

(34) Scholl, M.; Ding, S.; Lee, C. W.; Grubbs, R. H., Synthesis and Activity of a New Generation of Ruthenium-Based Olefin Metathesis Catalysts Coordinated with 1,3-Dimesityl-4,5-dihydroimidazol-2-ylidene Ligands. *Org. Lett.* **1999**, *1*, 953–956.

(35) Jafarpour, L.; Schanz, H.-J.; Stevens, E. D.; Nolan, S. P., Indenylidene-Imidazolylidene Complexes of Ruthenium as Ring-Closing Metathesis Catalysts. *Organometallics* **1999**, *18*, 5416–5419.

(36) Garber, S. B.; Kingsbury, J. S.; Gray, B. L.; Hoveyda, A. H., Efficient and Recyclable Monomeric and Dendritic Ru-Based Metathesis Catalysts. *J. Am. Chem. Soc.* **2000**, *122*, 8168–8179.

(37) Michrowska, A.; Bujok, R.; Harutyunyan, S.; Sashuk, V.; Dolgonos, G.; Grela, K., Nitro-Substituted Hoveyda-Grubbs Ruthenium Carbenes: Enhancement of Catalyst Activity through Electronic Activation. *J. Am. Chem. Soc.* **2004**, *126*, 9318–9325.

(38) Thiel, V.; Hendann, M.; Wannowius, K.-J.; Plenio, H., On the Mechanism of the Initiation Reaction in Grubbs-Hoveyda Complexes. *J. Am. Chem. Soc.* **2012**, *134*, 1104–1114.

(39) Hopkinson, M. N.; Richter, C.; Schedler, M.; Glorius, F., An Overview of N-Heterocyclic Carbenes. *Nature* **2014**, *510*, 485–496.

(40) Soleilhavoup, M.; Bertrand, G., Cyclic (Alkyl)(Amino)Carbenes (CAACs): Stable Carbenes on the Rise. *Acc. Chem. Res.* **2015**, *48*, 256–266.

(41) Arduengo, A. J.; Harlow, R. L.; Kline, M., A Stable Crystalline Carbene. *J. Am. Chem. Soc.* **1991**, *113*, 361–363.

(42) Back, O.; Henry-Ellinger, M.; Martin, C. D.; Martin, D.; Bertrand, G., $^{31}$P NMR Chemical Shifts of Carbene–Phosphinidene Adducts as an Indicator of the π-Accepting Properties of Carbenes. *Angew. Chem., Int. Ed.* **2013**, *52*, 2939–2943.

(43) Hey, D. A.; Reich, R. M.; Baratta, W.; Kühn, F. E., Current Advances on Ruthenium(II) N-Heterocyclic Carbenes in Hydrogenation Reactions. *Coord. Chem. Rev.* **2018**, *374*, 114–132.

(44) Smith, C. A.; Narouz, M. R.; Lummis, P. A.; Singh, I.; Nazemi, A.; Li, C.-H.; Crudden, C. M., N-Heterocyclic Carbenes in Materials Chemistry. *Chem. Rev.* **2019**, *119*, 4986–5056.

(45) Hameury, S.; de Fremont, P.; Braunstein, P., Metal Complexes with Oxygen-Functionalized NHC Ligands: Synthesis and Applications. *Chem. Soc. Rev.* **2017**, *46*, 632–733.

(46) Frey, G. D.; Dewhurst, R. D.; Kousar, S.; Donnadieu, B.; Bertrand, G., Cyclic (Alkyl)(Amino)Carbene Gold(I) Complexes: A Synthetic and Structural Investigation. *J. Organomet. Chem.* **2008**, *693*, 1674–1682.

(47) Fu, G. C.; Grubbs, R. H., The Application of Catalytic Ring-Closing Olefin Metathesis to the Synthesis of Unsaturated Oxygen Heterocycles. *J. Am. Chem. Soc.* **1992**, *114*, 5426–5427.

(48) The saturated lactone is marketed as Exaltolide (Firmenich), Cyclopentadecanolide (Symrise), Pentalide (Soda Aromatics), and Thibetolide (Givaudan). See: (a) Rowe, D. J. *Chemistry and Technology of Flavors and Fragrances*, CRC Press, Boca Raton, Florida, **2005**. For the first RCM route to this compound, see: (b) Fürstner, A.; Langemann, K., Conformationally Unbiased Macrocyclization Reactions by Ring Closing Metathesis. *J. Org. Chem.* **1996**, *61*, 3942–3943.

(49) Farina, V.; Horváth, A., Ring-Closing Metathesis in the Large-Scale Synthesis of Pharmaceuticals. In *Handbook of Metathesis*, Grubbs, R. H.; Wenzel, A. G., Eds. Wiley-VCH: Weinheim, 2015; Vol. 2, pp 633–658.

(50) Fandrick, K. R.; Savoie, J.; Jinhua, N. Y.; Song, J. J.; Senanayake, C. H., Challenges and Opportunities for Scaling the Ring-Closing Metathesis Reaction in the Pharmaceutical Industry. In *Olefin Metathesis – Theory and Practice*, Grela, K., Ed. Wiley: Hoboken, 2014; pp 349-366.

(51) For recent reviews of olefin metathesis in chemical biology, see: (a) Isenegger, P. G.; Davis, B. G., Concepts of Catalysis in Site-Selective Protein Modifications. *J. Am. Chem. Soc.* **2019**, *141*, 8005−8013. (b) Vinogradova, E. V., Organometallic Chemical Biology: An Organometallic Approach to Bioconjugation. *Pure Appl. Chem.* **2017**, *89*, 1619–1640. (c) Messina, M. S.; Maynard, H. D., Modification of Proteins using Olefin Metathesis. *Mater. Chem. Front.* **2020**, *4*, 1040–1051.

(52) Conrad, J. C.; Eelman, M. D.; Duarte Silva, J. A.; Monfette, S.; Parnas, H. H.; Snelgrove, J. L.; Fogg, D. E., Oligomers as Intermediates in Ring-Closing Metathesis. *J. Am. Chem. Soc.* **2007**, *129*, 1024–1025.

(53) Monfette, S.; Fogg, D. E., Equilibrium Ring-Closing Metathesis. *Chem. Rev.* **2009**, *109*, 3783–3816.

(54) van Lierop, B. J.; Lummiss, J. A. M.; Fogg, D. E., Ring-Closing Metathesis. In *Olefin Metathesis-Theory and Practice*, Grela, K., Ed. Wiley: Hoboken, NJ, 2014; pp 85–152.

(55) Gawin, R.; Tracz, A.; Chwalba, M.; Kozakiewicz, A.; Trzaskowski, B.; Skowerski, K., Cyclic Alkyl Amino Ruthenium Complexes—Efficient Catalysts for Macrocyclization and Acrylonitrile Cross Metathesis. *ACS Catal.* **2017**, *7*, 5443–5449.

(56) Sytniczuk, A.; Dąbrowski, M.; Banach, Ł.; Urban, M.; Czarnocka-Śniadała, S.; Milewski, M.; Kajetanowicz, A.; Grela, K., At Long Last: Olefin Metathesis Macrocyclization at High Concentration. *J. Am. Chem. Soc.* **2018**, *40*, 8895–8901.

(57) Shu, C.; Zeng, X.; Hao, M.-H.; Wei, X.; Yee, N. K.; Busacca, C. A.; Han, Z.; Farina, V.; Senanayake, C. H., RCM Macrocyclization Made Practical: An Efficient Synthesis of HCV Protease Inhibitor BILN 2061. *Org. Lett.* **2008**, *10*, 1303–1306.

(58) Yee, N. K.; Farina, V.; Houpis, I. N.; Haddad, N.; Frutos, R. P.; Gallou, F.; Wang, X.-J.; Wei, X.; Simpson, R. D.; Feng, X.; Fuchs, V.; Xu, Y.; Tan, J.; Zhang, L.; Xu, J.; Smith-Keenan, L. L.; Vitous, J.; Ridges, M. D.; Spinelli, E. M.; Johnson, M.; Donsbach, K.; Nicola, T.; Brenner, M.; Winter, E.; Kreye, P.; Samstag, W., Efficient Large-Scale Synthesis of BILN 2061, a Potent HCV

Protease Inhibitor, by a Convergent Approach Based on Ring-Closing Metathesis. *J. Org. Chem.* **2006**, *71*, 7133–7145.

(59) Tsantrizos, Y. S.; Ferland, J.-M.; McClory, A.; Poirier, M.; Farina, V.; Yee, N. K.; Wang, X.-j.; Haddad, N.; Wei, X.; Xu, J.; Zhang, L., Olefin Ring-Closing Metathesis as a Powerful Tool in Drug Discovery and Development – Potent Macrocyclic Inhibitors of the Hepatitis C Virus NS3 Protease. *J. Organomet. Chem.* **2006**, *691*, 5163–5171.

(60) Nicola, T.; Brenner, M.; Donsbach, K.; Kreye, P., First Scale-Up to Production Scale of a Ring Closing Metathesis Reaction Forming a 15-Membered Macrocycle as a Precursor of an Active Pharmaceutical Ingredient. *Org. Process Res. Dev.* **2005**, *9*, 513–515.

(61) Llinàs-Brunet, M.; Bailey, M. D.; Bolger, G.; Brochu, C.; Faucher, A.-M.; Ferland, J. M.; Garneau, M.; Ghiro, E.; Gorys, V.; Grand-Maître, C.; Halmos, T.; Lapeyre-Paquette, N.; Liard, F.; Poirier, M.; Rhéaume, M.; Tsantrizos, Y. S.; Lamarre, D., Structure−Activity Study on a Novel Series of Macrocyclic Inhibitors of the Hepatitis C Virus NS3 Protease Leading to the Discovery of BILN 2061. *J. Med. Chem.* **2004**, *47*, 1605–1608.

(62) Farina, V.; Shu, C.; Zeng, X.; Wei, X.; Han, Z.; Yee, N. K.; Senanayake, C. H., Second-Generation Process for the HCV Protease Inhibitor BILN 2061: A Greener Approach to Ru-Catalyzed Ring-Closing Metathesis. *Org. Process Res. Dev.* **2009**, *13*, 250–254.

(63) Calligari, P.; Bobone, S.; Ricci, G.; Bocedi, A., Molecular Investigation of SARS–CoV-2 Proteins and Their Interactions with Antiviral Drugs. *Viruses* **2020**, *12*.

(64) Chatel-Chaix, L.; Baril, M.; Lamarre, D., Pharmacology and Mechanisms of Action of Antiviral Drugs: Protease Inhibitors. In *Advanced Therapy for Hepatitis C*, McCaughan, G. W.; McHutchison, J.; Pawlotsky, J.-M., Eds. Wiley-Blackwell: Toronto, 2011.

(65) Kong, J.; Chen, C.-Y.; Balsells-Padros, J.; Cao, Y.; Dunn, R. F.; Dolman, S. J.; Janey, J.; Li, H.; Zacuto, M. J., Synthesis of the HCV Protease Inhibitor Vaniprevir (MK-7009) Using Ring-Closing Metathesis Strategy. *J. Org. Chem.* **2012**, *77*, 3820–3828.

(66) Sales of Simiprevir. Medivir: Interim Report, January – September 2014, Marketwatch. http://www.marketwatch.com/story/medivir-interim-report-january-september-2014-2014-11-20.

(67) Chatterjee, A. K.; Choi, T.-L.; Sanders, D. P.; Grubbs, R. H., A General Model for Selectivity in Olefin Cross Metathesis. *J. Am. Chem. Soc.* **2003**, *125*, 11360–11370.

(68) Bosma, R. H. A.; Van den Aardweg, F.; Mol, J. C., Cometathesis of Methyl Oleate and Ethylene; A Direct Route to Methyl Dec-9-Enoate. *J. Chem. Soc., Chem. Commun.* **1981**, 1132–1133.

(69) Higman, C. S.; Lummiss, J. A. M.; Fogg, D. E., Olefin Metathesis at the Dawn of Uptake in Pharmaceutical and Specialty Chemicals Manufacturing. *Angew. Chem., Int. Ed.* **2016**, *55*, 3552–3565.

(70) Bertin, P. A.; Gibbs, J. M.; Shen, C. K.-F.; Thaxton, C. S.; Russin, W. A.; Mirkin, C. A.; Nguyen, S. T., Multifunctional Polymeric Nanoparticles from Diverse Bioactive Agents. *J. Am. Chem. Soc.* **2006**, *128*, 4168–4169.

(71) Merrett, K.; Liu, W.; Mitra, D.; Camm, K. D.; McLaughlin, C. R.; Liu, Y.; Watsky, M. A.; Li, F.; Griffith, M.; Fogg, D. E., Synthetic Neoglycopolymer-Recombinant Human Collagen Hybrids as Biomimetic Crosslinking Agents in Corneal Tissue Engineering. *Biomaterials* **2009**, *30*, 5403–5408.

(72) Barrett, A. G. M.; Hopkins, B. T.; Koebberling, J., ROMPgel Reagents in Parallel Synthesis. *Chem. Rev.* **2002**, *102*, 3301–3323.

(73) Miki, K.; Oride, K.; Inoue, S.; Kuramochi, Y.; Nayak, R. R.; Matsuoka, H.; Harada, H.; Hiraoka, M.; Ohe, K., Ring-Opening Metathesis Polymerization-Based Synthesis of Polymeric Nanoparticles for Enhanced Tumor Imaging in vivo: Synergistic Effect of Folate-Receptor Targeting and Pegylation. *Biomaterials* **2010**, *31*, 934–942.

(74) Kolonko, E. M.; Kiessling, L. L., A Polymeric Domain That Promotes Cellular Internalization. *J. Am. Chem. Soc.* **2008**, *130*, 5626–5627.

(75) For selected recent advances in materials science applications, see: (a) Rizzo, A.; Peterson, G. I.; Bhaumik, A.; Kang, C.; Choi, T.-L., Sugar-Based Polymers from d-Xylose: Living Cascade Polymerization, Tunable Degradation, and Small Molecule Release. *Angew. Chem., Int. Ed.* **2021**, *60*, 849–855. (b) Foster, J. C.; Grocott, M. C.; Arkinstall, L. A.; Varlas, S.; Redding, M. J.; Grayson, S. M.; O'Reilly, R. K., It is Better with Salt: Aqueous Ring-Opening Metathesis Polymerization at Neutral pH. *J. Am. Chem. Soc.* **2020**, *142*, 13878–13885. (c) Debsharma, T.; Schmidt, B.; Laschewsky, A.; Schlaad, H., Ring-Opening Metathesis Polymerization of Unsaturated Carbohydrate Derivatives: Levoglucosenyl Alkyl Ethers. *Macromolecules* **2021**, *54*, 2720-2728. (d) Church, D. C.; Takiguchi, L.; Pokorski, J. K. Optimization of Ring-Opening Metathesis Polymerization (ROMP) under Physiologically Relevant Conditions. *Polym. Chem*. **2020**, *11*, 4492−4499. (e) Feist, J. D.; Xia, Y., Enol Ethers Are Effective Monomers for Ring-Opening Metathesis Polymerization: Synthesis of Degradable and Depolymerizable Poly(2,3-dihydrofuran). *J. Am. Chem. Soc.* **2020**, *142*, 1186-1189. (f) Varlas, S.; Foster, J. C.; O'Reilly, R. K., Ring-Opening Metathesis Polymerization-Induced Self-Assembly (ROMPISA). *Chem. Commun*. **2019**, *55*, 9066–9071. (g) Varlas, S.; Keogh, R.; Xie, Y.; Horswell, S. L.; Foster, J. C.; O'Reilly, R. K. Polymerization-Induced Polymersome Fusion. *J. Am. Chem. Soc.* **2019**, *141*, 20234−20248. (h) Debsharma, T.; Behrendt, F. N.; Laschewsky, A.; Schlaad, H., Ring-Opening Metathesis Polymerization of Biomass-Derived Levoglucosenol. *Angew. Chem., Int. Ed.* **2019**, *58*, 6718-6721. (i) Jung, K.; Ahmed, T. S.; Lee, J.; Sung, J. C.; Keum, H.; Grubbs, R. H.; Choi, T. L., Living beta-selective cyclopolymerization using Ru dithiolate catalysts. *Chem. Sci.* **2019**, *10*, 8955–8963. (j) Theunissen, C.; Ashley, M. A.; Rovis, T., Visible-Light-Controlled Ruthenium-Catalyzed Olefin Metathesis. *J. Am. Chem. Soc.* **2019**, *141*, 6791–6796. (k) Song, K.; Kim, K.; Hong, D.; Kim, J.; Heo, C. E.; Kim, H. I.; Hong, S. H., Highly Active Ruthenium Metathesis Catalysts Enabling Ring-Opening Metathesis Polymerization of Cyclopentadiene at Low Temperatures. *Nat. Commun.* **2019**, *10*, 3860. (l) Kang, E.-H.; Yu, S. Y.; Lee, I. S.; Park, S. E.; Choi, T.-L., Strategies to Enhance Cyclopolymerization using Third-Generation Grubbs Catalyst. *J. Am. Chem. Soc*. **2014**, *136*, 10508–10514. For applications in tissue engineering, see: (m) Merrett, K.; Liu, W.; Mitra, D.; Camm, K. D.; McLaughlin, C. R.; Liu, Y.; Watsky, M. A.; Li, F.; Griffith, M.; Fogg, D. E., Synthetic neoglycopolymer-recombinant human collagen hybrids as biomimetic crosslinking agents in corneal tissue engineering. *Biomaterials* **2009**, *30*, 5403–5408.

(76) Galan, B. R.; Giessert, A. J.; Keister, J. B.; Diver, S. T., Studies on the Mechanism of Intermolecular Enyne Metathesis: Kinetic Method and Alkyne Substituent Effects. *J. Am. Chem. Soc.* **2005**, *127*, 5762–5763.

(77) Gregg, T. M.; Keister, J. B.; Diver, S. T., Inhibitory Effect of Ethylene in Ene–Yne Metathesis: The Case for Ruthenacyclobutane Resting States. *J. Am. Chem. Soc.* **2013**, *135*, 16777–16780.

(78) Grotevendt, A. G. D.; Lummiss, J. A. M.; Mastronardi, M. L.; Fogg, D. E., Ethylene-Promoted versus Ethylene-Free Enyne Metathesis. *J. Am. Chem. Soc.* **2011**, *133*, 15918–15921.

(79) For leading reviews, see: (a) Schrodi, Y., Mechanisms of Olefin Metathesis Catalyst Decomposition and Methods of Catalyst Reactivation. In *Handbook of Metathesis*, Grubbs, R. H.; Wenzel, A. G., Eds. Wiley-VCH: Weinheim, 2015; pp 323–342. (b) Chadwick, J. C.; Duchateau, R.; Freixa, Z.; van Leeuwen, P. W. N. M. *Homogeneous Catalysts: Activity – Stability – Deactivation*, Wiley-VCH: Weinheim, 2011; pp 347–396.

(80) Tabari, D. S.; Tolentino, D. R.; Schrodi, Y., Reactivation of a Ruthenium-Based Olefin Metathesis Catalyst. *Organometallics* **2013**, *32*, 5–8.

(81) Engel, J.; Smit, W.; Foscato, M.; Occhipinti, G.; Törnroos, K. W.; Jensen, V. R., Loss and Reformation of Ruthenium Alkylidene: Connecting Olefin Metathesis, Catalyst Deactivation, Regeneration, and Isomerization. *J. Am. Chem. Soc.* **2017**, *139*, 16609–16619.

(82) Amoroso, D.; Snelgrove, J. L.; Conrad, J. C.; Drouin, S. D.; Yap, G. P. A.; Fogg, D. E., An Attractive Route to Olefin Metathesis Catalysts: Facile Synthesis of a Ruthenium Alkylidene Complex Containing Labile Phosphane Donors. *Adv. Synth. Catal.* **2002**, *344*, 757–763.

(83) Amoroso, D.; Yap, G. P. A.; Fogg, D. E., Deactivation of Ruthenium Metathesis Catalysts via Facile Formation of Face-Bridged Dimers. *Organometallics* **2002**, *21*, 3335–3343.

(84) Crabtree, R. H., Deactivation in Homogeneous Transition Metal Catalysis: Causes, Avoidance, and Cure. *Chem. Rev.* **2015**, *115*, 127–150.

(85) Lummiss, J. A. M.; McClennan, W. L.; McDonald, R.; Fogg, D. E., Donor-Induced Decomposition of the Grubbs Catalysts: An Intercepted Intermediate *Organometallics* **2014**, *33*, 6738–6741.

(86) McClennan, W. L.; Rufh, S. A.; Lummiss, J. A. M.; Fogg, D. E., A General Decomposition Pathway for Phosphine-Stabilized Metathesis Catalysts: Lewis Donors Accelerate Methylidene Abstraction. *J. Am. Chem. Soc.* **2016**, *138*, 14668−14677.

(87) Bailey, G. A.; Lummiss, J. A. M.; Foscato, M.; Occhipinti, G.; McDonald, R.; Jensen, V. R.; Fogg, D. E., Decomposition of Olefin Metathesis Catalysts by Brønsted Base: Metallacyclobutane Deprotonation as a Primary Deactivating Event. *J. Am. Chem. Soc.* **2017**, *139*, 16446–16449.

(88) Lummiss, J. A. M.; Beach, N. J.; Smith, J. C.; Fogg, D. E., Targeting an Achilles Heel in Olefin Metathesis: A Strategy for High-Yield Synthesis of Second-Generation Grubbs Methylidene Catalysts. *Catal. Sci. Technol.* **2012**, *2*, 1630–1632.

(89) Hong, S. H.; Day, M. W.; Grubbs, R. H., Decomposition of a Key Intermediate in Ruthenium-Catalyzed Olefin Metathesis Reactions. *J. Am. Chem. Soc.* **2004**, *126*, 7414–7415.

(90) Hong, S. H.; Wenzel, A. G.; Salguero, T. T.; Day, M. W.; Grubbs, R. H., Decomposition of Ruthenium Olefin Metathesis Catalysts. *J. Am. Chem. Soc.* **2007**, *129*, 7961–7968.

(91) Lummiss, J. A. M.; Botti, A. G. G.; Fogg, D. E., Isotopic Probes for Ruthenium-Catalyzed Olefin Metathesis. *Catal. Sci. Technol.* **2014**, *4*, 4210–4218.

(92) Lummiss, J. A. M.; Ireland, B. J.; Sommers, J. M.; Fogg, D. E., Amine-Mediated Degradation in Olefin Metathesis Reactions that Employ the Second-Generation Grubbs Catalysts. *ChemCatChem* **2014**, *6*, 459–463.

(93) Ireland, B. J.; Dobigny, B. T.; Fogg, D. E., Decomposition of a Phosphine-Free Metathesis Catalyst by Amines and Other Nitrogen Bases: Metallacyclobutane Deprotonation as a Major Deactivation Pathway. *ACS Catal.* **2015**, *5*, 4690−4698.

(94) Wang, H.; Goodman, S. N.; Dai, Q.; Stockdale, G. W.; Clark, W. M., Development of a Robust Ring-Closing Metathesis Reaction in the Synthesis of Sb-462795, a Cathepsin K Inhibitor. *Org. Process Res. Dev.* **2008**, *12*, 226–234.

(95) Schrock, R. R.; Hoveyda, A. H., Molybdenum and Tungsten Imido Alkylidene Complexes as Efficient Olefin-Metathesis Catalysts. *Angew. Chem., Int. Ed.* **2003**, *42*, 4592–4633.

(96) Ivin, K. J.; Mol, J. C., *Olefin Metathesis and Metathesis Polymerization*. Academic Press: New York, 1997.

(97) Schrock, R. R.; Sharp, P. R., Multiple Metal-Carbon Bonds. 7. Preparation and Characterization of $Ta(C_5H_5)_2(=CH_2)(CH_3)$, a Study of its Decomposition, and Some Simple Reactions. *J. Am. Chem. Soc.* **1978**, *100*, 2389–2399.

(98) Merrifield, J. H.; Lin, G.-Y.; Kiel, W. A.; Gladysz, J. A., Mechanism of Coupling of $=CH_2$ to $H_2C=CH_2$ at a Homogeneous $(C_5H_5)Re(NO)(PPh_3)^+$ Center. Remarkable Enantiomer Self-Recognition. *J. Am. Chem. Soc.* **1983**, *105*, 5811–5819.

(99) Robbins, J.; Bazan, G. C.; Murdzek, J. S.; O'Regan, M. B.; Schrock, R. R., Reduction of Molybdenum Imido-Alkyiidene Complexes in the Presence of Olefins to Give Molybdenum (IV) Complexes. *Organometallics* **1991**, *10*, 2902–2907.

(100) Fox, H. H.; Schrock, R. R.; O'Dell, R., Coupling of Terminal Olefins by Molybdenum(VI) Imido Alkylidene Complexes. *Organometallics* **1994**, *13*, 635–639.

(101) Tsang, W. C. P.; Hultzsch, K. C.; Alexander, J. B.; Bonitatebus, P. J., Jr.; Schrock, R. R.; Hoveyda, A. H., Alkylidene and Metalacyclic Complexes of Tungsten That Contain a Chiral Biphenoxide Ligand. Synthesis, Asymmetric Ring-Closing Metathesis, and Mechanistic Investigations. *J. Am. Chem. Soc.* **2003**, *125*, 2652–2666. Erratum: *J. Am. Chem. Soc.* **2003**, *125*, 6337.

(102) Lopez, L. P. H.; Schrock, R. R., Formation of Dimers that Contain Unbridged W(IV)/W(IV) Double Bonds. *J. Am. Chem. Soc.* **2004**, *126*, 9526–9527.

(103) Arndt, S.; Schrock, R. R.; Muller, P., Synthesis and Reactions of Tungsten Alkylidene Complexes That Contain the 2,6-Dichlorophenylimido Ligand. *Organometallics* **2007**, *26*, 1279–1290.

(104) Bailey, G. A.; Foscato, M.; Higman, C. S.; Day, C. S.; Jensen, V. R.; Fogg, D. E., Bimolecular Coupling as a Vector for Decomposition of Fast-Initiating Olefin Metathesis Catalysts. *J. Am. Chem. Soc.* **2018**, *140*, 6931–6944.

(105) Romero, P. E.; Piers, W. E., Direct Observation of a 14-Electron Ruthenacyclobutane Relevant to Olefin Metathesis. *J. Am. Chem. Soc.* **2005**, *127*, 5032–5033.

(106) Tsang, W. C. P.; Schrock, R. R.; Hoveyda, A. H., Evaluation of Enantiomerically Pure Binaphthol-Based Molybdenum Catalysts for Asymmetric Olefin Metathesis Reactions that Contain 3,3 '-Diphenyl- or 3,3 '-Dimesityl-Substituted Binaphtholate Ligands. Generation and Decomposition of Unsubstituted Molybdacyclobutane Complexes. *Organometallics* **2001**, *20*, 5658–5669.

(107) Tsang, W. C. P.; Jamieson, J. Y.; Aeilts, S. L.; Hultzsch, K. C.; Schrock, R. R.; Hoveyda, A. H., Investigations of Reactions Between Chiral Molybdenum Imido Alkylidene Complexes and Ethylene: Observation of Unsolvated Base-Free Methylene Complexes, Metalacyclobutane and Metalacyclopentane Complexes, and Molybdenum(IV) Olefin Complexes. *Organometallics* **2004**, *23*, 1997–2007.

(108) Nizovtsev, A. V.; Afanasiev, V. V.; Shutko, E. V.; Bespalova, N. B., Metathesis Catalysts Stability and Decomposition Pathway. *NATO Sci. Ser. II* **2007**, *243*, 125–135.

(109) Janse van Rensburg, W.; Steynberg, P. J.; Meyer, W. H.; Kirk, M. M.; Forman, G. S., DFT Prediction and Experimental Observation of Substrate-Induced Catalyst Decomposition in Ruthenium-Catalyzed Olefin Metathesis. *J. Am. Chem. Soc.* **2004**, *126*, 14332–14333.

# Chapter 2. Improving Synthetic Routes to Olefin Metathesis Catalysts

## 2.1. Context and Overview of Content

Clean, high-yield synthetic routes are essential for the reliable, cost-effective production of catalysts that enable reproducible performance. Described in this chapter are methods aimed at production of ruthenium catalysts stabilized by NHC or CAAC ligands, without the limitations in purity and yield associated with prior methods. Described first (Paper 1 in this chapter; Section 2.2) is an improved route to Ru-$H_2$IMes catalysts, including $^{13}$C-labelled isotopologues. That chemistry was undertaken at the outset of this thesis work, shortly after the opportunities associated with the CAAC catalysts was first reported, and hence focused solely on the NHC catalysts. Very recently, however, we applied these methodologies to production of CAAC catalysts. The latter work was begun in the course of the author's studies, but was enlarged and completed by Mr. Christian Blanco of this research group. Relevant aspects are described briefly in Section 2.3, Subsequent Advances.

### 2.1.1. Published Contributions

(1) Merrifield Resin-Assisted Routes to Second-Generation Metathesis Catalysts. D.L. Nascimento, E.C. Davy, D.E. Fogg.* *Catal. Sci. Technol.* **2018**, *8*, 1535-1544. (Full paper). Copyright 2018 Royal Society of Chemistry. Reprinted with permission.

*Abstract:* Phosphine-scavenging resins can significantly facilitate the synthesis of highly active Ru metathesis catalysts, including the second-generation Grubbs, Hoveyda, and indenylidene catalysts (**GII**, **HII**, **InII**). These catalysts are customarily prepared by ligand exchange of the corresponding first-generation catalysts with the N-heterocyclic carbene (NHC) $H_2$IMes. The $PCy_3$ coproduct is conventionally removed by pentane extraction, but the partial solubility of the desired Ru products can cause product losses of over 20%. Sequestration of the $PCy_3$ coproduct with CuCl is more efficient, but is undesirable given the potential for noninnocent copper residues. Use of the arylsulfonic acid resin Amberlyst-15 delivers near-quantitative catalyst yields, but the high acidity of the resin leads to problems with reproducibility and decomposition. An alternative approach is described, in which a neutral Merrifield resin (crosslinked polystyrene with pendant *p*-$C_6H_4CH_2I$ groups; **MF-I**) is used to sequester $PCy_3$ as the covalently-tethered benzylphosphonium salt. Addition of **MF-I** following complete ligand exchange effects quantitative uptake of free $PCy_3$ (and any residual free NHC) within 45 min at RT: the clean products are isolated by filtration, in ca. 95%

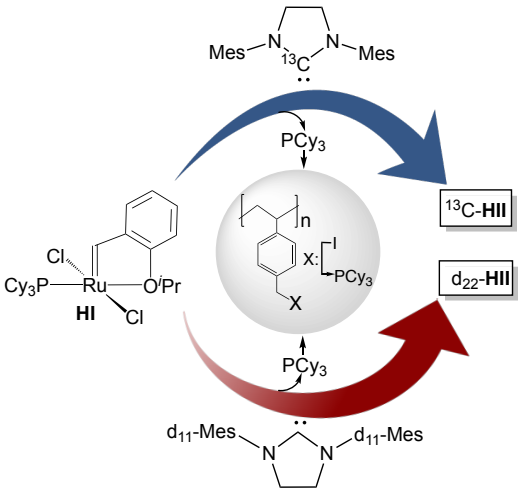

yield. These yields compare well with those obtained via the Amberlyst-15 route, without the challenges due to resin acidity. The efficacy of this methodology is demonstrated in the synthesis of isotopically-labelled derivatives of **HII**, in which the $H_2$IMes ligand bears a $^{13}$C-label at the carbene carbon, or perdeuterated mesityl rings.

(2) Routes to High-Performing Ru-Iodide Catalysts for Olefin Metathesis: Phosphine Lability Is Key to Efficient Halide Exchange. C.O. Blanco, D.L. Nascimento, D.E. Fogg,* *Organometallics*, ASAP. (Communication). Copyright 2021 American Chemical Society. Reprinted with permission.

*Abstract:* Clean, high-yield routes are described to ruthenium-diiodide catalysts recently shown to enable high productivity in olefin metathesis. For the second-generation Grubbs and Hoveyda catalysts (**GII**: $RuCl_2(H_2IMes)(PCy_3)(=CHPh)$; **HII**: $RuCl_2(H_2IMes)(=CHAr)$, Ar = $C_6H_4$-2-O$^i$Pr), slow salt metathesis is shown to arise from the low lability of the ancillary $PCy_3$ or ether ligands, which retards access to the four-coordinate intermediate required for efficient halide exchange. To exploit the lability of first-generation catalysts, diiodide complex $RuI_2(PCy_3)(=CHAr)$ **HI($I_2$)** was prepared by treating "Grubbs I" ($RuCl_2(PCy_3)_2(=CHPh)$, **GI**) with NaI, $H_2C$=CHAr **SE**, and a phosphine-scavenging Merrifield-iodide (**MF-I**) resin. Subsequent installation of $H_2$IMes or cyclic (alkyl)(amino)carbene (CAAC) ligands afforded the second-generation iodide catalysts in good to excellent yields. Given the incompatibility of the nitro group with a free carbene, the iodo-Grela catalyst $RuI_2(H_2IMes)(=CHAr')$ (**nG($I_2$)**: Ar' = $C_6H_3$-2-O$^i$Pr-4-$NO_2$) was instead accessed by sequential salt metathesis of **GI** with NaI, installation of $H_2$IMes, and finally cross-metathesis with nitrostyrenyl ether $H_2C$=CHAr' **NSE** , with **MF-I** as phosphine scavenger. The bulky iodide ligands improve selectivity for macrocyclization in ring-closing metathesis.

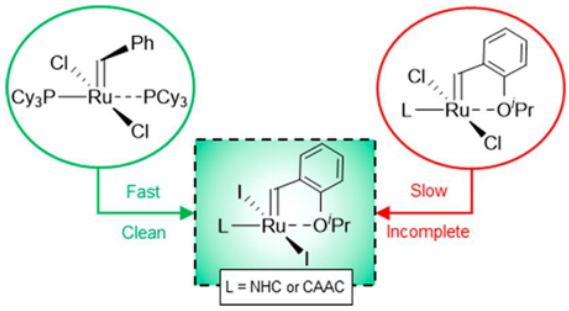


*Author Contributions:* Manuscript (1) was written by DN and DEF. All experiments were conducted by DN, apart from the synthesis of isotopically labelled ligands (carried out by ECD). Manuscript (2) was written by COB and DEF. Preliminary experiments were developed by DN, based on a hypothesized correlation between ligand lability and rate of halide exchange, and expanded and completed by COB.

*References for Chapter 2 begin on p. 40*

## 2.2. Merrifield Resin-Assisted Routes to Second-Generation Catalysts for Olefin Metathesis

### 2.2.1. Introduction

Olefin metathesis offers powerful, versatile methodologies for the catalytic assembly of carbon-carbon bonds.[1,2] Ruthenium metathesis catalysts bearing an *N*-heterocyclic carbene (NHC) ligand, long embraced for synthetic purposes in academia, have now begun to see uptake in pharmaceutical manufacturing.[3] Despite prominent recent advances highlighting the potential of alternative ligand sets, particularly cyclic (alkyl)(amino) carbenes,[4-10] the "second-generation" Grubbs and Hoveyda catalysts **GII** and **HII** (Chart 2.1) continue to dominate current use. Clean, reproducible, high-yield routes to such complexes, as well as indenylidene analogue **InII**, are therefore of interest.

**Chart 2.1. Metathesis catalysts discussed. Top: first-generation Ru catalysts, precursors to (bottom) the second-generation catalysts in dominant use.**

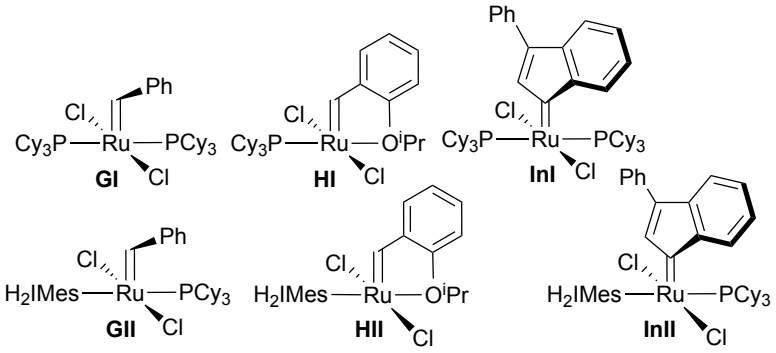


These catalysts are typically accessed via ligand exchange reactions, in which a $PCy_3$ ligand present in the corresponding first-generation complex is replaced with $H_2IMes$. Classically, such routes rely on in situ generation and installation of $H_2IMes$, via treatment of the imidazolinium salt $H_2IMes$•HX (X = Cl or $HBF_4$) with a strong base such as KO$^t$Bu, NaH, or potassium *t*-amylate ($KOCMe_2Et$).[11] Depicted in Scheme 2.1 is the original, still widely cited, synthesis of **GII** via this approach.[12]

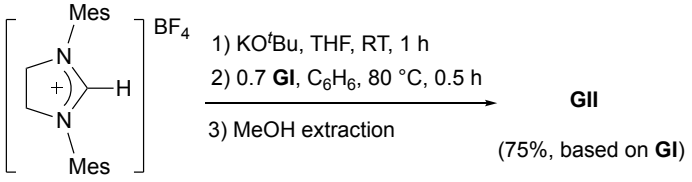


**Scheme 2.1. Synthesis of GII via in situ liberation and installation of $H_2IMes$.**

*References for Chapter 2 begin on p. 40*

The continuing popularity of in situ NHC generation is surprising, given the problems pointed out in early reports.[13,14] Challenges include the negative impact on catalytic activity of **GII** of unreacted NHC•HX (Scheme 2.2a; this reagent is used in excess to achieve full conversion of the ruthenium precursor), as well as residual alkali metal salts, likewise used in excess.[13] Reaction of **GI** with excess KO$^t$Bu generates Ru(O$^t$Bu)$_2$(PCy$_3$)(=CHPh) (Scheme 2.2b),[13] a complex known to exhibit minimal metathesis activity.[15] Extraction of excess base with methanol is also problematic, however, as this generates Ru hydride contaminants,[13,14] including isomerization-active[16] **Ru-1**: Scheme 2.2c. (This may plausibly occur via formation of methoxide ion, which reacts with **GI** and **GII** much more rapidly than does methanol itself).[17] Further, loss of the benzylidene ligand has been observed on adventitious admission of air during synthesis of **GII**[13] (Scheme 2.2d). Unintended exposure to air is a perennial risk for Schlenk reactions carried out at reflux, underscoring the convenience and reliability of the room-temperature, glovebox operations below.

Finally, no consensus exists on the reliability of operation via the NHC•HCl vs NHCs•HBF$_4$ salts. Bantreil and Nolan reported lower yields of the IMes analogue of **GII** on use of IMes•HCl, in place of IMes•HBF$_4$,[18] but the opposite claim has also been made.[13,19] Relevant in this context is Grela's comment that the yield of **GII** is extremely sensitive to the purity of the H$_2$IMes•HBF$_4$ reagent.[20] It should be noted that although the high crystallinity of H$_2$IMes•HBF$_4$ is a valuable aid to purification,[11,18] this salt must be rigorously dried to remove water remaining from its synthesis, which otherwise hydrolyzes the free NHC as it is generated (Scheme 2.2e).[21]

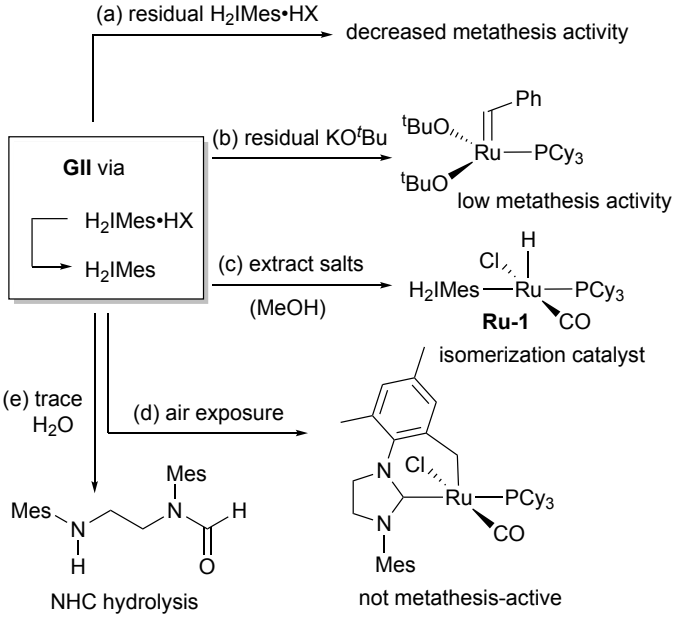


**Scheme 2.2. Exemplary problems in synthesis of GII via in situ liberation of H$_2$IMes.**

High-yield routes to the leading Ru-$H_2$IMes metathesis catalysts (Table 2.1) typically utilize alternative sources of $H_2$IMes. Such sources include $H_2$IMes•$CO_2$,[22] which stands out among the many NHC adducts used to access metal-NHC derivatives for the innocuousness of the $CO_2$ byproduct.[23] Delaude and coworkers reported the synthesis of **GII** and **HII** by refluxing **GI** or **HI** with $H_2$IMes•$CO_2$, followed by chromatographic workup (Table 2.1, entries 1-2).[22,24]
We previously reported a convenient route involving reaction with free $H_2$IMes, and workup by addition of the acidic resin Amberlyst-15 (Figure 2.1a) to scavenge the $PCy_3$ byproduct.[21] This procedure offered two key advances over standard methods. First, use of the isolated free NHC (an approach pioneered by Nolan with IMes as pro-ligand)[18,25] prevents side-reactions arising from in situ liberation of the NHC.[26] Secondly, the use of Amberlyst-15 as a $PCy_3$ scavenger, originally described in a patent procedure by Verpoort and co-workers,[27] and since adopted by our group and others for removal of $PCy_3$ or nitrogen bases,[21,28,29] contributes greatly to the simplicity and convenience of workup. Thus, workup requires only filtering off the resin once scavenging is complete, and evaporation of the filtrate.

This straightforward purification procedure is considerably more time- and resource-efficient than removing the $PCy_3$ byproduct by column chromatography or extracting with pentane or hexanes.[12,30] Amberlyst-assisted workup improves isolated yields by 20% or more for **GII**, and ca. 15% for **HII**, vs pentane extraction.[21] It also eliminates problems associated with the use of CuCl as a phosphine scavenger (Table 2.1, entries 2, 3, 5), as detailed below.

**Table 2.1. Reported high-yield routes (>90%) to GII, HII, and InII.**

| entry | catalyst (precursor) | NHC source | $PCy_3$ removal method | yield (scale)[a] | ref |
|---|---|---|---|---|---|
| 1 | **GII** (**GI**) | $H_2$IMes•$CO_2$ (1.5 equiv) | chromatography | 90% (1 g) | 22 |
| 2 | **HII** (**HI**) | $H_2$IMes•$CO_2$ (1.2 equiv) | 1.2 CuCl; chromatography | 95% (0.4 g) | 22 |
| 3 | **HII** (**HI**) | $H_2$IMes•$HBF_4$ (1.2 equiv) + KO-$CMe_2$Et (1.3 equiv) | 1.8 CuCl recrystallize | 92% (18 g) | 20 |
| 4 | **GII** (**GI**) | $H_2$IMes•$HC_6F_5$ (1.5 equiv) | chromatography | 91% (0.16 g) | 31 |
| 5 | **HII** (**GII**) | n/a[b] | 1.3 CuCl; chromatography | 97% (5 mg) | 32 |
| 6 | **GII** (**GI**) | 1 $H_2$IMes (1.1 equiv) | Amberlyst; "filter-strip" | 96% (2.4 g) | 21 |
| 7 | **HII** (**HI**) | $H_2$IMes (1.1 equiv) | Amberlyst; "filter-strip" | 98% (4 g) | 21 |
| 8 | **InII** (**InI**) | $H_2$IMes (1.1 equiv) | Amberlyst; "filter-strip" | 95% (1 g) | 21 |

[a] Scale based on Ru precursor as limiting reagent. [b] Accessed by cross-metathesis (CM) of **GII** with 1,2 isoproxy-2-propenylbenzene. For strategic limitations to synthesis of **HII** via ligand exchange of **GI**, followed by metathesis of **GII**, see Scheme 2.5 and associated discussion.

While CuCl is commonly used as an aid to workup, Hoveyda's original report commented that it complicates chromatographic purification of **HII**.[30] Grela and co-workers circumvented this

problem by developing a successful recrystallization procedure, used in one of the largest-scale syntheses of **HII** reported in the open literature (Table 2.1, entry 3).[20] This success notwithstanding, a copper-free scavenging protocol is highly desirable, particularly with an eye to deploying these metathesis catalysts in the pharmaceutical sector in compliance with current Good Manufacturing Practices (GMP). Cu(I) halides mediate many catalytic transformations,[33] and trace amounts of Cu are notorious for their capacity to engage in unanticipated catalytic and/or redox chemistry.[33b,34-36] Copper, even more so than iron, is one of the usual culprits in undesired oxidations of pharmaceutical compounds catalyzed by trace metal impurities.[36]

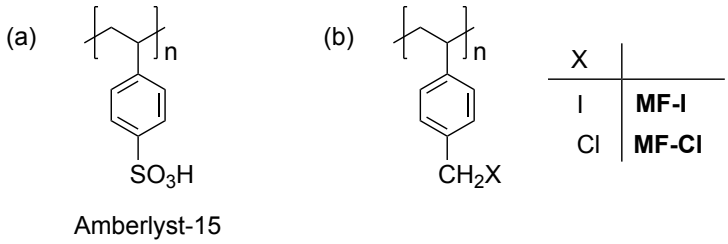


**Figure 2.1. Molecular structures of: (a) Amberlyst; (b) Merrifield resins.**

Sustained use of the alternative Amberlyst scavenging protocols, however, revealed limitations arising from the high acidity of the *p*-toluene sulfonic acid (pTSA)[37] groups on the resin. While the original experiments suggested that **GII** was stable toward Amberlyst-15 over 2 h in THF at RT,[21] problems with reproducibility and catalyst decomposition emerged in subsequent use, as detailed below. We therefore sought an alternative approach aimed at retaining the high yields and convenience of resin-enabled "filter-and-strip" workup, while circumventing the problems arising from the highly acidic pTSA scavenger.

Attractive from this perspective are Merrifield resins (e.g. **MF-I**, Figure 2.1b), benzyl halide-functionalized polystyrenes originally developed to assist solid-phase synthesis.[38,39] The Lipshutz group successfully employed in situ-generated **MF-I** to purify cross-coupling products synthesized via Ni or Pd catalysis.[40] Morris and co-workers found it advantageous to isolate the resin, which they used to sequester $PPh_3$ byproducts (and trace phosphine oxides) generated during synthesis of ruthenium hydride complexes.[41] Inspired by these successes, we examined the utility of the Merrifield resin **MF-I** in ligand-exchange routes to **GII**, **HII**, and **InII**, selected as the dominant metathesis catalysts in current use. Here we report the success of this approach, illustrated with synthesis of all three of these benchmark catalysts, as well as isotopically-labelled **HII**, in which the $H_2$IMes ligand bears a $^{13}$C-label at the carbene carbon, or perdeuterated mesityl rings.

### 2.2.2. Results and Discussion

**Problems with Amberlyst-15.** Initial problems with the Amberlyst-15 methodology were manifested in stoichiometric irreproducibility. Specifically, higher proportions of Amberlyst-15 were required (relative to our originally-optimized 4:1 ratio of resin pTSA groups vs Ru),[21] to completely scavenge free $PCy_3$. The stoichiometry of the resin reaction is, unsurprisingly, highly sensitive to storage conditions. While glovebox storage maximizes convenience, the avidity of the resin for volatile base (pyridines, amines) was apparent even when Amberlyst-15 was stored in well-taped vials, and opened only after purging the glovebox atmosphere. Beyond the requirement for additional resin when using Amberlyst-15 handled under these conditions, additional, unidentified signals were evident in $^{31}P\{^1H\}$ NMR spectra of **GII** "purified" via workup with this material (Figure A.9). Best practices thus involve bringing in fresh resin for each use, and ensuring that the stock supply is stored in a cabinet free of chemical vapours.

Even with clean resin, however, decomposition was occasionally apparent on treating **GII** with Amberlyst-15 in THF. In one case, 15% loss of **GII** was detected by integration of the alkylidene singlet against an internal standard, after stirring a clean sample of the catalyst with the resin in THF for 2 h. While Amberlyst-15 is much more aggressive toward **GII** alone than during workup, when free $PCy_3$ and **GII** are simultaneously present, this highlights undesirable potential risks.

**Synthesis of the Merrifield-Iodide Resin.** Preliminary experiments indicated that the benzyl chloride resin **MF-Cl** can sequester free $PCy_3$, but that reaction is inconveniently slow. Even for resin that is relatively lightly (1%) crosslinked with divinylbenzene, which permits better swelling, 30% $PCy_3$ remained after 20 h exposure to the resin at RT in THF. We therefore abandoned direct use of **MF-Cl**, instead converting it into the more electrophilic iodide resin **MF-I** via the established[40,41] reaction with NaI. Sub-stoichiometric proportions of NaI were used (Scheme 2.3), to ensure that the product resin is free of residual alkali iodide, which could contribute to formation of ruthenium iodide products.[41-43]

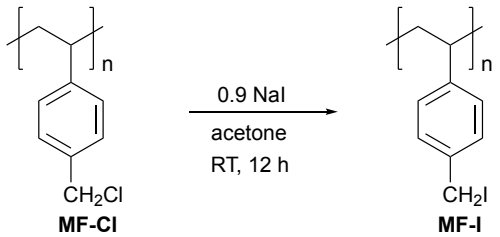


**Scheme 2.3. Synthesis of the Merrifield iodide resin.**

**Merrifield Resin-Assisted Synthesis of GII.** In examining the capacity of **MF-I** as an aid to workup, we first focused on the transformation of **GI** into **GII** by reaction with free $H_2IMes$

(Scheme 2.4). Adding the resin once exchange is complete enables removal of both the $PCy_3$ byproduct, and residual free NHC (which is used in 10% excess in these reactions, to ensure complete conversion of **GI**). THF was chosen as the reaction medium: chlorinated solvents are precluded by their reactivity toward the free NHC,[21,44] while aromatic solvents limit resin swelling,[45,46] retarding the $S_N2$ scavenging reaction.[21] It should be noted that greater bead fragility results from the choice of lightly crosslinked resins to aid in swelling. Controlled stirring rates (ca. 240 rpm) were therefore employed, to limit mechanical damage to the beads, and conserve consistent reaction stoichiometry and rates.

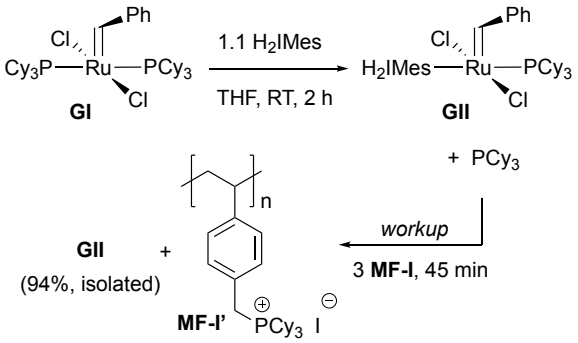


**Scheme 2.4. Merrifield resin-assisted synthesis of GII.**

Addition of a twofold excess of **MF-I**, relative to **GI**, effected complete removal of free $PCy_3$ within 1.5 h, as judged by $^{31}P\{^1H\}$ NMR analysis. This period was reduced to 45 min by increasing the resin stoichiometry to 3:1. Reactions on preparative scale (3 g; Scheme 2.4) proceeded smoothly under these conditions, with complete reaction after 45 min. The mixture was immediately filtered through Celite to remove the phosphonium iodide-bearing resin **MF-I'**. (Minimizing exposure times of the catalyst to the resin is a precaution against salt metathesis, the onset of which can be observed on extended reaction: e.g. 1% at 8 h). The product was washed through the Celite pad with further THF, and the filtrate was evaporated. This procedure afforded clean **GII** (for spectra, see Figure A.1) as a microcrystalline powder in 94% yield after drying. This is comparable to the yields obtained using the Amberlyst-15 resin. In comparison, workup by pentane extraction afforded **GII** in 75% isolated yield.[12]

**Merrifield Resin-Assisted Synthesis of HII**. The second-generation Hoveyda catalyst **HII** can be accessed from **GI** by either of the pathways shown in Scheme 2.5. Route A commences with synthesis of the first-generation Hoveyda catalyst **HI** via cross-metathesis of **GI** with *o*-isopropoxystyrene **SE**. **HI** is then converted into the target **HII** by ligand exchange with $H_2$IMes. In the alternative Route B, ligand exchange of **GI** is carried out first, forming **GII**, and the styrenyl ether ligand is then installed via cross-metathesis with **SE**.

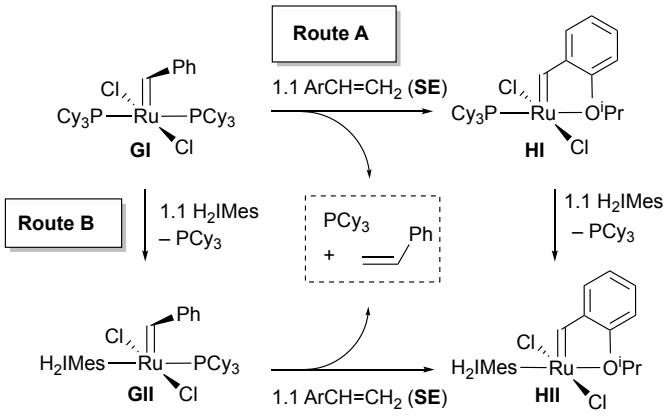


**Scheme 2.5. Strategies for synthesis of HII. Route A (preferred): metathesis with SE, then ligand exchange. Route B: ligand exchange, then metathesis. Ar = *o*-$C_6H_4$-O*i*Pr.**

Importantly, however, the styrene co-product of metathesis has no affinity for the resin (and nor do any stilbenes resulting from self-metathesis). To remove these byproducts, the Ru product must be purified by chromatography or extraction, either of which removes the $PCy_3$ coproduct along with styrene. There is thus no benefit to using the resin for post-metathesis workup (that is, after Step 1 of Route A, or Step 2 of Route B).

Finally, losses of 15-20% (extraction) or up to 10% (chromatography) are typically incurred in purification. Route A is therefore strategically preferable, in that maximum loss occurs in the first step, where the premium on materials and labour is least. The NHC ligand – synthesis of which is more demanding than that of **SE**, even when the NHC is not isotopically labelled – is then installed in the second stage of reaction. Accordingly, the studies below focused on the capacity of **MF-I** to improve yields in the *second* step of Route A, the transformation of **HI** into **HII** via ligand exchange.

A challenge in the synthesis of **HII**, described in the original study by Blechert and co-workers,[47] is slow chelation of the ether group following reaction of **HI** with $H_2$IMes. The initial product is a $\kappa^1$-isopropoxystyrene intermediate with a dangling ether oxygen (**HII$^P$**; Scheme 2.6), chelation of which is inhibited by the low lability characteristic of $PCy_3$ trans to an NHC ligand.[48,49] Formation of **HII** is commonly driven by addition of CuCl and heating. Resin treatment proves an effective alternative. In this approach, a more specific embodiment of the strategy exemplified in Scheme 2.5 above, **HI** was treated with $H_2$IMes for 2 h at RT to effect transformation to **HII$^P$**. Addition of excess **MF-I** and heating for 2 h at 40 °C afforded clean **HII** as a green powder in 96% yield (Figure A.2), after workup as above. In comparison, the original route delivered **HII** in 85% yield after chromatographic purification.[30]

*References for Chapter 2 begin on p. 40*

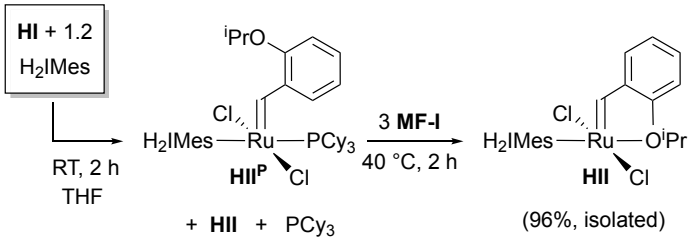


**Scheme 2.6. Merrifield resin-assisted synthesis of HII.**

**Merrifield Resin-Assisted Synthesis of InII.** Synthesis of **InII** was undertaken via the procedure established for the IMes analogue.[50] Accordingly, an orange-brown solution of **InI** and $H_2$IMes in hexanes was heated at 60 °C (Scheme 2.7). Within ca. 10 min, the **InII** product began to deposit as a red-brown precipitate. $^{31}P\{^1H\}$ NMR analysis of the supernatant confirmed conversion of **InI** to **InII** and free $PCy_3$ after 2.5 h. Also present were two minor, unidentified singlets (45.7 and –4.6 ppm in $CDCl_3$; 3% of total integration).*

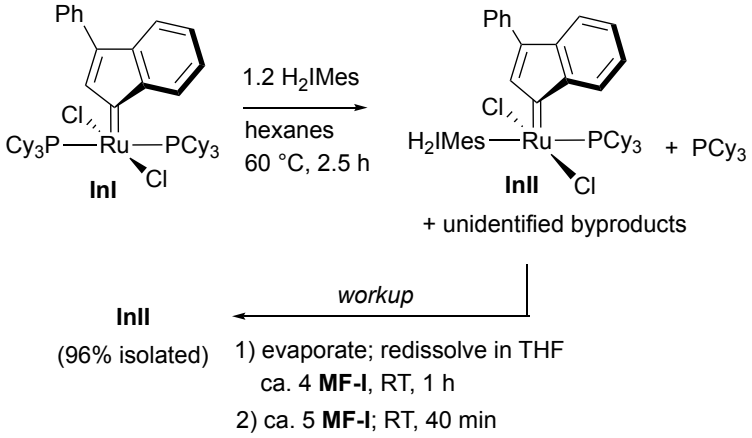


**Scheme 2.7. Synthesis of InII.**

To scavenge the free $PCy_3$, the solvent was evaporated on the Schlenk line, the residue was dissolved in THF, and a fourfold excess of **MF-I** was added. No free $PCy_3$ remained after stirring at RT for 1 h, as judged by NMR analysis, though traces of the byproducts remained (ca. 1% of total integration). Filtering and stirring with further **MF-I** for 40 min completely removed these species. Workup as before, by filtering through Celite to remove the resin, washing the product through with THF, and evaporating the filtrate, afforded clean **InII** as microcrystalline red-brown powder in 96% yield. In comparison, the Amberlyst route gave **InII** in 95% isolated yield;

*When this reaction was carried out in THF, rather than hexanes, a further pair of $^{31}P$ NMR doublets was observed even prior to complete consumption of **InI**. $^{31}P\{^1H\}$ NMR (121 MHz, $CDCl_3$) 49.7 (d, $^3J_{PP}$ = 43.9 Hz, 2% of total integration; unknown **i**), 45.7 (s, 1%; unknown **ii**), 43.4 (d, $^3J_{PP}$ = 45.6 Hz; 2%, unknown **iii**); 32.7 (s, 17%, **InI**); 26.9 (s, 62%, **InII**); 11.3 (s, $PCy_3$, 10%); –4.6 (s, 7%; unknown **iv**).

Delaude's $H_2$IMes•$CO_2$ route, with chromatographic workup, gave 86%,[22] and Nolan's synthesis of the IMes analogue, with pentane extraction of the $PCy_3$ byproduct, proceeded in 79% yield.[50]

**Halide Exchange.** A potential concern at the outset of these studies was formation of Ru-iodide derivatives of the targeted catalysts, via exchange of the chloride ligands (Figure 2.2a). Halide exchange was observed in the Morris study, which deliberately exploited the phenomenon to synthesize the iodo catalyst RuHI(BINAP)($PPh_3$).[41] In the context of metathesis, control over exchange is essential, given the impact of the anionic ligands on catalyst activity.[42,43,51]

To probe the potential for resin-induced halide exchange, the catalysts were stirred with a fourfold excess of **MF-I** at RT in THF, with dimethyl terephthalate (DMT) present as an NMR integration standard. This test, carried out with the isolated catalysts in the absence of any free $PCy_3$, is deliberately more aggressive than the scavenging reaction, in which uptake of $PCy_3$ damps the reactivity of the resin, as noted above. As shown in Figure 2.2b, no change was observed for **InII** after 8 h. For **HII**, no change was evident at 6 h, but 1% of the known[42] mono-iodide species **HII(I)** was detected at 8 h, as a singlet at 16.29 ppm. For **GII**, a similar small proportion of **GII(I)** was likewise present at 8 h. The latter species was assigned based on its transient formation on the independently-examined reaction of **GII** with NaI, en route to known[52] **GII($I_2$)**. Of greater concern was the observation of an as-yet unidentified decomposition pathway for **GII**, which caused slow loss of the benzylidene signal. No decomposition was evident at 2 h, however, or – more pertinently – on the 45-minute timescale of the Merrifield-scavenging chemistry described above (see Figures A.1–A.3). Nevertheless, this underscores the importance of removing **MF-I** promptly, particularly for **GII**, once $PCy_3$ scavenging is complete.

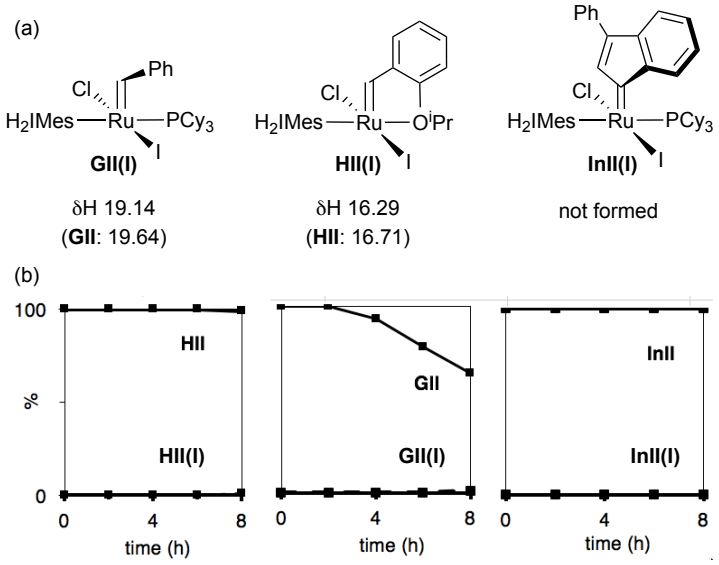


**Figure 2.2. (a) Observed (GII(I), HII(I)) or prospective (InII(I)) mono-iodide species following reaction of isolated GII, HII, or InII with MF-I (4 equiv; 8 h, RT). (b) Assessing decomposition and halide exchange vs DMT as internal standard.**

*References for Chapter 2 begin on p. 40*

**Merrifield Resin-Assisted Synthesis of Isotopically-Labelled Metathesis Catalysts.** In a final set of experiments, we deployed these methodologies to aid in synthesis of isotopically labelled metathesis catalysts. We were particularly interested in derivatives of **HII** containing $^{13}$C-labelled $H_2$IMes and $d_{22}$-$H_2$IMes, which could (respectively) report on the retention and/or activation of the NHC ligand during catalysis. The Piers group described a route to $d_{22}$-$H_2$IMes, in which the mesityl groups are fully deuterated,[53] and used this ligand to confirm that C–H activation of the Mes *o*-methyl groups is key to decomposition of the Piers catalyst, $[RuCl_2(H_2IMes)(=CHPR_3]X$ (R, X = various alkyl groups and counter-anions). $^{13}$C-labelled $H_2$IMes, in which the label is sited at the carbene carbon, has not been reported, although a number of reports describe the corresponding *unsaturated*, $^{13}$C-labelled NHCs, including $^{13}$C-IMes.[54] Studies with the latter have demonstrated the potential for important insights into reaction chemistry involving the NHC ligand during catalysis. Ruthenium catalysts for olefin metathesis have been prepared with a $^{13}$C label at the benzylidene,[55,56] methylidene,[57] and indenylidene[58] carbons, and at the metallacyclobutane ring carbons.[59,60] The present work is the first report of a metathesis catalyst in which the NHC ligand bears a $^{13}$C-label at the carbene carbon, directly bound to the Ru center. The $^{13}$C-NHC ligand can thus report directly on the stability of the Ru-NHC bond, on oxidation or attack at the NHC carbon, and (via, e.g., $^3J_{CH}$ coupling) on other spin-active ligands present on the metal.

Arduengo's now-classic synthetic route to non-labelled $H_2$IMes begins with cyclization of *N*,*N*'-dimesitylethane-1,2-diamine (NNDD) with triethyl orthoformate, the latter being used as both solvent and carbon source.[11,61] As use of the labelled orthoformate as solvent is cost-prohibitive, and probe reactions in alternative solvents proved unsatisfactory, we turned to $^{13}$C-labelled paraformaldehyde, $^{13}(CH_2O)_n$, the carbon source utilized to access $^{13}$C-IMes and related unsaturated NHCs.[54c–e] Thus, a suspension of diamine NNDD and $^{13}(CH_2O)_n$ (1.2 equiv; Scheme 2.8a) in DME was stirred for 20 h at RT, after which the crude product was treated with *N*-bromosuccinimide to afford labelled imidazolinium bromide $^{13}$C-$H_2$IMes•HBr. The latter was converted into the labelled free carbene by treatment with NaH. Ligand exchange of **HI** with $^{13}$C-$H_2$IMes was carried out as described above, with the **MF-I** workup enabling access to clean **$^{13}$C-HII** in 93% yield (Scheme 2.8b). The corresponding reaction with $d_{22}$-$H_2$IMes was carried out to obtain deuterium-labelled **$d_{22}$-HII** in 92% yield.

*References for Chapter 2 begin on p. 40*

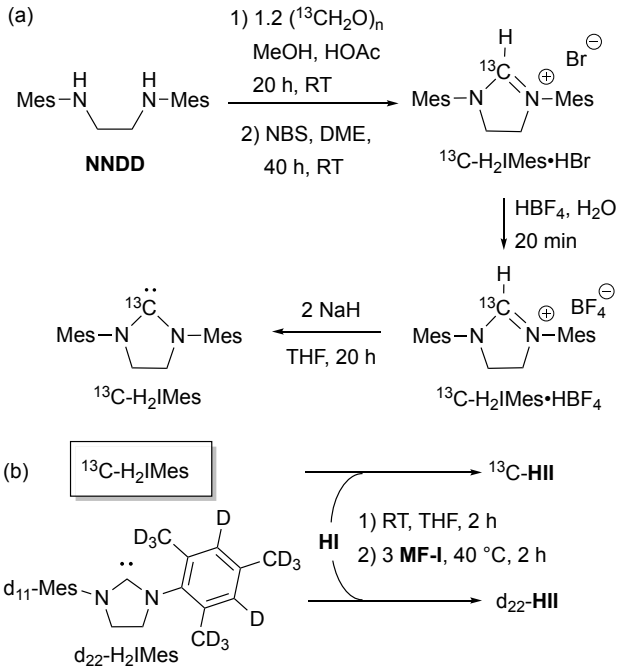


**Scheme 2.8. (a) Synthesis of $^{13}$C-labelled $H_2$IMes.[a] (b) Resin-assisted synthesis of isotopically-labelled HII. [a] NBS = *N*-bromosuccinimide, DME = dimethoxyethane.**

### 2.2.3. Conclusions

The foregoing describes an efficient route to second-generation metathesis catalysts, in which the neutral Merrifield resin **MF-I** greatly improves the convenience and reliability of purification. Addition of resin once ligand exchange of **GI**, **HI** or **InI** with free $H_2$IMes is complete results in sequestration of the free $PCy_3$ coproduct as the covalently-tethered benzylphosphonium salt. Excess NHC is likewise removed, and the clean products can be isolated by filtration in near-quantitative yields. The high yields are due to the convenient "filter-and-strip" workup, in place of standard pentane extraction or chromatographic purification methods, which are cumbersome and reduce final yields by up to ca. 20%. The Merrifield resin-assisted synthesis improves on process reliability relative to the prior resin workup, in which the highly acidic Amberlyst-15 resin was used to sequester $PCy_3$: it also obviates use of CuCl, residues of which are undesirable, particularly from the perspective of deploying these catalysts in pharmaceutical manufacturing. The efficacy of the new methodology was demonstrated in the synthesis of isotopically-labelled derivatives of **HII**, bearing a $^{13}$C label at the carbene carbon ($^{13}$C-$H_2$IMes), or perdeuterated mesityl rings ($d_{22}$-$H_2$IMes). Efficient access to the labelled catalysts adds powerful capabilities for the mechanistic exploration of catalyst performance, including studies of catalyst decomposition.

### 2.2.4. Experimental Details

**General Procedures.**
Reactions were carried out under $N_2$ in a glovebox at room temperature (25 ±2 °C), unless otherwise specified. Solvents ($C_6H_6$, hexanes, $CH_2Cl_2$ and THF) were dried and degassed using a Glass Contour solvent purification system and stored under $N_2$ over 4 Å molecular sieves. $C_6D_6$, $CDCl_3$ (Cambridge Isotopes) and deionized $H_2O$ were freeze-pump-thaw degassed (5x), and the deuterated solvents were stored under $N_2$ over 4 Å molecular sieves for at least 12 h prior to use. NaI (99.5% purity) and Merrifield resin **MF-Cl** (4.5 mmol/g Cl loading; 1% cross-linked with divinylbenzene; 200–400 mesh) were purchased from Sigma-Aldrich and used as received. **GI**,[62] *N,N'*-dimesitylethane-1,2-diamine NNDD,[63] and free $H_2$IMes[64] were prepared by the reported methods. Free $H_2$IMes was stored in the freezer (–35 °C) under $N_2$. NMR spectra were recorded on a Bruker Avance 300 NMR spectrometer at 23 ± 2 °C, and referenced to the residual proton signals of the deuterated solvents ($^1$H). Chemical shifts (δ), measured in parts per million (ppm), are reported relative to TMS ($^1$H, $^{13}$C) or 85% external $H_3PO_4$ ($^{31}$P) at 0 ppm.

**Synthetic Procedures.**

**Synthesis of MF-I from MF-Cl.** Reaction carried out using the reported procedure,[41] using lower proportions of NaI. **MF-Cl** (4.24 g, 19.1 mmol) was suspended in acetone (20 mL), and NaI (2.28 g, 17.2 mmol; 0.9 equiv) was added. The suspension was stirred for 16 h in air, after which the resin was filtered off and washed successively with $H_2O$ (4 x 100 mL), and acetone (2 x 100 mL). Yield after drying: 6.11 g (quantitative)**.**

**Resin-Assisted Synthesis of GII by Ligand Exchange.** Solid white $H_2$IMes (1.23 g, 4.01 mmol, 1.1 equiv) was added to a solution of **GI** (3.00 g, 3.64 mmol, 1 equiv) in 80 mL THF. A colour change from purple to red occurred on stirring for 5 min at RT. Stirring was continued for 2 h, after which conversion to **GII** was complete (NMR). **MF-I** (3.63 g, 10.9 mmol, 3 equiv) was then added to sequester free $PCy_3$, and the mixture was stirred for 45 min. No free $PCy_3$ remained after this time. The resin was then filtered off (Celite), and **GII** was washed through with THF (3 x 3 mL). The filtrate was evaporated under vacuum to afford 2.91 g of clean red **GII** (94%). NMR chemical shifts agree with values reported in $C_6D_6$.[48] Key values are reproduced here for convenience. $^{31}$P{$^1$H} NMR ($C_6D_6$, 121 MHz): δ 30.1 (s, *P*$Cy_3$).$^1$H NMR ($C_6D_6$, 300 MHz): δ 19.64 (s, 1H, Ru=C*H*Ph).

**Resin-Assisted Synthesis of HII by Ligand Exchange.** Solid $H_2$IMes (1.84 g, 5.99 mmol, 1.2 equiv) was added to a brown solution of **HI** (3.00 g, 4.99 mmol, 1 equiv) in 30 mL THF. The solution was stirred for 2 h at RT, at which point no colour change was evident, but conversion to **HII** and **HII$^P$** was complete. $^{31}$P{$^1$H} NMR (THF, 300 MHz): δ 30.6 (s, **HII$^P$**), 10.9 (s, $PCy_3$); ratio 4:1. **MF-I** (4.65 g, 14.0 mmol, 2.8 equiv) was added, and the reaction was heated at 40 °C. After 2 h, the solution was dark green, and both transformation to **HII** and sequestration of $PCy_3$

were complete. The mixture was filtered through Celite, and the product was washed through with THF (3 x 3 mL). The combined filtrate was stripped of solvent to afford **HII** as a spectroscopically clean green solid (2.99 mg, 96%; Figure A.2). NMR values agree with those reported.[30] That for the benzylidene proton is provided here for convenience. $^{1}$H NMR ($C_6D_6$, 300 MHz): δ 16.71 (s, 1H, Ru=C*H*Ph).

**Resin-Assisted Synthesis of InII by Ligand Exchange.** Reaction adapted from the reported procedure for the IMes analogue.[50] Thus, solid **InI** (0.31 g, 0.33 mmol, 1 equiv) was added to a stirred solution of $H_2$IMes (0.12 g, 0.39 mmol, 1.2 equiv) in hexanes (40 mL), and the mixture was heated to 60 °C. After 2.5 h, the colour had changed from orange-brown to dark red, and a red-brown precipitate had deposited. No **InI** remained in the solution, but two unassigned $PCy_3$ derivatives were present; $^{31}P\{^{1}H\}$ NMR ($CDCl_3$, 300 MHz): 45.7 (s), – 4.6 (s); ratio 3:1; 3% of total integrated intensity. Evaporation of the solvent gave a dark red powder. This was re-suspended in THF (20 mL) to form a slurry, to which **MF-I** (0.47 g, 1.43 mmol, 4.3 equiv) was added. The mixture was stirred at RT for 1 h, then filtered (Celite). The product was washed through with THF (3 x 2 mL). No free $PCy_3$ remained in the filtrate, though traces of the byproducts remained (ca. 1% of total integration). These disappeared on adding further **MF-I** (0.59 g, 1.77 mmol, 5.4 equiv) and stirring for 40 min. The resin was separated as before. Evaporation of the filtrate gave 0.30 g **InII** as a spectroscopically clean red-brown solid (96%; Figure A.3). The $^{31}P\{^{1}H\}$ NMR chemical shift is in good agreement with that reported in $C_6D_6$.[65] $^{31}P\{^{1}H\}$ NMR ($CDCl_3$, 121 MHz): δ 26.9 (s, *P*$Cy_3$).

**Synthesis of $^{13}$C-Labelled $H_2$IMes•HBr.** In air. $^{13}$C-Paraformaldehyde (61 mg, 1.97 mmol, 1.3 equiv) was added to a solution of *N,N'*-dimesitylethane-1,2-diamine (434 mg, 1.46 mmol) in 10 mL methanol. Acetic acid (0.17 mL, 2.97 mmol; 2.0 equiv) in 2 mL methanol was added dropwise to the stirred reaction mixture. Stirring was continued for 10 h, after which the solvent was removed under vacuum to afford the cyclic product. This was dissolved in DME (6 mL) and treated with *N*-bromosuccinimide (305 mg, 1.71 mmol; 1.1 equiv). A white precipitate deposited over 40 h, which was filtered off and washed with cold DME (3x). Yield: 468 mg (82%). NMR chemical shifts are in reasonable agreement with values reported for the chloride salt in dmso-$d_6$,[61] with the addition of $^{13}$C splitting. $^{1}$H NMR ($CDCl_3$, 300 MHz, 298 K): δ 8.87 (d, $^{1}J_{HC}$ = 204 Hz, 1H, NC*H*N), 6.92 (s, 4H, Mes C*H*), 4.61 (s, 4H, C$H_2$), 2.37 (s, 12H, Mes *o*-$CH_3$), 2.26 (s, 6H, Mes *p*-$CH_3$). $^{13}C\{^{1}H\}$ NMR ($CDCl_3$, 75.5 Hz, 298 K): δ 159.0 (N*C*HN), 140.6 (Mes *C*), 135.0 (Mes *C*), 130.1 (Mes *C*H), 52.0 (*C*$H_2$), 21.0 (Mes *p*-*C*$H_3$), 18.1 (Mes *o*-*C*$H_3$).

**Synthesis of $^{13}$C-$H_2$IMes•$HBF_4$.** In air; variant on the method reported for the unsaturated salt.[18] The dibromide salt (0.460 g, 1.18 mmol) was stirred vigorously in 50 mL water to effect complete dissolution. After 20 min, a solution of $HBF_4$ (40% w/w in water; 0.80 mL, 4.37 mmol; 3.4 equiv) was added dropwise. The product precipitated as a white solid, which was filtered off, suspended in $Et_2O$, filtered again, and dried for two days to ensure complete removal of water

prior to liberating the free carbene. Yield: 0.420 g (90%). $^1$H NMR ($CDCl_3$, 300 mHz, 298 K): δ 7.90 (d, $^1J_{HC}$ = 205 Hz, 1H, NC*H*N), 6.96 (br s, 4H, Mes C*H*), 4.52 (s, 4H, C$H_2$), 2.34 (s, 12H, Mes *o*-$CH_3$, 2.29 (s, 6H, Mes *p*-$CH_3$). $^{13}$C{$^1$H} NMR ($CDCl_3$, 75.5 MHz, 298K): δ 158.6 (NCHN), 141.2 (Mes *C*), 134.9 (Mes *C*), 130.2 (Mes *C*), 51.9 (*C*$H_2$), 21.1 (Mes *p*-*C*$H_3$), 17.7 (Mes *o*-*C*$H_3$).

**Synthesis of Free $^{13}$C-$H_2$IMes.** In the glovebox, NaH (33 mg, 1.31 mmol; 3.3 equiv) was added to a suspension of $^{13}$C-labelled $H_2$IMes•$HBF_4$ (156 mg (0.425 mmol) in 15 mL THF. The reaction was stirred for 18 h before filtering through Celite. The filtrate was stripped to dryness. The residue was redissolved in benzene, filtered through Celite, and stripped of solvent to yield a tan solid. Yield: 88 mg (63%). NMR chemical shifts are consistent with reported[61] values, with the addition of the $^{13}$C splitting indicated. $^1$H NMR ($C_6D_6$, 300 MHz, 298 K): δ 6.82 (s, 4H, Mes C*H*), 3.26 (s, 4H, C$H_2$), 2.29 (s, 12H, Mes *o*-C$H_3$), 2.16 (s, 6H, Mes *p*-C$H_3$). $^{13}$C{$^1$H} NMR ($C_6D_6$, 75.5 MHz, 298 K): δ 243.5 (N*C*N), 139.2 (d, $^2J_{CC}$ = 9.7 Hz, Mes $C_i$), 135.8 (d, $^3J_{CC}$ = 1.3 Hz, Mes $C_i$), 129.4 (Mes *C*H), 50.3 (d, $^2J_{CC}$ = 75.6 Hz, C$H_2$), 20.5 (Mes *p*-*C*$H_3$), 17.7 (Mes *o*-*C*$H_3$).

**Resin-Assisted Synthesis of $^{13}$C-HII.** As for the synthesis of **HII** above, but by reaction of $^{13}$C-$H_2$IMes (8 mg, 0.013 mmol, 1.1 equiv) with **HI** (14 mg, 0.023 mmol, 1 equiv) in 2 mL THF, and workup with **MF-I** (25 mg, 0.075 mmol, 3 equiv). Yield: 14 mg, 93%. NMR chemical shifts agree with those above, barring additional splitting due to the $^{13}$C label.

**Resin-Assisted Synthesis of $d_{22}$-HII.** As for **HII**, using $d_{22}$-$H_2$IMes (11.5 mg, 0.035 mmol, 1.4 equiv) with **HI** (15.1 mg, 0.025 mmol, 1 equiv) in 3 mL THF, and treating with **MF-I** (25 mg, 0.075 mmol, 3 equiv). Yield of **$d_{22}$-HII**: 15 mg, 92%. NMR chemical shifts agree with the values above for non-labelled **HII**, barring the absence of those due to the mesityl rings.

**Control Experiments: Halide Exchange with MF-I.**

**Representative procedure.** A solution of **GII** (10 mg, 0.01 mmol, 1 equiv) and DMT (2.3 mg, 0.01 mmol, 1 equiv) in THF (1 mL) was stirred at RT for 5 min. $^1$H NMR analysis of an aliquot (stripped to dryness and suspended in $C_6D_6$) was used to establish the initial integration ratio of substrate to DMT. This material was evaporated, redissolved (THF) and returned to the reaction mixture. **MF-I** (16.0 mg, 0.04 mmol, 4 equiv) was added, and the reaction was stirred at RT for 8 h. Aliquots were taken every 2 h to assess loss of **GII** and formation of **GII(I)**. $^1$H NMR ($C_6D_6$, 300 MHz, at 8 h): δ 19.64 (s, 1H, Ru=C*H*Ph for **GII**, 99%), 19.43 (s, 1H, Ru=C*H*Ph for **GII(I)**, 1%). A similar procedure was used for **HII** and **InII**. For **InII**, which has no benzylidene proton, an isolated signal of the indenylidene ring protons was used (see Figure A.3a).

## 2.3. Subsequent Advances: Applications of the Merrifield Resin in Synthesis of Ruthenium Diiodide Metathesis Catalysts

Recent work focused on deployment of these resin-based methodologies as an aid to synthesis of Hoveyda-class diiodide catalysts bearing NHC and CAAC ligands. Such catalysts can improve mRCM productivity,[43,66] selectivity for metathesis of terminal vs internal olefins,[67] and robustness to the ethylene co-product in metathesis of terminal olefins.[68] Existing routes involving salt metathesis of second-generation catalysts with KI in methanol result in inefficient halide exchange.[42,43,69] They are procedurally cumbersome (requiring multiple workup stages), and commonly result in up to 5% partially-iodated products. The limited solubility of the ruthenium reagents in methanol is one obvious challenge,[70] but even less satisfactory results are reported in organic media (or on use of [$^n$Bu$_4$N]I instead of an alkali metal iodide).[42]

We originally conceived of the Merrifield-iodide resin as a means of effecting *both* halide exchange (building on an advance by Morris and co-workers)[41] and phosphine sequestration. Iodation was inefficient, however, and we therefore resorted to use of NaI in THF[52] for the salt metathesis step. The key advance, however, lay in use of the labile first-generation catalysts as precursors for halide exchange, with installation of the NHC or CAAC ligand in a subsequent step. This is important because, as suggested in earlier work by Nicholas Beach of this research group,[17b] salt metathesis proceeds most efficiently via a four-coordinate species resulting from dechelation of a $PCy_3$ or ether ligand.

Accordingly, Christian Blanco effected clean conversion to **HI($I_2$)** in 86% yield by stirring **GI** with NaI (4 equiv) in THF at RT, and then treating it with o-isopropoxy styrene and **MF-I** at 50 °C (Scheme 2.9). Transformation of **HI($I_2$)** into its second-generation derivative was achieved via a two-step procedure. To prevent attack by the nucleophilic carbene on the resin, **MF-I** was added as a phosphine scavenger only once ligand exchange was complete. This approach afforded **HII($I_2$)** in ca. 93% yield and excellent purity. The iodo-Grela catalyst **nG($I_2$)** was accessed by a related procedure. In this case, the styrenyl ether group was installed after the $H_2$IMes ligand, to prevent nucleophilic attack by the free carbene on the nitro functionality. Workup again relied on **MF-I** as a phosphine scavenger, affording **nG($I_2$)** in 77% net yield over the three reactions: that is, salt metathesis, NHC installation, and cross-metathesis.

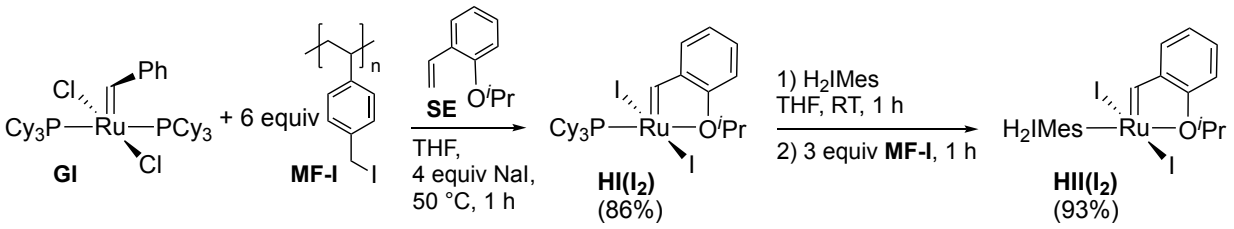


**Scheme 2.9. Synthesis of diiodide HI($I_2$) and HII($I_2$) catalysts using MF-I.**

*References for Chapter 2 begin on p. 40*

## 2.4. References


(1) Grela, K., *Olefin Metathesis-Theory and Practice*. Wiley: Hoboken, NJ, 2014.
(2) Grubbs, R. H.; Wenzel, A. G., *Handbook of Metathesis*. 2nd ed.; Wiley-VCH: Weinheim, 2015.
(3) Higman, C. S.; Lummiss, J. A. M.; Fogg, D. E., Olefin Metathesis at the Dawn of Uptake in Pharmaceutical and Specialty Chemicals Manufacturing. *Angew. Chem., Int. Ed.* **2016**, *55*, 3552–3565.
(4) Morvan, J.; Mauduit, M.; Bertrand, G.; Jazzar, R., Cyclic (Alkyl)(amino)carbenes (CAACs) in Ruthenium Olefin Metathesis. *ACS Catal.* **2021**, *11*, 1714–1748.
(5) Melaimi, M.; Jazzar, R.; Soleilhavoup, M.; Bertrand, G., Cyclic (Alkyl)(amino)carbenes (CAACs): Recent Developments. *Angew. Chem., Int. Ed.* **2017**, *56*, 10046–10068.
(6) Nascimento, D. L.; Gawin, A.; Gawin, R.; Guńka, P. A.; Zachara, J.; Skowerski, K.; Fogg, D. E., Integrating Activity with Accessibility in Olefin Metathesis: An Unprecedentedly Reactive Ruthenium-Indenylidene Catalyst Bearing a Cyclic Alkyl Amino Carbene. *J. Am. Chem. Soc.* **2019**, *141*, 10626–10631.
(7) Kajetanowicz, A.; Chwalba, M.; Gawin, A.; Tracz, A.; Grela, K., Non-Glovebox Ethenolysis of Ethyl Oleate and FAME at Larger Scale Utilizing a Cyclic (Alkyl)(Amino)Carbene Ruthenium Catalyst. *Eur. J. Lipid Sci. Technol.* **2019**, 1900263.
(8) Gawin, R.; Tracz, A.; Chwalba, M.; Kozakiewicz, A.; Trzaskowski, B.; Skowerski, K., Cyclic Alkyl Amino Ruthenium Complexes—Efficient Catalysts for Macrocyclization and Acrylonitrile Cross Metathesis. *ACS Catal.* **2017**, *7*, 5443–5449.
(9) Gawin, R.; Kozakiewicz, A.; Guńka, P. A.; Dąbrowski, P.; Skowerski, K., Bis(Cyclic Alkyl Amino Carbene) Ruthenium Complexes: A Versatile, Highly Efficient Tool for Olefin Metathesis. *Angew. Chem., Int. Ed.* **2017**, *56*, 981–986.
(10) Zhang, J.; Song, S.; Wang, X.; Jiao, J.; Shi, M., Ruthenium-Catalyzed Olefin Metathesis Accelerated by the Steric Effect of the Backbone Substituent in Cyclic (Alkyl)(Amino) Carbenes. *Chem. Commun.* **2013**, *49*, 9491–9493.
(11) Hans, M.; Lorkowski, J.; Demonceau, A.; Delaude, L., Efficient Synthetic Protocols for the Preparation of Common N-Heterocyclic Carbene Precursors. *Beilstein J. Org. Chem.* **2015**, *11*, 2318–2325.
(12) Scholl, M.; Ding, S.; Lee, C. W.; Grubbs, R. H., Synthesis and Activity of a New Generation of Ruthenium-Based Olefin Metathesis Catalysts Coordinated with 1,3-Dimesityl-4,5-dihydroimidazol-2-ylidene Ligands. *Org. Lett.* **1999**, *1*, 953–956.
(13) Trnka, T. M.; Morgan, J. P.; Sanford, M. S.; Wilhelm, T. E.; Scholl, M.; Choi, T.-L.; Ding, S.; Day, M. W.; Grubbs, R. H., Synthesis and Activity of Ruthenium Alkylidene Complexes Coordinated with Phosphine and N-Heterocyclic Carbene Ligands. *J. Am. Chem. Soc.* **2003**, *125*, 2546–2558.
(14) Fürstner, A.; Ackermann, L.; Gabor, B.; Goddard, R.; Lehmann, C. W.; Mynott, R.; Stelzer, F.; Thiel, O. R., Comparative Investigation of Ruthenium-Based Metathesis Catalysts Bearing N-Heterocyclic Carbene (NHC) Ligands. *Chem. – Eur. J.* **2001**, *7*, 3236–3253.
(15) Sanford, M. S.; Henling, L. M.; Day, M. W.; Grubbs, R. H., Ruthenium-Based Four-Coordinate Olefin Metathesis Catalysts. *Angew. Chem., Int. Ed.* **2000**, *39*, 3451–3453.
(16) van Lierop, B. J.; Lummiss, J. A. M.; Fogg, D. E., Ring-Closing Metathesis. In *Olefin Metathesis-Theory and Practice*, Grela, K., Ed. Wiley: Hoboken, NJ, 2014; pp 85–152.
(17) Decomposition of **GII** into hydride species by direct reaction with methanol is unlikely on short exposure at RT. See: (a) Beach, N. J.; Camm, K. D.; Fogg, D. E., Hydrogenolysis versus Methanolysis of First- and Second-Generation Grubbs Catalysts: Rates, Speciation, and Implications for Tandem Catalysis. *Organometallics* **2010**, *29*, 5450–5455. A more likely culprit is methoxide formed in situ on use of methanol to extract unreacted base. For reactions of **GII** with methoxide, see (b) Beach, N. J.; Lummiss, J. A. M.; Bates, J. M.; Fogg, D. E., Reactions of Grubbs Catalysts with Excess Methoxide: Formation of Novel Methoxyhydride Complexes. *Organometallics* **2012**, *31*, 2349–2356. (c) Dinger, M. B.; Mol, J. C., Degradation of the Second-

Generation Grubbs Metathesis Catalyst with Primary Alcohols and Oxygen. *Eur. J. Inorg. Chem.* **2003**, 2827–2833.
(18) Bantreil, X.; Nolan, S. P., Synthesis of N-heterocyclic Carbene Ligands and Derived Ruthenium Olefin Metathesis Catalysts. *Nature Protoc.* **2011**, *6*, 69–77.
(19) Jafarpour, L.; Hillier, A. C.; Nolan, S. P., Ru-NHC Improved One-Pot Synthesis of Second-Generation Ruthenium Olefin Metathesis Catalysts. *Organometallics* **2002**, *21*, 442–444.
(20) Bieniek, M.; Michrowska, A.; Gulajski, L.; Grela, K., A Practical Larger Scale Preparation of Second-Generation Hoveyda-Type Catalysts. *Organometallics* **2007**, *26*, 1096–1099.
(21) van Lierop, B. J.; Reckling, A. M.; Lummiss, J. A. M.; Fogg, D. E., High-Yield, High-Purity Routes to Second-Generation Ru Metathesis Catalysts from Commercially Available Precursors. *ChemCatChem* **2012**, *4*, 2020–2025.
(22) Sauvage, X.; Demonceau, A.; Delaude, L., Imidazol(in)ium-2-carboxylates as N-Heterocyclic Carbene Precursors for the Synthesis of Second Generation Ruthenium Metathesis Catalysts. *Adv. Synth. Catal.* **2009**, *351*, 2031–2038.
(23) A bicarbonate adduct also holds promise. See: (a) Fèvre, M.; Pinaud, J.; Leteneur, A.; Gnanou, Y.; Vignolle, J.; Taton, D.; Miqueu, K.; Sotiropoulos, J.-M., Imidazol(in)ium Hydrogen Carbonates as a Genuine Source of N-Heterocyclic Carbenes (NHCs): Applications to the Facile Preparation of NHC Metal Complexes and to NHC-Organocatalyzed Molecular and Macromolecular Syntheses. *J. Am. Chem. Soc.* **2012**, *134*, 6776–6784. However, a recent report suggests the $CO_2$ adducts may be more efficient as sources of the free NHC. See: (b) Fevre, M.; Coupillaud, P.; Miqueu, K.; Sotiropoulos, J.-M.; Vignolle, J.; Taton, D., Imidazolium Hydrogen Carbonates versus Imidazolium Carboxylates as Organic Precatalysts for N-Heterocyclic Carbene Catalyzed Reactions. *J. Org. Chem.* **2012**, *77*, 10135–10144.
(24) Wang, Z. J.; Jackson, W. R.; Robinson, A. J., A Simple and Practical Preparation of an Efficient Water Soluble Olefin Metathesis Catalyst. *Green Chem.* **2015**, *17*, 3407–3414.
(25) Huang, J.; Stevens, E. D.; Nolan, S. P.; Petersen, J. L., Olefin Metathesis-Active Ruthenium Complexes Bearing a Nucleophilic Carbene Ligand. *J. Am. Chem. Soc.* **1999**, *121*, 2674–2678.
(26) Use of the free NHC offers a clean, straightforward alternative, providing care is taken to use dry solvents. The free NHCs are readily hydrolyzed by water, although they are stable to oxygen. See ref 21 and: Denk, M. K.; Rodezno, J. M.; Gupta, S.; Lough, A. J., Synthesis and reactivity of subvalent compounds Part 11. Oxidation, Hydrogenation and Hydrolysis of Stable Diamino Carbenes. *J. Organomet. Chem.* **2001**, *617-618*, 242–253.
(27) Process for preparation of ruthenium-based carbene catalysts with chelating alkylidene ligands Umicore AG & Co. KG, Germany; Ghent University. 2011-Eur. Pat. 300 2011091980; WO 2011/091980 Al; PCT/EP2011/000300. Monsaert, S. F.; Verpoort, F. W. C. Process for preparation of ruthenium-based carbene catalysts with chelating alkylidene ligands. WO Patent App. WO 2011/091980 Al; CA+ 383210.
(28) Engle, K. M.; Lu, G.; Luo, S.-X.; Henling, L. M.; Takase, M. K.; Liu, P.; Houk, K. N.; Grubbs, R. H., Origins of Initiation Rate Differences in Ruthenium Olefin Metathesis Catalysts Containing Chelating Benzylidenes. *J. Am. Chem. Soc.* **2015**, *137*, 5782−5792.
(29) Kos, P.; Savka, R.; Plenio, H., Fast Olefin Metathesis: Synthesis of 2-Aryloxy-Substituted Hoveyda-Type Complexes and Application in Ring-Closing Metathesis. *Adv. Synth. Catal.* **2013**, *355*, 439 – 447.
(30) Garber, S. B.; Kingsbury, J. S.; Gray, B. L.; Hoveyda, A. H., Efficient and Recyclable Monomeric and Dendritic Ru-Based Metathesis Catalysts. *J. Am. Chem. Soc.* **2000**, *122*, 8168–8179.
(31) Blum, A. P.; Ritter, T.; Grubbs, R. H., Synthesis of N-Heterocylic Carbene-Containing Metal Complexes from 2-(Pentafluorophenyl)imidazolidines. *Organometallics* **2007**, *26*, 2122–2124.
(32) Bujok, R.; Bieniek, M.; Masnyk, M.; Michrowska, A.; Sarosiek, A.; Stepowska, H.; Arlt, D.; Grela, K., Ortho- and Para-Substituted Hoveyda-Grubbs Carbenes. An Improved Synthesis of Highly Efficient Metathesis Initiators. *J. Org. Chem.* **2004**, *69*, 6894–6896.

(33) (a) Shimkin, K. W.; Watson, D. A., Recent Developments in Copper-Catalyzed Radical Alkylations of Electron-Rich π-Systems. *Beilstein J. Org. Chem.* **2015**, *11*, 2278–2288; see also other papers in this Thematic Series on copper catalysis in organic synthesis. (b) Allen, S. E.; Walvoord, R. R.; Padilla-Salinas, R.; Kozlowski, M. C., Aerobic Copper-Catalyzed Organic Reactions. *Chem. Rev.* **2013**, *113*, 6234–6458. (c) Monnier, F.; Taillefer, M., Catalytic C-C, C-N, and C-O Ullmann-Type Coupling Reactions. *Angew. Chem., Int. Ed.* **2009**, *48*, 6954–6971. (d) Reymond, S.; Cossy, J., Copper-Catalyzed Diels−Alder Reactions. *Chem. Rev.* **2008**, *108*, 5359–5406. (e) For an illuminating overview of developments in copper-mediated synthesis, see: van Koten, G., Organocopper Compounds: From Elusive to Isolable Species. *Organometallics* **2012**, *31*, 7634–7646.

(34) Buchwald, S. L.; Bolm, C., On the Role of Metal Contaminants in Catalyses with $FeCl_3$. *Angew. Chem. Int. Ed.* **2009**, *48*, 5586 – 5587.

(35) Stanbury, D. M., Recent Advances in Electron-Transfer Reactions. In *Adv. Inorg. Chem.*, van Eldik, R., Ed. Elsevier: Amsterdam, 2003; Vol. 54, pp 351–393.

(36) Ahuja, S.; Alsante, K. M., *Handbook of Isolation and Characterization of Impurities in Pharmaceuticals*. Elsevier2003.

(37) A p$K_a$ of –2.8 is reported for *p*-toluene sulfonic acid in water. See: Guthrie, J. P., *Can. J. Chem.* **1978**, *56*, 2342–2354.

(38) Sabatino, G.; Papini, A. M., Advances in Automatic, Manual and Microwave-Assisted Solid-Phase Peptide Synthesis. *Curr. Opin. Drug Discov. Devel.* **2008**, *11*, 762–770.

(39) Vaino, A. R.; Janda, K. D., Solid-Phase Organic Synthesis: A Critical Understanding of the Resin *J. Comb. Chem.* **2000**, *2*, 579–596.

(40) Lipshutz, B. H.; Blomgren, P. A., Efficient Scavenging of $Ph_3P$ and $Ph_3P$=O with High-Loading Merrifield Resin. *Org. Lett.* **2001**, *3*, 1869–1871.

(41) Zhao, X.; Ivanova, N.; Hadzovic, A.; Zimmer-De Iuliis, M.; Lough, A. J.; Morris, R. H., Use of an Iodide-Modified Merrifield Resin in the Synthesis of Ruthenium Hydride Complexes. The Structure of RuHI((R)-binap)($PPh_3$). *Organometallics* **2008**, *27*, 503–508.

(42) Pump, E.; Fischer, R. C.; Slugovc, C., Halide Exchange in Second-Generation cis-Dihalo Ruthenium Benzylidene Complexes. *Organometallics* **2012**, *31*, 6972−6979.

(43) Tracz, A.; Matczak, M.; Urbaniak, K.; Skowerski, K., Nitro-Grela-Type Complexes Containing Iodides – Robust and Selective Catalysts for Olefin Metathesis Under Challenging Conditions. *Beilstein J. Org. Chem.* **2015**, *11*, 1823–1832.

(44) Arduengo, A. J.; Davidson, F.; Dias, H. V. R.; Goerlich, J. R.; Khasnis, D.; Marshall, W. J.; Prakasha, T. K., An Air Stable Carbene and Mixed Carbene “Dimers". *J. Am. Chem. Soc.* **1997**, *119*, 12742–12749.

(45) Birr, C., *Aspects of the Merrifield Peptide Synthesis*. Springer-Verlag: New York, 1978.

(46) Kates, S. F.; Albericio, F., *Solid-Phase Synthesis, A Practical Guide*. Marcel Dekker: New York, 2000.

(47) Gessler, S.; Randl, S.; Blechert, S., Synthesis and Metathesis Reactions of a Phosphine-Free Dihydroimidazole Carbene Ruthenium Complex. *Tetrahedron Lett.* **2000**, *41*, 9973–9976.

(48) Lummiss, J. A. M.; Higman, C. S.; Fyson, D. L.; McDonald, R.; Fogg, D. E., The Divergent Effects of Strong NHC Donation in Catalysis. *Chem. Sci.* **2015**, *6*, 6739–6746.

(49) Lability is significantly reduced for the $PCy_3$ ligand, vs $PPh_3$, for both alkylidene and hydridocarbonyl complexes. For closely comparable Ru systems, see: (a) Dharmasena, U. L.; Foucault, H. M.; dos Santos, E. N.; Fogg, D. E.; Nolan, S. P., N-Heterocyclic Carbenes as Activating Ligands for Hydrogenation and Isomerization of Unactivated Olefins. *Organometallics* **2005**, *24*, 1056–1058. (b) Conrad, J. C.; Yap, G. P. A.; Fogg, D. E., Concise Route to Highly Reactive Ruthenium Metathesis Catalysts Containing a Labile Donor and an N-Heterocyclic Carbene (NHC) Ligand. *Organometallics* **2003**, *22*, 1986–1988. For an excellent computational analysis of metal-phosphorus bonding and backbonding, see: (c) Fey, N.; Orpen, A. G.; Harvey, J. N., Building ligand knowledge bases for organometallic chemistry: Computational Description Of

Phosphorus(III)-Donor Ligands and the Metal–Phosphorus Bond. *Coord. Chem. Rev.* **2009**, *253*, 704–722.
(50) Jafarpour, L.; Schanz, H.-J.; Stevens, E. D.; Nolan, S. P., Indenylidene-Imidazolylidene Complexes of Ruthenium as Ring-Closing Metathesis Catalysts. *Organometallics* **1999**, *18*, 5416–5419.
(51) Monfette, S.; Camm, K. D.; Gorelsky, S. I.; Fogg, D. E., Electronic Effects of the Anionic Ligand in Ruthenium-Catalyzed Olefin Metathesis. *Organometallics* **2009**, *28*, 944–946.
(52) Sanford, M. S.; Love, J. A.; Grubbs, R. H., Mechanism and Activity of Ruthenium Olefin Metathesis Catalysts. *J. Am. Chem. Soc.* **2001**, *123*, 6543–6554.
(53) Leitao, E. M.; Dubberley, S. R.; Piers, W. E.; Wu, Q.; McDonald, R., Thermal Decomposition Modes for Four-Coordinate Ruthenium Phosphonium Alkylidene Olefin Metathesis Catalysts. *Chem. – Eur. J.* **2008**, *14*, 11565–11572.
(54) (a) Emsermann, J.; Arduengo, A. J., III; Opatz, T., Synthesis of Highly Substituted 2-$^{13}$C-Imidazolium Salts and Metal NHC Complexes for the Investigation of Electronic Unsymmetry by NMR. *Synthesis* **2013**, *45*, 2251–2264. (b) Praetorius, J. M.; Crudden, C. M., N-Heterocyclic Carbene Complexes Of Rhodium: Structure, Stability And Reactivity. *Dalton Trans.* **2008**, 4079–4094. (c) Pucino, M.; Mougel, V.; Schowner, R.; Fedorov, A.; Buchmeiser, M. R.; Copéret, C., Cationic Silica-Supported N-Heterocyclic Carbene Tungsten Oxo Alkylidene Sites: Highly Active and Stable Catalysts for Olefin Metathesis. *Angew. Chem., Int. Ed.* **2016**, *55*, 4300–4302. (d) Su, H.-L.; Perez, L. M.; Lee, S.-J.; Reibenspies, J. H.; Bazzi, H. S.; Bergbreiter, D. E., Studies of Ligand Exchange in N-Heterocyclic Carbene Silver(I) Complexes. *Organometallics* **2012**, *31*, 4063–4071. (e) Ramnial, T.; Abernethy, C. D.; Spicer, M. D.; McKenzie, I. D.; Gay, I. D.; Clyburne, J. A. C., A Monomeric Imidazol-2-ylidene-Silver(I) Chloride Complex: Synthesis, Structure, and Solid State $^{109}$Ag and $^{13}$C CP/MAS NMR Characterization. *Inorg. Chem.* **2003**, *42*, 1391–1393.
(55) Marciniec, B.; Rogalski, S.; Potrzebowski, M. J.; Pietraszuk, C., Ruthenium Carbene Siloxide Complexes Immobilized on Silica: Synthesis and Catalytic Activity in Olefin Metathesis. *ChemCatChem* **2011**, *3*, 904–910.
(56) Bates, J. M.; Lummiss, J. A. M.; Bailey, G. A.; Fogg, D. E., Operation of the Boomerang Mechanism in Olefin Metathesis Reactions Promoted by the Second-Generation Hoveyda Catalyst. *ACS Catal.* **2014**, *4*, 2387−2394.
(57) Lummiss, J. A. M.; Botti, A. G. G.; Fogg, D. E., Isotopic Probes for Ruthenium-Catalyzed Olefin Metathesis. *Catal. Sci. Technol.* **2014**, *4*, 4210–4218.
(58) Jimenez, L. R.; Tolentino, D. R.; Gallon, B. J.; Schrodi, Y., Development of a Method for the Preparation of Ruthenium Indenylidene-Ether Olefin Metathesis Catalysts. *Molecules* **2012**, *17*, 5675–5689.
(59) Romero, P. E.; Piers, W. E., Mechanistic Studies on 14-Electron Ruthenacyclobutanes: Degenerate Exchange with Free Ethylene. *J. Am. Chem. Soc.* **2007**, *129*, 1698–1704.
(60) Romero, P. E.; Piers, W. E., Direct Observation of a 14-Electron Ruthenacyclobutane Relevant to Olefin Metathesis. *J. Am. Chem. Soc.* **2005**, *127*, 5032–5033.
(61) Arduengo, A. J.; Krafczyk, R.; Schmutzler, R.; Craig, H. A.; Goerlich, J. R.; Marshall, W. J.; Unverzagt, M., Imidazolylidenes, Imidazolinylidenes and Imidazolidines. *Tetrahedron* **1999**, *55*, 14523–14534.
(62) Schwab, P.; Grubbs, R. H.; Ziller, J. W., Synthesis and Applications of $RuCl_2(=CHR')(PR_3)_2$: The Influence of the Alkylidene Moiety on Metathesis Activity. *J. Am. Chem. Soc.* **1996**, *118*, 100–110.
(63) Wanzlick, H.-W.; Lachmann, B.; Schikora, E., Chemie nucleophiler Carbene, VIII: Zur Bildung und Reaktivitat des Bis-[ l.3diphenyl-imidazolidinylide]. *Chem. Ber.* **1965**, 3170–3177.
(64) Arduengo, A. J.; Harlow, R. L.; Kline, M., A Stable Crystalline Carbene. *J. Am. Chem. Soc.* **1991**, *113*, 361–363.
(65) Monsaert, S.; Drozdzak, R.; Dragutan, V.; Dragutan, I.; Verpoort, F., Indenylidene-Ruthenium Complexes Bearing Saturated N-Heterocyclic Carbenes: Synthesis and Catalytic Investigation in Olefin Metathesis Reactions. *Eur. J. Inorg. Chem.* **2008**, 432–440.

(66) Blanco, C.; Sims, J.; Nascimento, D. L.; Goudreault, A. Y.; Steinmann, S. N.; Michel, C.; Fogg, D. E., The Impact of Water on Ru-Catalyzed Olefin Metathesis: Potent Deactivating Effects Even at Low Water Concentrations. *ACS Catal.* **2021**, *11*, 893−899.
(67) Nechmad, N. B.; Phatake, R.; Ivry, E.; Poater, A.; Lemcoff, N. G., Unprecedented Selectivity of Ruthenium Iodide Benzylidenes in Olefin Metathesis Reactions. *Angew. Chem., Int. Ed.* **2020**, *59*, 3539–3543.
(68) For a recent overview of the impact of ethylene, see: (a) Hoveyda, A. H.; Liu, Z.; Qin, C.; Koengeter, T.; Mu, Y., Impact of Ethylene on Efficiency and Stereocontrol in Olefin Metathesis: When to Add It, When to Remove It, and When to Avoid It. *Angew. Chem., Int. Ed.* **2020**, *59*, 22324−22348. The detrimental effect in ring-closing macrocyclization is particularly severe. See: (b) Monfette, S.; Eyholzer, M.; Roberge, D. M.; Fogg, D. E., Getting RCM Off the Bench: Reaction-Reactor Matching Transforms Metathesis Efficiency in the Assembly of Large Rings. *Chem. – Eur. J.* **2010**, *16*, 11720–11725. For early reports of problems, see: (c) Burdett, K. A.; Harris, L. D.; Margl, P.; Maughon, B. R.; Mokhtar-Zadeh, T.; Saucier, P. C.; Wasserman, E. P., Renewable Monomer Feedstocks via Olefin Metathesis: Fundamental Mechanistic Studies of Methyl Oleate Ethenolysis with the First-Generation Grubbs Catalyst. *Organometallics* **2004**, *23*, 2027–2047.
(69) Wappel, J.; Urbina-Blanco, C. A.; Abbas, M.; Albering, J. H.; Saf, R.; Nolan, S. P.; Slugovc, C., Halide Exchanged Hoveyda-Type Complexes in Olefin Metathesis. *Beilstein J. Org. Chem.* **2010**, *6*, 1091–1098.
(70) Other potential challenges arise from decomposition of Ru metathesis catalysts by methanol when base is present. For a review in the context of biomaterials applications, see: (a) Camm, K. D.; Fogg, D. E., From Drug Cocktails to Tissue Engineering: Synthesis of ROMP Polymers for Biological Applications. In *NATO Sci. Ser. II*, Imamoglu, Y.; Dragutan, V., Eds. Springer Verlag: Berlin, 2007; Vol. 243, pp 285–303). Importantly, however, direct reaction with methanol in the absence of base is rather slow at RT, although both **GI** and **GII** are rapidly decomposed by *methoxide* at RT. See ref 17 and: (b) Dinger, M. B.; Mol, J. C., Degradation of the First-Generation Grubbs Metathesis Catalyst with Primary Alcohols, Water, and Oxygen. Formation and Catalytic Activity of Ruthenium(II) Monocarbonyl Species. *Organometallics* **2003**, *22*, 1089–1095.

# Chapter 3. Decomposition of the Active Species in Ruthenium-Catalyzed Olefin Metathesis

## 3.1. Context and Overview of Content

At the outset of this thesis work, the breakthrough productivity attainable with the CAAC catalysts was a new discovery, and its basis was unknown. Armed with a clear picture of the major decomposition pathways (Chapter 1), and with pristine catalysts synthesized in-house (as described in Chapter 2), we set out to clarify the properties underlying this remarkable behaviour. The importance of pristine catalyst lies in the fact that this excludes the possibility of decomposition by adventitious poisons. We were thus able to focus on the decomposition pathways inherent to the active species: that is, β-hydride elimination from the metallacyclobutane, and bimolecular coupling of the methylidene. This work drew on experimental methodologies pioneered by Gwen Bailey in her doctoral studies in the Fogg group, which enabled direct examination of the active species.

The initial question (see Paper 1; Section 3.2) was whether one or both of these pathways was inhibited for the CAAC catalysts. On confirming that β-hydride elimination is prevented, but that the susceptibility to bimolecular decomposition is in fact heightened, the second question was why. The answer turns out to be very simple. The critical feature is the high trans influence associated with the CAAC ligands, which form stronger metal-ligand bonds than the NHCs. This property promotes bimolecular decomposition, as outlined in Paper 2 (Section 3.3). It also explains the resistance of the CAAC catalysts to β-hydride elimination. The latter point is covered briefly under the heading “Subsequent Advances to Section 3.3”, as it is the subject of a manuscript now in preparation.

A final question was whether the CAAC catalysts differ significantly from their NHC predecessors in terms of their robustness to nucleophiles and Brønsted base, two of the major “induced decomposition” pathways discussed in Chapter 1. In Paper 3 (Section 3.4), they are shown to be significantly more robust.

These contributions are listed in Section 3.1.1 below, following which each paper is presented in its published form.

*References for Chapter 3 begin on p. 92*

### 3.1.1. Published Contributions

(1) Origin of the Breakthrough Productivity of Ruthenium-CAAC Catalysts in Olefin Metathesis (CAAC = Cyclic Alkyl Amino Carbene). D.L. Nascimento, D.E. Fogg.* *J. Am. Chem. Soc.* **2019**, *141*, 19236-19240. (Communication). Copyright 2019 American Chemical Society. Reprinted with permission.

*Abstract:* Examined herein is the basis for the outstanding metathesis productivity of leading CAAC catalysts relative to their important N-heterocyclic carbene (NHC) predecessors, as recently demonstrated in the topical contexts of metathesis macrocyclization and the ethenolysis of renewable oils. The difference is traced to the stability to decomposition of the metallacyclobutane (MCB) intermediate. The CAAC catalysts are shown to undergo little to no β–H elimination of the MCB ring, a pathway to which the $H_2$IMes catalyst are highly susceptible. Unexpectedly, however, the CAAC catalysts are found to be *more* susceptible to bimolecular coupling of the key intermediate $RuCl_2(CAAC)(=CH_2)$, a reaction that culminates in elimination of the methylidene ligand as ethylene. Thus, an NMR study of transiently-stabilized $RuCl_2(L)(py)(=CH_2)$ complexes (L = CAAC or $H_2$IMes) revealed bimolecular decomposition of the CAAC derivative within 5 min at RT, as compared to a timescale of hours for the $H_2$IMes analogue. The remarkable productivity of the CAAC catalysts is thus due to their resistance to β-elimination, which enables their use at ppm loadings, and to the retarding effect of these low catalyst concentrations on bimolecular decomposition.

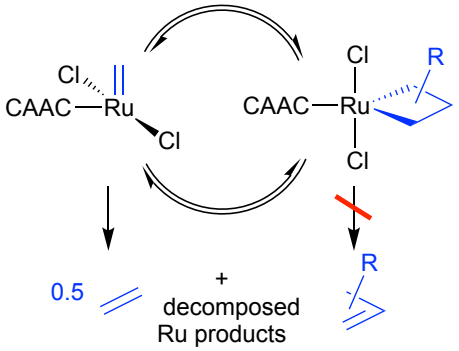


(2) Bimolecular Coupling in Olefin Metathesis: Correlating Structure and Decomposition for Leading and Emerging Ruthenium-Carbene Catalysts. D. L. Nascimento, M. Foscato, G. Occhipinti, V. R. Jensen,* D. E. Fogg.* *J. Am. Chem. Soc.* **2021**, accepted. (Communication). Copyright 2021 American Chemical Society. Reprinted with permission.

*Abstract:* Bimolecular decomposition has long been recognized as a fundamental challenge in olefin metathesis. Emerging ruthenium–cyclic(alkyl)(amino)carbene (CAAC) catalysts, which enable breakthrough advances in productivity and general robustness, are now known to be extraordinarily susceptible to this pathway. The details of the process have hitherto been obscure. The present study provides the first detailed mechanistic insights into the steric and electronic factors that govern bimolecular decomposition. In a combined experimental and theoretical study, we examine decomposition of the key active species, $RuCl_2(L)(py)(=CH_2)$ **mBpy** (in which L is the

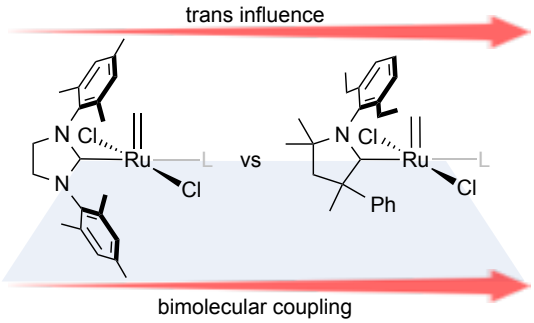

N-heterocyclic carbene (NHC) $H_2$IMes, or a CAAC ligand: the latter vary in the NAr group (NMes, N-2,6-$Et_2C_6H_3$, or N-2-Me,6-$^iPrC_6H_3$) and the substituents on the quaternary site flanking the carbene carbon (i.e., $CMe_2$ or CMePh)). The transiently-stabilized pyridine adducts **mBpy** were isolated by cryogenic generation of the metallacyclobutanes, addition of pyridine, and precipitation. All are shown to decompose via second-order kinetics at –10 °C. The most vulnerable CAAC species decompose more than a thousand-fold faster than the $H_2$IMes analogue. Computational studies reveal that the key factor underlying accelerated decomposition of the CAAC derivatives is their stronger trans influence, which increases the transient concentration of the 14-electron methylidene species, $RuCl_2(L)(=CH_2)$ **B**. Fast catalyst initiation, a major design goal in olefin metathesis, thus has the negative consequence of accelerating decomposition. Inhibiting bimolecular decomposition offers major opportunities to transform catalyst productivity and utility, and to realize the outstanding promise of olefin metathesis.

(3) Challenging Metathesis Catalysts with Nucleophiles and Brønsted Base: The Stability of State-of-the-Art Catalysts to Attack by Amines. D. L. Nascimento, I. Reim, M. Foscato, V. R. Jensen,* D. E. Fogg* *ACS Catal.* **2020**, 10, 19, 11623-11633. (Full paper). Copyright 2020 American Chemical Society. Reprinted with permission.

*Abstract*: Critical to advancing the uptake of olefin metathesis in leading contexts, including pharmaceutical manufacturing, is identification of highly active catalysts that resist decomposition. Amines constitute an aggressive challenge to ruthenium metathesis catalysts. Examined here is the impact of DBU (1,8-diazabicyclo[5.4.0]undec-7-ene), morpholine, *n*-butylamine, and triethylamine on Ru metathesis catalysts that represent the current state of the art, including cyclic alkyl amino carbene (CAAC) and N-heterocyclic carbene (NHC) complexes. Accordingly, the amine-tolerance of the nitro-Grela catalyst $RuCl_2(H_2IMes)(=CHAr)$ (**nG**; Ar = $C_6H_4$-2-O$^i$Pr-5-$NO_2$) is compared with that of its CAAC analogues **nGC1$^{Ph}$** and **nGC2$^{Me}$**, and the Hoveyda-class $RuCl_2$(**C2$^{Me}$**)(=CHAr') **HC2$^{Me}$** (Ar' = $C_6H_4$-2-O$^i$Pr). In **C1$^{Ph}$**, the carbene carbon is flanked by an N-2,6-$Et_2C_6H_3$ group and a CMePh quaternary carbon; in **C2$^{Me}$**, by an N-2-iPr-6-$MeC_6H_3$ group and a $CMe_2$ quaternary carbon. The impact of 1 equiv amine per Ru on turnover numbers (TON) in ring-closing metathesis of diethyl diallylmalonate was assessed at 9 ppm Ru, at RT and 70 °C. The deleterious impact of amines followed the trend $NEt_3$ ~$NH_2{}^nBu$<<DBU~morpholine. Morpholine is shown to decompose **nGC1$^{Ph}$** by nucleophilic abstraction of the methylidene ligand; DBU, by proton abstraction from the metallacyclobutane. Decomposition was minimized at 70 °C, at which **nGC1$^{Ph}$** enabled TONs of ca. 60,000 even in the presence of morpholine or DBU, vs ca. 80,000 in the absence of base. Unexpectedly, $H_2$IMes catalyst **nG** delivered 70-90% of the performance of **nGC1$^{Ph}$** at high temperatures, and underwent decomposition by Brønsted base at a similar rate. Density functional theory (DFT) analysis shows that this similarity is due

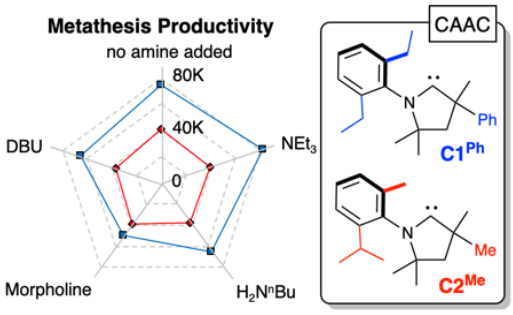

to comparable net electron-donation by the $H_2$IMes and **C1$^{Ph}$** ligands. Catalysts bearing the smaller **C2$^{Me}$** ligand were comparatively insensitive to amines, owing to rapid, preferential bimolecular decomposition.

(4) Exploring the Metathesis Productivity of Olefin Metathesis Catalysts: A High Trans-Influence Carbene Prevents Decomposition via β-Hydride Elimination. G. Occhipinti, M. Foscato, D. L. Nascimento, D. E. Fogg, V. R. Jensen.* *Manuscript in preparation*.

*Abstract*: Ruthenium–cyclic alkyl amino carbene (CAAC) catalysts can deliver dramatically higher productivities in olefin metathesis than their important N-heterocyclic carbene (NHC) predecessors. A key reason is the reduced susceptibility of the key metallacyclobutane intermediate to decomposition via β-elimination. The factors responsible for this greater robustness are unknown. To uncover them, we compared the metathesis of styrene and ethylene, vs β-H elimination, for Grela-type catalysts bearing an NHC ($H_2$IMes) or a CAAC ligand (**C1$^{Ph}$** or **C2$^{Me}$**). In the CAAC ligand **C1$^{Ph}$**, the carbene carbon is flanked by an N(2,6-diethylphenyl) group and a quaternary CMePh; in **C2$^{Me}$**, by an N(2-isopropyl-6-methylphenyl) group and a quaternary $CMe_2$. Density functional theory (DFT) calculations show that because the β-C-H bond of the metallacyclobutane (MCB) occupies a site trans to the CAAC or NHC, the susceptibility to β-hydride elimination is determined largely by the trans influence of this carbene. The stronger trans influence of **C1$^{Ph}$** and **C2$^{Me}$**, vs $H_2$IMes, is manifested in higher barriers to β-H elimination, accounting for the reduced susceptibility of the CAAC catalysts to this decomposition reaction. The carbene trans influence also influences the selectivity for metathesis of styrene (a representative 1-olefin), over unproductive cycling with ethylene. Whereas the transition-state geometry for styrene metathesis has significant MCB character, the transition state for ethylene metathesis has greater π-complex character. In the latter TS, bound ethylene is positioned largely trans to the carbene ligand: for the CAAC catalysts, the transition state for ethylene metathesis is thus destabilized relative to that for styrene metathesis, increasing selectivity for *productive* metathesis. The calculations predict that these effects are greater for **C1$^{Ph}$** than **C2$^{Me}$**. Replacing one quaternary methyl with a phenyl group increases the steric bulk and the trans-influence of the CAAC, and thus the barrier to ethylene self-metathesis and to β-H elimination. This substitution also reduces electrostatic repulsion between the quaternary alkyl moiety and the α-methylene of the MCB, stabilizing this intermediate as well as the transition state for styrene self-metathesis. Overall, the replacement of a methyl with a phenyl group increases selectivity for productive metathesis and retards decomposition via β-H elimination, leading to a more efficient and productive catalyst.

*Author Contributions:* In all cases but Contribution (4), the manuscripts were written by DN and DEF, with computational contributions by VRJ in (2) and (3). Manuscript (4) was written by GO, DEF, and VRJ. All experimental work, including that in (4), was designed by DN and DEF, and conducted by DN.

*References for Chapter 3 begin on p. 92*

## 3.2. Origin of the Breakthrough Productivity of Ruthenium-CAAC Catalysts in Olefin Metathesis

### 3.2.1. Introduction

Ruthenium-catalyzed olefin metathesis, widely embraced as a core methodology in organic synthesis,[1,2] is now beginning to see uptake in pharmaceutical manufacturing.[3] The demands of process chemistry are bringing new recognition to long-standing challenges of catalyst productivity.[4] While steps can be taken to circumvent decomposition induced by extraneous contaminants,[3,5] *intrinsic* decomposition is a more fundamental problem.

Two such pathways have been established for the dominant N-heterocyclic carbene (NHC) catalysts: β-elimination of the ruthenacyclobutane (Scheme 3.1a),[6,7] and bimolecular coupling of methylidene **B** (Scheme 3.1b).[8,9] Particularly vulnerable to β-elimination is the unsubstituted ruthenacyclobutane **A**[10] formed on reaction of **B** with the ethylene co-product generated in metathesis of terminal olefins. Ethylene has been shown to limit metathesis yields in multiple contexts,[11] most prominently process chemistry[12,13] and continuous-flow metathesis.[14]

**Scheme 3.1. Intrinsic decomposition pathways established for phosphine-free Ru-$H_2$IMes metathesis catalysts.**

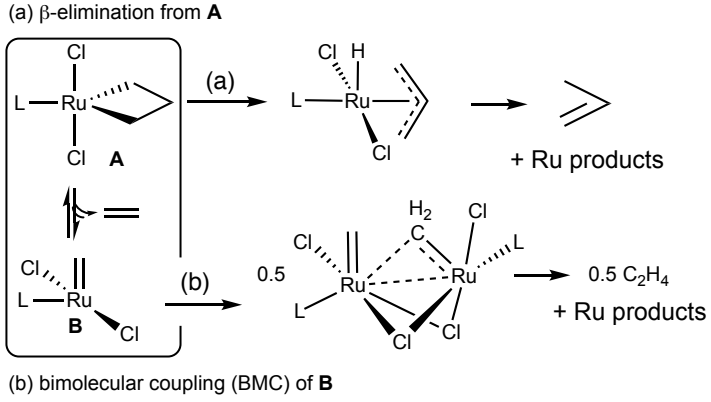


Striking, therefore, is the extraordinary productivity demonstrated for metathesis catalysts bearing a cyclic alkyl amino carbene (CAAC; Chart 3.1) in place of an NHC ligand.[15-19] Even in ethenolysis – that is, generation of α-olefins from unsaturated internal olefins of plant or algal origin,[3a,20-23] under an *atmosphere* of ethylene – turnover numbers (TONs) as high as 340,000 could be achieved using a CAAC catalyst.[16] This represents a level of efficiency 2 orders of magnitude higher than that attained with leading $H_2$IMes catalysts[15] under standard conditions of metathesis.

*References for Chapter 3 begin on p. 92*

**Chart 3.1. Metathesis catalysts discussed.**

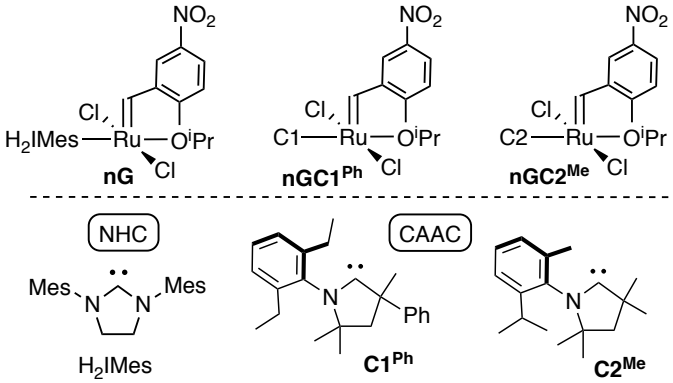


The origin of this remarkable performance has received little study to date. Grubbs and Bertrand proposed that **B-C1$^{Ph}$**, the CAAC analogue of intermediate **B-H$_2$IMes**, may be more stable to insertion of the N-aryl substituent into the Ru=CH$_2$ bond (for ligand structures, see Chart 3.1).[16] Lemcoff and co-workers[24] pointed out that the CAAC catalysts cause significantly less C=C migration: as the latter side-reaction is promoted by decomposed catalyst,[25] this is indirect evidence for the greater stability of the CAAC catalysts. We speculated that the resistance to C=C isomerization, as well as the remarkable ethenolysis productivity noted above, reports on the capacity of the propagating species to resist the decomposition pathways of Scheme 3.1. In a study of state-of-the-art CAAC catalysts, we demonstrate that β-elimination is indeed dramatically suppressed, although bimolecular coupling remains operative.

### 3.2.2. Results and Discussion

We began by evaluating the susceptibility of **nGC1$^{Ph}$** to bimolecular coupling. This catalyst was chosen for study given its record-setting productivity in macrocyclic ring-closing metathesis (mRCM),[17-19] and its striking tolerance for the contaminants present in technical-grade ethylene in ethenolysis,[19] relative to methyl-substituted **C2$^{Me}$** [16] (Chart 3.1). Steric protection by the phenyl group at the quaternary CAAC carbon in the **C1$^{Ph}$** ligand appears to improve its stability to contaminants,[19] and we queried whether this might also inhibit bimolecular coupling.

We thus set out to assess the susceptibility to bimolecular coupling of methylidene intermediate RuCl$_2$(**C1$^{Ph}$**)(=CH$_2$) (**B-C1$^{Ph}$**), relative to its H$_2$IMes analogue **B-H$_2$IMes**. The hallmark for this coupling reaction is release of ethylene. We recently developed a protocol for quantitation of the ethylene product, via synthesis and cryogenic isolation of transiently-stabilized pyridine adducts of **mGIII** (e.g. RuCl$_2$(H$_2$IMes)(py)(=CH$_2$), **mGIII**), and controlled decomposition of the adducts in the presence of an internal standard.[8]

Accordingly, we undertook synthesis of the CAAC-methylidene complex **mC1$^{Ph}$**: see Scheme 3.2. Key precursors to these complexes are the Piers-class phosphonium alkylidene catalysts (see **PC1$^{Ph}$**), which *irreversibly* eliminate the phosphonium ylide **12** on reaction with ethylene.[26] This effects quantitative formation of the metallacyclobutane (MCB), which in turn permits access to

the target methylidene species. The recently reported[19] indenylidene dimer **InC1$^{Ph}$** offers a convenient alternative to the benzylidene complexes typically used to synthesize the carbide precursors to the Piers catalysts.[10,27-29] Treatment of **InC1$^{Ph}$** with Feist's ester and P$^i$Pr$_3$ gave the CAAC carbide **CbC1$^{Ph}$**, which upon protonation with triflic acid generated the CAAC-Piers catalyst **PC1$^{Ph}$**.

**Scheme 3.2. Synthesis of methylidene complex mC1$^{Ph}$.**

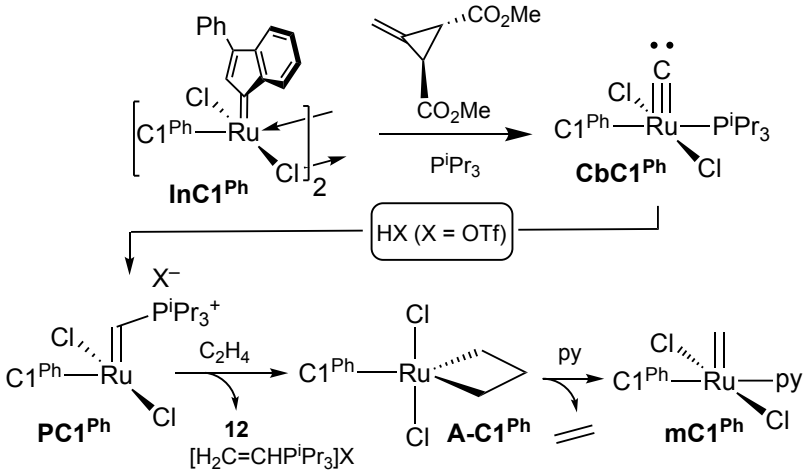


With **PC1$^{Ph}$** in hand, we generated the 14-electron MCB **A-C1$^{Ph}$** in situ, via the methodology developed by Piers for $H_2$IMes analogue **A-H$_2$IMes**.[28] To guard against premature decomposition of the MCB, we introduced ethylene at –78 °C, rather than at –50 °C as in the original report. Nevertheless, formation of **A-C1$^{Ph}$** was complete within 10 min. Addition of cold py triggered immediate retro-addition, and trapped the methylidene species **B-C1$^{Ph}$** as the py adduct **mC1$^{Ph}$**. The phosphonium salt **12** was then precipitated with cold pentane and filtered off under vacuum, enabling isolation of **mC1$^{Ph}$** free of both **12** and ethylene.

Controlled decomposition of the $H_2$IMes and CAAC methylidene complexes **mGIII** and **mC1$^{Ph}$** (Figure 3.1) was carried out in parallel, to probe their relative susceptibility to bimolecular coupling under directly comparable conditions. NMR tubes were filled to 80% capacity with the catalyst solutions, to limit volatilization of $C_2H_4$.[•] After measuring an initial $^1$H NMR spectrum at –20 °C (a temperature at which both complexes are stable), the samples were immediately warmed to 23 °C. Much faster decomposition was observed for CAAC derivative **mC1$^{Ph}$**, with complete disappearance of the alkylidene signal within <5 min (Figure 3.1a). Decomposition of the $H_2$IMes analogue **mGIII**, in comparison, was only 95% complete after 3 h. Ethylene, the

[•] Restricting the headspace in the NMR tube to 20% of the total tube volume represents a balance between tube rupture and retention of $C_2H_4$ in solution. For a resource on safe handling of cryogenic liquids, including a discussion on condensable gases, see: Kuespert, D. R., *Research Laboratory Safety*. de Gruyter: Haarlem, NL, 2016; pp 55–63. Losses to the headspace occur over a timescale of hours. For **mGIII**, 76% $C_2H_4$ was detected when decomposition was complete within 20 min.[8]

marker for bimolecular coupling, was observed in 81% or 75% yield, respectively (Figure 3.1b), and no propene was evident, indicating the absence of β-elimination. The ethylene yields represent lower limits, owing to diffusion into the headspace. It should be noted that the high Ru concentrations required for rapid NMR analysis (20 mM) accelerate bimolecular reaction, exaggerating absolute rates of decomposition. However, the increased susceptibility of the CAAC catalyst to bimolecular decomposition is maintained under catalytic conditions, at micromolar Ru concentrations and lower: see later.

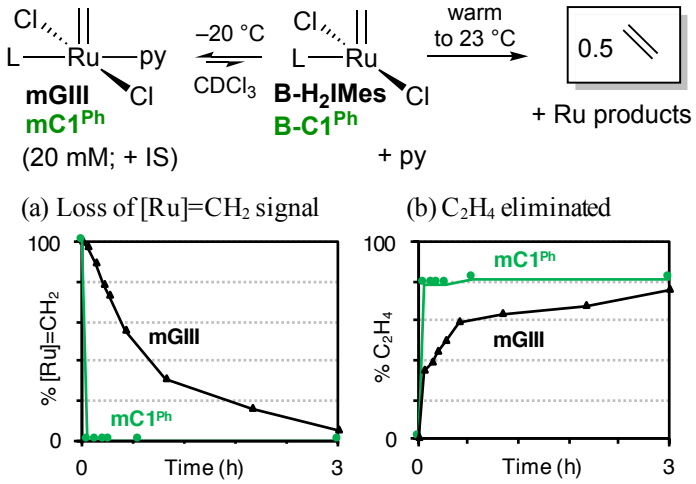


**Figure 3.1. Assessing the susceptibility to bimolecular coupling of the CAAC and $H_2$IMes methylidene complexes, mC1$^{Ph}$ and mGIII, respectively. IS = internal standard.**

The data of Figure 3.1 demonstrate that the metathesis-active intermediate **B-C1$^{Ph}$** is not merely susceptible to bimolecular decomposition, but that it is *more* so than the corresponding $H_2$IMes derivative. This was initially unexpected: given the low lability of the CAAC catalysts, relative to their $H_2$IMes analogues,[19,30] we anticipated that slower pyridine (py) dissociation would retard liberation and bimolecular coupling of **B-C1$^{Ph}$**. The observed trend implies that the coupling step, rather than py loss, is rate-determining.

The CAAC ligands are both more nucleophilic (σ-donating), and more electrophilic (π-accepting) than diaminocarbenes.[31,32] While the balance between these properties as they relate to the Ru catalysts has not yet been examined, strong ligand donicity is central to the high metathesis activity of these carbene catalysts. Of interest is the possibility that the electrophilicity of the Ru center is heightened relative to the $H_2$IMes analogue, promoting bimolecular decomposition (i.e., attack on **B-C1$^{Ph}$** by the dative chloride donors of a second **B-C1$^{Ph}$** unit). Py re-uptake would likewise be favoured, but this reaction is reversible, whereas dimerization is followed by rapid, irreversible elimination of ethylene (Scheme 3.1a).[8] Steric factors may also be relevant, however. The bulk of the CAAC ligands relative to NHCs is not clear-cut,[33] but the

extended "wingstips" of $H_2$IMes, with its mesityl *p*-methyl group, could potentially retard bimolecular coupling.

Of note, early studies of CAAC catalysts revealed incomplete RCM of standard substrates at catalyst loadings of 1-5 mol%.[34] This limited performance may reflect the propensity of the CAAC catalysts for bimolecular coupling at high Ru concentrations. Consistent with this inference, two subsequent literature reports reveal increased productivity as CAAC loadings are reduced.[16,19] To probe this point, and to complement the NMR study above, the productivities of the $H_2$IMes and CAAC catalysts were compared under conditions of catalysis, in the self-metathesis of styrene at 50 °C. We find a slight increase in TON for **nG** when the catalyst loading is increased from 1 ppm to 50 ppm (from 19,300 to 19,600). In contrast, TONs for **nGC1$^{Ph}$** decline fourfold (from 27,800 at 1 ppm to 6,500 at 50 ppm). Clearly, both systems participate in bimolecular decomposition, but the CAAC catalyst is significantly more sensitive.

The data so far indicate that the standout performance of the CAAC catalysts does not arise from resistance to bimolecular decomposition. We therefore sought to examine their susceptibility to the second major decomposition pathway discussed above: unimolecular decomposition via β-elimination of the MCB ring (Scheme 3.1b). In this case, the behaviour of the CAAC and NHC derivatives was compared by examining two top-performing CAAC catalysts, **nGC1$^{Ph}$** and **nGC2$^{Me}$**, in parallel with the Grela catalyst **nG**. The latter has long been valued for its outstanding performance in ring-closing and cross-metathesis.[1-3] The enhanced lability, and hence enhanced initiation efficiency, conferred by the nitro group *para* to the ether donor (see Chart 3.1) is a critical asset in the Ru-CAAC catalyst platform, given the much slower initiation noted above.[19,30]

Styrene self-metathesis (Figure 3.2), if carried out at Ru concentrations sufficient for NMR detection, offers an invaluable probe of MCB decomposition.[35] β-Elimination of the MCB ring generates unique propenyl markers ($H_2C$=$CHCH_2R$; R = H, Ph), which are readily distinguished from the products of metathesis (e.g. RHC=CHR) by the odd number of backbone carbons present. Styrene ensures the validity of this experiment because, unlike most 1-olefins, it cannot isomerize, and is therefore unable to generate "false" propenyl markers via isomerization prior to metathesis.[8] In addition, its relatively low reactivity ensures complete catalyst conscription even at 1 mol% Ru,[35] maximizing yields of the organic products of decomposition. Filling the NMR tubes to 80% capacity is again important, to limit loss of volatile propene to the headspace.

As shown in Figure 3.2a, and consistent with prior reports for this and related Ru-NHC catalysts,),[7] **nG** readily undergoes β-elimination. Propenes were detected in 51% yield relative to the starting charge of **nG**. (Bimolecular coupling is presumed to account for the balance, but its ethylene marker is masked by the ethylene liberated in metathesis). In striking contrast, essentially zero propenes were eliminated from the CAAC catalysts (2% for **nGC1$^{Ph}$**; 0% for

**nGC2$^{Me}$**). The CAAC ligand thus confers near-complete resistance to β-elimination. We speculate that heightened σ-donicity could potentially stabilize the metallacyclobutane, and hence raise the energy barrier to elimination.

The rapid catalyst decomposition evident in the decay curves of Figure 3.2b further underscores the ease with which all of these methylidene intermediates undergo bimolecular decomposition at high (20 mM) catalyst concentrations. The slower net disappearance of **nGC2$^{Me}$** is an artifact of slower initiation of the dimethyl-CAAC catalysts.[18]

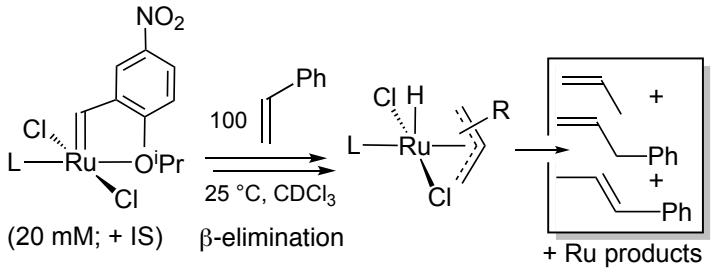


(a) Propene formation via β-elimination. (b) Loss of [Ru]=CHAr signal.

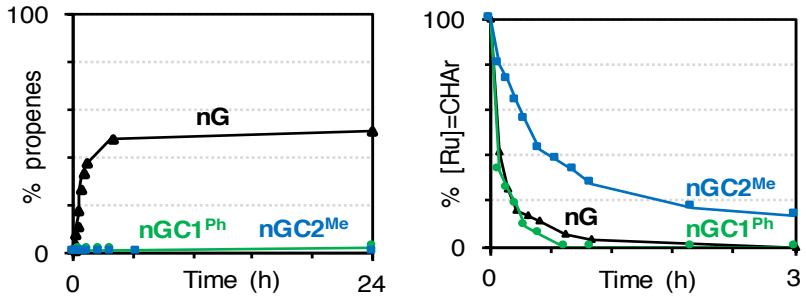


**Figure 3.2. Contribution of β-elimination (propene formation) to catalyst decomposition. Metathesis products ($C_2H_4$, stilbene) not shown.**

### 3.2.3. Conclusion

These findings have several important implications. First, the remarkable productivity of the CAAC catalysts is clearly due to the stability of the ruthenacycle to β-elimination, not to the resistance of the methylidene intermediate to bimolecular coupling. Indeed, the CAAC catalysts are *more* susceptible to bimolecular decomposition. Importantly, however, because they resist β-elimination, the CAAC catalysts can be used at much lower catalyst loadings, which in turn minimizes bimolecular decomposition. The remarkable productivity of these catalysts thus originates in the fact that at low catalyst loadings, both of the decomposition pathways of Scheme 3.1 are inhibited.

*References for Chapter 3 begin on p. 92*

Fundamental studies now under way seek to deepen our understanding of the factors that influence the stability of the CAAC catalysts to β-elimination, as well as their susceptibility to bimolecular decomposition. Likewise of keen interest is their robustness to Brønsted base, water, and other contaminants to which the NHC catalysts are vulnerable.[35-37] Nevertheless, these catalysts hold great promise for the broader implementation of metathesis methodologies, particularly in contexts where ethylene is required, or where its removal cannot be efficiently achieved.

### 3.2.4. Experimental Details for Section 3.2

**General Procedures.** Reactions were carried out under $N_2$ using glovebox or Schlenk techniques, unless otherwise noted. HPLC-grade solvents ($C_6H_6$, $CH_2Cl_2$, *n*-hexane) were dried and degassed using a Glass Contour solvent purification system, and stored under $N_2$ over 4 Å molecular sieves for at least 18 h prior to use. EtOAc (reagent grade) was washed with 5% $Na_2CO_3$, brine, distilled over $MgSO_4$ and then $P_2O_5$. Pentane (HPLC grade) was distilled likewise and stored as above. $CDCl_3$ (Cambridge Isotopes) was degassed by 5 freeze/pump/thaw cycles, and stored as above. Feist's ester,[38] **nGC2$^{Me}$**,[17] **InC1$^{Ph}$**,[19] and **mGIII**[8] were prepared by literature methods. The CAAC salt **C2$^{Me}$•BF$_4$** was kindly supplied by Umicore; the catalysts **nG** and **nGC1$^{Ph}$** by Apeiron Synthesis. CuCl (Aldrich, 99%) was stored in the glovebox and opened only after purging. P$^i$Pr$_3$ (Fischer, 98%) was stored in the glovebox freezer at –35 °C. Ethylene (BOC Gases; Linde, 99.9%) and internal standards dimethyl terephthalate (DMT, Aldrich, 99%) and 1,3,5-trimethoxybenzene (TMB, Aldrich, 99%) were used as received.

NMR spectra were recorded on Avance 300, Avance II 300 or Avance II 500 spectrometers at 23±2 °C, except where otherwise specified. Chemical shifts are reported in ppm, and referenced to the residual proton or carbon signals of the solvent. For $^{31}$P NMR, $H_3PO_4$ (85%) at 0 ppm was used as external standard. MALDI mass spectra were collected on a Bruker UltrafleXtreme MALDI-TOF/TOF mass spectrometer. Solutions of matrix (pyrene) and analyte (20:1) were prepared such that the final concentration of matrix and analyte was ca. 100 mM and 5 mM, respectively. A 1 μL aliquot of the mixed solution was spotted on the MALDI target plate and allowed to evaporate by the dried-droplet method.[39] Spectra were calibrated externally using the peaks for pyrene (*m/z* 202.078) and $H_2$IMes•H$^+$ (*m/z* 307.217).

**Catalyst Synthesis**

**Synthesis of [RuCl$_2$(CAAC)P(i Pr)$_3$(≡C:)], CbC1$^{Ph}$.** To a brown solution of **InC1$^{Ph}$** (138 mg, 0.202 mmol) and Feist's ester (40.0 mg, 0.235 mmol, 1.2 equiv) in 4 mL $CH_2Cl_2$ was slowly added a solution of P$^i$Pr$_3$ (49.0 μL, 0.26 mmol, 1.3 equiv) in 1 mL $CH_2Cl_2$. The solution was transferred to an oil bath at 35 °C and stirred for 2 h, after which the solution was dark red, and complete conversion to the carbide **CbC1$^{Ph}$** was evident by TLC analysis (solvent system 1:1 EtOAc: *n*-hexane; **InC1$^{Ph}$** Rf = 0.50; carbide **CbC1$^{Ph}$** Rf = 0.81). The volatiles were removed

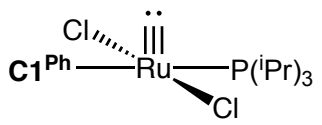

under vacuum, and the residue was taken up in 1:1:2 $CH_2Cl_2$:EtOAc:*n*-hexane, and chromatographed on $NEt_3$-deactivated silica with 1:1 EtOAc:*n*-hexane as eluant. The orange band was collected and stripped of solvent to afford a light brown solid. This was dissolved in *n*-hexane (0.5 mL) and chilled (–35 °C) for 2 h, after which a pale yellow solid was filtered off, washed with pentane (–35 °C, 1 mL), dried, and sublimed at 50 °C under reduced pressure for 1.5 h. Yield: 86 mg, 60%. $^1$H NMR ($CDCl_3$, 300 MHz): δ 7.73 (d, $^3J_{HH}$ = 6.4 Hz, 2H, *m*-C*H* of **C1$^{Ph}$** Ar), 7.45–7.31 (m, 5H, C*H* of **C1$^{Ph}$** Ph), 7.24 (t, $^3J_{HH}$ = 7.1 Hz, 1H, *p*-C*H* of **C1$^{Ph}$** Ar), 2.98 (m, 3H, C$H_2$ of **C1$^{Ph}$** Ar and backbone C$H_2$ of **C1$^{Ph}$**, overlapping), 2.78 –2.49 (m, 5H, C*H* of $^i$Pr$_3$ and C$H_2$ of **C1$^{Ph}$** Ar, overlapping), 2.33 (s, 4H, backbone C$H_2$ of **C1$^{Ph}$** and C$H_3$ of **C1$^{Ph}$**, overlapping), 1.58 (s, 3H, C$H_3$ of **C1$^{Ph}$**, overlapping), 1.53 (s, 3H, C$H_3$ of **C1$^{Ph}$**, overlapping), 1.20 (m, 24H, C$H_3$ of **C1$^{Ph}$** Ar, C$H_3$ of $^i$Pr$_3$, overlapping). $^{31}$P{$^1$H} ($CDCl_3$, 121 MHz): δ 39.57 (s, 1P, *P*($^i$Pr)$_3$). $^{13}$C{$^1$H} NMR ($CDCl_3$, 125 MHz): δ 478.56 (Ru≡*C*:), 263.53, 262.87, 142.82, 142.68, 141.88, 139.30, 129.32, 128.90, 128.22, 126.93, 126.27, 126.18, 65.12, 50.96, 31.19, 28.97, 28.20, 26.04, 24.55, 21.88, 21.71, 19.35, 19.15, 14.86, 14.41. MALDI-TOF MS (pyrene matrix), *m/z*: [**CbC1$^{Ph}$**–Cl,$^i$Pr]$^+$ 585.149 (calculated: 585.162 for $C_{30}H_{43}ClNPRu$). For fully-assigned NMR spectra, see Figures A.14–A.18.

**Synthesis of [RuCl$_2$(CAAC)(=CHP($^i$Pr)$_3$)]OTf (PC1$^{Ph}$).** Conducted by minor modification of the reported[38] procedure. To a stirred yellow solution of carbide **CbC1$^{Ph}$** (61 mg, 0.087 mmol) in 4 mL $CH_2Cl_2$ was added a solution of HOTf (8.0 μL, 0.087 mmol, 1.0 equiv) in 1.5 mL $CH_2Cl_2$, causing an immediate colour change to dark-green. The mixture was stirred for 45 min at RT, after which the solvent was removed under vacuum. Addition of pentane (3 mL) and vigorous stirring yielded a fine green precipitate, which was filtered off, washed with pentane (2 x 1 mL) and dried. Yield: 64.5 mg (87%). $^1$H NMR ($CDCl_3$, 500 MHz): δ 18.67 (d, $^2J_{HP}$ = 35.3 Hz, 1H, Ru=C*H*), 7.83 (s br, 2H, *m*-CH of **C1$^{Ph}$** Ar), 7.54 (m, 3H, *p*-C*H* of **C1$^{Ph}$** Ar and *o*-C*H* of **C1$^{Ph}$** Ph), 7.49 (dd, $^3J_{HH}$ = 22.3, 7.7 Hz, 2H, *m*-C*H* of **C1$^{Ph}$** Ph), 7.43 (t, $^3J_{HH}$ = 7.3 Hz, 1H, *p*-C*H* of **C1$^{Ph}$** Ph), 2.96 (m, 3H, C*H* of $^i$Pr$_3$), 2.82 (s br, 1H, backbone C$H_2$ of **C1$^{Ph}$**), 2.71 –2.44 (m, 5H, C$H_2$ of **C1$^{Ph}$** Ar and backbone C$H_2$ of **C1$^{Ph}$**, overlapping), 2.06 (s, 3H, C$H_3$ of **C1$^{Ph}$**), 1.53 (s, 3H, C$H_3$ of **C1$^{Ph}$**), 1.36 (s, 3H, C$H_3$ of **C1$^{Ph}$**), 1.29 (t, $^3J_{HH}$ = 7.4 Hz, 3H, C$H_3$ of **C1$^{Ph}$** Ar), 1.28 (t, $^3J_{HH}$ = 7.5 Hz, 3H, C$H_3$ of **C1$^{Ph}$** Ar), 1.12 (dt, $^3J_{HH}$ = 16.6, 6.6 Hz, 18H, C$H_3$ of $^i$Pr$_3$). $^{31}$P{$^1$H} ($CDCl_3$, 121 MHz): δ 57.74 (s, 1P, *P*($^i$Pr)$_3$) $^{13}$C{$^1$H} NMR ($CDCl_3$, 125 MHz): δ 141.60, 136.29, 130.73, 128.56, 128.00, 127.61, 126.27, 121.93, 119.39, 64.02, 31.70, 29.69, 28.15, 26.73, 25.39, 22.77, 22.49, 22.19, 17.97, 16.92, 14.34. MALDI-TOF MS (pyrene matrix), *m/z*: [**PC1$^{Ph}$**–Cl,OTf]$^+$ 629.289 (calculated: 629.258 for $C_{33}H_{51}ClNPRu$). For fully-assigned NMR spectra, see Figures A.19–A.24.

**Synthesis of [RuCl$_2$(CAAC)(py)$_n$(=CH$_2$)] (mC1$^{Ph}$).** Conducted by minor modification of the reported[8] procedure. In a 10 mL Schlenk flask, a dark-green solution of **PC1$^{Ph}$** (100 mg, 0.117 mmol) in $CH_2Cl_2$ (850 μL, 138 mM Ru) was

prepared and frozen in liquid $N_2$. The headspace was freeze-pump-thaw degassed, and thawed under ethylene at –78 °C, causing a colour change to dark red. The reaction was stirred for 10 min, after which a cold (–78 °C) solution of pyridine (17.0 μL, 0.211 mmol, 1.8 equiv) in 400 μL pentane was dribbled down the flask wall (ca. 10 sec). A colour change to dark green, then brown was observed. The mixture was stirred for a further 10 min, after which cold pentane (5 mL) was added from a reservoir held at –116 °C (liquid $N_2$–ethanol bath), via a cannula chilled with dry ice. A brown-yellow precipitate deposited, consisting chiefly of the phosphonium ylid, with some **mC1$^{Ph}$**. The $C_2H_4$ supply was closed off, the system was opened to $N_2$, and an $N_2$-filled Schlenk frit / receiver flask assembly was quickly attached to the reaction flask against a flow of $N_2$. Inversion of the assembly gave an orange filtrate, leaving a brown solid on the frit. Vacuum was applied to precipitate the phosphonium-salt-free **mC1$^{Ph}$** as a pale yellow solid. The assembly was removed to the glovebox, and the precipitate was immediately transferred to a vial for storage at -35 °C until use. Yield 15 mg (20%). $^1$H NMR ($CDCl_3$, 500 MHz, – 20 °C): δ 18.35 (s, 2H, Ru=C$H_2$), 9.06 (d, $^3J_{HH}$ = 5.8 Hz, 3H, *o*-C*H* of py'), 8.12 (d, $^3J_{HH}$ = 6.0 Hz, 2H, *o*-C*H* of py), 7.73 –7.66 (m, 2H, *m*-C*H* of py'), 7.64 (t, $^3J_{HH}$ = 8.0 Hz, 1H, *p*-C*H* of py'), 7.47 (m, 2H, *m*-C*H* of py), 7.41 (t, $^3J_{HH}$ = 8.0 Hz, 1H, *p*-C*H* of py'), 7.30 (m, 3H, *m*-C*H* of **C1$^{Ph}$** Ar and *p*-C*H* of **C1$^{Ph}$** Ph, overlapping with $CHCl_3$), 7.18 (m, 2H, *o*-C*H* of **C1$^{Ph}$** Ph), 7.07 (d, $^3J_{HH}$ = 7.5 Hz, 1H, *p*-C*H* of **C1$^{Ph}$** Ar), 6.97 –6.90 (m, 2H, *m*-C*H* of **C1$^{Ph}$** Ph), 3.35 –3.21 (m, 2H, C$H_2$ of **C1$^{Ph}$** Ar), 2.96 (d, $^2J_{HH}$ = 12.3 Hz, 1H, backbone C$H_2$ of **C1$^{Ph}$**), 2.93 –2.79 (m, 2H, C$H_2$ of **C1$^{Ph}$** Ar), 2.56 (d, $^2J_{HH}$ = 11.6 Hz, 1H, backbone C$H_2$ of **C1$^{Ph}$**), 2.30 (s, 3H, C$H_3$ of **C1$^{Ph}$**), 2.04 (s, 3H, C$H_3$ of **C1$^{Ph}$**), 1.58 (s, 3H, C$H_3$ of **C1$^{Ph}$**), 1.39 (t, $^3J_{HH}$ = 7.2 Hz, 3H, C$H_3$ of **C1$^{Ph}$** Ar), 0.98 (t, $^3J_{HH}$ = 6.9 Hz, 3H, C$H_3$ of **C1$^{Ph}$** Ar). $^{13}$C{$^1$H} NMR ($CDCl_3$, 125 MHz): δ 267.61, 161.58, 158.48, 156.99, 155.68, 155.28, 153.87, 153.47, 153.09, 152.71, 144.74, 143.75, 142.82, 142.47, 141.80, 138.83, 138.05, 136.32, 135.17, 134.32, 134.21, 133.50, 133.02, 131.51, 127.89, 127.80, 126.88, 125.83, 125.40, 125.12, 124.81, 124.14, 123.98, 123.91, 123.68, 123.43, 122.84, 122.36, 122.03, 121.31, 121.13, 119.28, 118.39, 78.01, 76.47, 72.57, 71.91, 71.89, 49.30, 44.75, 34.59, 31.74, 31.40, 31.30, 30.87, 29.07, 28.88, 27.72, 25.50, 25.19, 24.77, 23.71, 23.60, 22.83, 21.45, 20.73, 17.05, 15.01, 14.47, 14.44, 14.37, 13.69, 13.57, 11.73. For fully-assigned NMR spectra, see Figures A.25–A.27.

**Catalysis Experiments**

**Representative Procedure for Self-Metathesis of Styrene at 50 ppm of nGC1$^{Ph}$:** A mixture of styrene (46.0 μL, 0.400 mmol) and dodecane (91.0 μL, 0.401 mmol, 1 equiv; internal standard for GC analysis) was diluted with 1.85 mL $C_6H_6$ to give a final concentration of 200 mM styrene. The reaction vial was transferred to an oil bath pre-heated to 50 °C and stirred for ca. 10 min to ensure thermal equilibration. A 50 μL aliquot was removed for GC-FID analysis to establish the starting ratio of styrene to dodecane. **nGC1$^{Ph}$** (14.0 μL of a stock solution of 10.0 mg **nGC1$^{Ph}$** in 10.0 mL $C_6H_6$; 0.020 μmol, 0.005 mol%) was added to the stirred solution. After 24 h, an aliquot was removed, quenched[40] with KTp in THF (10.0 mg/mL; 10 equiv vs starting Ru), and analyzed by GC-FID. Table 3.1 shows the TONs obtained for each catalyst.

**nG (50 ppm):** As above, with **nG** (13.4 μL of a stock solution of 10.0 mg **nG** in 10.0 mL $C_6H_6$; 0.020 μmol, 0.005 mol%).
**nGC1$^{Ph}$ (1 ppm).** A stock solution of **nGC1$^{Ph}$ (**10.0 mg in 10.0 mL $C_6H_6$) was diluted 1,000x, resulting in a final concentration of 14.6 μM Ru. From this, 27.0 μL (0.394 x $10^{-6}$ mmol, 0.0001 mol%) was added to the reaction.

**nG (1 ppm).** As **nGC1$^{Ph}$**; final concentration of 14.9 μM Ru; 0.402 x $10^{-6}$ mmol (0.0001 mol%) was added to the reaction.

**Table 3.1. Turnover numbers in self-metathesis of styrene for nG and nGC1$^{Ph}$.**

| Catalyst | mol% Ru (ppm) | TON (x$10^3$) |
|---|---|---|
| **nG** | 0.005 (50) | 19.6 |
| **nGC1$^{Ph}$** | 0.005 (50) | 6.5 |
| **nG** | 0.0001 (1) | 19.3 |
| **nGC1$^{Ph}$** | 0.0001 (1) | 27.8 |

**Catalyst Decomposition Experiments: β-Elimination**

**Representative Procedure for β-Elimination from nG:** Solid **nG** (30 mg, 0.044 mmol) and 40 mg of DMT (0.21 mmol, 4.7 equiv) were added to a J-Young tube. $CDCl_3$ (1.7 mL) was added and the NMR sample was taken to the spectrometer to acquire the initial **nG**:IS ratio. The NMR sample was returned to the glovebox, where styrene (504 μL, 4.40 mmol, 100 equiv) was added to give a 20 mM Ru solution, and the timer was started immediately. The NMR tube was shaken periodically. After 3 h, the NMR tube was attached to a mechanical rotator (10 rpm) to effect mixing. For starting and ending spectra, see Figure A.10.

**nGC1$^{Ph}$:** As above, with **nGC1$^{Ph}$** (30 mg, 0.044 mmol), DMT (10 mg, 0.051 mmol, 1.2 equiv) and styrene (504 μL, 4.40 mmol, 100 equiv). For starting and ending spectra, see Figure A.11.

**nGC2$^{Me}$:** As above, with **nGC2$^{Me}$** (27 mg, 0.043 mmol), DMT (10 mg, 0.051 mmol, 1.2 equiv) and styrene (504 μL, 4.40 mmol, 102 equiv). For starting and ending spectra, see Figure A.12.

**Catalyst Decomposition Experiments: Bimolecular Coupling (BMC)**
**Representative Procedure for BMC of CAAC Methylidene Complex mC1$^{Ph}$:** Solid **mC1$^{Ph}$** (29 mg, 0.044 mmol) and ca. 50 mg of DMT (0.26 mmol, 5.9 equiv) were added to a cold NMR tube bedded in a chilled (−35 °C) sand-bath. Cold $CDCl_3$ (2.2 mL) was added, resulting in a 20 mM Ru solution. The tube was sealed, transferred to the instrument room in a dry-ice acetone bath (−78 °C), quickly shaken and inserted into an NMR probe precooled to −20 °C. After determining the initial ratio of **mC1$^{Ph}$** vs IS, the NMR sample was removed from the

spectrometer, set in a water bath (23 °C) behind a blast shield and shaken periodically while the spectrometer was warmed. After 5 min, the sample was returned to the spectrometer, at 23 °C.

---

## 3.3. Bimolecular Coupling in Olefin Metathesis: Correlating Structure and Decomposition for Leading and Emerging Ruthenium-Carbene Catalysts

### 3.3.1. Introduction

Olefin metathesis offers exceptional versatility in the catalytic assembly of carbon-carbon bonds.[1,2] Recent advances hold great promise for overcoming productivity challenges in frontier applications ranging from pharmaceutical manufacturing[3] to materials science[41,42] and chemical biology.[43] Notwithstanding the groundbreaking impact of the dominant Ru-$H_2$IMes catalysts, their facile decomposition is a fundamental limitation.[44] Of major importance, therefore, is the breakthrough performance of cyclic (alkyl)(amino) carbene derivatives (CAAC; Chart 3.2).[32,45] These catalysts show unprecedented productivity in the transformation of renewable fatty acids into α-olefins by cross-metathesis with ethylene ('ethenolysis'),[16,18,19,46] as first reported by Bertrand and Grubbs in 2015,[16] and in macrocyclization via ring-closing metathesis[17-19] (mRCM), a process of keen interest for the production of antiviral drugs.[3]

**Chart 3.2. Catalysts and carbene ligands discussed.**[a]

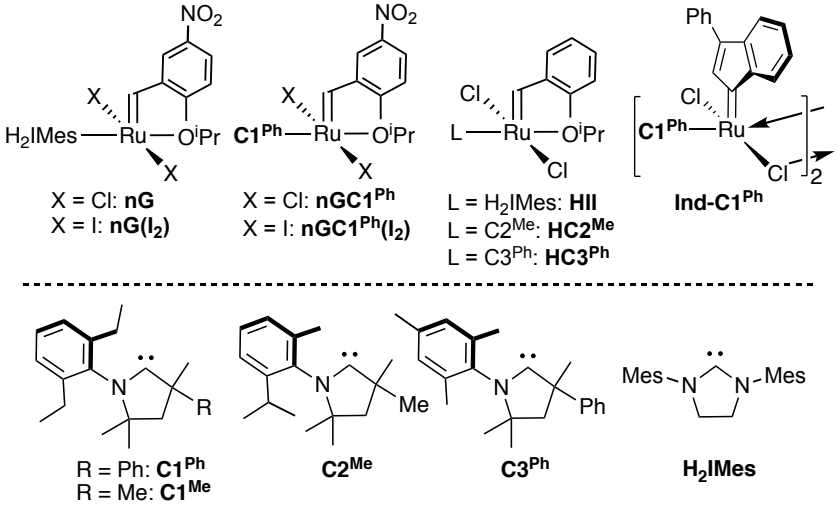


[a]The CAAC labelling system adopted (C#$^R$) defines ligand families by common NAr moiety. The superscript R specifies the 4th substituent on the quaternary site α to the carbene carbon.

We recently demonstrated[47] that the Ru-$H_2$IMes catalysts decompose via bimolecular coupling (Scheme 3.3a) – a pathway previously regarded as improbable for second-generation Ru catalysts – in addition to β-hydride elimination of the metallacyclobutane ring (Scheme 3.3b).[6] The CAAC catalysts, in comparison, resist β-hydride elimination,[47] but appear to be highly

sensitive to bimolecular decomposition, as judged from striking declines in metathesis productivity as catalyst loadings are increased.[48] In studies of transiently-stabilized methylidene species, we demonstrated that bimolecular coupling is faster for CAAC species $RuCl_2$(**C1**$^{Ph}$)(=$CH_2$)(py) (**mC1**$^{Ph}$) than its $H_2$IMes analogue **mGIII**.[49] To date, the factors that govern this pathway remain poorly understood. Indeed, although bimolecular coupling is a general vector for decomposition of both early and late transition methylidene species,[4,50] many details remain obscure. Here we present an experimental and computational study that provides the first detailed insight into the process, and its sensitivity to the nature of the neutral carbene. These findings are expected to aid both strategic planning and de novo catalyst design.[51,52]

**Scheme 3.3. Intrinsic decomposition pathways. (a) Bimolecular decomposition. (b) β-hydride elimination.**[a]

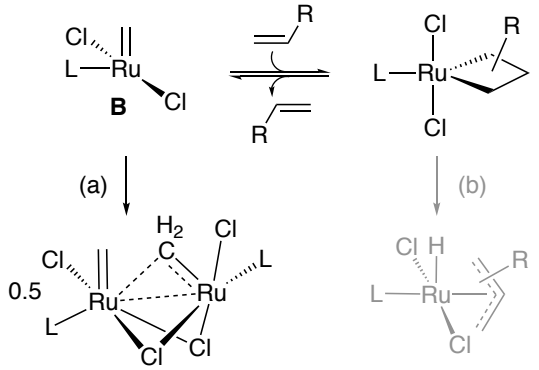


[a] Path (b) was found to be negligible for L = **C1**$^{Ph}$ and **C2**$^{Me}$: see text.

The key experimental evidence for bimolecular coupling of $RuCl_2$(L)(py)(=$CH_2$) (L = $H_2$IMes and **C1**$^{Ph}$) in our prior work was the observation that ethylene was liberated in ca. 75% yield.[47] Essential for quantitation was rapid warming of the samples from –20 °C to RT, to minimize loss of ethylene to the headspace. In the present study, we sought to probe the relevant structure–decomposition relationships, by assessing the relative susceptibility to bimolecular coupling of the series of CAAC and $H_2$IMes complexes shown in Chart 3.2. We began with a kinetics study of the isothermal decomposition of these transiently-stabilized complexes at –10 °C.

### 3.3.2. Results and Discussion

The methylidene species were synthesized via the cryogenic protocol of Scheme 3.4,[47] in which the Piers phosphonium alkylidenes **P**$^{X}$ is treated with ethylene to form the metallacyclobutane **A**$^{X}$, then with pyridine to collapse the ring and form the pyridine adducts **mBpy**$^{X}$. The phosphonium ylide coproduct, [$H_2$C=CHP$^{i}$Pr$_3$]OTf, was precipitated by cannula addition of cold (–110 °C) hexanes, and removed by filtration. Evaporation of the filtrate enabled isolation of the py adducts for all but **mC2**$^{Me}$. The latter was formed, as indicated by observation of the diagnostic $^1$H NMR signal for the [Ru]=C$H_2$ group at 18.35 ppm (Figure A.37), but was too unstable to isolate.

**Scheme 3.4. Synthesis of transiently-stabilized methylidene complexes $RuX_2(L)(py)(=CH_2)$, $mBpy^X$.** [a]

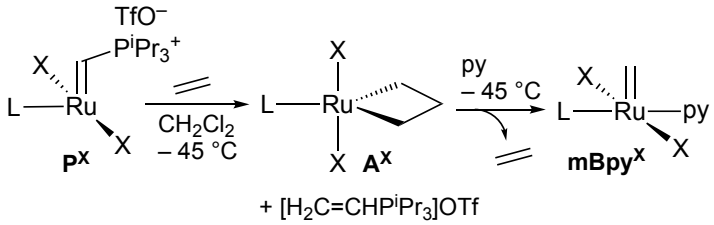


[a]X = Cl in all cases except $RuI_2(\mathbf{C1^{Ph}})(py)(=CH_2)$.

With this set of 5 methylidene complexes in hand, we undertook NMR studies to establish their relative susceptibility to bimolecular decomposition. Accordingly, each was redissolved at –35 °C in a solution of $CDCl_3$ containing an integration standard of known concentration. The samples were warmed to –10 °C, and their rates of decomposition were monitored from the decline in the intensity of the methylidene signal relative to that for the internal standard. Second-order kinetics were observed (Figure 3.3), confirming that decomposition is dominated by bimolecular coupling. The second-order rate constants spanned 3 orders of magnitude, with coupling being slowest for **mGIII**, and >>1 200 times faster for $\mathbf{mC2^{Me}}$. The lower limit for the latter is set by the rate for $\mathbf{mC1^{Me}}$, the fastest-decomposing species for which a rate could be measured.

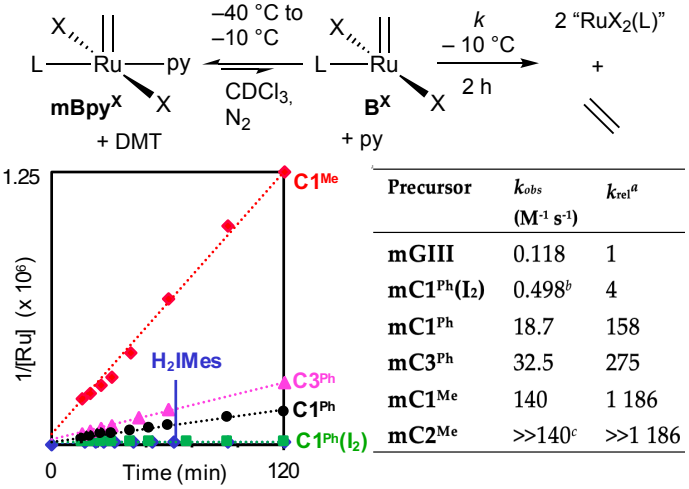


| Precursor | $k_{obs}$ ($M^{-1}$ $s^{-1}$) | $k_{rel}$[a] |
|---|---|---|
| **mGIII** | 0.118 | 1 |
| $\mathbf{mC1^{Ph}(I_2)}$ | 0.498[b] | 4 |
| $\mathbf{mC1^{Ph}}$ | 18.7 | 158 |
| $\mathbf{mC3^{Ph}}$ | 32.5 | 275 |
| $\mathbf{mC1^{Me}}$ | 140 | 1 186 |
| $\mathbf{mC2^{Me}}$ | >>140[c] | >>1 186 |

**Figure 3.3. Second-order plot for bimolecular decomposition, and tabulated rate constants ($k_{obs}$). Average of 2 trials. [a]$k_{rel}$ = rate constants normalized to that for the slowest-decomposing system, mGIII. [b]A similar rate (0.444 $M^{-1}s^{-1}$) was observed in $C_7D_8$. [c]A lower limit is given for $\mathbf{mC2^{Me}}$, which decomposed too rapidly to isolate.**

Figure 3.4 highlights the impact of individual structural features on rates of decomposition. We first consider the impact of the NAr *o*-aryl substituents, for CAAC ligands bearing a CMePh

group adjacent to the carbene carbon (Figure 3.4a). The N-mesityl complex **mC3$^{Ph}$** decomposes at twice the rate of its N-diethylphenyl (N-DEP) analogue **mC1$^{Ph}$**. That is, the rate of coupling is doubled by removing just one methylene unit from each *o*-substituent. (The mesityl *p*-methyl substituent in **C3$^{Ph}$** may also play a role, for example increasing σ-donation slightly relative to **C1$^{Ph}$**, but this effect is presumed to be minor). Faster decomposition with diminishing NAr bulk would account for the lower productivity reported for multiple catalyst classes (Hoveyda, Grela, and bis-CAAC platforms) when the **C1$^{Ph}$** ligand is replaced with **C3$^{Ph}$**.[16-18]

Truncation of the quaternary CMePh group to $CMe_2$ (**mC1$^{Ph}$** vs **mC1$^{Me}$**; Figure 3.4b) triggers both steric and electronic impacts. The N-DEP group is then too small to retard coupling, and **mC1$^{Me}$** decomposes nearly 10× faster than **mC1$^{Ph}$**. In keeping with this trend, turnover numbers reported for **C1$^{Me}$** catalysts are consistently lower than those for their **C1$^{Ph}$** analogues, for reactions ranging from ethenolysis to acrylonitrile metathesis.[16-18,53]

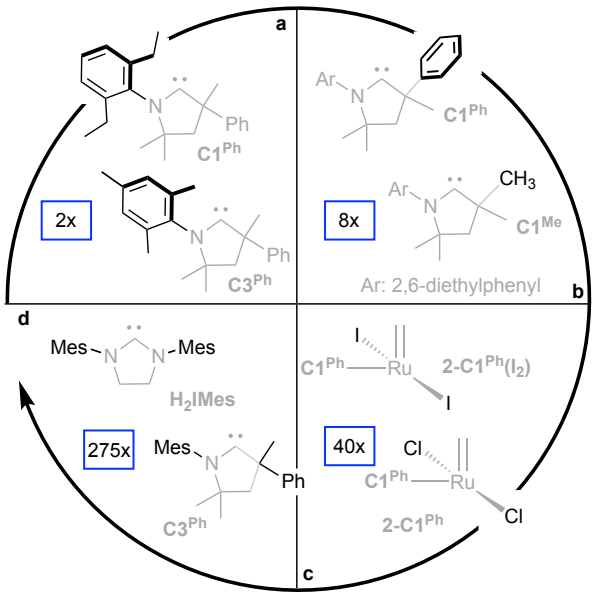


**Figure 3.4. Relative rates (text in blue boxes) of bimolecular decomposition. Shown in black are the key structural elements being compared: (a) NAr substituents. (b) Substitution at $C_\alpha$ (the quaternary center α to the carbene carbon). (c) The anionic ligand: chloride vs iodide. (d) NHC vs CAAC: $H_2$IMes vs its closest analogue, C3$^{Ph}$.**

Particularly rapid decomposition is seen for **mC2$^{Me}$**, despite the presence of one relatively bulky *o*-$^{i}$Pr substituent. Computational examination (see below) revealed that the latter in fact promotes pyridine loss to form the four-coordinate species **B-C2$^{Me}$**, while being insufficient to impede coupling. The extreme sensitivity of the **C2$^{Me}$** catalysts to bimolecular decomposition is implied by multiple experimental studies, as we have noted elsewhere.[47,54] Perhaps most striking is the

negative impact of increased catalyst loadings on TONs for **HC2$^{Me}$** even at <5 ppm catalyst.* Indeed, bimolecular coupling of **HC2$^{Me}$** appears to be so rapid at 70 °C that nucleophilic abstraction of the methylidene ligand is unable to compete, even when aggressive[55] nucleophiles such as unencumbered primary amines are employed).[54]

An inherent tradeoff is thus apparent between the steric protection required to retard bimolecular decomposition, and the steric accessibility required for fast initiation and turnover. As illustrated in Figure 3.4c, replacing the chloride ligands in the **C1$^{Ph}$** derivative by iodide slows the rate of decomposition 40-fold. Iodide catalysts, long dismissed for their lower reactivity, have recently been shown to offer productivity superior to their faster-initiating analogues in demanding contexts that require long catalyst lifetimes.[56-59] Retarded bimolecular decomposition is clearly an important component of this robustness, although it should be noted that it remains operative for **nG(I$_2$)** even at micromolar catalyst concentrations.[48b] Slowly-initiating CAAC-iodide metathesis catalyst may thus be of keen interest for metathesis of accessible olefinic bonds, although few such complexes have yet been developed.[45,60]

We come last to a more difficult comparison (Figure 3.4d), between **mGIII** and its closest CAAC analogue, **mC3$^{Ph}$**. The superficially minor replacement of one $H_2$IMes N-mesityl group by a CMePh unit dramatically increases the rate constant for decomposition, by 275×. Multiple parameters are affected by the transformation of an NHC to even a closely corresponding CAAC ligand, a point that has seen much recent discussion.[33,45,61-63] To probe the specific impact on bimolecular decomposition, we turned to computational analysis.

A density functional theory (DFT) analysis of the bimolecular coupling of **mGIII** reveals a complex overall mechanism. Key intermediates and transition states are shown in Scheme 3.5. Full exploration for the CAAC complexes is hampered by the multitude of isomers arising from the unsymmetrical nature of the carbene, and the chiral centers present in **C1$^{Ph}$** and **C3$^{Ph}$**. We therefore limited study of the CAAC systems to the Ru species shown, with bimetallic structures further limited to the diasteromeric dimers and transition states of **mC3$^{Ph}$**. Even with these restrictions, the study included 16 unique structures for the C–C bond-forming transition state (**TS$_{CC}$**) alone. The free energies in Table 3.2 were calculated using experimental catalyst concentrations.

* The outstanding performance of **HC2$^{Me}$** vs **HC1$^{Ph}$** in ethenolysis of methyl oleate is striking in light of the extreme sensitivity of the **C2$^{Me}$** catalysts to decomposition. Relevant in this context is the hindered nature of the substrate, the greater steric accessibility of the active species for the **C2$^{Me}$** catalyst, and the fact that TONs dropped from 340 000 to 180 000 on increasing catalyst loadings from 1 ppm to 3 ppm.[16]

*References for Chapter 3 begin on p. 92*

**Scheme 3.5. Key steps in the bimolecular decomposition of mBpy$^{X}$ identified by DFT calculations.**

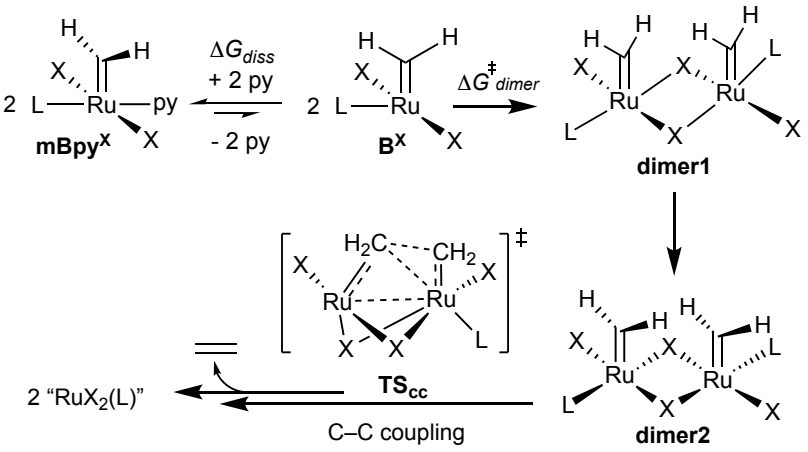


**Table 3.2 Calculated free energies for pyridine loss, dimerization, and buried volume**[a]

| Starting Complex | Pyridine Loss, $\Delta G_{diss}$ | Dimerization, $\Delta G^{\ddagger}_{dimer}$ | Buried Volume, %$V_{bur}$[b] |
|---|---|---|---|
| **mGIII** | 7.6 | 19.5 | 81.9 |
| **mC1$^{Ph}$(I$_2$)** | 4.4 | 13.2 | 88.6 |
| **mC1$^{Ph}$** | 3.9 | 12.3 | 83.7 |
| **mC3$^{Ph}$** | 3.8 | 12.1 | 82.6 |
| **mC1$^{Me}$** | 0.4 | 5.1 | 83.7 |
| **mC2$^{Me}$** | –2.0 | 0.4 | 82.8 |

[a]Free energies in kcal/mol vs $G$(**mBpy$^{X}$**), calculated for the most stable rotamers of **mBpy$^{X}$** and **B$^{X}$** at experimental catalyst concentrations (**mGII**: 1.4 mM, **mC1$^{Ph}$(I$_2$)**: 0.59 mM, **mC1$^{Ph}$**: 0.061 mM, **mC3$^{Ph}$**: 0.027 mM, **mC1$^{Me}$**: 0.01 mM). $\Delta G_{diss} = G(\mathbf{B}^{X}) + G(\text{py}) - G(\mathbf{mBpy}^{X})$; $\Delta G^{\ddagger}_{dimer} = 2\times\Delta G_{diss} + \Delta G^{\ddagger}_{diff}$ where $\Delta G^{\ddagger}_{diff}$ is the estimated lower limit for the free-energy barrier (4.4 kcal/mol). See Appendix for details. [b]$\%V_{bur}$ = fraction of the first coordination sphere (radius 3.5 Å) that is occupied in **B$^{X}$**.[64]

The calculations suggest that bimolecular decomposition is controlled by a few key steps (Scheme 3.5). Even the initial ligand dissociation is important, as indicated by the inverse correlation between the rate constants for decomposition in Figure 3.3, and the free-energy changes for pyridine dissociation in Table 3.2. Thus, the highest penalty for loss of pyridine ($\Delta G_{diss}$ = 7.6 kcal/mol) is found for **mGIII**, which is experimentally most resistant to bimolecular decomposition. Pyridine binding is 3.2–9.6 kcal/mol weaker in the CAAC complexes, and the Ru–N bond distances are 3–6 pm longer (see Table 3.2 and DFT-optimized structures in Figure 3.5). The impact of this difference will be doubled in the relative decomposition rates, as two pyridine ligands must be lost for a single dimer to form.

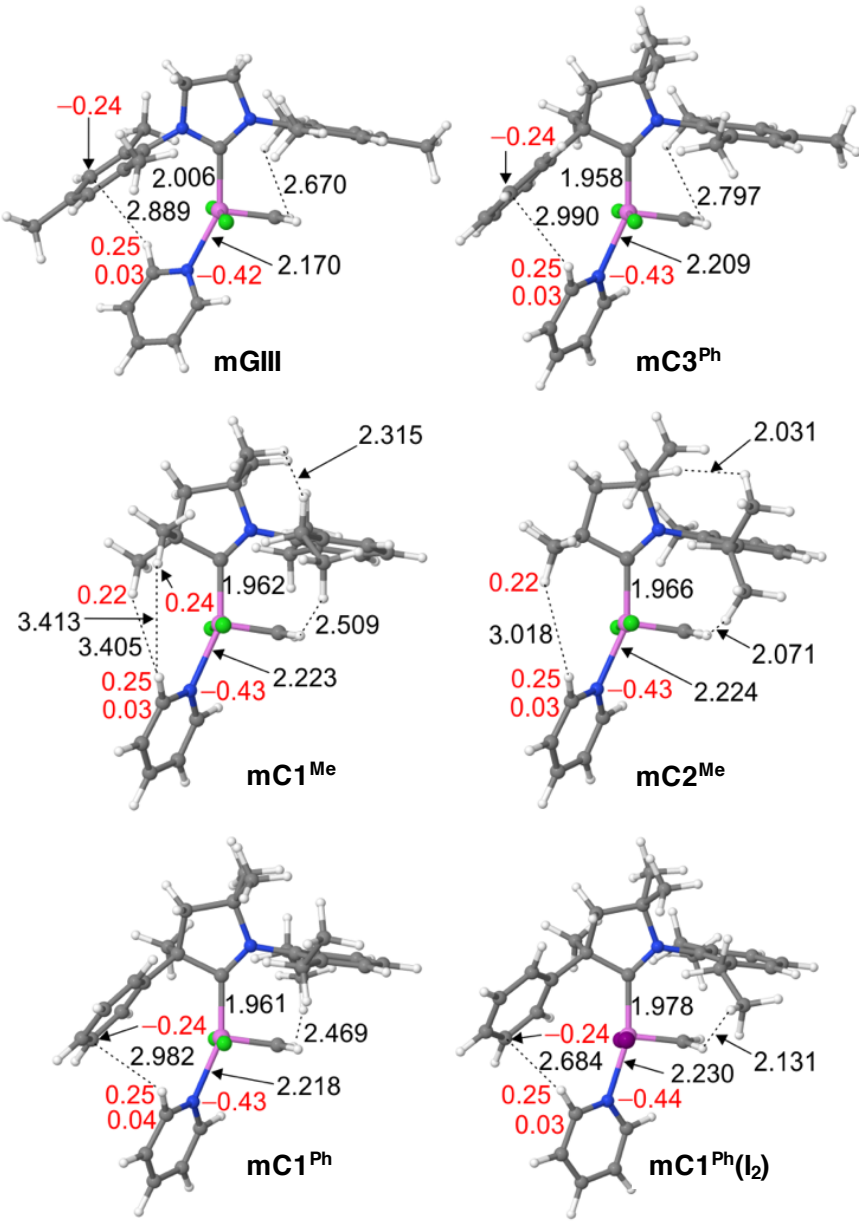


**Figure 3.5. Selected atomic distances (Å) for py adducts mBpy$^{X}$ (DFT-optimized geometries). Ru: pink; Cl: green; I: violet; C: grey; N: blue; H: white). Natural charges (*e*) of selected atoms in red.**

Weakening of the Ru–py bonds in the CAAC complexes is due chiefly to the enhanced σ-donor and π-acceptor character of this carbene class,[32] which increases the trans influence of the CAAC ligands relative to NHCs. In **mC1$^{Ph}$(I$_2$)**, the most stable of the CAAC species shown in Figure 3.3, the trans influence of **C1$^{Ph}$** is attenuated by the Ru–C$_{carbene}$ bond elongation induced by the bulky iodide ligands. The significant steric impact is evident from the much higher buried volume calculated for this complex (Table 3.2). The Ru–py bond in the iodide complex is hence

0.5 kcal/mol stronger than that in its chloride analogue **mC1$^{Ph}$**, contributing to the reduced susceptibility to bimolecular decomposition.

A much weaker Ru–py bond is seen in **mC1$^{Me}$** and, to an even greater extent, in **mC2$^{Me}$**. Given the broad similarity in calculated buried volumes (*%$V_{bur}$*; Table 3.2) for the various CAAC ligands,[65] this instability is unlikely to be steric in origin. Rather, we suggest that the key feature that distinguishes both **C1$^{Me}$** and **C2$^{Me}$** is the absence of an aromatic quaternary substituent that can participate in polar CH–π interactions[66,67] with the pyridine ligand in **mBpy$^{X}$**. In the most stable conformers of **mC2$^{Me}$** and **mC1$^{Me}$**, the N-aryl group is syn to the methylidene, precluding such interaction. In the **C1$^{Ph}$** and **H$_2$IMes** complexes, in comparison, an electron-rich aromatic ring is positioned to engage in hydrogen-bonding and donor–acceptor bonding with the electron-deficient *o*-H and *o*-C pyridine atoms (natural charges = 0.25 *e* (H), 0.03–0.04 *e* (C); Figure 3.5).*

Importantly, these stabilizing interactions are not restricted to the pyridine ligand: they are likewise expected for bound olefin, owing to Ru-induced polarization of the sp$^2$ C–H bonds. The consequent reduction in the concentration of the 14-electron species would limit bimolecular decomposition.† For the CAAC catalysts to achieve these effects, however, a quaternary aromatic group is essential. In **mC1$^{Me}$** and **mC2$^{Me}$**, the hydrogen atoms of the quaternary methyl groups bear a positive charge, as do the pyridine *o*-H and *o*-C atoms: this and the minimum Me—pyridine interatomic distances (>3 Å; Figure 3.5) reflect the absence of attractive interactions.
An additional factor affecting **mC2$^{Me}$**, beyond the absence of stabilizing polar CH–π interactions, is steric repulsion associated with the NAr *o*-isopropyl substituent. The latter is within ca. 2 Å of both the methylidene ligand and the methyl groups on the carbene backbone. This steric repulsion is relieved by pyridine dissociation and 90° rotation of the methylidene group to form **B-C2$^{Me}$**. The observed instability of **mC2$^{Me}$** is thus due to a combination of steric and electronic factors.

The second-order kinetics evident in Figure 3.3 indicate that pyridine dissociation is not rate-limiting. Detailed calculations on **mGIII** and **mC3$^{Ph}$** instead suggest that the rate-determining step is coupling of two molecules of 14-electron **B$^{X}$** to form **dimer1** (Scheme 3.5), in which a chloride from each Ru atom serves as a dative ligand to the other Ru atom. Within this dimer, the geometry of the individual Ru centers in **B$^{X}$** is largely conserved, including the essentially

---

* These interactions include donor–acceptor bonding, with the filled π orbitals of the aromatic carbene substituents donating into the π* and s* orbitals of the pyridine N=C and *o*-C–H bonds, respectively.

† Other donor ligands, such as the isopropoxy group in the leading Grela and Hoveyda catalyst platforms, are also expected to participate in such stabilizing interactions, and may indeed contribute to the slow initiation of such CAAC precatalysts. For example, interatomic distances as short as ca. 2.8 Å are seen between the phenyl ring of the **C1$^{Ph}$** ligand and the chelated isopropoxy donor in the X-ray crystal structure of **nGC1$^{Ph}$**.[17]

orthogonal disposition of the methylidene ligand relative to the $RuCl_2$ plane. The minimal geometrical adaption needed for **B-H$_2$IMes** and **B-C3$^{Ph}$** suggests little to no enthalpic cost to formation of **dimer1** from **B$^X$**. A lower bound for the barrier to dimerization can be obtained by assuming that the rate is diffusion-controlled. Rate constants for diffusion in common organic solvents are on the order of $4 \times 10^9$ $s^{-1}$,[68] from which a barrier ($\Delta G^{\ddagger}_{diff}$) of 4.4 kcal/mol can be extracted from the Eyring equation. Summing this value and the free energies of two 14-electron complexes **B$^X$** gives an estimated overall barrier to dimerization $\Delta G^{\ddagger}_{dimer}$ of ca. 19.5 kcal/mol for **mGIII** and 12.1 kcal/mol for **mC3$^{Ph}$**, relative to four-coordinate methylidenes.

In contrast, the ensuing rearrangement from **dimer1** to the more stable, tightly bonded **dimer2** is practically barrierless. In the latter structure, the methylidene groups return to a conformation aligned with the $RuCl_2$ plane. All subsequent steps are likewise facile compared to the initial dimerization. That is, the barrier to C–C bond formation via **TS$_{CC}$** is lower than that for formation of **dimer1**, as is the subsequent formation of an ethylene-bridged Ru dimer, rearrangement to a $\eta^2$-ethylene complex, and release of ethylene and Ru decomposition products. The calculations for **mGIII** and **mC3$^{Ph}$** thus strongly suggest that the most energy-demanding step in bimolecular decomposition from the 14-electron complexes **B$^X$** is the formation of **dimer1**, rather than coupling of the methylidene units. Quantitative agreement between the calculated barriers $\Delta G^{\ddagger}_{dimer}$ and the experimental rate constants cannot be expected, given the exclusion of enthalpic contributions to the dimerization of **B$^X$** (see above), the standard errors expected for DFT-calculated free-energy differences (2–5 kcal/mol), and the exponential (Eyring) relationship between barriers and rate constants. However, the kinetic bottleneck predicted computationally is supported by the qualitative, rank-order agreement between the calculated barriers and the experimental rate constants, as well as the fact that the observed second-order kinetics (Figure 3.6) are consistent with dimerization as the rate-determining step in the overall reaction.

### 3.3.3. Conclusion

Bimolecular catalyst decomposition has long been recognized as a fundamental challenge in olefin metathesis. Leading ruthenium–carbene catalysts, initially thought to be immune, are now known to be extraordinarily susceptible, even at ppm catalyst loadings. The foregoing provides the first detailed mechanistic insights into the process, and the steric and electronic factors that govern decomposition. An experimental "catalyst susceptibility ranking" was established for the most productive CAAC and NHC catalysts, and qualitatively reproduced via DFT analysis, which revealed that dimerization of the 14-electron complex **B$^X$** is rate-determining. A major component of this barrier is ligand dissociation to generate **B$^X$**, dimerization of which is retarded surprisingly little even by relatively bulky carbene ligands. Fast catalyst initiation, aimed at rapid generation of metathesis-active **B$^X$**, is thus inextricably connected to accelerated bimolecular decomposition for state-of-the-art NHC and (particularly) CAAC catalysts. The striking susceptibility of the latter to bimolecular decomposition is shown to originate in the high trans

influence of the CAAC ligand, which promotes formation of $\mathbf{B^X}$, and necessitates very low catalyst concentrations to restrict bimolecular decomposition. Prevention of this major decomposition reaction offers major opportunities to transform catalyst productivity and utility, and to realize the outstanding promise of olefin metathesis.

### 3.3.4. Experimental Details for Section 3.2

**General Procedures.** Reactions were carried out under $N_2$ using glovebox or Schlenk techniques. HPLC-grade $CH_2Cl_2$, *n*-hexane, $C_6H_6$ were dried and degassed using a Glass Contour solvent purification system, toluene by distillation from Na: all were stored under $N_2$ over 4 Å molecular sieves for at least 18 h prior to use. NMR solvents ($CDCl_3$, $C_6D_6$ and $C_7D_8$: Cambridge Isotopes) were degassed (freeze/pump/thaw; 5x), and stored as above. CAAC salts[18] and Feist's ester[38] were prepared by literature methods. Known Hoveyda-class CAAC complexes,[16,57] carbide complexes $[RuCl_2(L)PR_3(\equiv C:)]$ and Piers catalysts $[RuCl_2(L)(=CHPR_3)]OTf$ (L = $H_2$IMes, R = Cy);[10,38] L = $\mathbf{C1^{Me}}$,[5] or $\mathbf{C1^{Ph}}$,[47] R = $^i$Pr) were synthesized by literature methods. Ethylene (BOC Gases; Linde, 99.9%), internal standard dimethyl terephthalate (DMT, Aldrich, 99%) and $P^iPr_3$ (Alfa, 98%) were used as received. The latter was stored in the glovebox freezer until use.

NMR spectra were recorded on Avance II 500 spectrometers at 23±0.2 °C, unless otherwise specified. Chemical shifts are reported in ppm, referenced to the residual proton or carbon signals of the solvent. MALDI mass spectra were collected on a Bruker UltrafleXtreme MALDI-TOF/TOF mass spectrometer. Solutions of matrix (pyrene) and analyte (20:1) were prepared such that the final concentration of matrix and analyte was ca. 100 mM and 5 mM, respectively. A 1 μL aliquot of the mixed solution was spotted on the MALDI target plate and allowed to evaporate by the dried-droplet method.[39] Spectra were calibrated internally with pyrene (*m/z* 202.078). Details of computational calculations, which were carried out by co-workers, are omitted from the Appendix.

#### Synthesis of Ru Complexes

**Synthesis of Carbide Complexes $RuX_2(CAAC)(P^iPr3)(\equiv C:)$, CbX**

Higher yields of the CAAC carbide complexes were obtained, relative to our prior route,[69] by starting with the known Hoveyda-CAAC complexes rather than the indenylidene CAAC dimer (Scheme 3.6). Washing the product with *n*-hexane sufficed to remove the organic side-products, where our original procedure required chromatography to remove a species that gave rise to a broad aromatic signal.

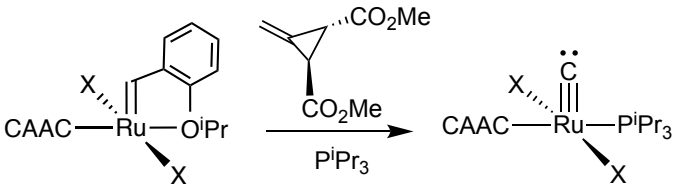

**Scheme 3.6. Synthesis of the CAAC-Carbide Complexes**

**Representative Procedure for Synthesis of $RuCl_2(C1^{Ph})(P^iPr_3)(\equiv C:)$, $CbC1^{Ph}$.** To a green solution of $HC1^{Ph}$ (130 mg, 0.203 mmol) and Feist's ester (55 mg, 0.32 mmol, 1.6 equiv) in 3 mL $CH_2Cl_2$ was added a solution of $P^iPr_3$ (53 mg, 0.33 mmol, 1.6 equiv) in 1 mL $CH_2Cl_2$. The solution was transferred to an oil bath at 35 °C and stirred for 20 h to give a dark yellow solution in which complete conversion to $CbC1^{Ph}$ was evident ($^1$H NMR). The volatiles were removed under vacuum, and the residue was taken up in *n*-hexane (2 mL). The suspension was stirred vigorously until a fine powder resulted. The suspension was chilled (–35 °C) for 2 h, after which the pale-yellow solid was filtered off, washed with *n*-hexane (–35 °C, 1 mL), dried, and sublimed at 60 °C under reduced pressure for 2 h. Yield: 117 mg, 82%. The $^1$H NMR data in $CDCl_3$ agree with values reported.[69] Particularly diagnostic is the most downfield signal: δ 7.73 (d, $^3J_{HH}$ = 6.4 Hz, 2H, *m*-C*H* of $C1^{Ph}$ Ar)

**Synthesis of $CbC2^{Me}$:** As in the representative procedure, with $HC2^{Me}$ (112 mg, 0.194 mmol), Feist's ester (45 mg, 0.27 mmol, 1.4 equiv) and $P^iPr_3$ (44 mg, 0.28 mmol, 1.4 equiv). $^1$H NMR showed complete consumption of starting material after 6 h of reaction. Product obtained as a pale-yellow solid. Yield after workup: 84 mg (72%). For NMR spectra (including the assigned $^1$H spectrum), see Figures A.28a and b.

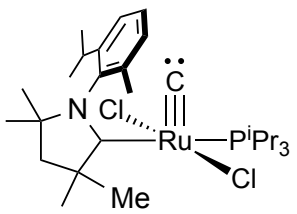


$^1$H NMR ($CDCl_3$, 500 MHz): δ 7.29 (d, $^3J_{HH}$ = 4.5 Hz, 2H, *m*-C*H* of $C2^{Me}$ Ar), 7.14 (t, $^3J_{HH}$ = 4.6 Hz, 1H, *p*-C*H* of $C2^{Me}$ Ar), 3.05 (sept, $^3J_{HH}$ = 6.5 Hz, 1H, C*H* of $C2^{Me}$ $^i$Pr), 2.74 (m, 3H, C*H* of $P^iPr_3$), 2.42 (s, 3H, C$H_3$ of $C2^{Me}$), 2.09 (d, $^2J_{HH}$ = 3.3 Hz, 2H, backbone C$H_2$ of $C2^{Me}$), 1.75 (d, $^3J_{HH}$ = 16.9 Hz, 6H C$H_3$ of $C2^{Me}$ $^i$Pr), 1.47 (s, 3H, C$H_3$ of $C2^{Me}$ or C$H_3$ of $P^iPr_3$), 1.41 (s, 3H, C$H_3$ of $C2^{Me}$ or C$H_3$ of $P^iPr_3$), 1.34 (m, 21H, C$H_3$ of $P^iPr_3$ and $C2^{Me}$, overlapping), 1.17 (d, *J* = 6.4 Hz, 3H, C$H_3$ of $C2^{Me}$ or C$H_3$ of $P^iPr_3$). $^{13}$C{$^1$H} NMR ($CDCl_3$, 125 MHz): δ 474.0, 266.5, 265.9, 147.5, 138.5, 137.1, 129.0, 128.9, 125.1, 80.1, 58.4, 52.3, 31.0, 30.8, 30.5, 28.7, 28.4, 26.5, 24.4, 22.9, 21.7, 19.7, 19.6. MALDI-TOF MS (pyrene matrix), *m/z*: $[CbC2^{Me}]^+$ 601.127 (calculated for $C_{28}H_{48}Cl_2NPRu$: 601.194).

**Synthesis of $CbC3^{Ph}$:** As in the representative procedure, with $HC3^{Ph}$ (148 mg, 0.237 mmol), Feist's ester (52 mg, 0.31 mmol, 1.3 equiv) and $P^iPr_3$ (51 mg, 0.32 mmol, 1.4 equiv). $^1$H NMR showed complete consumption of starting material after 2 h of reaction. Product obtained as a beige solid. Yield after workup: 130 mg (84%). For NMR spectra (including the assigned $^1$H spectrum), see Figures A.29a and b.

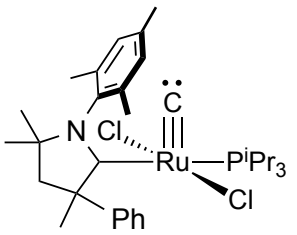


$^1$H NMR ($CDCl_3$, 500 MHz): Note. Signals are broad, causing small deviations in integration. δ 7.82 (s br, 2H, *m* or *p*-C*H* of $C3^{Ph}$ Ph), 7.66 (s br, 1H, *m*-C*H* of $C3^{Ph}$ Ar or *p*-C*H* of $C3^{Ph}$ Ph), 7.42 – 7.17 (m br, 4H, *m* or *p*-C*H* of $C3^{Ph}$ Ph and C*H*$Cl_3$, overlapping), 6.93 (s br, 1H, *m*-C*H* of $C3^{Ph}$ Ar or *p*-C*H* of $C3^{Ph}$ Ph), 6.86 (s br, 1H, *m*-C*H* of $C3^{Ph}$ Ar or *p*-C*H* of $C3^{Ph}$ Ph), 2.66 (s br, 3H, C*H* of $P^iPr_3$), 2.47 (m br, 6H, C$H_3$ of $C3^{Ph}$), 2.39 (s br, 4H, C$H_3$ and backbone C$H_2$ of $C3^{Ph}$), 2.26 (s br, 4H, C$H_3$ of $C3^{Ph}$), 1.58 (s br, 1H, backbone C$H_2$ of $C3^{Ph}$), 1.46 (s br, 3H, C$H_3$

of **C3$^{Ph}$**), 1.28 (s br, 2H, C$H_3$ of **C3$^{Ph}$**), 1.13 (m br, 20H, C$H_3$ of P$^i$Pr$_3$). $^{13}$C{$^1$H} NMR ($CDCl_3$, 125 MHz): δ 435.0, 265.1, 264.4, 148.4, 138.2, 136.0, 135.7, 130.3, 130.3, 130.0, 129.4, 128.3, 126.89, 126.9, 126.5, 81.7, 80.4, 66.4, 54.9, 29.8, 29.5, 28.9, 25.0, 24.2, 21.8, 21.6, 20.8, 19.3. MALDI-TOF MS (pyrene matrix), *m/z*: [**CbC3$^{Ph}$**–Cl,$^i$Pr]$^+$ 517.109 (calc'd for $C_{29}H_{41}ClNPRu$: 517.171).

**Synthesis of CbC1$^{Ph}$(I$_2$):** As in the representative procedure, with minor modifications: **HC1$^{Ph}$(I$_2$)** (193 mg, 0.235 mmol), Feist's ester (61 mg, 0.36 mmol, 1.5 equiv), P$^i$Pr$_3$ (57 mg, 0.36 mmol, 1.5 equiv). Toluene was used as solvent and the reaction was stirred at 80 °C for 22 h, at which time no starting material remained. Yield of brown product after workup: 176 mg (88%). For NMR spectra (including the assigned $^1$H spectrum), see Figures A.30a and b.

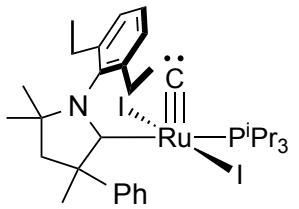


$^1$H NMR ($C_6D_6$, 500 MHz): δ 7.79 (d, $^3J_{HH}$ = 7.5 Hz, 2H, C$H$ of **C1$^{Ph}$** Ar or Ph), 7.34 (t, $^3J_{HH}$ = 7.9 Hz, 2H, C$H$ of **C1$^{Ph}$** Ar or Ph), 7.18 (s, 2H, C$H$ of **C1$^{Ph}$** Ar or Ph), 7.13 (d, $^3J_{HH}$ = 8.1 Hz, 1H, C$H$ of **C1$^{Ph}$** Ar or Ph), 7.05 (t, $^3J_{HH}$ = 7.6 Hz, 1H, *p*-C$H$ of **C1$^{Ph}$** Ar or Ph), 3.64 (dq, $^3J_{HH}$ = 15.0, 7.4 Hz, 1H, C$H_2$ of **C1$^{Ph}$** Ar), 3.45 (dq, $^3J_{HH}$ = 14.6, 7.3 Hz, 1H, C$H_2$ of **C1$^{Ph}$** Ar), 3.08 (m, 3H, C$H$ of P$^i$Pr$_3$), 2.88 (d, $^2J_{HH}$ = 12.3 Hz, 1H, backbone C$H_2$ of **C1$^{Ph}$**), 2.73 (dq, $^3J_{HH}$ = 14.7, 7.3 Hz, 2H, C$H_2$ of **C1$^{Ph}$** Ar), 2.42 (s, 3H, backbone C$H_3$ of **C1$^{Ph}$**), 1.69 (d, $^2J_{HH}$ = 12.3 Hz, 1H, backbone C$H_2$ of **C1$^{Ph}$**), 1.39 (t, $^3J_{HH}$ = 7.4 Hz, 3H, C$H_3$ of **C1$^{Ph}$** Ar), 1.34 (t, $^3J_{HH}$ = 7.4 Hz, 3H, C$H_3$ of **C1$^{Ph}$** Ar), 1.28 (dd, $^3J_{HH}$ = 13.4, 7.3 Hz, 6H, C$H_3$ of P$^i$Pr$_3$ and backbone C$H_3$ of **C1$^{Ph}$**, overlapping), 1.18 – 1.11 (m, 15H, C$H_3$ of P$^i$Pr$_3$). $^{13}$C{$^1$H} NMR ($C_6D_6$, 125 MHz): δ 269.6, 269.0, 147.7, 144.1, 142.1, 139.5, 129.4, 129.2, 127.0, 126.8, 126.6, 79.0, 67.4, 67.4, 36.2, 28.0, 27.0, 25.8, 25.5, 25.4, 20.4, 20.3, 15.8, 15.0. MALDI-TOF MS (pyrene matrix), *m/z*: [**CbC1$^{Ph}$–I$_2$**]$^+$ 593.211 (calc'd for $C_{33}H_{50}NPRu$: 593.272).

**Synthesis of Piers Complexes [RuX$_2$(CAAC)(=CHP($^i$Pr)$_3$)]OTf, P$^X$**

**Representative Procedure for Synthesis of [RuCl$_2$(C1$^{Ph}$)(=CHP$^i$Pr$_3$)]OTf PC1$^{Ph}$.** The Piers complexes were prepared according to the method reported for **C1$^{Ph}$** [69] (Scheme 3.7; reproduced here for convenience). To a stirred yellow solution of **CbC1$^{Ph}$** (117 mg, 0.166 mmol) in 4 mL $CH_2Cl_2$ was added a solution of HOTf (27 mg, 0.18 mmol, 1.1 equiv) in 1.5 mL $CH_2Cl_2$. The solution immediately turned dark-green. The mixture was stirred for 45 min at RT, after which the solvent was removed under vacuum. Addition of *n*-hexane (2 mL) and vigorous stirring yielded a fine green precipitate, which was filtered off, washed with *n*-hexane (2 mL) and dried. Yield: 127 mg (89%). The $^1$H NMR data in $CDCl_3$ agree with values reported.[69] Key alkylidene signal: δ 18.67 (d, $^2J_{HP}$ = 35.3 Hz, 1H, Ru=C$H$).

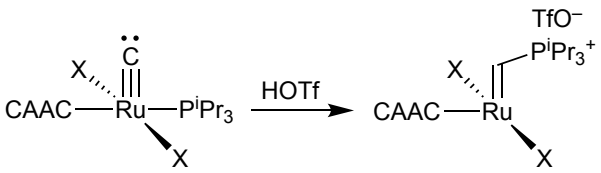

**Scheme 3.7. Synthesis of Piers Complexes from the Corresponding Carbides**

**Synthesis of PC2$^{Me}$**: As above, with **CbC2$^{Me}$** (70 mg, 0.116 mmol) and HOTf (18 mg, 0.12 mmol, 1 equiv). Product obtained as a light-green solid. Yield after workup: 75 mg (80%). For NMR spectra (including the assigned $^1$H spectrum), see Figures A.31a and b.

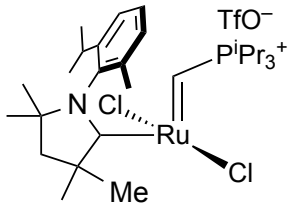


$^1$H NMR ($CDCl_3$, 500 MHz): δ 18.12 (d, $^2J_{HP}$ = 41.9 Hz, 1H, Ru=C*H*), 7.60 – 7.49 (m, 2H, *m*-C*H* of **C2$^{Me}$** Ar), 7.34 (d, $^3J_{HH}$ = 7.3 Hz, 1H, *p*-C*H* of **C2$^{Me}$** Ar), 3.20 – 3.11 (m, 3H, C*H* of P$^i$Pr$_3$), 3.10–3.05 (m, 1H, C*H* of **C2$^{Me}$** $^i$Pr), 2.30 (d, $^2J_{HH}$ = 1.6 Hz, 2H, backbone C$H_2$ of **C2$^{Me}$**), 2.22 (s, 3H, C$H_3$ of **C2$^{Me}$**), 2.18 (s, 3H, C$H_3$ of **C2$^{Me}$**), 2.13 (s, 3H, C$H_3$ of **C2$^{Me}$**), 1.46 (s, 3H, C$H_3$ of **C2$^{Me}$**), 1.39 – 1.34 (m, 6H, C$H_3$ of **C2$^{Me}$** and C$H_3$ of P$^i$Pr$_3$, overlapping), 1.30 (m, 5H, C$H_3$ of P$^i$Pr$_3$), 1.22 (m, 6H, C$H_3$ of P$^i$Pr$_3$), 0.87 (d, $^3J_{HH}$ = 6.6 Hz, 3H, C$H_3$ of P$^i$Pr$_3$). $^{13}$C{$^1$H} NMR ($CDCl_3$, 125 MHz): δ 254.6, 232.6, 148.4, 136.9, 130.3, 130.2, 126.6, 81.1, 51.9, 29.6, 29.3, 29.0, 28.7, 26.6, 24.3, 24.0, 23.9, 18.3, 18.2, 14.3. MALDI-TOF MS (pyrene matrix), *m/z*: [**PC2$^{Me}$–Cl,H**]$^+$ 715.171 (calc'd for $C_{29}H_{48}ClF_3NO_3PRuS$: 715.178).

**Synthesis of PC3$^{Ph}$:** As above, with **CbC3$^{Ph}$** (70 mg, 0.116 mmol) and HOTf (18 mg, 0.12 mmol, 1 equiv). Product obtained as a green solid. Yield after workup: 113 mg (82%). For NMR spectra (including the assigned $^1$H spectrum), see Figures A.32a and b.

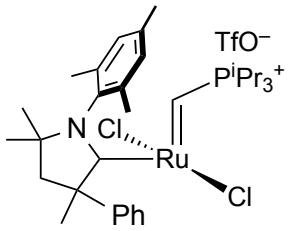


$^1$H NMR ($CDCl_3$, 500 MHz): δ 18.74 (d, $^2J_{HP}$ = 34.0 Hz, 1H, Ru=C*H*), 7.79 (s, 1H, *m*-C*H* of **C3$^{Ph}$** Mes), 7.53 (t, $^3J_{HH}$ = 7.7 Hz, 2H, *m*-C*H* of **C3$^{Ph}$** Ph), 7.38 (t, $^3J_{HH}$ = 7.5 Hz, 1H, *p*-C*H* of **C3$^{Ph}$** Ph), 7.26 (s, 1H, *m*-C*H* of **C3$^{Ph}$** Mes), 7.12 (d, $^3J_{HH}$ = 10.0 Hz, 2H, *o*-C*H* of **C3$^{Ph}$** Ph), 2.94 (m, 3H, C*H* of P$^i$Pr$_3$), 2.77 (s, 1H, backbone C$H_2$ of **C3$^{Ph}$**), 2.49 (d, $^2J_{HH}$ = 13.3 Hz, 1H, backbone C$H_2$ of **C3$^{Ph}$**), 2.38 (m, 9H, C$H_3$ of **C3$^{Ph}$**), 2.03 (s, 3H, C$H_3$ of **C3$^{Ph}$**), 1.50 (s, 3H, C$H_3$ of **C3$^{Ph}$**), 1.39 (s, 3H, C$H_3$ of **C3$^{Ph}$**), 1.11 (m, 18H, C$H_3$ of P$^i$Pr$_3$). $^{13}$C{$^1$H} NMR ($CDCl_3$, 125 MHz): δ 241.9, 140.5, 137.9, 136.5, 134.7, 131.4, 131.2, 130.6, 128.6, 126.3, 81.2, 64.0, 31.7, 30.5, 29.6, 28.1, 22.8, 22.1, 21.8, 21.1, 17.9, 17.8, 17.7, 14.3. MALDI-TOF MS (pyrene matrix), *m/z*: [**PC3$^{Ph}$–Cl, OTf**]$^+$ 615.201 (calc'd for $C_{32}H_{49}ClNPRu$: 615.233).

**Synthesis of PC1$^{Ph}$(I$_2$):** As above, with minor modifications: **CbC1$^{Ph}$(I$_2$)** (174 mg, 0.205 mmol) and HOTf (34 mg, 0.23 mmol, 1.1 equiv). $C_6H_6$ was chosen as the solvent to avoid possible halide exchange during reaction, which was stirred for 2.5 h at RT. Product obtained as an olive-green solid. Yield after workup: 179 mg (87%). For analysis, $CD_2Cl_2$ was used as the product is only sparingly soluble in $C_6D_6$. For NMR spectra (including the assigned $^1$H spectrum), see Figures A.33a and b.

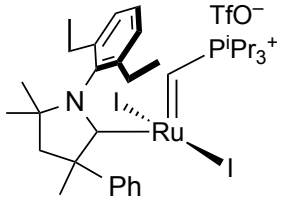


$^1$H NMR ($CD_2Cl_2$, 500 MHz): δ 16.66 (d, $^2J_{HP}$ = 30.1 Hz, 1H, Ru=C*H*), 8.71 (s br, 2H, C*H* of **C1$^{Ph}$** Ar or Ph), 8.10 (m br, 3H, C*H* of **C1$^{Ph}$** Ar or Ph), 8.03 – 7.88 (m br, 3H, C*H* of **C1$^{Ph}$** Ar or Ph), 3.70 (s br, 1H, backbone C*H* of **C1$^{Ph}$**), 3.44 (m, 3H, C*H* of P$^i$Pr$_3$), 3.31 – 3.23 (s br, 1H,

backbone C*H* of **C1$^{Ph}$**), 3.17 (m br, 1H, C$H_2$ of **C1$^{Ph}$** Ar), 3.07 (m br, 1H, C$H_2$ of **C1$^{Ph}$** Ar), 2.95 (m, 2H, C$H_2$ of **C1$^{Ph}$** Ar), 2.09 (d br, $^3J_{HH}$ = 5.7 Hz 3H, C$H_3$ of **C1$^{Ph}$** Ar), 1.92 (m, 7H, C$H_3$ of **C1$^{Ph}$** Ar and backbone, overlapping), 1.75 (m, 6H, C$H_3$ of **C1$^{Ph}$** backbone), 1.63 (m, 19H, C$H_3$ of P$^i$Pr$_3$). $^{13}$C{$^1$H} NMR ($CD_2Cl_2$, 125 MHz): δ 248.9, 146.6, 142.8, 142.1, 137.6, 132.7, 131.5, 130.6, 128.4, 124.3, 81.1, 63.4, 33.3, 32.1, 31.4, 28.4, 28.0, 25.5, 21.9, 21.6, 19.9, 19.6, 19.0, 18.8, 18.2, 17.2, 17.0, 14.3, 14.1. MALDI-TOF MS (pyrene matrix), *m/z*: [**PC1$^{Ph}$(I$_2$)**]$^+$ 721.130 (calc'd for $C_{33}H_{51}INPRu$: 721.184).

### Synthesis of Pyridine Adducts RuX$_2$(L)(py)$_n$(=CH$_2$), mBpy$^X$

The pyridine adducts were prepared according to the method reported for **mC1$^{Ph}$** and **mGIII** (Scheme 3.8).[8,69] For convenience, a representative procedure is provided for **mC1$^{Ph}$**.

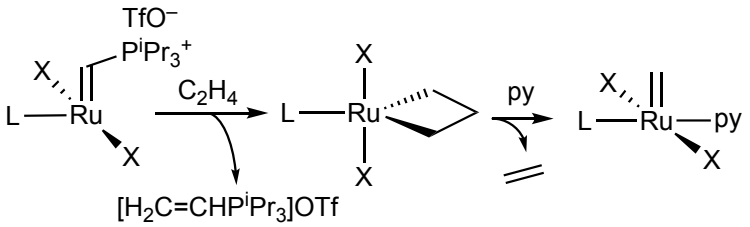


**Scheme 3.8. Synthesis of Pyridine Adducts from the Corresponding Piers Complexes**

**Representative Procedure for Synthesis of RuCl$_2$(C1$^{Ph}$)(py)(=CH$_2$), mC1$^{Ph}$** In a 10 mL Schlenk flask, a dark-green solution of the **PC1$^{Ph}$** (100 mg, 0.117 mmol) in 2 mL $CH_2Cl_2$ was frozen in $N_{2(l)}$. The sample was freeze-pump-thaw degassed 3x, and thawed under 1 atm ethylene at –45 °C (MeCN–dry ice bath). The resulting dark red solution was stirred for 15 min, briefly exposed to vacuum to remove ethylene, then stirred under $N_2$. A solution of pyridine (18.7 μL, 0.231 mmol, 2 equiv) in 500 μL *n*-hexane, chilled in an ethanol-$N_{2(l)}$ cold bath (–110 to –80 °C), was then added via syringe as a slow dribble down the flask wall (ca. 10 sec). The solution rapidly turned dark green, then brown-yellow. The mixture was stirred for a further 10 min. Cold *n*-hexane (4 mL; –110 to –80 °C) was then added using a dry-ice-chilled cannula. The mixture was stirred for 10 min to precipitate the phosphonium salt [$H_2C$=CHP$^i$Pr$_3$]OTf as a brown solid, leaving an orange supernatant. The latter was filtered cold, and the orange filtrate was immediately stripped to dryness at –45 °C to afford yellow **mC1$^{Ph}$**. The flask containing solid **mC1$^{Ph}$** was transferred to a –35 °C freezer inside a glovebox until use.

NMR data for **mC1$^{Ph}$** and **mGIII** agree with values reported.[69] For NMR spectra, see Figures A.34–A.37. Key [Ru]=C$H_2$ signals: $^1$H NMR ($CDCl_3$, 500 MHz, –40 °C): **mC1$^{Ph}$**, δ 18.35 ppm; **mH$_2$IMes**, δ 18.76 ppm; **mC1$^{Me}$**, δ 17.98 ppm; **mC3$^{Ph}$**, δ 18.31 ppm; **mC1$^{Ph}$**, δ 16.73 ppm; **mC2$^{Me}$**, 18.22 ppm (not isolated, generated in situ).

**Bimolecular Coupling of Methylidene Complex mBpy$^{X}$**

The procedure for the coupling reaction is summarized in Scheme 3.9. In our original study, the objective was quantitation of ethylene evolved from **mC1$^{Ph}$**, and considerations of purity were minor.[69] The solid methylidene complex **mC1$^{Ph}$** was thus not purified to remove the phosphonium salt [$H_2C$=CHP$^{i}$Pr$_3$]OTf. In the present kinetics study, the phosphonium salt was removed (see above) to improve accuracy in the concentrations of **mBpy$^{X}$**. The resulting powder had a high static charge, and could not be weighed: moreover, the CAAC complexes were obtained in very low yields owing to their much faster decomposition. Samples were therefore made up by adding a known volume of cold $CDCl_3$ to the Schlenk flask to dissolve the complex, and transferring the solution to an NMR tube containing a known volume of a stock solution of DMT. To protect against warming, the IS stock solution, NMR tubes, pipettes, $CDCl_3$ and sand-bath were stored in the glovebox freezer (–35 °C) for at least 12 h prior to use. To ensure accuracy in NMR integration, the recycle delay (d1) was raised to 0.1 sec from 0.01 sec.

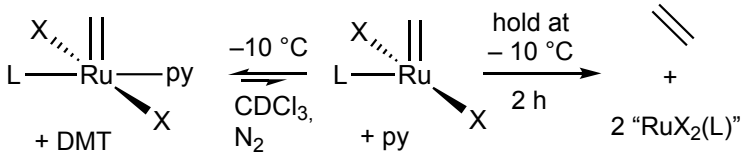


**Scheme 3.9. Bimolecular decomposition: coupling of methylidene species.**

**Representative Procedure for Bimolecular Coupling of mC1$^{Ph}$:** The Schlenk flask containing solid **mC1$^{Ph}$** was removed from the glovebox freezer and bedded in a cold sand-bath (chilled to −35 °C by storing in the freezer overnight). To a J-Young NMR tube also bedded in the sand-bath was added cold DMT (20.0 μL of a stock solution of 10 mg DMT in 1 mL $CDCl_3$; 1.03 μmol); NMR integration standard (IS). Solid **mC1$^{Ph}$** was dissolved in cold $CDCl_3$ (0.6 mL) and transferred to the NMR tube via a chilled pipette. The NMR tube was sealed, transported to the NMR facility in a dry-ice acetonitrile bath (−45 °C), then quickly shaken and inserted into an NMR probe precooled to −40 °C. The initial integration ratio of **mC1$^{Ph}$** vs IS was measured, after which the NMR probe was warmed to –10 °C to effect liberation of four-coordinate **B-C1$^{Ph}$**. After an initial 15 min period for thermal equilibration, loss of the [Ru]=C$H_2$ NMR signal was measured over time: see Figure 3.3 in the main text.

The same procedure was carried out for **mC1$^{Me}$**, **mC3$^{Ph}$** and **mC1$^{Ph}$**. For $H_2$IMes complex **mGIII**, a higher volume of 1.2 mL $CDCl_3$ was used to reduce the headspace, to ensure that any propenes formed via β-H elimination could be detected (none were observed).

*References for Chapter 3 begin on p. 92*

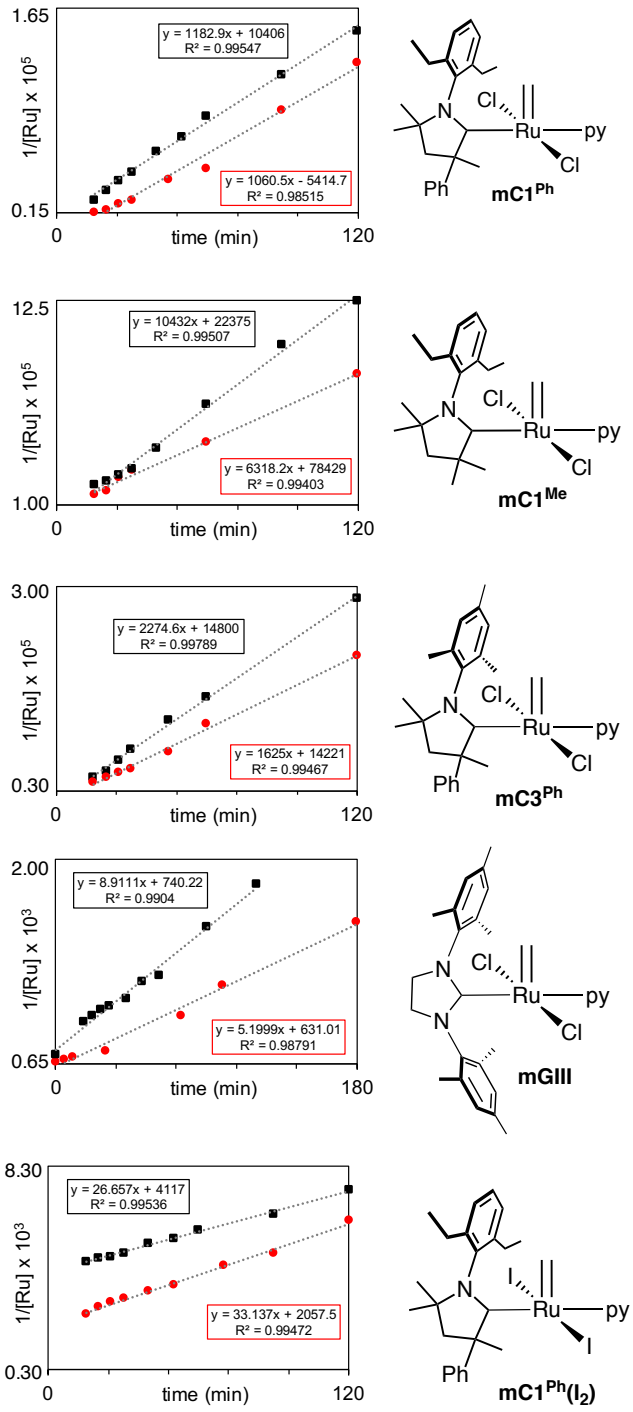


**Figure 3.6. Second-order plots for BMC reaction at –10 °C.**

### 3.3.5. Subsequent Advances Relevant to Section 3.3

The discovery of the stronger trans influence of the CAAC ligands, relative to $H_2$IMes, has further profound implications for β-H elimination. As the principal element of that work is a

DFT study by co-workers (the subject of a manuscript now in preparation), only the key conclusion is outlined here. In short, the transition state for this decomposition pathway involves a structure in which the β-C-H bond of the metallacyclobutane is sited trans to the CAAC or NHC ligand. The susceptibility to β-hydride elimination is determined largely by the trans influence of this carbene. The significantly higher trans influence of the CAAC ligands increases the energy of this transition state, reducing susceptibility to this decomposition reaction.

---

## 3.4. Challenging Metathesis Catalysts with Nucleophiles and Brønsted Base: The Stability of State-of-the-Art Catalysts to Attack by Amines

### 3.4.1. Introduction

Widely embraced in organic synthesis, olefin metathesis has now begun to emerge in pharmaceutical manufacturing, particularly for the production of antiviral therapeutics.[3] Among the most important catalysts used in the latter context is the nitro-Grela complex **nG** (Chart 3.3),[70] which is stabilized by an N-heterocyclic carbene (NHC) ligand.

**Chart 3.3. Metathesis catalysts discussed.**

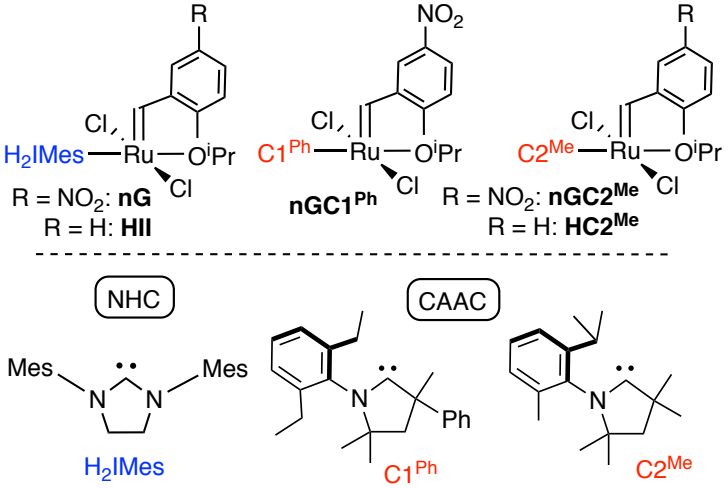


Large-scale implementation, however, brings new demands for robustness, reliability, and mechanistic understanding (the latter encompassing both intended and unintended chemistries).[71a] From this perspective, olefin metathesis falls short of other catalytic methodologies, such as hydrogenation and cross-coupling, which are now mainstays of pharmaceutical manufacturing.[71] Grubbs' pioneering development of ruthenium metathesis catalysts,[72] with their dramatically improved tolerance for oxygen and water relative to their group 6 predecessors, was *the* development that put olefin metathesis into the hands of the practicing organic chemist. Nevertheless, reports of the instability of the active species date back nearly 20 years.[50b,11,73,74] Like the majority of metathesis catalysts, the Ru-NHC catalysts readily

degrade via β-elimination of the metallacyclobutane ring from $\mathbf{A^R}$ (Scheme 3.10a), and bimolecular coupling of [Ru]=CHR intermediates (Scheme 3.10b).[7,47]

These challenges provide context for the breakthrough importance of cyclic alkyl amino carbene (CAAC) derivatives that resist β-elimination[47] notwithstanding efforts to reverse catalyst decomposition.[75] Dramatically higher turnover numbers (TON) have been achieved with Ru-CAAC catalysts, relative to their NHC predecessors, in high-profile applications that include macrocyclization and the production of α-olefins from renewable oleate esters.[16,18,19] Importantly, the improved productivity achieved by shutting down β-elimination permits use of lower catalyst concentrations, which in turn diminishes bimolecular decomposition. The resulting step-change in efficiency has the further potential to alleviate challenges to continuous-flow metathesis.[14,76,77]

**Scheme 3.10. Major intrinsic decomposition pathways established for Ru-$H_2$IMes metathesis catalysts.[a]**

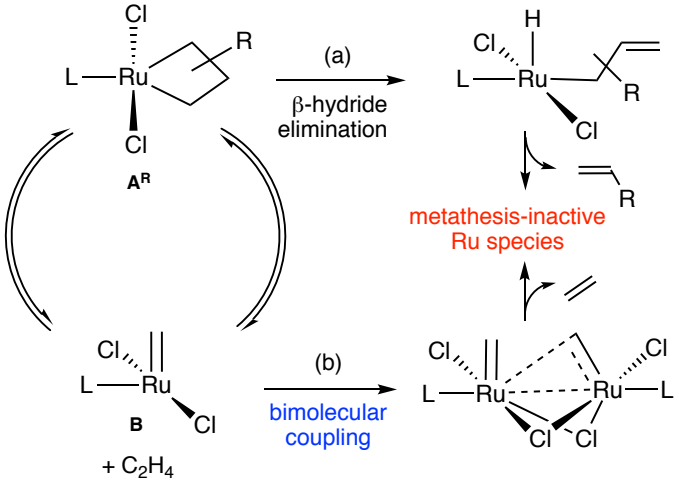


[a] An additional ring-expansion pathway has been established for olefins bearing an α-alkyl substituent.[75a]

To date, however, little study has focused on the susceptibility of the CAAC catalysts to decomposition by exogenous agents.[78] Of particular importance are amines. Amines may be present as minor contaminants (for example, morpholine is reportedly present in ppm levels in technical-grade toluene),[79a] or as functional groups on the substrate, and hence present in very high proportions relative to the catalyst. The ubiquity of nitrogen centers in active pharmaceutical ingredients (APIs) underscores the importance of understanding their unintended reaction chemistry.[80] Even trace amines can have a major impact on the viability of metathesis reactions. Morpholine and DBU contaminants were shown to severely degrade the performance of early ruthenium catalysts in process chemistry campaigns at Boehringer-Ingelheim[79a] and GlaxoSmithKline.[79b] More generally, problematic catalyst performance has led to the widespread adoption of protection strategies for primary or secondary amines and amides,[81] as well as pyridines.[82]

*References for Chapter 3 begin on p. 92*

We have established two major pathways by which amines attack the metathesis-active species. These are deprotonation of $\mathbf{A^R}$ (Scheme 3.11a),[35-37] and nucleophilic abstraction of the methylidene ligand from **B** (by, e.g., $NH_2{}^nBu$; Scheme 3.11b; related chemistry has been established for $PCy_3$-stabilized catalysts).[36,55,83]

**Scheme 3.11. Amine-induced decomposition pathways.**

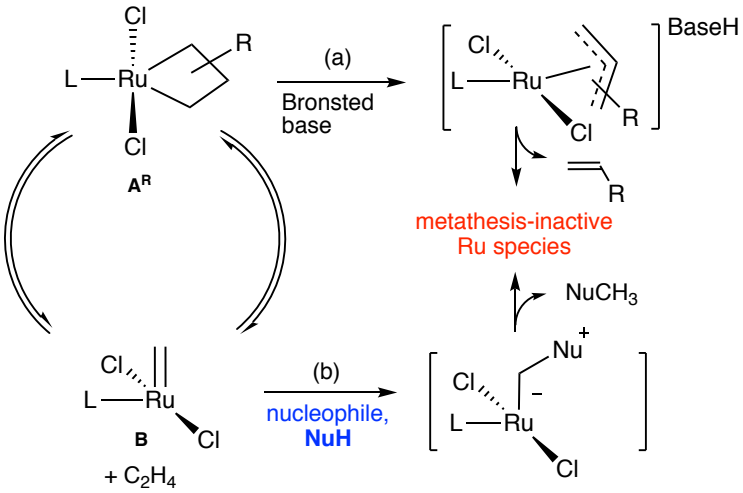


These pathways are curtailed where basicity and nucleophilicity are limited. For example, anilines are not only compatible with Ru-catalyzed metathesis, but can be valuable ancillary ligands.[84] Tertiary amines are likewise widely regarded as innocuous, owing to steric protection of the nitrogen site,[81a,b] but scattered reports, including recent model studies,[36] suggest that even these may trigger catalyst decomposition. Here we examine the productivity of leading NHC and CAAC catalysts (Chart 3.3) when challenged by amines of varying size, basicity and nucleophilicity.

### 3.4.2. Results and Discussion

**Impact of amines on metathesis productivity.** In the present work, we focused on the impact of amines of widely differing bulk and basicity.[85] Three of these have been established as problematic in pharma and elsewhere (see Chart 3.4 and discussion above). As well, $NEt_3$ was evaluated, in light of ambiguities concerning whether tertiary amines are in fact innocuous.[36,86] Catalysts surveyed are selected as representing the current state of the art: they include the CAAC complexes $\mathbf{nGC1^{Ph}}$, $\mathbf{nGC2^{Me}}$, and $\mathbf{HC2^{Me}}$ (which collectively afford the highest metathesis TONs reported to date),[16-19] and the important, widely-used NHC analogue **nG**.

**Chart 3.4. Amines examined, and p$K_a$ of the conjugate acid.**

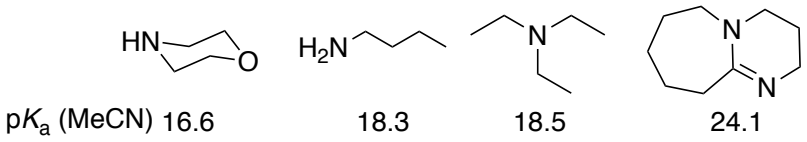


The benchmark substrate diethyl diallylmalonate (**2**, Figure 3.7) was chosen for these studies, because its exceptional ease of cyclization means that any agents that inhibit RCM merit attention. Reactions were undertaken in toluene (now the most widely used solvent for metathesis),[86b] in the presence of 1 equiv amine per Ru. In the TON studies, we employed catalyst loadings of 9 ppm (0.0009 mol% Ru), both to ensure that the impact of added amine is not masked by excessive catalyst loadings, and to approximate targeted catalyst loadings. To assess whether heat reinforces or mitigates negative impacts, RCM was carried out at 25 and 70 °C.

The radar plots of Figure 3.7 give a direct visual comparison of productivity for all four catalysts, and the impact of amine on each. The maximum TON attained in the *absence* of amine is indicated on the vertical radial line, with each of the remaining "spokes" depicting the impact of a specific amine. Greater deviations from the outermost point toward the center signify lower productivity, i.e. a greater negative impact.

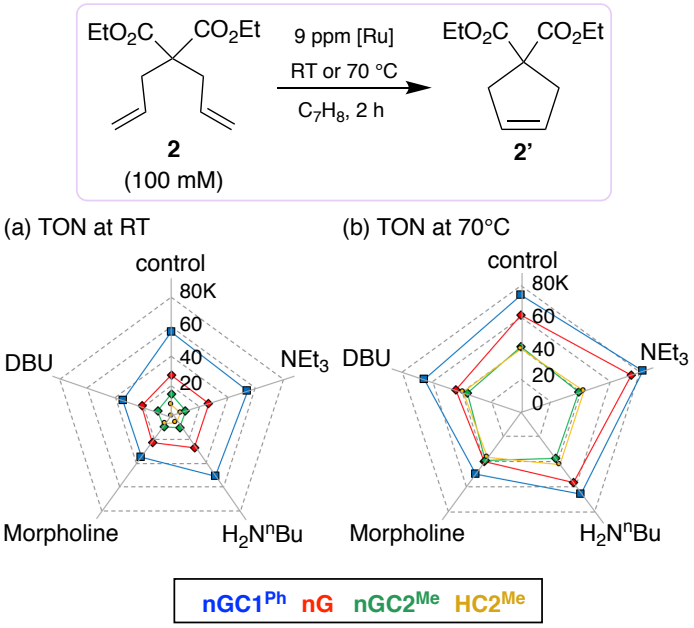


**Figure 3.7. Radar plots showing impact of amine on TON (1 equiv vs Ru). (a) At RT: $TON_{max}$ ca. 60,000. (b) At 70 °C: $TON_{max}$ ca. 80,000.**

*References for Chapter 3 begin on p. 92*

As no direct comparison of all four catalysts has previously been reported, we begin by analyzing their performance in the control reaction: that is, in the absence of amine (vertical spoke). The outermost data-point on the pentagonal line indicates the maximum TON achieved using the top-performing catalyst **nGC1$^{Ph}$**: 56,700 at RT (Figure 3.7a), or 74,400 at 70 °C (Figure 3.7b). The maximum TON for $H_2$IMes analogue **nG**, in comparison, was 27,800 or 61,100, at RT or 70 °C, respectively. The drop relative to **nGC1$^{Ph}$** reflects the vulnerability of the NHC catalysts to β-hydride elimination (see Scheme 3.10a), a decomposition pathway to which the CAAC catalysts are nearly immune.[69] Of note, however, the difference in performance between **nG** and **nGC1$^{Ph}$** is far less in this reaction than in the contexts noted above.

Least productive were **nGC2$^{Me}$** and **HC2$^{Me}$**, with TONs of 14,400 and 7,800, respectively (a difference that disappears at higher temperature, as the slower initiation of **HC2$^{Me}$** is erased: both catalysts then deliver a TON of ca. 40,000). We attribute this drop in productivity to the poor steric protection conferred by the small quaternary $CMe_2$ group of **C2$^{Me}$**, and consequently faster bimolecular decomposition (Scheme 3.10b). While bimolecular decomposition of the **C2$^{Me}$** derivative has not been directly examined, the fact that TONs *decrease* for **C2$^{Me}$** derivatives when catalyst loadings are tripled from 1 to 3 ppm suggests an even greater vulnerability with decreasing CAAC size.[16]

The trend in catalyst productivity was unaffected in the presence of amine, with **nGC1$^{Ph}$** remaining most productive. A deleterious impact was observed in all cases, however, increasing in the order $NEt_3$ ~ $NH_2{}^nBu$ << morpholine ~ DBU. For $NH_2{}^nBu$ and $NEt_3$, this impact was relatively minor. This is important given model studies with Ru-$H_2$IMes catalysts, which indicated nucleophilic abstraction of the methylidene ligand by $NH_2{}^nBu$,[55] and MCB deprotonation by $NEt_3$,[36] on reaction with 10 equiv styrene and amine. The present work demonstrates that under conditions more relevant to catalysis, decomposition by $NEt_3$ and $NH_2{}^nBu$ does not significantly compete with metathesis. Morpholine and DBU caused greater declines in TON (ca. 40% at RT for **nGC1$^{Ph}$**), but this could generally be mitigated by use of high temperatures, most significantly for DBU.

Also noteworthy is the *beneficial* impact of small proportions of $NEt_3$ at 70 °C: this increased TONs relative to the base-free control by ca. 10%, for both **nGC1$^{Ph}$** and **nG**. (When the proportion of base was increased from 1 to 10 equiv vs **nGC1$^{Ph}$**, however, the TON dropped by 4,000). Improved TONs were likewise observed for an independent batch of **2**, albeit at a slightly lower level. In contrast, no improvement was seen for two other substrates (styrene and a pro-lactone: see Table 3.5), suggesting that the beneficial impact of $NEt_3$ is due to suppression of contaminants present in **2**. Beller, Kadyrov and co-workers have noted that, despite its benchmark status, diene **2** contains a wide range of contaminants (including butanedioic acid and 2-acetyl-2-allylpent-4-enoic acid).[87] They established the beneficial impact of several additives, although amines were omitted. The observed decline in TONs when a larger excess of $NEt_3$ was

added presumably reflects MCB deprotonation. We previously demonstrated that $NEt_3$ is able to deprotonate $\mathbf{A^R}$, albeit more slowly than stronger bases such as Proton Sponge.[36]

The discussion so far has focused on the core issue from a synthetic perspective: identification of catalysts and conditions that deliver highest TON despite the presence of amine. **nGC1$^{Ph}$** emerges as the top-performing candidate, and high temperatures as beneficial. Unexpectedly, however, $H_2$IMes catalyst **nG** does not fall far short, delivering 70-90% of the TONs of **nGC1$^{Ph}$** at 70 °C. This contrasts with the orders-of-magnitude superiority of CAAC vs NHC catalysts in ethenolysis, and their ca. 5-fold superiority in mRCM.[16,17,19]

Also striking is the performance of the **C2$^{Me}$** catalysts, for which Figure 3.7b indicates essentially no impact for any amine at 70 °C. This "tolerance" is due to much faster decomposition by amine-independent pathways, most probably bimolecular decomposition, to which these sterically less protected catalysts are particularly susceptible, as noted above. Catalyst decomposition has previously been shown to follow unique pathways for sufficiently small carbene ligands.[88] Given that other decomposition pathways overtake those induced by amine in the present case, the **C2$^{Me}$** catalysts are omitted from further analysis.

If stronger σ-donation results in a more electron-rich Ru center for the CAAC catalysts vs their $H_2$IMes analogues, **nGC1$^{Ph}$** might be expected to resist attack by nucleophiles or Brønsted base to a greater extent than **nG**. To probe this point, we plot in Figure 3.8 the amine-tolerance of **nGC1$^{Ph}$** and **nG** independent of inherent catalyst productivity: that is, as the *percent* of activity retained in the presence of amine. Unexpectedly, comparable amine-tolerance is evident, despite the steric and electronic distinctions between the **C1$^{Ph}$** and the $H_2$IMes ligands. Although **nGC1$^{Ph}$** is slightly more sensitive to morpholine and DBU at RT, the differences are erased at 70 °C; indeed, the CAAC catalyst exhibits slightly higher stability to DBU. This point is examined computationally below.

*References for Chapter 3 begin on p. 92*

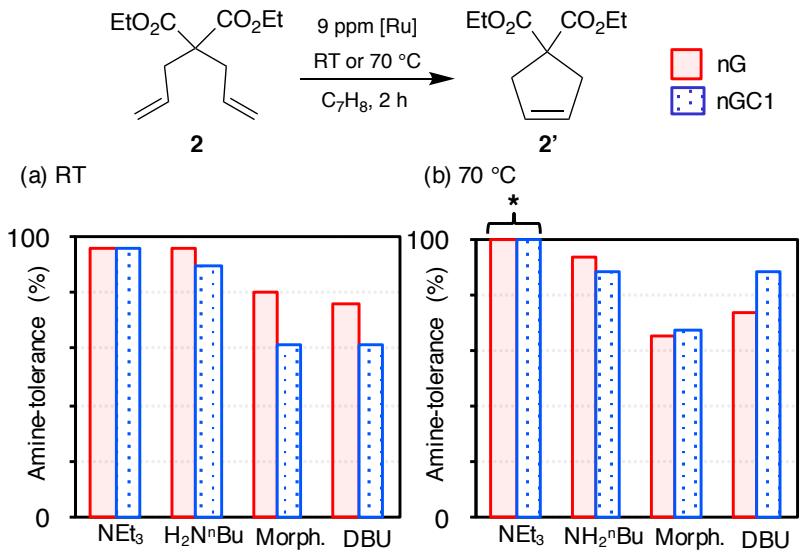


**Figure 3.8. Amine-tolerance of nG and nGC1$^{Ph}$ in RCM of 2 (100 mM). (a) At RT; (b) At 70 °C. Amine-tolerance =[100 – ($TON_{control}$ – $TON_{amine}$)/ $TON_{control}$] x 100. *The value for $NEt_3$ in (b) exceeds 100 (nG: 122%; nGC1$^{Ph}$: 110%), indicating that the TON is higher than that in the control experiment. See discussion in text.**

A final set of experiments examined important mechanistic points for the two most deleterious amines. Here we wished to extract the rate at which DBU decomposes **nG** and **nGC1$^{Ph}$**, relative to the background β-hydride elimination, and to establish the pathway by which morpholine effects decomposition. The decomposition pathway for DBU was previously examined for **HII**. Unsurprisingly, given the high basicity of DBU (by far the strongest base examined: see the p$K_a$ values of Chart 3.3), it deprotonates the metallacyclobutane intermediate **A$^R$** (Scheme 3.11a).[36] An important question, however, is the relative rate of deprotonation relative to competing β-H-elimination (Scheme 3.10a). Both reactions liberate propenes. To assess their respective rates, we measured the total yield of propenes during metathesis of styrene, and subtracted that formed via β-hydride elimination (Figure 3.9).

Deprotonation is clearly very rapid for **nG**, as indicated by the elimination of >50% propenes within 5 min in the presence of DBU, vs 2% in its absence. Disappearance of alkylidene signals is complete in 30 min. In comparison, 34% deprotonation is seen within 5 min for CAAC catalyst **nGC1$^{Ph}$** (which, as noted above, undergoes essentially no β-H elimination). Deprotonation reaches nearly 60% by 30 min. This should be viewed as a lower limit, however, given the propensity to competing bimolecular coupling at the 20 mM Ru concentrations required for this experiment. The latter accounts for the plateau in propene yields at ca. 10 min. Nevertheless, it appears that **nG** and **nGC1$^{Ph}$** are readily attacked by DBU (Figure 3.9c), at broadly similar rates. This implies that the distinct electronic properties of the CAAC ligand[31-33,89] do not greatly affect the vulnerability of the MCB. This point is probed by computational analysis in the final section.

*References for Chapter 3 begin on p. 92*

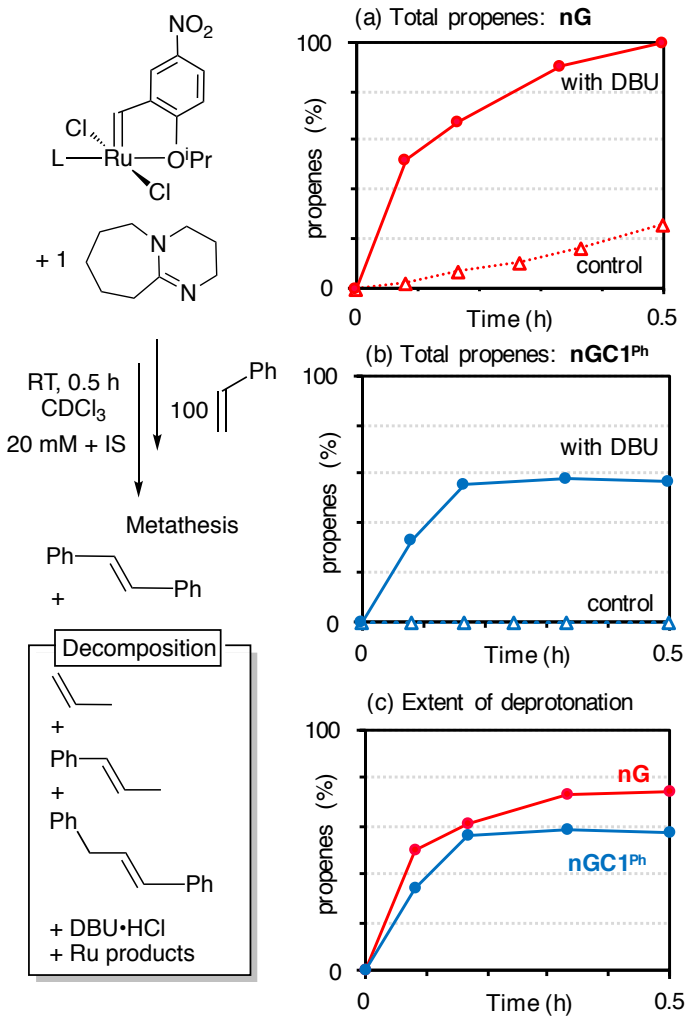


**Figure 3.9. Assessing rates of MCB deprotonation relative to β-H elimination for nG and nGC1$^{Ph}$ (NMR analysis; 20 mM Ru), showing propene products and yields.**

The mechanism by which morpholine decomposes metathesis catalysts, somewhat surprisingly, has not been explored. Only ca. 5% propenes was observed on repeating the experiment of Figure 3.9 with **nGC1$^{Ph}$** and morpholine (Figure A.38). MCB deprotonation is evidently a minor pathway, consistent with the low basicity of morpholine indicated in Chart 3.4. We therefore examined the possibility that morpholine engages in nucleophilic abstraction of the methylidene from **B**, as previously shown for the primary amine $NH_2{}^nBu$ (Scheme 3.11b).[35]

To probe this point, a CAAC derivative of the Piers catalyst (see **PC1$^{Ph}$**, Scheme 3.12) was treated with ethylene at –45 °C in $CDCl_3$. Because the Piers catalysts initiate irreversibly (that is, the bulky phosphonium ylide released from the benzylidene resists re-uptake), they afford clean entry to the active species. Injection of cold morpholine caused the solution to immediately change colour from dark red to orange-brown, and an alkylidene signal assigned to a morpholine adduct was detected at 18.57 ppm.[47] After warming to 25 °C to complete formation and

decomposition of the **Ru-2** intermediate, N-methylmorpholine **13** was observed in 43% yield. The balance is presumed to be due to bimolecular coupling, which is markedly more aggressive for **B-C1$^{Ph}$** than its $H_2$IMes analogue.[47] Neither propenes nor morpholine•HCl from deprotonation of **A-C1$^{Ph}$** were observed, consistent with the deleterious role of morpholine stemming from its nucleophilicity, rather than its Brønsted basicity.

**Scheme 3.12. Confirming methylidene abstraction by morpholine.**

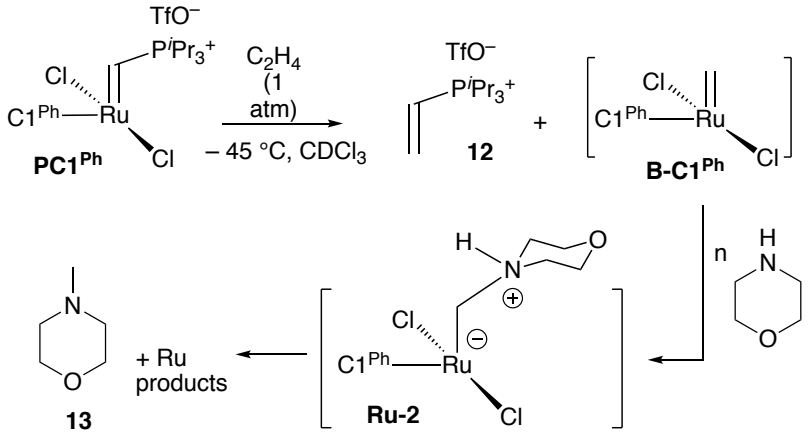


**Computational Studies.** Density functional theory (DFT) analysis was undertaken to probe the susceptibility of **nG** to deprotonation by DBU, as compared to β-elimination or continued metathesis (i.e. retro-addition to eliminate ethylene). These pathways, with the corresponding energy barriers in brackets, are shown in Scheme 3.13. Deprotonation of **A-H$_2$IMes** led to a single transition state for proton transfer to DBU (**TS-1**), with a free energy of 12.6 kcal/mol relative to **nG**, as compared to 12.0 kcal/mol for concerted bond breaking and rotation of ethylene (which represents the upper bound for continued metathesis: see Supporting Information), and 26.7 kcal/mol for β-elimination. Thus, deprotonation is predicted to be much faster than β-elimination, in agreement with the experimental results in Figure 3.9.

*References for Chapter 3 begin on p. 92*

**Scheme 3.13. Calculated Free Energies for Reactions of MCB Intermediate A-$H_2$IMes. (a) Metathesis (Retro-Addition). (b) β-Hydride Elimination. (c) Deprotonation by DBU.**[a]

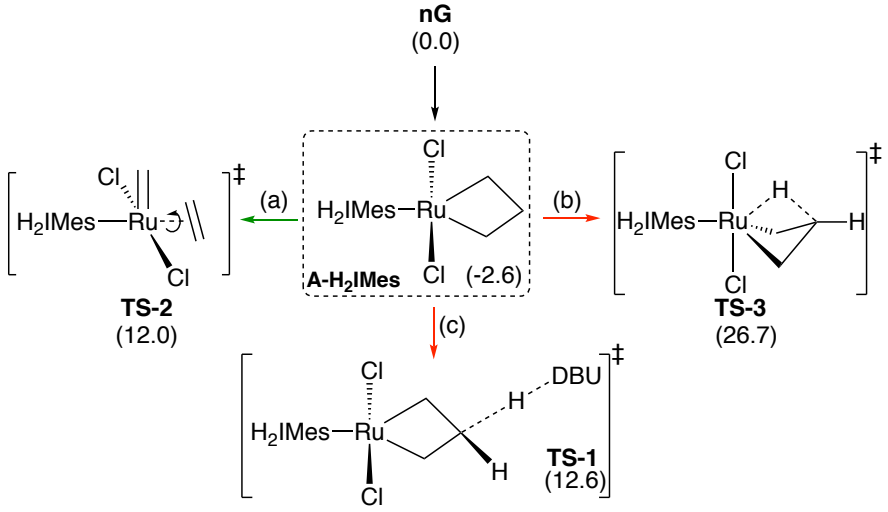


[a] Given in brackets are activation free energies (kcal/mol vs **nG,** calculated using the PBE-D3BJ-SMD computational model with chloroform as solvent.

For the CAAC system, the complexity of analysis is significantly increased by the lack of symmetry in the **C1$^{Ph}$** ligand. We therefore focused on assessing the barrier to deprotonation of the metallacyclobutane **A-C1$^{Ph}$**, for comparison with the $H_2$IMes system. Proton transfer to DBU from **A-C1$^{Ph}$** can proceed via four isomers of comparable energy. The calculated free energy barriers for deprotonation were 14–20 kcal/mol relative to the precatalyst, depending on isomer, solvent, and functional. Importantly, however, the barrier for the most favorable pathway from **nGC1$^{Ph}$** is very similar to that for **nG** (within 1.4 kcal/mol, relative to the precatalyst, or 0.3 kcal/mol, relative to the MCB), and DBU is thus predicted to deprotonate the MCB at similar rates, as indeed observed experimentally.

The thermodynamics of proton abstraction likewise indicate similar acidity for the **C1$^{Ph}$** and $H_2$IMes intermediates. To exploit error cancellation, we evaluated the energetics of the acid-base equilibrium between each MCB and its conjugate base, the allylic anion **Ru-3-$H_2$IMes** or **Ru-3-C1$^{Ph}$** (Scheme 3.14). With a calculated reaction Gibbs free energy of 2.0-3.7 kcal/mol, depending on the computational model used, the equilibrium favours the deprotonated **C1$^{Ph}$**-complex **Ru-3-C1$^{Ph}$** to a small extent. In short, the acidity of the **nG** and **nGC1$^{Ph}$** MCB intermediates is predicted to be comparable.

**Scheme 3.14. Assessing relative acidity of the MCB β-H for the C1$^{Ph}$ and H$_2$IMes systems.**[a]

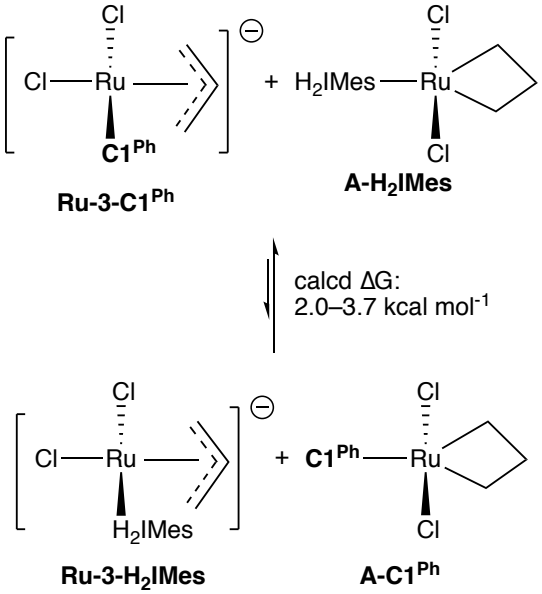


[a]Calculated using the PBE-D3BJ-SMD computational model with chloroform as solvent.

The similar propensity of the **nG** and **nGC1$^{Ph}$** systems to deprotonation by base was initially unexpected. Although CAAC ligands are better π-acceptors than NHCs, their net electron-donor capacity (that is, the difference between σ-donation and π-back-donation) is consistently described as better than that of the NHC ligands.[32] Increased electron-donation from the carbene might be expected to reduce the acidity of the MCB β-proton in **nGC1$^{Ph}$**. However, minimal differences are seen in the Tolman electronic parameter (TEP; the ν(CO) stretching frequencies of Ni(CO)$_3$(L) complexes)[90] for representative CAACs and their NHC counterparts,[33,91] suggesting that any increase in *overall* donating capacity for the CAACs may be modest.

Natural charge analysis indeed indicates that **C1$^{Ph}$** and H$_2$IMes donate essentially the same number of electrons in the MCB intermediate (0.496 for **A-H$_2$IMes**, and 0.484 for **A-C1$^{Ph}$**). Thus, despite the significant differences in the electronic properties of the CAAC and NHC ligands, the better σ-donor capacity of the CAACs is offset by their better π-acceptor properties.[32,33] Comparable net electron-donation to the ruthenacyclobutane fragment of **nG** and **nGC1$^{Ph}$** accounts for their similar susceptibility to proton abstraction by base.

### 3.4.3. Conclusion

Amines are ubiquitous as functional groups and contaminants in olefin metathesis. The foregoing describes the impact of selected amines on state-of-the-art catalysts containing CAAC and NHC ligands. The amines studied were chosen for the documented risk they pose to metathesis productivity, or, in the case of the tertiary amine NEt$_3$, to test a widely-presumed innocuousness. The order of increasing negative impact was NEt$_3$ ~ NH$_2$$^n$Bu << morpholine ~ DBU, with NEt$_3$ and NH$_2$$^n$Bu showing very minor effects, and DBU and morpholine being much more damaging. In general, deleterious effects diminished at elevated temperatures. The impact of amine does not

group by mode of decomposition. Thus, $NEt_3$ and DBU, both of which act by deprotonating the MCB, represent the least and one of the most deleterious amines, respectively, and irrespective of temperature. Similarly, morpholine is much more aggressive than the primary amine $NH_2{}^n$Bu, although both decompose the catalysts by nucleophilic attack on the [Ru]=CHR moiety.

The CAAC catalyst **nGC1$^{Ph}$** proved most productive in the presence of amines, with TONs up to ca. 50,000 to 80,000. Unexpectedly competitive performance was observed for the $H_2$IMes analogue **nG**, which delivered TONs ranging from 70–90% those attained with **nGC1$^{Ph}$**. The difference in TON between the CAAC and NHC catalysts in the test reaction employed here (RCM of diethyl diallylmalonate **2**) is much less substantial than in more challenging reactions, however, and greater margin of difference in amine-sensitivity may thus be apparent in other contexts. Nevertheless, **nG** and **nGC1$^{Ph}$** were found to undergo deprotonation by base at broadly comparable rates. On the basis of DFT calculations, this similarity is attributed to comparable net electron-donation by the $H_2$IMes and **C1$^{Ph}$** ligands. The Ru centers in the metallacyclobutane intermediates are consequently comparably electron-rich, and the β-protons of the MCB are hence similar in their acidity and susceptibility to abstraction by base.
Finally, the **C2$^{Me}$** catalysts were found to be least productive, but also least sensitive to amine. A simple explanation accounts for this initially puzzling observation: it does not indicate that the smaller **C2$^{Me}$** catalysts are in fact immune to attack by amines, but that bimolecular decomposition is considerably faster. The latter reaction thus out-competes decomposition by amines where the carbene is sufficiently small.

### 3.4.4. Experimental Details for Section 3.4

**General Experimental Procedures.** Reactions were carried out under $N_2$ using glovebox or Schlenk techniques, unless otherwise noted. Toluene (Fisher, HPLC grade) was distilled over $P_2O_5$ and stored under $N_2$ over 4 Å molecular sieves for at least 18 h prior to use. $CDCl_3$ (Cambridge Isotopes) was degassed by 5 freeze/pump/thaw cycles, and stored as above. Diethyl diallylmalonate (**2**, TCI, 98%) and styrene (**11**, Sigma, >99%) were degassed similarly, and stored in the glovebox freezer (–35 °C). $NH_2{}^n$Bu (Alfa, 99%), morpholine (Sigma, >99.5%), DBU (Alfa, 99%) and $NEt_3$ (Sigma, >99.5%) were degassed and stored under $N_2$. Literature methods were used to prepare diene **1**,[92] macrolactone **1'**[92] and catalysts **nGC2$^{Me}$**,[18] **HC2**,[16] **nG**[70] and **PC1$^{Ph}$**;[47] **nGC1$^{Ph}$** was kindly supplied by Apeiron Synthesis. Ethylene (BOC Gases; Linde, 99.9%) and internal standard dimethyl terephthalate (DMT, Aldrich, 99%) were used as received. $^1$H NMR spectra were recorded on Avance II 500 spectrometer at 23 °C, unless otherwise specified. Chemical shifts are reported in ppm, and referenced to the residual proton signal of the deuterated solvent. RCM experiments were analyzed using an Agilent 7890A gas chromatograph (GC) equipped with auto-sampler, flame ionization detector (FID) and Agilent HP-5 polysiloxane column (30 m length, 320 μm diameter). Calibration curves of peak areas versus concentration were established for substrates and products in the relevant concentration regimes,

using ca. 1:1 (w/w) sample versus dodecane as internal standard; for NMR analysis they were confirmed by integration vs dodecane.

**Catalysis Experiments.** Stock solutions of each amine were prepared by dissolving 2.0 μL of the amine in $C_7H_8$ (20.0 mL), and diluting a 1.0 mL aliquot to 10.0 mL with $C_7H_8$. All were stored in the glovebox freezer (–35 °C) and allowed to come to thermal equilibrium at RT for ca. 20 min before use. For experiments probing the impact of amine, these stock solutions were added immediately prior to catalyst addition. Stock solutions of catalyst were prepared immediately prior to use (10 mg catalyst in 20.0 mL $C_7H_8$, and diluting a 1.0 mL aliquot to 10.0 mL with $C_7H_8$. Heated reactions were carried out in a degassed oil bath in the glovebox at 70 ±1 °C, with thermal equilibration for 10 min prior to catalyst addition.

**Representative Procedure for RCM of Diethyl Diallylmalonate (2) with nGC1$^{Ph}$.** (a) Control experiment. To **2** (97.0 μL, 0.400 mmol) and dodecane (91.0 μL, 0.400 mmol, 1 equiv; internal standard for GC analysis) was added 3.76 mL $C_7H_8$ to give a final concentration of 100 mM **2**. A 100 μL aliquot was removed for GC-FID analysis to establish the initial ratio of **2** to dodecane. To the stirred solution was added **nGC1$^{Ph}$** (49.0 μL of a stock solution of 10 mg **nGC1$^{Ph}$** in 200 mL; serial dilutions, see above; 3.6 nmol, 0.0009 mol%). After 2 h, an aliquot was removed, quenched with KTp[40] (10 mg/mL in THF; 10 equiv vs starting Ru), and analyzed by GC-FID. (b) $NH_2{}^nBu$: As above, with $NH_2{}^nBu$ (36.0 μL, 3.64 nmol, 1 equiv) and 3.73 mL $C_7H_8$. (c) Morpholine: As above, with morpholine (32.0 μL, 3.66 nmol, 1 equiv) and 3.73 mL $C_7H_8$. (d) DBU: As above, with DBU (54.0 μL, 3.61 nmol, 1 equiv) and 3.71 mL $C_7H_8$. (e) $NEt_3$: As above, with 1 or 10 equiv $NEt_3$ (50.0 μL, 3.60 nmol, 1 equiv in 3.71 mL $C_7H_8$, or 502 μL, 36.0 nmol, 10 equiv in 3.26 mL $C_7H_8$). For radar plot, see Figure 3.7; for numerical data, see Tables 3.3a and 3.4.

**Representative Procedure for RCM of pro-lactone 1 with nGC1$^{Ph}$.** (a) Control experiment. As above, using pro-lactone **1** (22.8 μL, 0.075 mmol) and dodecane (17.0 μL, 0.075 mmol, 1 equiv) diluted with 14.9 mL $C_7H_8$ to a final concentration of 5 mM **1**. To the stirred solution was added a solution of **nGC1$^{Ph}$** (30.8 μL of a stock solution of 10 mg **nGC1$^{Ph}$** in 200 mL; serial dilutions, see above; 2.25 μmol, 0.003 mol%). (b) $NEt_3$: As in the control experiment, with $NEt_3$ (31.4 μL, 2.25 μmol, 1 equiv). For numerical data, see Table 3.3b.

**Representative Procedure for self-metathesis of styrene 11 with nGC1$^{Ph}$.** (a) Control experiment. As above, using styrene **11** (91.7 μL, 0.800 mmol) and dodecane (182 μL, 0.800 mmol, 1 equiv) diluted with 3.11 mL $C_7H_8$ to give a final concentration of 200 mM **11**. Catalyst: **nGC1$^{Ph}$** (54.8 μL of a stock solution of 10 mg **nGC1$^{Ph}$** in 20 mL; 0.040 μmol, 0.005 mol%). (b) $NEt_3$: As in the control experiment, with $NEt_3$: 558 μL, 0.040 μmol, 1 equiv. For numerical data, see Table 3.3b.

**Representative Procedure: MCB Decomposition by β-Elimination**. (a) From **nGC1$^{Ph}$**: In a minor adaptation of the reported method,[47] **nGC1$^{Ph}$** (30 mg, 0.044 mmol) and ca. 10 mg DMT (0.051 mmol, 1 equiv) was dissolved in $CDCl_3$ (1.69 mL) in a J-Young NMR tube. The **nGC1$^{Ph}$**:IS ratio was measured ($^1$H NMR). Styrene (500 μL, 4.36 mmol, 100 equiv) was added (glovebox) to give a solution 20 mM in Ru, and the timer was immediately started. The NMR tube was shaken periodically over 30 min, then attached to a mechanical rotator (10 rpm) for sustained mixing. (b) From **nG**: As above, with **nG** (30 mg, 0.045 mmol). (c) From **nGC2$^{Me}$**: As above, with **nGC2$^{Me}$** (27 mg, 0.043 mmol).

**Representative Procedure: MCB Decomposition by Deprotonation.** (a) From **nGC1$^{Ph}$**: As above, with **nGC1$^{Ph}$** (30 mg, 0.044 mmol), DMT (10 mg, 0.051 mmol, 1 equiv), $CDCl_3$ (1.69 mL), styrene (500 μL, 4.36 mmol, 100 equiv) and DBU (6.6 μL, 0.045 mmol, 1 equiv). (b) From **nG**: As above, with **nG** (30 mg, 0.045 mmol), DMT (10 mg, 0.051 mmol, 1 equiv), $CDCl_3$ (1.69 mL), styrene (500 μL, 4.36 mmol, 97 equiv) and DBU (6.7 μL, 0.045 mmol, 1 equiv).

**Assessing Methylidene Abstraction from PC1$^{Ph}$ by Morpholine:** To **PC1$^{Ph}$** (15 mg, 0.018 mmol) and DMT (ca. 10 mg, 0.020 mmol, 1 equiv) in a J-Young NMR tube was added $CDCl_3$ (0.6 mL). The initial ratio of **PC1$^{Ph}$**:IS was measured, and the NMR sample was transferred to a Kontes flask with a stir bar. The NMR tube was rinsed with 0.4 mL $CDCl_3$, the washings also being transferred to the Kontes flask. The green-brown solution was transferred to the Schlenk line, where it was degassed (FPT; 3x), thawed under ethylene at –45 °C (MeCN-dry ice) to afford a dark red-brown solution, and stirred for 15 min. A chilled (–45 °C) solution of morpholine (4.5 μL, 0.052 mmol, 3 equiv) in 0.8 mL $CDCl_3$ was then injected, resulting in a final Ru concentration of 9.7 mM. The orange-brown solution was stirred for 20 min, then transferred by syringe into a pre-chilled Rotoflo NMR tube, which was inserted into the spectrometer set to –40 °C for $^1$H NMR analysis. The probe was warmed to 25 °C and the sample was allowed to thermally equilibrate for 10 min prior to $^1$H NMR analysis.

*References for Chapter 3 begin on p. 92*

**Tabulated Turnover Numbers.**

**Table 3.3a. Turnover numbers (x $10^3$) in RCM of 2 (numerical data for Figure 3.7).**

| Catalyst | Temp | Control | $NEt_3$ | $H_2N^nBu$ | Morpholine | DBU |
|---|---|---|---|---|---|---|
| **nG** | RT | 27.8 | 26.7 | 26.7 | 22.2 | 21.1 |
| **nGC1$^{Ph}$** | RT | 56.7 | 54.4 | 51.1 | 34.4 | 34.4 |
| **nGC2$^{Me}$** | RT | 14.4 | 10.0 | 10.0 | 8.90 | 10.0 |
| **HC2$^{Me}$** | RT | 7.80 | 6.70 | 5.60 | 6.70 | 0.00 |
| **nG** | 70 °C | 61.1 | 74.4 | 56.7 | 40.0 | 44.4 |
| **nGC1$^{Ph}$** | 70 °C | 74.4 | 82.2 | 65.6 | 50.0 | 65.6 |
| **nGC2$^{Me}$** | 70 °C | 41.1 | 38.9 | 37.8 | 38.9 | 36.7 |
| **HC2$^{Me}$** | 70 °C | 40.0 | 42.2 | 42.2 | 36.7 | 38.9 |

**Table 3.4. Impact of added $NEt_3$ on turnover numbers (x $10^3$) for the reactions shown. Catalysis by nGC1$^{Ph}$ at 70 °C.**

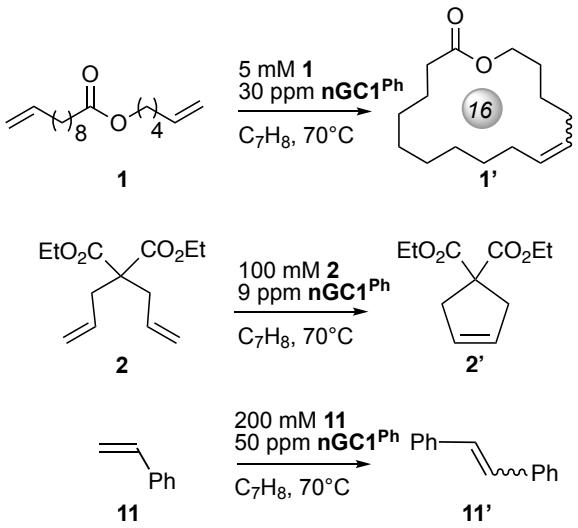


| Substrate | TON Control | + 1 equiv $NEt_3$ | + 10 equiv $NEt_3$ |
|---|---|---|---|
| **1** | 20.7 | 20.7 | – |
| **2** | 74.4 | 82.2 | – |
| **2**[a] | 71.1 | 75.6 | 66.7 |
| **11** | 2.2 | 2.2 | – |

[a] Experiment carried out with a second batch of substrate **2**, likewise supplied by TCI at 98% purity.

*References for Chapter 3 begin on p. 92*

**Table 3.5. Amine-tolerance (%) vs base-free control reaction (numerical data for Figure 3.8).**

| Catalyst | Temp | $NEt_3$ | $H_2N^nBu$ | Morpholine | DBU |
|---|---|---|---|---|---|
| **nG** | RT | 96 | 96 | 80 | 76 |
| **nGC1$^{Ph}$** | RT | 96 | 90 | 61 | 61 |
| **nG** | 70 °C | 100 | 93 | 65 | 73 |
| **nGC1$^{Ph}$** | 70 °C | 100 | 88 | 67 | 88 |

**Computational Details**. Density functional theory (DFT) calculations were performed with revisions B.01[93] and C.01[94] of the Gaussian 16 suite of programs. For the $H_2$IMes-coordinated catalyst **nG**, prior input geometries were adopted.[36] For the **C1$^{Ph}$** analogue **nGC1$^{Ph}$**, these geometries were modified using Spartan 16.[95] Conformational searches were performed using the MMFF force field[96] as implemented in Spartan 16 by freezing the coordination geometry of the Ru center while exploring torsional degrees of freedom for the **C1$^{Ph}$** ligand. The allylic species were obtained by deprotonation at $C_\beta$ of the MCBs.

Molecular geometries were optimized using the ωB97XD functional,[97] which generates geometries for ruthenium metathesis catalysts and other homogeneous catalysts in very good agreement with those of X-ray diffraction.[98] Numerical integration was performed using the Gaussian "ultrafine" grid using valence double-ζ quality basis sets (see below). For the Ru atoms, the Stuttgart/Cologne 28-electron relativistic effective core potentials (ECP28MDF)[99] with the corresponding correlation-consistent valence double-ζ plus polarization basis set (cc-pVDZ-PP)[99] were used as obtained from the Stuttgart/Cologne basis set repository.[100] All other atoms were described by correlation-consistent, valence double-ζ plus polarization basis sets (labeled cc-pVDZ[101] at the EMSL basis set exchange website).[102] All geometries were optimized without symmetry constraints to match default convergence criteria (max force $<4.5\cdot10^{-4}$ a.u., max RMS force $<3.0\cdot10^{-4}$ a.u., max displacement $<1.8\cdot10^{-3}$ a.u., max RMS displacement $<1.2\cdot10^{-3}$ a.u.) Default convergence criteria were used for the self-consistent field (SCF) procedure (RMS change in density matrix $<1.0\cdot10^{-8}$, max change in density matrix = $1.0\cdot10^{-6}$). Stationary points were characterized by the curvature of the analytically-calculated second-derivative (Hessian) matrix. Minima were confirmed to have real frequencies only; for transition states, a single imaginary frequency with a mode corresponding to the intended reaction coordinate was confirmed.

Thermal corrections to yield the Gibbs free energies were calculated within the ideal-gas, rigid-rotor, and harmonic oscillator approximations, barring precautions taken to avoid the divergent effects of very soft modes:[103] all frequencies below 100 $cm^{-1}$ were shifted to 100 $cm^{-1}$ when calculating the vibrational component of the entropy (quasi-harmonic oscillator approximation).[103,104]

*References for Chapter 3 begin on p. 92*

Single-point (SP) energy calculations were performed in the optimized geometries using the PBE[105] and M06-L[106] functionals in conjunction with the SMD continuum solvent model[107] to account for solvation effects, using default parameters for either benzene or chloroform as solvent. PBE calculations included Grimme's empirical D3 dispersion corrections with Becke-Johnson (BJ) damping.[108,109] Basis sets of valence quadruple-ζ level quality were used in the single-point calculations: Ru was described by the 28-electron relativistic effective core potential (ECP28MDF)[99] in conjunction with the corresponding correlation-consistent valence quadruple-ζ plus polarization basis set, augmented by diffuse functions (cc-pVQZ-PP)[99] from the Stuttgart/Cologne basis set repository.[102] All other atoms were described by correlation-consistent, valence quadruple-ζ plus polarization basis sets (cc-pVQZ[101] from the EMSL repository).[102] The single-point SCF convergence criteria were relaxed vs those of the geometry optimizations (to RMS change in density matrix $<1.0\cdot10^{-5}$, max change in density matrix $<1.0\cdot10^{-3}$).

Free energies in solution were calculated from the following:
$\boldsymbol{G_X} = \boldsymbol{E_X} + \Delta\boldsymbol{G}^{\boldsymbol{T=298.15\,K}}_{\boldsymbol{\omega B97XD,qh}} + \Delta\boldsymbol{G}^{\boldsymbol{T=298.15\,K}}_{\boldsymbol{1atm\rightarrow 1M}}$, where $\boldsymbol{E_X}$ is the SP energy calculated with the computational model X, where X = PBE-D3BJ-SMD(solvent), or M06L-SMD(solvent), and the solvent is either chloroform or benzene. $\boldsymbol{\Delta G}^{\boldsymbol{T=298.15\,K}}_{\boldsymbol{\omega B97XD,qh}}$ is the thermal correction to the Gibbs free energy calculated at the geometry-optimization level with the quasi-harmonic oscillator approximation as described above, and $\boldsymbol{\Delta G}^{\boldsymbol{T=298.15\,K}}_{\boldsymbol{1atm\rightarrow 1M}}$ is the standard state correction from the ideal gas at 1 atm to a 1 M solution (but exhibiting infinite-dilution, ideal-gas-like behavior), which is equal to 1.89 kcal/mol at RT.

Natural population analysis (NPA) was performed using the 7.0.7 version of the Natural Bond Orbital (NBO)[110] program and the electron density obtained from the PBE-D3BJ-SMD($CHCl_3$) SP energy calculations. The sum of the natural charges calculated for the fragment $RuCl_2(C_3H_6)$ in the metallacyclobutane intermediate of **nG** and **nGC1$^{Ph}$** is negative due to electron donation from $H_2$IMes and **C1$^{Ph}$**, respectively: this donation is defined as the number of electrons corresponding to the negative charge for $RuCl_2(C_3H_6)$.

## 3.5. References


(1) Grela, K., *Olefin Metathesis-Theory and Practice*. Wiley: Hoboken, NJ, 2014.

(2) Grubbs, R. H.; Wenzel, A. G., *Handbook of Metathesis*. 2nd ed.; Wiley-VCH: Weinheim, 2015.

(3) (a) Higman, C. S.; Lummiss, J. A. M.; Fogg, D. E. Olefin Metathesis at the Dawn of Uptake in Pharmaceutical and Specialty Chemicals Manufacturing. *Angew. Chem., Int. Ed.* **2016**, *55*, 3552–3565. (b) Yu, M.; Lou, S.; Gonzalez-Bobes, F., Ring-Closing Metathesis in Pharmaceutical Development: Fundamentals, Applications, and Future Directions. *Org. Process Res. Dev.* **2018**, *22*, 918−946. (c) Farina, V.; Horváth, A., Ring-Closing Metathesis in the Large-Scale Synthesis of Pharmaceuticals. In *Handbook of Metathesis*, Grubbs, R. H.; Wenzel, A. G., Eds. Wiley-VCH: Weinheim, 2015; Vol. 2, pp 633–658. (d) Fandrick, K. R.; Savoie, J.; Jinhua, N. Y.; Song, J. J.; Senanayake, C. H., Challenges and Opportunities for Scaling the Ring-Closing Metathesis Reaction in the Pharmaceutical Industry. In *Olefin Metathesis – Theory and Practice*, Grela, K., Ed. Wiley: Hoboken, 2014; pp 349-366. For recent examples of oncology or antiviral drug candidates, see: (e) St-Pierre, G.; Cherney, A. H.; Chen, W.; Dong, X.; Dornan, P. K.; Griffin, D. J.; Houk, K. N.; Lin, J. B.; Osgood, S.; Elipe, M. V. S.; Timmons, H. C.; Xie, Y.; Tedrow, J. S.; Thiel, O. R.; Smith, A. G., Accelerated Development of a Scalable Ring-Closing Metathesis to Manufacture AMG 176 Using a Combined High-Throughput Experimentation and Computational Modeling Approach. *Org. Process Res. Dev.* **2020**, *25*, 442–451. (f) Cink, R. D.; Lukin, K. A.; Bishop, R. D.; Zhao, G.; Pelc, M. J.; Towne, T. B.; Gates, B. D.; Ravn, M. M.; Hill, D. R.; Ding, C.; Cullen, S. C.; Mei, J. Z.; Leanna, M. R.; Henle, J.; Napolitano, J. G.; Nere, N. K.; Chen, S.; Sheikh, A.; Kallemeyn, J. M., Development of the Enabling Route for Glecaprevir via Ring-Closing Metathesis. *Org. Process Res. Dev.* **2020**, *24*, 183-200.

(4) (a) Schrodi, Y., Mechanisms of Olefin Metathesis Catalyst Decomposition and Methods of Catalyst Reactivation. In ref 2, pp 323–342. (b) Chadwick, J. C.; Duchateau, R.; Freixa, Z.; van Leeuwen, P. W. N. M., Alkene Metathesis. In *Homogeneous Catalysts: Activity – Stability – Deactivation*, Wiley-VCH: Weinheim, 2011; pp 347-396.

(5) In developing a production route to Simeprevir, Janssen chemists added methanesulfonic acid to neutralize basic impurities prior to mRCM. See: ref 3c. In **GII**-catalyzed acrylate metathesis, a sacrificial proton source can prevent deprotonation of the MCB by $PCy_3$-generated enolates. See: (a) Santos, A. G.; Bailey, G. A.; dos Santos, E. N.; Fogg, D. E., Overcoming Catalyst Decomposition in Acrylate Metathesis: Poly-phenol Resins as Enabling Agents for Phosphine-Stabilized Metathesis Catalysts. *ACS Catal.* **2017**, *7*, 3181−3189. (b) Bailey, G. A.; Fogg, D. E., Acrylate Metathesis via the Second-Generation Grubbs Catalyst: Unexpected Pathways Enabled by a $PCy_3$-Generated Enolate. *J. Am. Chem. Soc.* **2015**, *137*, 7318–7321. In enyne metathesis, rapid catalyst decomposition is inhibited by use of ethylene atmosphere. See: (c) Mori, M.; Sakakibara, N.; Kinoshita, A., Remarkable Effect of Ethylene Gas in the Intramolecular Enyne Metathesis of Terminal Alkynes. *J. Org. Chem.* **1998**, *63*, 6082–6083. The beneficial effect is due to inhibition of yne-yne reactions that result in catalyst decomposition. See: (d) Grotevendt, A. G. D.; Lummiss, J. A. M.; Mastronardi, M. L.; Fogg, D. E., Ethylene-Promoted versus Ethylene-Free Enyne Metathesis. *J. Am. Chem. Soc.* **2011**, *133*, 15918–15921.

(6) β-Hydride elimination was first explored within $d^0$ catalysts. For a recent overview, see (a) Schrock, R. R.; Copéret, C., Formation of High-Oxidation-State Metal–Carbon Double Bonds. *Organometallics* **2017**, *36*, 1884–1892. For leading references to its observation for silica-supported metathesis catalysts, see: (b) Leduc, A.-M.; Salameh, A.; Soulivong, D.; Chabanas, M.; Basset, J.-M.; Copéret, C.; Solans-Monfort, X.; Clot, E.; Eisenstein, O.; Boehm, V. P. W.; Roeper, M., Beta-H Transfer from the Metallacyclobutane: A Key Step in the Deactivation and Byproduct Formation for the Well-Defined Silica-Supported Rhenium Alkylidene Alkene Metathesis Catalyst. *J. Am. Chem. Soc.* **2008**, *130*, 6288–6297. (b) Solans-Monfort, X.; Copéret, C.; Eisenstein, O., Shutting Down Secondary Reaction Pathways: The Essential Role of the Pyrrolyl Ligand in

Improving Silica Supported $d^0$-$ML_4$ Alkene Metathesis Catalysts from DFT Calculations. *J. Am. Chem. Soc.* **2010**, *132*, 7750–7757.

(7) For unambiguous labelling evidence for b-elimination from the ruthenacyclobutane, see: (a) Romero, P. E.; Piers, W. E., Mechanistic Studies on 14-Electron Ruthenacyclobutanes: Degenerate Exchange with Free Ethylene. *J. Am. Chem. Soc.* **2007**, *129*, 1698–1704. For early experimental and computational evidence, see: (b) Nizovtsev, A. V.; Afanasiev, V. V.; Shutko, E. V.; Bespalova, N. B., Metathesis Catalysts Stability And Decomposition Pathway. *NATO Sci. Ser. II* **2007**, *243*, 125–135. (c) Janse van Rensburg, W. J.; Steynberg, P. J.; Meyer, W. H.; Kirk, M. M.; Forman, G. S., DFT Prediction and Experimental Observation of Substrate-Induced Catalyst Decomposition in Ruthenium-Catalyzed Olefin Metathesis. *J. Am. Chem. Soc.* **2004**, *126*, 14332–14333.

(8) Bailey, G. A.; Foscato, M.; Higman, C. S.; Day, C. S.; Jensen, V. R.; Fogg, D. E., Bimolecular Coupling as a Vector for Decomposition of Fast-Initiating Olefin Metathesis Catalysts. *J. Am. Chem. Soc.* **2018**, *140*, 6931–6944.

(9) Thiel, V.; Wannowius, K.-J.; Wolff, C.; Thiele, C. M.; Plenio, H., Ring-Closing Metathesis Reactions: Interpretation of Conversion–Time Data. *Chem. - Eur. J.* **2013**, *19*, 16403–16414.

(10) Keitz, B. K.; Grubbs, R. H., Probing the Origin of Degenerate Metathesis Selectivity via Characterization and Dynamics of Ruthenacyclobutanes Containing Variable NHCs. *J. Am. Chem. Soc.* **2011**, *133*, 16277–16284.

(11) Burdett, K. A.; Harris, L. D.; Margl, P.; Maughon, B. R.; Mokhtar-Zadeh, T.; Saucier, P. C.; Wasserman, E. P., Renewable Monomer Feedstocks via Olefin Metathesis: Fundamental Mechanistic Studies of Methyl Oleate Ethenolysis with the First-Generation Grubbs Catalyst. *Organometallics* **2004**, *23*, 2027–2047.

(12) Yee, N. K.; Farina, V.; Houpis, I. N.; Haddad, N.; Frutos, R. P.; Gallou, F.; Wang, X.-J.; Wei, X.; Simpson, R. D.; Feng, X.; Fuchs, V.; Xu, Y.; Tan, J.; Zhang, L.; Xu, J.; Smith-Keenan, L. L.; Vitous, J.; Ridges, M. D.; Spinelli, E. M.; Johnson, M.; Donsbach, K.; Nicola, T.; Brenner, M.; Winter, E.; Kreye, P.; Samstag, W., Efficient Large-Scale Synthesis of BILN 2061, a Potent HCV Protease Inhibitor, by a Convergent Approach Based on Ring-Closing Metathesis. *J. Org. Chem.* **2006**, *71*, 7133–7145.

(13) Nicola, T.; Brenner, M.; Donsbach, K.; Kreye, P., First Scale-Up to Production Scale of a Ring Closing Metathesis Reaction Forming a 15-Membered Macrocycle as a Precursor of an Active Pharmaceutical Ingredient. *Org. Process Res. Dev.* **2005**, *9*, 513–515.

(14) Monfette, S.; Eyholzer, M.; Roberge, D. M.; Fogg, D. E., Getting RCM Off the Bench: Reaction-Reactor Matching Transforms Metathesis Efficiency in the Assembly of Large Rings. *Chem. – Eur. J.* **2010**, *16*, 11720–11725.

(15) Schrodi, Y.; Ung, T.; Vargas, A.; Mkrtumyan, G.; Lee, C. W.; Champagne, T. M.; Pederson, R. L.; Hong, S. H., Ruthenium Olefin Metathesis Catalysts for the Ethenolysis of Renewable Feedstocks. *Clean Soil, Air, Water* **2008**, *36*, 669–673.

(16) Marx, V. M.; Sullivan, A. H.; Melaimi, M.; Virgil, S. C.; Keitz, B. K.; Weinberger, D. S.; Bertrand, G.; Grubbs, R. H., Cyclic Alkyl Amino Carbene (CAAC) Ruthenium Complexes as Remarkably Active Catalysts for Ethenolysis. *Angew. Chem., Int. Ed.* **2015**, *54*, 1919–1923.

(17) Gawin, R.; Tracz, A.; Chwalba, M.; Kozakiewicz, A.; Trzaskowski, B.; Skowerski, K., Cyclic Alkyl Amino Ruthenium Complexes—Efficient Catalysts for Macrocyclization and Acrylonitrile Cross Metathesis. *ACS Catal.* **2017**, *7*, 5443–5449.

(18) Gawin, R.; Kozakiewicz, A.; Guńka, P. A.; Dąbrowski, P.; Skowerski, K., Bis(Cyclic Alkyl Amino Carbene) Ruthenium Complexes: A Versatile, Highly Efficient Tool for Olefin Metathesis. *Angew. Chem., Int. Ed.* **2017**, *56*, 981–986.

(19) Nascimento, D. L.; Gawin, A.; Gawin, R.; Guńka, P. A.; Zachara, J.; Skowerski, K.; Fogg, D. E., Integrating Activity with Accessibility in Olefin Metathesis: An Unprecedentedly Reactive

Ruthenium-Indenylidene Catalyst Bearing a Cyclic Alkyl Amino Carbene. *J. Am. Chem. Soc.* **2019**, *141*, 10626–10631.

(20) Bidange, J.; Fischmeister, C.; Bruneau, C., Ethenolysis: A Green Catalytic Tool to Cleave Carbon–Carbon Double Bonds. *Chem. – Eur. J.* **2016**, *22*, 12226–12244.

(21) Chikkali, S.; Mecking, S., Refining of Plant Oils to Chemicals by Olefin Metathesis. *Angew. Chem., Int. Ed.* **2012**, *51*, 5802−5808.

(22) Hess, S. K.; Lepetit, B.; Kroth, P. G.; Mecking, S., Production of Chemicals from Microalgae Lipids – Status and Perspectives. *Eur. J. Lipid Sci. Technol.* **2018**, *120*, 1700152.

(23) For a recent study deploying a CAAC catalyst in ethenolysis of ethyl oleate on 1 L scale, see: (a) Kajetanowicz, A.; Chwalba, M.; Gawin, A.; Tracz, A.; Grela, K., Non-Glovebox Ethenolysis of Ethyl Oleate and FAME at Larger Scale Utilizing a Cyclic (Alkyl)(Amino)Carbene Ruthenium Catalyst. *Eur. J. Lipid Sci. Technol.* **2019**, 1900263. For the use of CAAC and fluorinated NHC catalysts for ethenolysis of the terpene squalene (which contains six trisubstituted olefinic units), see: (b) Byun, S.; Seo, H.; Choi, J.-H.; Ryu, J. Y.; Lee, J.; Chung, W.-j.; Hong, S., Fluoro-Imidazopyridinylidene Ruthenium Catalysts for Cross Metathesis with Ethylene. *Organometallics* **2019**, *38*, 4121–4132.

(24) Butilkov, D.; Frenklah, A.; Rozenberg, I.; Kozuch, S.; Lemcoff, N. G., Highly Selective Olefin Metathesis with CAAC-Containing Ruthenium Benzylidenes. *ACS Catal.* **2017**, *7*, 7634–7637.

(25) Molecular hydride species often cited as promoting competing isomerization are insufficiently reactive to do so. For a kinetics study, see: (a) Higman, C. S.; Plais, L.; Fogg, D. E., Isomerization During Olefin Metathesis: An Assessment of Potential Catalyst Culprits. *ChemCatChem* **2013**, *5*, 3548-3551. For **GII,** Ru nanoparticles have been implicated. See: (b) Higman, C. S.; Lanterna, A. E.; Marin, M. L.; Scaiano, J. C.; Fogg, D. E., Catalyst Decomposition During Olefin Metathesis Yields Isomerization-Active Ru Nanoparticles. *ChemCatChem* **2016**, *8*, 2446–2449. For a critical review of isomerization in metathesis, see (c) van Lierop, B. J.; Lummiss, J. A. M.; Fogg, D. E., Ring-Closing Metathesis. In ref 1; pp 85–152.

(26) For evidence that the vinylphosphonium salt [$H_2C$=CHP$Cy_3$]Cl (**12**) lost on reaction with ethylene does not re-enter metathesis, see: Leitao, E. M.; van der Eide, E. F.; Romero, P. E.; Piers, W. E.; McDonald, R., Kinetic and Thermodynamic Analysis of Processes Relevant to Initiation of Olefin Metathesis by Ruthenium Phosphonium Alkylidene Catalysts. *J. Am. Chem. Soc.* **2010**, *132*, 2784–2794.

(27) Carlson, R. G.; Gile, M. A.; Heppert, J. A.; Mason, M. H.; Powell, D. R.; Vander Velde, D.; Vilain, J. M., The Metathesis-Facilitated Synthesis of Terminal Ruthenium Carbide Complexes: A Unique Carbon Atom Transfer Reaction. *J. Am. Chem. Soc.* **2002**, *124*, 1580–1581.

(28) Romero, P. E.; Piers, W. E., Direct Observation of a 14-Electron Ruthenacyclobutane Relevant to Olefin Metathesis. *J. Am. Chem. Soc.* **2005**, *127*, 5032–5033.

(29) van der Eide, E. F.; Romero, P. E.; Piers, W. E., Generation and Spectroscopic Characterization of Ruthenacyclobutane and Ruthenium Olefin Carbene Intermediates Relevant to Ring Closing Metathesis Catalysis. *J. Am. Chem. Soc.* **2008**, *130*, 4485–4491.

(30) Anderson, D. R.; Ung, T.; Mkrtumyan, G.; Bertrand, G.; Grubbs, R. H.; Schrodi, Y., Kinetic Selectivity of Olefin Metathesis Catalysts Bearing Cyclic (Alkyl)(Amino)Carbenes. *Organometallics* **2008**, *27*, 563–566.

(31) Soleilhavoup, M.; Bertrand, G., Cyclic (Alkyl)(Amino)Carbenes (CAACs): Stable Carbenes on the Rise. *Acc. Chem. Res.* **2015**, *48*, 256–266.

(32) Melaimi, M.; Jazzar, R.; Soleilhavoup, M.; Bertrand, G., Cyclic (Alkyl)(amino)carbenes (CAACs): Recent Developments. *Angew. Chem., Int. Ed.* **2017**, *56*, 10046–10068.

(33) Paul, U. S. D.; Radius, U., What Wanzlick Did Not Dare To Dream: Cyclic (Alkyl)(amino)carbenes (CAACs) as New Key Players in Transition-Metal Chemistry. *Eur. J. Inorg. Chem.* **2017**, 3362–3375.

(34) Anderson, D. R.; Lavallo, V.; O'Leary, D. J.; Bertrand, G.; Grubbs, R. H., Synthesis and Reactivity of Olefin Metathesis Catalysts Bearing Cyclic (Alkyl)(Amino)Carbenes. *Angew. Chem., Int. Ed.* **2007**, *46*, 7262–7265.

(35) Ireland, B. J.; Dobigny, B. T.; Fogg, D. E., Decomposition of a Phosphine-Free Metathesis Catalyst by Amines and Other Nitrogen Bases: Metallacyclobutane Deprotonation as a Major Deactivation Pathway. *ACS Catal.* **2015**, *5*, 4690−4698.

(36) Bailey, G. A.; Lummiss, J. A. M.; Foscato, M.; Occhipinti, G.; McDonald, R.; Jensen, V. R.; Fogg, D. E., Decomposition of Olefin Metathesis Catalysts by Brønsted Base: Metallacyclobutane Deprotonation as a Primary Deactivating Event. *J. Am. Chem. Soc.* **2017**, *139*, 16446–16449.

(37) Guidone, S.; Songis, O.; Nahra, F.; Cazin, C. S. J., Conducting Olefin Metathesis Reactions in Air: Breaking the Paradigm. *ACS Catal.* **2015**, *5*, 2697–2701.

(38) Romero, P. E.; Piers, W. E.; McDonald, R., Rapidly Initiating Ruthenium Olefin-Metathesis Catalysts Angew. Chemie 2004 116, 6287-6291. *Angew. Chem., Int. Ed.* **2004**, *43*, 6161–6165.

(39) Bailey, G. A.; Fogg, D. E., Confronting Neutrality: Maximizing Success in the Analysis of Transition-Metal Catalysts by MALDI Mass Spectrometry. *ACS Catal.* **2016**, *6*, 4962–4971.

(40) Blacquiere, J. M.; Jurca, T.; Weiss, J.; Fogg, D. E., Time as a Dimension in High-Throughput Homogeneous Catalysis. *Adv. Synth. Catal.* **2008**, *350*, 2849–2855.

(41) For selected recent advances in materials science applications, see: (a) Rizzo, A.; Peterson, G. I.; Bhaumik, A.; Kang, C.; Choi, T.-L., Sugar-Based Polymers from d-Xylose: Living Cascade Polymerization, Tunable Degradation, and Small Molecule Release. *Angew. Chem., Int. Ed.* **2021**, *60*, 849–855. (b) Foster, J. C.; Grocott, M. C.; Arkinstall, L. A.; Varlas, S.; Redding, M. J.; Grayson, S. M.; O'Reilly, R. K., It is Better with Salt: Aqueous Ring-Opening Metathesis Polymerization at Neutral pH. *J. Am. Chem. Soc.* **2020**, *142*, 13878–13885. (c) Debsharma, T.; Schmidt, B.; Laschewsky, A.; Schlaad, H., Ring-Opening Metathesis Polymerization of Unsaturated Carbohydrate Derivatives: Levoglucosenyl Alkyl Ethers. *Macromolecules* **2021**, *54*, 2720-2728. (d) Church, D. C.; Takiguchi, L.; Pokorski, J. K. Optimization of Ring-Opening Metathesis Polymerization (ROMP) under Physiologically Relevant Conditions. *Polym. Chem*. **2020**, *11*, 4492−4499. (e) Feist, J. D.; Xia, Y., Enol Ethers Are Effective Monomers for Ring-Opening Metathesis Polymerization: Synthesis of Degradable and Depolymerizable Poly(2,3-dihydrofuran). *J. Am. Chem. Soc.* **2020**, *142*, 1186-1189. (f) Varlas, S.; Foster, J. C.; O'Reilly, R. K., Ring-Opening Metathesis Polymerization-Induced Self-Assembly (ROMPISA). *Chem. Commun*. **2019**, *55*, 9066–9071. (g) Varlas, S.; Keogh, R.; Xie, Y.; Horswell, S. L.; Foster, J. C.; O'Reilly, R. K. Polymerization-Induced Polymersome Fusion. J. Am. Chem. Soc. 2019, 141, 20234−20248. (h) Debsharma, T.; Behrendt, F. N.; Laschewsky, A.; Schlaad, H., Ring-Opening Metathesis Polymerization of Biomass-Derived Levoglucosenol. *Angew. Chem., Int. Ed.* **2019**, *58*, 6718-6721. (i) Jung, K.; Ahmed, T. S.; Lee, J.; Sung, J. C.; Keum, H.; Grubbs, R. H.; Choi, T. L., Living Beta-Selective Cyclopolymerization Using Ru Dithiolate Catalysts. *Chem. Sci.* **2019**, *10*, 8955–8963. (j) Theunissen, C.; Ashley, M. A.; Rovis, T., Visible-Light-Controlled Ruthenium-Catalyzed Olefin Metathesis. *J. Am. Chem. Soc.* **2019**, *141*, 6791–6796. (k) Song, K.; Kim, K.; Hong, D.; Kim, J.; Heo, C. E.; Kim, H. I.; Hong, S. H., Highly Active Ruthenium Metathesis Catalysts Enabling Ring-Opening Metathesis Polymerization of Cyclopentadiene at Low Temperatures. *Nat. Commun.* **2019**, *10*, 3860. (l) Kang, E.-H.; Yu, S. Y.; Lee, I. S.; Park, S. E.; Choi, T.-L., Strategies to Enhance Cyclopolymerization using Third-Generation Grubbs Catalyst. *J. Am. Chem. Soc*. **2014**, *136*, 10508–10514. For applications in tissue engineering, see: (m) Merrett, K.; Liu, W.; Mitra, D.; Camm, K. D.; McLaughlin, C. R.; Liu, Y.; Watsky, M. A.; Li, F.; Griffith, M.; Fogg, D. E., Synthetic Neoglycopolymer-Recombinant Human Collagen Hybrids as Biomimetic Crosslinking Agents In Corneal Tissue Engineering. *Biomaterials* **2009**, *30*, 5403–5408.

(42) For recent reviews, see: (a) Edwards, J. P.; Wolf, W. J.; Grubbs, R. H., The Synthesis of Cyclic Polymers by Olefin Metathesis: Achievements and Challenges. *J. Polym. Sci. A*. **2019**, *57*, 228–242. (b) Knall, A.-C.; Slugovc, C., Olefin Metathesis Polymerization. In *Olefin Metathesis-Theory and Practice*, Grela, K., Ed. Wiley: Hoboken, NJ, 2014; pp 269–284. (c) Dong, Y.; Matson, J. B.; Edgar, K. J., Olefin Cross-Metathesis in Polymer and Polysaccharide Chemistry. *Biomacromolecules* **2017**, *18*, 1661–1676. .

(43) For recent reviews of olefin metathesis in chemical biology, see: (a) Isenegger, P. G.; Davis, B. G., Concepts of Catalysis in Site-Selective Protein Modifications. *J. Am. Chem. Soc.* **2019**, *141*, 8005−8013. (b) Vinogradova, E. V., Organometallic Chemical Biology: An Organometallic Approach to Bioconjugation. *Pure Appl. Chem.* **2017**, *89*, 1619–1640. (c) Messina, M. S.; Maynard, H. D., Modification of Proteins using Olefin Metathesis. *Mater. Chem. Front.* **2020**, *4*, 1040–1051.

(44) Problems arising from decomposition of the readily-handled Ru catalysts are extensively documented in process chemistry in pharma (particularly for mRCM: ref 3), and in molecular biology, where bioconjugation is described as a race between metathesis and decomposition (ref 43a), requiring use of the Ru complex in significant stoichiometric excess. Perhaps more surprisingly, recent reports in materials applications likewise flag challenges arising from decomposition, notwithstanding the greater steric protection of the active species. See, for example, refs 41a–k.

(45) Morvan, J.; Mauduit, M.; Bertrand, G.; Jazzar, R., Cyclic (Alkyl)(amino)carbenes (CAACs) in Ruthenium Olefin Metathesis. *ACS Catal.* **2021**, *11*, 1714–1748.

(46) Biermann, U.; Bornscheuer, U. T.; Feussner, I.; Meier, M. A. R.; Metzger, J. O., Fatty Acids and their Derivatives as Renewable Platform Molecules for the Chemical Industry. *Angew. Chem., Int. Ed.* **2021**, Early View article, DOI 10.1002/anie.202100778.

(47) For quantitative experimental evidence of bimolecular decomposition of $RuCl_2(L)(=CH_2)$ (L = NHC, CAAC), see: ref 8 and: Nascimento, D. L.; Fogg, D. E., Origin of the Breakthrough Productivity of Ruthenium-CAAC Catalysts in Olefin Metathesis (CAAC = Cyclic Alkyl Amino Carbene). *J. Am. Chem. Soc.* **2019**, *141*, 19236–19240.

(48) For reports in which lower metathesis productivity can be seen at higher catalyst loadings, see refs 16-19 and: (a) Ton, S. J.; Fogg, D. E., The Impact of Oxygen on Leading and Emerging Ru-Carbene Catalysts for Olefin Metathesis: An Unanticipated Correlation Between Robustness and Metathesis Activity *ACS Catal.* **2019**, *9*, 11329−11334. (b) Blanco, C.; Sims, J.; Nascimento, D. L.; Goudreault, A. Y.; Steinmann, S. N.; Michel, C.; Fogg, D. E., The Impact of Water on Ru-Catalyzed Olefin Metathesis: Potent Deactivating Effects Even at Low Water Concentrations. *ACS Catal.* **2021**, *11*, 893−899.

(49) See ref 47. Disappearance of the methylidene signal for **mC1$^{Ph}$**, $RuCl_2$(**C1**)(py)($=CH_2$), was complete in <5 min at 23 °C in $CDCl_3$, vs just 2% of the corresponding **mGIII**. The latter complex was still observable after 3 h (5% vs internal standard). In both cases, ca. 80% ethylene was ultimately detected (a lower limit, owing to loss of ethylene to the headspace), confirming decomposition via bimolecular coupling.

(50) Facile bimolecular coupling of labile $PPh_3$-stabilized [Ru]=CHR catalysts can be inferred in many early reports in which stilbenes and related RHC=CHR byproducts, and in some cases relevant Ru dimers were observed. See, for example: (a) Schwab, P.; Grubbs, R. H.; Ziller, J. W. Synthesis and Applications of $RuCl_2(=CHR)(PR_3)_2$. *J. Am. Chem. Soc*. **1996**, *118*, 100−110) and a structurally characterized ruthenium dimer (see: (b) Amoroso, D.; Snelgrove, J. L.; Conrad, J. C.; Drouin, S. D.; Yap, G. P. A.; Fogg, D. E., An Attractive Route to Olefin Metathesis Catalysts: Facile Synthesis of a Ruthenium Alkylidene Complex Containing Labile Phosphane Donors. *Adv. Synth. Catal.* **2002**, *344*, 757–763). For second-generation catalysts, bimolecular coupling was long thought improbable, on the basis of the low concentrations of the 14-electron species arising from strong ligand binding. See ref 4.

(51) Foscato, M.; Jensen, V. R., Automated in Silico Design of Homogeneous Catalysts. *ACS Catal.* **2020**, *10*, 2354–2377.

(52) Foscato, M.; Venkatraman, V.; Jensen, V. R., DENOPTIM: Software for Computational de Novo Design of Organic and Inorganic Molecules. *J. Chem. Inf. Model.* **2019**, *59*, 4077–4082.

(53) Kaczanowska, K.; Trzaskowski, B.; Peszczyńska, A.; Tracz, A.; Gawin, R.; Olszewski, T. K.; Skowerski, K., Cross Metathesis with Acrylates: N-Heterocyclic Carbene (NHC)- Versus Cyclic Alkyl Amino Carbene (CAAC)-Based Ruthenium Catalysts, an Unanticipated Influence of the Carbene Type on Efficiency and Selectivity of the Reaction. *ChemCatChem* **2020**, *12*, 6366−6374.

(54) Nascimento, D. L.; Reim, I.; Foscato, M.; Jensen, V. R.; Fogg, D. E., Challenging Metathesis Catalysts with Nucleophiles and Brønsted Base: The Stability of State-of-the-Art Catalysts to Attack by Amines. *ACS Catal.* **2020**, *10*, 11623–11633.

(55) Basic aliphatic amines such as $NH_2{}^nBu$ abstract the benzylidene ligand from **GII** or **HII** even at RT. **GII**: (a) Lummiss, J. A. M.; Ireland, B. J.; Sommers, J. M.; Fogg, D. E., Amine-Mediated Degradation in Olefin Metathesis Reactions that Employ the Second-Generation Grubbs Catalysts. *ChemCatChem* **2014**, *6*, 459–463. **HII**: See ref 35. $^{13}$C-Labelling studies indicate that *n*-butylamine indeed competes with $PCy_3$ to abstract the methylidene ligand from the four-coordinate active species **B-$H_2$IMes**: (c) Lummiss, J. A. M.; Botti, A. G. G.; Fogg, D. E., Isotopic Probes for Ruthenium-Catalyzed Olefin Metathesis. *Catal. Sci. Technol.* **2014**, *4*, 4210–4218.

(56) Wappel, J.; Urbina-Blanco, C. A.; Abbas, M.; Albering, J. H.; Saf, R.; Nolan, S. P.; Slugovc, C., Halide Exchanged Hoveyda-Type Complexes in Olefin Metathesis. *Beilstein J. Org. Chem.* **2010**, *6*, 1091–1098.

(57) Tracz, A.; Matczak, M.; Urbaniak, K.; Skowerski, K., Nitro-Grela-Type Complexes Containing Iodides – Robust and Selective Catalysts for Olefin Metathesis Under Challenging Conditions. *Beilstein J. Org. Chem.* **2015**, *11*, 1823–1832.

(58) Nechmad, N. B.; Phatake, R.; Ivry, E.; Poater, A.; Lemcoff, N. G., Unprecedented Selectivity of Ruthenium Iodide Benzylidenes in Olefin Metathesis Reactions. *Angew. Chem., Int. Ed.* **2020**, *59*, 3539–3543.

(59) Torker, S.; Khan, R. K. M.; Hoveyda, A. H., The Influence of Anionic Ligands on Stereoisomerism of Ru Carbenes and Their Importance to Efficiency and Selectivity of Catalytic Olefin Metathesis Reactions. *J. Am. Chem. Soc.* **2014**, *136*, 3439−3455.

(60) Blanco, C.; Nascimento, D. L.; Fogg, D. E., Routes to High-Performing Ruthenium-Iodide Catalysts for Olefin Metathesis: Phosphine Lability Is Key to Efficient Halide Exchange. *Organometallics* **2021**, accepted.

(61) Falivene, L.; Cao, Z.; Petta, A.; Serra, L.; Poater, A.; Oliva, R.; Scarano, V.; Cavallo, L., Towards the Online Computer-Aided Design of Catalytic Pockets. *Nature Chem.* **2019**, *11*, 872–879.

(62) Gomez-Suarez, A.; Nelson, D. J.; Nolan, S. P., Quantifying and understanding the steric properties of N-heterocyclic carbenes. *Chem. Commun.* **2017**, *53*, 2650–2660.

(63) Paul, U. S. D.; Sieck, C.; Haehnel, M.; Hammond, K.; Marder, T. B.; Radius, U., Cyclic (Alkyl)(Amino)Carbene Complexes of Rhodium and Nickel and Their Steric and Electronic Parameters. *Chem. Eur. J.* **2016**, *22*, 11005–11014.

(64) Poater, A.; Cosenza, B.; Correa, A.; Giudice, S.; Ragone, F.; Scarano, V.; Cavallo, L., SambVca: A Web Application for the Calculation of the Buried Volume of N-Heterocyclic Carbene Ligands. *Eur. J. Inorg. Chem.* **2009**, 1759–1766.

(65) Buried volumes were calculated for the DFT-optimized geometries of $\mathbf{B^X}$, using Ru as the center of the sphere, thereby avoiding the skewed orientation of the unsymmetric CAAC ligands that Paul and Radius have flagged as a concern (ref 33).

(66) Hohenstein, E. G.; Sherrill, C. D., Effects of Heteroatoms on Aromatic π−π Interactions: Benzene−Pyridine and Pyridine Dimer. *J. Phys. Chem. A* **2009**, *113*, 878–886.

(67) Nishio, M., The CH/π Hydrogen Bond in Chemistry. Conformation, Supramolecules, Optical Resolution and Interactions Involving Carbohydrates. *Phys. Chem. Chem. Phys.* **2011**, *13*, 13873-13900.

(68) Fernández-Ramos, A.; Miller, J. A.; Klippenstein, S. J.; Truhlar, D. G., Modeling the Kinetics of Bimolecular Reactions. *Chem. Rev.* **2006**, *106*, 4518-4584.

(69) Nascimento, D. L.; Fogg, D. E., Origin of the Breakthrough Productivity of Ruthenium-CAAC Catalysts in Olefin Metathesis (CAAC = Cyclic Alkyl Amino Carbene). *J. Am. Chem. Soc.* **2019**, *141*, 19236–19240.

(70) Michrowska, A.; Bujok, R.; Harutyunyan, S.; Sashuk, V.; Dolgonos, G.; Grela, K., Nitro-Substituted Hoveyda-Grubbs Ruthenium Carbenes: Enhancement of Catalyst Activity through Electronic Activation. *J. Am. Chem. Soc.* **2004**, *126*, 9318–9325.

(71) (a) Hayler, J. D.; Leahy, D. K.; Simmons, E. M., A Pharmaceutical Industry Perspective on Sustainable Metal Catalysis. *Organometallics* **2019**, *38*, 36–46. (b) Ager, D. J.; de Vries, A. H. M.; de Vries, J. G., Asymmetric Homogeneous Hydrogenations at Scale. *Chem. Soc. Rev.* **2012**, *41*, 3340–3380. (c) Magano, J.; Dunetz, J. R., Large-Scale Applications of Transition Metal-Catalyzed Couplings for the Synthesis of Pharmaceuticals. *Chem. Rev.* **2011**, *111*, 2177–2250.

(72) Schwab, P.; Grubbs, R. H.; Ziller, J. W., Synthesis and Applications of $RuCl_2(=CHR')(PR_3)_2$: The Influence of the Alkylidene Moiety on Metathesis Activity. *J. Am. Chem. Soc.* **1996**, *118*, 100–110.

(73) Amoroso, D.; Yap, G. P. A.; Fogg, D. E., Deactivation of Ruthenium Metathesis Catalysts via Facile Formation of Face-Bridged Dimers. *Organometallics* **2002**, *21*, 3335–3343.

(74) Amoroso, D.; Yap, G. P. A.; Fogg, D. E., The Life, Death, and ROMP Activity of Ruthenium Complexes Containing the Basic, Chelating Diphosphine Bis(Dicyclohexyl)-1,4-Phosphinobutane. *Can. J. Chem.* **2001**, *79*, 958–963.

(75) A number of studies have sought to improve the productivity of the $H_2$IMes catalysts by reversing catalyst decomposition. Small proportions of a methylidene species, for example, were observed following decomposition of $RuCl_2$(*p*-cymene)($H_2$IMes) in the presence of ethylene and $PCy_3$. See: (a) Smit, W.; Foscato, M.; Occhipinti, G.; Jensen, V. R., Ethylene-Triggered Formation of Ruthenium Alkylidene from Decomposed Catalyst. *ACS Catal.* **2020**, *10*, 6788–6797. (b) Engel, J.; Smit, W.; Foscato, M.; Occhipinti, G.; Törnroos, K. W.; Jensen, V. R., Loss and Reformation of Ruthenium Alkylidene: Connecting Olefin Metathesis, Catalyst Deactivation, Regeneration, and Isomerization. *J. Am. Chem. Soc.* **2017**, *139*, 16609–16619. For details of the instability of the *p*-cymene starting complex, see: (c) Day, C. S.; Fogg, D. E., High-Yield Synthesis of a Long-Sought, Labile Ru-NHC Complex and Its Application to the Concise Synthesis of Second-Generation Olefin Metathesis Catalysts. *Organometallics* **2018**, *24*, 4551–4555. For prior efforts aimed at catalyst regeneration, see: (d) Tabari, D. S.; Tolentino, D. R.; Schrodi, Y., Reactivation of a Ruthenium-Based Olefin Metathesis Catalyst. *Organometallics* **2013**, *32*, 5–8.

(76) Lysenko, Z.; Maughon, B. R.; Mokhtar-Zadeh, T.; Tulchinsky, M. L., Stability of the First-Generation Grubbs Metathesis Catalyst in a Continuous Flow Reactor. *J. Organomet. Chem.* **2006**, *691*, 5197–5203.

(77) Skowerski, K.; Czarnocki, S. J.; Knapkiewicz, P., Tube-In-Tube Reactor as a Useful Tool for Homo- and Heterogeneous Olefin Metathesis under Continuous Flow Mode. *ChemSusChem* **2014**, *7*, 536–542.

(78) Exceptions: We recently demonstrated that certain **C1** catalysts resist decomposition by $O_2$ more than their $H_2$IMes analogues. See (a): Ton, S. J.; Fogg, D. E., The Impact of Oxygen on Leading and Emerging Ru-Carbene Catalysts for Olefin Metathesis: An Unanticipated Correlation Between Robustness and Metathesis Activity *ACS Catal.* **2019**, *9*, 11329−11334. The more facile attack of sodium cyanoborohydride on **HII**, vs a CAAC analogue, has also been reported. See: ref 24. More typically, contaminants are already present. Impurities in standard grades of ethylene, for example, were proposed to account for the higher productivity of CAAC catalysts bearing $\mathbf{C1^{Ph}}$, relative to

**C2$^{Me}$** derivatives, in oleate ethenolysis. See: ref 19. In striking contrast to the superiority of CAAC vs NHC catalysts in this reaction, $H_2$IMes catalysts greatly outperformed CAAC catalysts in ethenolysis of maleates. Whether this is due to impurities was not examined, however. See: (b) Engl, P. S.; Tsygankov, A.; Silva, J. D. J.; Lange, J.-P.; Copéret, C.; Togni, A.; Fedorov, A., Acrylate Esters by Ethenolysis of Maleate Esters with Ru Metathesis Catalysts: an HTE and a Technoeconomic Study. *Helv. Chim. Acta* **2020**, *103*, e2000035.

(79) (a) Nicola, T.; Brenner, M.; Donsbach, K.; Kreye, P., First Scale-Up to Production Scale of a Ring Closing Metathesis Reaction Forming a 15-Membered Macrocycle as a Precursor of an Active Pharmaceutical Ingredient. *Org. Process Res. Dev.* **2005**, *9*, 513–515. (b) Wang, H.; Goodman, S. N.; Dai, Q.; Stockdale, G. W.; Clark, W. M., Development of a Robust Ring-Closing Metathesis Reaction in the Synthesis of SB-462795, a Aathepsin K Inhibitor. *Org. Process Res. Dev.* **2008**, *12*, 226–234. These discoveries were made in campaigns using Hoveyda-class catalysts, $RuCl_2(L)[=CH(C_6H_4$-2-OiPr). The impact of morpholine was seen for the first-generation catalyst (L = $PCy_3$); that of DBU with its second-generation variant (L = $H_2$IMes).

(80) Vitaku, E.; Smith, D. T.; Njardarson, J. T., Analysis of the Structural Diversity, Substitution Patterns, and Frequency of Nitrogen Heterocycles among U.S. FDA Approved Pharmaceuticals. *J. Med. Chem.* **2014**, *57*, 10257–10274.

(81) For leading reviews, see: (a) Compain, P.; Hazelard, D., Synthesis of Amine-Containing Heterocycles by Metathesis Reactions: Recent Advances and Opportunities. *Top. Heterocyclic Chem*. **2015**, 1–43. (b) Compain, P. Olefin Metathesis of Amine-Containing Systems: Beyond the Current Consensus. *Adv. Synth. Catal.* **2007**, *349*, 1829–1846. For additional examples cited in review articles, see: (c) Deiters, A.; Martin, S. F. Synthesis of Oxygen- and Nitrogen-Containing Heterocycles by Ring-Closing Metathesis. *Chem. Rev*. **2004**, *104*, 2199–2238. For an early report noting the importance of protecting groups in RCM of amine-containing substrates, see: (d) Nguyen, S. T.; Grubbs, R. H.; Ziller, J. W., Synthesis and Activities of New Single-Component Ruthenium-Based Olefin Metathesis Catalysts. *J. Am. Chem. Soc*. **1993**, *115*, 9858–9859.

(82) (a) Lafaye, K.; Bosset, C.; Nicolas, L.; Guérinot, A.; Cossy, J., Lewis Basicity Modulation of N‑Heterocycles: A Key for Successful Cross-Metathesis. *Beilstein J. Org. Chem.* **2015**, *11*, 2223–2241. (b) Lafaye, K.; Nicolas, L.; Guérinot, A.; Reymond, S. b.; Cossy, J., Lewis Basicity Modulation of N-Heterocycles: A Key for Successful Cross-Metathesis. *Org. Lett.* **2014**, *16*, 4972−4975.

(83) Nucleophilic attack of $PCy_3$ on methylidene ligands in the resting-state species $RuCl_2(L)(PCy_3)(=CH_2)$ has been confirmed crystallographically (see: (a) Lummiss, J. A. M.; McClennan, W. L.; McDonald, R.; Fogg, D. E., Donor-Induced Decomposition of the Grubbs Catalysts: An Intercepted Intermediate *Organometallics* **2014**, *33*, 6738–6741) and spectroscopically (see: (b) McClennan, W. L.; Rufh, S. A.; Lummiss, J. A. M.; Fogg, D. E., A General Decomposition Pathway for Phosphine-Stabilized Metathesis Catalysts: Lewis Donors Accelerate Methylidene Abstraction. *J. Am. Chem. Soc.* **2016**, *138*, 14668−14677). This pathway can culminate in abstraction of the methylidene moiety as $[MePCy_3]Cl$. See: (c) Hong, S. H.; Wenzel, A. G.; Salguero, T. T.; Day, M. W.; Grubbs, R. H., Decomposition of Ruthenium Olefin Metathesis Catalysts. *J. Am. Chem. Soc.* **2007**, *129*, 7961–7968. For evidence of this pathway in catalysis, see: (d) Lummiss, J. A. M.; Ireland, B. J.; Sommers, J. M.; Fogg, D. E., Amine-Mediated Degradation in Olefin Metathesis Reactions that Employ the Second-Generation Grubbs Catalysts *ChemCatChem* **2014**, *6*, 459–463.

(84) Higman, C. S.; Nascimento, D.; Ireland, B. J.; Audorsch, S.; Bailey, G. A.; Fogg, D. E., Chelate-Assisted Ring-Closing Metathesis: A Strategy for Accelerating Macrocyclization at Ambient Temperatures. *J. Am. Chem. Soc.* **2018**, *140*, 1604−1607.

(85) Cox, B. G., *Acids and Bases: Solvent Effects on Acid-Base Strength*. Oxford University Press: Croydon, 2013.

(86) In some cases, failed reactions adduced as evidence that Ru catalysts are inhibited by tertiary amines may have other causes. In, e.g.: (a) Lee, K.L., Goh, J.B., Martin, S.F. *Tetrahedron Lett*. **2001**, *42*, 1635–1638, the failed metathesis of an exocyclic alkene could be predicted solely from the unreactivity of the first-generation Grubbs catalyst **GI** with geminally-substituted olefins. For a discussion, see ref 25c. In other cases, catalyst deactivation may be independent of the amine. For example, the failure of a NHC-binaphtholate catalyst in RCM synthesis of N-methylpiperidine derivatives (see: (b) Cortez, G. A.; Schrock, R. R.; Hoveyda, A. H., Efficient Enantioselective Synthesis of Piperidines through Catalytic Asymmetric Ring-Opening/Cross-Metathesis Reactions. *Angew. Chem., Int. Ed.* **2007**, *46*, 4534–4538) could reflect MCB deprotonation by an intramolecular Bronsted base (as established in ref 36), but may alternatively be due to formation of a metathesis-inactive piano-stool complexes. See: (d) Snelgrove, J. L.; Conrad, J. C.; Eelman, M. D.; Moriarty, M. M.; Yap, G. P. A.; Fogg, D. E., Inhibiting s-p Isomerization of Aryloxide Ligands in Late Transition-Metal Complexes. *Organometallics* **2005**, *24*, 103–109. Tertiary N-allylamines, however, appear genuinely susceptible to deallylation, albeit typically in refluxing toluene with high loadings of **GI** (5 mol%). **GII** is reportedly less effective. See (b) and: (e) Alcaide, B.; Almendros, P.; Luna, A., Grubbs' Ruthenium-Carbenes Beyond the Metathesis Reaction: Less Conventional Non-Metathetic Utility. *Chem. Rev.* **2009**, *109*, 3817–3858.

(87) Lübbe, C.; Dumrath, A.; Neumann, H.; Schäffer, M.; Zimmermann, R.; Beller, M.; Kadyrov, R., How Important are Impurities in Catalysis? An Example from Ring-Closing Metathesis. *ChemCatChem* **2014**, *6*, 684–688.

(88) Rufh, S.; Goudreault, A. Y.; Foscato, M.; Jensen, V. R.; Fogg, D. E., Rapid Decomposition of Olefin Metathesis Catalysts by a Truncated N-Heterocyclic Carbene (NHC): Unprecedentedly Efficient Catalyst Quenching and NHC Vinylation. *ACS Catal.* **2018**, *8*, 11822−11826.

(89) Munz, D., Pushing Electrons: Which Carbene Ligand for Which Application? *Organometallics* **2018**, *37*, 275−289.

(90) Tolman, C. A., Steric Effects of Phosphorus Ligands in Organometallic Chemistry and Homogeneous Catalysis. *Chem. Rev.* **1977**, *77*, 313–348.

(91) For example, an analogue of $\mathbf{C2^{Me}}$ bearing an N-2,6-$iPr_2C_6H_3$ group has a TEP value only 4 $cm^{-1}$ lower than IMes (2046 vs 2050 $cm^{-1}$). See ref 63 and: Dorta, R.; Stevens, E. D.; Scott, N. M.; Costabile, C.; Cavallo, L.; Hoff, C. D.; Nolan, S. P., Steric and Electronic Properties of N-Heterocyclic Carbenes (NHC): A Detailed Study on Their Interaction with $Ni(CO)_4$. *J. Am. Chem. Soc.* **2005**, *127*, 2485–2495.

(92) Fürstner, A.; Langemann, K., Macrocycles by Ring-Closing Metathesis. *Synthesis* **1997**, 792–803.

(93) Frisch, M. J.; Trucks, G. W.; Schlegel, H. B.; Scuseria, G. E.; Robb, M. A.; Cheeseman, J. R.; Scalmani, G.; Barone, V.; Petersson, G. A.; Nakatsuji, H.; Li, X.; Caricato, M.; Marenich, A. V.; Bloino, J.; Janesko, B. G.; Gomperts, R.; Mennucci, B.; Hratchian, H. P.; Ortiz, J. V.; Izmaylov, A. F.; Sonnenberg, J. L.; Williams; Ding, F.; Lipparini, F.; Egidi, F.; Goings, J.; Peng, B.; Petrone, A.; Henderson, T.; Ranasinghe, D.; Zakrzewski, V. G.; Gao, J.; Rega, N.; Zheng, G.; Liang, W.; Hada, M.; Ehara, M.; Toyota, K.; Fukuda, R.; Hasegawa, J.; Ishida, M.; Nakajima, T.; Honda, Y.; Kitao, O.; Nakai, H.; Vreven, T.; Throssell, K.; Montgomery Jr., J. A.; Peralta, J. E.; Ogliaro, F.; Bearpark, M. J.; Heyd, J. J.; Brothers, E. N.; Kudin, K. N.; Staroverov, V. N.; Keith, T. A.; Kobayashi, R.; Normand, J.; Raghavachari, K.; Rendell, A. P.; Burant, J. C.; Iyengar, S. S.; Tomasi, J.; Cossi, M.; Millam, J. M.; Klene, M.; Adamo, C.; Cammi, R.; Ochterski, J. W.; Martin, R. L.; Morokuma, K.; Farkas, O.; Foresman, J. B.; Fox, D. J., Gaussian 16 Rev. B.01: Wallingford, CT, 2016.

(94) Frisch, M. J.; Trucks, G. W.; Schlegel, H. B.; Scuseria, G. E.; Robb, M. A.; Cheeseman, J. R.; Scalmani, G.; Barone, V.; Petersson, G. A.; Nakatsuji, H.; Li, X.; Caricato, M.; Marenich, A. V.; Bloino, J.; Janesko, B. G.; Gomperts, R.; Mennucci, B.; Hratchian, H. P.; Ortiz, J. V.; Izmaylov, A. F.; Sonnenberg, J. L.; Williams; Ding, F.; Lipparini, F.; Egidi, F.; Goings, J.; Peng, B.; Petrone, A.;

Henderson, T.; Ranasinghe, D.; Zakrzewski, V. G.; Gao, J.; Rega, N.; Zheng, G.; Liang, W.; Hada, M.; Ehara, M.; Toyota, K.; Fukuda, R.; Hasegawa, J.; Ishida, M.; Nakajima, T.; Honda, Y.; Kitao, O.; Nakai, H.; Vreven, T.; Throssell, K.; Montgomery Jr., J. A.; Peralta, J. E.; Ogliaro, F.; Bearpark, M. J.; Heyd, J. J.; Brothers, E. N.; Kudin, K. N.; Staroverov, V. N.; Keith, T. A.; Kobayashi, R.; Normand, J.; Raghavachari, K.; Rendell, A. P.; Burant, J. C.; Iyengar, S. S.; Tomasi, J.; Cossi, M.; Millam, J. M.; Klene, M.; Adamo, C.; Cammi, R.; Ochterski, J. W.; Martin, R. L.; Morokuma, K.; Farkas, O.; Foresman, J. B.; Fox, D. J., Gaussian 16 Rev. C.01: Wallingford, CT, 2016.

(95) Spartan 16, Wavefunction, Inc.: Irvine, CA, 2016.

(96) Halgren, T. A., Merck Molecular Force Field. I. Basis, Form, Scope, Parameterization, and Performance of MMFF94. *J. Comput. Chem.* **1996**, *17*, 490–519.

(97) Chai, J.-D.; Head-Gordon, M., Long-Range Corrected Hybrid Density Functionals with Damped Atom-Atom Dispersion Corrections. *Phys. Chem. Chem. Phys.* **2008**, *10*, 6615–6620.

(98) Minenkov, Y.; Singstad, Å.; Occhipinti, G.; Jensen, V. R., The Accuracy of DFT-Optimized Geometries of Functional Transition Metal Compounds: A Validation Study of Catalysts for Olefin Metathesis and Other Reactions in The Homogeneous Phase. *Dalton Trans.* **2012**, *41*, 5526–5541.

(99) Peterson, K. A.; Figgen, D.; Dolg, M.; Stoll, H., Energy-Consistent Relativistic Pseudopotentials and Correlation Consistent Basis Sets for the 4d Elements Y–Pd. *J Chem. Phys.* **2007**, *126*, 124101.

(100) Energy-consistent pseudopotentials of the Stuttgart/Cologne Group, http://www.tc.uni-koeln.de/PP/clickpse.en.html.

(101) Dunning, T. H., Gaussian Basis Sets for Use in Correlated Molecular Calculations. I. The Atoms Boron Through Neon and Hydrogen. *J. Chem. Phys.* **1989**, *90*, 1007–1023.

(102) Schuchardt, K. L.; Didier, B. T.; Elsethagen, T.; Sun, L.; Gurumoorthi, V.; Chase, J.; Li, J.; Windus, T. L., Basis Set Exchange: A Community Database for Computational Sciences. *J. Chem. Inf. Model.* **2007**, *47*, 1045–1052.

(103) Ribeiro, R. F.; Marenich, A. V.; Cramer, C. J.; Truhlar, D. G., Use of Solution-Phase Vibrational Frequencies in Continuum Models for the Free Energy of Solvation. *J. Phys. Chem. B* **2011**, *115*, 14556–14562.

(104) Zhao, Y.; Truhlar, D. G., Computational Characterization And Modeling Of Buckyball Tweezers: Density Functional Study Of Concave–Convex π···π Interactions. *Phys. Chem. Chem. Phys.* **2008**, *10*, 2813–2818.

(105) Perdew, J. P.; Burke, K.; Ernzerhof, M., Generalized Gradient Approximation Made Simple. *Phys. Rev. Lett.* **1996**, *77*, 3865–3868.

(106) (a) Zhao, Y.; Truhlar, D. G., A New Local Density Functional for Main-Group Thermochemistry, Transition Metal Bonding, Thermochemical Kinetics, and Noncovalent Interactions. *J. Chem. Phys.* **2006**, *125*, 194101. (b) Zhao, Y.; Truhlar, D. G., Density Functionals with Broad Applicability in Chemistry. *Acc. Chem. Res.* **2008**, *41*, 157–167. (c) Zhao, Y.; Truhlar, D. G., Applications and Validations of the Minnesota Density Functionals. *Chem. Phys. Lett.* **2011**, *502*, 1–13.

(107) Marenich, A. V.; Cramer, C. J.; Truhlar, D. G., Universal Solvation Model Based on Solute Electron Density and on a Continuum Model of the Solvent Defined by the Bulk Dielectric Constant and Atomic Surface Tensions. *J. Phys. Chem. B.* **2009**, *113*, 6378–6396.

(108) Grimme, S.; Ehrlich, S.; Goerigk, L., Effect of the Damping Function in Dispersion Corrected Density Functional Theory. *J. Comput. Chem.* **2011**, *32*, 1456–1465.

(109) Smith, D. G. A.; Burns, L. A.; Patkowski, K.; Sherrill, C. D., Revised Damping Parameters for the D3 Dispersion Correction to Density Functional Theory. *J. Phys. Chem. Lett.* **2016**, *7*, 2197–2203.

(110) Glendening, E. D.; Badenhoop, J. K.; Reed, A. E.; Carpenter, J. E.; Bohmann, J. A.; Morales, C. M.; Karafiloglou, P.; Landis, C. R.; Weinhold, F., NBO 7.0.; Theoretical Chemistry Institute, University of Wisconsin, Madison, WI 2018.

# Chapter 4. Building on Insights into Decomposition: Catalyst Redesign

## 4.1. Context and Overview of Content

A number of the advances described so far offer important clues for improved catalyst design. Most general was the lesson emerging from studies of the Grubbs catalysts described in Chapter 1: that is, hazards associated with the $PCy_3$ ligand used to stabilize the five-coordinate precatalyst. Use of an ancillary ligand for the purpose of stabilizing a higher-coordinate precatalyst is ubiquitous in molecular catalysis. Commonly, however, the ligand is relatively innocuous once it is released to permit access to the active species. $PCy_3$ is an exception, as a potent nucleophile, as well as a Brønsted base. These properties result in undesired side-reactions arising from the free ligand.

An initial objective was therefore identification of alternative stabilizing ligands, which would be (1) more labile than the chelating ether ligand of the Hoveyda catalysts, and (2) innocuous once released. As these studies commenced at the outset of this thesis work, they focused on the then-dominant $H_2$IMes catalysts. It may be noted, however, that although the data in Chapter 3 suggest that the future in metathesis may belong to the CAAC catalysts, commercial deployment of these complexes is subject to intellectual-property restrictions. The $H_2$IMes derivatives may thus remain strategically important for the immediate future.

Described in Paper 1 (Section 4.2) is a novel ligand design centered on a 2,2'-*ortho*-dianiline (ODA) chelate. Additional, unanticipated advantages arising from the flexibility of this atropisomeric chelate lie in its capacity to collapse the metallacyclobutane ring, enabling the catalyst to rapidly exit a vulnerable state. An intriguing further advantage is the H-bonding capacity of this ligand, which can promote binding and cyclization of conformationally flexible dienes bearing polar sites.

A limitation associated with H-bonding, however, is increased sensitivity to trace water. This point is touched on briefly under the heading "Subsequent Advances to Section 4.2" (Paper 2). Nevertheless, the **DA** catalyst has since been adopted in pharmaceutical science for the production of DNA-encoded chemical libraries in aqueous media.[1]

An alternative approach, focusing on the synthesis of CAAC catalysts (Paper 3), deploys a dative chloride ligand to stabilize the precatalyst via a dimeric structure, in place of the usual Lewis-base donor ligands that offer access to monoruthenium complexes. This is an unorthodox approach, given early work by our group demonstrating that the chloride ligands can mediate bimolecular decomposition[2,3] (findings supported by the breaking results of Chapter 3,[4] which indicate that the CAAC catalysts are even more susceptible to this decomposition pathway than their NHC predecessors).[5] The key lies in use of a bulky indenylidene ligand in the precatalyst, which is immune to bimolecular coupling.

*References for Chapter 4 begin on p. 132*

These contributions are listed below, following which each paper is presented.

### 4.1.1. Published Contributions

(1) Chelate-Assisted Ring-Closing Metathesis: A Strategy for Accelerating Macrocyclization at Ambient Temperatures. C.S. Higman,^ D.L. Nascimento,^ B.J. Ireland, S.A. Audorsch, G.A. Bailey, R. McDonald, D.E. Fogg.* *J. Am. Chem. Soc.* **2018**, *140*, 1604-1607. ^Equal contributions. (Communication). Copyright 2018, American Chemical Society. Reprinted with permission.

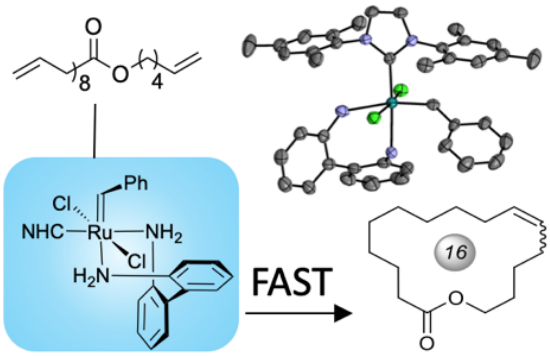


*Abstract:* Ring-closing metathesis (RCM) offers versatile catalytic routes to macrocycles, with applications ranging from perfumery to production of antiviral drugs. Unwanted oligomerization, however, is a long-standing challenge. Oligomers can be converted into the cyclic targets by catalysts that are sufficiently reactive to promote backbiting (e.g. Ru complexes of N-heterocyclic carbenes; NHCs), but catalyst decomposition limits yields and selectivity. Incorporation of a hemilabile *o*-dianiline (ODA) chelate into new catalysts of the form $RuCl_2$(NHC)(ODA)(=CHPh) accelerates macrocyclization, particularly for dienes bearing polar sites capable of H-bonding: it may also inhibit catalyst decomposition during metathesis. Significant improvements relative to prior Ru-NHC catalysts result, with fast macrocyclization of conformationally flexible dienes at room temperature.

(2) The Impact of Water on Ru-Catalyzed Olefin Metathesis: Potent Deactivating Effects Even at Low Water Concentrations. C.O. Blanco, J. Sims, D.L. Nascimento, A.Y. Goudreault, S.N. Steinmann, C. Michel,* D.E. Fogg.* *ACS Catal.*, **2021**, *11*, 893-899. (Communication). Copyright 2021, American Chemical Society. Reprinted with permission.

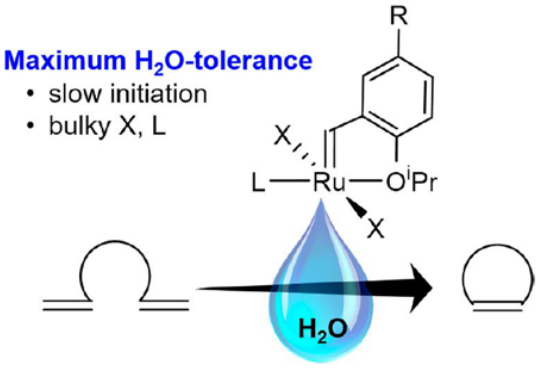


*Abstract:* Ruthenium catalysts for olefin metathesis are widely viewed as water-tolerant. Evidence is presented, however, that even low concentrations of water cause catalyst decomposition, severely degrading yields. Of 11 catalysts studied, fast-initiating examples (e.g., the Grela catalyst $RuCl_2(H_2IMes)(=CHC_6H_4\text{-}2\text{-}O^iPr\text{-}5\text{-}NO_2)$ were most affected. Highest water-tolerance was exhibited by slowly-initiating iodide and cyclic (alkyl)(amino)carbene derivatives. Computational investigations indicated that hydrogen-bonding of water to substrate can also play a role, by retarding cyclization relative to decomposition. These results have important implications for

olefin metathesis in organic media, where water is a ubiquitous contaminant, and for aqueous metathesis, which currently requires super-stoichiometric "catalyst" for demanding reactions.

(3) Integrating Activity with Accessibility in Olefin Metathesis: An Unprecedentedly Reactive Ruthenium-Indenylidene Catalyst. D.L. Nascimento, A. Gawin, R. Gawin, P.A. Gunka, J. Zachara, K. Skowerski, D.E. Fogg.* *J. Am. Chem. Soc.* **2019**, 141, 10626-10631. (Communication). Copyright 2019 American Chemical Society. Reprinted with permission.

*Abstract:* Access to leading olefin metathesis catalysts, including the Grubbs, Hoveyda, and Grela catalysts, ultimately rests on the non-scalable transfer of a benzylidene ligand from an unstable, impure aryldiazomethane. The indenylidene ligand can be reliably installed, but to date yields much less reactive catalysts. A fast-initiating, dimeric indenylidene complex (**InC1$^{Ph}$**) is reported, which reconciles high activity with scalable synthesis. Each Ru center in **InC1$^{Ph}$** is stabilized by a state-of-the-art cyclic alkyl amino carbene (CAAC, **C1$^{Ph}$**) and a bridging chloride donor: the lability of the latter elevates the reactivity of **InC1$^{Ph}$** to a level previously attainable only with benzylidene derivatives. Evaluation of initiation rate constants reveals that **InC1$^{Ph}$** initiates >250x faster than indenylidene catalyst **InII** ($RuCl_2(H_2IMes)(PCy_3)(Ind)$), and 65x faster than **UC** ($RuCl_2(\mathbf{C1^{Ph}})_2(Ind)$). The slow initiation previously regarded as characteristic of indenylidene catalysts is hence due to low ligand lability, not inherently slow cycloaddition at the Ru=CRR' site. In macrocyclization and "ethenolysis" of methyl oleate (i.e. transformation into α-olefins via cross-metathesis with $C_2H_4$), **InC1$^{Ph}$** is comparable or superior to the corresponding, breakthrough CAAC-benzylidene catalyst. In ethenolysis, **InC1$^{Ph}$** is 5x more robust to standard-grade (99.9%) $C_2H_4$ than the top-performing catalyst, probably reflecting steric protection at the quaternary CAAC carbon.

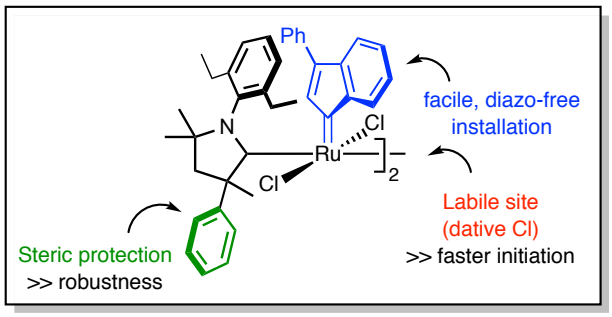


*Author Contributions:* Papers (1) and (3) were written by DN and DEF, with contributions by CH in (1). Experiments in (1) were conducted by DN (who conceived of the phenomenon of H-bonding assistance in macrocyclization) and CH. Paper 2 originated in high-throughput catalyst screening to probe the impact of water (DN and Alexandre Goudreault); these preliminary data were repeated by CB in higher-precision bench-scale experiments, and also expanded to a series of further catalysts. The initial synthetic procedure in (3) was developed by KS and RG, and further optimized by DN. Catalytic studies were carried out by DN, X-ray analysis by PG and JZ.

*References for Chapter 4 begin on p. 132*

## 4.2. Hydrogen-Bonding Assisted Macrocyclization at Room Temperature

### 4.2.1. Introduction

One of the most prominent advances enabled by olefin metathesis is the assembly of macrocyclic rings via ring-closing metathesis (RCM).[6] RCM is among the most versatile catalytic methodologies developed to date for the synthesis of diverse macrocyclic structures, entities of keen interest in the medicinal and fine-chemicals sectors.[6,7] Pioneering advances in total synthesis[8] demonstrated its power, and laid the foundation for widespread adoption. RCM macrocyclization has recently been exploited as a pivotal step in the assembly of several active pharmaceutical ingredients (APIs).[6]

Catalyst efficiency, however, remains a challenge.[9,10] While the Ru precatalysts (Chart 4.1) are often robust, productivity in demanding reactions is limited by decomposition of Ru intermediates, particularly active species **B-$H_2$IMes** and the unsubstituted metallacyclobutane **A-$H_2$IMes**. Exacerbating factors include high temperatures and the presence of ethylene (the usual co-product of metathesis, which increases the proportion of vulnerable, unproductive **A-$H_2$IMes**). Also problematic are the high dilutions required to favor macrocyclic products.[8,11] In general,[12] reduced concentrations retard metathesis, permitting catalyst decomposition to compete with RCM.

**Chart 4.1. Leading Ru metathesis catalysts and (inset) intermediates discussed.**

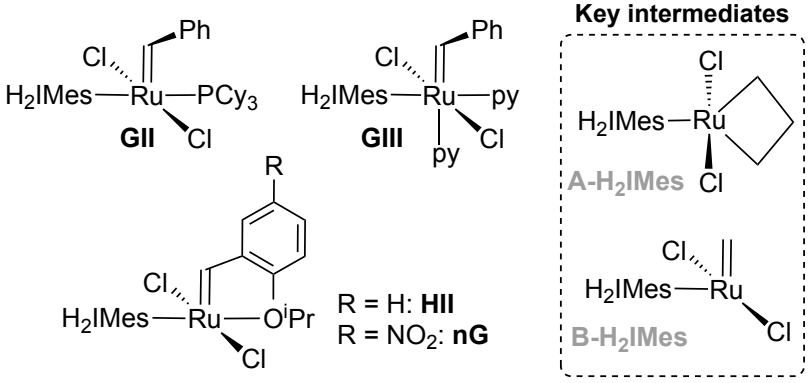


Competing catalyst decomposition is a particular challenge in macrocyclization of flexible dienes. For such substrates (e.g. **1**, Scheme 4.1; precursor to a leading synthetic musk),[13] the kinetic products are oligomers rather than the desired macrocycles (Scheme 4.1a vs 4.1b).[14,15] The macrocycles can be liberated via backbiting, if the catalyst is sufficiently active and long-lived, and if dilutions are high enough for the ring-chain equilibrium to favor the cyclic product (5 mM, in the case of **1**; Scheme 4.1c). However, metathesis at internal, chiefly *trans*-configured olefinic sites typically requires high temperatures or long reaction times. Either promotes catalyst decomposition, trapping a proportion of the potential product as oligomers.

*References for Chapter 4 begin on p. 132*

**Scheme 4.1. Ring-chain equilibrium in RCM of conformationally mobile dienes such as 1.**

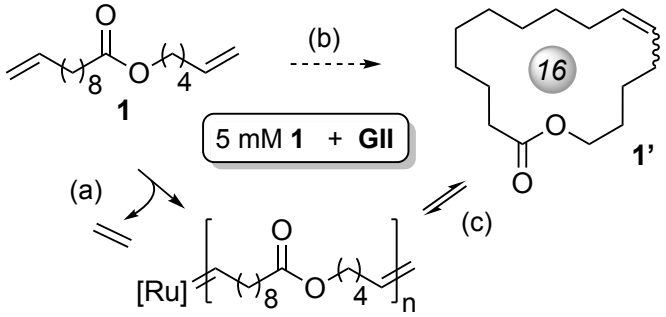


To date, high productivity has been attained only where decomposition is restrained by aggressively removing ethylene,[*20] adding the catalyst slowly or in several doses, and, in the extreme, stringently purifying reagents and solvent.[21] Barring such measures, catalyst loadings of 3-5 mol% are the norm for quantitative RCM of **1**.[11,15,22,23] Such loadings increase process costs, impede product isolation, and can degrade selectivity, owing to double-bond isomerization catalyzed by decomposed catalyst.[9,24] Here we describe a mechanistically-guided catalyst design strategy. Redesign of the stabilizing ancillary ligand realized our initial goal of fast, efficient macrocyclization at room temperature, while uncovering new capabilities that promote conformational preorganization of substrates bearing polar groups.

### 4.2.2. Results and Discussion

As a prime objective, we sought to identify a bidentate, hemilabile ligand (Scheme 4.2) that could permit facile entry into the catalytic cycle, while impeding decomposition of intermediates **A** and **B**. To prevent ligand-induced decomposition, we further stipulated that this ancillary ligand should possess limited nucleophilicity,[25] and low Brønsted basicity.[26] *o*-Dianiline (ODA) meets each of these criteria.[27,28] Treating **GIII** with ODA at RT resulted in immediate formation of the target catalyst **DA**, in 40% equilibrium yield. Ligand exchange was forced to completion by repeated azeotropic removal of pyridine, after which **DA** was isolated in ca. 80% yield by reprecipitating from $CH_2Cl_2$-hexanes. The IMes analog **DA'** was prepared likewise from **GIII'**. The analytical data are consistent with the structure shown. This assignment is further supported by crystallographic analysis of **DA'**, X-ray quality crystals of which deposited from toluene-hexanes at –30 °C.

[*] Catalysts bearing cyclic (alkyl)(amino) carbene ligands are significantly more tolerant toward ethylene.[16-19]

*References for Chapter 4 begin on p. 132*

**Scheme 4.2. Synthesis of *o*-dianiline (ODA) catalysts, and ORTEP plot showing perspective view of DA'.**[a]

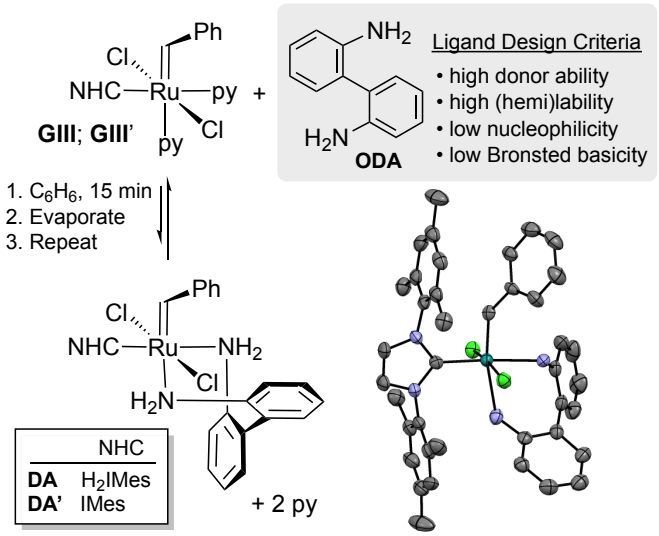


[a]Non-hydrogen atoms are represented by Gaussian ellipsoids (30% probability level). Hydrogen atoms and solvent omitted. **GIII**: NHC = $H_2$IMes; **GIII'**: NHC = IMes.

Figure 4.1 shows the accelerating effect of the ODA ligand on macrocyclization of **1**. For **DA**, RCM yields were quantitative at 2 h. NHC backbonding and rotation[29] have minimal impact, as indicated by the similar performance of IMes complex **DA'**. Of the benchmark catalysts in Chart 4.1, none enabled complete RCM, but the Grela catalyst **nG** performed best, with ca. 90% **1'**.

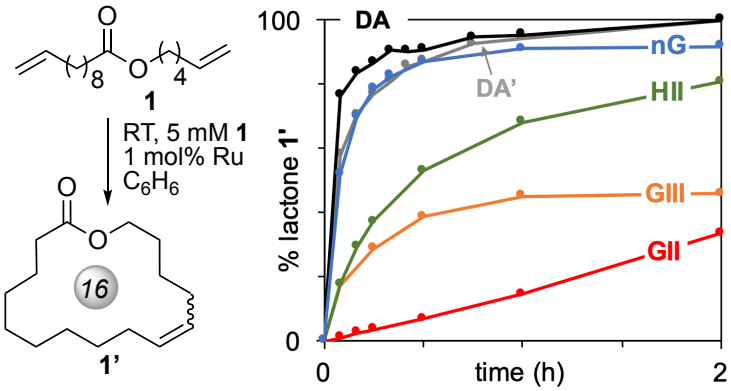


**Figure 4.1. Assessing catalyst performance in RCM of diene 1 to yield lactone 1'.**

RCM by **HII** and **GII** is slower, consistent with retarded initiation vs the ODA catalysts or **nG**, as well as recapture of active species **A** by isopropoxystyrene[30] or $PCy_3$[12,29a] (respectively). RCM by **GIII** terminates at <50%, despite rapid entry into the catalytic cycle enabled by the lability of pyridine. We recently demonstrated that the pyridine ligand is too labile to stabilize intermediate **A** against bimolecular coupling and loss of methylidene as ethylene (Scheme 4.3a).[5] The

chelating ODA ligand, in contrast, appears to retard coupling. Importantly, adding ODA to solutions of **GIII** at the high dilutions essential for RCM of **1** did not improve RCM yields,* implying that **DA** itself forms **B'** (Scheme 4.3b) as the active species, not **B**. N–H---Cl hydrogen bonding[31] may help to retain the ODA ligand in the metal coordination sphere. We speculate that recoordination of the dangling $NH_2$ moiety in intermediate **A'** also promotes rapid reformation of **B'**.[5] A similar phenomenon may well account for the high macrocyclization efficiency of RuCl($\kappa^2$-O,Br-$OC_6Br_5$)(IMes)(py).[32]

**Scheme 4.3. (a) Decomposition of GIII by coupling of A. (b) Proposed role for the hemilabile ODA ligand in inhibiting decomposition. L = $H_2$IMes.**

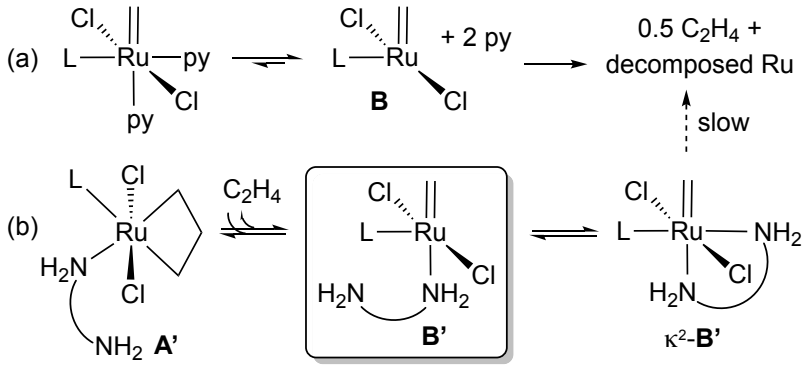


The rate difference between **DA** and **nG** in RCM of **1** is enhanced at 0.1 mol% catalyst (Table 4.1, entries 1–2~~; for rate curves, See Appendix~~). Only slightly higher conversions are seen for **DA** at 60 °C (entry 3), probably indicating thermally-induced loss of ODA and accelerated decomposition. Experiments with dienes bearing polar sites indicate that H-bonding represents an additional advantage of the ODA ligand, beyond initiation and longevity. Thus, while **DA** and **nG** show comparable performance in RCM of readily-cyclized diethyl diallylmalonate **2**, **DA** is dramatically faster in RCM of polyether **3** to give 14-membered **3'** (entry 5). H-bonding may assist both substrate binding, and (via conformational pre-organization) the macrocyclization step.[14,33]

Consistent with this hypothesis, the **DA** / **nG** performance difference diminishes as the number of polar sites on the diene decreases (see **4**, entry 6). (Also of note for **3** and **4** is the absence of C=C isomerization, despite the propensity of allyl ether substrates to such bond migration).[9] Unexpectedly, tosyl-protected amine **5** is also more readily cyclized by **DA**, probably reflecting H-bonding to a tosyl oxygen. Diamide **6**, which likewise yields a 15-membered ring but benefits from additional polar sites, cyclizes much more readily than **5** at a concentration tenfold higher.

---

* Yield of **1'** at 2 h with 0.05 mol% **GIII**; other conditions as in Figure 4.1: 19%. With 2 equiv ODA added: 19%. At 6 h: no change.

**Table 4.1. RCM performance of DA vs nG.**[a]

| Entry | Diene | RCM Product | Conditions | Ru-1 Conv. | Ru-1 Yield | nG Conv. | nG Yield |
|---|---|---|---|---|---|---|---|
| 1 | **1** | **1'** | 1 mol% Ru RT, 1 h | Q | Q | Q | 92 |
| 2 | **1** | **1'** | 0.1 mol% Ru RT, 1 h | 95 | 85 | 91 | 80 |
| 3[b] | **1** | **1'** | 0.1 mol% Ru 60 °C, 15 min | 99 | 86 | | |
| 4 | **2** | **2'** | 0.05 mol% Ru RT, 0.2 M, 30 min | Q | Q | Q | Q |
| 5 | **3** | **3'** | 1 mol% Ru RT, 0.5 mM, 1 h | Q | 97 | 65 | 63 |
| 6 | **4** | **4'** | 1 mol% Ru RT, 0.5 mM, 1 h | 98 | 70 | 82 | 58 |
| 7 | **5** | **5'** | 1 mol% Ru RT, 0.5 mM, 1 h | Q | 61 | 86 | 36 |
| 8 | **6** | **6'** | 1 mol% Ru RT, 0.5 h | Q | Q | Q | 66 |

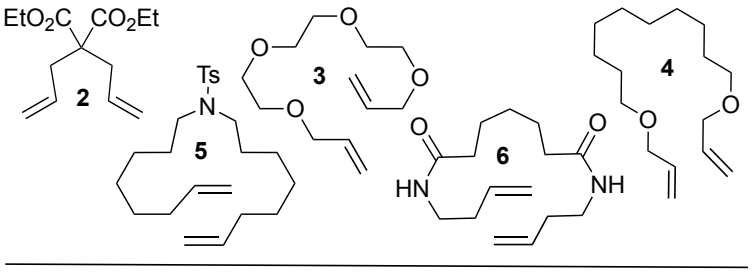


[a]5 mM diene, unless otherwise stated. Q = quantitative. [b]Cf. **GII**: 97% conversion, 79% yield.

### 4.2.3. Conclusion

The foregoing describes the first efficient Ru-catalyzed synthesis of macrocycles via room-temperature RCM. New catalysts incorporating a hemilabile *o*-dianiline ligand, $RuCl_2(NHC)(\kappa^2$-ODA)(=CHPh), exhibit high activity, including fast conversion of oligomers into the desired macrocycles, without the need for elevated temperatures. Proposed as key functions of the ODA ligand are fast initiation, retarded decomposition, and H-bonding to polar sites in the substrates, the last of which may aid both substrate binding and preorganization. Particularly for dienes capable of H-bonding interactions, the performance of the ODA catalysts greatly surpasses that of the leading second-generation catalysts **nG**, **GII** and **HII**. The use of a hemilabile, H-bonding ligand to assist RCM represents a new, potentially general paradigm for improved efficiency in RCM macrocyclization of functionalized dienes.

*References for Chapter 4 begin on p. 132*

### 4.2.4. Experimental Details for Section 4.2

**General Procedures.** Reactions were carried out under $N_2$ in a glovebox or Schlenk line, unless otherwise indicated. For glovebox and Schlenk line procedures, solvents (HPLC grade: $C_6H_6$, $C_7H_8$, hexanes, $CH_2Cl_2$, THF) were dried and degassed using a Glass Contour solvent purification system, and stored under $N_2$ over 4 Å molecular sieves for at least 16 h prior to use. Pentane (HPLC grade) was distilled over $MgSO_4$, then $P_2O_5$. For aerobic benchtop procedures, solvents used were standard laboratory grade. The NMR solvents $C_6D_6$ and $CDCl_3$ (Cambridge Isotopes) were freeze/pump/thaw degassed and stored under $N_2$ over 4 Å molecular sieves for at least 12 h prior to use. Potassium tris(1-pyrazolyl)borohydride (KTp; TCI), *p*-toluenesulfonamide (Aldrich, 99%), 8-bromo-1-octene (Aldrich, 97%), tetra-*N*-butylammonium iodide (Aldrich, 99%), 3-buten-1-amine (Alfa Aesar, 97%), triethylamine (Alfa Aesar, 99%), and pimeloyl chloride (Aldrich, 98%) were used as received. Metathesis catalysts **GIII**,[34] **GIII'**,[34] **GII**,[35] and **HII**[35] were prepared by literature methods, as were *o*-dianiline ligand ODA;[36] dienes **1**,[37] **3**,[38] and **4**;[39] and macrocycles **1'** and **2'** (for GC-FID calibration).[37,40] The nitro-Grela catalyst **nG** was generously provided by Apeiron Synthesis. Liquid RCM substrates (including diethyl diallylmalonate **2**, Aldrich, 98%), decane and dodecane (GC internal standards; both Aldrich, anhydrous, 99%) were freeze/pump/thaw degassed and stored under $N_2$ in the glovebox.

Analyte quantification was effected using Agilent 6890 or 7890A gas chromatographs (GC) equipped with autosamplers, flame ionization detectors (FID) and Agilent HP-5 polysiloxane columns (30 m length, 320 μm diameter). Calibration curves of peak areas versus concentration were established for the starting diene and macrocyclic products in the relevant concentration regimes, with ca. 1:1 (w/w) sample versus decane or dodecane as internal standard. Yields were determined from the integrated peak areas versus internal standard. Reported values are averages of two trials (±2%). For the diamide substrate **6** and its RCM product **6'**, the poor solubility of the isolated solids precluded construction of accurate calibration curves. Instead, the absence of oligomers was confirmed by $^1$H NMR, MALDI-TOF MS, and TLC following RCM with **DA** (Table 4.1, entry 8), from which the yield of **6'** was deemed quantitative. The percent yield for **nG** was then calculated as the fraction of the response observed for **DA**.

NMR spectra were recorded on Avance 300, Avance II 300, or Avance 500 NMR spectrometers at 23 ±2 °C, unless otherwise indicated. Chemical shifts are reported in ppm, and referenced to the residual proton or carbon signals of the solvent. MALDI mass spectra were collected on a Bruker UltrafleXtreme MALDI-TOF/TOF mass spectrometer. Mixed solutions of matrix and analyte were prepared in 30:70 [v/v] acetonitrile : 0.1% TFA in water, such that the final concentration of matrix and analyte as ca. 50 mM and 0.1 mM, respectively. A 1 μL aliquot of the mixed solution was spotted on the MALDI target plate and allowed to evaporate by the dried-droplet method. Spectra were calibrated internally using the peaks for the matrix (CHCA•$H^+$: *m/z* 190.0499) and $H_2$IMes•$H^+$ (residual from RCM; *m/z* 307.2174).

**Synthesis of *o*-Dianiline (ODA) Complexes**

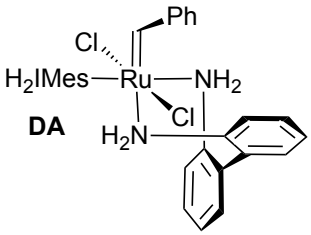


**$RuCl_2(H_2IMes)(ODA)(=CHPh)$, DA:** In the glovebox, a solution of *o*-dianiline (ODA; 55 mg, 0.30 mmol, 1.0 equiv) in 1 mL $C_6H_6$ was added to a green solution of GIII (218 mg, 0.300 mmol, 1.0 equiv) in 4 mL $C_6H_6$. After 15 min, an equilibrium mixture of the desired **DA**, **GIII** and ODA was present. Partial azeotropic removal of pyridine was effected by evaporation of the solvent, following which the residue was redissolved in fresh $C_6H_6$, stirred for 15 min, and subjected to vacuum as before. This process was repeated until consumption of **GIII** was complete ($^1$H NMR; 10 iterations). The resulting green solid was reprecipitated from $CH_2Cl_2$–hexanes and washed with hexanes (3 x 3 mL). Yield after drying: 180 mg (80%). $^1$H NMR ($CDCl_3$, 500 MHz, –20 °C): δ 18.49 (s, 1H, [Ru]=C*H*Ph), 8.73 (br s, 1H, Ph *o*-C*H*), 7.56 (t, $^3J_{HH}$ = 6 Hz, 1H, Ph *p*-C*H*), 7.40 (br s, 1H, Ph *o*-C*H*), 7.35 (s, 1H, Mes C*H*), 7.32–7.22 (overlapping m, 3H, Ph *m*-C*H* and ODA C*H*), 7.15–6.79 and 7.08 (overlapping m and s, 6H, 5 ODA *CH* and Mes C*H*), 6.78 (s, 1H, Mes C*H*), 6.58 (d, $^3J_{HH}$ = 9 Hz, 1H, ODA *o*-C*H*), 6.19 (s, 1H, Mes C*H*), 5.93 (br s, 1H, ODA *o*-C*H*), 4.69 (br s, 1H, ODA N*H*), 4.44 (br s, 1H, ODA N*H*), 4.32 (br s, 1H, ODA N*H*), 4.17–4.02 (m, 1H, NHC NC$H_2$), 4.02–3.89 (overlapping m, 2H, NHC NC$H_2$), 3.89–3.67 (overlapping m, 2H, ODA N*H* and NHC NC$H_2$), 2.75 (s, 3H, Mes *o*-$CH_3$), 2.67 (s, 3H, Mes *o*-$CH_3$), 2.53 (s, 3H, Mes *p*-$CH_3$), 2.34 (s, 3H, Mes *p*-$CH_3$), 2.02 (s, 3H, Mes *o*-$CH_3$), 1.90 (s, 3H, Mes *o*-$CH_3$). $^{13}$C{$^1$H} NMR ($C_6D_6$, 125.8 MHz, –20 °C): δ 307.5 ([Ru]=*C*HPh), 215.7 ($C_{NHC}$), 151.7 (Ph $C_{ipso}$), 141.0, 139.4, 139.2, 138.9, 138.4, 138.0, 137.9, 137.6, 136.7, 130.3, 130.1, 129.9, 129.7, 129.6, 129.3, 129.0, 128.8, 128.6, 128.3, 128.2, 127.5, 127.4, 127.1 (ODA *o*-*C*–Ar), 126.3 (ODA *o*-*C*–Ar), 123.8 (ODA *m*-*C*H), 122.3 (ODA *o*-*C*H), 121.1 (ODA *o*-*C*H), 120.8, 51.3 (NHC N*C*$H_2$), 50.8 (NHC N*C*$H_2$), 21.2 (Mes *p*-*C*$H_3$), 20.9 (Mes *o*-*C*$H_3$), 19.5 (Mes *o*-*C*$H_3$), 19.4 (Mes *o*-*C*$H_3$), 18.8 (Mes *p*-*C*$H_3$), 18.2 (Mes *o*-*C*$H_3$). IR (ATR, cm$^{-1}$): ν(N-H) 3346 (s), 3324 (m), 3258 (m). Anal. Calcd. for $C_{40}H_{44}N_4Cl_2Ru$: C, 63.82; H, 5.89; N, 7.44. Found: C, 63.81; H, 6.06; N, 7.66.

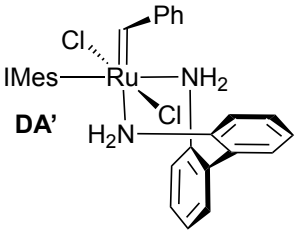


**$RuCl_2(IMes)(ODA)(=CHPh)$, DA':** Reaction was carried out as for **DA**, but starting from **GIII'** (217 mg, 0.300 mmol), and with only three dissolution/ evaporation cycles. The product was dissolved in THF, filtered through Celite, and stripped of solvent prior to recrystallizing from toluene-hexanes. Yield after drying: 105 mg (58%). X-ray quality crystals deposited from toluene–hexanes at –30 °C. $^1$H NMR ($CDCl_3$, 500.1 MHz, –20 °C): δ 18.49 (s, 1H, [Ru]=C*H*Ph), 8.81 (br s, 1H, Ph *o*-C*H*), 7.59 (t, $^3J_{HH}$ = 7 Hz, 1H, Ph *p*-CH), 7.42 (br s, 1H, Ph *o*-C*H*), 7.37 (s, 1H, Mes C*H*), 7.33–7.22 (overlapping m, 3H, Ph *m*-C*H* and ODA C*H*), 7.11 (s, 1H, Mes C*H*), 7.08–6.89 (overlapping m and s, 7H, ODA C*H* and NHC C*H*), 6.83 (s, 1H, Mes C*H*), 6.65 (d, $^3J_{HH}$ = 8 Hz, 1H, ODA *o*-C*H*), 6.23 (s, 1H, Mes C*H*), 5.89 (br s, 1H, ODA *o*-C*H*), 4.87 (d, $^3J_{HH}$ = 9 Hz, 1H, ODA N*H*), 4.63 (d, $^3J_{HH}$ = 8 Hz, 1H, ODA N*H*), 4.51 (d, $^3J_{HH}$ = 8 Hz, 1H, ODA N*H*), 3.82 (d, $^3J_{HH}$ = 9 Hz, 1H, ODA N*H*), 2.57 (s, 3H, Mes *o*-C$H_3$), 2.42 (s, 3H, Mes *p*-C$H_3$), 2.38 (s, 3H, Mes *o*-C$H_3$), 2.30 (s, 3H, Mes *p*-C$H_3$),

*References for Chapter 4 begin on p. 132*

2.06 (s, 3H, Mes *o*-C$H_3$), 1.70 (s, 3H, Mes *o*-C$H_3$). $^{13}C\{^1H\}$ NMR ($CDCl_3$, 125.8 MHz, –20 °C): δ 308.7 ([Ru]=*C*HPh), 181.6 ($C_{NHC}$), 152.4 (Ph, $C_{ipso}$), 141.3 (ODA $C_{ipso}$), 140.3 (ODA $C_{ipso}$), 139.0, 138.84, 138.82, 138.2, 137.4, 137.3, 137.2, 136.5, 130.4, 130.2, 130.0, 129.8, 129.6, 129.5, 128.8, 128.64, 128.63, 127.7 (ODA *o*-*C*–Ar), 127.6, 127.4 (ODA *o*-*C*–Ar), 125.4, 124.6, 124.1 (ODA *m*-*C*H), 122.7 (ODA *m*-*C*H), 121.4 (ODA *o*-*C*H), 121.1 (ODA *o*-*C*H), 21.5 (Mes *o*-*C*$H_3$), 21.2 (Mes *o*-*C*$H_3$), 19.4 (Mes *o*-*C*$H_3$), 19.3 (Mes *p*-*C*$H_3$), 18.7 (Mes *p*-*C*$H_3$), 18.2 (Mes *o*-*C*$H_3$). IR (ATR, $cm^{-1}$): ν(N-H) 3358 (s), 3342 (m), 3320 (m), 3254 (m). Anal. Calcd. for $C_{40}H_{42}N_4Cl_2Ru$: C, 63.99; H, 5.64; N, 7.46. Found: C, 64.13; H, 5.90; N, 7.11.

## Synthesis of Dienes and Macrocycles

### Synthesis of Dienes

**Diene *N,N*-di(oct-7-enyl)-*p*-toluenesulfonamide (5):** Tosyl diene **5** was prepared according to the reported protocol for the di(hexenyl) analog,[41] but with chromatographic conditions adapted for the larger diene. On the bench, a 250 mL round-bottom flask was charged with *p*-toluenesulfonamide (3.0 g, 18 mmol, 1.0 equiv), 8-bromo-1-octene (9.2 mL, 55 mmol, 3.0 equiv), tetra-*N*-butylammonium iodide (6.6 g, 18 mmol, 1.0 equiv), NaOH (3.6 g, 91 mmol, 5.0 equiv), $C_6H_6$ (100 mL), and water (6 mL). The resulting homogeneous yellow solution was heated to reflux for 2.5 h, after which time TLC indicated clean conversion to the desired product ($R_f$ 0.65, 2:1 hexanes/ethyl acetate). The solution was extracted with ethyl acetate (100 mL). The combined organic fractions were washed with brine and water (100 mL each), dried ($MgSO_4$), and concentrated to dryness, affording crude diene **5** as a yellow oil (4.36 g, 62%). A portion of the crude product was purified by flash column chromatography (70% $CH_2Cl_2$ / pentane; 18 cm x 3.5 cm column), affording pure diene **5** as a colourless oil. $^1H$ NMR ($CDCl_3$, 300 MHz): δ 7.67 (d, $^3J_{HH}$ = 8.3 Hz, $^4J_{HH}$ = 1.8 Hz, 2H, Ar C*H*), 7.28 (d, $^3J_{HH}$ = 8.0 Hz, 2H, Ar C*H*), 5.87–5.71 (m, 2H, =C*H*), 4.98 (dm, $^3J_{HH}$ = 19 Hz, 2H, =C*H*), 4.93 (dm, $^3J_{HH}$ = 11 Hz, 2H, =C*H*), 3.08 (t, $^3J_{HH}$ = 7.5 Hz, 4H, NC$H_2$), 2.41 (s, 3H, Ts C$H_3$), 2.02 (m, 4H, C$H_2$), 1.57–1.43 (m, 4H, C$H_2$), 1.41–1.19 (m, 12H, C$H_2$). The $^1H$ NMR data for **5** are in good agreement with the literature data for the corresponding di(hexenyl) analog,[41] with the exception of the aliphatic signals (1.41–1.19), which integrate to 12H for **5**.

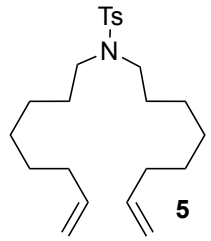

**5**

**Diene *N,N*-di(4-buten-1-yl)-1,5-pentanediamide (6):** Diamide **6** was prepared according to the reported protocol for synthesis of diaryl malonyl diamides.[42] Thus, an oven-dried 100 mL 3-neck round-bottom flask was charged with dry THF (10 mL), 3-buten-1-amine (0.32 g, 4.6 mmol, 2.1 equiv), and triethylamine (0.43 g, 4.3 mmol, 2.0 equiv) on the Schlenk line. The solution was cooled to 0 °C, and a solution of pimeloyl chloride (0.42 g, 2.2 mmol, 1.0 equiv) in dry THF (10 mL) was added via dropping funnel over 10 min. A white precipitate appeared instantly. The reaction was stirred for a further 1.5 h, and then aqueous HCl (4 M solution; 7.5 mL) was added dropwise, resulting in vigorous gas

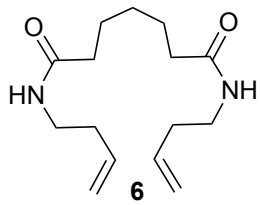

**6**

evolution. The reaction was allowed to warm to RT, stirred for an additional 30 min, and then filtered and concentrated to dryness. Ethyl acetate (70 mL) and water (20 mL) were added to the filtrate, the aqueous phase was extracted with ethyl acetate (3 x 70 mL), and the combined organic phase was washed with saturated $NaHCO_3$ (70 mL). Drying ($MgSO_4$) and evaporation of the solvent afforded diamide 6 as a crystalline white solid (0.38 g, 67%). Diamide **6** was used in subsequent RCM protocols without further purification. $^1$H NMR ($CDCl_3$, 300 MHz): δ 5.82–5.67 (m, 2H, =C*H*), 5.50 (br s, 2H, N*H*), 5.13–5.06 (overlapping m, 4H, =C$H_2$), 3.32 (q, $^3J_{HH}$ = 6.1 Hz, 4H, C$H_2$NH), 2.26 (q, $^3J_{HH}$ = 6.8 Hz, 4H, C$H_2$), 2.16 (t, $^3J_{HH}$ = 7.3 Hz, 4H, C$H_2$), 1.64 (quint, $^3J_{HH}$ = 7.6 Hz, 4H, C$H_2$), 1.34 (quint, $^3J_{HH}$ = 7.4 Hz, 4H, C$H_2$). $^{13}$C{$^1$H} ($CDCl_3$, 75 MHz): δ 172.8 (*C*=O), 135.2 (=*C*H), 117.1 (=C$H_2$), 38.3 (NC$H_2$), 36.3, 33.7, 28.5, 25.1. For full assignments, see Figures A.46a and b. MALDI-TOF MS (CHCA matrix), *m/z*: [**6**•H]$^+$ 267.208 (calculated: 267.207 for $C_{15}H_{27}N_2O_2^+$).

**Synthesis of Macrocycles**

For the synthetic procedures described below, stock solutions of **DA** (10 mg / mL, 13 mM in $C_6H_6$) were freshly prepared.

**Cyclic ether 1,4,7,10-tetraoxacyclotetradec-3-ene (3'):** In the glovebox, a solution of tetraether diene **3** (28 mg, 0.12 mmol, 1.0 equiv) and dodecane (27 μL, 0.12 mmol, 1.0 equiv) in 240 mL $C_6H_6$ was prepared (0.5 mM $[3]_0$). **DA** stock solution (90 μL; 0.90 mg, 0.0012 mmol, 1.0 mol%) was added, and the reaction was stirred at RT. Complete consumption of diene was evident by GC-FID within 15 min, together with formation of two new products assigned to *E*- and *Z*-**3'**. A single product was evident by TLC, consistent with co-elution of the *E*/*Z* isomers, and the absence of any oligomers (100% $Et_2O$; $R_f$ 0.25). The reaction was quenched (KTp solution in THF; 10 equiv vs starting Ru; glovebox)[43] and then concentrated to dryness on the bench. Purification by flash column chromatography (100% $Et_2O$; 20 cm x 1.5 cm column) in air afforded cyclic tetraether **3'** as a gray oil (19 mg, 79%; 67/33 *E*/*Z*). $^1$H NMR ($CDCl_3$, 300 MHz): δ 5.97 (m, 2H, =C*H* of *E*-**3'**), 5.74 (m, 1H, =C*H* of *Z*-**3'**), 4.28 (m, 2H, =CHC$H_2$O of *Z*-**3'**), 4.06 (m, 4H, =CHC$H_2$O of *E*-**3'**), 3.73–3.59 (m, 18H, OC$H_2$C$H_2$O of *E*- and *Z*-**3'**). The $^1$H NMR data for *Z*-**3'** are in good agreement with the literature values;[38] those for *E*-**3'** are shifted relative to the known *Z*-isomer, but are otherwise in close correspondence.

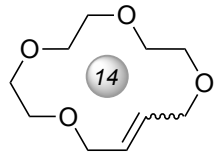

**3'**

**Cyclic ether 1,6-dioxacyclohexadec-3-ene (4'):** The reaction was carried out as for tetraether **3'** above, only starting with diene **4** (31 mg, 0.12 mmol). Near-complete consumption of diene (95%) and formation of a major new product was evident by GC-FID at 30 min, after which the proportion of diene and product did not change. TLC revealed a major product ($R_f$ 0.50) together with a small amount of starting diene ($R_f$ 0.70) and a minor impurity ($R_f$ 0.40) presumed to be an oligomeric product (30:70 ethyl acetate/hexanes). The reaction was quenched (KTp) and concentrated to dryness as above. Purification by column chromatography (15:85 $Et_2O$ in

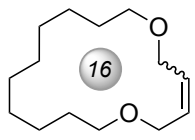

**4'**

*References for Chapter 4 begin on p. 132*

hexanes; 20 cm x 1.5 cm column) in air afforded cyclic diether **4'** as a colourless oil (15 mg, 56%; 96/4 *E*/*Z*). The $^{1}$H NMR data for *E*- and *Z*-**4'** are in good agreement with the literature values.[39]

**Cyclic tosylamide *N*-toluenesulfonyl-azacyclopentadec-8-ene (5'):** The reaction was carried out as for cyclic tetraether **3'** above, only starting with tosyl diene 5 (47 mg, 0.12 mmol), and with additional **DA** stock solution (45 μL, 0.12 mmol, 0.5 mol%) added at 1.5 h. Complete consumption of diene was evident by GC-FID after 2 h, together with formation of two new products assigned as *E*- and *Z*-**5'**. A single spot was evident by TLC, consistent with co-elution of the *E*/*Z* isomers, and the absence of oligomers (70:30 $CH_2Cl_2$/pentane; $R_f$ 0.35). The reaction was quenched (KTp) and concentrated in vacuo as above. The spent Ru was removed by passing through a silica plug (70/30 $CH_2Cl_2$/pentane as eluent) in air, affording pure cyclic tosylamide **5'** as a colourless oil (5 mg, 12%, 65/35 *E*/*Z*). $^{1}$H NMR ($CDCl_3$, 300 MHz): δ 7.68 (m, 2H, Ar C*H*), 7.28 (m, 2H, Ar C*H*), 5.33 (m, 2H, =C*H*), 3.07 (q, $^{3}J_{HH}$ = 6.9 Hz, 4H, NC$H_2$), 2.41 (s, 3H, Ar C$H_3$), 2.03 (m, 4H, C$H_2$), 1.64–1.46 (m, 4H, C$H_2$), 1.45–1.25 (m, 12H, $CH_2$). The $^{1}$H NMR data for **5'** are in good agreement with the literature data for the 21-membered analog,[44] with the exception of the aliphatic signals (1.45–1.25), which integrate to 12H for **5'**. Separate signals for *E*- and *Z*-**5'** were not observed, probably because of signal overlap.

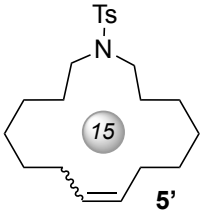


**Cyclic di-lactam cyclopentadecene-6,12-diamide (6'):** In the glovebox, a solution of diamide diene **6** (144 mg, 0.5 mmol) in $CH_2Cl_2$ (100 mL) was prepared (5 mM $[6]_0$). **DA** stock solution (762 μL, 0.01 mmol, 2 mol%) was added, and the colour changed from green to yellow over 1 h. A single major product was evident at this stage by TLC ($R_f$ 0.20), as was a small amount of starting diene ($R_f$ 0.60; 60/40 acetone/ethyl acetate). A further 100 μL **DA** stock was added, and the reaction was stirred for a further 2.5 h, after which TLC revealed complete consumption of starting material and oligomer. The reaction was quenched (KTp), prompting a colour change from green to blue over 30 min. The solvent was evaporated on the bench (rotovap), and the residue was resuspended in $CH_2Cl_2$ (10 mL), filtered, and dried in vacuo to afford pure **6'** as a white crystalline solid (80 mg, 67%, 95/5 *E*/*Z*). $^{1}$H NMR ($CDCl_3$, 300 MHz): δ 5.81 (br s, 2H, N*H*), 5.49 and 5.44 (2 m, 2H, =C*H* for *E*- and *Z*-**6'**), 3.39 (m, 4H, NC$H_2$), 2.28–2.13 (overlapping m, 8H, C$H_2$), 1.64 (m, 4H, C$H_2$), 1.29 (quint, $^{3}J_{HH}$ = 7.0 Hz, 2H, C$H_2$). $^{13}$C{$^{1}$H} NMR ($CDCl_3$, 75 MHz): 173.5 (s, *C*=O), 129.6 (s, =*C*H), 38.7 (s), 35.7 (s), 32.6 (2 s), 27.2 (s), 23.8 (s). For full assignments, see Figures A.47a and b. MALDI-TOF MS (CHCA matrix), *m/z*: [**6'**•H]$^{+}$ 239.174 (calculated: 239.175 for $C_{13}H_{23}N_2O_2^{+}$).

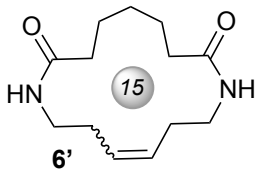


**Catalytic Experiments**

The following representative procedures utilized freshly-prepared stock solutions of **DA** (10 mg / mL, 13 mM) in $C_6H_6$.

**RCM of 5 mM starting [diene]:** In the glovebox, a substrate stock solution was prepared by dissolving diene **1** (100 mg, 0.396 mmol, 1.0 equiv) and dodecane (91 μL, 0.40 mmol, 1.0 equiv) in $C_6H_6$ (2.00 mL total volume; 0.200 mM). An aliquot was removed for GC-FID analysis to establish the starting ratio of substrate to decane. Then, 390 μL of substrate stock solution (0.075 mmol) was diluted to 15.0 mL in $C_6H_6$ (5 mM $[\mathbf{1}]_0$), and **DA** stock solution (5.7 μL, 0.057 mg, 0.075 nmol, 0.1 mol%) was added to the stirred solution. Aliquots were removed periodically from the stirred reaction, quenched with KTp, and analyzed by GC-FID.

**RCM at 0.5 mM starting [diene]:** In the glovebox, a substrate stock solution was prepared by dissolving diene **4** (17.0 mg, 0.0667 mmol, 1.0 equiv) and dodecane (15 μL, 0.0667 mmol, 1.0 equiv) in $C_6H_6$ (1.00 mL total volume; 66.7 mM). An aliquot of the stock solution was removed for GC-FID analysis to establish the starting ratio of substrate to decane. Then, 300 μL of substrate stock was diluted to 40 mL in $C_6H_6$ (0.5 mM $[\mathbf{4}]_0$), and **DA** stock solution (15 μL, 0.20 μmol, 1.0 mol%) was added. The reaction progress was monitored as in the representative procedure immediately above.

### 4.2.5. Subsequent Advances on Section 4.2: The Janus Face of Hydrogen-Bonding

**1) Impact of water on DA:** The advantages of the **DA** catalyst outlined above motivated colleagues in pharma to explore its use in research and development operations. Unexpectedly, they observed much less satisfactory performance. We speculated that the difference might arise from the fact that our work was carried out in rigorously dry solvents, in keeping with standard organometallic practice. In broader synthetic practice, water is a ubiquitous, little-regarded contaminant. Water has the potential to disrupt H-bonding of the catalyst to substrates: in addition, we considered that it might contribute to catalyst decomposition. These factors could account for the inconsistent performance of **DA**.

To probe this point, the author (in collaboration with Mr. Alexandre Goudreault of this research group) undertook high-throughput screening to assess the impact of water on mRCM using **DA** and **nG**. As expected, **DA** proved more sensitive – consistent with stronger H-bonding of water to a dangling $NH_2$ functionality – but both catalysts were found to be negatively affected.

Shown in Figure 4.2 are data from subsequent, higher-precision bench-scale experiments, carried out by Mr. Christian Blanco. Even for **nG**, mRCM yields in the presence of water were dramatically lower than those in the anhydrous reactions. For example, 30% mRCM was observed in the presence of 0.1% v/v water, as compared to 87% in dry toluene. More robust is the iodide analogue **nG(I$_2$)**; this finding led to pursuit of clean synthetic routes to the iodide catalysts described in Chapter 2.[45] The CAAC catalysts proved most water-tolerant of the systems examined: as this work goes beyond the author's contributions, however, other than catalyst synthesis, readers are referred to the published work for details.[46]

*References for Chapter 4 begin on p. 132*

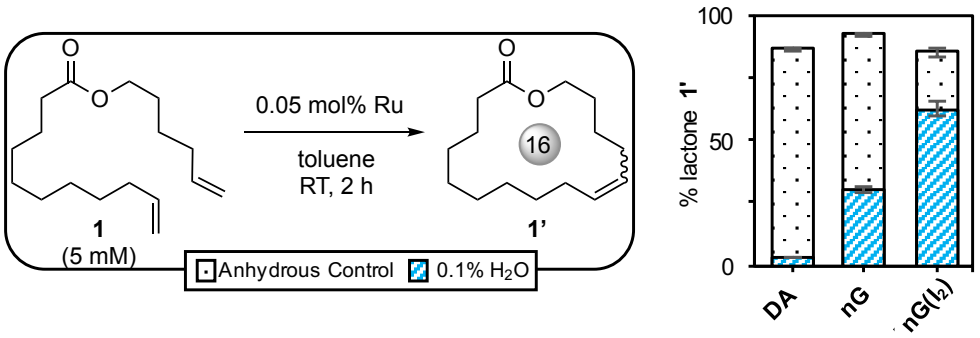


**Figure 4.2. Impact of water on mRCM by DA, nG, and nG($I_2$) catalysts.**

**2) Evidence for H-bonding of DA:** Evident in the X-ray crystal structure of the precatalyst **DA** are intramolecular HN–H...Cl H-bonding interactions. The bond distance of 2.74 Å (Figure 4.3a) suggests an interaction of moderate strength. H-bonding may thus help retain the **ODA** ligand within the coordination sphere of the metal even if both N-donor sites dissociate. NOESY-NMR analysis of a polyether-alkylidene species derived from **DA** indicates retention of the H-bonding interaction in solution. The alkylidene complex was generated by treating **DA** with a mono-alkene analogue of polyether **3** in $CDCl_3$ at –10 °C (Figure 4.3b). Interactions between the **ODA** N$H_2$ and the OC$H_3$ of the substrate were observed, albeit of small intensity, possibly due to partial deuteration of the aniline $NH_2$ protons by the solvent. Use of $C_7D_8$ could enable improved resolution and intensity.

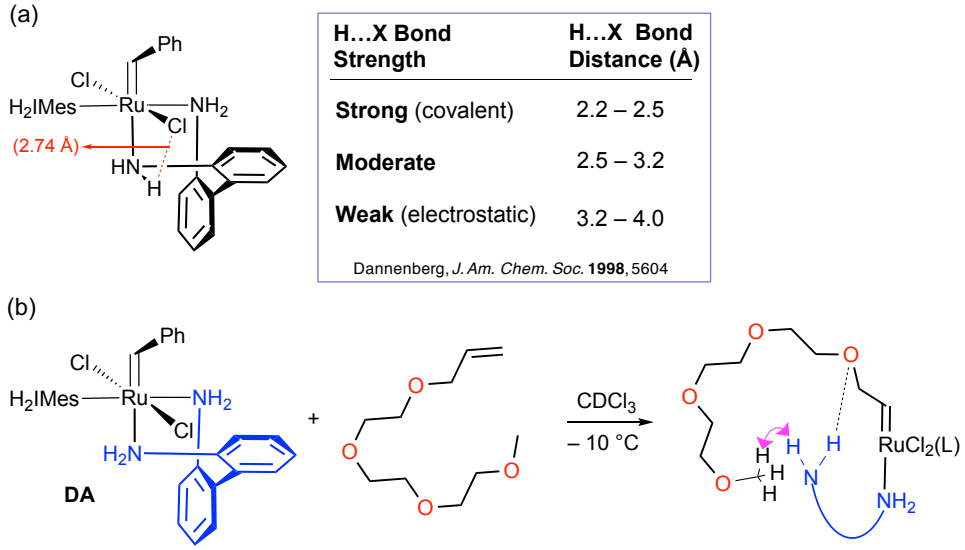


**Figure 4.3. Evidence for H-bonding of the *o*-dianiline ligand. (a) In precatalyst DA. (b) Within a trapped alkylidene species obtained by metathesis of a long-chain 1-olefin.**

**3) Synthesis of DA analogues:** Ligand modulation can transform catalyst productivity. With **DA** as a benchmark, we sought to install other chelating ligands via the same approach, to determine the impact of different chelating ligands on catalyst productivity. Figure 4.4.a shows the various **DA** analogues for which synthesis was attempted. For the first of these, **BrDA**, we expected higher lability in light of the electron-withdrawing bromine atom. Surprisingly, clean conversion to the desired product was achieved after 10 cycles of pyridine evaporation (as cmpared to?? for **DA**). For **HODA**, we speculated that the phenol group, a better H-bond donor, might improve ligand retention. In fact, it showed increased lability: even on increasing to 15 azeotrope cycles, 6% **GIII** remained. For **MeODA**, in contrast, the strongly-donating MeO groups enabled complete conversion within only 7 azeotrope cycles, and the catalyst was isolated in ca. 50% yield for a 66 mg scale reaction. Finally, impeding rotation of the atropisomeric ligand hampers isolation. Installation of **mDA** was incomplete even after ca. 20 cycles, with 10% **GIII** still evident by $^{1}$H NMR analysis. The importance of ligand flexibility is suggested by unpublished work by Carolyn Higman of this research group: efforts to synthesize the bipy analogue of **DA** resulted in decomposition, presumably owing to unfavourable steric interactions with the NHC ligand.

Neither the **BrDA** nor the **HODA** catalysts was isolated in these forays into alternative ligand sets, and their metathesis activity was thus not examined. The **mDA** derivative performed poorly in mRCM of **1** (Figure 4.4.b), consistent with facile ligand loss. For **MeODA,** stronger ligand binding could account for the slightly lower rate of metathesis observed. Nonetheless, this catalyst achieved similar performance than **DA** at 2 h.

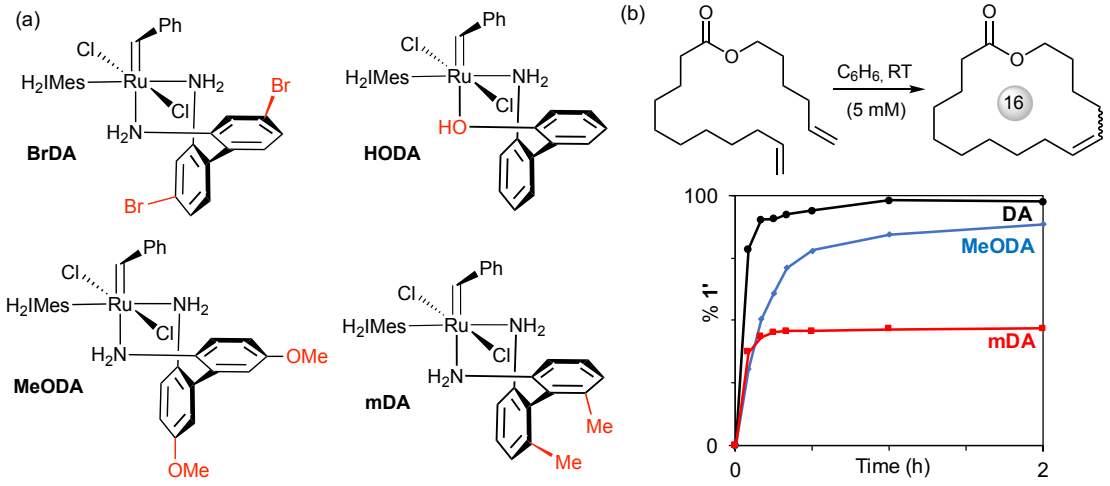


**Figure 4.4. (a) Synthesis of DA analogues. (b) Macrocyclization of 1 comparing DA with analogues.**

---

## 4.3. Fast-Initiating Indenylidene Catalyst Bearing a CAAC Ligand

### 4.3.1. Introduction

Reported herein is a ruthenium metathesis catalyst that integrates breakthrough productivity with a robust, reliably-installed indenylidene ligand. The advent of large-scale olefin metathesis processes in pharmaceutical manufacturing,[6] and the associated demand for catalyst supply on scale, bring to the fore long-neglected challenges in scalable catalyst synthesis. Chief among these is the means by which the critical Ru=CRR' site is introduced.

Interest extends beyond the important N-heterocyclic carbene[47] (NHC) complexes to new cyclic alkyl amino carbene (CAAC)[48] catalysts: Chart 4.2. While metathesis in process chemistry[6] is dominated by NHC catalysts (**HII**, **nG**),[49-51] bench-scale studies report exceptional productivity for CAAC catalysts in macrocyclic ring-closing metathesis (mRCM)[21a] and cross-metathesis (CM) routes to α-olefins from renewable oils.[16,17,19,52] The CAAC catalysts thus hold significant potential in the pharmaceutical and renewable-feedstock sectors.[6,52-54]

**Chart 4.2. Literature metathesis catalysts discussed.**

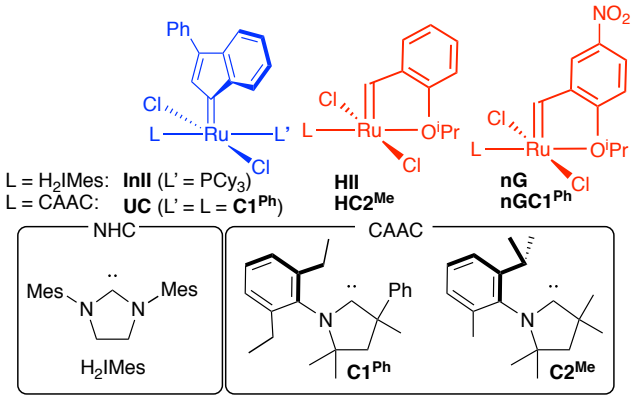


A long-standing challenge, however, is the tradeoff between metathesis activity, vs the efficiency of catalyst synthesis. Most active are Ru-benzylidene catalysts (red; Chart 4.2).[16,21a] Despite attempts to develop alternative synthetic methodologies,[55] optimal routes to benzylidene catalysts continue to rest on the reaction of a Ru precursor with an aryldiazomethane, typically $PhCHN_2$.[56,57] $PhCHN_2$ is toxic and unstable (indeed, potentially explosive),[58] to an extent that prevents purification. Its low purity, in turn, limits stoichiometric control over benzylidene transfer.[2,3,57,59] Significant limitations to process scalability result.

Indenylidene catalysts (blue, Chart 4.2) enable straightforward, convenient, reliable installation of the Ru-carbon double bond, via the high-yield reaction of Ru precursors with propargyl alcohol.[60,61] However, study of the NHC derivatives, most extensively **InII**, reveals very inefficient initiation.[40,62-71] Slow loss of the stabilizing donor ($PCy_3$, for **InII**) impedes entry into the catalytic cycle at room temperature (RT), even for the readily-cyclized diene diethyl diallylmalonate **2**.[17,67-69] Elevated temperatures are required to elicit high activity, promoting catalyst degradation. Here we report the novel CAAC-indenylidene catalyst **InC1$^{Ph}$**, a labile chloride-bridged dimer, which overturns this long-accepted limitation. **InC1$^{Ph}$** exhibits

unprecedented activity in demanding metathesis reactions (indeed, at a level comparable to the Grela-class catalyst **nGC1$^{Ph}$**), establishing that high-performing metathesis catalysts can be accessed via simple, safe, scalable chemistry.

It should be noted that **nGC1$^{Ph}$** is itself accessible without recourse to diazo technology, via CM of the commercial indenylidene catalyst **UC** with the chelating *β*-methylstyrene reagent **NSE'**, when CuCl is added to abstract the "extra" CAAC ligand (Scheme 4.4a).[21a] Limitations, however, are the <40% yield, compounded by the multistep, low-yielding synthesis of **NSE'**.[72,73] We queried whether *omitting* **NSE'** might enable access to dimeric **InC1$^{Ph}$**, in which the precatalyst is stabilized by a dative Cl interaction. The high lability, and consequently high metathesis activity, conferred by dative chloride bonds has been recognized since Herrmann's pioneering work on bimetallic metathesis catalysts containing one [Ru]=CHR site.[74] While bimolecular elimination of the alkylidene moiety as RCH=CHR is a documented risk for dimers containing *two* [Ru]=CHR sites,[2,5,75] this reaction is highly sensitive to alkylidene bulk.[5,76] We thus regarded the disubstituted indenylidene ligand as a potentially key asset in blocking alkylidene elimination.

### 4.3.2. Results and Discussion

We treated **UC** with CuCl (Scheme 4.4b) in the absence of additional donors. A **C1$^{Ph}$** ligand was successfully abstracted at 40 °C, enabling transformation of **UC** into dimeric **InC1$^{Ph}$** in ca. 80% isolated yield. The structure of **InC1$^{Ph}$** is supported by X-ray analysis. Consistent with the critical role of indenylidene bulk in inhibiting bimolecular decomposition, the corresponding reaction of CuCl with the second-generation Grubbs catalyst $RuCl_2(H_2IMes)(PCy_3)(=CHPh)$ led to rapid elimination of stilbene. In the absence of CuCl, this reaction requires days at 60 °C.[77]

*References for Chapter 4 begin on p. 132*

**Scheme 4.4 Synthesis of InC1$^{Ph}$.**

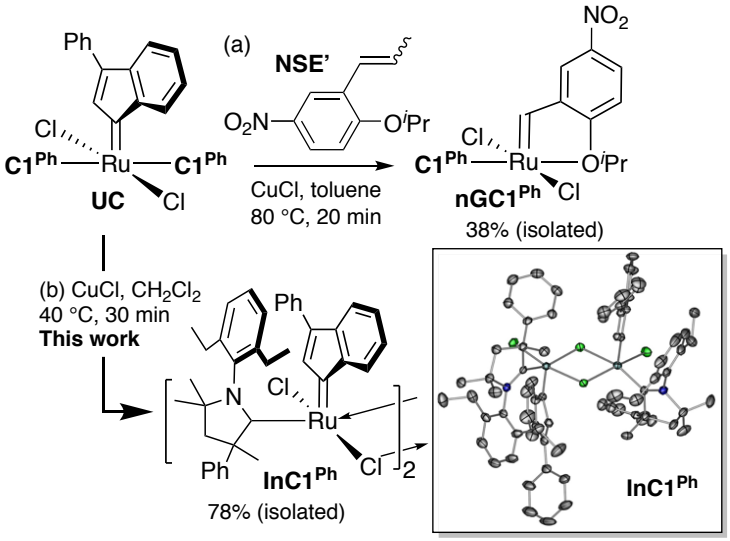


The metathesis activity of **InC1$^{Ph}$** was benchmarked against key CAAC and NHC catalysts in RCM of diethyl diallylmalonate **2**. Comparison with the state-of-the-art catalyst **nGC1$^{Ph}$** gives insight into the relative reactivity of the indenylidene and chelating *p*-nitrobenzylidene ligands.[21a] Comparison with **UC** reports on the impact of replacing a CAAC donor with a much more labile dative chloride, while comparison of **nGC1$^{Ph}$** with its $H_2$IMes analogue **nG** probes the impact of the carbene. Catalyst loadings were chosen in light of prior studies of RCM of **2** via indenylidene catalyst **InII**.[17,40,64-71] We suspected that the reported TONs (ca. 20–2,000) might under-report catalyst productivity, given near-quantitative conversions. Initial catalyst loadings were therefore reduced to 0.005 mol% (i.e. 50 ppm Ru relative to **2**; cf. 5–0.05 mol% in the literature reports). The resulting data are summarized in Figure 4.5a.

*References for Chapter 4 begin on p. 132*

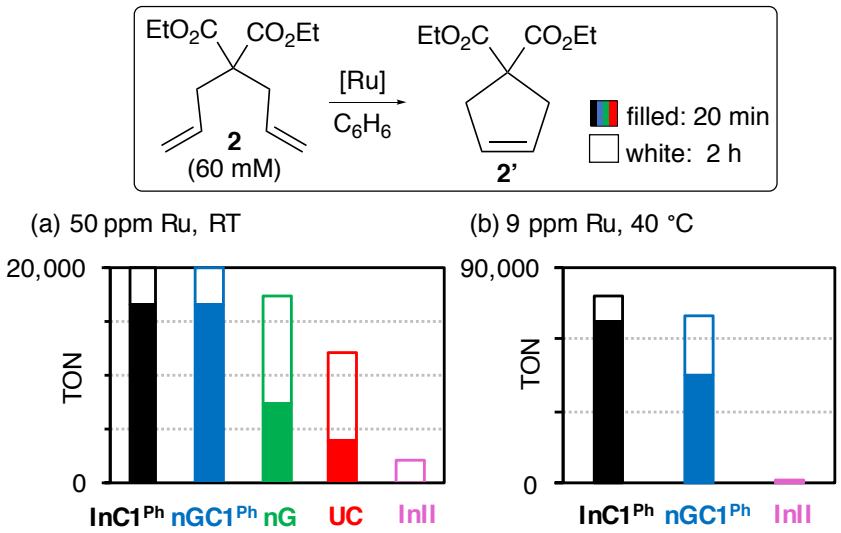


**Figure 4.5. Turnover numbers (TON) at 2 h in RCM of 2. For numerical values, see Table 4.4. Catalyst loadings are based on 2 active Ru centers in InC1$^{Ph}$.**

Unexpectedly, **InC1$^{Ph}$** exhibited RCM activity comparable to the leading catalyst **nGC1$^{Ph}$** at RT at this loading, and slightly *higher* activity at 9 ppm Ru and 40 °C. The basis for this difference is discussed below. **InC1$^{Ph}$** also outperformed **nG** and **InII**, in keeping with the trend established for $H_2$IMes vs CAAC catalysts,[16,17] which may arise from faster decomposition of the $H_2$IMes complexes.[78]

A further inhibiting factor for **InII** is the low lability characteristic of phosphines trans to an NHC ligand,[29a,79] which limits TONs to 2,000 at 50 ppm Ru. The higher RT productivity of **UC** (TON 12,000) suggests that the **C1$^{Ph}$** ligand in **UC** is more labile than the $PCy_3$ ligand in **InII** (confirmed below), though catalyst lifetime is almost certainly also relevant. Of note, this TON is nearly 60% of that measured for **nG** under the same conditions (17,200), despite the higher lability expected for the styrenyl ether ligand in **nG**, vs a strongly-bound CAAC donor.[80]

As a metathesis reaction manifold of significant current interest, we next turned to macrocyclization. Substrates such as prolactone **1** (Figure 4.6) are challenging because the ester functionality contributes the sole conformational bias toward cyclization.[37] Oligomers are hence typically formed as the kinetic products, but can be recycled into macrocycles if catalyst activity and longevity permit.[15,81] High dilutions (5 mM, in the case of **1**) are essential to exert an entropic bias sufficient to shift the ring-chain equilibrium in favour of the macrocyclic rings.[14,15] (Carrying out mRCM of **1** at 20 mM, for example, yields ca. 40% oligomers).[21a] A catalyst loading of 0.01 mol% thus corresponds to sub-micromolar concentrations of Ru. Combined with the internal, predominantly trans-substituted nature of the oligomeric olefins, this offers a stringent test of catalyst performance.

*References for Chapter 4 begin on p. 132*

Notwithstanding these challenges, **InC1$^{Ph}$** enabled fast, selective mRCM at 0.01 mol% Ru, achieving TONs of ca. 9,000 within 10 min at 40 °C (Figure 4.6). **nGC1$^{Ph}$** and **UC** exhibited similar, slower, performance, while the productivity of $H_2$IMes catalyst **nG** was ca. 30% lower, and **InII** failed to react. At RT, **InC1$^{Ph}$** enabled quantitative mRCM within 20 min at 0.05 mol%, where **UC** reacted much more slowly (44% yield at 2 h; Figure 4.7).

At 0.002 mol% and 40 °C (Figure 4.6b), a TON of 27,500 was measured for **InC1$^{Ph}$** (the highest yet reported for a Ru catalyst at dilutions compatible with selective mRCM).* In comparison, the record TON for NHC catalysts in this reaction is 16,000, achieved by Kadyrov at 80 °C and 8 mM **1**, with rigorously purified diene and solvent, and aggressive removal of ethylene to limit catalyst decomposition.[21e] Under more standard conditions, reported TONs are ≤500.[21]

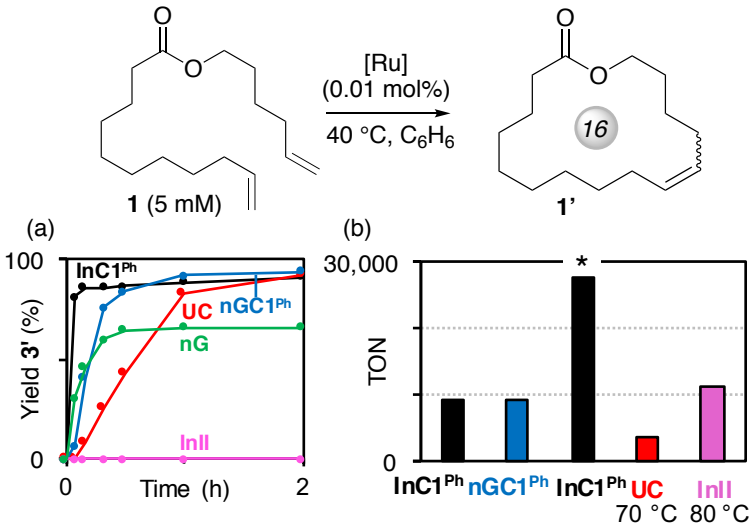


**Figure 4.6. mRCM of 1 at 40 °C. (a) Rate profiles and (b) maximum TONs at 0.01 or (*) 0.002 mol% Ru, shown alongside the best reported TONs for UC[17] and InII.[21e] For the RT plot and numerical data, see Figure 4.7 and Table 4.5.**

Improved stability to ethylene appears to be an important contributor to the exceptional productivity of the CAAC catalysts. This tolerance opens the door to ethenolysis of unsaturated lipids,[6] a reaction of keen interest for the production of α-olefins from renewable plant or algal oils.[6,52-54] Outstanding performance has been reported in ethenolysis of methyl oleate (**MO**) with CAAC catalysts,[16-19] particularly **HC2$^{Me}$**.[16] However, **HC2$^{Me}$** may be highly sensitive to impurities. Costly, very high grade (99.995%) ethylene was required for maximum productivity, and a 40–70% drop in TON was reported on using 99.95 or 99.99% $C_2H_4$.[16,17] We utilized affordable, technical-grade $C_2H_4$ (99.9%) to probe the robustness of **InC1$^{Ph}$** relative to this breakthrough catalyst.

* A TON of 62,000 could be achieved with **nGC1$^{Ph}$** at higher concentrations (20 mM **1**) at 70 °C.[21a]

*References for Chapter 4 begin on p. 132*

Table 4.2 shows the impact of ethylene pressures on cross-metathesis (CM) yields at 40 °C in neat **MO**. A pressure of 200 psi proved optimal (entries 1–4), possibly indicating a trade-off between ethylene solubility and the cumulative impact of poisons. Importantly, however, **InC1$^{Ph}$** appears significantly more robust than **HC2$^{Me}$**, as indicated by TON values of 50,000 and 10,000 (respectively) at 200 psi. Steric protection may be higher for **C1$^{Ph}$**, in which the quaternary carbon flanking the carbene site bears a methyl and a phenyl group, as compared with two methyl groups in **C2$^{Me}$** (Chart 4.2).

**nGC1$^{Ph}$** delivered CM yields similar to **InC1$^{Ph}$**, though higher conversions of **MO**. The balance was due to 1,18-dimethyl 9-octadecenoate **9** and 9-octadecene **10**, formed via self-metathesis (SM) of **MO** or its ethenolysis products.

**Table 4.2. Ethenolysis of methyl oleate: cross-metathesis (CM) and self-metathesis (SM).**[a]

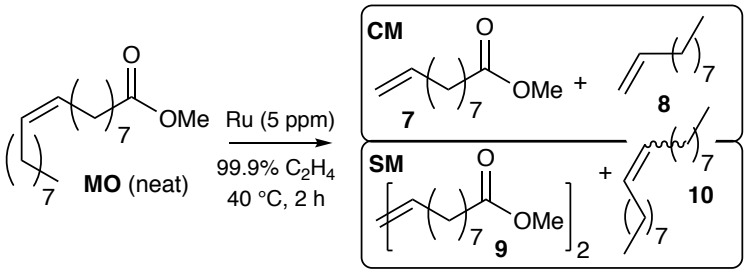


| Entry | Catalyst | Pressure (psi) | %Conv. (% Yield) | TON |
|---|---|---|---|---|
| 1 | **InC1$^{Ph}$** | 20 | 16 (3) | 6,000 |
| 2 | **InC1$^{Ph}$** | 110 | 39 (20) | 40,000 |
| 3 | **InC1$^{Ph}$** | 200 | 28 (25) | 50,000 |
| 4 | **InC1$^{Ph}$** | 400 | 18 (8) | 16,000 |
| 5 | **nGC1$^{Ph}$** | 200 | 39 (23) | 46,000 |
| 6 | **HC2$^{Me}$** | 200 | 9 (5) | 10,000 |

[a] 5 ppm catalyst = 0.0005 mol% Ru. TON based on **7**/**8**. Quantified by $^{1}$H NMR analysis (Figure A.48).

The impressive activity of **InC1$^{Ph}$** documented above attests to the lability of the dative chloride donor, relative to the stabilizing ligands present in indenylidene catalysts such as **InII** and **UC**. It also supports the case made by Cavallo, Nolan and co-workers, on the basis of DFT analysis, that slow initiation of **InII** and related catalysts is due to slow ligand loss, not the resistance of the indenylidene moiety to cycloaddition.[69b,82,83]

*References for Chapter 4 begin on p. 132*

To examine this key point, we measured initiation rate constants ($k_1$) for **InC1$^{Ph}$** and selected other catalysts, via the irreversible reaction with *tert*-butyl vinyl ether (tBVE; Table 4.3).[69b,84] The bulk of tBVE retards metathesis to experimentally convenient rates.*

As expected, initiation was fastest with benzylidene complex **nGC1$^{Ph}$** (in which the inductive effect of the *p*-$NO_2$ substituent increases the lability of the ether donor),[51] and slowest with **UC** and **InII**. Notable is the 260x faster initiation of **InC1$^{Ph}$** relative to **InII**, and 65x relative to **UC**. Indeed, **nGC1$^{Ph}$** initiates only 3.5x faster than **InC1$^{Ph}$**, despite the steric barrier to metathesis at the disubstituted Ru=CRR' site. Clearly, incorporating a labile dative ligand greatly diminishes the barrier to indenylidene initiation, even relative to a classically fast-initiating[51] benzylidene ligand.

Also striking is the slightly *slower* overall rate of metathesis for **nGC1$^{Ph}$** vs **InC1$^{Ph}$** (Figs. 2a, 4.5), despite threefold faster initiation. As the two catalysts generate the same active species, the lower net activity of **nGC1$^{Ph}$** suggests recapture of free 4-nitro-2-isopropoxystyrene **NSE** by the active species. The rate difference is maintained even at 40 °C and sub-micromolar concentrations of Ru and **NSE** (Figure 4.6b). While heat and high dilutions amplify engagement of **nGC1$^{Ph}$** in metathesis, they are insufficient to inhibit re-uptake of **NSE**.[30]

**Table 4.3. Initiation rates in CM with tBVE.**[a]

| entry | catalyst | type | $k_i$ ($s^{-1}$) | $k_{rel}$ vs **InII** |
|---|---|---|---|---|
| 1 | **nGC1$^{Ph}$** | Ru=CHPh | $7.50 \times 10^{-4}$ | 903 |
| 2 | **InC1$^{Ph}$** | Ru=CRR' | $2.15 \times 10^{-4}$ | 259 |
| 3 | **UC** | Ru=CRR' | $3.33 \times 10^{-6}$ | 4 |
| 4 | **InII** | Ru=CRR' | $0.83 \times 10^{-6}$ | 1 |

[a] 30 equiv tBVE; measured in $CDCl_3$, 23 °C.

### 4.3.3. Conclusion

A tradeoff has long existed between the ease with which an alkylidene ligand can be installed at Ru centers, and the activity of the resulting catalysts. The need for scalable, high-yield routes to metathesis catalysts, which obviate the unreliability and risk of diazoalkane methodologies, is becoming urgent with the increasing demand for catalyst supply on scale. The foregoing overturns the long-standing view that the synthetic accessibility of Ru-indenylidene catalysts is incompatible with high metathesis activity. Catalyst **InC1$^{Ph}$** exhibits a level of activity previously attainable only with benzylidene catalysts, indicating that the "fundamental"

* Reaction with ethyl vinyl ether was dramatically faster. For **nGC1$^{Ph}$**, for example, reaction with 100 EVE was complete in <1 min at 23 °C.

*References for Chapter 4 begin on p. 132*

unreactivity of prior indenylidene catalysts merely reflects the low lability of the stabilizing ligands. In reconciling high metathesis activity with straightforward, reliable, safe installation of the alkylidene ligand, this advance is anticipated to create new opportunities in olefin metathesis.

### 4.3.4. Experimental Details for Section 4.3

**General Procedures.** Reactions were carried out under $N_2$ in a glovebox or Schlenk line, unless otherwise noted. HPLC-grade solvents ($C_6H_6$, *n*-hexane, $CH_2Cl_2$) dried and degassed using a Glass Contour solvent purification system, and stored under $N_2$ over 4 Å molecular sieves for 16 h prior to use. Pentane (HPLC grade) and EtOAc (reagent grade) were distilled over $MgSO_4$, then $P_2O_5$, and stored as above. $CDCl_3$ (Cambridge Isotopes) was freeze/pump/thaw degassed and stored as above. Potassium tris(1-pyrazolyl)borohydride (KTp; TCI), was used as received to quench metathesis by the reported method.[43] Metathesis catalysts **InC1$^{Ph}$** [77] and **HC2$^{Me}$** [16] were prepared by literature methods, as were diene **1**[37] and macrocycle **1'**,[37] (for GC-FID calibration). The nitro-Grela catalyst **nG**, its CAAC analogue **nGC1$^{Ph}$**, and "Ultracat" **UC** were supplied by Apeiron Synthesis. Diethyl diallylmalonate (**2**, Aldrich, 98%) and methyl oleate (**MO**, Aldrich, 99%) were freeze/pump/thaw degassed and stored over activated neutral alumina prior to use. CuCl was freshly prepared from $CuCl_2$ according to the published procedure.[85] Decane and dodecane (GC internal standards; both Aldrich, anhydrous, 99%) were freeze/pump/thaw degassed and stored under $N_2$ in the glovebox. Ethylene gas (BOC Gases; Linde group, 99.9% purity) was used as received.

Ethenolysis reactions were conducted in machined steel autoclaves equipped with glass liners, rupture disks, and Ashcroft pressure gauges. Reactions at 110 psi or lower were conducted in a vessel with a pressure capacity of 200 psi; those at 200–600 psi in a vessel with a pressure capacity of 1– 2,000 psi. In all cases, the maximum pressure was less than 2/3 of the rated maximum.

NMR spectra were recorded on Avance 300 or Avance II 300 spectrometers at 23 ±2 °C, unless otherwise indicated. Chemical shifts are reported in ppm, and referenced to the residual proton or carbon signals of the solvent. RCM experiments were analyzed using Agilent 6890 or 7890A gas chromatographs (GC) equipped with auto-samplers, flame ionization detectors (FID) and Agilent HP-5 polysiloxane column (30 m length, 320 μm diameter). Calibration curves of peak areas versus concentration were established for the starting dienes and cyclic products in the relevant concentration regimes, with ca. 1:1 (w/w) sample versus decane (for mRCM experiments) or dodecane (for RCM of **2**) as internal standard. Ethenolysis experiments were analyzed by $^1$H NMR integration against 1,3,5-trimethoxybenzene (TMB) as internal standard.

**Synthesis of [RuCl$_2$(CAAC)(=Ind)]$_2$ (InC1$^{Ph}$) by Ligand Abstraction from UC with CuCl.** *Note:* our standard synthesis was carried out using dry solvents in the glovebox. Shown below, at the request of a referee, is a convenient Schlenk-line synthesis using minimally purified solvents, which was carried out without adverse effects on purity or yield.

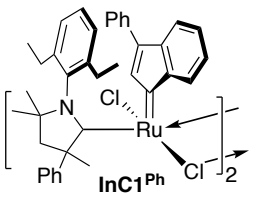

**InC1$^{Ph}$**

Solid **UC** (5.01 g, 5.00 mmol) and freshly prepared CuCl (1.04 g, 10.5 mmol, 2.1 equiv) were added to a 100 mL round-bottom flask equipped with a magnetic stir-bar and a reflux condenser. The flask was connected to a Schlenk line, and the air atmosphere was exchanged for argon by three evacuation-backfill cycles. Addition of $CH_2Cl_2$ (33 mL; degassed by sparging with Ar) gave a dark red solution. The assembly was connected to an oil bubbler, transferred to an oil bath set at 43 °C, and stirred under a gentle flow of argon for 30 min, over which time it turned dark brown. TLC analysis (silica gel, 1:1:0.075 EtOAc:cyclohexane:$NEt_3$) confirmed complete conversion of **UC** into **InC1$^{Ph}$**. The brown mixture was filtered through Celite in air. The Celite was washed with additional $CH_2Cl_2$ (10 mL), and the combined filtrate was stripped of solvent under vacuum. The residue was taken up in $Et_2O$ (100 mL), and the initially gummy solid was converted to a fine powder by spatula grinding combined with vigorous stirring. The crude product was filtered off using a standard Schott frit, washed with $Et_2O$ (6 x 25 mL) and MeOH (4 x 10 mL), and dried under vacuum overnight. Brown **InC1$^{Ph}$** was obtained as a microcrystalline solid. Yield: 2.65 g (78%). NMR data are given for the major rotamer (ind = indenylidene). For fully-assigned $^1$H NMR and 2D spectra with numbered $^1$H nuclei, see Section S3.

$^1$H NMR ($CDCl_3$, 300 MHz): δ 8.82 (d, $^3J_{HH}$ = 7.4 Hz, 2H, [Ru]=CCC*H* of ind), 8.12 (s, 4H, *o*-C*H* of **C1$^{Ph}$** Ph), 7.53 (d, $^3J_{HH}$ = 8.9 Hz, 4H, *m*-C*H* of **C1$^{Ph}$** Ph), 7.47 (t, $^3J_{HH}$ = 7.4 Hz, 2H, ind CC*H*), 7.32 (m, 6H, *o*-C*H* of ind Ph; ind CCHC*H*), 7.23 (t, $^3J_{HH}$ = 7.6 Hz, 3H, ind *p*-C*H* + C*H*$Cl_3$), 7.02 (d, $^3J_{HH}$ = 7.2 Hz, 2H, *p*-C*H* of ind Ph), 6.95–6.85 (m, 4H, *m*-C*H* of **C1$^{Ph}$** Ar), 6.77–6.65 (m, 6H, *m*-C*H* of ind Ph; *p*-C*H* of **C1$^{Ph}$** Ph), 6.50 (t, $^3J_{HH}$ = 7.7 Hz, 2H, *p*-C*H* of **C1$^{Ph}$** Ar), 5.89 (s, 2H, [Ru]=CC*H*), 3.10 (dq, $^3J_{HH}$ = 15.2, 7.6 Hz, 2H, C$H_2$ of **C1$^{Ph}$** Ar), 2.88 (q, $^3J_{HH}$ = 8.4, 7.8 Hz, 2H, C$H_2$ of **C1$^{Ph}$** Ar), 2.75 (d, $^3J_{HH}$ = 12.6 Hz, 2H, **C1$^{Ph}$** C$H_2$), 2.44 (s, 6H, **C1$^{Ph}$** C$H_3$), 2.14 (d, $^3J_{HH}$ = 12.5 Hz, 2H, **C1$^{Ph}$** C$H_2$), 1.70 (q, $^3J_{HH}$ = 7.3 Hz, 4H, C$H_2$ of **C1$^{Ph}$** Ar), 1.50 (t, $^3J_{HH}$ = 7.4 Hz, 6H, C$H_3$ of **C1$^{Ph}$** Ar), 1.43 (s, 6H, **C1$^{Ph}$** C$H_3$), 0.93 (s, 6H, **C1$^{Ph}$** C$H_3$), 0.54 (t, $^3J_{HH}$ = 7.4 Hz, 6H, C$H_3$ of **C1$^{Ph}$** Ar). $^{13}$C{$^1$H} NMR ($CDCl_3$, 75 MHz): δ 303.93 ([Ru]=*C*), 302.31 ([Ru]=*C*), 263.56 (*C* **C1$^{Ph}$**), 263.28 (*C* **C1$^{Ph}$**), 148.13, 146.17, 143.99, 143.72, 143.43, 143.30, 142.60, 141.38, 141.30, 140.32, 139.82, 139.42, 138.96, 138.05 ([Ru]=C*C*H), 136.54, 135.80, 135.60, 134.81, 131.67, 132.03, 130.75 ([Ru]=CC*C*H), 130.14, 129.62 (**C1$^{Ph}$** Ar *p*-*C*H), 129.47, 129.44, 129.04, 128.78, 128.66, 128.45, 128.13, 127.89, 127.80, 127.40, 126.78, 126.42, 125.73, 125.44, 124.82, 124.75, 124.21 (**C1$^{Ph}$** Ph *o*-*C*H), 118.07 (ind Ph *p*-*C*H), 117.65, 78.54, 78.23, 65.84, 65.43, 44.50, 43.95 (Ar *C*$H_2$), 31.81, 31.75 (**C1$^{Ph}$** *C*$H_3$), 30.88 (**C1$^{Ph}$** *C*$H_3$), 27.93, 27.84 (**C1$^{Ph}$** *C*$H_3$), 24.27 (*C*$H_2$ of **C1$^{Ph}$** Ar ), 24.01, 23.87 (*C*$H_2$ of **C1$^{Ph}$** Ar), 23.66, 13.39 (*C*$H_3$ of **C1$^{Ph}$** Ar), 13.10 (*C*$H_3$ of **C1$^{Ph}$** Ar), 12.69, 12.51. ESI-MS (MeCN+0.1% formic acid; *m/z* 1369.36 ([M–Cl+NC$CH_3$]$^+$; calcd 1369.02).

**Catalysis.** Stock catalyst solutions of known concentration in $CH_2Cl_2$ were prepared immediately prior to use. Heated reactions were carried out in a degassed oil bath in the

glovebox at 40 ± 1 °C, with a 10 minutes period for thermal equilibration prior to catalyst addition.

**Representative Procedure for RCM of Diethyl Diallylmalonate 2.** A mixture of **2** (58.0 μL, 0.240 mmol) and dodecane (54.5 μL, 0.240 mmol, 1 equiv; internal standard for GC analysis) was diluted in 3.90 mL $C_6H_6$ to give a final concentration of 60.0 mM **2**. A 150 μL aliquot was removed for GC-FID analysis to establish the starting ratio of **2** to dodecane. **InC1$^{Ph}$** (2.40 μL of a stock solution of 10.2 mg **InC1$^{Ph}$** in 3.00 mL $CH_2Cl_2$; 0.012 μmol, 0.005 mol%) was added to the stirred solution. Aliquots were removed periodically, quenched[43] with KTp in THF (10.0 mg/mL; 10 equiv vs starting Ru), and analyzed by GC-FID. A histogram appears in Figure 4.5 above; Table 4.4 gives numerical data.

**Table 4.4. Turnover numbers in RCM of diethyl diallylmalonate 2.**

| **Catalyst** | TON at 50 ppm (0.005 mol% Ru), RT | | TON at 9 ppm (0.0009 mol% Ru), 40 °C | |
|---|---|---|---|---|
| | 20 min | 2 h | 20 min | 2 h |
| **InC1$^{Ph}$** | 16,600 | 20,000 | 68,000 | 78,000 |
| **nGC1$^{Ph}$** | 16,600 | 20,000 | 46,000 | 70,000 |
| **nG** | 7,200 | 17,200 | – | – |
| **UC** | 3,800 | 12,000 | – | – |
| **InII** | 0 | 2,000 | 0 | 0 |

**Representative Procedure for mRCM of Diene 1:** As above, using pro-lactone **1** (17.9 μL, 0.075 mmol) and decane (14.6 μL, 0.075 mmol; internal standard) diluted with $C_6H_6$ (14.9 mL) to 5 mM **1**. To the stirred solution was added a solution of the catalyst (102 μL: stock solution 10.0 mg **InC1$^{Ph}$** in 20.0 mL $CH_2Cl_2$ (required for full solubility of **InC1$^{Ph}$**); 0.038 μmol, 0.05 mol%).

Figure 4.7 shows rate curves at 23 °C. Table 4.5 provides data to complement those in the histogram shown in Figure 4.6b of the main text. Both also supply values for the dianiline catalyst **DA**. For convenient comparison with the literature, catalyst loadings are shown in both mol% and ppm.

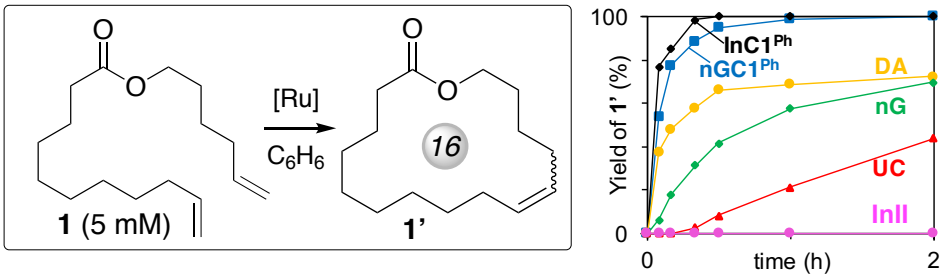


**Figure 4.7. Catalyst performance in mRCM of 1 at 23 °C (0.05 mol% Ru).**

**Table 4.5. Turnover numbers in mRCM of pro-lactone 1.**

| Catalyst | Cat. Loading | Temp. (°C) | [1] | Conv. (Yield) | TON | Reference |
|---|---|---|---|---|---|---|
| **InC1$^{Ph}$** | 0.01 mol% (100 ppm) | 40 | 5 mM | 100 (92) | 9,200 | This work |
| **InC1$^{Ph}$** | 0.002 (20) | 40 | 5 mM | 56 (55) | 27,500 | This work |
| **nGC1$^{Ph}$** | 0.01 (100) | 40 | 5 mM | 100 (94) | 9,400 | This work |
| **InC1$^{Ph}$** | 0.05 (500) | 23 | 5 mM | 75 (72) | 1,440 | This work |
| **nGC1$^{Ph}$** | 0.0045 (45) | 70 | 5 mM | 99 (98) | 21,800 | 21a |
| **UC** | 0.025 (250)[a] | 70 | 5 mM | 95 (91) | 3,640 | 17 |
| **InII** | 0.0075 (75) | 80 | 8 mM | 100 (83) | 11,100 | 21e |

[a]Catalyst added in 5 portions.

**Representative Procedure for Ethenolysis of Methyl Oleate, MO:** In the glovebox, **MO** (1 mL, 0.874 g, 2.95 mmol) and a solution of TMB (ca. 10 mg, 0.059 mmol, 0.02 equiv; internal standard) in $CH_2Cl_2$ (100 μL) were added to a glass-lined pressure reactor equipped with a stirring bar. The clear, colourless solution was stirred at 40 °C for ca. 5 min to ensure total dissolution of the internal standard, after which an aliquot was removed for $^1$H NMR analysis to establish the initial **MO**:TMB ratio. After cooling to RT, **InC1$^{Ph}$** (20 μL of a stock solution of 10.0 mg **InC1$^{Ph}$** in 20.0 mL $CH_2Cl_2$; 0.015 μmol, 0.0005 mol%) was added.

The reactor was assembled, transferred from the glovebox to an oil bath pre-heated to 40 °C, and connected to a cylinder of ethylene (99.9% purity). The gas line was purged 3x, and the reactor was pressurized to 200 psi. After 2 h, the reactor was vented and KTp (10 equiv vs starting Ru) was added to quench reaction. The mixture was stirred for 1 min, after which a ca. 0.1 mL aliquot was removed for NMR analysis. To ensure that any volatile olefins formed by isomerization were retained, vacuum was not used to remove $CH_2Cl_2$: instead, the sample was diluted with ca. 0.6 mL $CDCl_3$.

The conversion of **MO**, and the yields of **7**/**8** were determined by $^1$H NMR analysis ($CDCl_3$), based on the integration for the olefinic peaks for **MO** (Figure A.48: 5.33 ppm, red) and **7**/**8** (5.78 ppm; overlapping, blue), relative to the internal standard TMB (6.07 ppm). Also quantified,

where present, were self-metathesis products **9** and **10** (assignment confirmed by GC-MS). The average of 2 trials (± 3%) is reported.

**Initiation rate of InC1$^{Ph}$:** In the glovebox, **InC1$^{Ph}$** (10.0 mg, 0.0150 mmol) and TMB (ca. 1 mg, 0.007 mmol, 0.8 equiv) were dissolved in 500 μL $CDCl_3$ in an NMR tube equipped with a screw-cap septum seal. The NMR tube was closed, wrapped with Parafilm, and transferred to the NMR instrument to measure the initial ratio of catalyst to TMB. *t*-Butyl vinyl ether (tBVE, 58.0 μL, 0.439 mmol, 30 equiv) was then injected via a gas-tight syringe, the NMR tube was again sealed with Parafilm, and the tube was inverted several times. Immediately after injecting tBVE, the timer was started. The spectrum was then measured. The NMR tube was removed from the probe and inverted repeatedly over the 1 h experiment. Decreases in catalyst concentration were measured from the integrated intensity of the well-isolated indenylidene signal H2 at 5.89 ppm. Rate and first-order plots appear in Figure 4.8.

**Initiation rate of UC and InII:** As above, with the following modifications: DMT was used as internal standard, and a J-Young NMR tube was used to minimize solvent evaporation over the 48 h reaction period. After the initial ratio of catalyst to DMT was measured, the NMR tube was returned to the glovebox, where tBVE was added. A mechanical rotator was used to mix the solution between NMR measurements.

*References for Chapter 4 begin on p. 132*

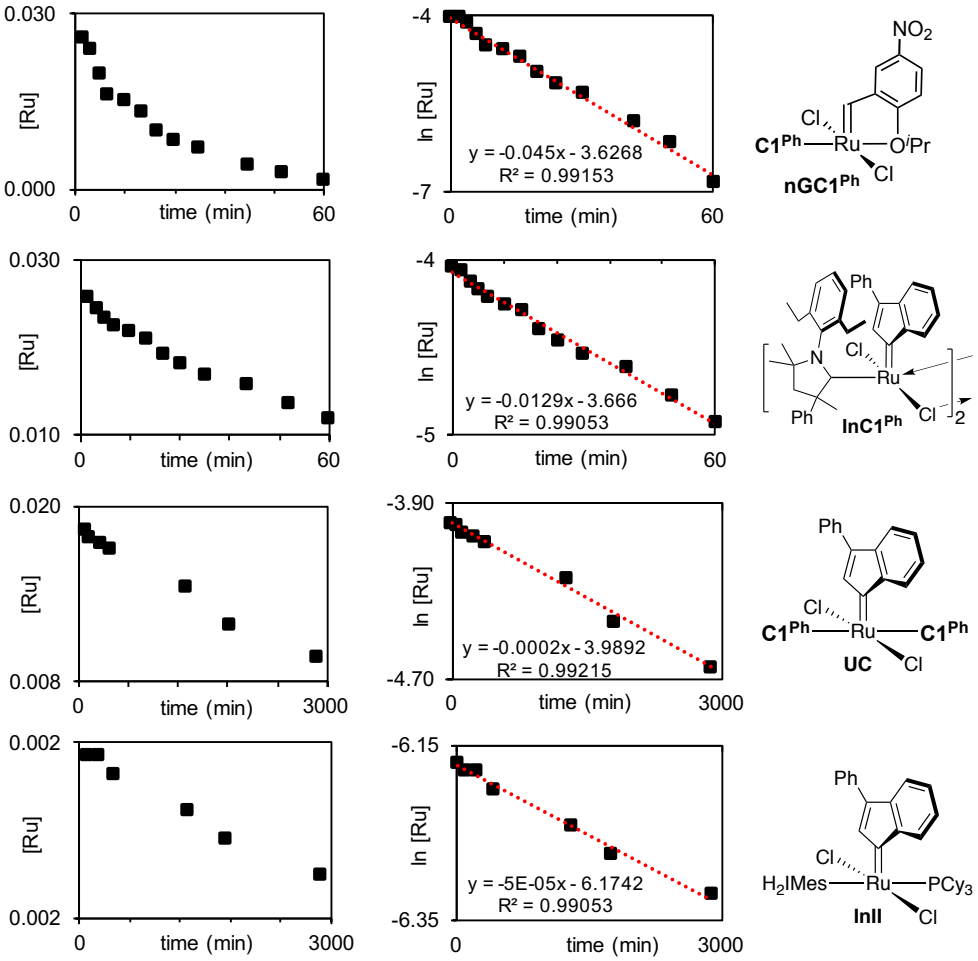


**Figure 4.8 Time profiles (left) and first-order plots (right) for reaction of catalysts with tBVE at 23 °C. Measured over 1 h for nGC1$^{Ph}$ and InC1$^{Ph}$, and over 48 h for UC and InII.**

### 4.3.5. Subsequent Advances on Section 4.3

**1) $O_2$ tolerance of InC1$^{Ph}$:** The water-sensitivity of even classic dichloride ruthenium catalysts (Section 4.2) was initially unexpected. In light of those findings, Ms. Stephanie Ton of this research group conducted studies aimed at assessing the extent and mechanism of oxygen-sensitivity (Figure 4.9). The CAAC catalysts described above were provided to her by the author to include in screening. Of note, **InC1$^{Ph}$** and **nGC1$^{Ph}$** emerged as the most oxygen-tolerant of the catalysts examined, outperforming all NHC catalysts studied, as well as the bis-CAAC catalyst **UC**.[86]

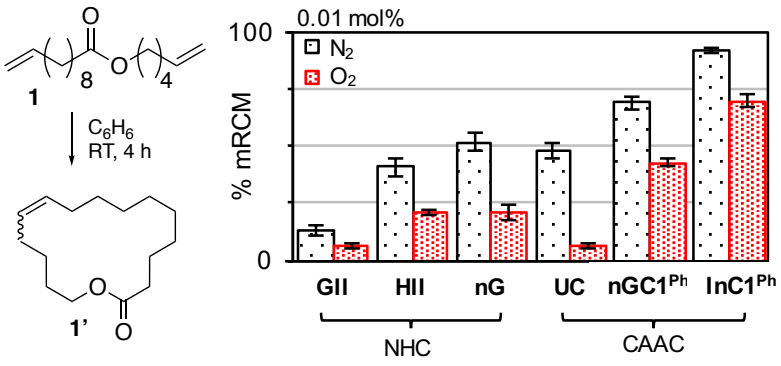


**Figure 4.9. Impact of $O_2$ in macrocyclization of 1.**

**2) ODA installation on InC1$^{Ph}$:** Preliminary experiments showed that installation of the **ODA** ligand on **InC1$^{Ph}$** was possible, as judged by $^1$H NMR analysis. However, the same rate profile was obtained in mRCM of **1** by **InC1$^{Ph}$** and **DAC1$^{Ph}$** (Figure 4.10), suggesting loss of the **ODA** ligand to generate the identical 4-coordinate species in solution. Ligand redesign to enable retention was not pursued in this thesis work, but offers clear opportunities for advance.

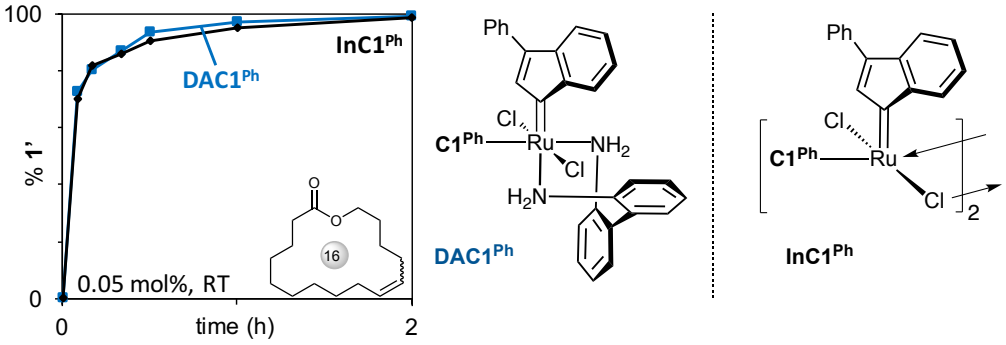


**Figure 4.10. Comparison between DAC1$^{Ph}$ and InC1$^{Ph}$ in macrocyclization of 1.**

## 4.4. References


(1) Monty, O. B. C.; Nyshadham, P.; Bohren, K. M.; Palaniappan, M.; Matzuk, M. M.; Young, D. W.; Simmons, N., Homogeneous and Functional Group Tolerant Ring-Closing Metathesis for DNA-Encoded Chemical Libraries. *ACS Comb. Sci.* **2020**, *22*, 80-88.

(2) Amoroso, D.; Yap, G. P. A.; Fogg, D. E., Deactivation of Ruthenium Metathesis Catalysts via Facile Formation of Face-Bridged Dimers. *Organometallics* **2002**, *21*, 3335–3343.

(3) Amoroso, D.; Snelgrove, J. L.; Conrad, J. C.; Drouin, S. D.; Yap, G. P. A.; Fogg, D. E., An Attractive Route to Olefin Metathesis Catalysts: Facile Synthesis of a Ruthenium Alkylidene Complex Containing Labile Phosphane Donors. *Adv. Synth. Catal.* **2002**, *344*, 757–763.

(4) Nascimento, D. L.; Foscato, M.; Occhipinti, G.; Jensen, V. R.; Fogg, D. E., Bimolecular Coupling in Olefin Metathesis: Correlating Structure and Decomposition for Leading and Emerging Ruthenium-Carbene Catalysts. *J. Am. Chem. Soc.* **2021**, accepted.

(5) Bailey, G. A.; Foscato, M.; Higman, C. S.; Day, C. S.; Jensen, V. R.; Fogg, D. E., Bimolecular Coupling as a Vector for Decomposition of Fast-Initiating Olefin Metathesis Catalysts. *J. Am. Chem. Soc.* **2018**, *140*, 6931–6944.

(6) (a) Higman, C. S.; Lummiss, J. A. M.; Fogg, D. E. Olefin Metathesis at the Dawn of Uptake in Pharmaceutical and Specialty Chemicals Manufacturing. *Angew. Chem., Int. Ed.* **2016**, *55*, 3552–3565. (b) Yu, M.; Lou, S.; Gonzalez-Bobes, F., Ring-Closing Metathesis in Pharmaceutical Development: Fundamentals, Applications, and Future Directions. *Org. Process Res. Dev.* **2018**, *22*, 918−946. (c) Farina, V.; Horváth, A., Ring-Closing Metathesis in the Large-Scale Synthesis of Pharmaceuticals. In *Handbook of Metathesis*, Grubbs, R. H.; Wenzel, A. G., Eds. Wiley-VCH: Weinheim, 2015; Vol. 2, pp 633–658. (d) Fandrick, K. R.; Savoie, J.; Jinhua, N. Y.; Song, J. J.; Senanayake, C. H., Challenges and Opportunities for Scaling the Ring-Closing Metathesis Reaction in the Pharmaceutical Industry. In *Olefin Metathesis – Theory and Practice*, Grela, K., Ed. Wiley: Hoboken, 2014; pp 349-366. For recent examples of oncology or antiviral drug candidates, see: (e) St-Pierre, G.; Cherney, A. H.; Chen, W.; Dong, X.; Dornan, P. K.; Griffin, D. J.; Houk, K. N.; Lin, J. B.; Osgood, S.; Elipe, M. V. S.; Timmons, H. C.; Xie, Y.; Tedrow, J. S.; Thiel, O. R.; Smith, A. G., Accelerated Development of a Scalable Ring-Closing Metathesis to Manufacture AMG 176 Using a Combined High-Throughput Experimentation and Computational Modeling Approach. *Org. Process Res. Dev.* **2020**, *25*, 442–451. (f) Cink, R. D.; Lukin, K. A.; Bishop, R. D.; Zhao, G.; Pelc, M. J.; Towne, T. B.; Gates, B. D.; Ravn, M. M.; Hill, D. R.; Ding, C.; Cullen, S. C.; Mei, J. Z.; Leanna, M. R.; Henle, J.; Napolitano, J. G.; Nere, N. K.; Chen, S.; Sheikh, A.; Kallemeyn, J. M., Development of the Enabling Route for Glecaprevir via Ring-Closing Metathesis. *Org. Process Res. Dev.* **2020**, *24*, 183-200.

(7) (a) Villar, E. A.; Beglov, D.; Chennamadhavuni, S.; Porco, J. A.; Kozakov, D.; Vajda, S.; Whitty, A., How proteins bind macrocycles. *Nat. Chem. Biol.* **2014**, *10*, 723-731 (b) Heinis, C., Tools and Rules for Macrocycles. *Nat. Chem. Biol.* **2014**, *10*, 696-698. (c) Giordanetto, F.; Kihlberg, J., Macrocyclic Drugs and Clinical Candidates: What Can Medicinal Chemists Learn from Their Properties? *J. Med. Chem.* **2014**, *57*, 278-295.

(8) (a) Furstner, A., Metathesis in Total Synthesis. *Chem. Commun.* **2011**, *47*, 6505–6511. (b) Fürstner, A., Olefin metathesis and beyond. *Angew. Chem., Int. Ed.* **2000**, *39*, 3012–3043. (c) Nicolaou, K. C.; Bulger, P. G.; Sarlah, D., Metathesis Reactions in Total Synthesis. *Angew. Chem., Int. Ed.* **2005**, *44*, 4490–4527. (d) Rivkin, A.; Cho, Y. S.; Gabarda, A. E.; Yoshimura, F.; Danishefsky, S. J., Application of Ring-Closing Metathesis Reactions in the Synthesis of Epothilones. *J. Nat. Prod.* **2004**, *67*, 139–143. (e) Cossy, J.; Arseniyadis, S.; Meyer, C., *Metathesis in Natural Product Synthesis: Strategies, Substrates and Catalysts*. Wiley-VCH: Weinheim, 2010.

(9) van Lierop, B. J.; Lummiss, J. A. M.; Fogg, D. E., Ring-Closing Metathesis. In *Olefin Metathesis-Theory and Practice*, Grela, K., Ed. Wiley: Hoboken, NJ, 2014; pp 85–152.

(10) For leading reviews, see: (a) Schrodi, Y., Mechanisms of Olefin Metathesis Catalyst Decomposition and Methods of Catalyst Reactivation. In *Handbook of Metathesis*, Grubbs, R. H.; Wenzel, A. G., Eds. Wiley-VCH: Weinheim, 2015; pp 323–342. (b) Chadwick, J. C.; Duchateau, R.; Freixa, Z.; van Leeuwen, P. W. N. M. *Homogeneous Catalysts: Activity – Stability – Deactivation*, Wiley-VCH: Weinheim, 2011; pp 347–396.

(11) Gradillas, A.; Perez-Castells, J., Macrocyclization by Ring-Closing Metathesis in the Total Synthesis of Natural Products: Reaction Conditions and Limitations. *Angew. Chem., Int. Ed.* **2006**, *45*, 6086–6101.

(12) An exception is **GII**, for which $PCy_3$ loss is rate-determining. See: Sanford, M. S.; Love, J. A.; Grubbs, R. H. *J. Am. Chem. Soc.* **2001**, *123*, 6543–6554.

(13) The saturated lactone is marketed as Exaltolide (Firmenich), Cyclopentadecanolide (Symrise), Pentalide (Soda Aromatics), and Thibetolide (Givaudan). See: (a) Rowe, D. J. *Chemistry and Technology of Flavors and Fragrances*, CRC Press, Boca Raton, Florida, **2005**. For the first RCM route, see: (b) (1) Fürstner, A.; Langemann, K., Conformationally Unbiased Macrocyclization Reactions by Ring Closing Metathesis. *J. Org. Chem.* **1996**, *61*, 3942–3943.

(14) Conrad, J. C.; Eelman, M. D.; Duarte Silva, J. A.; Monfette, S.; Parnas, H. H.; Snelgrove, J. L.; Fogg, D. E., Oligomers as Intermediates in Ring-Closing Metathesis. *J. Am. Chem. Soc.* **2007**, *129*, 1024–1025.

(15) Monfette, S.; Fogg, D. E., Equilibrium Ring-Closing Metathesis. *Chem. Rev.* **2009**, *109*, 3783–3816.

(16) Marx, V. M.; Sullivan, A. H.; Melaimi, M.; Virgil, S. C.; Keitz, B. K.; Weinberger, D. S.; Bertrand, G.; Grubbs, R. H., Cyclic Alkyl Amino Carbene (CAAC) Ruthenium Complexes as Remarkably Active Catalysts for Ethenolysis. *Angew. Chem., Int. Ed.* **2015**, *54*, 1919–1923.

(17) Gawin, R.; Kozakiewicz, A.; Guńka, P. A.; Dąbrowski, P.; Skowerski, K., Bis(Cyclic Alkyl Amino Carbene) Ruthenium Complexes: A Versatile, Highly Efficient Tool for Olefin Metathesis. *Angew. Chem., Int. Ed.* **2017**, *56*, 981–986.

(18) Zhang, J.; Song, S.; Wang, X.; Jiao, J.; Shi, M., Ruthenium-Catalyzed Olefin Metathesis Accelerated by the Steric Effect of the Backbone Substituent in Cyclic (Alkyl)(Amino) Carbenes. *Chem. Commun.* **2013**, *49*, 9491–9493.

(19) Schrodi, Y.; Ung, T.; Vargas, A.; Mkrtumyan, G.; Lee, C. W.; Champagne, T. M.; Pederson, R. L.; Hong, S. H., Ruthenium Olefin Metathesis Catalysts for the Ethenolysis of Renewable Feedstocks. *Clean Soil, Air, Water* **2008**, *36*, 669–673.

(20) Rigorous ethylene removal is feasible on bench scale, but is impeded by mass transfer on manufacturing scale. Sparging with $N_2$ at 1,000 L $h^{-1}$ was reported to incompletely remove ethylene from 2,400 L solvent. See: Yee, N. K.; Farina, V.; Houpis, I. N.; Haddad, N.; Frutos, R. P.; Gallou, F.; Wang, X.-J.; Wei, X.; Simpson, R. D.; Feng, X.; Fuchs, V.; Xu, Y.; Tan, J.; Zhang, L.; Xu, J.; Smith-Keenan, L. L.; Vitous, J.; Ridges, M. D.; Spinelli, E. M.; Johnson, M.; Donsbach, K.; Nicola, T.; Brenner, M.; Winter, E.; Kreye, P.; Samstag, W. *J. Org. Chem*. **2006**, *71*, 7133–7145.

(21) For yields of >90% **1'** achieved at 0.3–0.5 mol% Ru via slow catalyst addition (and, for NHC catalysts, ethylene removal), see: (a) Gawin, R.; Tracz, A.; Chwalba, M.; Kozakiewicz, A.; Trzaskowski, B.; Skowerski, K. *ACS Catal.* **2017**, *7*, 5443–5449. (b) Tracz, A.; Matczak, M.; Katarzyna; Urbaniak; Skowerski, K. *Beilstein J. Org. Chem.* **2015**, *11*, 1823–1832. (c) Skowerski, K.; Kasprzycki, P.; Bieniek, M.; Olszewski, T. K. *Tetrahedron* **2013**, *69*, 7408–7415. (d) Monfette, S.; Eyholzer, M.; Roberge, D. M.; Fogg, D. E. *Chem. – Eur. J.* **2010**, *16*, 11720–11725. Rigorous purification of **1** and solvent, drying to <2 ppm $H_2O$, ultrasonic degassing, and aggressively removing ethylene gave 80-88% **1'** at 0.008 mol% Ru, the balance being chiefly oligomers. See: (e) Kadyrov, R. *Chem. – Eur. J.* **2013**, *19*, 1002–1012.

(22) In several API routes in ref 6, peptide residues in the diene, in conjunction with judicious *N*-protection, create a conformational bias toward RCM at >50 mM diene, enabling lower catalyst

loadings. The effect is substrate-dependent, however. See, e.g.: (a) Sundararaju, B.; Sridhar, T.; Achard, M.; Sharma, G. V. M.; Bruneau, C. *Eur. J. Org. Chem.* **2013**, 6433–6442. (b) Jiang, Y.; Andrews, S. W.; Condroski, K. R.; Buckman, B.; Serebryany, V.; Wenglowsky, S.; Kennedy, A. L.; Madduru, M. R.; Wang, B.; Lyon, M.; Doherty, G. A.; Woodard, B. T.; Lemieux, C.; Geck Do, M.; Zhang, H.; Ballard, J.; Vigers, G.; Brandhuber, B. J.; Stengel, P.; Josey, J. A.; Beigelman, L.; Blatt, L.; Seiwert, S. D. *J. Med. Chem.* **2014**, *57*, 1753–1769. A clever alternative means of suppressing oligomerization involves the imposition of spatial constraints via a mesoporous foam. See: (c) Jee, J.-E.; Cheong, J. L.; Lim, J.; Chen, C.; Hong, S. H.; Lee, S. S. *J. Org. Chem.* **2013**, *78*, 3048−3056.

(23) Martí-Centelles, V.; Pandey, M. D.; Burguete, M. I.; Luis, S. V., Macrocyclization Reactions: The Importance of Conformational, Configurational, and Template-Induced Preorganization. *Chem. Rev.* **2015**, *115*, 8736−8834.

(24) (a) Larionov, E.; Li, H.; Mazet, C. *Chem. Commun.* **2014**, *50*, 9816–9826. (b) Nam, Y. H.; Snapper, M. L., Ruthenium-Catalyzed Tandem Metathesis/Non-Metathesis Processes. In *Handbook of Metathesis*, Grubbs, R. H.; Wenzel, A. G., Eds. Wiley-VCH: Weinheim, 2015; pp 311–380. (c) Fustero, S.; Simón-Fuentes, A.; Barrio, P.; Haufe, G. *Chem. Rev.* **2015**, *115*, 871−930. (d) Lampa, A.; Ehrenberg, A. E.; Vema, A.; Åkerblom, E.; Lindeberg, G.; Helena Danielson, U.; Karlén, A.; Sandström, A. *Bioorg. Med. Chem.* **2011**, *19*, 4917-4927. (e) Schmidt, B.; Hauke, S. *Eur. J. Org. Chem.* **2014**, 1951–1960. (f) Marhold, M.; Stillig, C.; Fröhlich, R.; Haufe, G. *Eur. J. Org. Chem.* **2014**, 5777–5785. (g) Schmidt, B. *Eur. J. Org. Chem.* **2004**, 1865–1880.

(25) Nucleophilic amines can abstract the alkylidene ligand: (a) Lummiss, J. A. M.; Botti, A. G. G.; Fogg, D. E. *Catal. Sci. Technol.* **2014**, *4*, 4210–4218. (b) Lummiss, J. A. M.; Ireland, B. J.; Sommers, J. M.; Fogg, D. E. *ChemCatChem* **2014**, *6*, 459–463. Nucleophilic phosphines can likewise attack the [Ru]=CHR carbon: (c) Werner, H.; Stuer, W.; Weberndorfer, B.; Wolf, J. *Eur. J. Inorg. Chem.* **1999**, 1707–1713. (d) Hansen, S. M.; Rominger, F.; Metz, M.; Hofmann, P. *Chem. – Eur. J.* **1999**, *5*, 557–566. (e) Hong, S. H.; Wenzel, A. G.; Salguero, T. T.; Day, M. W.; Grubbs, R. H. *J. Am. Chem. Soc.* **2007**, *129*, 7961–7968. (f) Galan, B. R.; Pitak, M.; Keister, J. B.; Diver, S. T. *Organometallics* **2008**, *27*, 3630–3632. (g) Lummiss, J. A. M.; McClennan, W. L.; McDonald, R.; Fogg, D. E. *Organometallics* **2014**, *33*, 6738–6741. (h) McClennan, W. L.; Rufh, S.; Lummiss, J. A. M.; Fogg, D. E. *J. Am. Chem. Soc.* **2016**, *138*, 14668−14677.

(26) (a) Bailey, G. A.; Lummiss, J. A. M.; Foscato, M.; Occhipinti, G.; McDonald, R.; Jensen, V. R.; Fogg, D. E. Decomposition of Olefin Metathesis Catalysts by Brønsted Base: Metallacyclobutane Deprotonation as a Primary Deactivating Event. *J. Am. Chem. Soc.* **2017**, *139*, 16446–16449. (b) Ireland, B. J.; Dobigny, B. T.; Fogg, D. E. Decomposition of a Phosphine-Free Metathesis Catalyst by Amines and Other Nitrogen Bases: Metallacyclobutane Deprotonation as a Major Deactivation Pathway. *ACS Catal.* **2015**, *5*, 4690−4698.

(27) Aniline is significantly less nucleophilic than pyridine. Values on the Mayr nucleophilicity scale: 12.99 vs 11.05; both in $H_2O$. See: http://www.cup.lmu.de/oc/mayr/reaktionsdatenbank/.

(28) The conjugate acid of ODA has a p$K_a$ value of 3.81 (cf. 5.25 for pyridine). See: (a) Grantham, P. H.; Weisburger, E. K.; Weisburger, J. H., Ionization Constants of Derivatives of Fluorene and Other Polycyclic Compounds. *J. Org. Chem.* **1961**, *26*, 1008–1017. (b) Örnskov, E.; Linusson, A.; Folestad, S. *J. Pharm. Biomed. Anal.* **2003**, *33*, 379–391.

(29) (a) Lummiss, J. A. M.; Higman, C. S.; Fyson, D. L.; McDonald, R.; Fogg, D. E. *Chem. Sci.* **2015**, *6*, 6739–6746. (b) Vummaleti, S. V. C.; Nelson, D. J.; Poater, A.; Gomez-Suarez, A.; Cordes, D. B.; Slawin, A. M. Z.; Nolan, S. P.; Cavallo, L. *Chem. Sci.* **2015**, 6, 1895–1904. (c) Back, O.; Henry-Ellinger, M.; Martin, C. D.; Martin, D.; Bertrand, G. *Angew. Chem., Int. Ed.* **2013**, *52*, 2939 –2943.

(30) Facile re-uptake of isopropoxystyrene was originally proposed in: (a) Kingsbury, J. S.; Harrity, J. P. A.; Bonitatebus, P. J.; Hoveyda, A. H., A Recyclable Ru-Based Metathesis Catalyst. *J. Am. Chem. Soc.* **1999**, *121*, 791–799. This long-debated "boomerang" mechanism was recently demonstrated in kinetics and isotopic labelling studies. See: (b) Griffiths, J. R.; Keister, J. B.; Diver, S. T., From

Resting State to the Steady State: Mechanistic Studies of Ene−Yne Metathesis Promoted by the Hoveyda Complex. *J. Am. Chem. Soc.* **2016**, *138*, 5380−5391. (c) Bates, J. M.; Lummiss, J. A. M.; Bailey, G. A.; Fogg, D. E., Operation of the Boomerang Mechanism in Olefin Metathesis Reactions Promoted by the Second-Generation Hoveyda Catalyst. *ACS Catal.* **2014**, *4*, 2387−2394. Of note, *electron-deficient* styrenyl ethers were reported to resist recapture in $H_2$IMes complexes. See: (d) Vorfalt, T.; Wannowius, K. J.; Thiel, V.; Plenio, H., How Important Is the Release–Return Mechanism in Olefin Metathesis? *Chem. – Eur. J.* **2010**, *16*, 12312–12315.

(31) For examples of inter-ligand E–H—Cl hydrogen bonding (E = N, O), and its impact on selectivity in catalysis, see: (a) Roşca, D.-A.; Radkowski, K.; Wolf, L. M.; Wagh, M.; Goddard, R.; Thiel, W.; Fürstner, A., Ruthenium-Catalyzed Alkyne trans-Hydrometalation: Mechanistic Insights and Preparative Implications. *J. Am. Chem. Soc.* **2017**, *139*, 2443–2455. (b) Rummelt, S. M.; Cheng, G.-J.; Gupta, P.; Thiel, W.; Fürstner, A., Hydroxy-Directed Ruthenium-Catalyzed Alkene/Alkyne Coupling: Increased Scope, Stereochemical Implications, and Mechanistic Rationale. *Angew. Chem. Int. Ed.* **2017**, *56*, 3599–3604. (c) Rummelt, S. M.; Radkowski, K.; Roşca, D.-A.; Fürstner, A., Interligand Interactions Dictate the Regioselectivity of trans-Hydrometalations and Related Reactions Catalyzed by [Cp*RuCl]. Hydrogen Bonding to a Chloride Ligand as a Steering Principle in Catalysis. *J. Am. Chem. Soc.* **2015**, *137*, 5506–5519.

(32) Conrad, J. C.; Parnas, H. H.; Snelgrove, J. L.; Fogg, D. E., Highly Efficient Ru-Pseudohalide Catalysts for Olefin Metathesis. *J. Am. Chem. Soc.* **2005**, *127*, 11882–11883.

(33) Fürstner, A.; Langemann, K., Total Syntheses of (+)-Ricinelaidic Acid Lactone and of (-)-Gloeosporone Based on Transition-Metal-Catalyzed C-C Bond Formations. *J. Am. Chem. Soc.* **1997**, *119*, 9130–9136.

(34) Sanford, M. S.; Love, J. A.; Grubbs, R. H., A Versatile Precursor for the Synthesis of New Ruthenium Olefin Metathesis Catalysts. *Organometallics* **2001**, *20*, 5314–5318.

(35) van Lierop, B. J.; Reckling, A. M.; Lummiss, J. A. M.; Fogg, D. E., High-Yield, High-Purity Routes to Second-Generation Ru Metathesis Catalysts from Commercially Available Precursors. *ChemCatChem* **2012**, *4*, 2020–2025.

(36) Jung, K.-H.; Kim, H.-K.; Lee, G. H.; Kang, D.-S.; Park, J.-A.; Kim, K. M.; Chang, Y.; Kim, T.-J., Gd Complexes of Macrocyclic Diethylenetriaminepentaacetic Acid (DTPA) Biphenyl-2,2'-bisamides as Strong Blood-Pool Magnetic Resonance Imaging Contrast Agents. *J. Med. Chem.* **2011**, *54*, 5385–5394.

(37) Fürstner, A.; Langemann, K., Macrocycles by Ring-Closing Metathesis. *Synthesis* **1997**, 792–803.

(38) Marsella, M. J.; Maynard, H. D.; Grubbs, R. H., Template-directed ring-closing metathesis: synthesis and polymerization of unsaturated crown ether analogs. *Angew. Chem., Int. Ed. Engl.* **1997**, *36*, 1101–1103.

(39) Matsuda, H.; Watanabe, S.; Yamamoto, K., New Macrocyclic Musk Compounds. *Chem. Biodiversity* **2004**, *1*, 1985–1991.

(40) Clavier, H.; Nolan, S. P., N-Heterocyclic Carbene and Phosphine Ruthenium Indenylidene Precatalysts: A Comparative Study in Olefin Metathesis. *Chem. – Eur. J.* **2007**, *13*, 8029–8036.

(41) Arisawa, M.; Kato, C.; Kaneko, H.; Nishida, A.; Nakagawa, M., Concise synthesis of azacycloundecenes using ring-closing metathesis (RCM). *Perkin 1* **2000**, 1873–1876.

(42) Habash, M.; Taha, M. O., Ligand-Based Modelling Followed by Synthetic Exploration Unveil Novel Glycogen Phosphorylase Inhibitory Leads. *Bioorg. Med. Chem.* **2011**, *19*, 4746–4771.

(43) Blacquiere, J. M.; Jurca, T.; Weiss, J.; Fogg, D. E., Time as a Dimension in High-Throughput Homogeneous Catalysis. *Adv. Synth. Catal.* **2008**, *350*, 2849–2855.

(44) Lacombe, F.; Radkowski, K.; Seidel, G.; Fürstner, A., (E)-Cycloalkenes and (E,E)-Cycloalkadienes by Ring Closing Diyne- or Enyne–Yne Metathesis/Semi-Reduction. *Tetrahedron* **2004**, *60*, 7315–7324.

(45) Blanco, C.; Nascimento, D. L.; Fogg, D. E., Routes to High-Performing Ruthenium-Iodide Catalysts for Olefin Metathesis: Phosphine Lability Is Key to Efficient Halide Exchange. *Organometallics* **2021**, accepted.

(46) Blanco, C.; Sims, J.; Nascimento, D. L.; Goudreault, A. Y.; Steinmann, S. N.; Michel, C.; Fogg, D. E., The Impact of Water on Ru-Catalyzed Olefin Metathesis: Potent Deactivating Effects Even at Low Water Concentrations. *ACS Catal.* **2021**, *11*, 893−899.

(47) Arduengo, A. J., Looking for Stable Carbenes: The Difficulty in Starting Anew. *Acc. Chem. Res.* **1999**, *32*, 913–921.

(48) Soleilhavoup, M.; Bertrand, G., Cyclic (Alkyl)(Amino)Carbenes (CAACs): Stable Carbenes on the Rise. *Acc. Chem. Res.* **2015**, *48*, 256–266.

(49) Garber, S. B.; Kingsbury, J. S.; Gray, B. L.; Hoveyda, A. H., Efficient and Recyclable Monomeric and Dendritic Ru-Based Metathesis Catalysts. *J. Am. Chem. Soc.* **2000**, *122*, 8168–8179.

(50) Gessler, S.; Randl, S.; Blechert, S., Synthesis and Metathesis Reactions of a Phosphine-Free Dihydroimidazole Carbene Ruthenium Complex. *Tetrahedron Lett.* **2000**, *41*, 9973–9976.

(51) Grela, K.; Harutyunyan, S.; Michrowska, A., A Highly Efficient Ruthenium Catalyst for Metathesis Reaction. *Angew. Chem. Int. Ed.* **2002**, *41*, 4038–4040.

(52) Hess, S. K.; Lepetit, B.; Kroth, P. G.; Mecking, S., Production of Chemicals from Microalgae Lipids – Status and Perspectives. *Eur. J. Lipid Sci. Technol.* **2018**, *120*, 1700152.

(53) Bidange, J.; Fischmeister, C.; Bruneau, C., Ethenolysis: A Green Catalytic Tool to Cleave Carbon–Carbon Double Bonds. *Chem. – Eur. J.* **2016**, *22*, 12226–12244.

(54) Biermann, U.; Bornscheuer, U. T.; Feussner, I.; Meier, M. A. R.; Metzger, J. O., Fatty Acids and their Derivatives as Renewable Platform Molecules for the Chemical Industry. *Angew. Chem., Int. Ed.* **2021**, Early View article, DOI 10.1002/anie.202100778.

(55) For a summary of early attempts to circumvent the diazo technology, see: (a) Fogg, D. E.; Foucault, H. M., Ring-Opening Metathesis Polymerization. In *Comprehensive Organometallic Chemistry III,* Crabtree, R. H.; Mingos, D. M. P., Eds. Elsevier: Oxford, 2007; Vol. 11, pp 623–652. For a recent route to Ru thiolate-alkylidene complexes enabled by aryl vinyl sulfides, see: (b) Dahcheh, F.; Stephan, D. W., A New Route to Ruthenium Thiolate Alkylidene Complexes. *Organometallics* **2013**, *32*, 5253−5255.

(56) Schwab, P.; Grubbs, R. H.; Ziller, J. W., Synthesis and Applications of $RuCl_2(=CHR')(PR_3)_2$: The Influence of the Alkylidene Moiety on Metathesis Activity. *J. Am. Chem. Soc.* **1996**, *118*, 100–110.

(57) More rarely, $ArCHN_2$ is used (Ar = $C_6H_4$-*o*-O$^i$Pr). For its reaction with $RuCl_2(PPh_3)_3$, see ref 30a. With $RuCl_2$(*p*-cymene): Day, C. S.; Fogg, D. E., High-Yield Synthesis of a Long-Sought, Labile Ru-NHC Complex and Its Application to the Concise Synthesis of Second-Generation Olefin Metathesis Catalysts. *Organometallics* **2018**, *24*, 4551–4555.

(58) Sammakia, T., Phenyldiazomethane. In *Encyclopedia of Reagents for Organic Synthesis*, John Wiley & Sons: Hoboken, NJ, 2001.

(59) Exacerbating the problem, use of the diazoalkane reagent in excess triggers alkylidene elimination as (e.g.) PhCH=CHPh. See: Amoroso, D.; Fogg, D. E., Ring-Opening Metathesis Polymerization via Ruthenium Complexes of Chelating Diphosphines. *Macromolecules* **2000**, *33*, 2815–2818.

(60) Harlow, K. J.; Hill, A. F.; Wilton-Ely, J. D. E. T., The First Coordinatively Unsaturated Group 8 Allenylidene Complexes: Insights into Grubbs' vs Dixneuf-Furstner Olefin Metathesis Catalysts. *J. Chem. Soc., Dalton Trans.* **1999**, 285–292.

(61) Boeda, F.; Clavier, H.; Nolan, S., Ruthenium–Indenylidene Complexes: Powerful Tools for Metathesis Transformations. *Chem. Commun.* **2008**, 2726–2740.

(62) Dixneuf, H. P.; Bruneau, C., Ruthenium Indenylidene Catalysts for Alkene Metathesis. In *Handbook of Metathesis*, Grubbs, R. H.; Wenzel, A. G., Eds. Wiley-VCH: Weinheim, 2015; Vol. 1, pp 389–416.

(63) Lozano-Vila, A. M.; Monsaert, S.; Bajek, A.; Verpoort, F., Ruthenium-Based Olefin Metathesis Catalysts Derived from Alkynes. *Chem. Rev.* **2010**, *110*, 4865–4909.

(64) Monsaert, S.; Drozdzak, R.; Dragutan, V.; Dragutan, I.; Verpoort, F., Indenylidene-Ruthenium Complexes Bearing Saturated N-Heterocyclic Carbenes: Synthesis and Catalytic Investigation in Olefin Metathesis Reactions. *Eur. J. Inorg. Chem.* **2008**, 432–440.

(65) Clavier, H.; Urbina-Blanco, C. A.; Nolan, S. P., Indenylidene Ruthenium Complex Bearing a Sterically Demanding NHC Ligand: An Efficient Catalyst for Olefin Metathesis at Room Temperature. *Organometallics* **2009**, *28*, 2848–2854.

(66) Clavier, H.; Petersen, J. L.; Nolan, S. P., A Pyridine-Containing Ruthenium–Indenylidene Complex: Synthesis and Activity in Ring-Closing Metathesis. *J. Organomet. Chem.* **2006**, *691*, 5444–5447.

(67) Jafarpour, L.; Schanz, H.-J.; Stevens, E. D.; Nolan, S. P., Indenylidene-Imidazolylidene Complexes of Ruthenium as Ring-Closing Metathesis Catalysts. *Organometallics* **1999**, *18*, 5416–5419.

(68) Bieniek, M.; Michrowska, A.; Usanov, D. L.; Grela, K., An Attempt to Provide a User's Guide to the Galaxy of Benzylidene, Alkoxybenzylidene, and Indenylidene Ruthenium Olefin Metathesis Catalysts. *Chem. – Eur. J.* **2008**, *14*, 806–818.

(69) Pyridine- and $PPh_3$-stabilized indenylidene catalysts are reported to exhibit even lower room-temperature activity than **M2**. See refs 27, 28. A DFT study concluded that their slow initiation is due to reduced steric pressure in the precatalyst. See: Urbina-Blanco, C. A.; Poater, A.; Lebl, T.; Manzini, S.; Slawin, A. M. Z.; Cavallo, L.; Nolan, S. P., The Activation Mechanism of Ru–Indenylidene Complexes in Olefin Metathesis. *J. Am. Chem. Soc.* **2013**, *135*, 7073–7079.

(70) Yu, B.; Li, Y.; He, X.; Hamad, F. B.; Ding, F.; Van Hecke, K.; Yusubov, M. S.; Verpoort, F., SIMes/$PCy_3$ Mixed Ligand-Coordinated Alkyl Group-Tagged Ruthenium Indenylidene Complexes: Synthesis, Characterization and Metathesis Activity. *Appl. Organomet. Chem.* **2018**, *32*, e4548.

(71) Smoleń, M.; Marczyk, A.; Kośnik, W.; Trzaskowski, B.; Kajetanowicz, A.; Grela, K., Ruthenium-Catalysed Olefin Metathesis in Environmentally Friendly Solvents: 2-Methyltetrahydrofuran Revisited. *Eur. J. Org. Chem.* **2019**, 640–646.

(72) Bieniek, M.; Michrowska, A.; Gulajski, L.; Grela, K., A Practical Larger Scale Preparation of Second-Generation Hoveyda-Type Catalysts. *Organometallics* **2007**, *26*, 1096–1099.

(73) Knapkiewicz, P.; Skowerski, K.; Jaskólska, D. E.; Barbasiewicz, M.; Olszewski, T. K., Nitration Under Continuous Flow Conditions: Convenient Synthesis of 2‑Isopropoxy-5-nitrobenzaldehyde, an Important Building Block in the Preparation of Nitro-Substituted Hoveyda−Grubbs Metathesis Catalyst. *Org. Process Res. Dev.* **2012**, *16*, 1430–1435.

(74) Weskamp, T.; Kohl, F. J.; Hieringer, W.; Gleich, D.; Herrmann, W. A., Highly Active Ruthenium Catalysts for Olefin Metathesis: The Synergy of N-Heterocyclic Carbenes and Coordinatively Labile Ligands. *Angew. Chem., Int. Ed.* **1999**, *38*, 2416–2419.

(75) For kinetics evidence for bimolecular decomposition, see: Thiel, V.; Wannowius, K.-J.; Wolff, C.; Thiele, C. M.; Plenio, H., Ring-Closing Metathesis Reactions: Interpretation of Conversion–Time Data. *Chem. - Eur. J.* **2013**, *19*, 16403–16414.

(76) This may seem to run counter to the successful deployment of chloride-bridged dimers in ring-opening metathesis polymerization. See: (a) Hansen, S. M.; Volland, M. A. O.; Rominger, F.; Eisentrager, F.; Hofmann, P., A New Class of Ruthenium Carbene Complexes: Synthesis and Structures of Highly Efficient Catalysts for Olefin Metathesis. *Angew. Chem., Int. Ed.* **1999**, *38*,

1273–1276. The difference reflects the resistance of bulky [Ru]=CHR groups to bimolecular elimination.

(77) Higman, C. S.; Nascimento, D.; Ireland, B. J.; Audorsch, S.; Bailey, G. A.; Fogg, D. E., Chelate-Assisted Ring-Closing Metathesis: A Strategy for Accelerating Macrocyclization at Ambient Temperatures. *J. Am. Chem. Soc.* **2018**, *140*, 1604−1607.

(78) Butilkov, D.; Frenklah, A.; Rozenberg, I.; Kozuch, S.; Lemcoff, N. G., Highly Selective Olefin Metathesis with CAAC-Containing Ruthenium Benzylidenes. *ACS Catal.* **2017**, *7*, 7634–7637.

(79) Dharmasena, U. L.; Foucault, H. M.; dos Santos, E. N.; Fogg, D. E.; Nolan, S. P., N-Heterocyclic Carbenes as Activating Ligands for Hydrogenation and Isomerization of Unactivated Olefins. *Organometallics* **2005**, *24*, 1056–1058.

(80) Weskamp, T.; Schattenmann, W. C.; Spiegler, M.; Herrmann, W. A., A Novel Class of Ruthenium Catalysts for Olefin Metathesis. *Angew. Chem., Int. Ed.* **1998**, *37*, 2490–2493.

(81) Such simple "olfactory lactones" were recently isolated at higher concentrations, by distilling off the cyclic product to shift the ring-chain equilbrium. See: Sytniczuk, A.; Dąbrowski, M.; Banach, Ł.; Urban, M.; Czarnocka-Śniadała, S.; Milewski, M.; Kajetanowicz, A.; Grela, K., At Long Last: Olefin Metathesis Macrocyclization at High Concentration. *J. Am. Chem. Soc.* **2018**, *40*, 8895–8901.

(82) Voccia, M.; Nolan, S. P.; Cavallo, L.; Poater, A., The Activity of Indenylidene Derivatives in Olefin Metathesis Catalysts. *Beilstein J. Org. Chem.* **2018**, *14*, 2956–2963.

(83) Computational studies of **M2** derivatives predict that increasing indenylidene bulk accelerates initiation by increasing steric pressure on the dissociating $PCy_3$ ligand. See: (a) Voccia, M.; Nolan, S. P.; Cavallo, L.; Poater, A., The Activity of Indenylidene Derivatives in Olefin Metathesis Catalysts. *Beilstein J. Org. Chem.* **2018**, *14*, 2956–2963. The rigidity of the conventional indenylidene ligand is presumed to limit such steric pressure relative to the conformationally mobile benzylidene ligand. Steric pressure exerted by the [Ru]=CHPh group has been shown to be central to the 275x faster loss of $PCy_3$ from **GII** vs its methylidene analogue $RuCl_2(H_2IMes)(PCy_3)(=CH_2)$. See: (b) Lummiss, J. A. M.; Perras, F. A.; Bryce, D. L.; Fogg, D. E., Sterically-Driven Metathesis: The Impact of Alkylidene Substitution on the Reactivity of the Grubbs Catalysts. *Organometallics* **2016**, *35*, 691–698.

(84) Engle, K. M.; Lu, G.; Luo, S.-X.; Henling, L. M.; Takase, M. K.; Liu, P.; Houk, K. N.; Grubbs, R. H., Origins of Initiation Rate Differences in Ruthenium Olefin Metathesis Catalysts Containing Chelating Benzylidenes. *J. Am. Chem. Soc.* **2015**, *137*, 5782−5792.

(85) Keller, R. N.; Wycoff, H. D., Copper(1) Chloride. *Inorg. Synth.* **1964**, *2*, 1–4.

(86) Ton, S. J.; Fogg, D. E., The Impact of Oxygen on Leading and Emerging Ru-Carbene Catalysts for Olefin Metathesis: An Unanticipated Correlation Between Robustness and Metathesis Activity *ACS Catal.* **2019**, *9*, 11329−11334.

# Chapter 5. Conclusions and Future Directions

## 5.1. Conclusions.

Molecular catalysis is a vital area in modern chemistry, with a central role in the development of sustainable chemical practices. Efficient new catalysts are essential to provide the new tools and capabilities required for demanding contexts at the frontiers of 21st century science. Critical, however, is an expanded perspective on catalyst efficiency. The overwhelming focus of current efforts is catalyst initiation and turnover. However, the active species in catalysis are typically highly reactive entities that can undergo a myriad of reactions, of which the desired, productive reactions are merely a subset. The haste to develop faster-initiating and reactive catalysts without deeper scrutiny can propagate inherent design flaws, by neglecting unintended off-cycle pathways that culminate in catalyst deactivation and decomposition. Catalyst decomposition – at best – limits efficiency: at worst, it promotes side-reactions that undermine the synthetic objectives.

This thesis is situated toward the close of an important cycle in the history of olefin metathesis, and the beginning of a new one. Studies of catalyst decomposition go back to the dawn of molecular metathesis catalysis: they formed a prominent part of Schrock's pioneering studies,[1,2] as well as those by other eminent researchers in the 1980s.[3] A small but influential group continued such studies in the context of $d^0$ metathesis catalysts, including silica-supported examples.[4-6] Within the ruthenium catalysts, however, such studies fell into abeyance, perhaps because the ruthenium catalysts had been billed as "robust" since their inception. As early as 2001,[*] our research group pointed out risks associated with inherent decomposition pathways, and the critical importance of understanding catalyst decomposition in order to identify relevant principles for catalyst design.[7,8] Even so, a detailed mechanistic program of study was initiated only in 2012, when Justin Lummiss of this research group developed the first clean, high-yield synthesis of $RuCl_2(NHC)(PCy_3)(=CH_2)$, **mGII**, the off-cycle resting-state species formed by the second-generation Grubbs catalysts.[9] The insights enabled by his detailed study of this complex were outlined in Chapter 1. They laid the groundwork for subsequent advances focusing on decomposition of on-cycle species, including those in the present thesis.

## 5.2. Future Directions

**5.2.1. Improving Catalyst Synthesis.** Clean catalyst synthesis is critical for accurate mechanistic analysis. To ensure quality control, this requires synthesis in-house. High-yielding routes are hence also essential, to limit the time spent "bringing up material". This thesis work began with development of a methodology to improve yields and purity in synthesis of second-

[*] "Catalyst Design for Olefin Metathesis and Tandem Catalysis"; lecture by Prof. Fogg at the *International Symposium on Olefin Metathesis*, Cambridge MA, August 2001.

*References for Chapter 5 begin on p. 145*

generation metathesis catalysts. Chapter 2 described the development of a synthetic protocol involving a Merrifield resin as a phosphine scavenger. The simple "filter-and-strip" workup enabled by the resin accelerated and simplified catalyst production, while increasing yields relative to the state of the art.

The Merrifield-resin protocol is likely to remain essential for the production of metathesis catalysts from $PCy_3$-stabilized precursors. (Alternatively, phosphine-free precursors are highly desirable: a promising example is under study by Ms. Eliza Boisvert). Still challenging, however, are routes to the CAAC catalysts, which suffer from poor yields and cumbersome, multistep workup (often including chromatographic purification, which risks partial decomposition on the column, and reduces isolated yields). Low yields and extensive decomposition during workup are all too common. The low yields are almost certainly due in part to the conditions required for in situ generation of the free CAAC using strong base (e.g., KHMDS, LiHMDS), at 80 °C. It is unclear, however, that the problem is primarily decomposition, as opposed to failed generation of the free CAAC, or CAAC dimerization via the Wanzlick equilibrium.

This underscores a major current limitation of the CAAC ligands: the fact that to date, only those with bulky groups (e.g., N(2,6-diisopropylaryl)) flanking the carbene carbon can be isolated as the free CAAC. As noted in Chapter 2, in situ generation and installation of free carbenes comes at a high price in terms of catalyst cleanliness. Effort was therefore directed at isolating free CAACs bearing *o*-diethyl N-aryl groups. The higher HOMO and lower LUMO of the CAACs, relative to NHCs, mean that rigorously dry solvent is essential (and possibly flame-dried glassware). Even with such precautions, attempted isolation has so far yielded only coloured oils that gave low yields of CAAC-containing products on reaction with Ru precursors. A potential alternative is use of the CAAC–$CO_2$ adducts, a strategy that showed some success with the NHC analogues (Chapter 2), but has apparently not yet been attempted with the CAACs.

The uncertain yields of the in situ-generated CAACs hampers stoichiometric control in synthesis of mono-CAAC products via ligand exchange. Synthesis of bis-CAAC derivatives does not face the same limitation, because the CAAC precursor can be used in large excess. Such products were used to access mono-CAAC species, via abstraction of one CAAC ligand with CuCl. As noted in Chapter 2, however, residual copper is a concern for applications in pharma, owing to the persistence and potent activity of copper complexes in numerous undesired pathways. In light of the high Lewis basicity of CAACs, **MF-I** could offer an alternative CAAC-scavenging strategy. A potential concern, if high temperatures or prolonged reaction are required, is unintended halide exchange. However, diiodide-CAAC catalysts (prepared deliberately via the **MF-I** + NaI route) may also be of interest in the near term, as the combination of the indenylidene moiety and bulkier iodides could retard bimolecular coupling. Longer-term solutions to the latter problem will be returned to below.

*References for Chapter 5 begin on p. 145*

Importantly, the iodide complexes could offer routes to catalysts bearing small CAAC ligands, which offer potential breakthroughs for metathesis of sterically congested olefins (see next section). Grubbs and Bertrand commented on difficulties in obtaining complexes of **C3$^{Me}$** (in which the CAAC carbene carbon is flanked by an N-mesityl group and a dimethyl-substituted quaternary site).[10] Noting that they were unable to get even small amounts of the desired product, they suggested facile dimerization. Very recently, however, Mr. Christian Blanco synthesized the iodide complex **HC3$^{Me}$** in 80% yield.[11] The difference presumably reflects faster dechelation of the ether moiety, owing to the iodide bulk. Salt metathesis of this and related species could offer the first entry point to chlororuthenium catalysts bearing small CAAC ligands.

### 5.2.2. New Criteria for Catalyst Design

**Curbing Bimolecular Decomposition.** Prior to this thesis work, detailed understanding of catalyst decomposition in Ru-catalyzed olefin metathesis was limited to the $H_2$IMes catalysts. These catalysts will likely remain important in the near term, as many of the most relevant examples are no longer subject to intellectual property restrictions, but the CAAC catalysts appear likely to displace them. The breakthrough productivity of the latter was shown in Chapter 3 to originate in their resistance to β-H elimination, one of the two major "intrinsic decomposition" pathways. This stability holds the key to the astonishing productivity of the CAAC catalysts in metathesis reactions involving ethylene. Also demonstrated was their remarkable robustness to poisons, particularly nucleophilic, basic amines. Unexpectedly, however, the CAAC catalysts proved much more susceptible to bimolecular coupling. This translates into extreme sensitivity to catalyst loadings – thus, paradoxically, dramatically higher metathesis productivity at *lower* catalyst loadings. While desirable from the perspective of potential catalyst productivity, this is a core weakness for utilization, because the exquisite sensitivity of metathesis yields to concentrations results in unpredictable performance. Indeed, excessive catalyst loadings, and hence high concentrations (ca. 10 mM Ru), contributed to the strikingly poor performance originally reported for the CAAC catalysts (incomplete RCM of diethyl-diallylmalonate **2** – arguably the most facile cyclization reaction in metathesis chemistry – at catalyst loadings of 1-5 mol%).[12] Essential for uptake by the synthetic community are strategies for curbing bimolecular coupling of the CAAC catalysts.

Such strategies are a clear priority in the near term. Most straightforward would be replacement of the chloride ligands by pseudohalide ligands such as aryloxides, a strategy pioneered by our group[13,14] following the discovery that the chloride ligands enable bimolecular decomposition.[7,8] Catalyst immobilization offers a further, well-developed solution, albeit one that so far has failed to improve the productivity of molecular metathesis catalysts. In a recent review of immobilization strategies for metathesis and hydrogenation catalysis, de Vries and Farina deliver a robust critique of the negative impact on activity and productivity.[15] These weaknesses are inevitable, where the metallacyclobutane can undergo unimolecular decomposition. Immobilization strategies take on new relevance with the advent of catalysts that are immune to

β-hydride elimination. The latter advance, in conjunction with the heightened robustness of the CAAC catalysts to poisons, opens the first true opportunities for supported Ru metathesis catalysts (see section 5.2.3).

Particularly intriguing possibilities are raised by immobilization of catalysts bearing *small* CAAC ligands. At present, the extreme susceptibility of such complexes to bimolecular coupling (BMC) is predicted to render them functionally unusable. A survey should be undertaken to assess this point by, for example, measuring the maximum TONs attainable with **nGC3$^{Me}$** (synthesized via diiodo analogue as proposed above) vs **nGC3$^{Ph}$** and **nGC1$^{Ph}$**. While TONs are expected to improve as catalyst concentrations decrease, the levels required to inhibit BMC are predicted to be so low that trace impurities quench metathesis activity. Suppressing BMC via immobilization is anticipated to be critical to harnessing small CAAC catalysts for key transformations in which minimizing steric bulk is essential.

**Design Opportunities for Stereoselective Metathesis.** CAAC catalysts bearing pseudohalide ligands may offer solutions to current challenges in Z-selective metathesis. At present, high catalyst loadings are necessary, yields are often modest, and stereoselectivity is typically eroded as conversions increase. Indeed, even the most widely used Z-selective catalyst requires loadings of 7.5 mol% to furnish macrocycles in yields of 36–65%.[16] The high loadings are a clear indicator of catalyst decomposition, and the decomposed products are almost undoubtedly responsible for the drop in stereoselectivity at high conversions. The presence of water or oxygen further limits selectivity.[17,18] Cumulatively, these challenges limit success and uptake. Mr. Christian Blanco and Ms. Stephanie Ton, respectively, showed that CAAC catalysts offer significantly higher tolerance for water[17] and oxygen.[19] Robust pseudohalide derivatives based on Ru-CAAC platforms are likely to offer significant opportunities for stereoselective metathesis.

**Fundamental Criteria for Ligand Design.** Since 1999, olefin metathesis has been dominated by Ru-NHC complexes, the reactivity of which rests on the heightened σ-donicity of the carbene ligands relative to their phosphine predecessors. Now under way is a transition to CAAC ligands with improved σ-donating and π-accepting ability. Arguably the broadest implication of Chapter 4 is the net impact of these combined properties: at its simplest, it calls for strongly donating, high trans-influence ligands. As noted above, however, this is a double-edged sword: it enables resistance to β-H elimination, but promotes bimolecular decomposition. These simple guidelines offer a key metric for the identification of new candidate ligand families, but highlight the critical importance of minimizing the obscuring effect of accelerated bimolecular coupling. With that caveat in place, high trans-influence ligands are likely to reshape ligand design in olefin metathesis.

*References for Chapter 5 begin on p. 145*

### 5.2.3. New Applications Frontiers

**Process Chemistry.** Described in Chapter 4 were new catalyst architectures that offer opportunities in important reaction contexts. The dianiline-stabilized catalyst **DA** significantly improved yields in macrocyclization of conformationally flexible dienes bearing donor ligands. Polar groups ubiquitous in mRCM in pharma are thus transformed from threat to opportunity, so long as water is removed from the reaction medium. Polyphenol resins deployed by our group to mitigate decomposition arising from Bronsted base may offer opportunities in this context as well.[20]

**Flow Chemistry.** The advances described above are anticipated to transform the powerful Ru-CAAC catalysts into the most reliable OM tools to date for organic synthesis. Of added interest are opportunities in flow chemistry. Ethylene-induced decomposition has been a fundamental challenge to the implementation of flow methodologies for olefin metathesis. Our group and others have reported engineering solutions to the mass transfer challenges associated with ethylene removal. These range from continuous stirred-tank reactors[21] to tube-in-tube[22,23] and pervaporation reactors.[24] These approaches, while often ingenious, require specialized equipment inaccessible to the broader community. Anchored CAAC catalysts offer tremendous opportunity for olefin metathesis using conventional plug-flow reactors.

**Biorefinery Applications of Immobilized CAAC Catalysts.** An important niche opportunity that emerges from immobilization of small CAAC catalysts (which, as noted above, are extremely susceptible to bimolecular decomposition), is the successful metathesis of sterically demanding substrates. An illustrative opportunity is the metathetical transformation of lignin-derived stilbenes.[25] Noted in Chapter 1 was the urgent need to transition from petrochemicals to low-impact renewables as a carbon source for the chemical industry. In that context, valorization of waste lignin biomass has been a tantalizing prospect for many years.[26] Of keen interest is the potential access to high-value phenolic styrene building blocks via cross-metathesis of stilbenes with ethylene. While ethenolysis is a reaction manifold in which the CAACs normally excel (Chapter 4), preliminary experiments now being pursued by Ms. Eliza-Jayne Boisvert revealed *zero* product for **HC1$^{Ph}$** in this reaction, which involves a sterically congested trans-disubstituted olefin. Preferential reaction with ethylene is presumed to increase the proportion of the [Ru]=$CH_2$ intermediate, and hence bimolecular decomposition. Small, immobilized CAACs would open new doors for these and other transformations of sterically encumbered dienes.

More broadly, the superior performance of the CAAC catalysts in ethenolysis brings within reach the long-standing goal of producing α-olefins from plant oils. A more potent proposition, however, is the use of robust, water-tolerant CAAC catalysts for harnessing algae lipids as feedstocks. As a truly "green" biorefinery methodology, this would greatly expand opportunities for olefin metathesis in sustainable chemistry.

*References for Chapter 5 begin on p. 145*

**High Throughput Experimentation (HTE).** The resistance of the CAAC catalysts to decomposition by ethylene makes them the first plausible candidates for HTE screening of metathesis catalysts. HTE catalyst screening is now routine in pharmaceutical R&D, and has been expanding in academia. Indeed, the uOttawa Centre for Catalysis Research and Innovation has some of the most sophisticated such tools in academia worldwide: while our group led their acquisition, the deleterious impact of ethylene in sealed small vessels meant that HTE data did not faithfully reproduce "real" catalyst behaviour. Elimination of this problem at last opens the door to HTE screening in olefin metathesis.

**Chemical Biology.** Implementation of olefin metathesis in chemical biology has long been desired, with applications to peptide and protein modification attaining highest visibility.[27,28] Applications to the assembly of DNA-encoded chemical libraries offer compelling new opportunities for advanced drug scouting programs in pharmaceutical R&D.[29,30] Indeed, the **DA** catalyst was found by colleagues at the Baylor College of Medicine to significantly improve catalyst performance in on-DNA RCM.[29] **DA** out-performed other metathesis catalysts in these contexts, despite use of water as a solvent.

All these contexts, however, require ruthenium as reagent (sometimes in startlingly high stoichiometric excess). As noted repeatedly throughout this thesis, the problems of catalyst decomposition are compounded by the ability of the decomposed catalyst to cause side-reactions. Whether the Ru products formed in water cause side-reactions, and the role of water in decomposing the catalyst, are under current study by Mr. Christian Blanco of this research group. Use of fluorophore-modified **ODA** ligands could be invaluable in assessing whether the ligand is displaced by water, and whether strategies for improving Ru bond strengths should be prioritized. The ability of the Ru complexes to degrade DNA underscores the importance of long-lived, *catalytic* olefin metathesis in these contexts. The water-tolerance of the CAAC catalysts is predicted to offer powerful new opportunities in areas at the interface of synthetic chemistry and chemical biology.

*References for Chapter 5 begin on p. 145*

## 5.3. References


(1) Schrock, R. R.; Copéret, C., Formation of High-Oxidation-State Metal–Carbon Double Bonds. *Organometallics* **2017**, *36*, 1884–1892.

(2) Schrock, R. R., Multiple Metal-Carbon Bonds for Catalytic Metathesis Reactions (Nobel Lecture). *Angew. Chem., Int. Ed.* **2006**, *45*, 3748–3759.

(3) For leading reviews, see: (a) Schrodi, Y., Mechanisms of Olefin Metathesis Catalyst Decomposition and Methods of Catalyst Reactivation. In *Handbook of Metathesis*, Grubbs, R. H.; Wenzel, A. G., Eds. Wiley-VCH: Weinheim, 2015; pp 323–342. (b) Chadwick, J. C.; Duchateau, R.; Freixa, Z.; van Leeuwen, P. W. N. M. *Homogeneous Catalysts: Activity – Stability – Deactivation*, Wiley-VCH: Weinheim, 2011; pp 347–396.

(4) Gordon, C. P.; Raynaud, C.; Anderson, R. A.; Copéret, C.; Eisenstein, O., Carbon-13 NMR Chemical Shift: A Descriptor for Electronic Structure and Reactivity of Organometallic Compounds. *Acc. Chem. Res.* **2019**, *52*, 2278–2289.

(5) Solans-Monfort, X.; Copéret, C.; Eisenstein, O., Shutting Down Secondary Reaction Pathways: The Essential Role of the Pyrrolyl Ligand in Improving Silica Supported d0-ML4 Alkene Metathesis Catalysts from DFT Calculations. *J. Am. Chem. Soc.* **2010**, *132*, 7750–7757.

(6) Leduc, A.-M.; Salameh, A.; Soulivong, D.; Chabanas, M.; Basset, J.-M.; Copéret, C.; Solans-Monfort, X.; Clot, E.; Eisenstein, O.; Boehm, V. P. W.; Roeper, M., beta-H Transfer from the Metallacyclobutane: a Key Step in the Deactivation and Byproduct Formation for the Well-Defined Silica-Supported Rhenium Alkylidene Alkene Metathesis Catalyst. *J. Am. Chem. Soc.* **2008**, *130*, 6288–6297.

(7) Amoroso, D.; Yap, G. P. A.; Fogg, D. E., Deactivation of Ruthenium Metathesis Catalysts via Facile Formation of Face-Bridged Dimers. *Organometallics* **2002**, *21*, 3335–3343.

(8) Amoroso, D.; Snelgrove, J. L.; Conrad, J. C.; Drouin, S. D.; Yap, G. P. A.; Fogg, D. E., An Attractive Route to Olefin Metathesis Catalysts: Facile Synthesis of a Ruthenium Alkylidene Complex Containing Labile Phosphane Donors. *Adv. Synth. Catal.* **2002**, *344*, 757–763.

(9) Lummiss, J. A. M.; Beach, N. J.; Smith, J. C.; Fogg, D. E., Targeting an Achilles Heel in Olefin Metathesis: A Strategy for High-Yield Synthesis of Second-Generation Grubbs Methylidene Catalysts. *Catal. Sci. Technol.* **2012**, *2*, 1630–1632.

(10) Marx, V. M.; Sullivan, A. H.; Melaimi, M.; Virgil, S. C.; Keitz, B. K.; Weinberger, D. S.; Bertrand, G.; Grubbs, R. H., Cyclic Alkyl Amino Carbene (CAAC) Ruthenium Complexes as Remarkably Active Catalysts for Ethenolysis. *Angew. Chem., Int. Ed.* **2015**, *54*, 1919–1923.

(11) Blanco, C.; Nascimento, D. L.; Fogg, D. E., Routes to High-Performing Ruthenium-Iodide Catalysts for Olefin Metathesis: Phosphine Lability Is Key to Efficient Halide Exchange. *Organometallics* **2021**, *40*, 1811–1816.

(12) Anderson, D. R.; Lavallo, V.; O'Leary, D. J.; Bertrand, G.; Grubbs, R. H., Synthesis and Reactivity of Olefin Metathesis Catalysts Bearing Cyclic (Alkyl)(Amino)Carbenes. *Angew. Chem., Int. Ed.* **2007**, *46*, 7262–7265.

(13) Conrad, J. C.; Amoroso, D.; Czechura, P.; Yap, G. P. A.; Fogg, D. E., The First Highly Active, Halide-Free Ruthenium Catalyst for Olefin Metathesis. *Organometallics* **2003**, *22*, 3634–3636.

(14) Conrad, J. C.; Parnas, H. H.; Snelgrove, J. L.; Fogg, D. E., Highly Efficient Ru-Pseudohalide Catalysts for Olefin Metathesis. *J. Am. Chem. Soc.* **2005**, *127*, 11882–11883.

(15) Hubner, S.; de Vries, J. G.; Farina, V., Why Does Industry Not Use Immobilized Transition Metal Complexes as Catalysts? *Adv. Synth. Catal.* **2016**, *358*, 3–25.

(16) Rosebrugh, L. E.; Herbert, M. B.; Marx, V. M.; Keitz, B. K.; Grubbs, R. H., Highly Active Ruthenium Metathesis Catalysts Exhibiting Unprecedented Activity and Z-Selectivity. *J. Am. Chem. Soc.* **2013**, *135*, 1276–1279.

(17) Blanco, C.; Sims, J.; Nascimento, D. L.; Goudreault, A. Y.; Steinmann, S. N.; Michel, C.; Fogg, D. E., The Impact of Water on Ru-Catalyzed Olefin Metathesis: Potent Deactivating Effects Even at Low Water Concentrations. *ACS Catal.* **2021**, *11*, 893−899.

(18) Max, H.; Goldberg, J. M.; Johns, A.; Fogg, D. E., Z-Selective Olefin Metathesis Catalysts: Stereoselectivity and Decomposition. manuscript in preparation.
(19) Ton, S. J.; Fogg, D. E., The Impact of Oxygen on Leading and Emerging Ru-Carbene Catalysts for Olefin Metathesis: An Unanticipated Correlation Between Robustness and Metathesis Activity *ACS Catal.* **2019**, *9*, 11329−11334.
(20) Santos, A. G.; Bailey, G. A.; dos Santos, E. N.; Fogg, D. E., Overcoming Catalyst Decomposition in Acrylate Metathesis: Poly-phenol Resins as Enabling Agents for Phosphine-Stabilized Metathesis Catalysts. *ACS Catal.* **2017**, *7*, 3181−3189.
(21) Monfette, S.; Eyholzer, M.; Roberge, D. M.; Fogg, D. E., Getting RCM Off the Bench: Reaction-Reactor Matching Transforms Metathesis Efficiency in the Assembly of Large Rings. *Chem. – Eur. J.* **2010**, *16*, 11720–11725.
(22) Skowerski, K.; Czarnocki, S. J.; Knapkiewicz, P., Tube-in-Tube Reactor as a Useful Tool for Homo- and Heterogeneous Olefin Metathesis under Continuous Flow Mode. *ChemSusChem* **2014**, *7*, 536–542.
(23) Morvan, J.; McBride, T.; Curbet, I.; Colombel-Rouen, S.; Roisnel, T.; Crévisy, C.; Browne, D. L.; Mauduit, M., Continuous Flow Z-Stereoselective Olefin Metathesis: Development and Applications in the Synthesis of Pheromones and Macrocyclic Odorant Molecules. *Angew. Chem. Int. Ed.* **2021**, ASAP article.
(24) Breen, C. P.; Parrish, C.; Shangguan, N.; Majumdar, S.; Murnen, H.; Jamison, T. F.; Bio, M. M., A Scalable Membrane Pervaporation Approach for Continuous Flow Olefin Metathesis. *Org. Proc. Res. Dev.* **2020**, *24*, 2298–2303.
(25) Lahive, C. W.; Deuss, P. J.; Lancefield, C. S.; Sun, Z.; Cordes, D. B.; Young, C. M.; Tran, F.; Slawin, A. M. Z.; Vries, J. G. d.; Kamer, P. C. J.; Westwood, N. J.; Barta, K., Advanced Model Compounds for Understanding Acid-Catalyzed Lignin Depolymerization: Identification of Renewable Aromatics and a Lignin-Derived Solvent. *J. Am .Chem. Soc.* **2016**, *138*, 8900−8911.
(26) Sun, Z.; Fridrich, B. l.; Santi, A. d.; Elangovan, S.; Barta, K., Bright Side of Lignin Depolymerization: Toward New Platform Chemicals. *Chem. Rev.* **2018**, *118*, 614−678.
(27) Messina, M. S.; Maynard, H. D., Modification of Proteins Using Olefin Metathesis. *Mater. Chem. Front.* **2020**, *4*, 1040–1051.
(28) Isenegger, P. G.; Davis, B. G., Concepts of Catalysis in Site-Selective Protein Modifications. *J. Am. Chem. Soc.* **2019**, *141*, 8005−8013.
(29) Monty, O. B. C.; Nyshadham, P.; Bohren, K. M.; Palaniappan, M.; Matzuk, M. M.; Young, D. W.; Simmons, N., Homogeneous and Functional Group Tolerant Ring-Closing Metathesis for DNA-Encoded Chemical Libraries. *ACS Comb. Sci.* **2020**, *22*, 80-88.
(30) Lu, X.; Fan, L.; Phelps, C. B.; Davie, C. P.; Donahue, C. P., Ruthenium Promoted on-DNA Ring-Closing Metathesis and Cross-Metathesis. *Bioconjugate Chem.* **2017**, *28*, 1625−1629.

# Appendices

## A. NMR Spectra

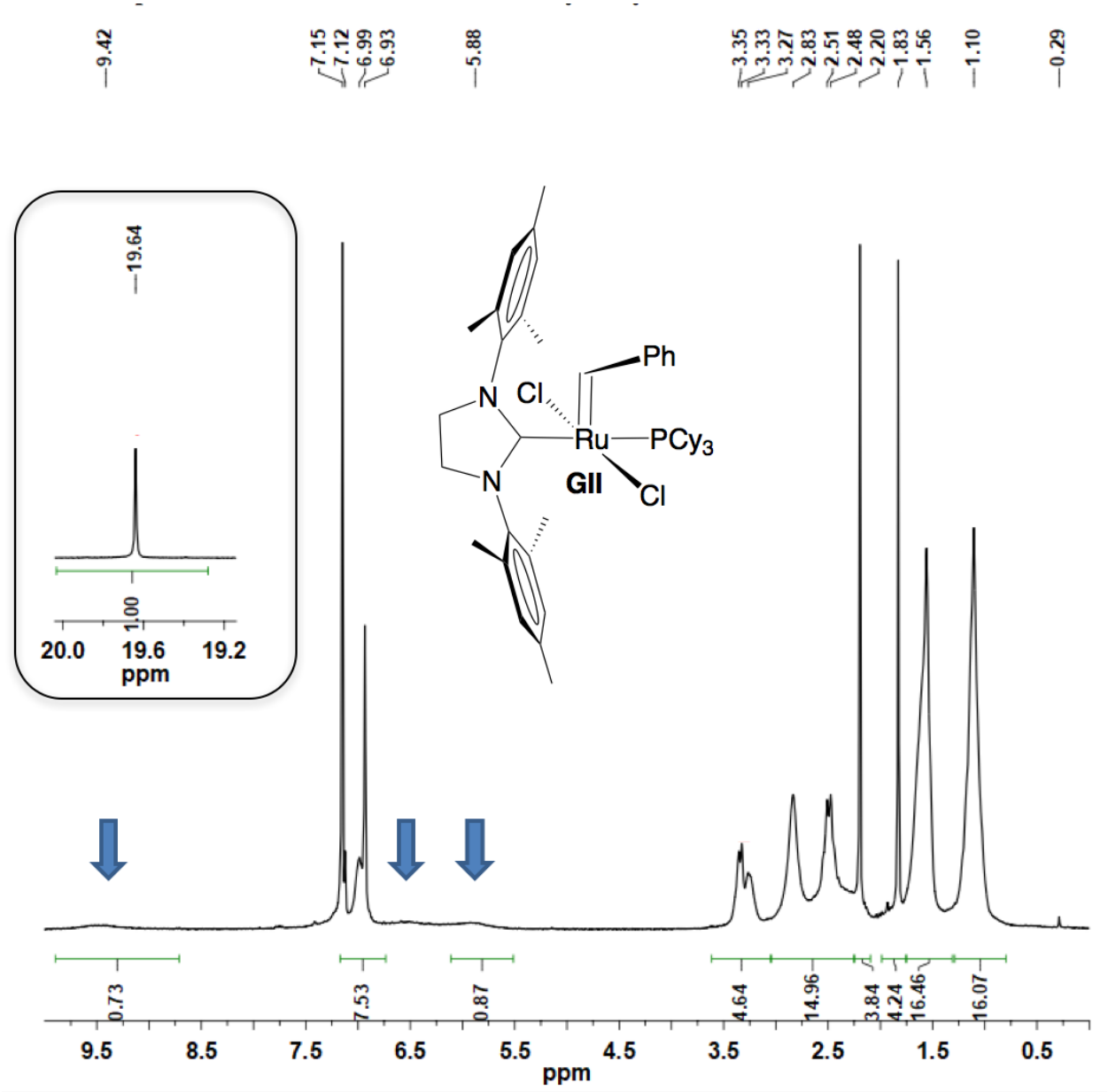


**Figure A.1a.** $^{1}$H NMR spectrum ($C_6D_6$, 300 MHz) of **GII**, prepared from **GI** by ligand exchange and worked up using **MF-I** to scavenge free $PCy_3$. Arrows denote the broad signals arising from rotation of the aromatic rings.

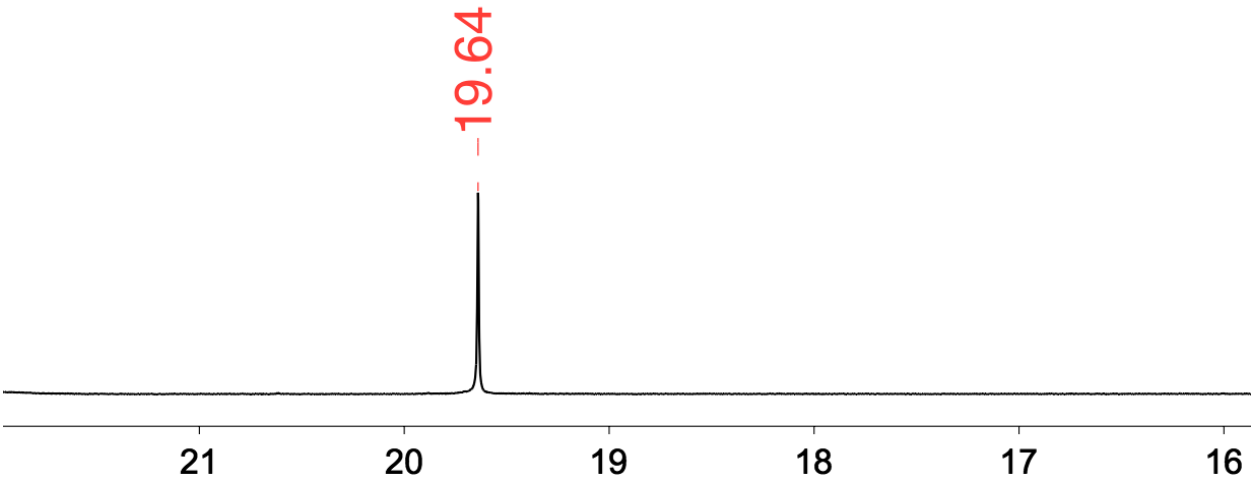


**Figure A.1b.** Expanded alkylidene region for the spectrum of Fig. A.1a, showing the absence of additional signals.

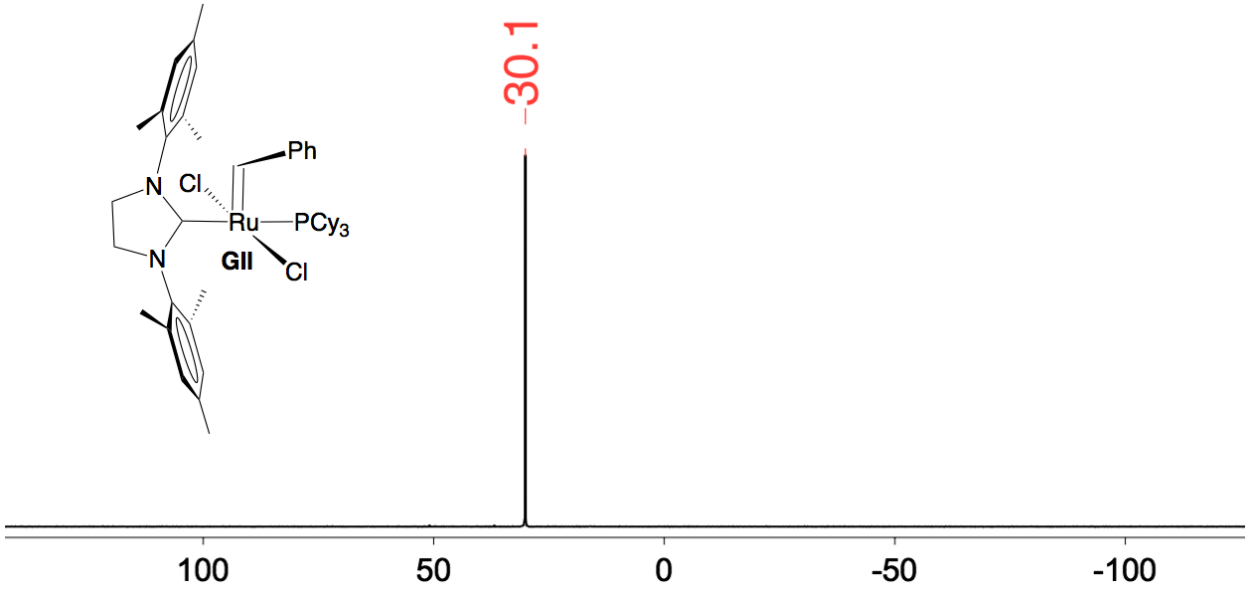


**Figure A.1c.** $^{31}P\{^{1}H\}$ NMR spectrum ($C_6D_6$, 121.2 MHz) of **GII**, prepared from **GI** by ligand exchange and worked up using **MF-I** to scavenge free $PCy_3$.

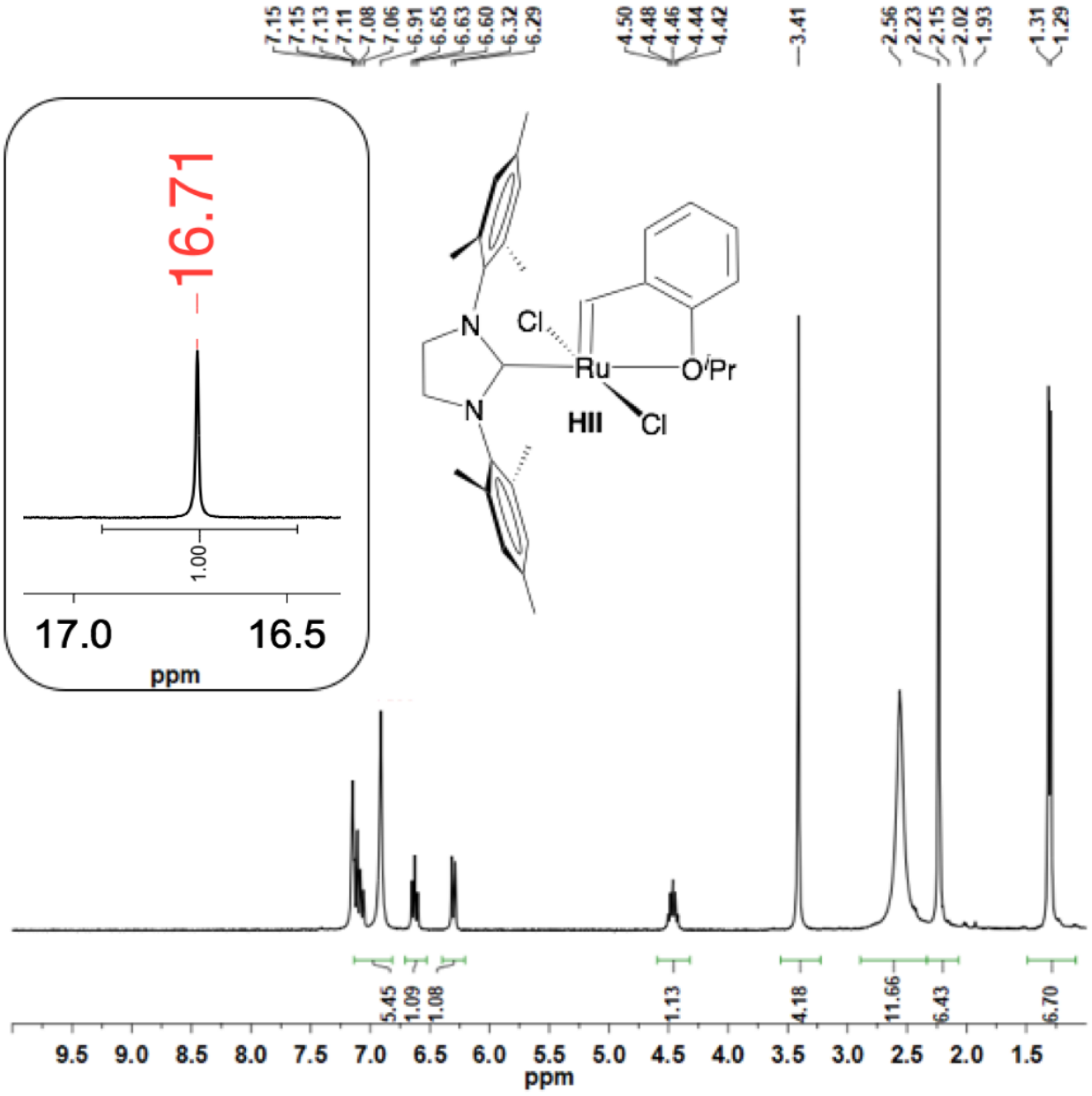


**Figure A.2a.** $^1$H NMR spectrum ($C_6D_6$, 300 MHz) of **HII**, prepared from **HI** by ligand exchange and worked up using **MF-I** to scavenge free $PCy_3$.

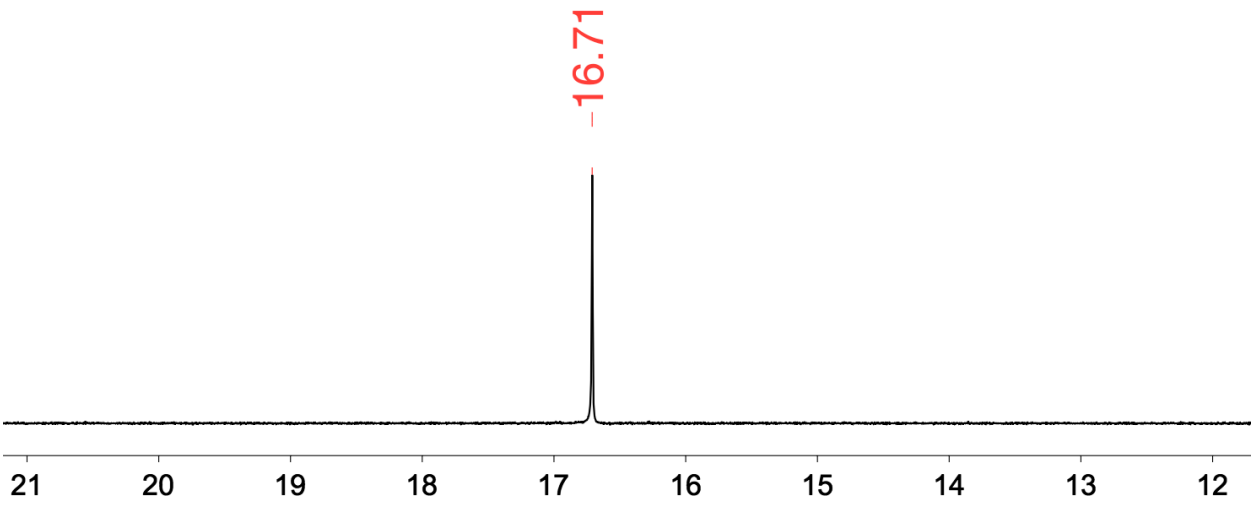


**Figure A.2b.** Full alkylidene region for the spectrum of Fig. A.2a, showing the absence of additional signals.

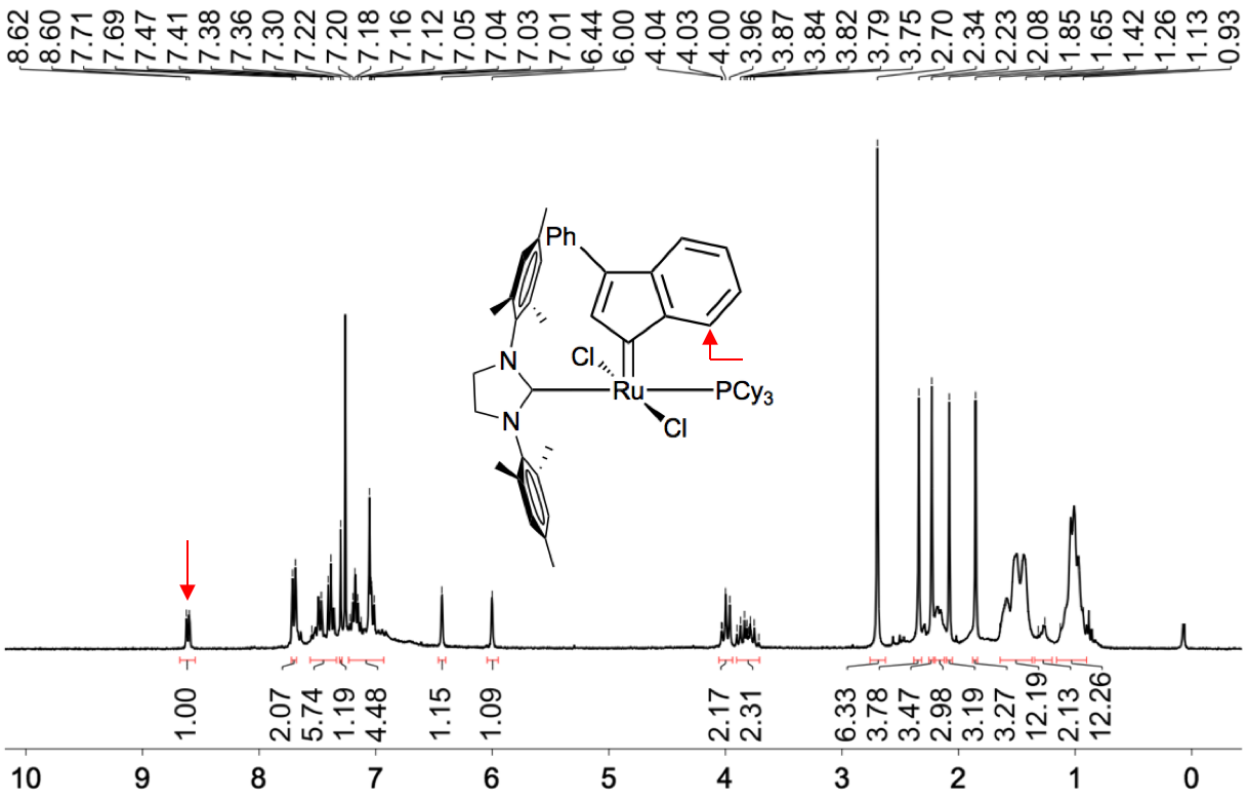


**Figure A.3a.** $^{1}$H NMR spectrum ($CDCl_3$, 300 MHz) of **InII**, prepared from **InI** by ligand exchange and worked up using **MF-I** to scavenge free $PCy_3$. Arrow indicates the location of the proton used to confirm the stability of **InII** in decomposition experiments.

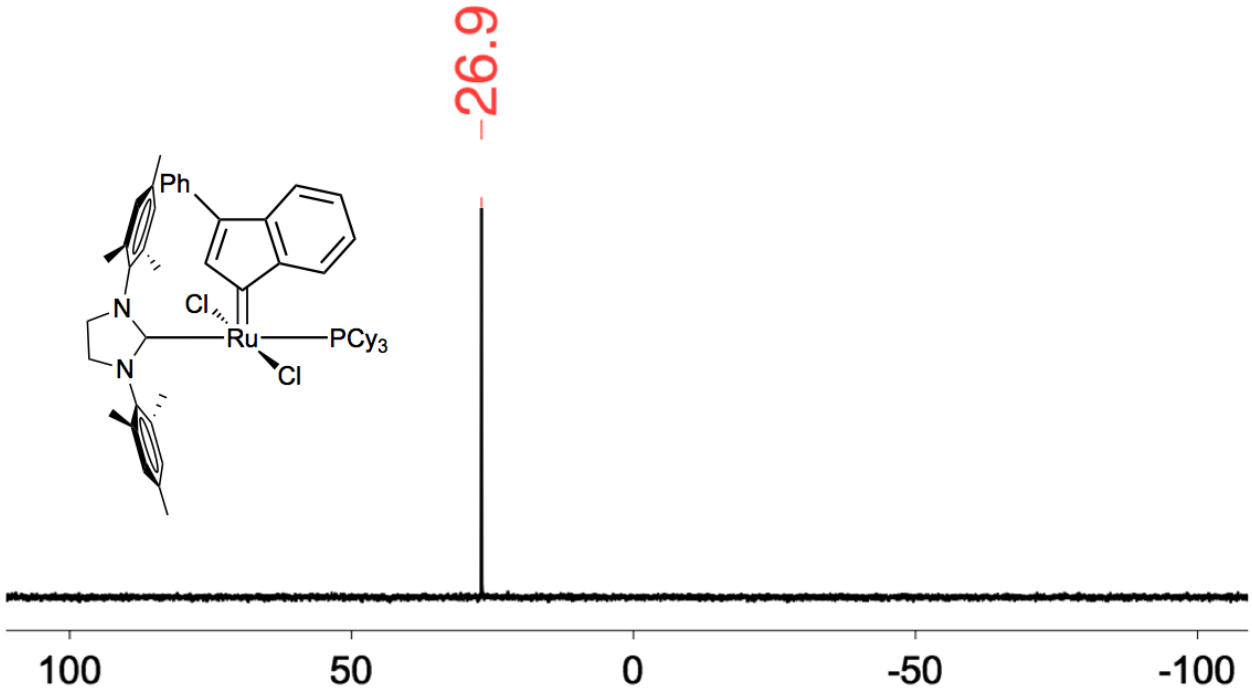


**Figure A.3b.** $^{31}P\{^{1}H\}$ NMR spectrum ($CDCl_3$, 121.2 MHz) of **InII**, prepared from **InI** by ligand exchange and worked up using **MF-I** to scavenge free $PCy_3$.

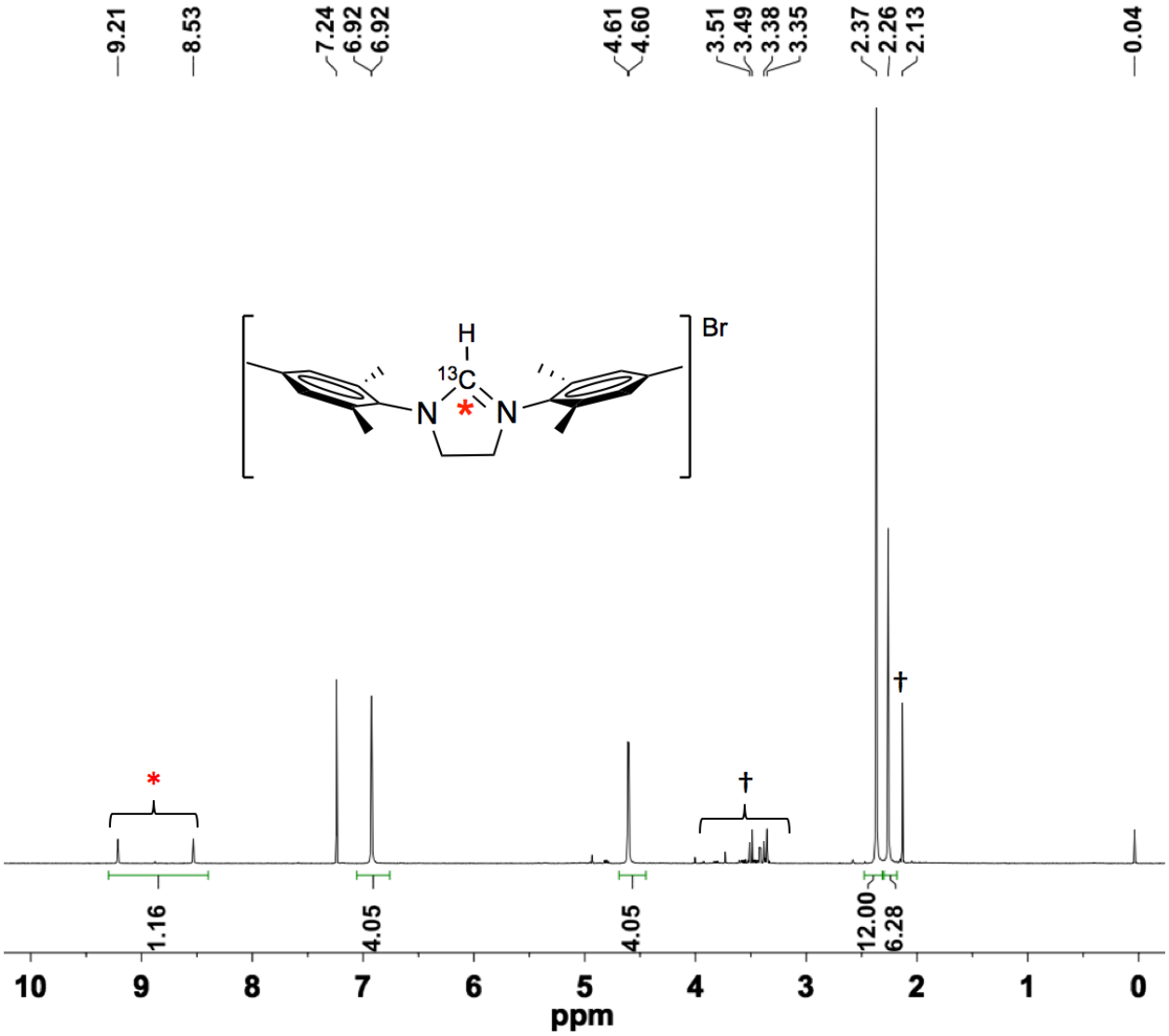


**Figure A.4a.** $^{1}$H NMR spectrum (300 MHz, $CDCl_3$) of **$^{13}$C-H$_2$IMes•HBr** (* = $^{13}$C*H* doublet showing $^{1}J_{CH}$ coupling of 204 Hz; (†) = solvent and *N*-bromosuccinimide impurities removed in the next step).

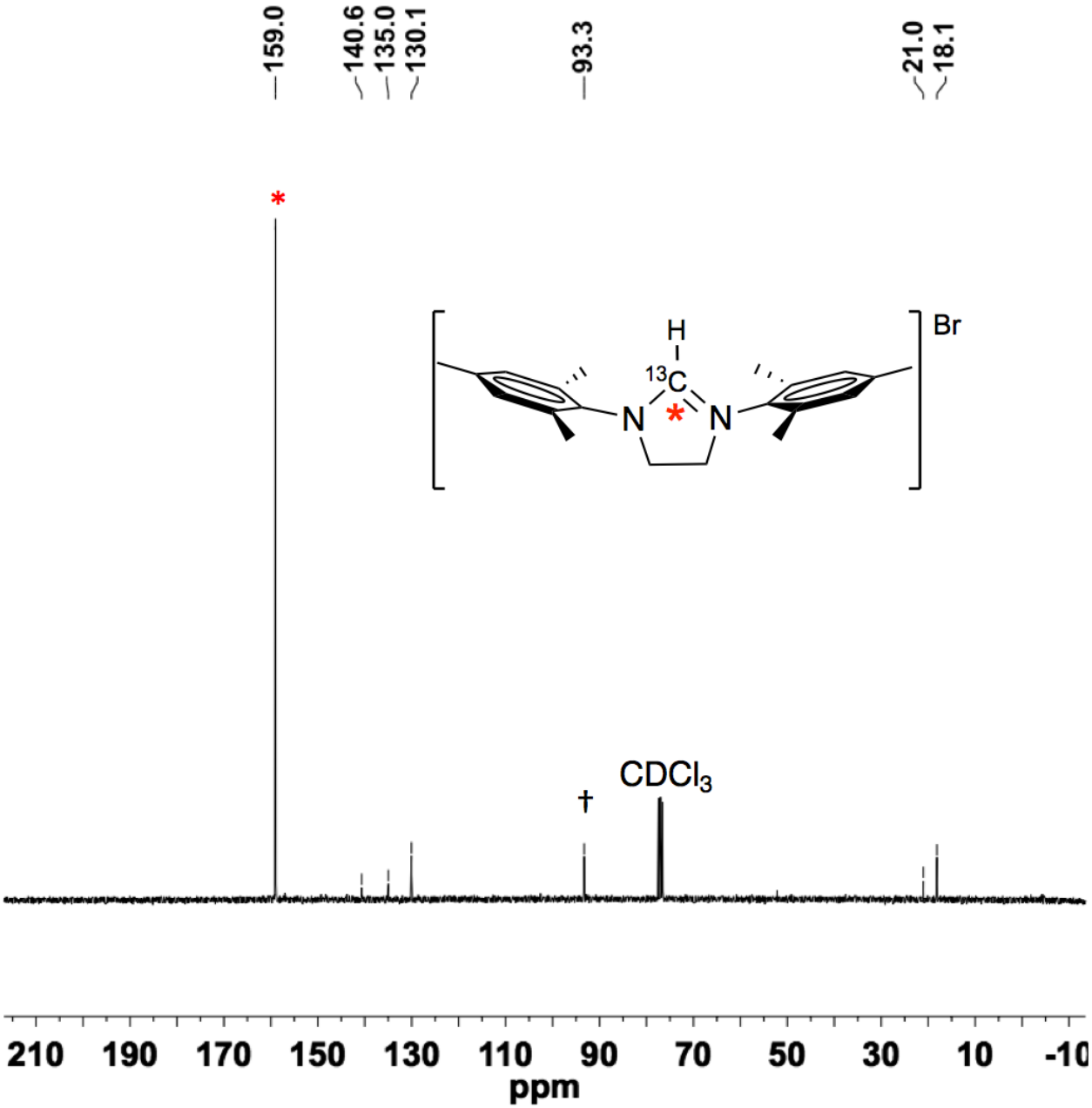


**Figure A.4b.** $^{13}C\{^{1}H\}$ NMR spectrum ($CDCl_3$, 75.5 MHz) of **$^{13}$C-H$_2$IMes•HBr** (* = $^{13}C$-labelled carbon). (†) designates unidentified impurity.

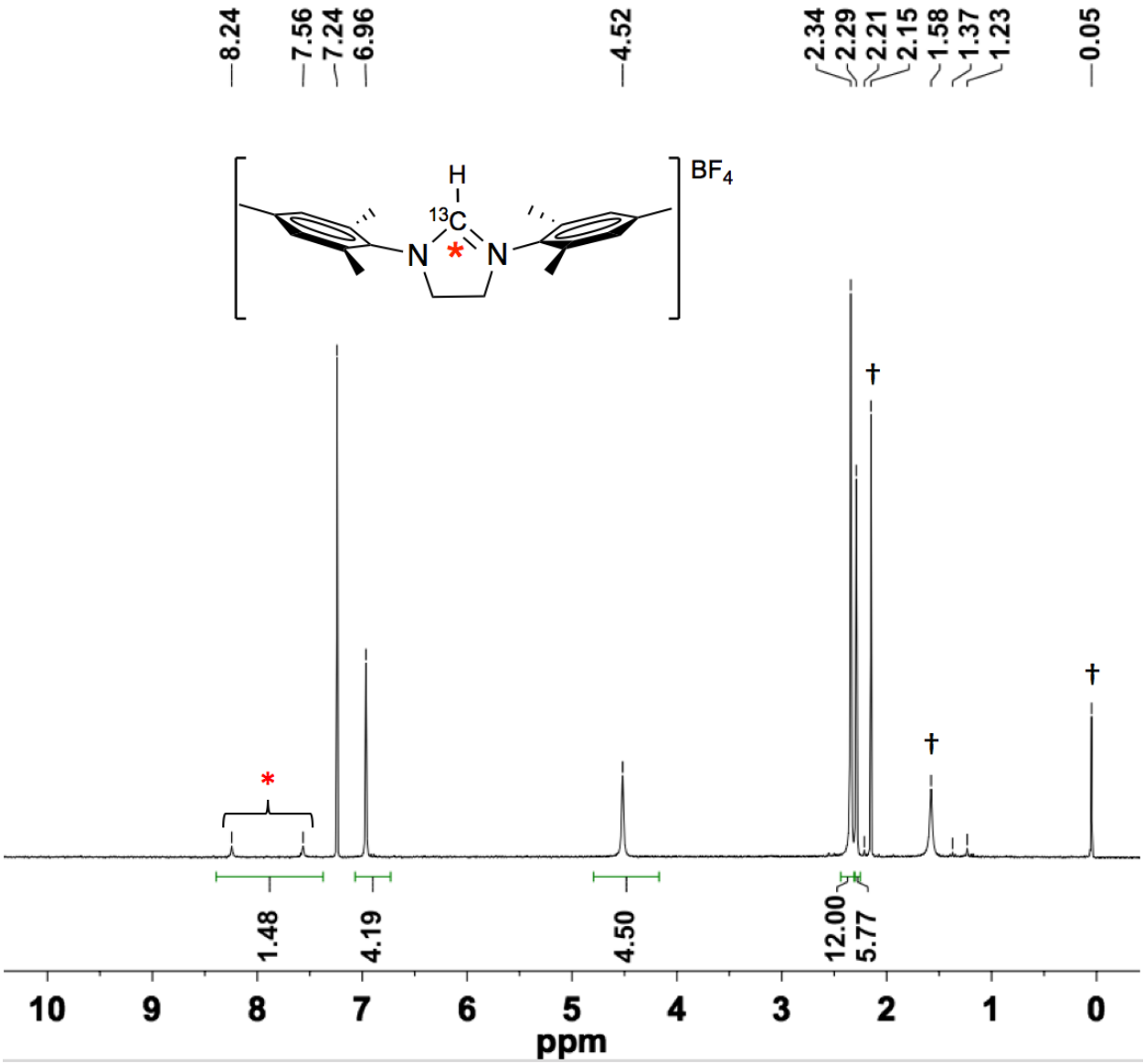


**Figure A.5a.** $^{1}$H NMR spectrum (300 MHz, $CDCl_3$) of **$^{13}$C-H$_2$IMes•HBF$_4$** (* = $^{13}$C*H* doublet showing $^{1}J_{CH}$ coupling of 205 Hz; (†) = acetone, water, and silicon grease impurities).

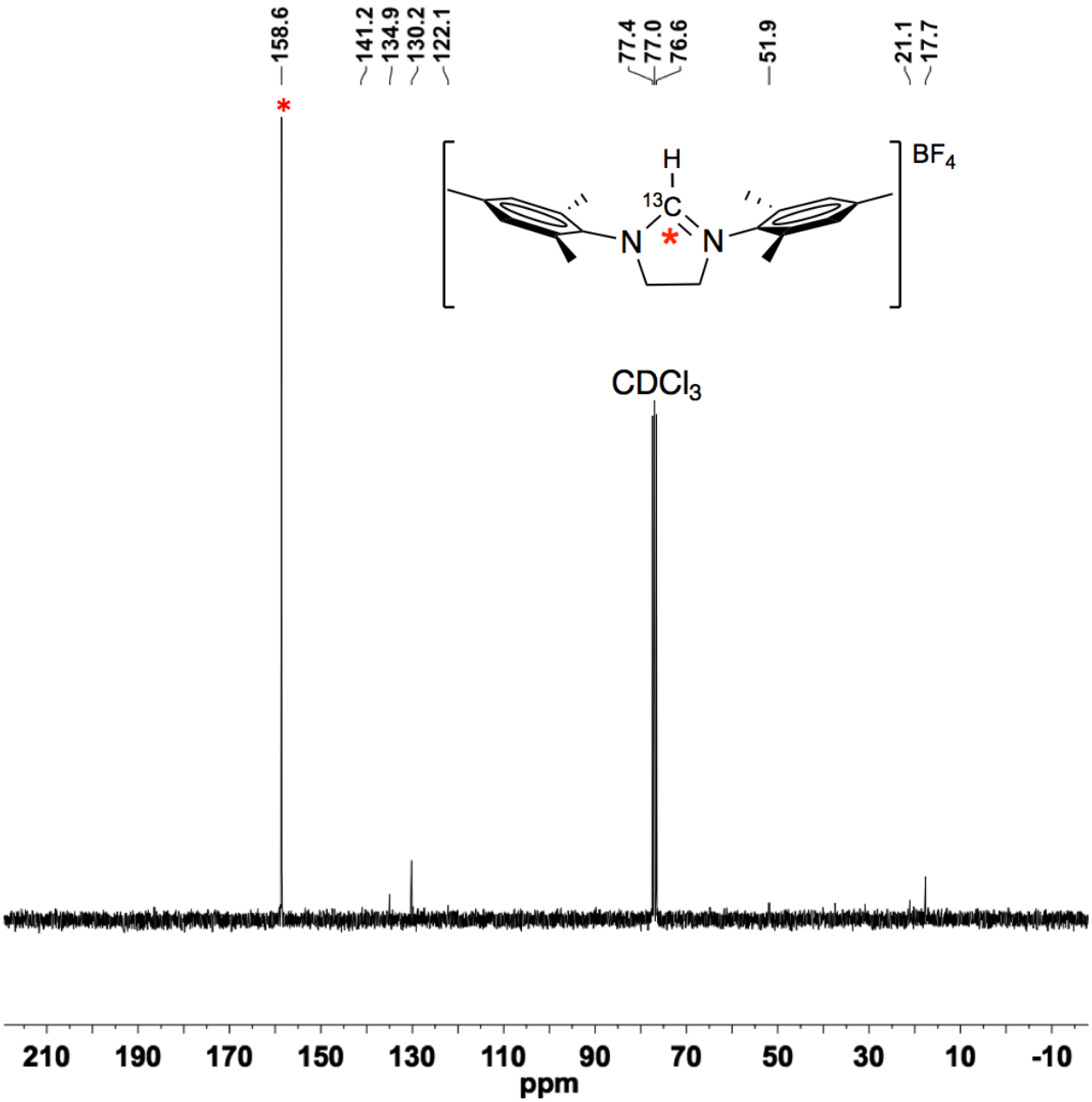


**Figure A.5b.** $^{13}C\{^{1}H\}$ NMR spectrum ($CDCl_3$, 75.5 MHz) of **$^{13}$C-H$_2$IMes•HBF$_4$** (* = $^{13}C$-labelled carbon).

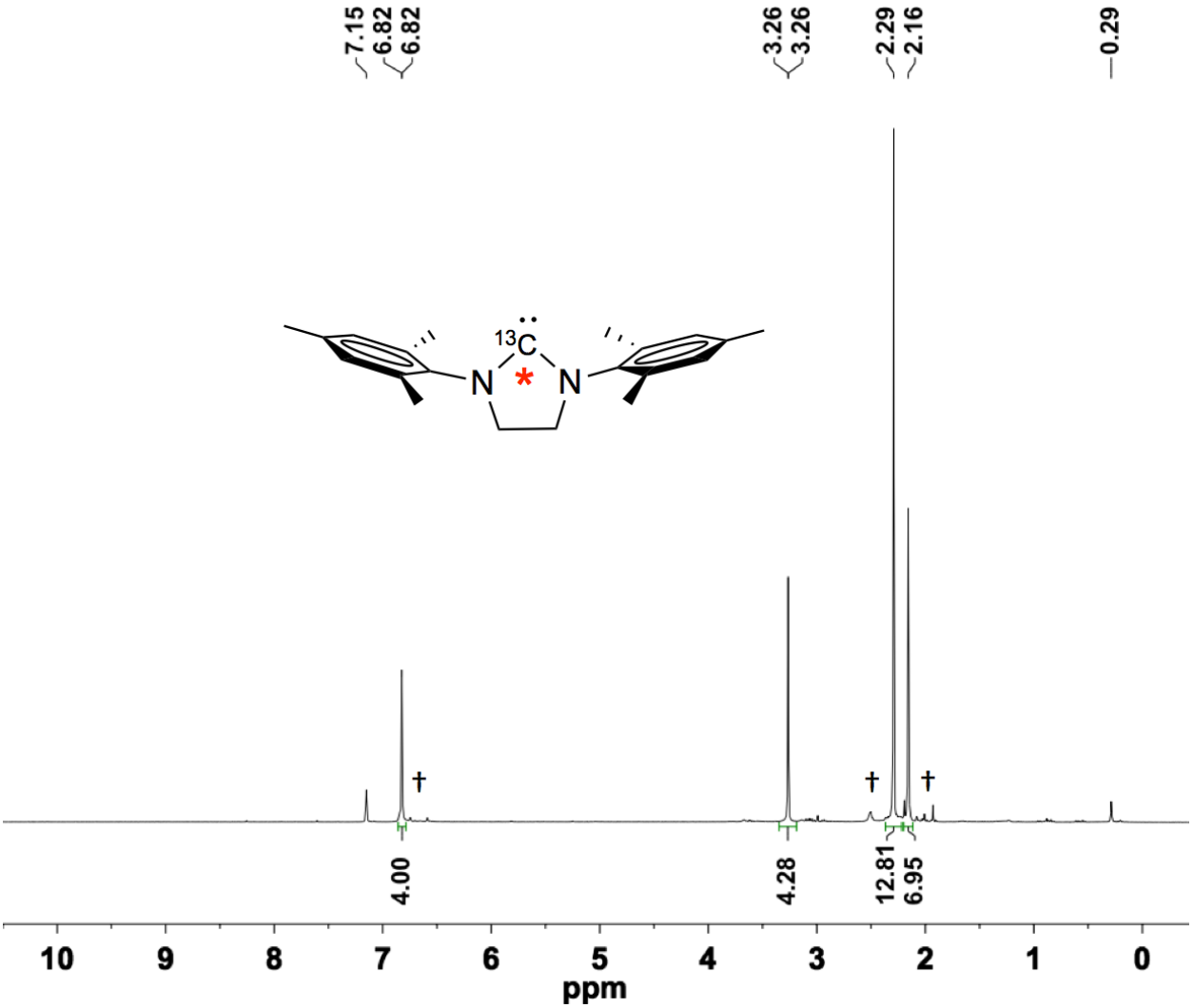


**Figure A.6a.** $^{1}$H NMR spectrum ($C_6D_6$, 300 MHz) of free **$^{13}$C-$H_2$IMes**; (†) = impurity generated by hydrolysis from residual water in deuterated solvent.

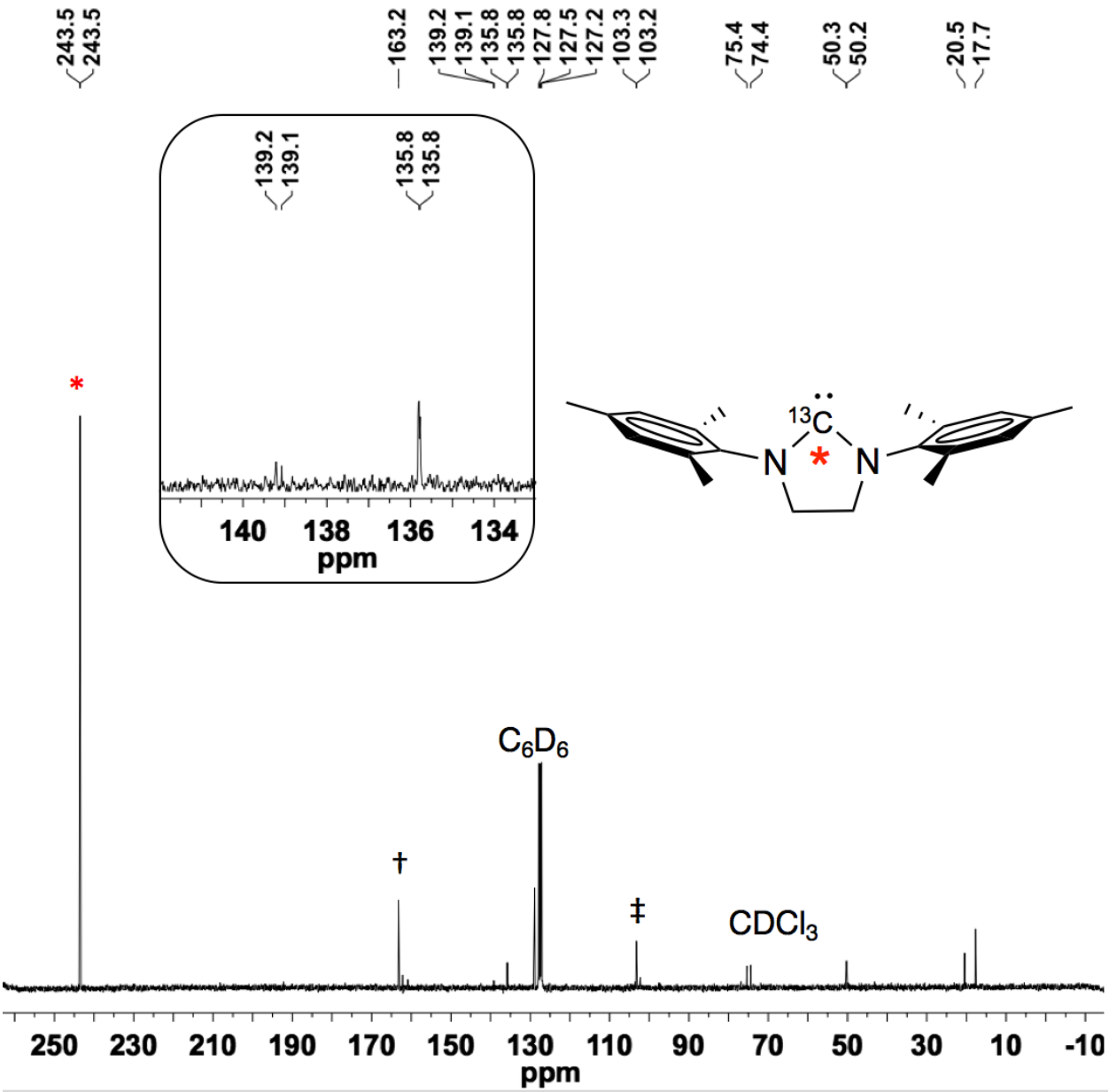


**Figure A.6b.** $^{13}C\{^{1}H\}$ NMR spectrum ($C_6D_6$, 75.5 MHz) of **$^{13}$C-H$_2$IMes** (* = $^{13}C$-labelled carbon; (†) = impurity generated by hydrolysis from residual water in deuterated solvent. (‡) = unidentified impurity).

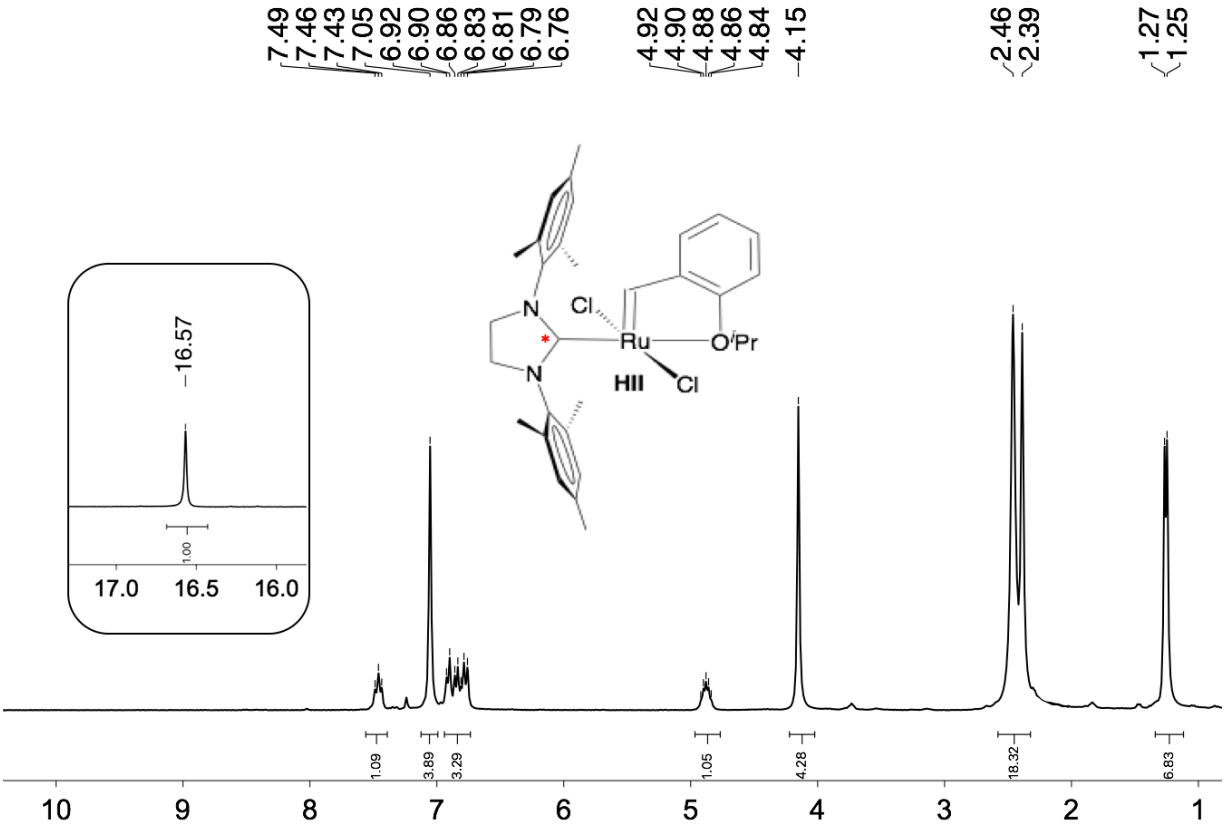


**Figure A.7a.** $^{1}$H NMR spectrum ($CDCl_3$, 300 MHz) of **$^{13}$C-HII** (* = $^{13}$*C*-labelled carbon).

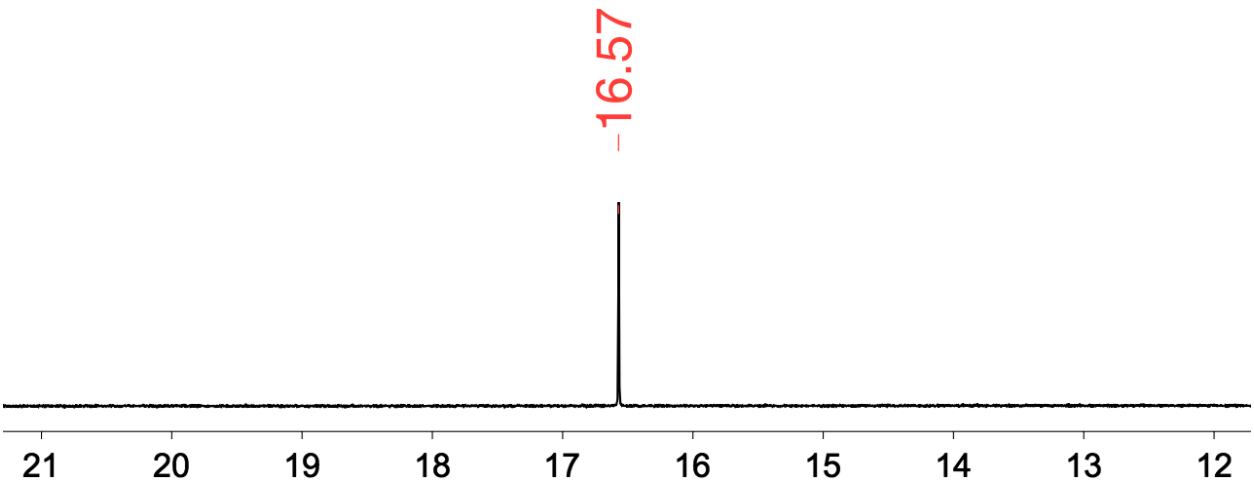


**Figure A.7b.** Full alkylidene region for the spectrum of Fig. A.7a, showing the absence of additional signals.

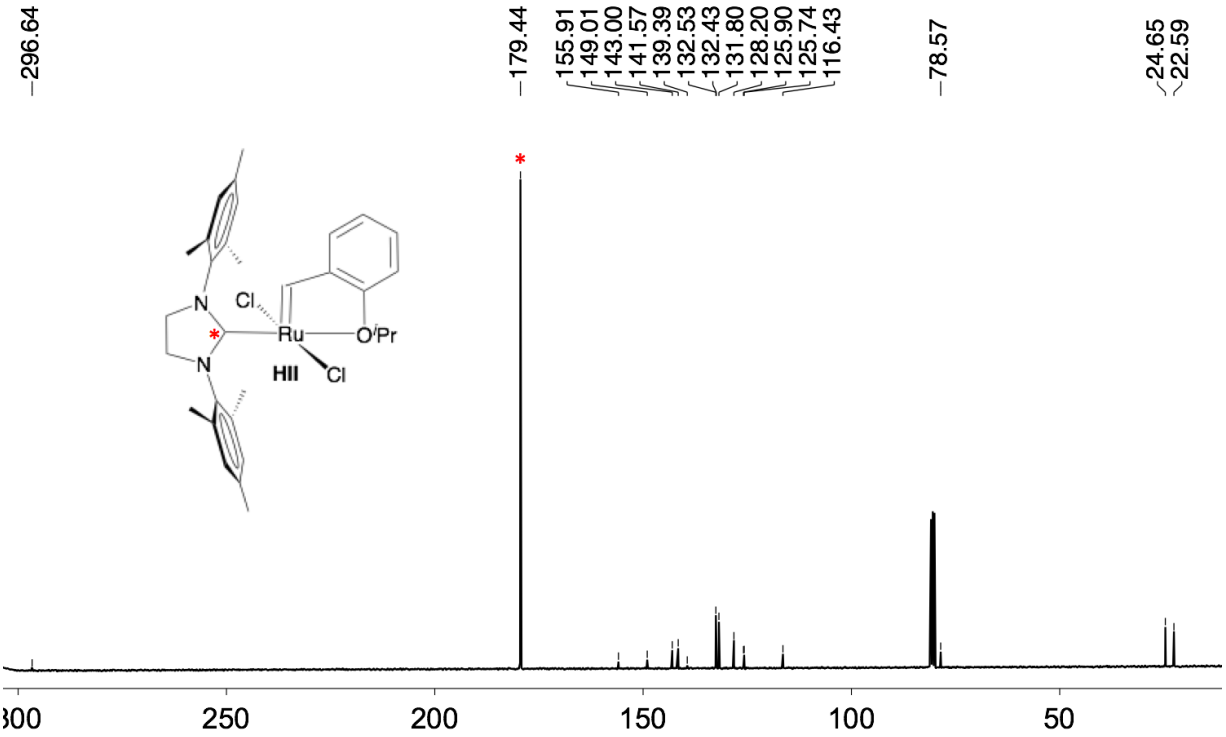


**Figure A.7c.** $^{13}C\{^1H\}$ NMR spectrum ($CDCl_3$, 75.5 MHz) of **$^{13}$C-HII** (* = $^{13}C$-labelled carbon).

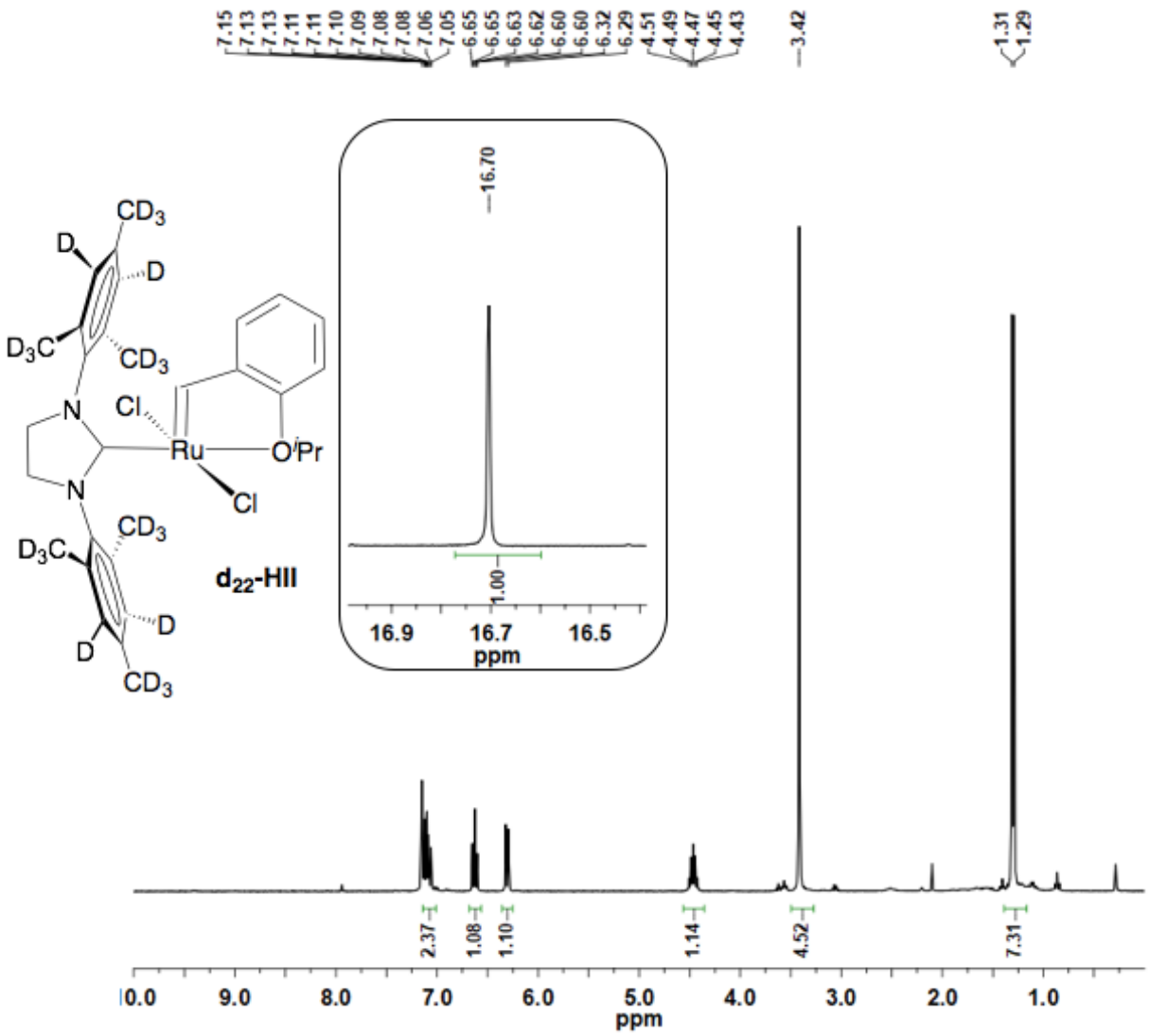


**Figure A.8a.** $^{1}$H NMR spectrum ($C_6D_6$, 300 MHz) of **$d_{22}$-HII**.

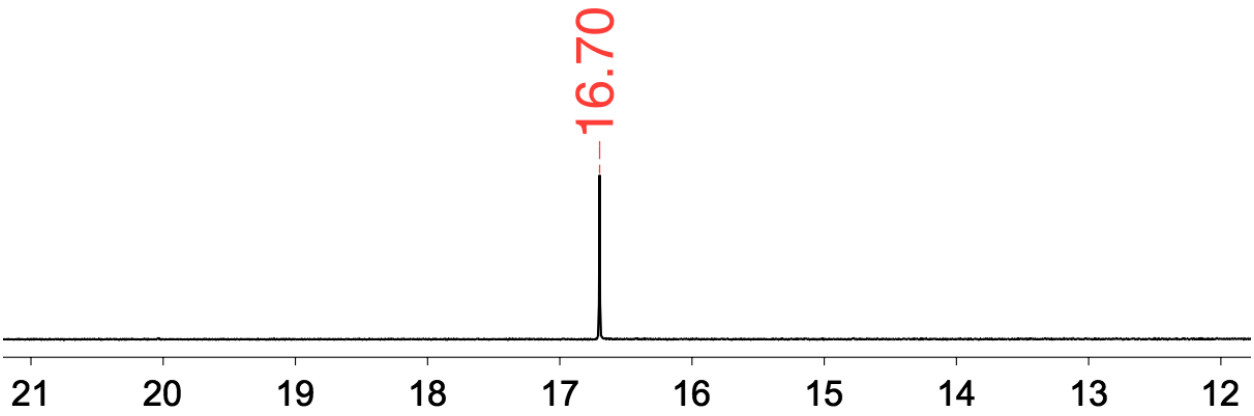


**Figure A.8b.** Full alkylidene region for the spectrum of Fig. A.8a, showing the absence of additional signals.

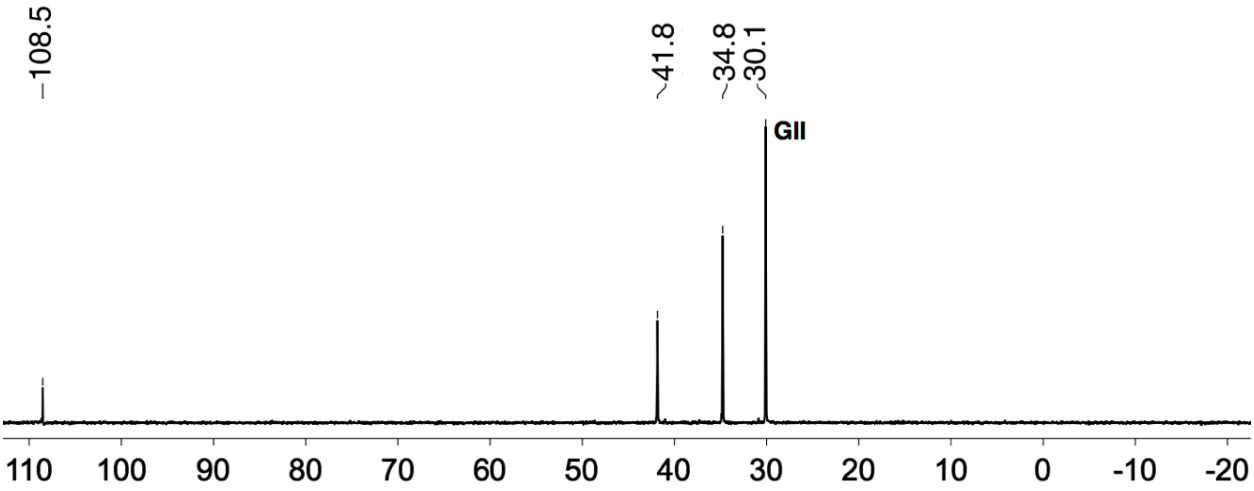


**Figure A.9.** $^{31}P\{^{1}H\}$ NMR spectrum ($C_6D_6$, 121.2 MHz) showing impurities present in a sample of **GII** prepared via Amberlyst-15 workup, using resin stored in the glovebox.

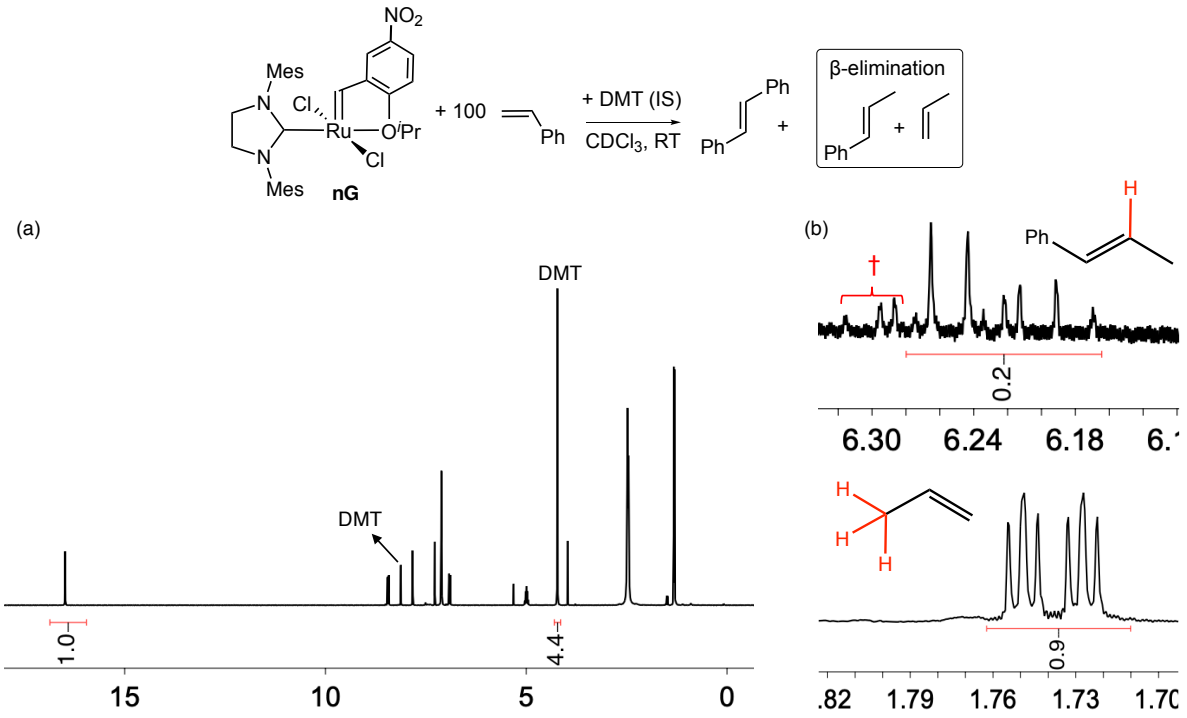


**Figure A.10.** $^{1}$H NMR spectra ($CDCl_3$, 300 MHz) for reaction of **nG** with styrene: assessing β-elimination. (a) Initial. DMT = internal standard (IS). (b) Propene region at 24 h: 51% yield vs. IS. Top: β-methyl styrene; bottom: propene. (†) = unknown.

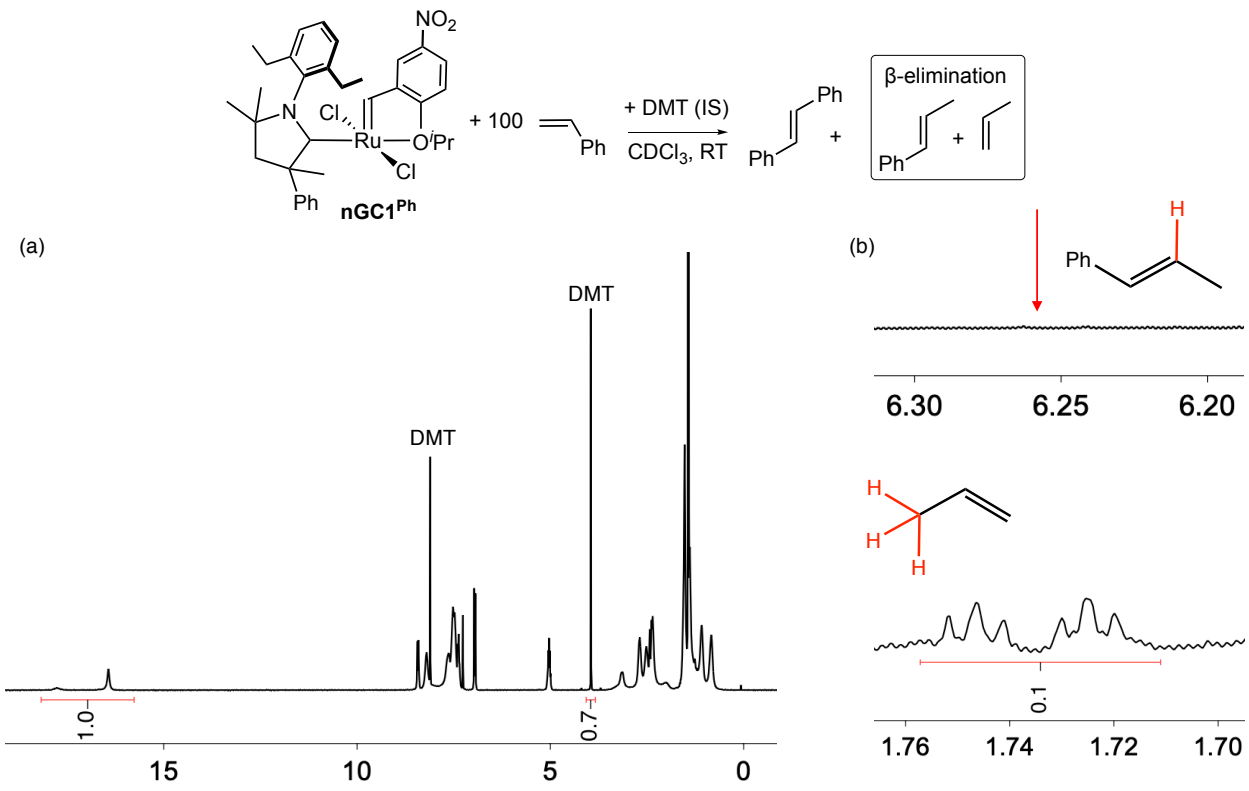


**Figure A.11.** $^{1}$H NMR spectra ($CDCl_3$, 300 MHz) of β-elimination reaction of **nGC1$^{Ph}$**. (a) Initial. DMT = IS. (b) Propene region at 24 h: yield 2% vs. IS. Top: 0% β-methyl styrene; bottom: 2% propene. Red arrow indicates the expected location of the proton shown in red.

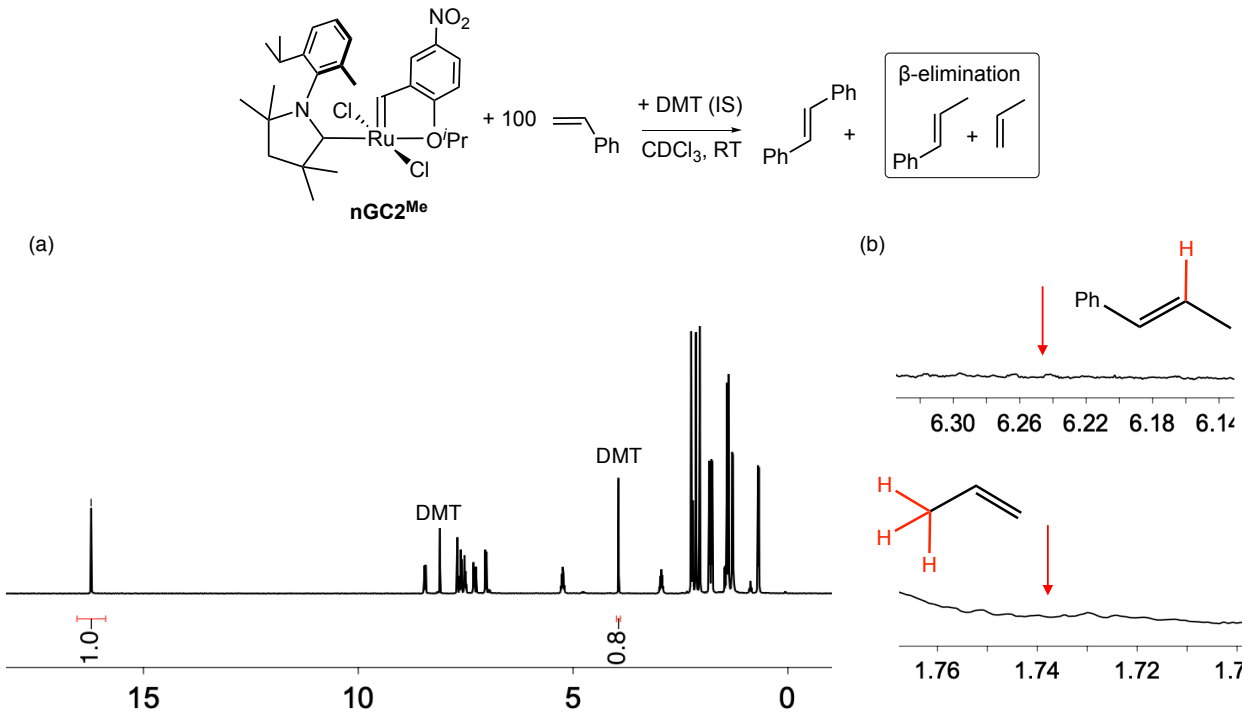


**Figure A.12.** $^{1}$H NMR spectrum ($CDCl_3$, 300 MHz) of β-elimination reaction of **nGC2$^{Me}$**. (a) Initial. DMT = IS. (b) Propene region at 24 h: net yield 0% vs. IS. Top: β-methyl styrene; bottom: propene; both absent. Red arrows indicate the expected location of the proton shown in red.

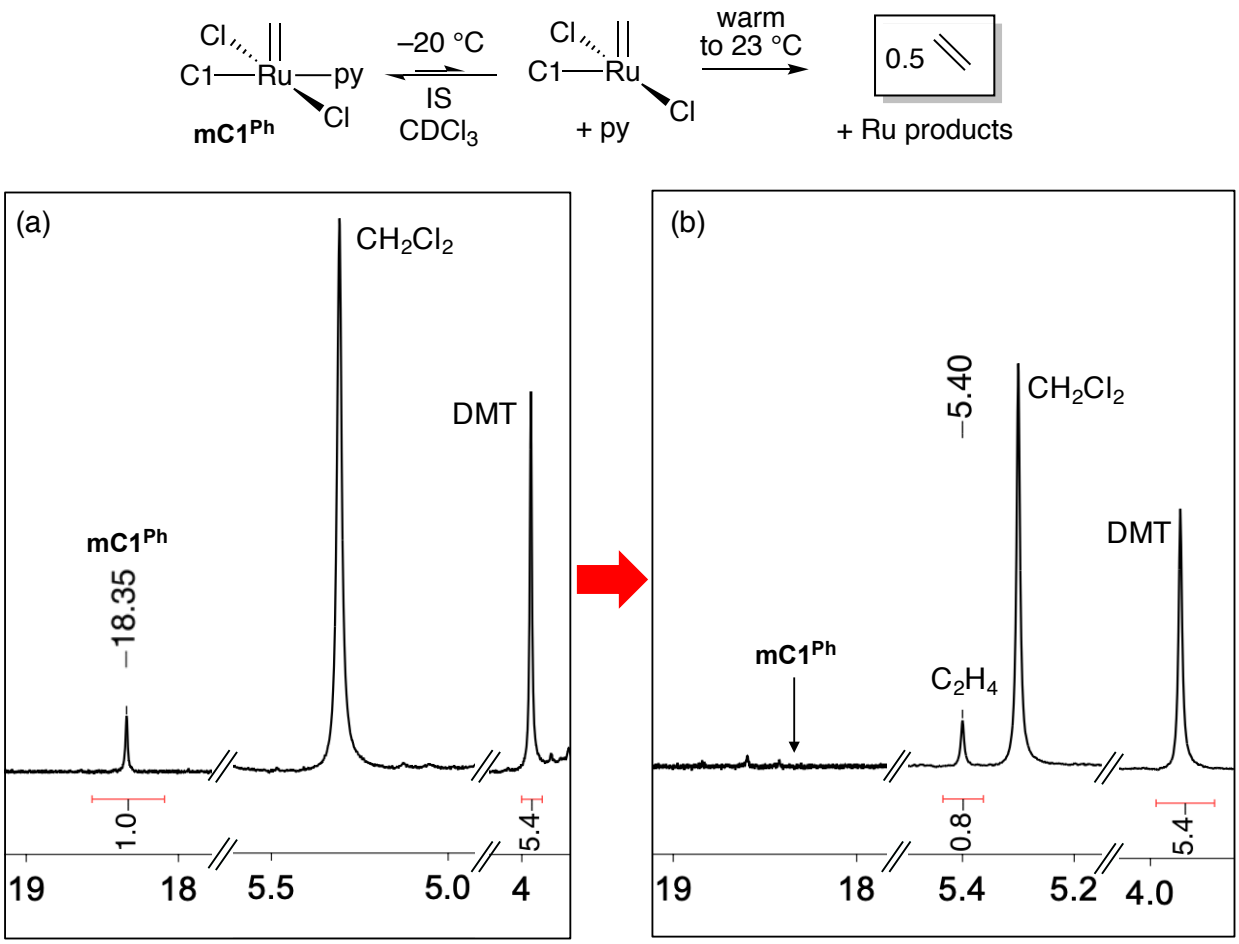


**Figure A.13.** $^{1}$H NMR spectrum ($CDCl_3$, 500 MHz) assessing bimolecular coupling of **mC1$^{Ph}$**. (a) Initial ratio of **mC1$^{Ph}$** vs. DMT, confirming removal of the $C_2H_4$ used in the synthesis. (b) Total disappearance of **mC1$^{Ph}$** and appearance of $C_2H_4$ from bimolecular coupling. Note absence of propene derived from β-elimination of the unsubstituted MCB.

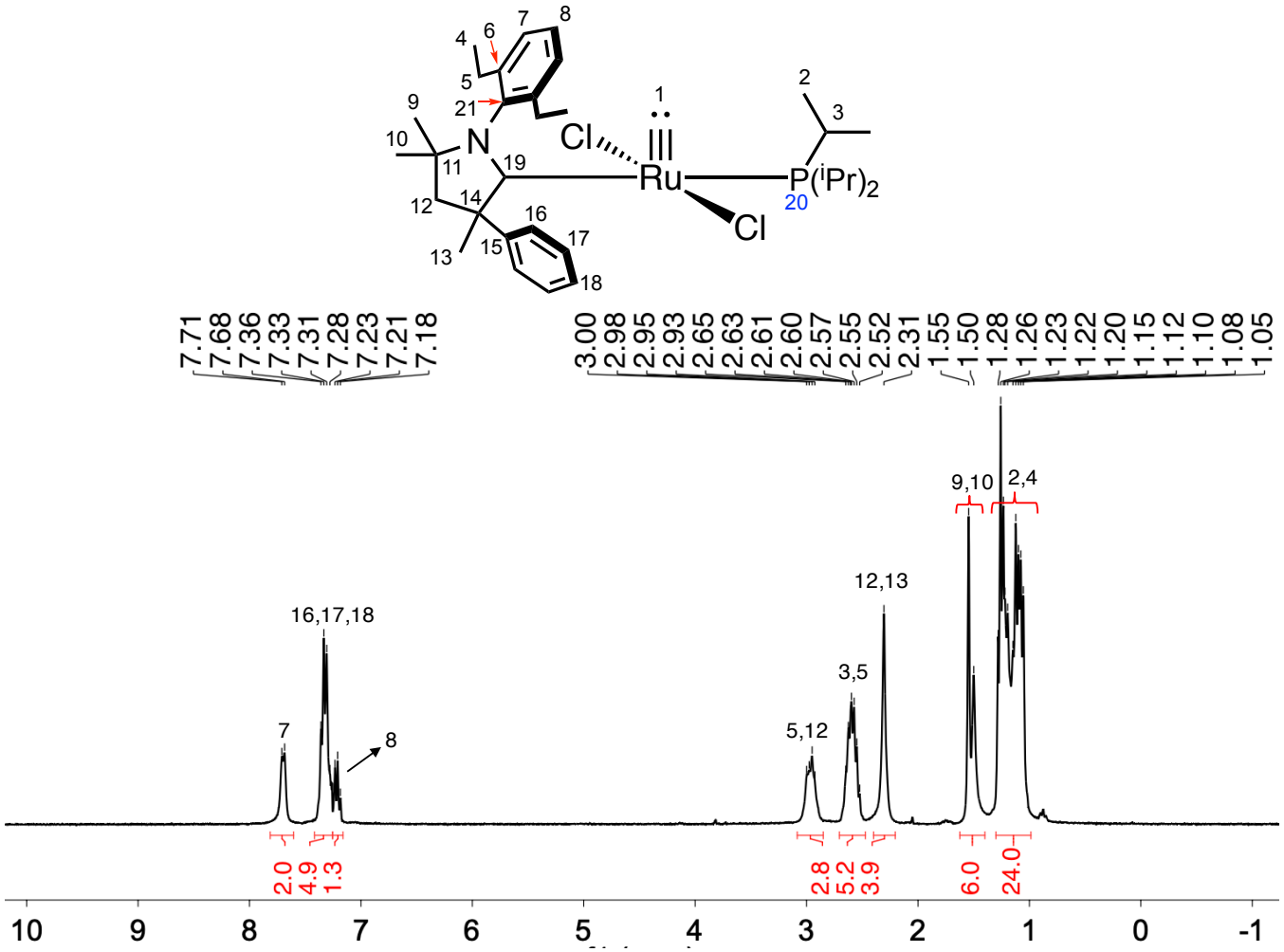


**Figure A.14.** $^{1}$H NMR spectrum ($CDCl_3$, 300 MHz) of **CbC1$^{Ph}$**.

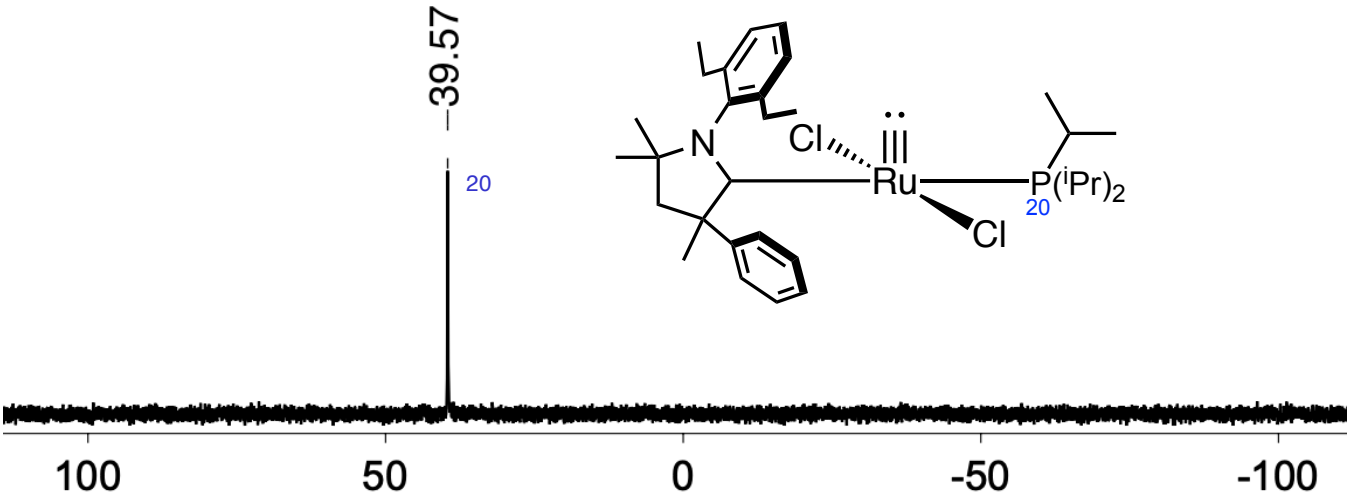


**Figure A.15.** $^{31}P\{^{1}H\}$ NMR spectrum ($CDCl_3$, 121 MHz) of **CbC1**$^{\mathbf{Ph}}$.

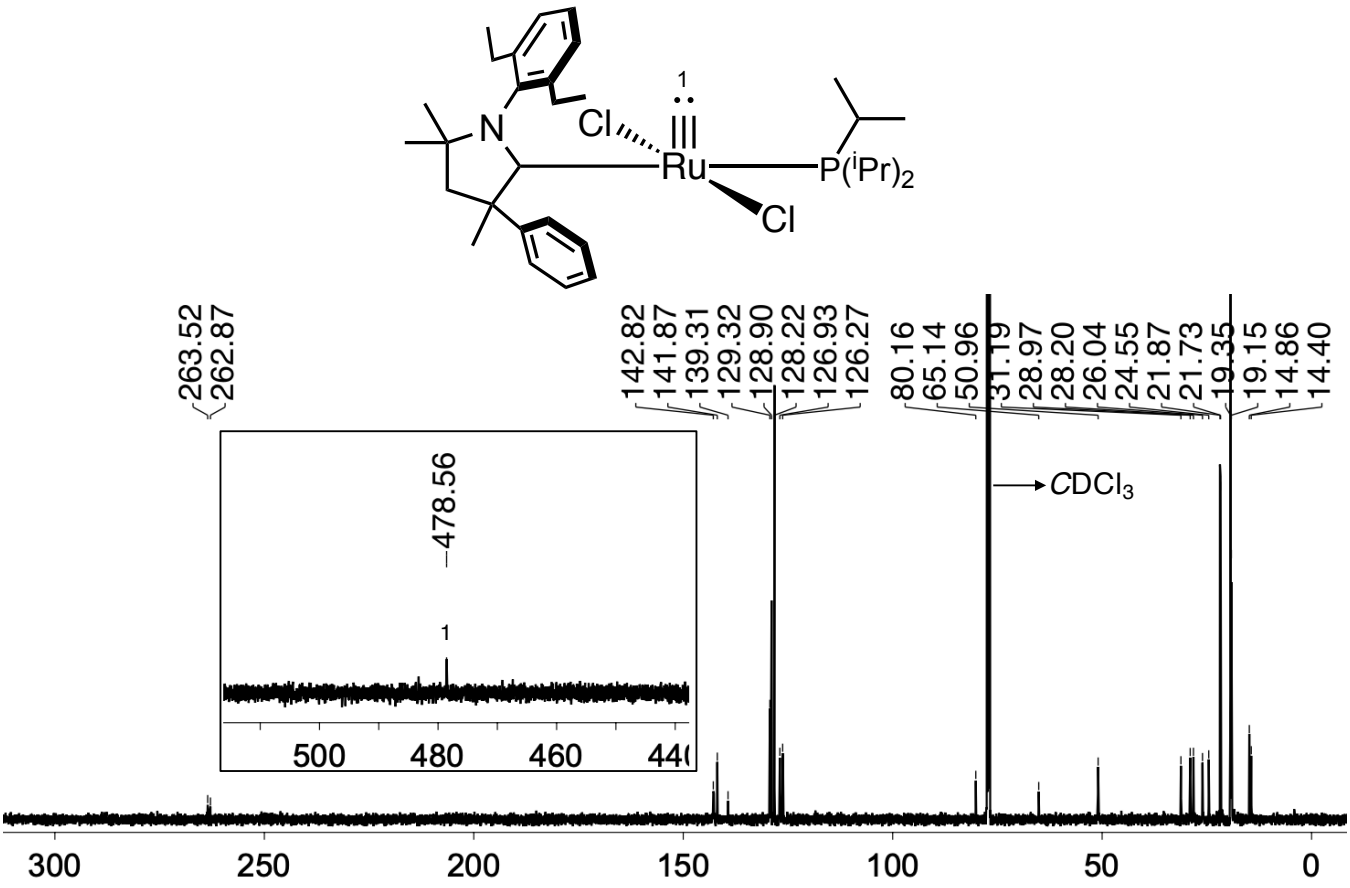


**Figure A.16.** $^{13}C\{^{1}H\}$ NMR spectrum ($CDCl_3$, 125 MHz) of **CbC1$^{Ph}$**. Inset shows the carbide peak.

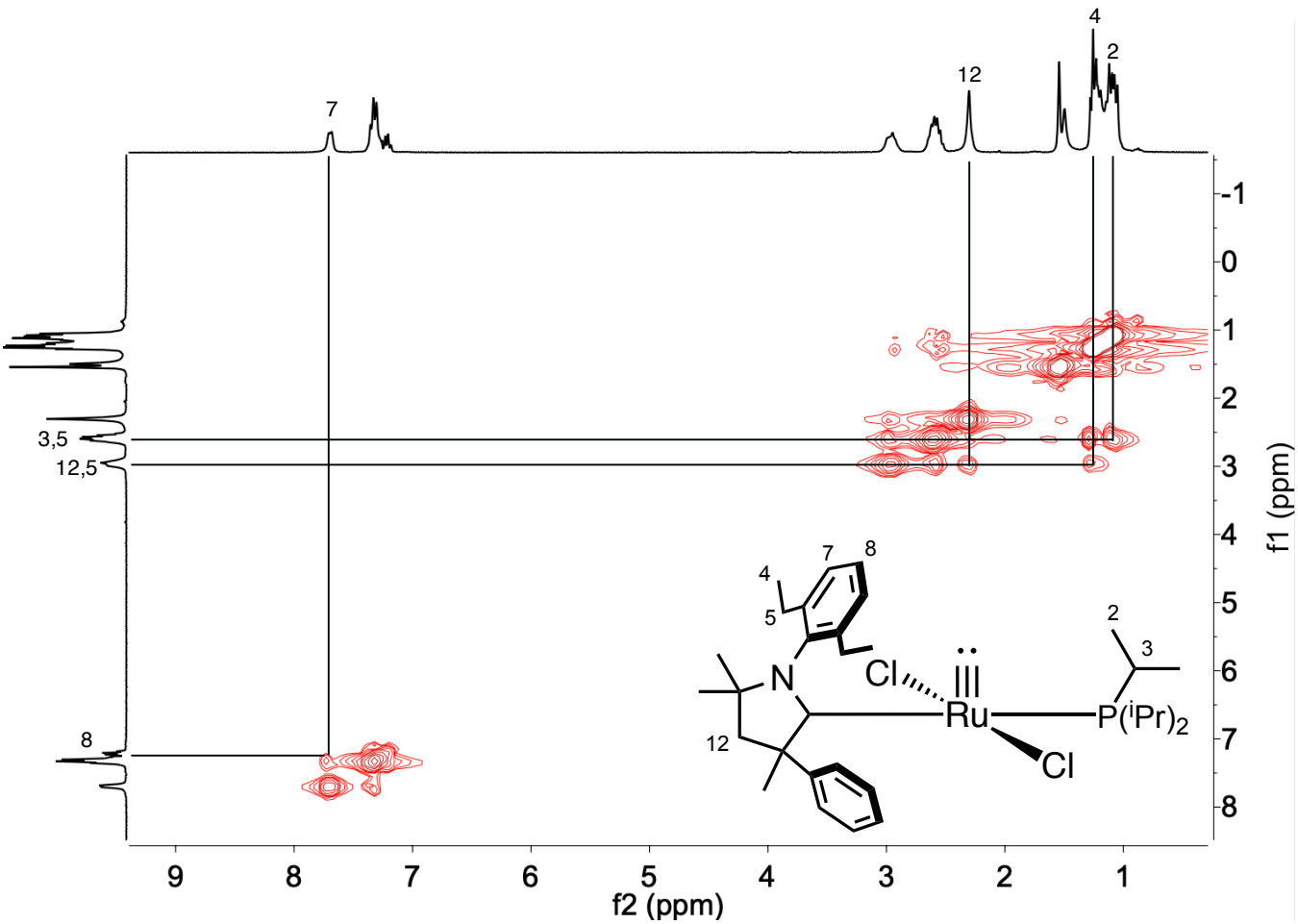


**Figure A.17.** $^{1}$H-$^{1}$H COSY NMR spectrum ($CDCl_3$, 500 MHz) of **CbC1$^{Ph}$**.

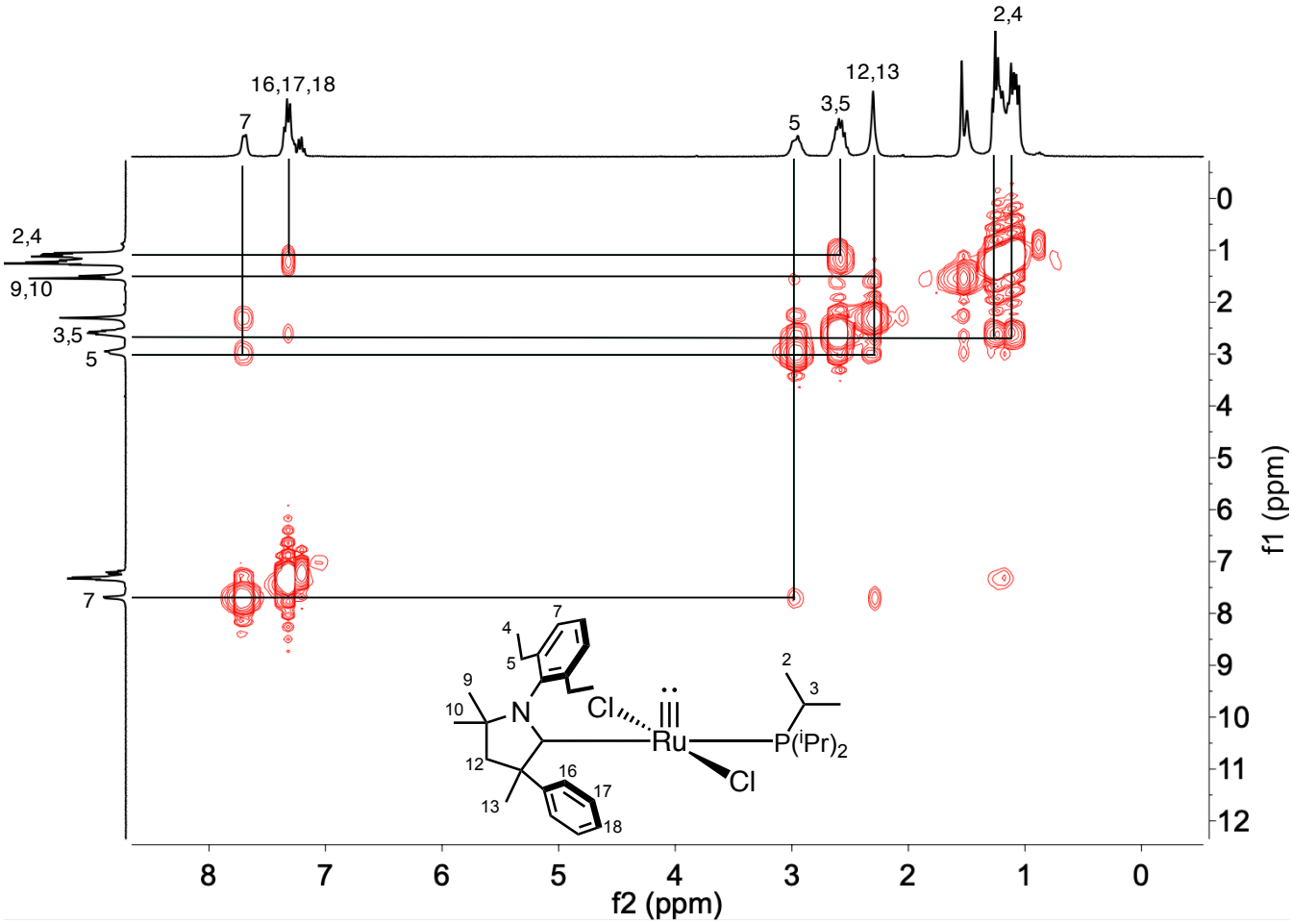


**Figure A.18.** $^{1}$H-$^{1}$H NOESY NMR spectrum ($CDCl_3$, 500 MHz) of **CbC1$^{Ph}$**.

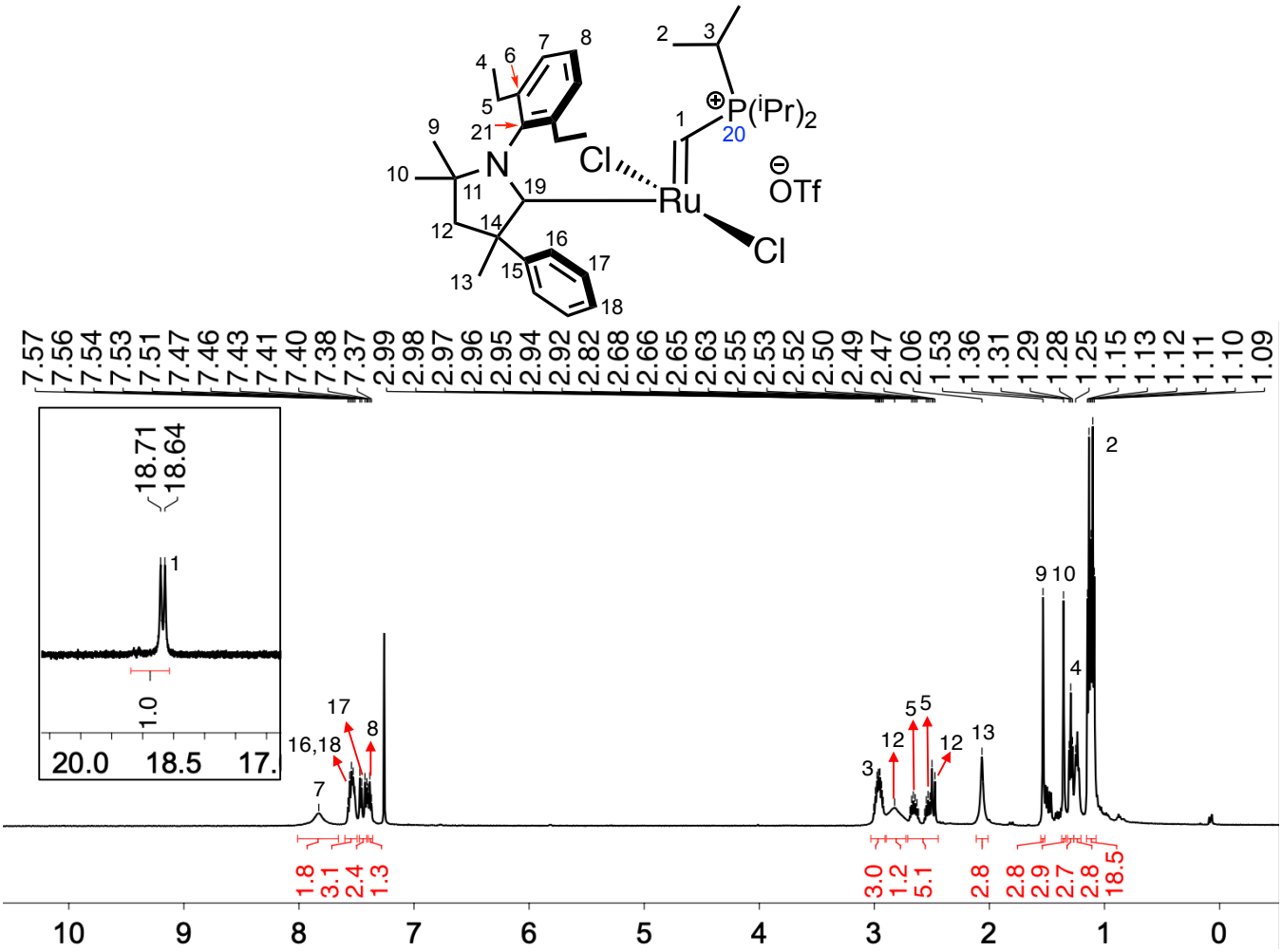


**Figure A.19.** $^{1}$H NMR spectrum ($CDCl_3$, 500 MHz) of **PC1$^{Ph}$**. Inset shows the alkylidene region.

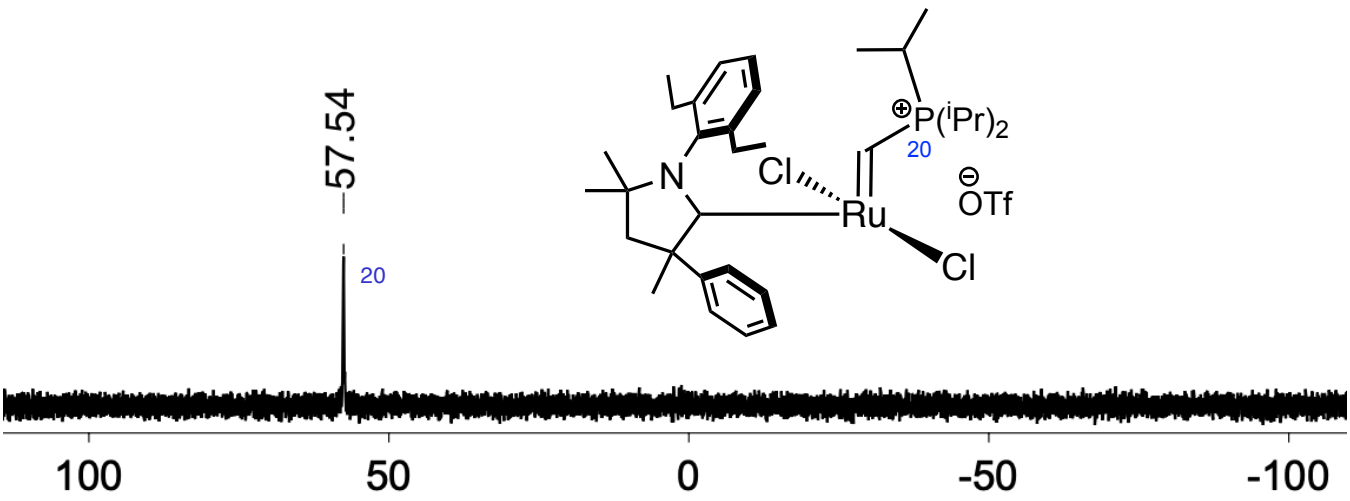


**Figure A.20.** $^{31}P\{^{1}H\}$ NMR spectrum ($CDCl_3$, 121 MHz) of **PC1$^{Ph}$**.

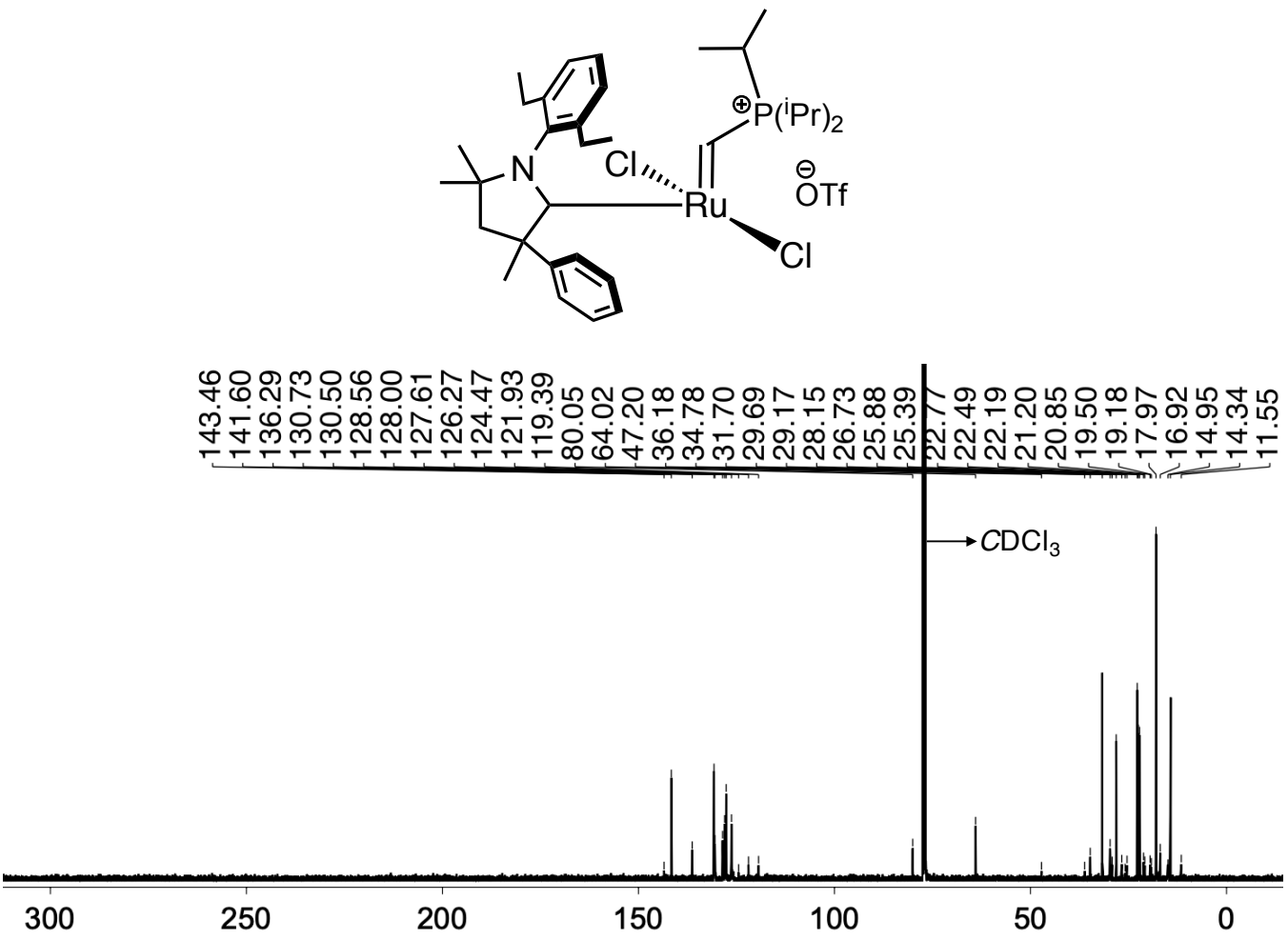


**Figure A.21.** $^{13}C\{^{1}H\}$ NMR spectrum ($CDCl_3$, 125 MHz) of **PC1$^{Ph}$**.

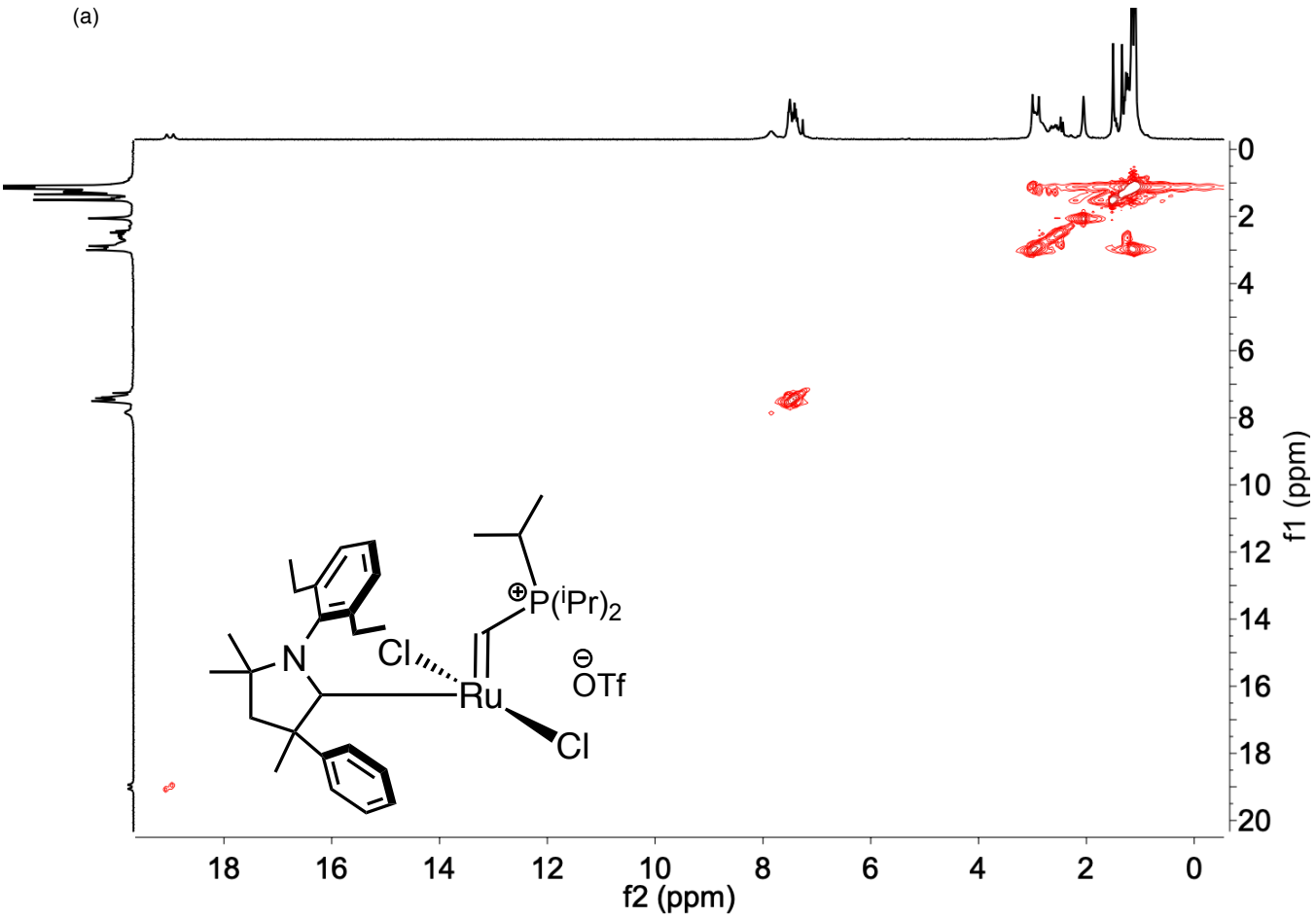


**Figure A.22.** Full $^{1}$H-$^{1}$H COSY NMR spectrum ($CDCl_3$, 300 MHz) of **PC1$^{Ph}$**.

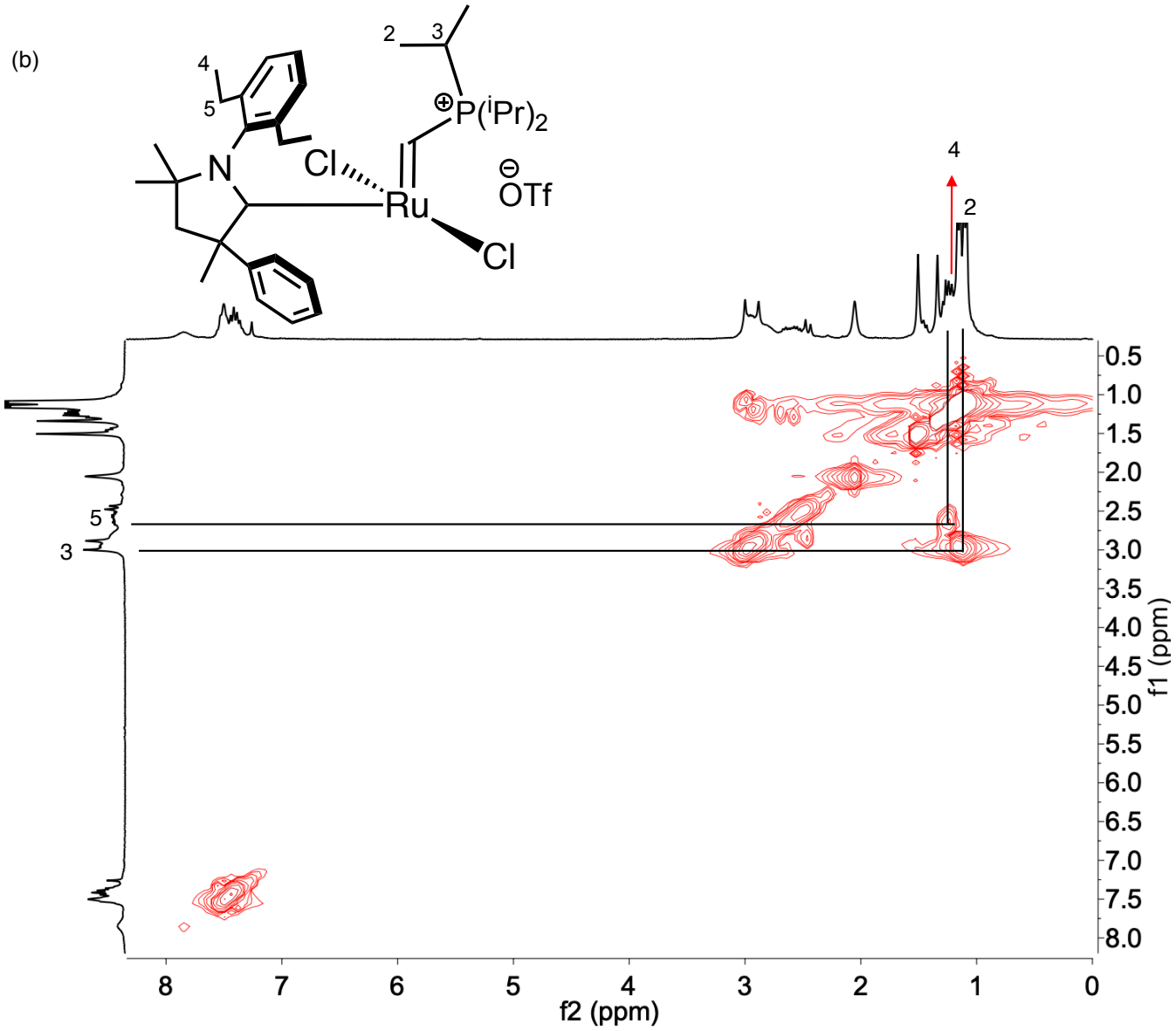


**Figure A.23.** Inset of $^{1}$H-$^{1}$H COSY NMR spectrum ($CDCl_3$, 300 MHz) of **PC1$^{Ph}$** showing the correlation between numbered peaks.

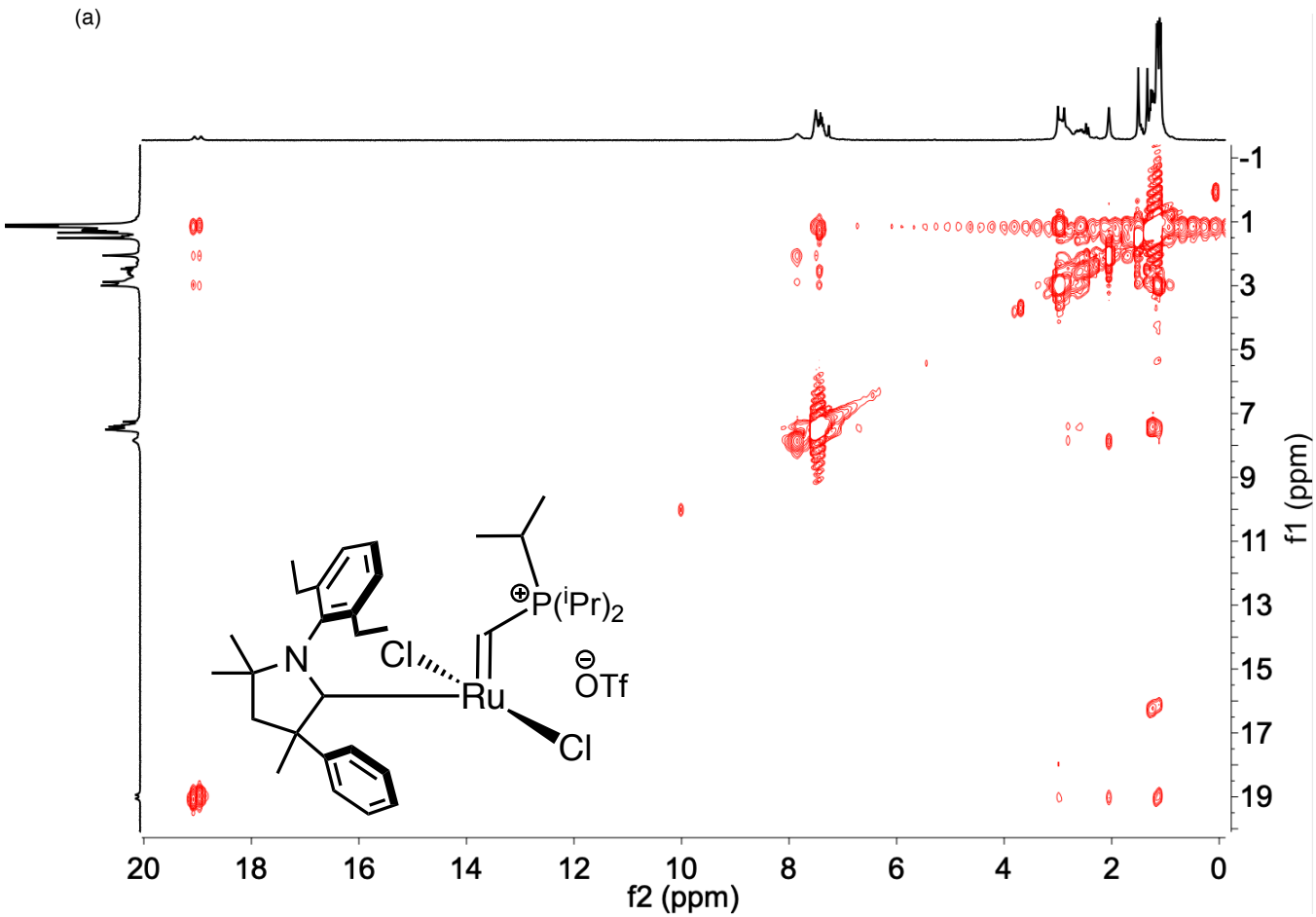


**Figure A.24a.** Full $^{1}$H-$^{1}$H NOESY NMR spectrum ($CDCl_3$, 300 MHz) of **PC1$^{Ph}$**.

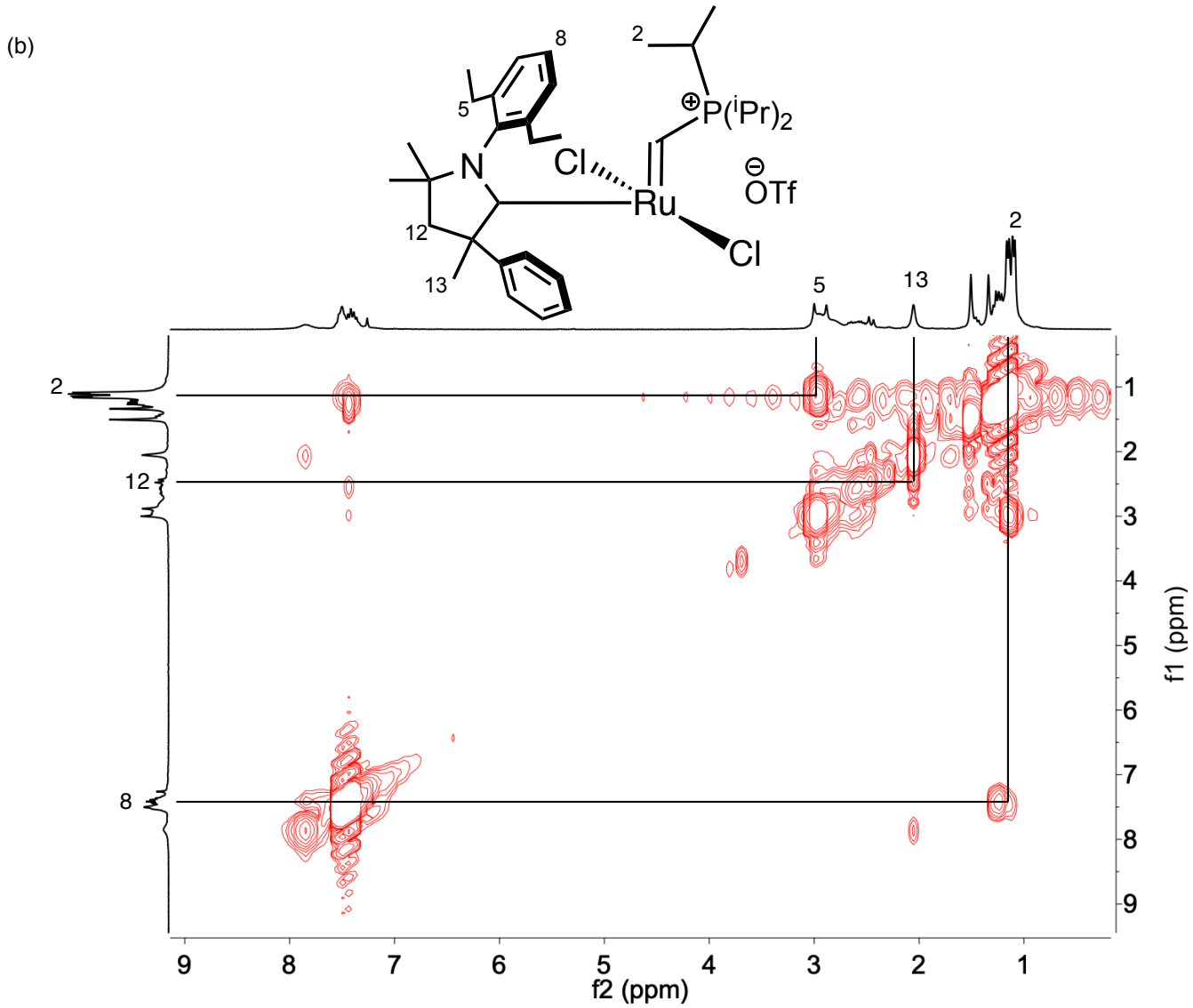


**Figure A.24b.** Inset of $^{1}$H-$^{1}$H NOESY NMR spectrum ($CDCl_3$, 300 MHz) of **PC1$^{Ph}$** showing the correlation between the numbered peaks.

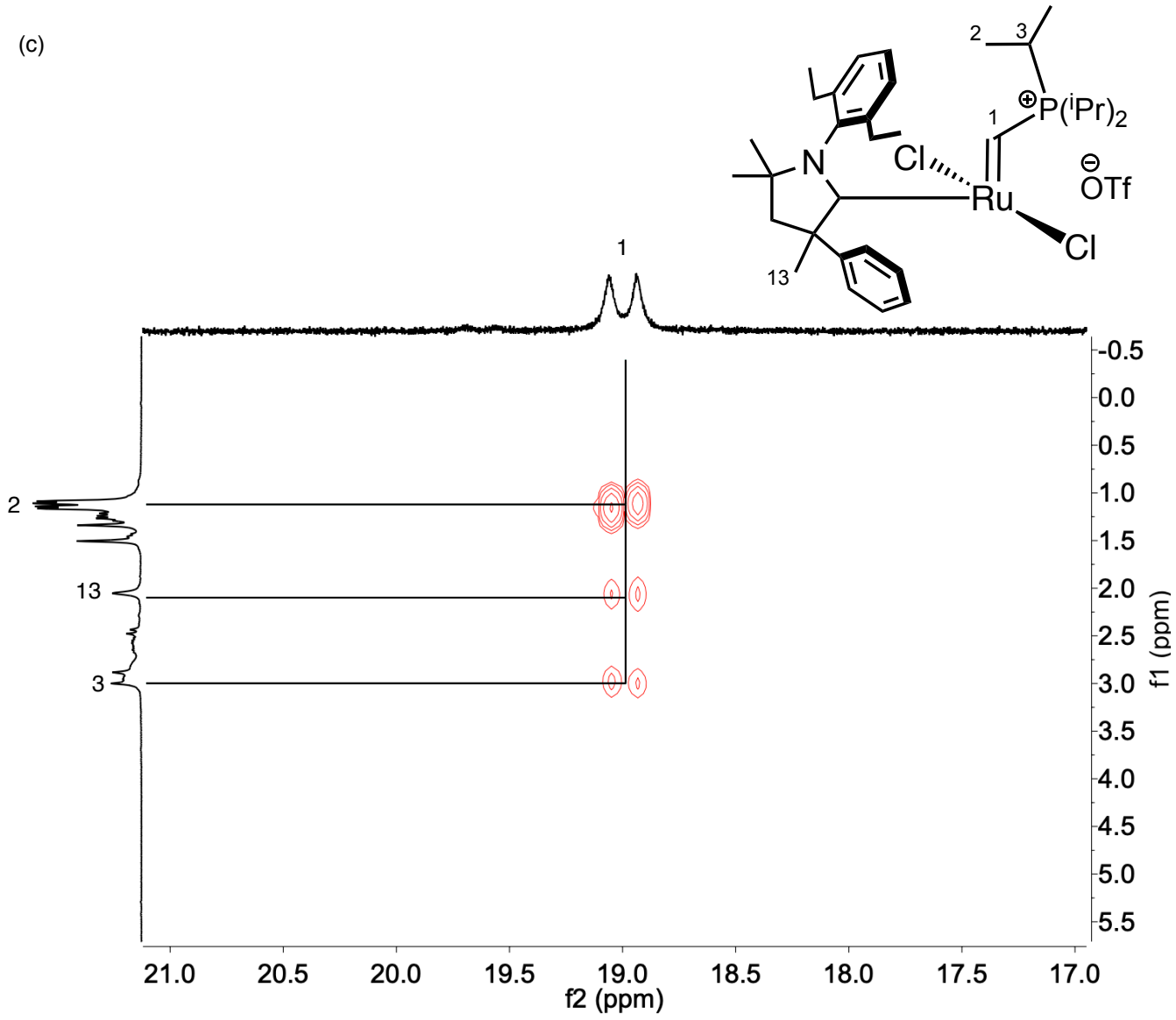


**Figure A.24c.** Inset of $^{1}$H-$^{1}$H NOESY NMR spectrum ($CDCl_3$, 300 MHz) of **PC1$^{Ph}$** showing the correlation between the numbered peaks.

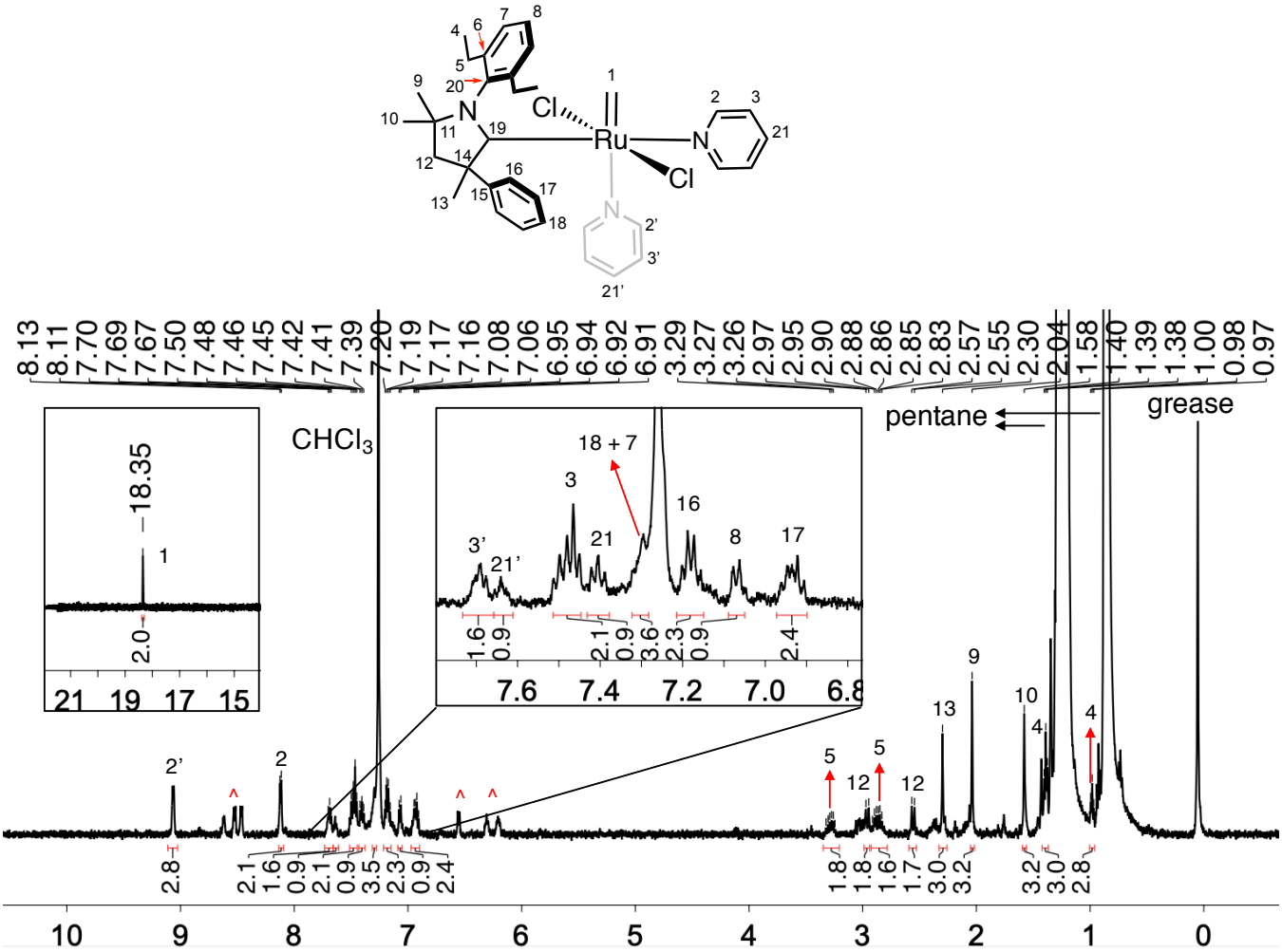


**Figure A.25.** $^{1}$H NMR spectrum ($CDCl_3$, 500 MHz, –20 °C) of isolated **mC1$^{Ph}$**. Left inset shows the alkylidene region; right inset shows the expanded aromatic region. A 2:1 mono / bis-pyridine mixture was obtained. Peaks for the second pyridine (shown in gray) are designated with a prime symbol. The symbol (^) denotes unassigned impurities.

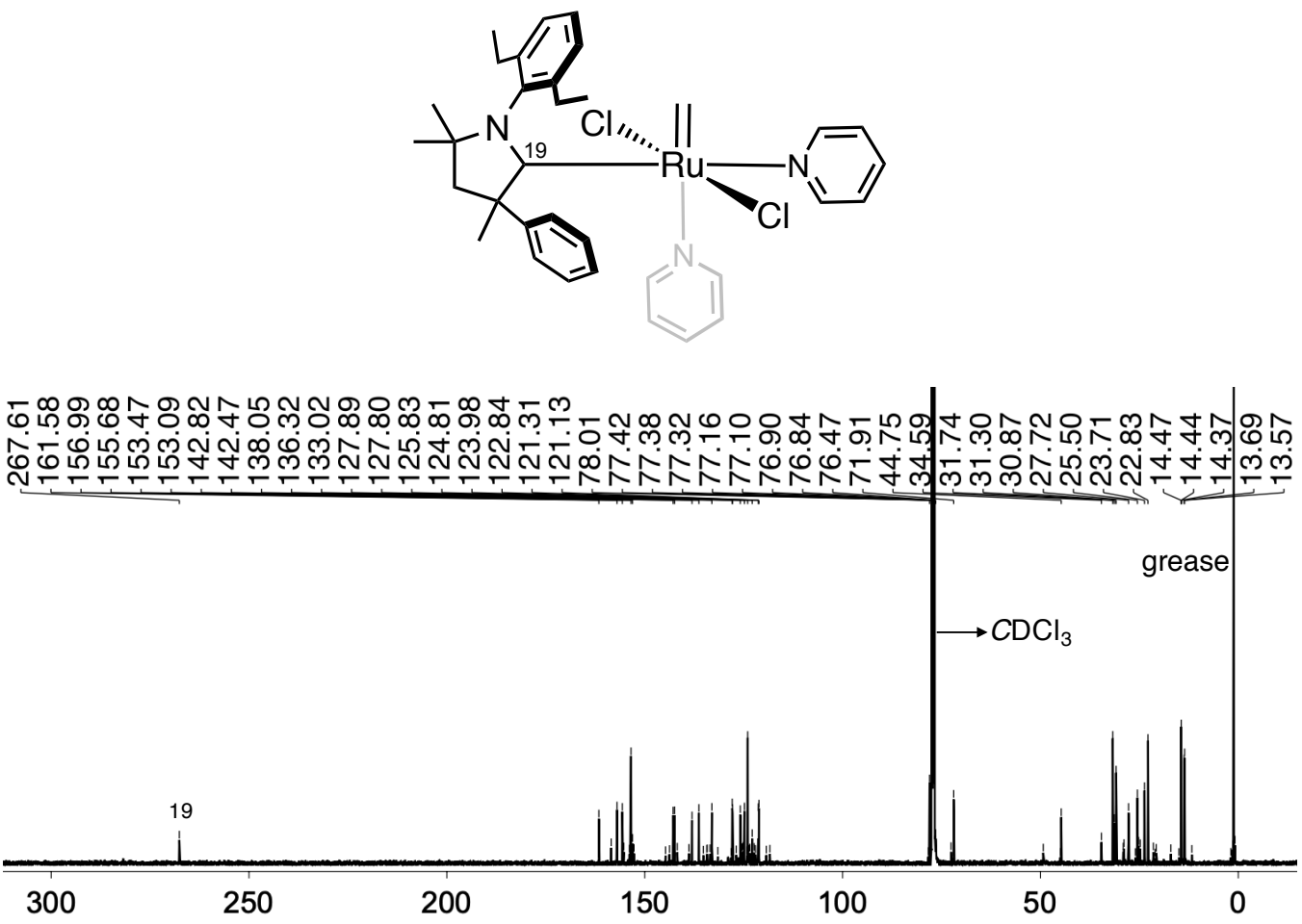


**Figure A.26.** $^{13}C\{^{1}H\}$ NMR spectrum ($CDCl_3$, 125 MHz, –40 °C) of **mC1$^{Ph}$**.

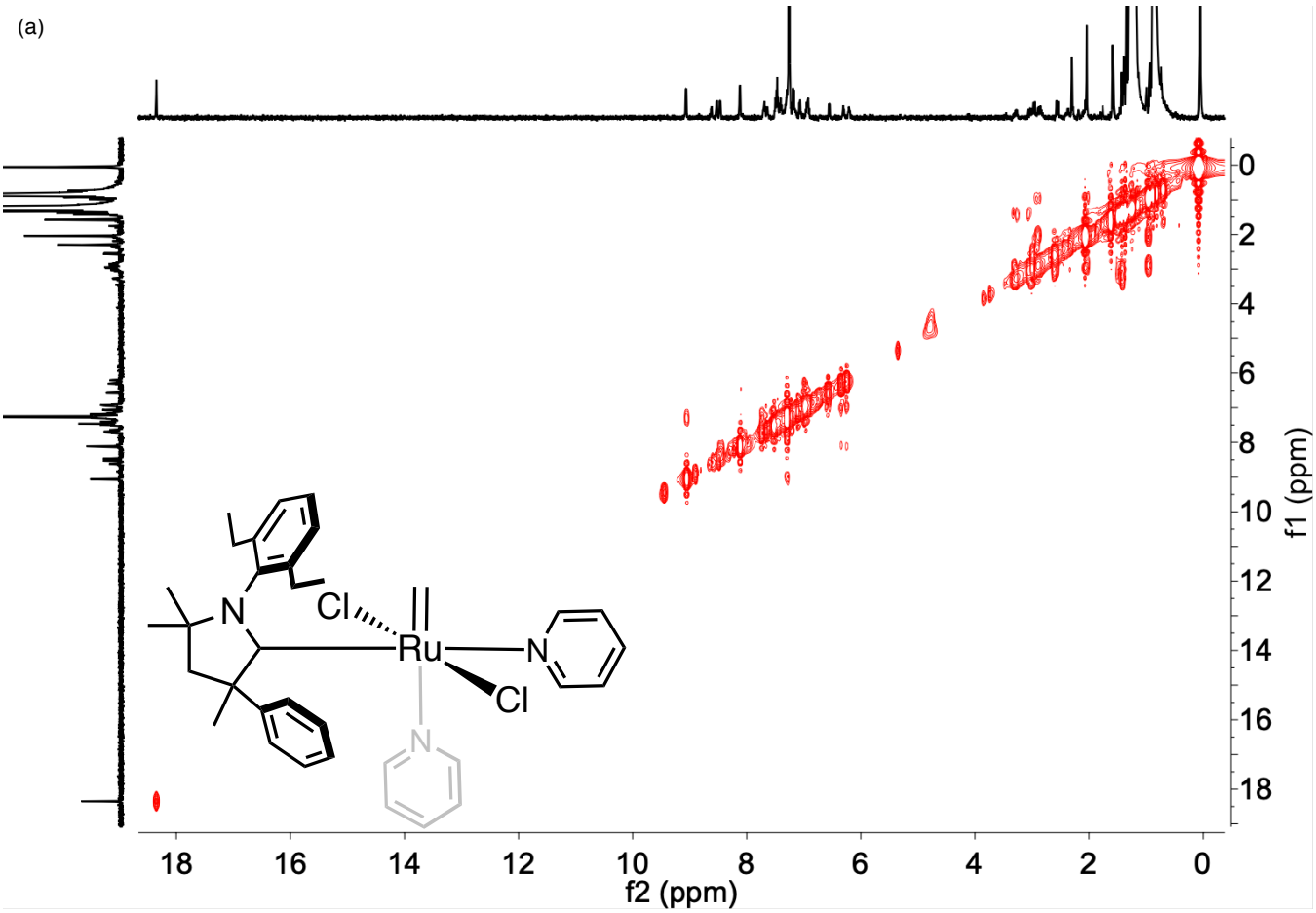


**Figure A.27a.** Full $^{1}$H-$^{1}$H COSY NMR spectrum ($CDCl_3$, 500 MHz, –40 °C) of **mC1$^{Ph}$**.

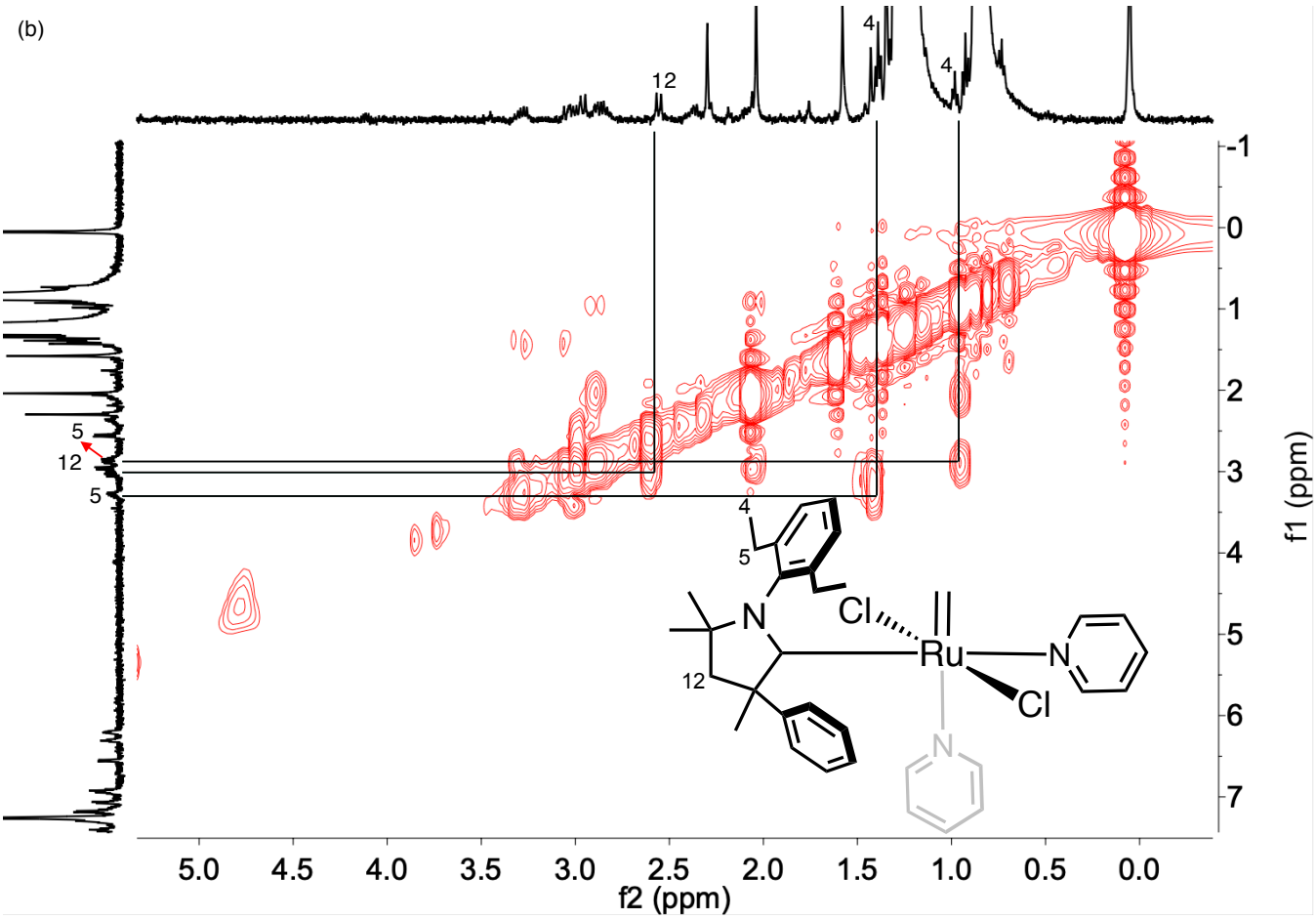


**Figure A.27b.** Inset of $^{1}$H-$^{1}$H COSY NMR spectrum ($CDCl_3$, 500 MHz, –40 °C) of **mC1$^{Ph}$**, showing the correlation between the numbered peaks

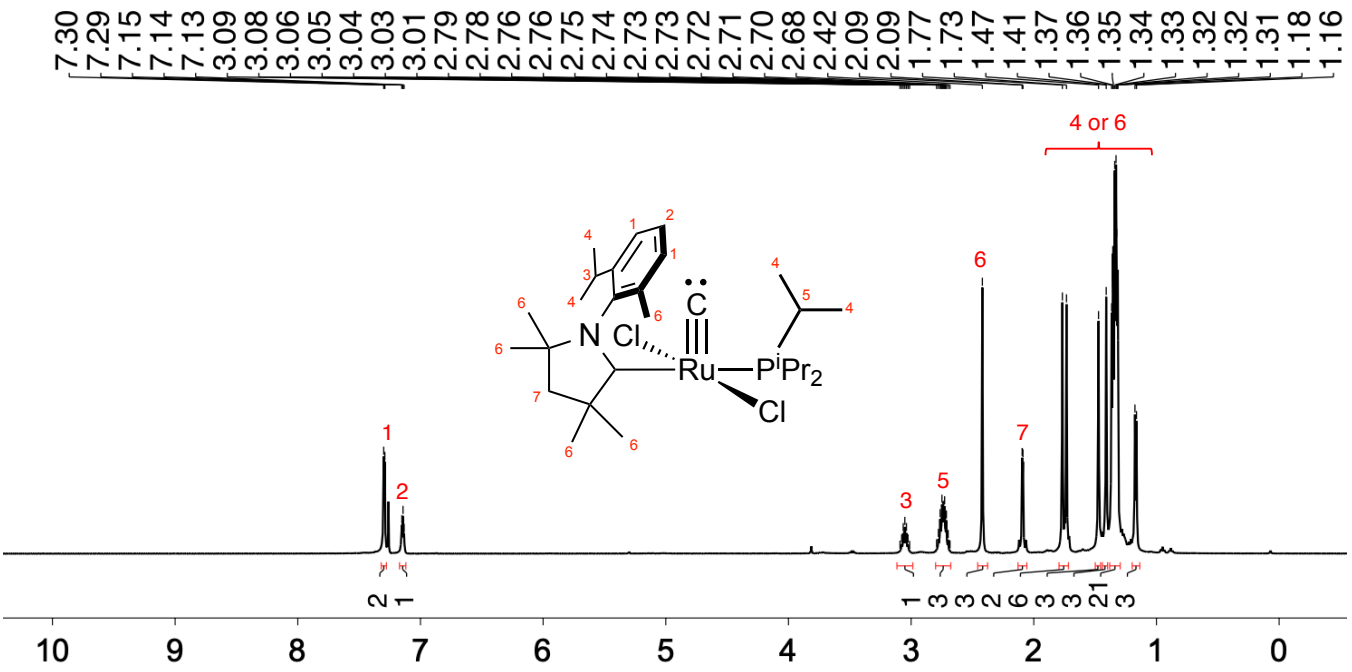


**Figure A.28a.** $^{1}$H NMR spectrum ($CDCl_3$, 500 MHz) of **CbC2$^{Me}$**.

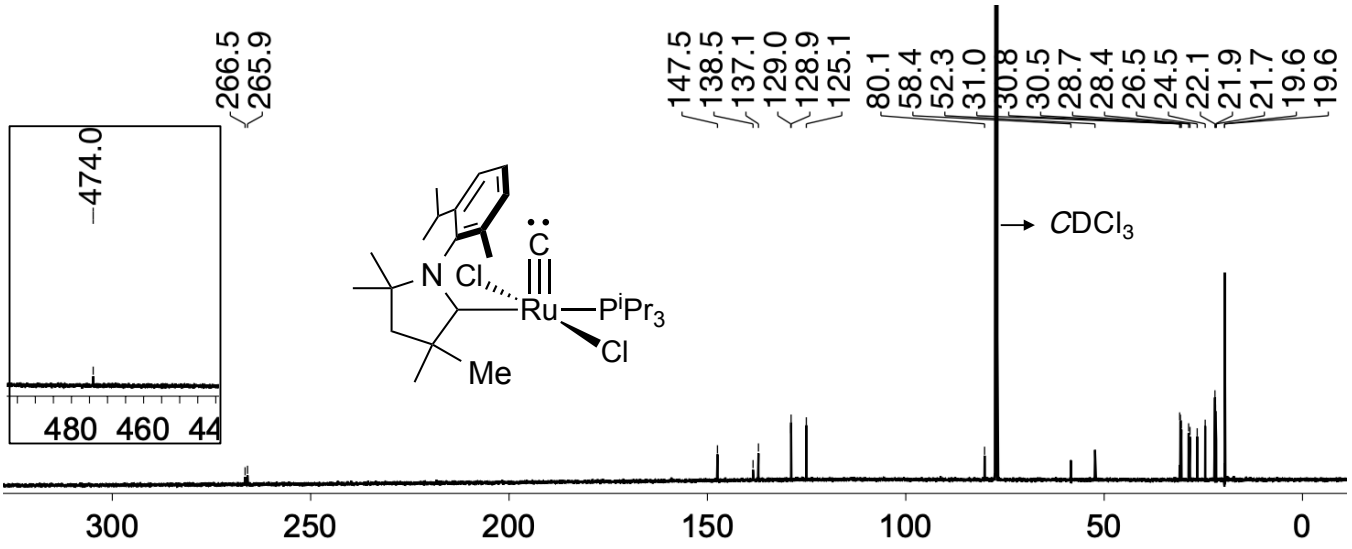


**Figure A.28b.** $^{13}C\{^{1}H\}$ NMR spectrum ($CDCl_3$, 125 MHz) of **CbC2$^{Me}$**. Inset shows the carbide carbon.

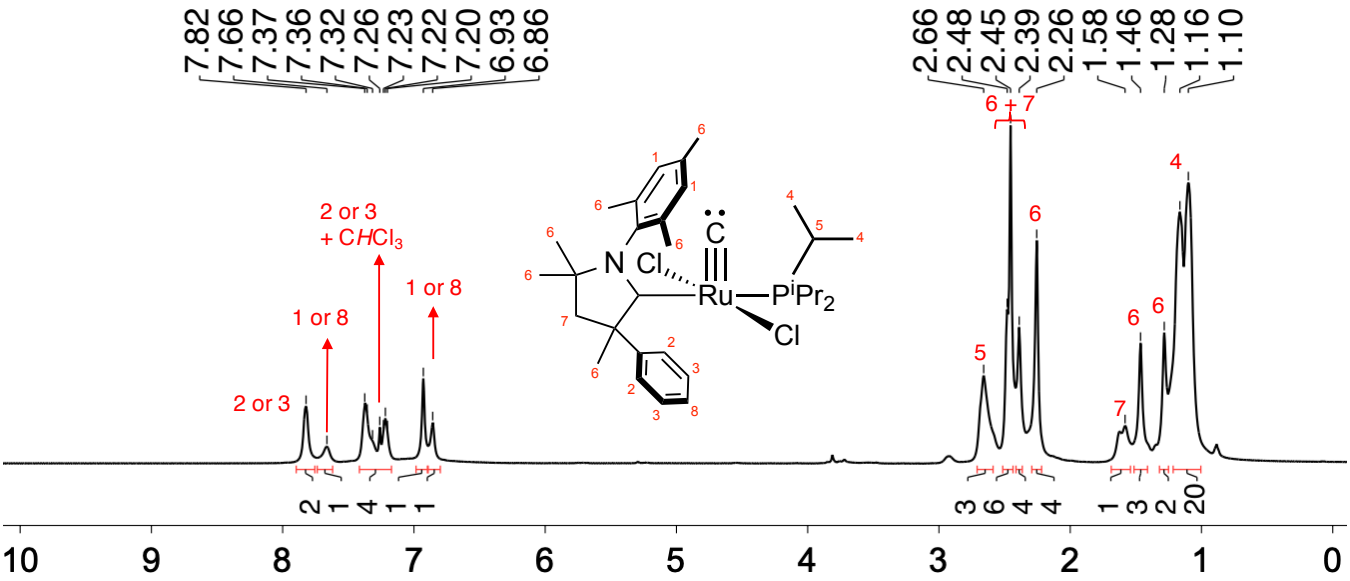


**Figure A.29a.** $^{1}$H NMR spectrum ($CDCl_3$, 500 MHz) of **CbC3$^{Ph}$**.

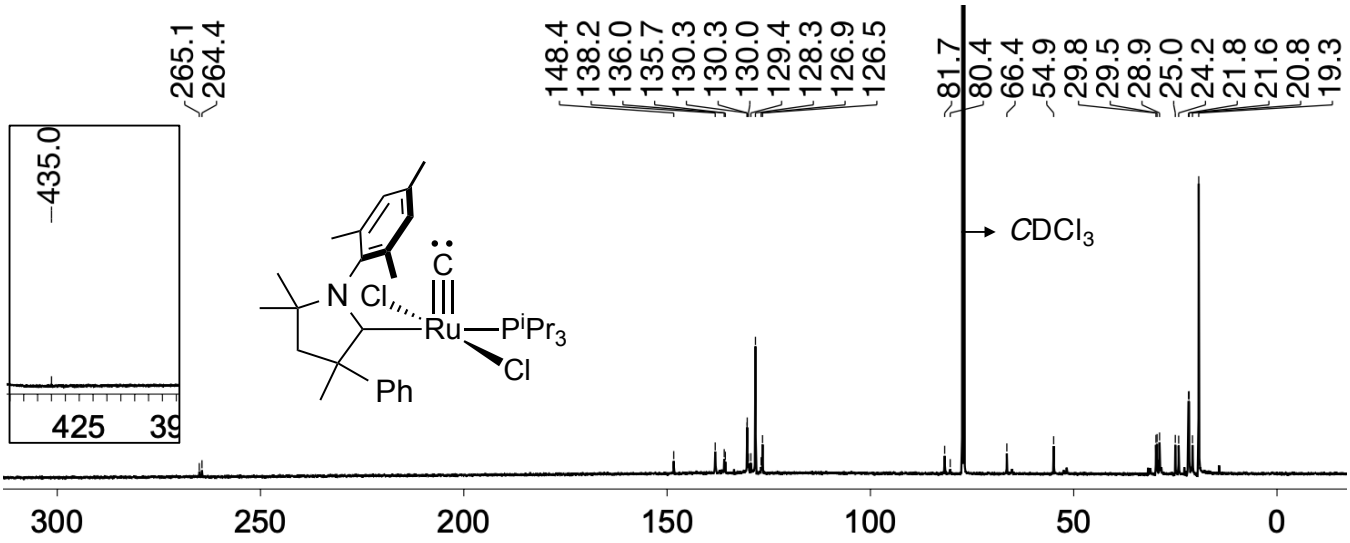


**Figure A.29b.** $^{13}$C{$^{1}$H} NMR spectrum ($CDCl_3$, 125 MHz) of **CbC3$^{Ph}$**. Inset shows carbide carbon.

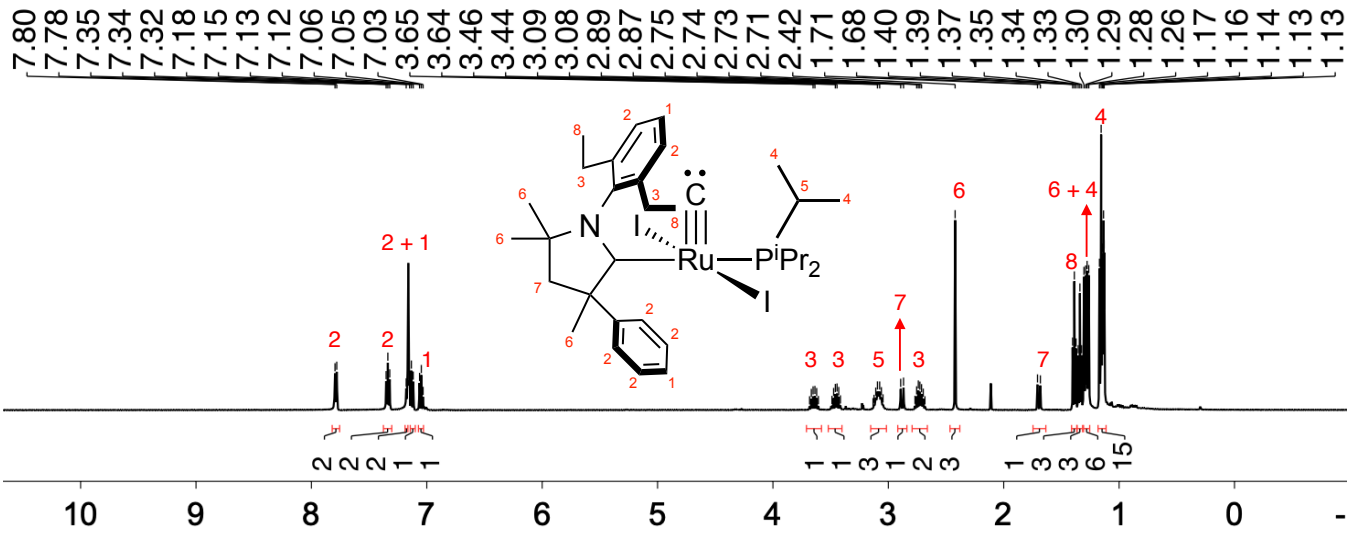

**Figure A.30a.** $^{1}$H NMR spectrum ($C_6D_6$, 500 MHz) of **CbC1$^{Ph}$(I$_2$)**.

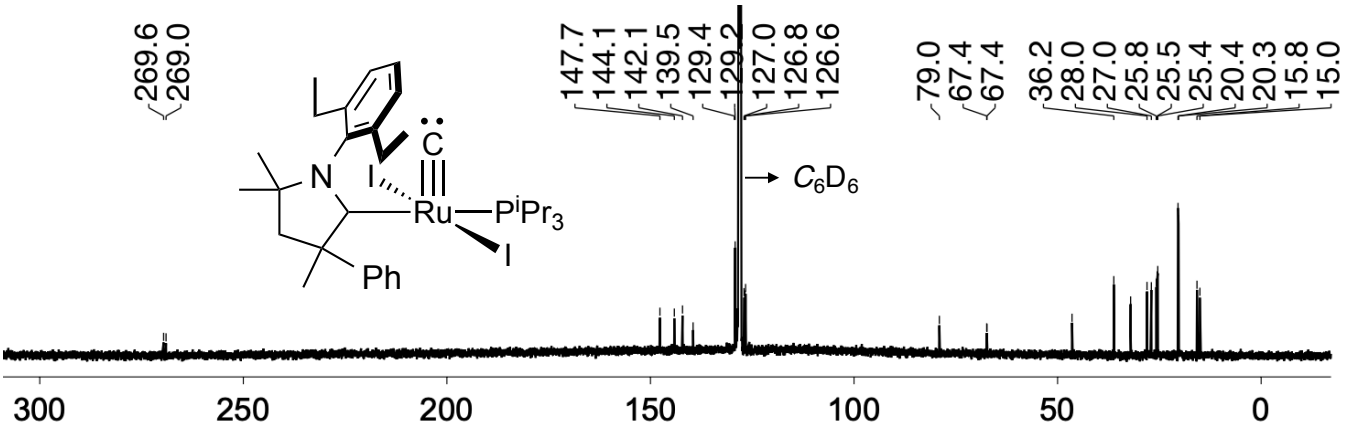

**Figure A.30b.** $^{13}$C{$^{1}$H} NMR spectrum ($C_6D_6$, 125 MHz) of **CbC1$^{Ph}$(I$_2$)**. Carbide signal not observed.

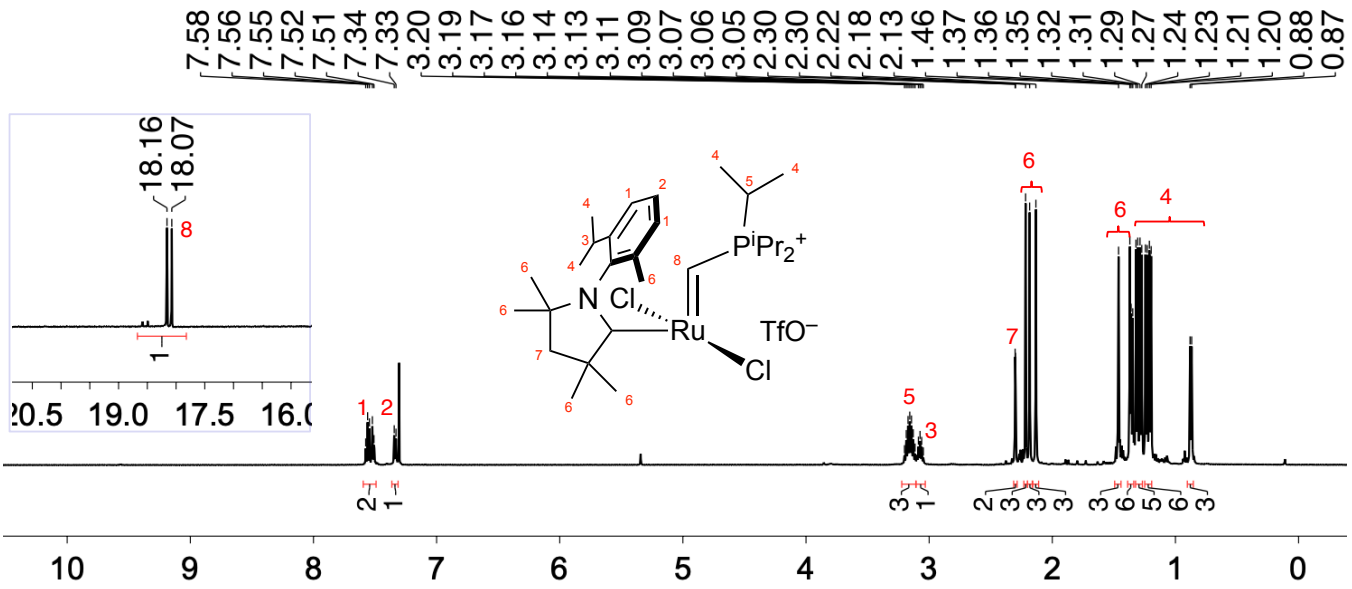


**Figure A.31a.** $^{1}$H NMR spectrum ($CDCl_3$, 500 MHz) of **PC2$^{Me}$**.

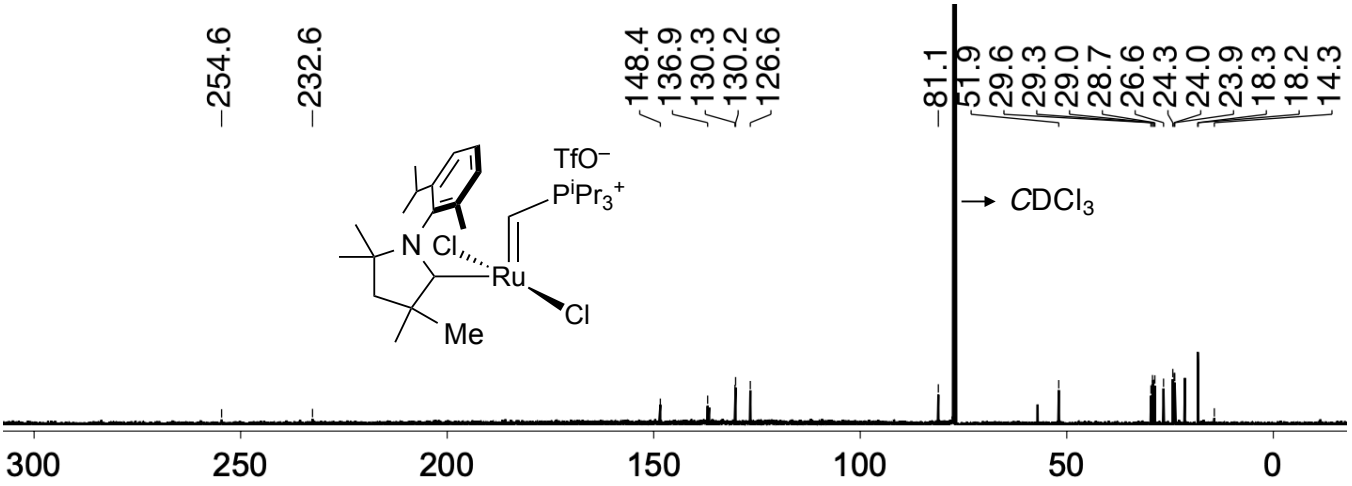


**Figure A.31b.** $^{13}$C{$^{1}$H} NMR spectrum ($CDCl_3$, 125 MHz) of **PC2$^{Me}$**.

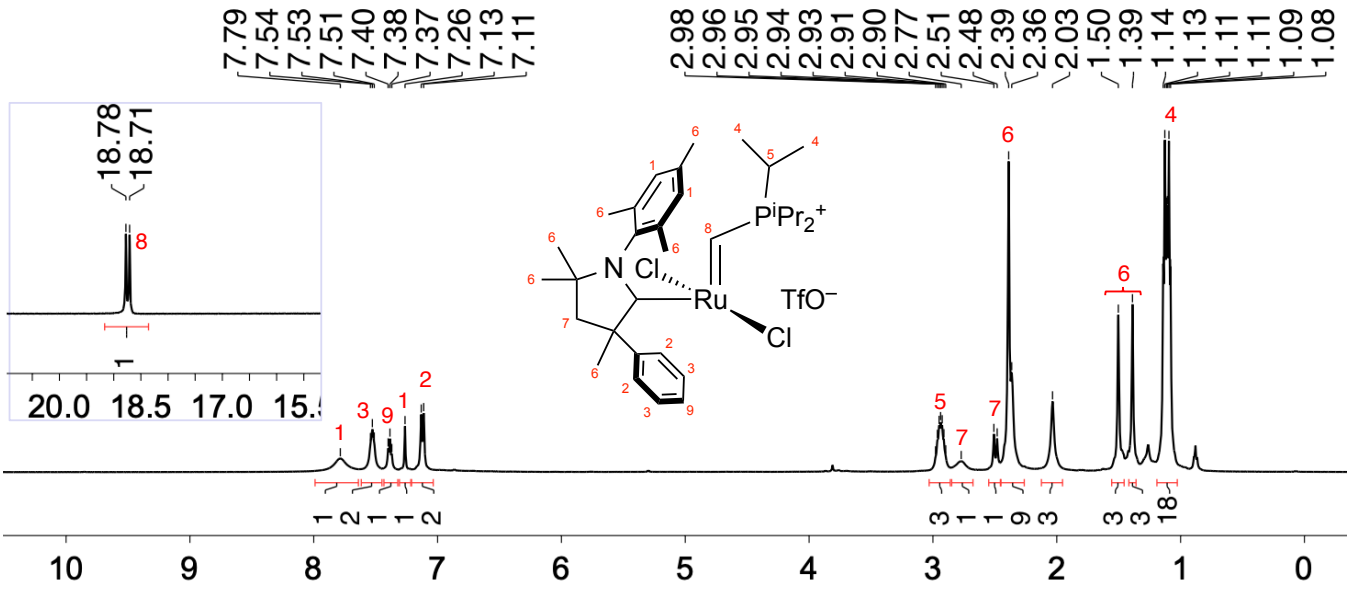


**Figure A.32a.** $^{1}$H NMR spectrum ($CDCl_3$, 500 MHz) of **PC3$^{Ph}$**.

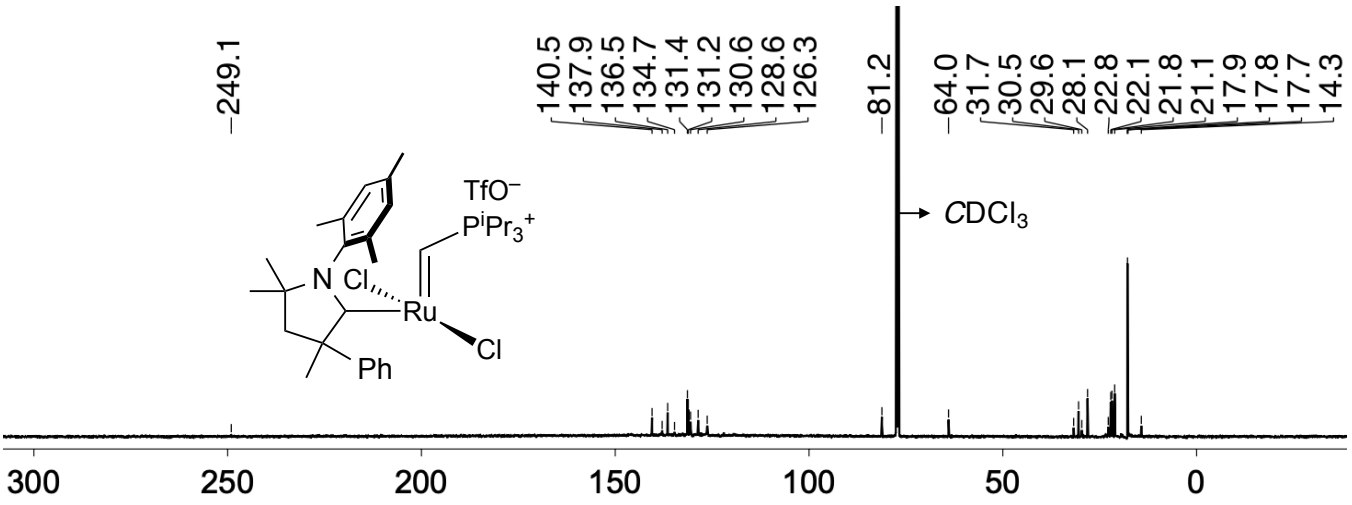


**Figure A.32b.** $^{13}$C{$^{1}$H} NMR spectrum ($CDCl_3$, 125 MHz) of **PC3$^{Ph}$**.

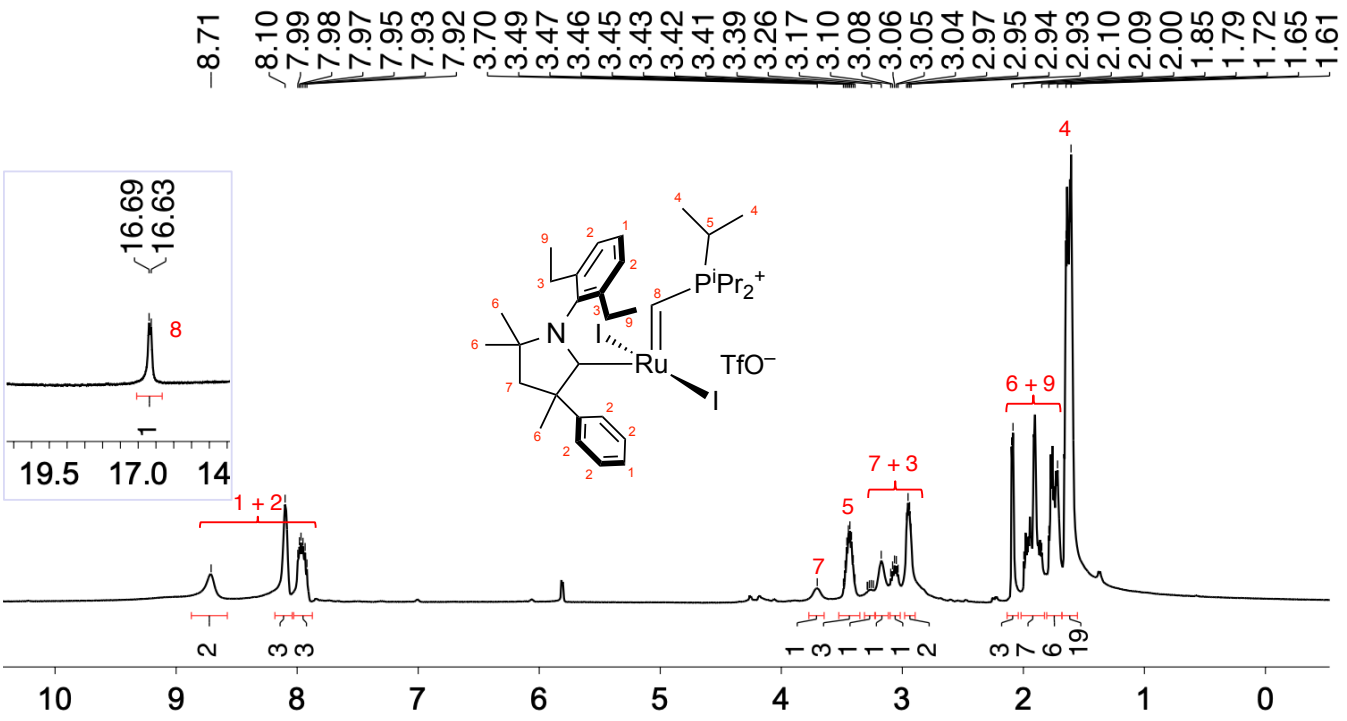


**Figure A.33a.** $^{1}H$ NMR spectrum ($CD_2Cl_2$, 500 MHz) of **PC1$^{Ph}$**.

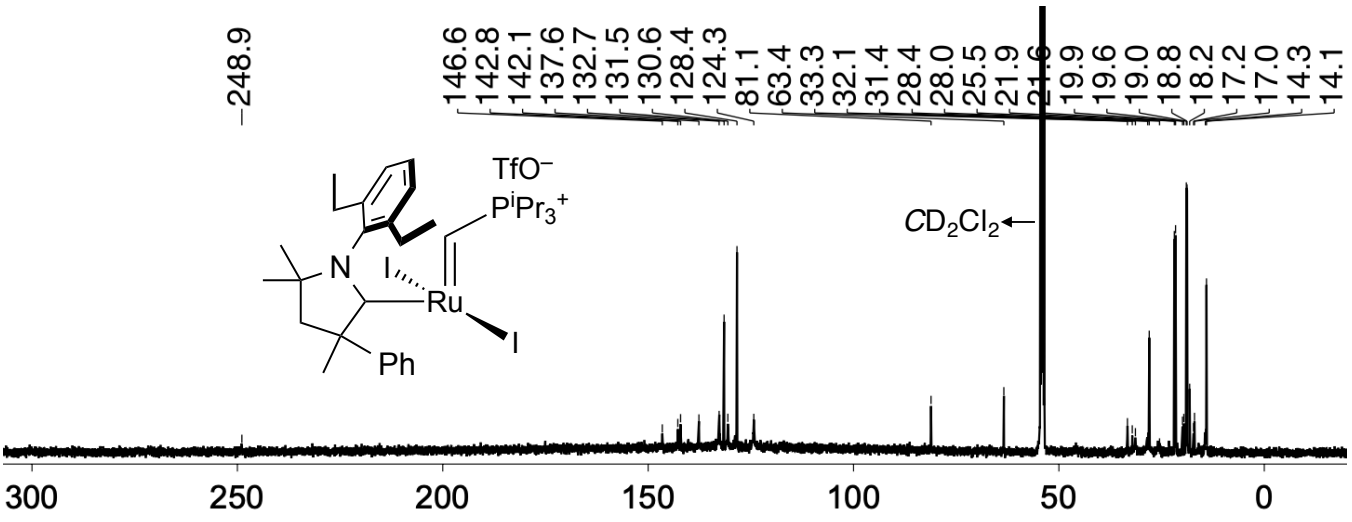


**Figure A.33b.** $^{13}C\{^{1}H\}$ NMR spectrum ($CD_2Cl_2$, 125 MHz) of **PC1$^{Ph}$(I$_2$)**.

Pyridine-stabilized methylidene complexes

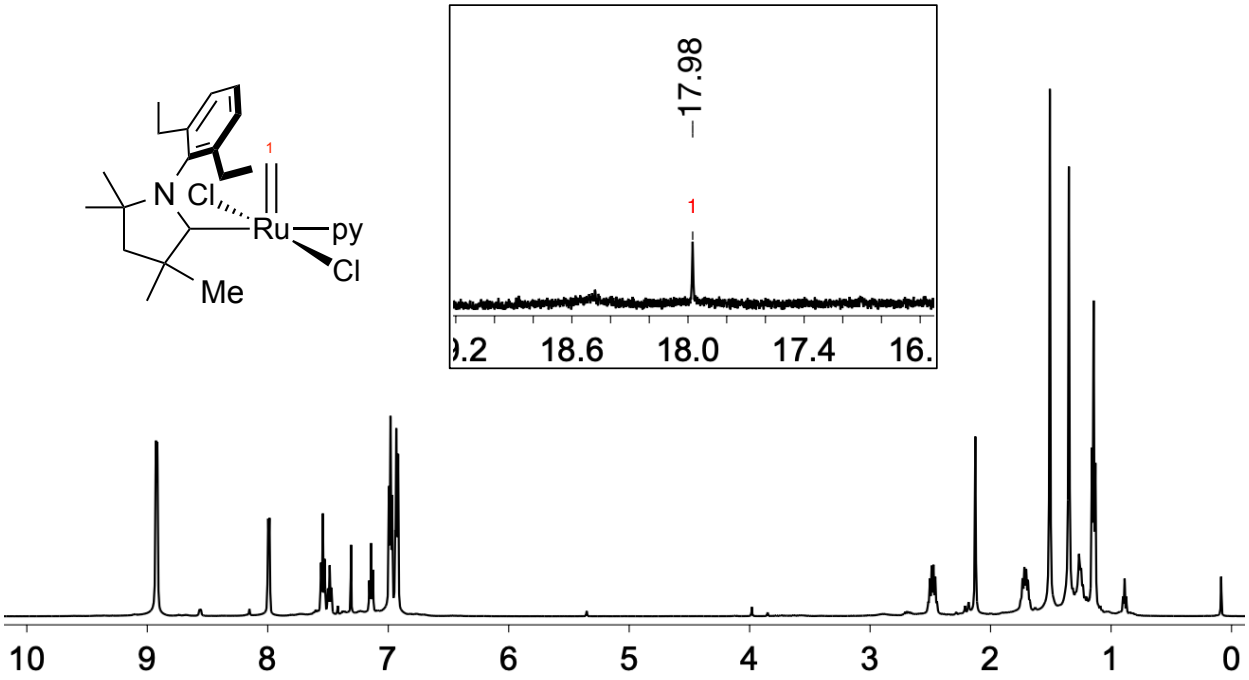


**Figure A.34.** $^{1}$H NMR spectrum ($CDCl_3$, 500 MHz) of **mC1**$^{Me}$ at –40 °C. The instability of the complex hindered the acquisition of $^{13}$C NMR over the course of 7 h at –40 °C.

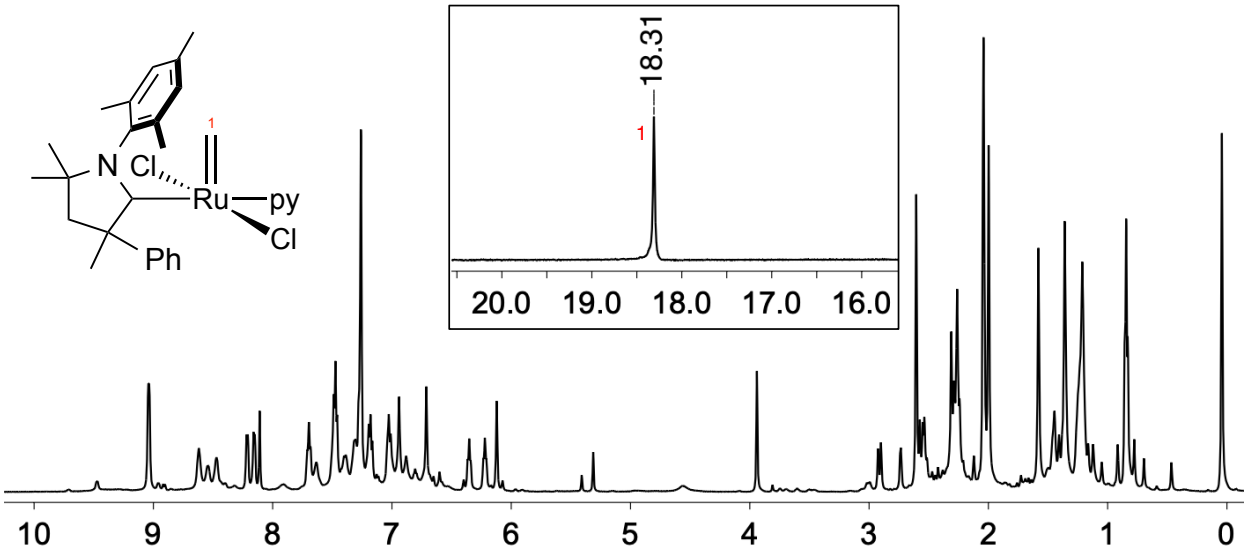


**Figure A.35.** $^{1}$H NMR spectrum ($CDCl_3$, 500 MHz) of **mC3**$^{Ph}$ at –40 °C. The instability of the complex hindered the acquisition of $^{13}$C NMR over the course of 7 h at –40 °C.

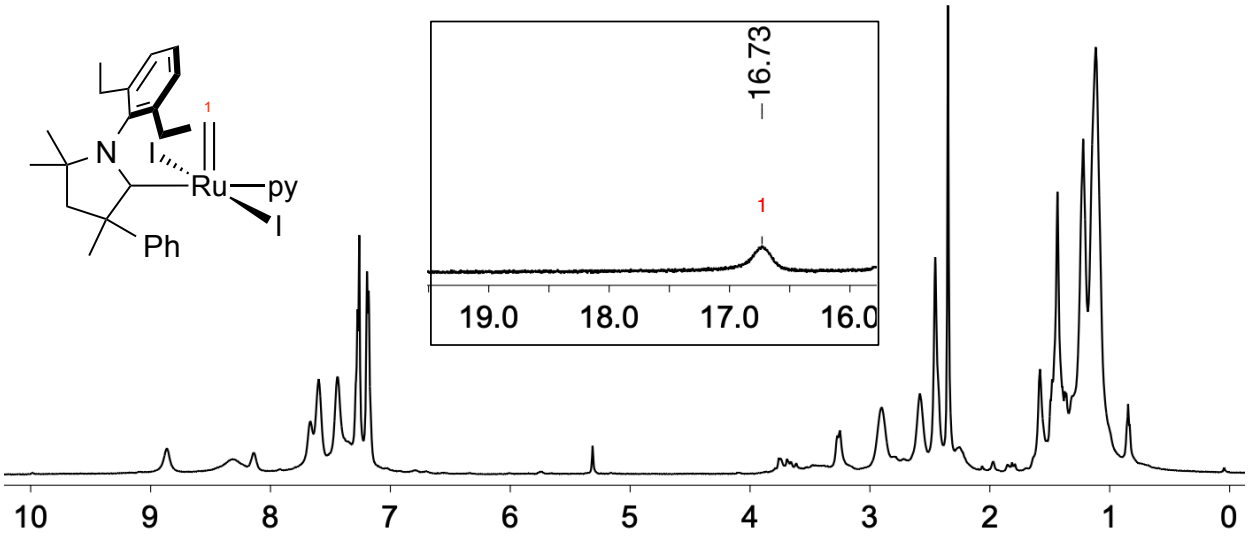


**Figure A.36a.** $^{1}$H NMR spectrum ($CDCl_3$, 500 MHz) of **mC1$^{Ph}$(I$_2$)** at –40 °C.

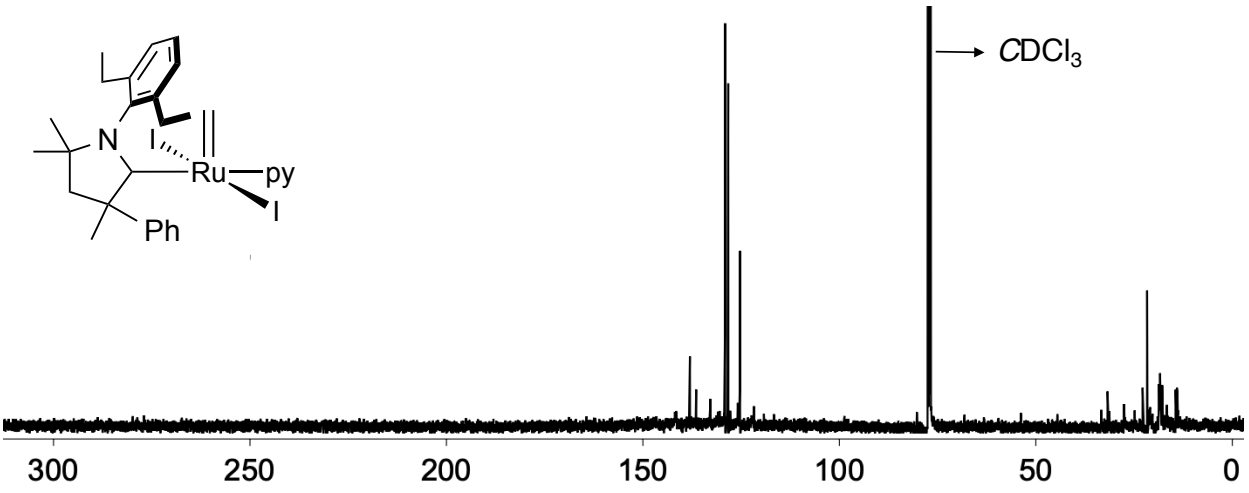


**Figure A.36b.** $^{13}$C{$^{1}$H} NMR spectrum ($CDCl_3$, 125 MHz) of **mC1$^{Ph}$(I$_2$)** at –40 °C.

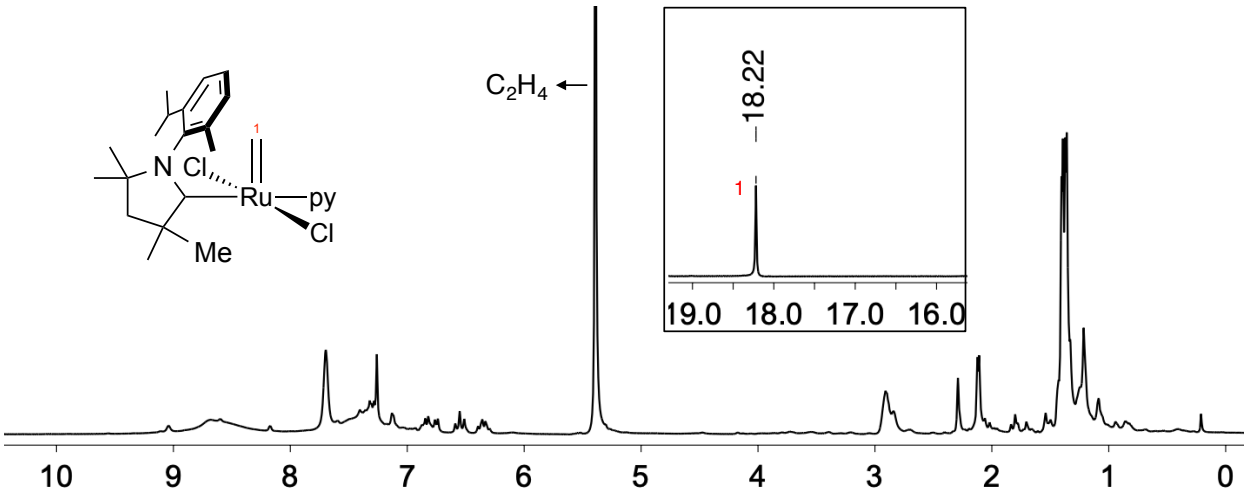


**Figure A.37.** $^{1}$H NMR spectrum ($CDCl_3$, 500 MHz) showing in situ generation of **mC2$^{Me}$** at –40 °C

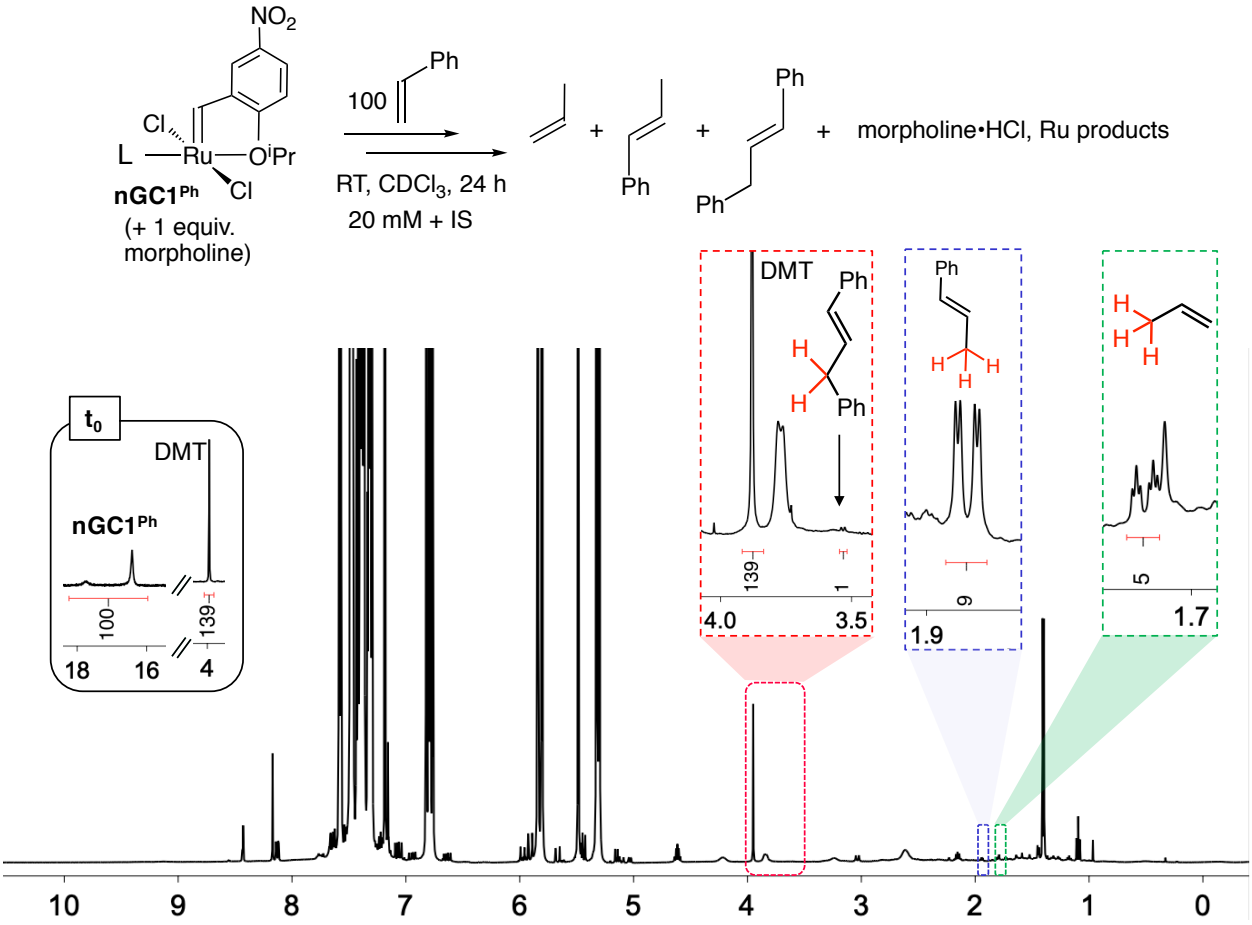


**FigureA.38.** $^{1}$H NMR spectrum ($CDCl_3$, 500 MHz) at 24 h for reaction at top: assessing proton abstraction by morpholine. Inset at left shows the initial ratio of **nGC1** to DMT (internal standard; IS). Spectrum shows ca. 5% propenes; 3% β-methyl styrene (blue); 0.5% (E)-$PhCH{=}CHCH_2Ph$ (red); 2% propene (green).

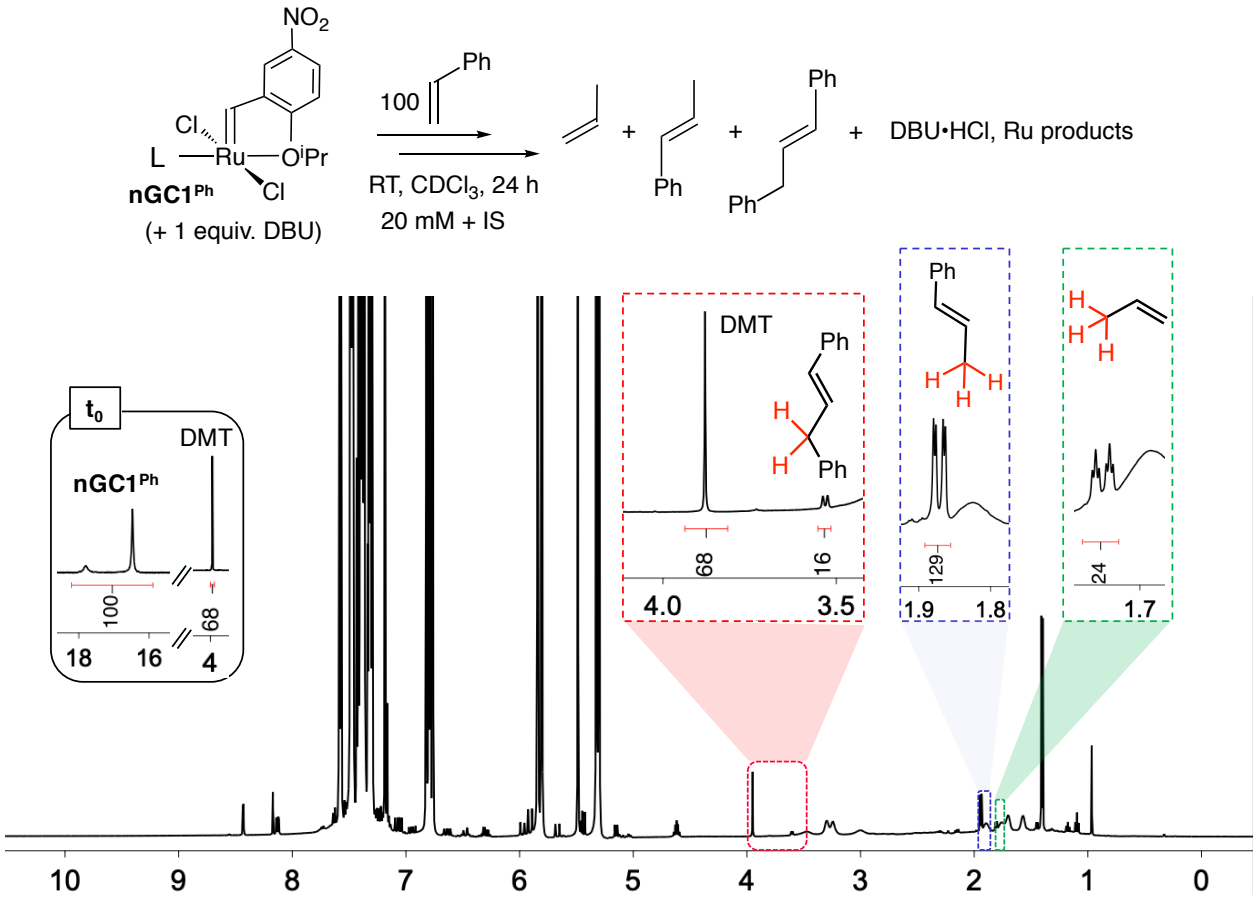


**Figure A.39.** $^{1}$H NMR spectrum ($CDCl_3$, 500 MHz) at 24 h for reaction at top: assessing proton abstraction by DBU. Inset at left shows the initial ratio of **nGC1** to DMT (internal standard; IS). Spectrum shows 59% propenes; 43% β-methyl styrene (blue); 8% (E)-PhCH=CHCH$_2$Ph (red); 8% propene (green).

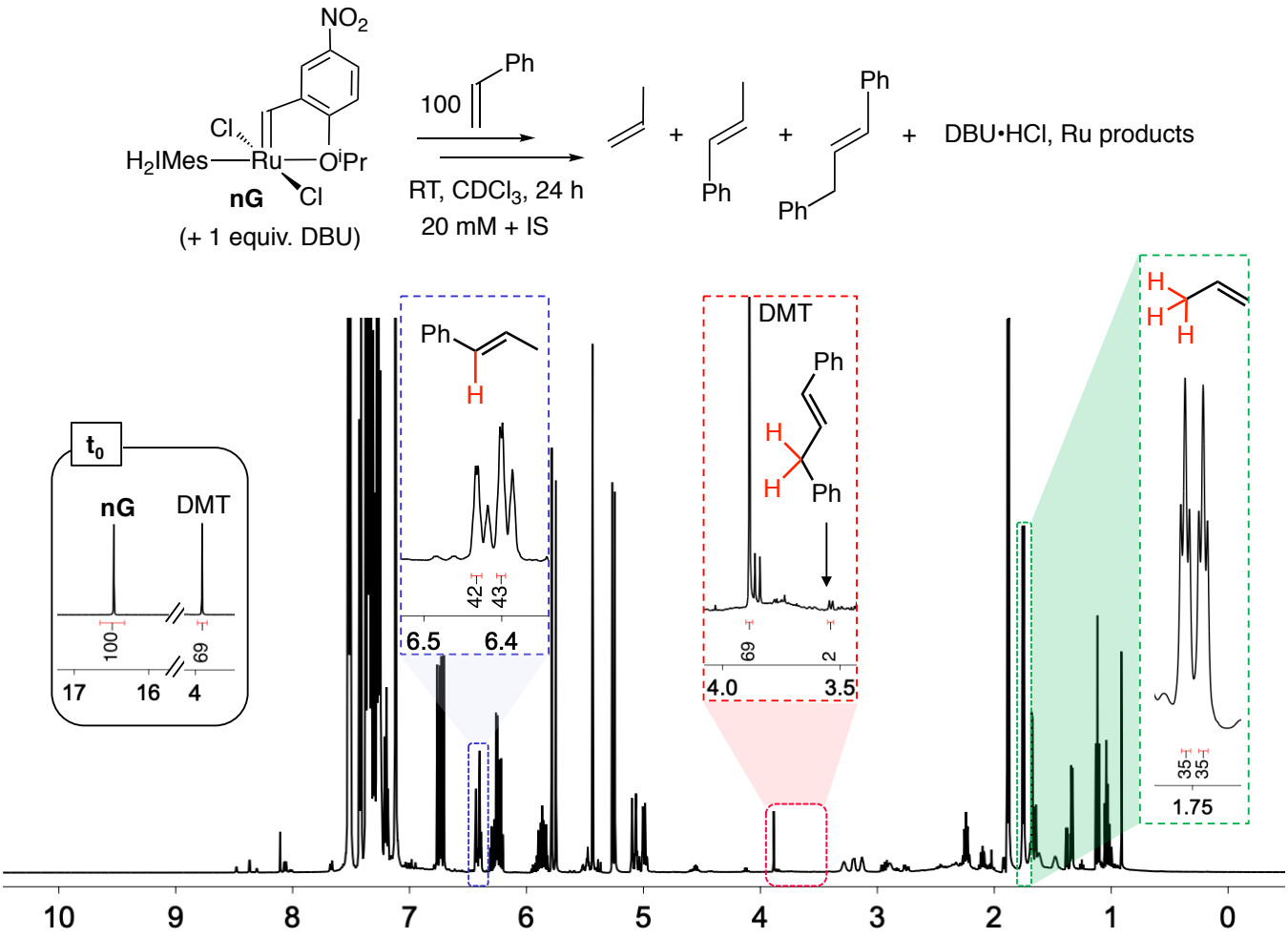


**Figure A.40.** $^{1}$H NMR spectrum ($CDCl_3$, 500 MHz) at 24 h for reaction at top: assessing proton abstraction by DBU. Inset at left shows the initial ratio of **nG** to DMT (internal standard; IS). Spectrum shows 100% propenes; 85% β-methyl styrene (blue); 1% (E)-PhCH=CHCH$_2$Ph (red); 23% propene (green).

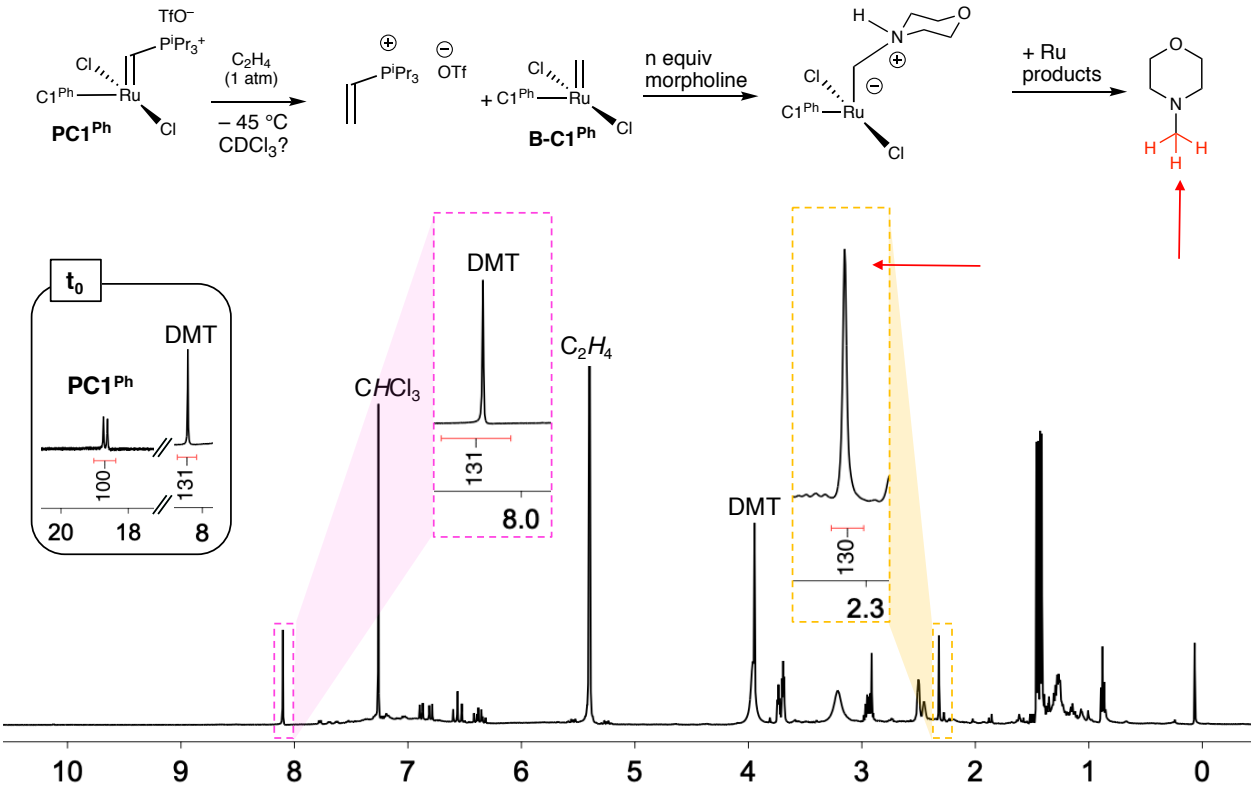


**Figure A.41.** Crude $^{1}$H NMR spectrum ($CDCl_3$, 500 MHz) for reaction of **PC1$^{Ph}$** with $C_2H_4$ followed by addition of morpholine: assessing methylidene abstraction by morpholine. $t_0$ inset shows initial ratio of **PC1$^{Ph}$** : DMT (internal standard; IS). Spectrum at RT: 43% 4-methylmorpholine vs. IS.

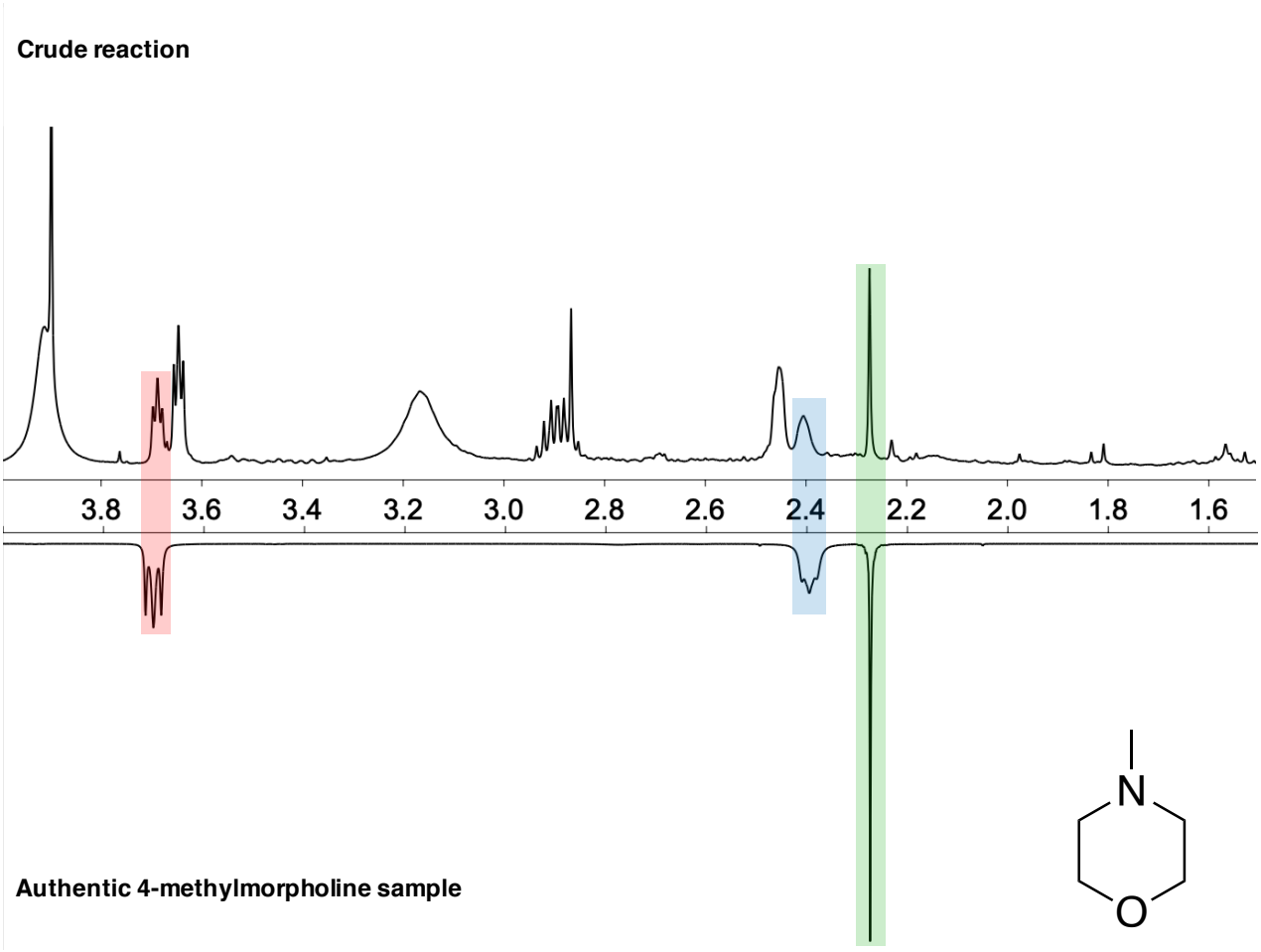


**Figure A.42.** $^{1}H$ NMR spectra ($CDCl_3$, 500 MHz) for reaction of **PC1$^{Ph}$** with $C_2H_4$ followed by addition of morpholine. Inverted: authentic sample of 4-methylmorpholine.

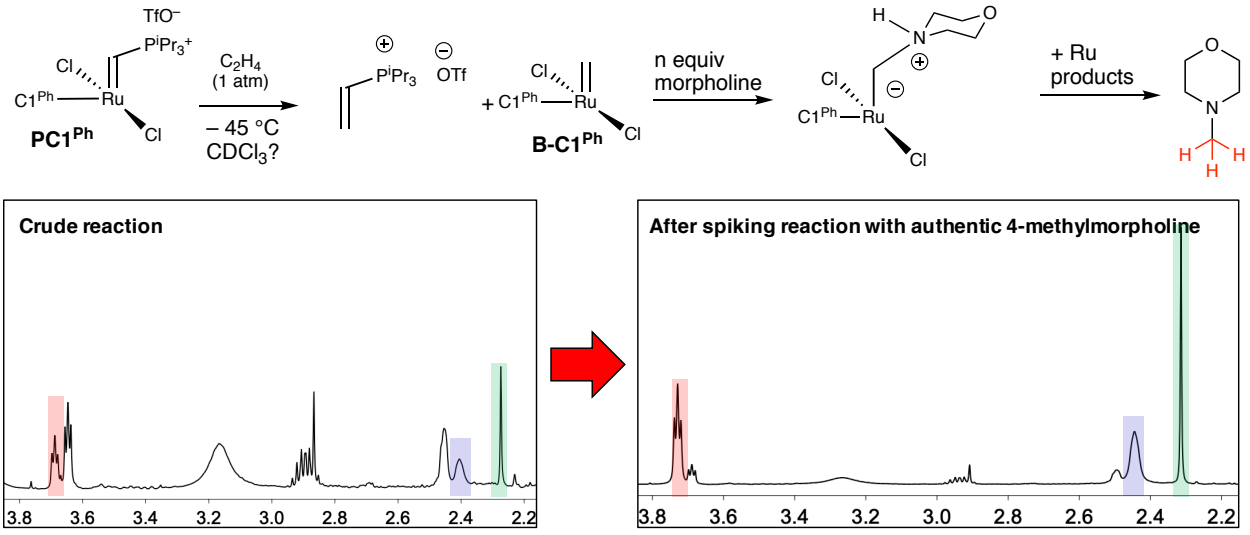


**Figure A.43.** $^{1}$H NMR spectra ($CDCl_3$, 500 MHz). Left: Spectrum of crude reaction of **PC1$^{Ph}$** with $C_2H_4$ and morpholine. Right: Spiking of reaction with authentic 4-methylmorpholine confirming assignment of signals in spectrum of crude product.

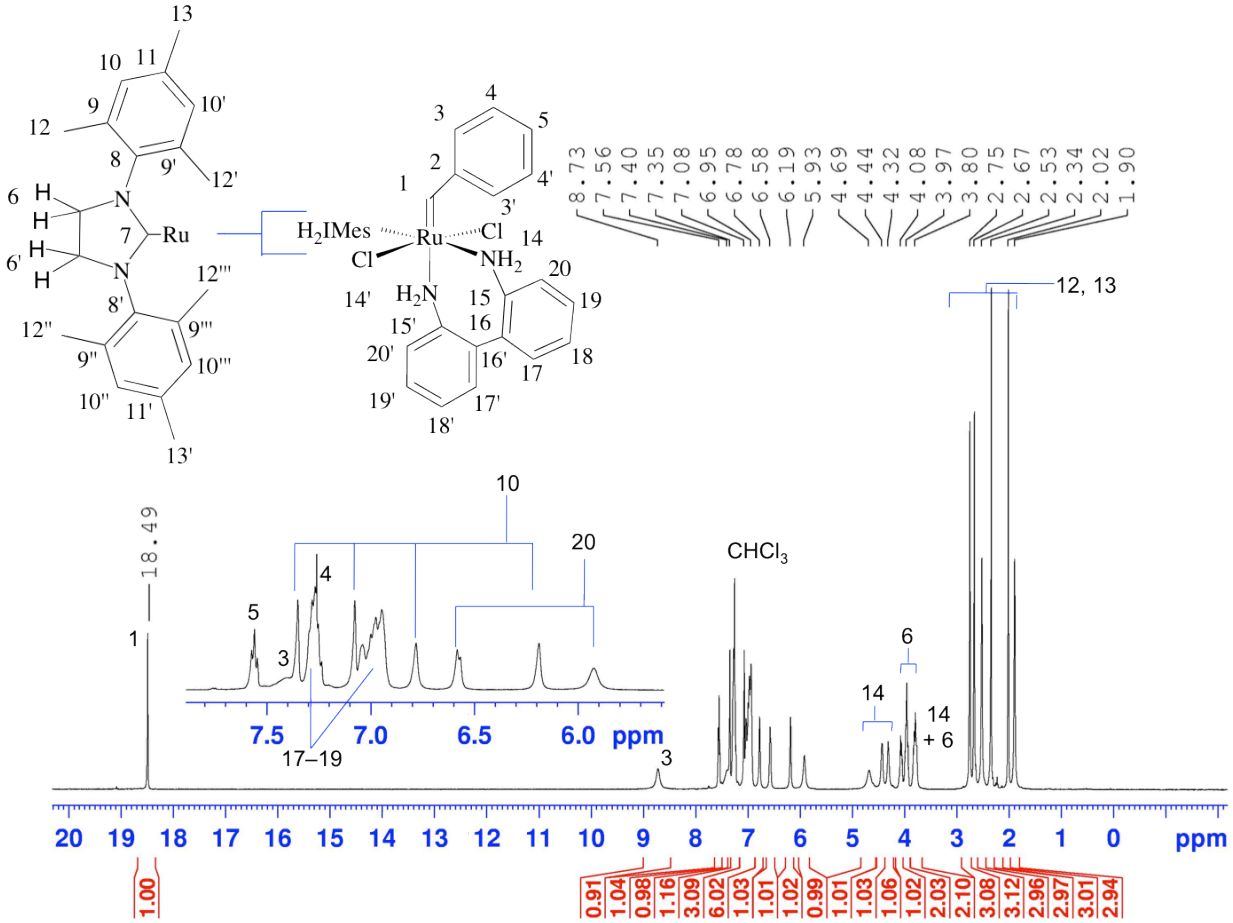


**Figure A.44a.** $^{1}$H NMR spectrum of $RuCl_2(H_2IMes)(ODA)(=CHPh)$ **DA** ($CDCl_3$, 500.1 MHz, –20 °C).

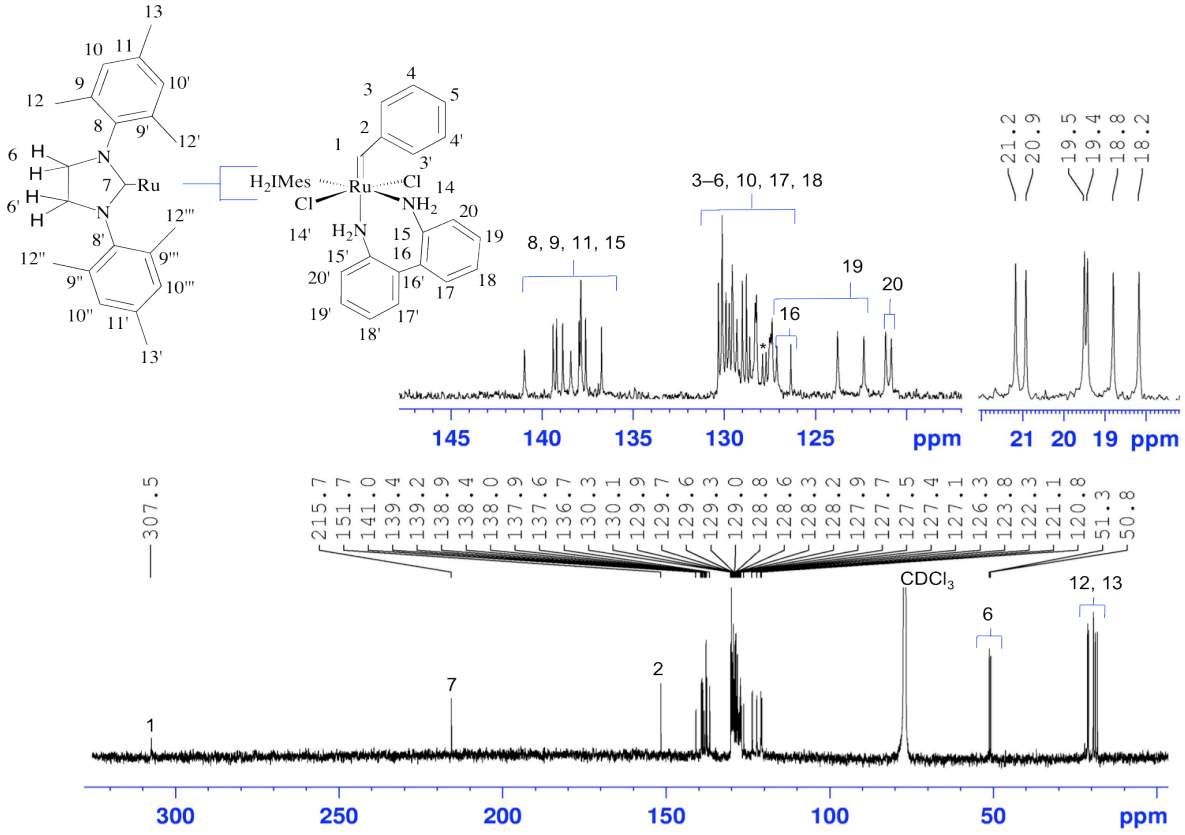


**Figure A.44b.** $^{13}C\{^{1}H\}$NMR spectrum of $RuCl_2(H_2IMes)(ODA)(=CHPh)$ **DA** ($CDCl_3$, 125.8 MHz, –20 °C).

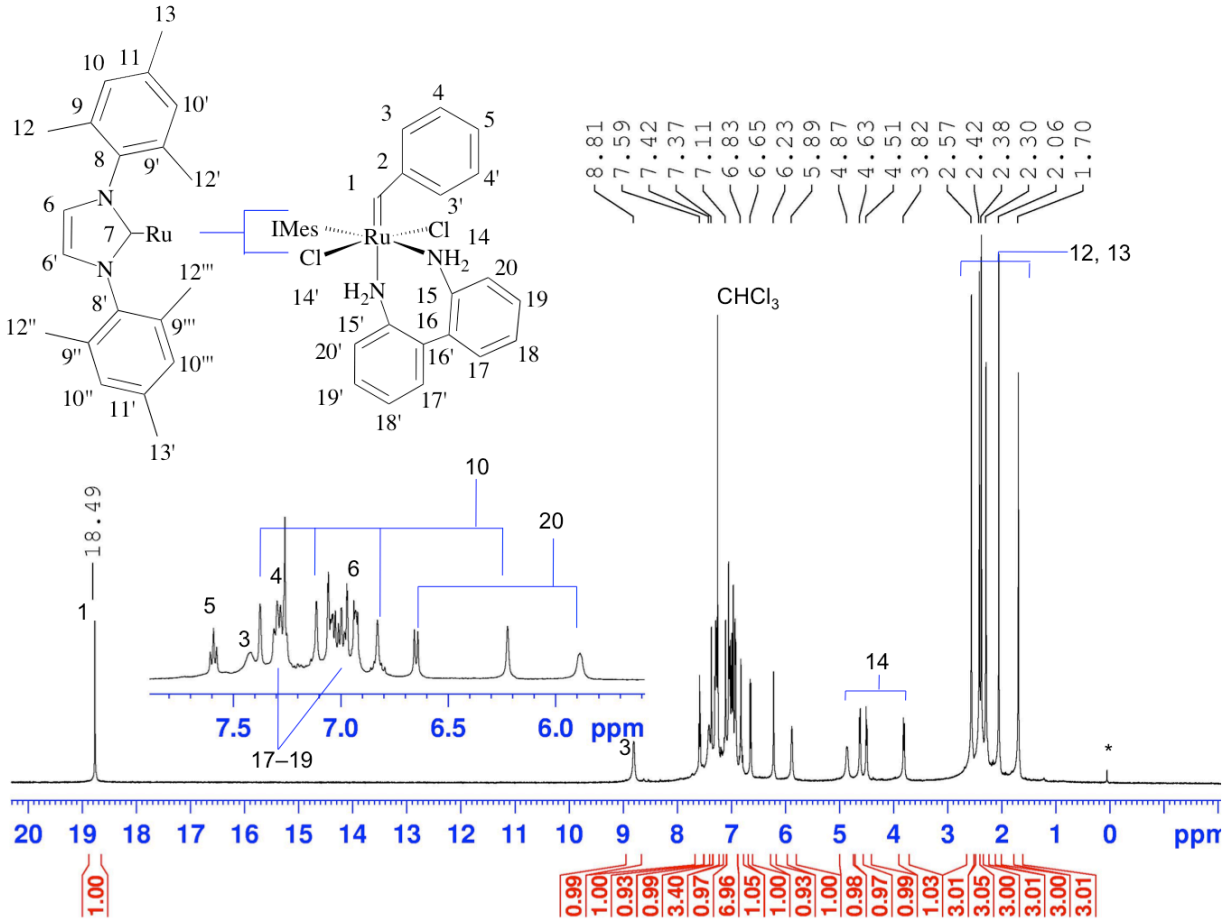


**Figure A.45a.** $^{1}$H NMR spectrum of $RuCl_2$(IMes)(ODA)(=CHPh) **DA'** ($CDCl_3$, 500.1 MHz, –20 °C, * silicone grease).

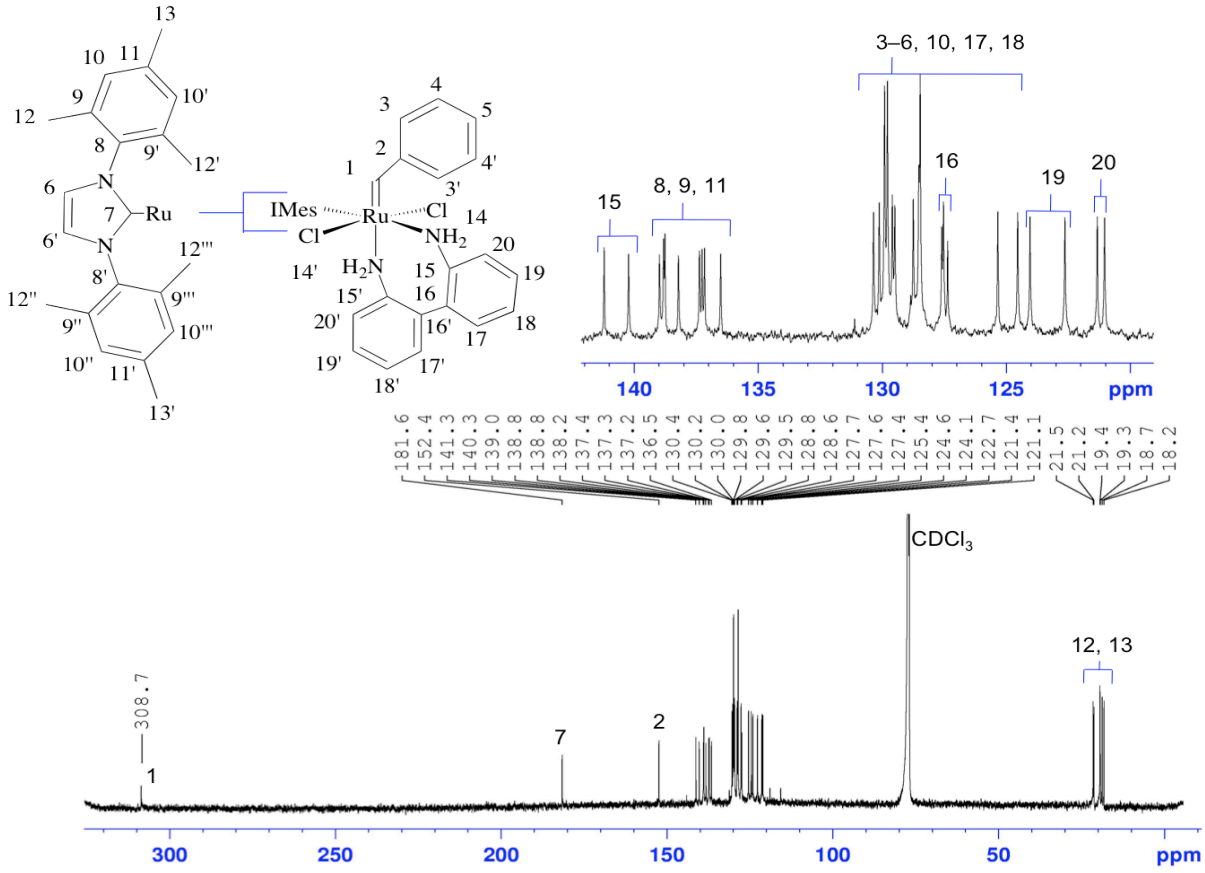


**Figure A.45b.** $^{13}C\{^{1}H\}$ NMR spectrum of $RuCl_2(IMes)(ODA)(=CHPh)$ **DA'** ($CDCl_3$, 125.8 MHz, –20 °C).

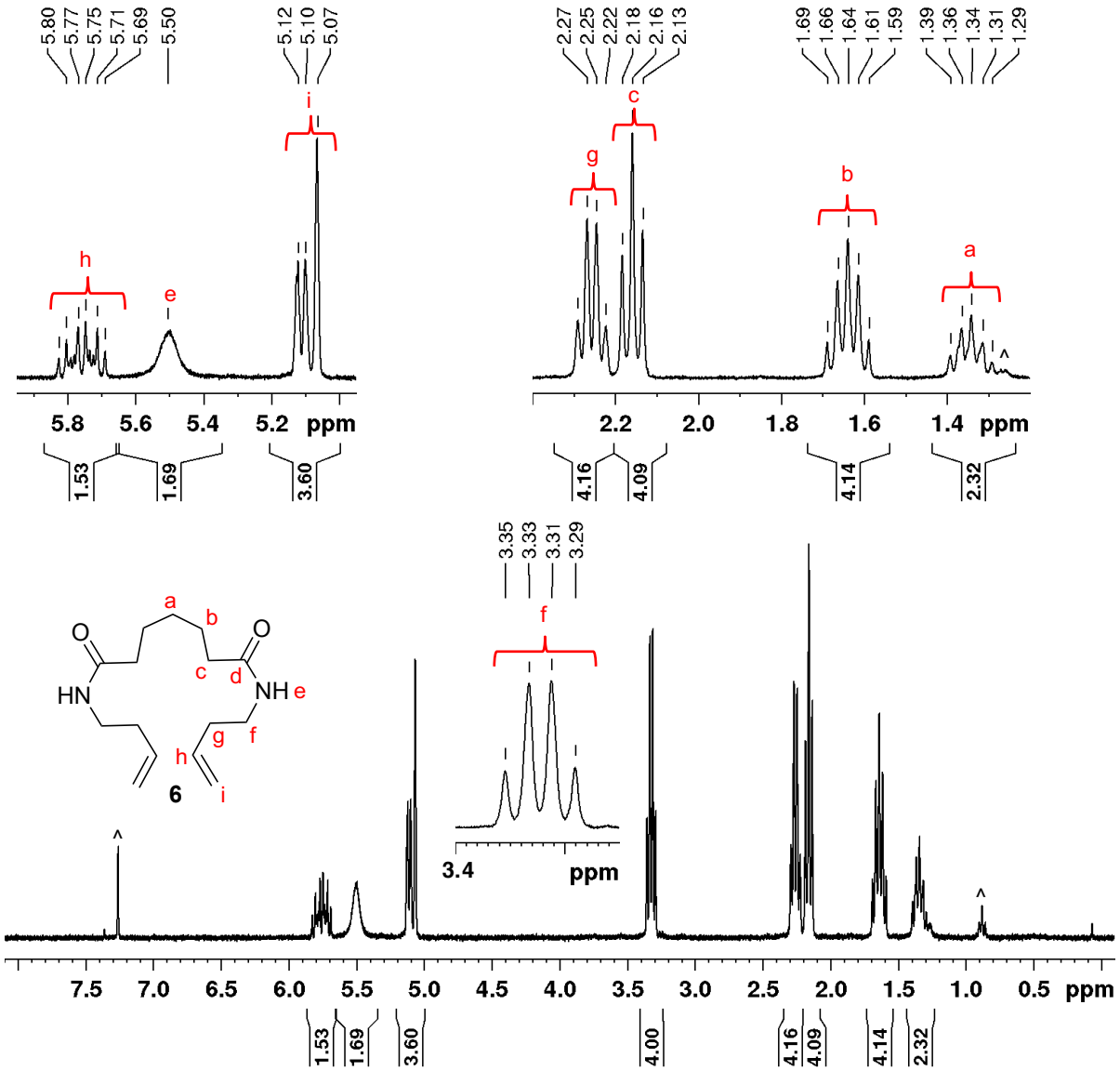


**Figure A.46a.** $^{1}$H NMR spectrum for diene *N,N*-di(4-buten-1-yl)-1,5-pentanediamide (**6**; $CDCl_3$, 300 MHz). ^Denotes residual solvents ($CHCl_3$, hexanes).

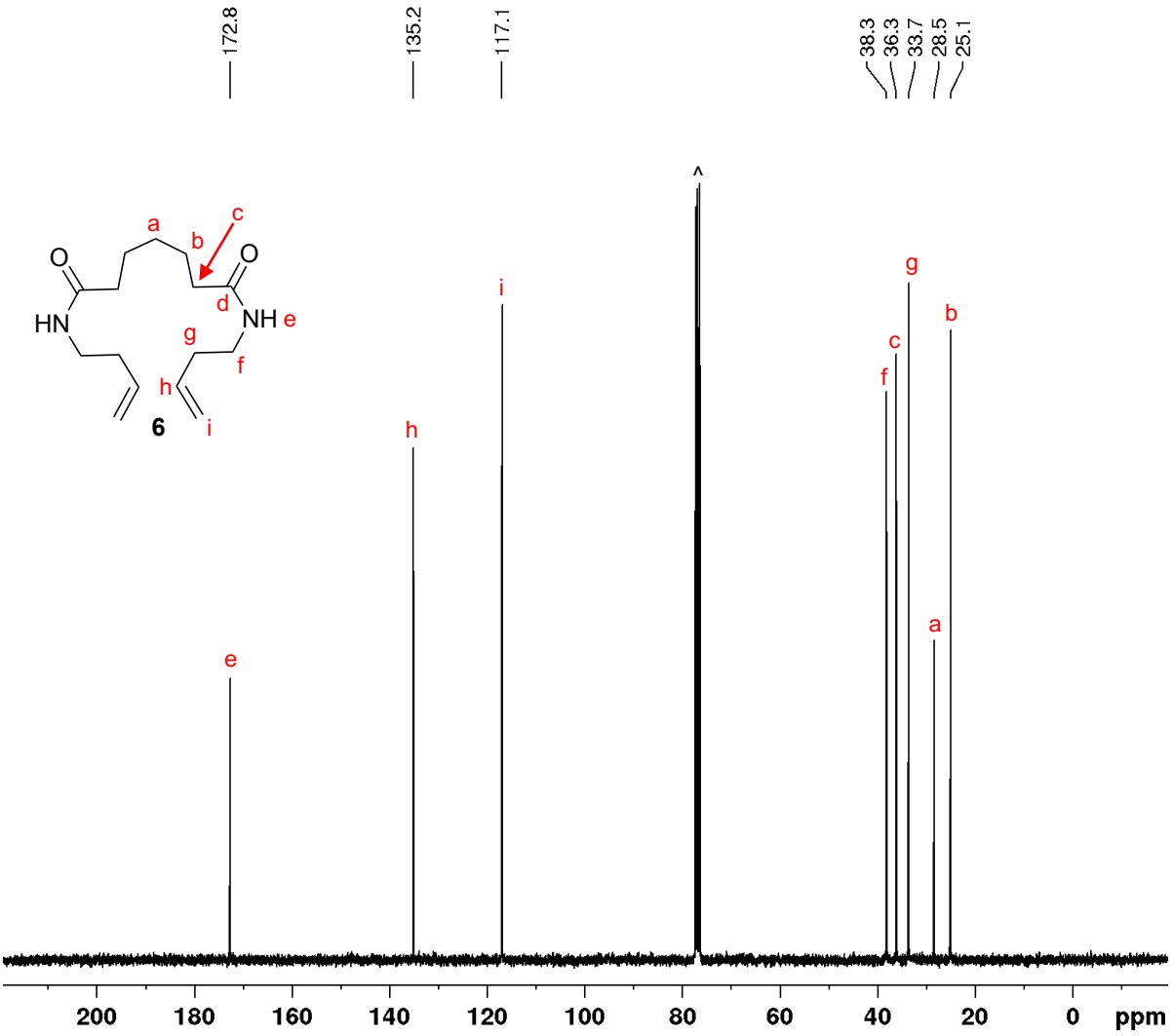


**Figure A.46b.** $^{13}C$ NMR spectrum for diene *N,N*-di(4-buten-1-yl)-1,5-pentanediamide (**6**; $CDCl_3$, 300 MHz). ^Denotes signals arising from the *C*$DCl_3$ solvent.

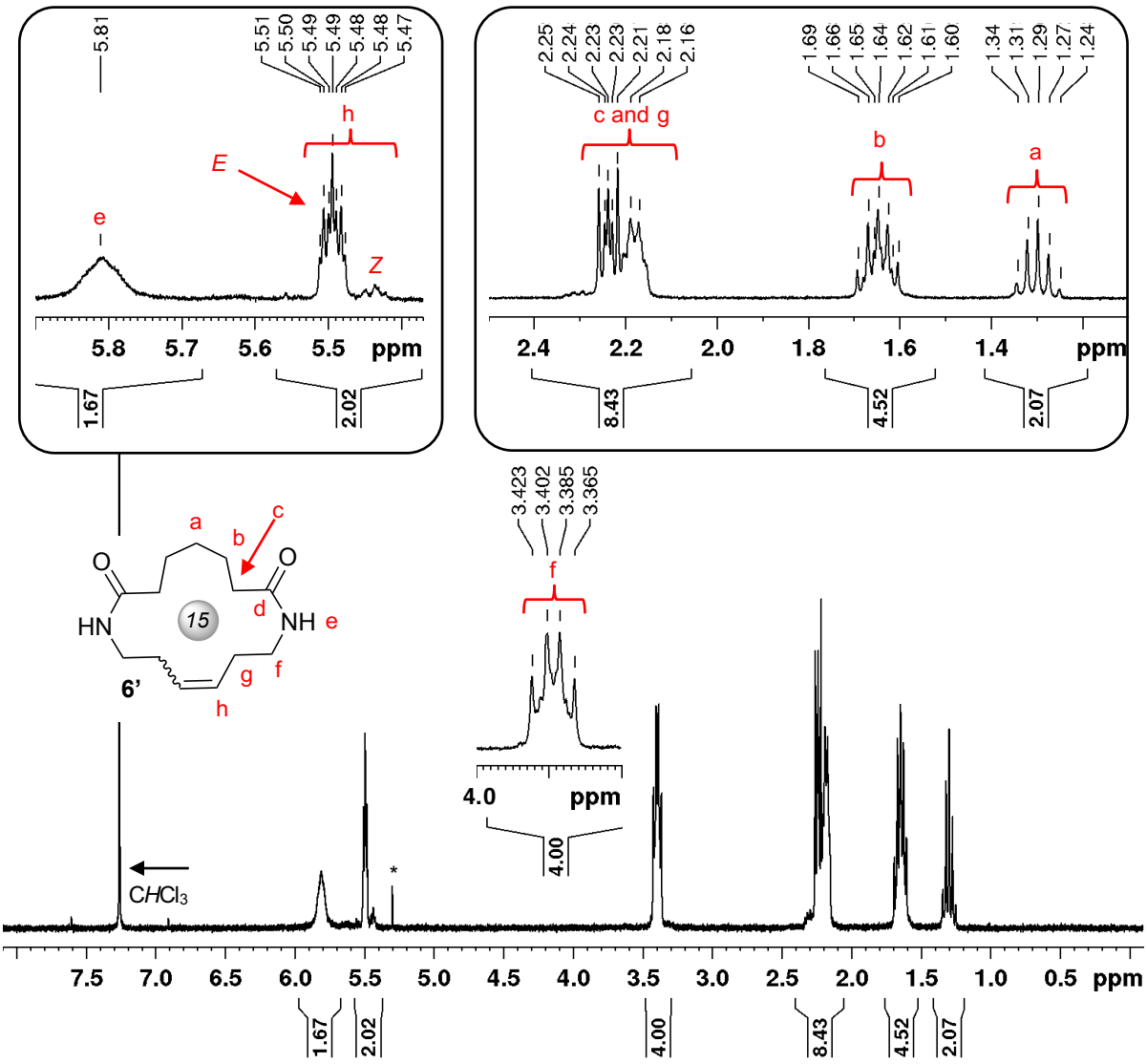


**Figure A.47a.** $^{1}$H NMR spectrum for cyclic dilactam cyclopentadecene-6,12-diamide (**6'**; $CDCl_3$, 300 MHz). *Denotes residual $CH_2Cl_2$.

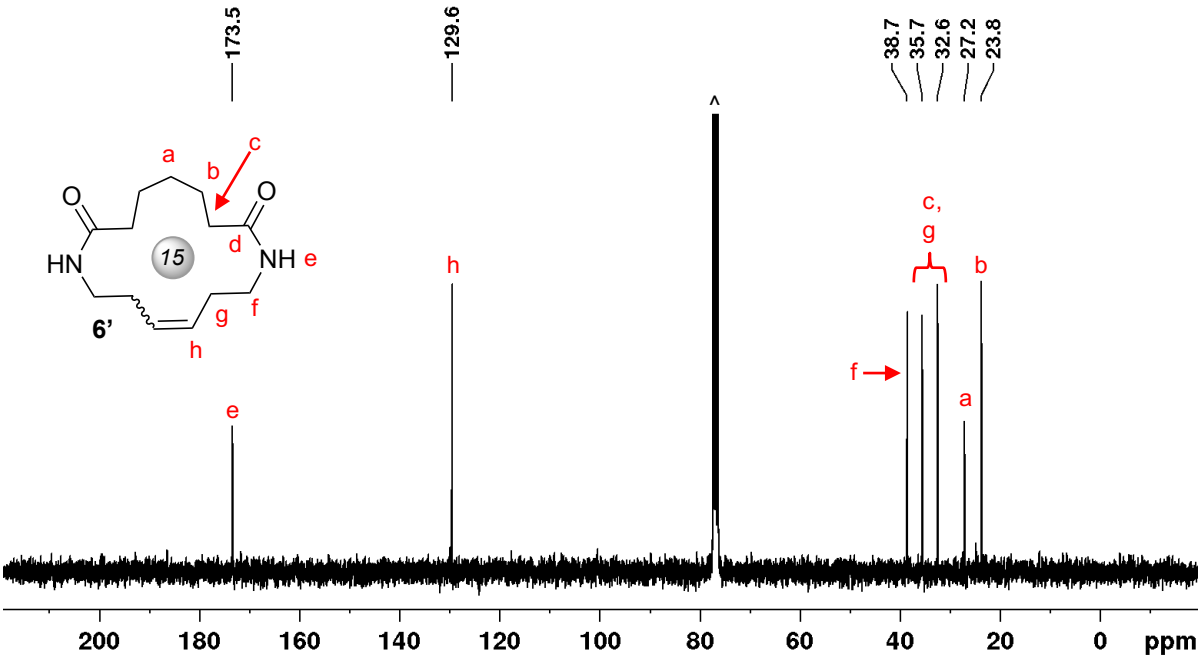


**Figure A.47b.** $^{13}C$ NMR spectrum for cyclic dilactam cyclopentadeene-6,12-diamide (**6'**; $CDCl_3$, 300 MHz). ^Denotes signals arising from the *C*$DCl_3$ solvent.

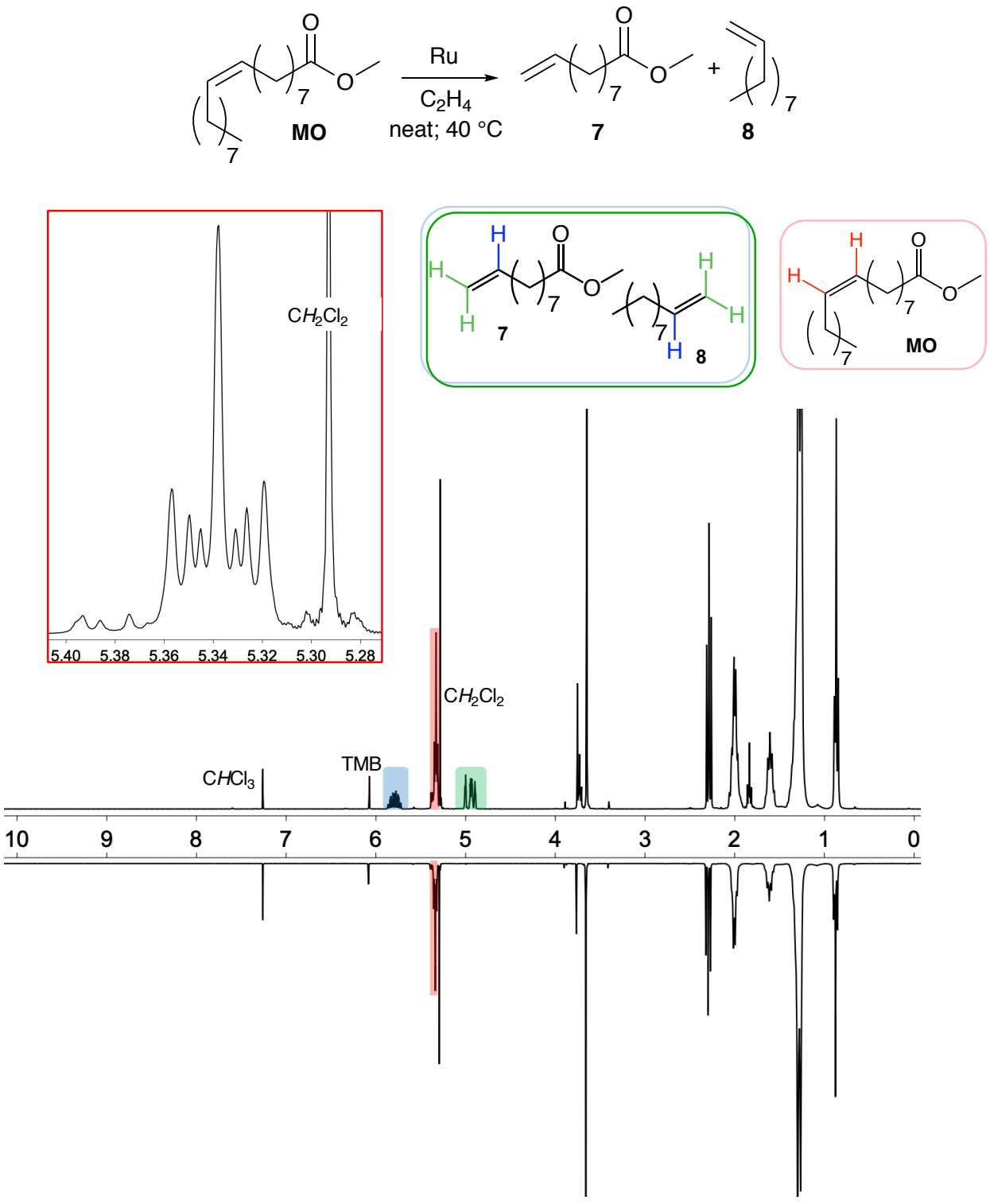


**Figure A.48.** $^{1}$H NMR spectra ($CDCl_3$, 300 MHz) for ethenolysis of methyl oleate, **MO**. Top: After 2 h of reaction with **InC1$^{Ph}$** at 200 psi ethylene, 40 °C. Inset demonstrates that the olefinic signals for **MO** can be integrated free of trace $CH_2Cl_2$. Bottom: Spectrum of **MO** and TMB.

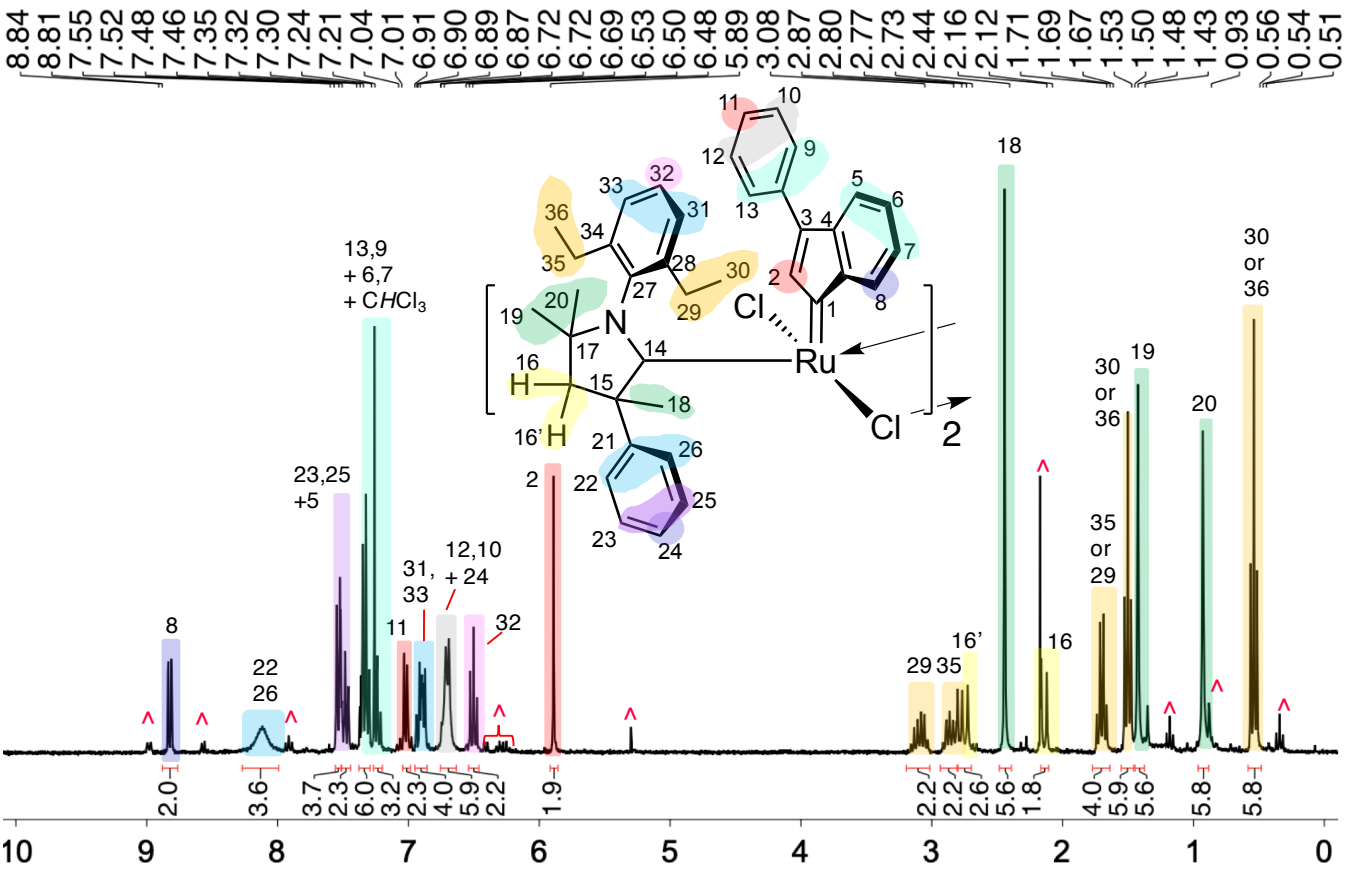


**Figure A.49a.** $^{1}$H NMR spectrum ($CDCl_3$, 300 MHz) of $[RuCl_2(\mathbf{C1^{Ph}})(=Ind)]_2$ **InC1$^{Ph}$**. The symbol ^ denotes rotamers.

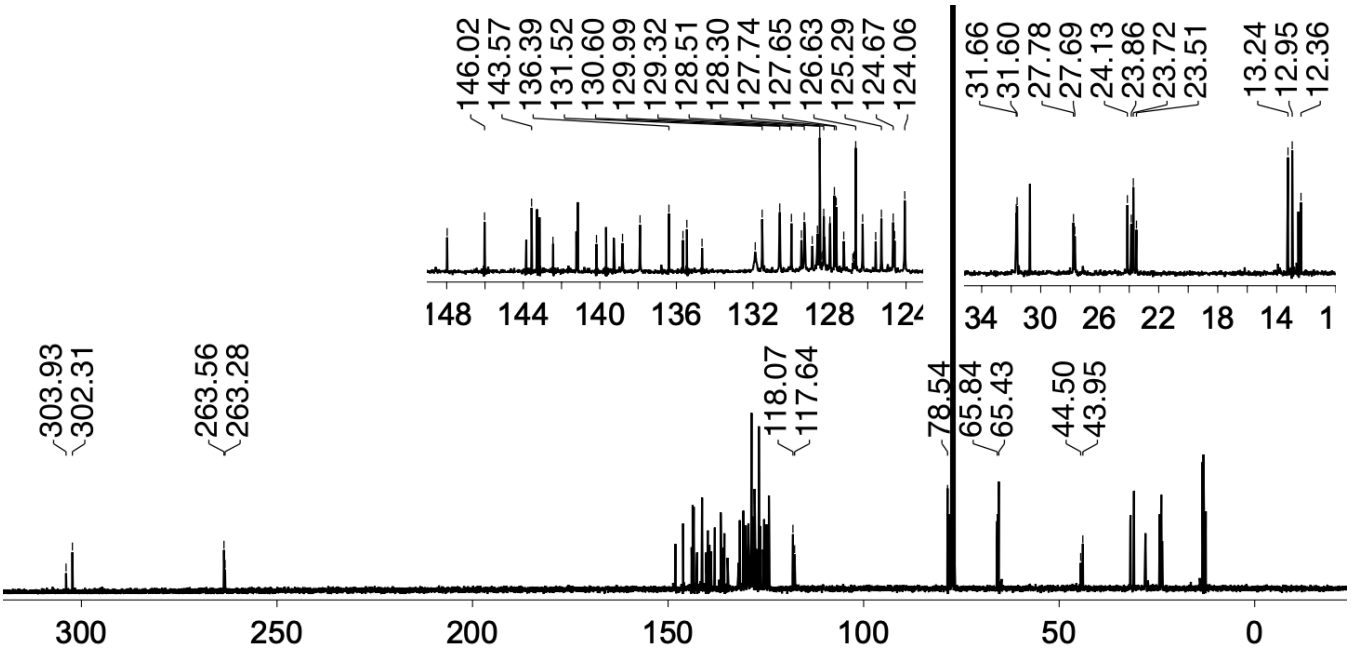


**Figure A.49b.** $^{13}C\{^{1}H\}$ NMR spectrum ($CDCl_3$, 75 MHz) of $[RuCl_2(\mathbf{C1^{Ph}})(=Ind)]_2$ **InC1$^{Ph}$**.

(a)

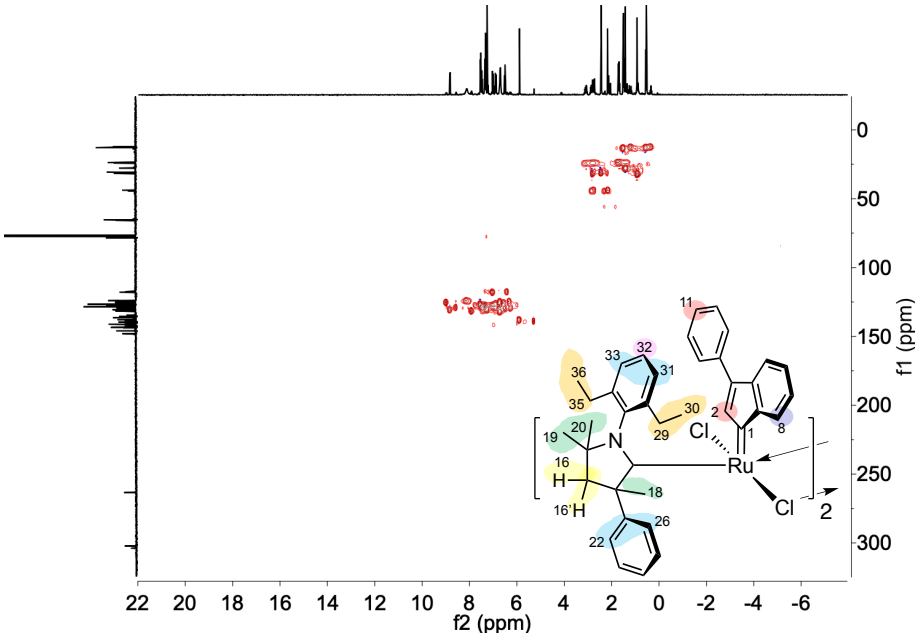


(b)

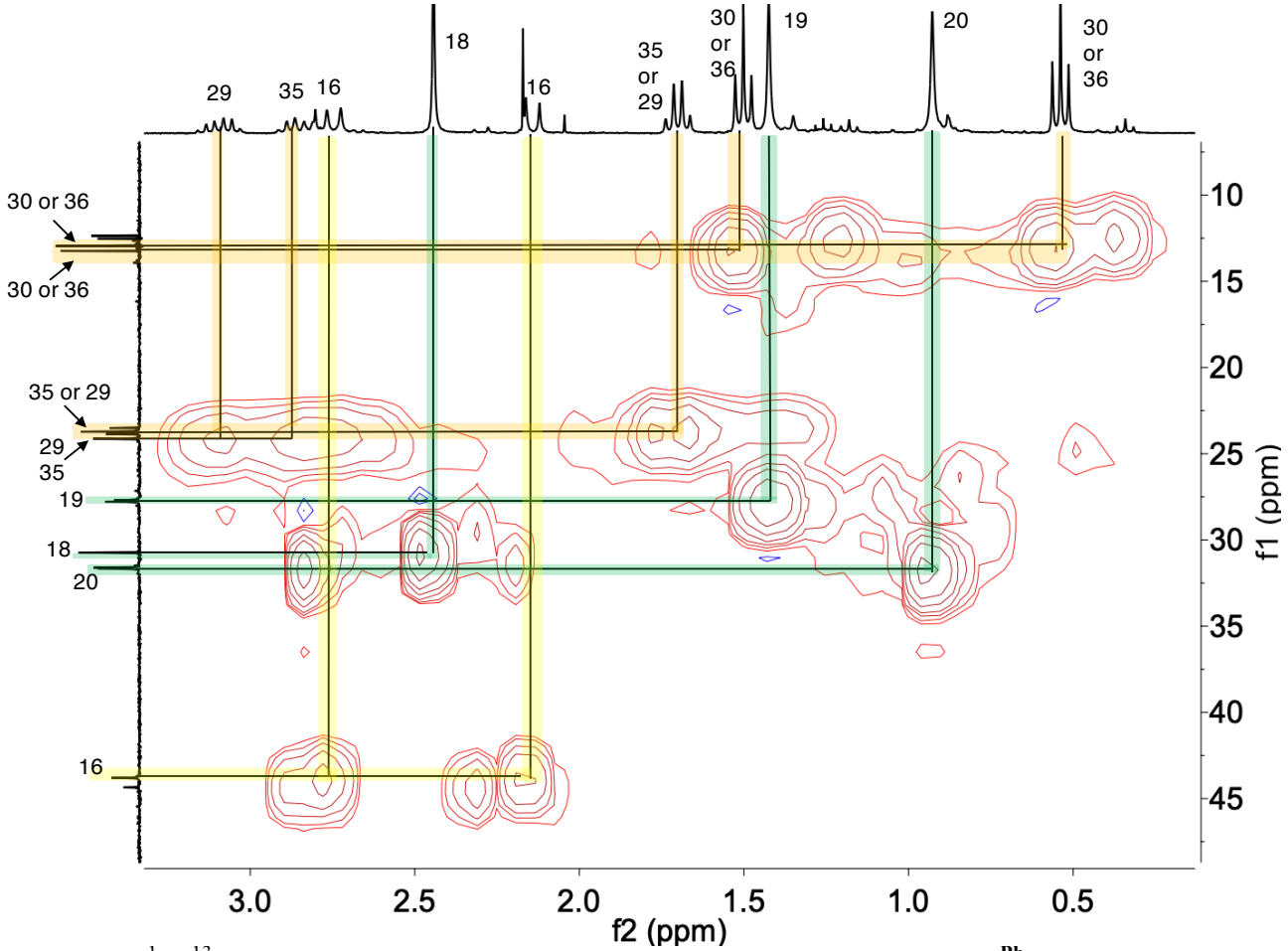


**Figure A.49c.** (a) $^{1}$H-$^{13}$C HSQC NMR spectrum ($CDCl_3$, 300 MHz) of $[RuCl_2(\mathbf{C1^{Ph}})(=Ind)]_2$ **InC1$^{Ph}$**.
(b) Expanded aliphatic region. For the expanded aromatic region, see continuation next page.

(c)

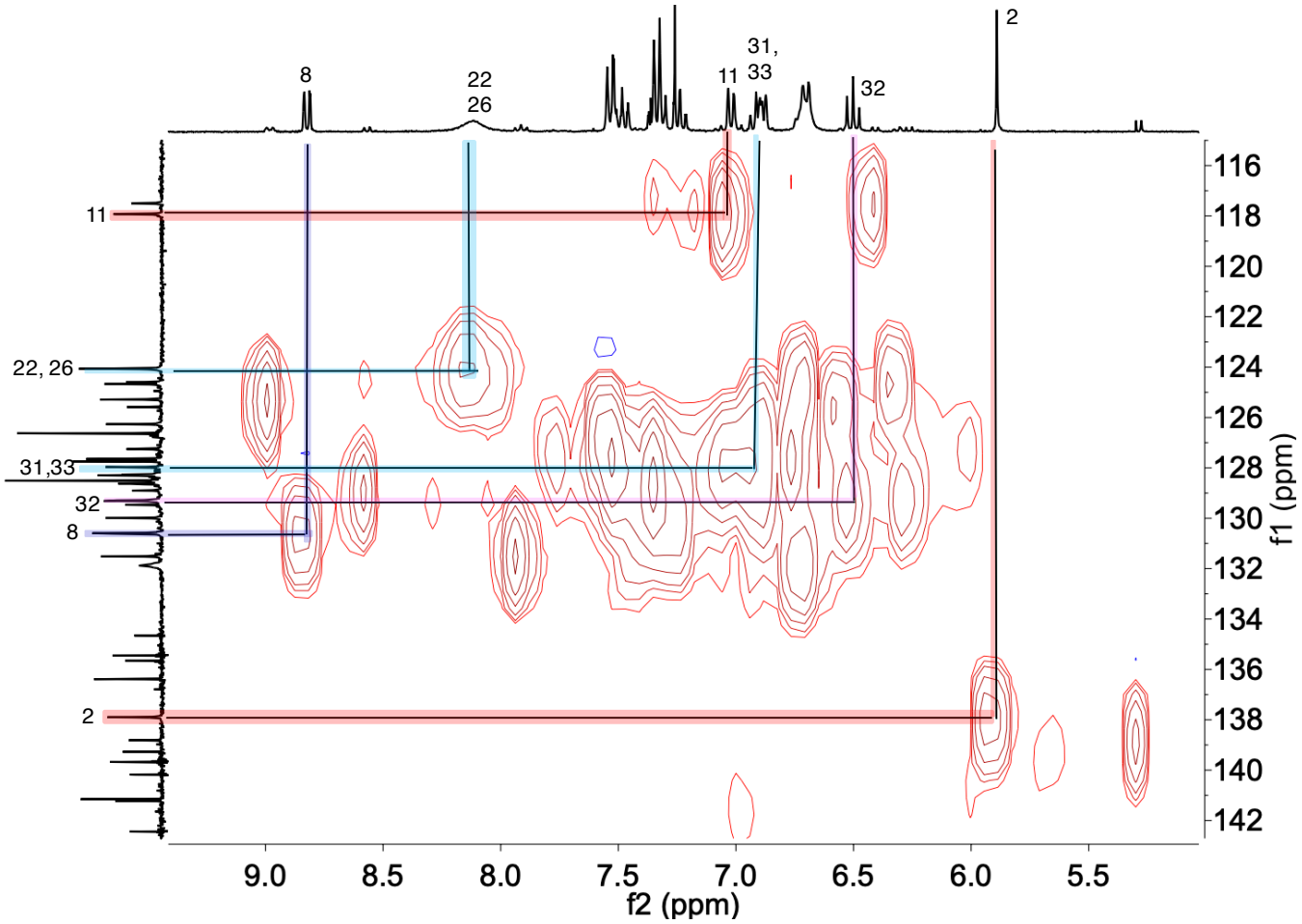


**Figure A.49d.** (c) $^{1}$H-$^{13}$C HSQC NMR spectrum ($CDCl_3$, 300 MHz) of $[RuCl_2(\mathbf{C1^{Ph}})(=Ind)]_2$ **InC1$^{Ph}$**. Expanded aromatic region.

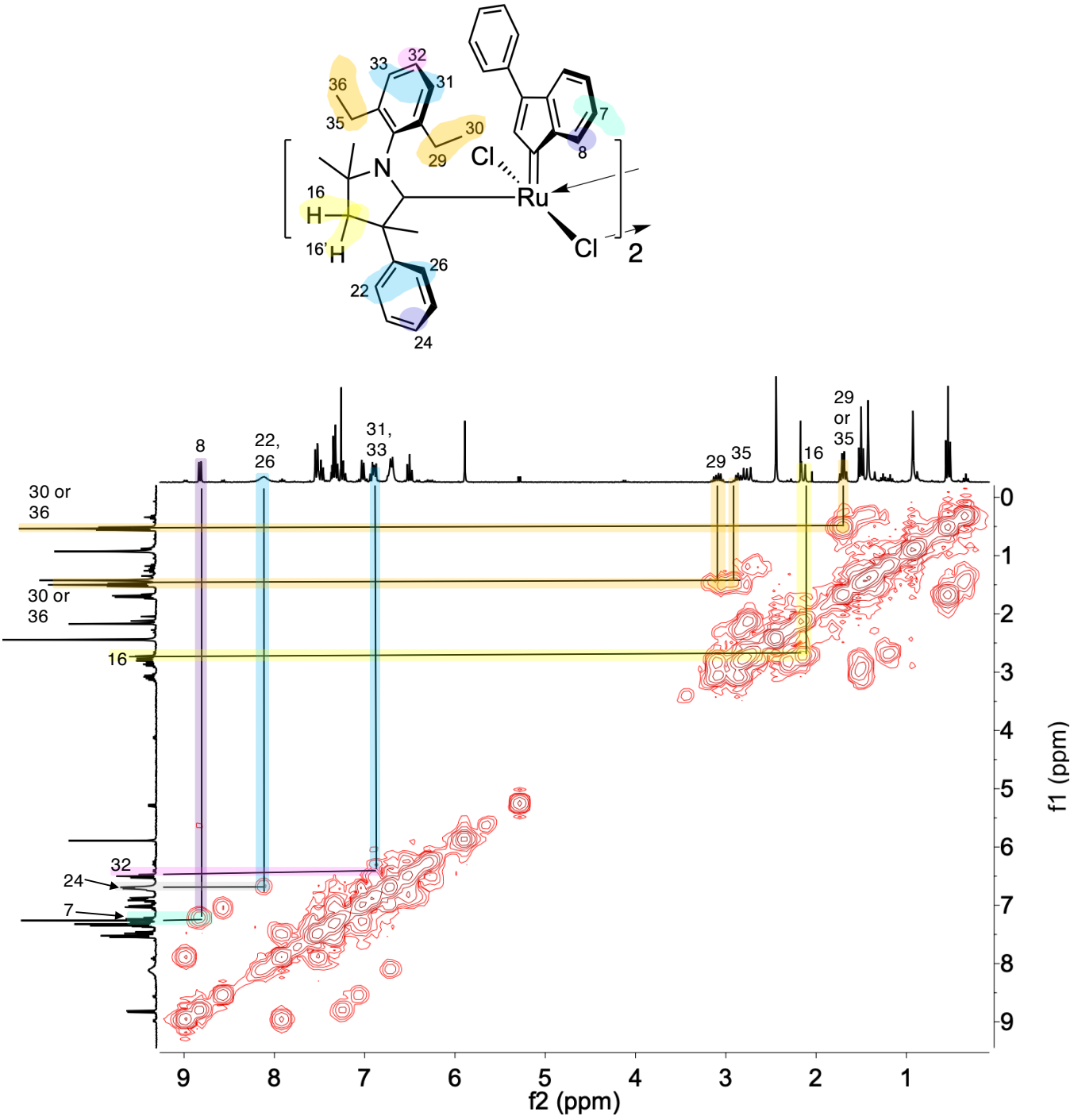


**Figure A.49e.** $^{1}$H-$^{1}$H COSY NMR spectrum ($CDCl_3$, 300 MHz) of $[RuCl_2(\mathbf{C1^{Ph}})(=Ind)]_2$ **InC1$^{Ph}$**. Numbers above/beside correlation lines correspond to the $^{1}$H protons highlighted in the structure.

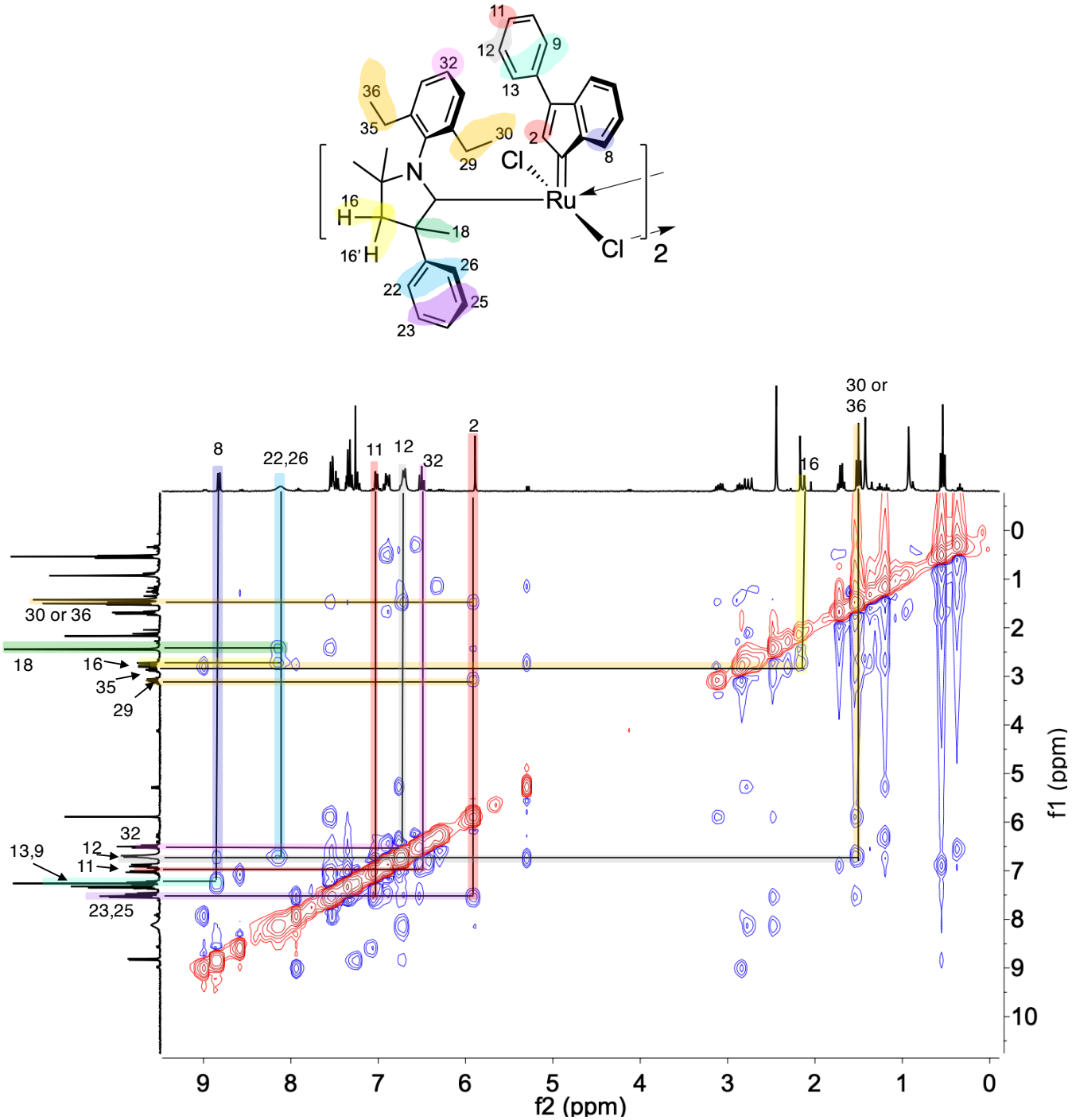


**Figure A.49f.** $^{1}$H-$^{1}$H NOESY NMR spectrum ($CDCl_3$, 300 MHz) of $[RuCl_2(\mathbf{C1}^{Ph})(=Ind)]_2$ **InC1**$^{Ph}$.

## B. Crystallographic Data

### B.1. X-Ray Crystallographic Analysis of DA'.

**Table B.1.** Crystallographic Experimental Details

| | |
|---|---|
| ***A. Crystal Data*** | |
| formula | $C_{54}H_{58}Cl_2N_4Ru$ |
| formula weight | 935.01 |
| crystal dimensions (mm) | 0.24 × 0.18 × 0.13 |
| crystal system | orthorhombic |
| space group | $P2_12_12_1$ (No. 19) |
| unit cell parameters[a] | $a$ 11.0709 (13) (Å) |
| | $b$ 17.884 (2) (Å) |
| | $c$ 23.464 (3) (Å) |
| | $V$ 4645.8 (9) (Å$^3$) |
| | $Z$ 4 |
| $\rho_{calcd}$ (g cm$^{-3}$) | 1.337 |
| $\mu$ (mm$^{-1}$) | 0.493 |
| ***B. Data Collection and Refinement Conditions*** | |
| diffractometer | Bruker PLATFORM/APEX II CCD[b] |
| radiation ($\lambda$ [Å]) | graphite-monochromated Mo Kα (0.71073) |
| temperature (°C) | –100 |
| scan type | ω scans (0.3°) (20 s exposures) |
| data collection $2\theta$ limit (deg) | 52.90 |
| total data collected | 37416 (-13 ≤ $h$ ≤ 13, -22 ≤ $k$ ≤ 22, -29 ≤ $l$ ≤ 29) |
| independent reflections | 9567 ($R_{int}$ = 0.0742) |
| number of observed reflections (*NO*) | 7693 [$F_o^2 \geq 2\sigma(F_o^2)$] |

| | |
|---|---|
| structure solution method | Patterson/structure expansion (*DIRDIF–2008*[c]) |
| refinement method | full-matrix least-squares on $F^2$ (*SHELXL–97*)[12] |
| absorption correction method | Gaussian integration (face-indexed) |
| range of transmission factors | 0.9395–0.8891 |
| data/restraints/parameters | 9567 / 6[e] / 516 |
| Flack absolute structure parameter[f] | –0.03(5) |
| goodness-of-fit (*S*)[g] [all data] | 1.084 |
| final *R* indices[h] | |
| $R_1$ [$F_o^2 \geq 2\sigma(F_o^2)$] | 0.0587 |
| $wR_2$ [all data] | 0.1597 |
| largest difference peak and hole | 1.520 and –1.142 e Å$^{-3}$ |

[a]Obtained from least-squares refinement of 9919 reflections with $4.32° < 2\theta < 43.88°$.

[b]Programs for diffractometer operation, data collection, data reduction and absorption correction were those supplied by Bruker.

[c]Beurskens, P. T.; Beurskens, G.; de Gelder, R.; Smits, J. M. M.; Garcia-Granda, S.; Gould, R. O. (2008). The *DIRDIF-2008* program system. Crystallography Laboratory, Radboud University Nijmegen, The Netherlands.

[e]Distances involving the methyl carbon positions within the two conformers of the disordered solvent toluene molecule were restrained: d(C20S–C21S) = d(C30S–C31S) = 1.50(1) Å; d(C20S···C22S) = d(C20S···C26S) = d(C30S···C32S) = [d](C30S···C36S) = 2.52(1) Å. The phenyl rings of these solvent toluene molecules were refined as idealized regular hexagons with C–C bond distances of exactly 1.39 Å and ring bond angles of exactly 120.0º.

[f](a) Flack, H. D. *Acta Crystallogr.* **1983**, *A39*, 876–881; (b) Flack, H. D.; Bernardinelli, G. *Acta Crystallogr.* **1999**, *A55*, 908–915; (c) Flack, H. D.; Bernardinelli, G. *J. Appl. Cryst.* **2000**, *33*, 1143–1148. The Flack parameter will refine to a value near zero if the structure is in the correct configuration and will refine to a value near one for the inverted configuration.

**Table B.2.** Selected Interatomic Distances (Å)

| Atom1 | Atom2 | Distance | Atom1 | Atom2 | Distance |
|---|---|---|---|---|---|
| Ru | Cl1 | 2.3903(14) | C14 | C15 | 1.365(10) |
| Ru | Cl2 | 2.4233(14) | C14 | C18 | 1.489(10) |
| Ru | N3 | 2.253(4) | C15 | C16 | 1.366(9) |
| Ru | N4 | 2.390(5) | C16 | C19 | 1.521(9) |
| Ru | C1 | 2.048(5) | C21 | C22 | 1.400(8) |
| Ru | C4 | 1.847(6) | C21 | C26 | 1.394(8) |
| N1 | C1 | 1.373(7) | C22 | C23 | 1.359(9) |
| N1 | C2 | 1.388(7) | C22 | C27 | 1.486(9) |
| N1 | C11 | 1.438(7) | C23 | C24 | 1.408(10) |
| N2 | C1 | 1.387(7) | C24 | C25 | 1.389(10) |
| N2 | C3 | 1.393(7) | C24 | C28 | 1.477(10) |
| N2 | C21 | 1.430(7) | C25 | C26 | 1.382(9) |
| N3 | C31 | 1.436(8) | C26 | C29 | 1.520(9) |
| N4 | C41 | 1.421(7) | C31 | C32 | 1.400(8) |
| C2 | C3 | 1.318(9) | C31 | C36 | 1.381(9) |
| C4 | C5 | 1.481(8) | C32 | C33 | 1.385(8) |
| C5 | C6 | 1.381(9) | C32 | C42 | 1.497(9) |
| C5 | C10 | 1.404(8) | C33 | C34 | 1.378(10) |
| C6 | C7 | 1.386(9) | C34 | C35 | 1.340(11) |
| C7 | C8 | 1.389(10) | C35 | C36 | 1.386(10) |
| C8 | C9 | 1.377(10) | C41 | C42 | 1.405(8) |
| C9 | C10 | 1.398(9) | C41 | C46 | 1.378(8) |
| C11 | C12 | 1.399(9) | C42 | C43 | 1.390(8) |
| C11 | C16 | 1.403(8) | C43 | C44 | 1.379(10) |

| | | | | | |
|---|---|---|---|---|---|
| C12 | C13 | 1.408(9) | C44 | C45 | 1.388(9) |
| C12 | C17 | 1.499(9) | C45 | C46 | 1.388(9) |
| C13 | C14 | 1.383(11) | | | |

**Table B.3.** Selected Interatomic Angles (degrees)

| **Atom1** | **Atom2** | **Atom 3** | **Angle** | **Atom1** | **Atom2** | **Atom3** | **Angle** |
|---|---|---|---|---|---|---|---|
| Cl1 | Ru | Cl2 | 168.98(5) | C12 | C13 | C14 | 121.4(6) |
| Cl1 | Ru | N3 | 83.92(15) | C13 | C14 | C15 | 119.3(6) |
| Cl1 | Ru | N4 | 87.81(12) | C13 | C14 | C18 | 118.3(7) |
| Cl1 | Ru | C1 | 90.25(14) | C15 | C14 | C18 | 122.4(7) |
| Cl1 | Ru | C4 | 103.16(17) | C14 | C15 | C16 | 122.1(7) |
| Cl2 | Ru | N3 | 92.19(14) | C11 | C16 | C15 | 118.7(6) |
| Cl2 | Ru | N4 | 81.25(12) | C11 | C16 | C19 | 119.6(6) |
| Cl2 | Ru | C1 | 93.31(15) | C15 | C16 | C19 | 121.7(6) |
| Cl2 | Ru | C4 | 87.06(17) | N2 | C21 | C22 | 118.2(5) |
| N3 | Ru | N4 | 76.71(17) | N2 | C21 | C26 | 118.7(5) |
| N3 | Ru | C1 | 174.0(2) | C22 | C21 | C26 | 122.7(6) |
| N3 | Ru | C4 | 89.2(2) | C21 | C22 | C23 | 117.7(6) |
| N4 | Ru | C1 | 101.81(19) | C21 | C22 | C27 | 121.3(5) |
| N4 | Ru | C4 | 161.22(19) | C23 | C22 | C27 | 120.9(6) |
| C1 | Ru | C4 | 93.5(2) | C22 | C23 | C24 | 122.2(6) |
| C1 | N1 | C2 | 112.4(5) | C23 | C24 | C25 | 117.9(6) |
| C1 | N1 | C11 | 128.5(5) | C23 | C24 | C28 | 122.1(7) |
| C2 | N1 | C11 | 118.8(5) | C25 | C24 | C28 | 120.0(7) |
| C1 | N2 | C3 | 111.2(5) | C24 | C25 | C26 | 122.1(7) |
| C1 | N2 | C21 | 129.8(4) | C21 | C26 | C25 | 117.3(6) |
| C3 | N2 | C21 | 119.0(5) | C21 | C26 | C29 | 121.2(6) |

| | | | | | | | |
|---|---|---|---|---|---|---|---|
| Ru | N3 | C31 | 119.4(4) | C25 | C26 | C29 | 121.5(6) |
| Ru | N4 | C41 | 125.6(4) | N3 | C31 | C32 | 120.2(5) |
| Ru | C1 | N1 | 129.0(4) | N3 | C31 | C36 | 120.2(6) |
| Ru | C1 | N2 | 128.8(4) | C32 | C31 | C36 | 119.5(6) |
| N1 | C1 | N2 | 101.9(4) | C31 | C32 | C33 | 119.1(6) |
| N1 | C2 | C3 | 106.8(5) | C31 | C32 | C42 | 121.6(5) |
| N2 | C3 | C2 | 107.7(5) | C33 | C32 | C42 | 119.2(5) |
| Ru | C4 | C5 | 134.9(4) | C32 | C33 | C34 | 120.1(7) |
| C4 | C5 | C6 | 123.4(5) | C33 | C34 | C35 | 120.6(7) |
| C4 | C5 | C10 | 118.4(5) | C34 | C35 | C36 | 120.9(7) |
| C6 | C5 | C10 | 118.2(5) | C31 | C36 | C35 | 119.6(7) |
| C5 | C6 | C7 | 120.9(6) | N4 | C41 | C42 | 119.8(5) |
| C6 | C7 | C8 | 120.2(7) | N4 | C41 | C46 | 120.8(5) |
| C7 | C8 | C9 | 120.4(6) | C42 | C41 | C46 | 119.4(5) |
| C8 | C9 | C10 | 118.9(6) | C11 | C12 | C17 | 122.0(6) |
| C5 | C10 | C9 | 121.3(6) | C13 | C12 | C17 | 120.9(6) |
| N1 | C11 | C12 | 118.7(5) | C12 | C13 | C14 | 121.4(6) |
| N1 | C11 | C16 | 119.5(5) | C32 | C42 | C41 | 121.5(5) |
| C12 | C11 | C16 | 121.3(5) | C32 | C42 | C43 | 120.6(5) |
| C11 | C12 | C13 | 117.0(6) | C41 | C42 | C43 | 117.8(6) |
| Cl1 | Ru | Cl2 | 168.98(5) | C42 | C43 | C44 | 122.9(7) |
| Cl1 | Ru | N3 | 83.92(15) | C43 | C44 | C45 | 118.6(6) |
| Cl1 | Ru | N4 | 87.81(12) | C44 | C45 | C46 | 119.5(6) |
| C11 | C12 | C17 | 122.0(6) | C41 | C46 | C45 | 121.7(6) |
| C13 | C12 | C17 | 120.9(6) | | | | |

**X-Ray Crystallographic Analysis of InC1$^{Ph}$.**

Single crystals of **InC1$^{Ph}$** were grown from $CH_2Cl_2$/MeOH at 4 °C. A suitable crystal was selected under a polarizing microscope and glued to a cactus needle with a two-component epoxy resin. Diffraction data were collected on a Rigaku Oxford Diffraction Gemini A Ultra diffractometer at RT using MoKα radiation. CrysAlis$^{PRO}$ was used for data collection and reduction.[12] The structure was determined via the Olex2 software suite using ShelXT and ShelXL for intrinsic phasing and structure refinement by least-squares minimization, respectively.[13-15] The terminal carbon atoms of two ethyl groups exhibited disorder, which was modeled: the crystal structure contained voids with solvent molecules so heavily disordered that a structural model could not be refined for them. The SQUEEZE procedure implemented in PLATON was therefore utilized. A void of 356 Å, centered at ½, 0, 0 and containing 105 electrons, was identified, and the crystal structure was refined against the squares of structure factors from which the contribution of the electron density from the disordered solvent was removed. Hydrogen atoms were placed at calculated positions. Additional refinement details are provided in Table S3 and the cif file. CCDC-1884543 contains the supplementary crystallographic data for this paper; these data can be obtained free of charge from The Cambridge Crystallographic Data Centre via https://www.ccdc.cam.ac.uk/structures/.

**InC1$^{Ph}$** crystallizes in the monoclinic $P2_1/n$ space group, with one $Ru_2Cl_4(CAAC)_2(indenylidene)_2$ dimer per asymmetric unit. The Ru centers exhibit distorted square pyramidal coordination geometry. The coordination sphere contains three chloride ligands, one CAAC, and an apical indenylidene ligand. The two Ru units are bridged via two chloride anions which form the common edge of the square-based pyramid. The apices of the two condensed coordination polyhedra are located on opposite sides of the $Ru_2Cl_4$ mean plane (Figure S5). Selected bond lengths involving Ru are presented in Table S4.

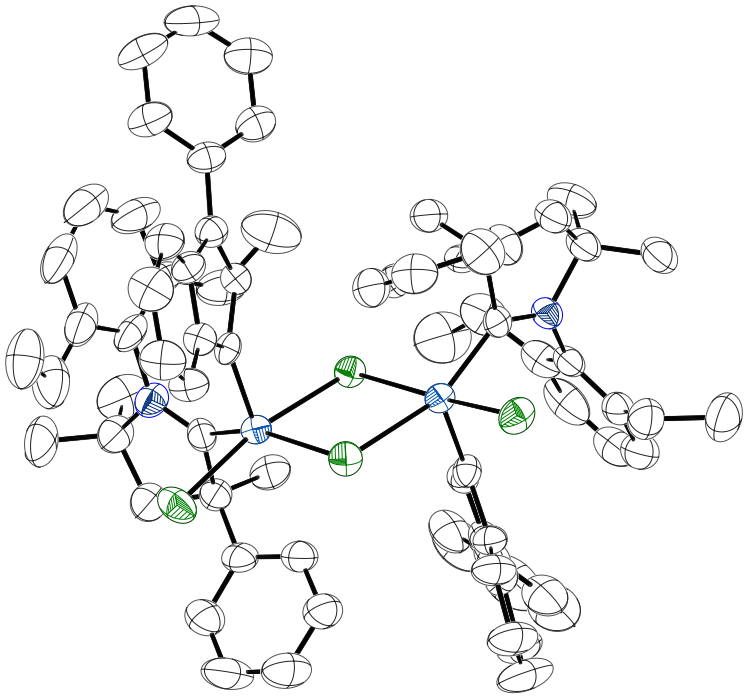

**Figure B.1.** ORTEP diagram of **InC1$^{Ph}$**. Hydrogen atoms omitted for clarity; only major components of the disordered ethyl groups shown. Atomic displacement parameters shown at the 50% probability level.

**Table B.4.** Crystal data and structure refinement for **InC1$^{Ph}$**.

| Identification code | **InC1$^{Ph}$** |
|---|---|
| Empirical formula | $C_{76}H_{78}Cl_4N_2Ru_2$ |
| Formula weight | 1363.34 |
| $T$ /K | 293 |
| Crystal system | monoclinic |
| Space group | $P2_1/n$ |
| $a$/Å | 20.2004(7) |
| $b$/Å | 13.0402(4) |
| $c$/Å | 27.5306(8) |
| $\alpha$/° | 90 |
| $\beta$/° | 105.534(3) |
| $\gamma$/° | 90 |
| $V$/Å$^3$ | 6987.1(4) |
| $Z$ | 4 |
| $\rho_{calc}$ /g/cm$^3$ | 1.296 |
| $\mu$/mm$^{-1}$ | 0.627 |
| $F$(000) | 2816.0 |
| Crystal size/mm$^3$ | 0.14 × 0.07 × 0.04 |
| Radiation | MoKα ($\lambda$ = 0.71073 Å) |
| 2Θ range for data collection/° | 6.722 to 52 |
| Index ranges | $-24 \le h \le 24$, $-16 \le k \le 16$, $-33 \le l \le 33$ |
| Reflections collected | 80301 |
| Independent reflections | 13693 [$R_{int}$ = 0.1093, $R_{sigma}$ = 0.1051] |
| Data/restraints/parameters | 13693/15/789 |
| Goodness-of-fit on $F^2$ | 0.962 |
| Final $R$ indexes [$I \ge 2\sigma(I)$] | $R_1$ = 0.0502, $wR_2$ = 0.0875 |
| Final $R$ indexes [all data] | $R_1$ = 0.1068, $wR_2$ = 0.1055 |
| Largest diff. peak/hole / eÅ$^{-3}$ | 0.66/−0.38 |

**Table B.5.** Bond lengths involving Ru for **InC1$^{Ph}$**.

| **Atom** | **Atom** | **Length (Å)** | **Atom** | **Atom** | **Length (Å)** |
|---|---|---|---|---|---|
| Ru1 | Cl1 | 2.3421(11) | Ru2 | Cl2 | 2.3644(11) |
| Ru1 | Cl3 | 2.4785(11) | Ru2 | Cl3 | 2.4871(11) |
| Ru1 | Cl4 | 2.4240(11) | Ru2 | Cl4 | 2.4200(10) |
| Ru1 | C1 | 1.975(4) | Ru2 | C41 | 1.974(4) |
| Ru1 | C25 | 1.854(4) | Ru2 | C65 | 1.869(4) |